Graduate Texts in Physics

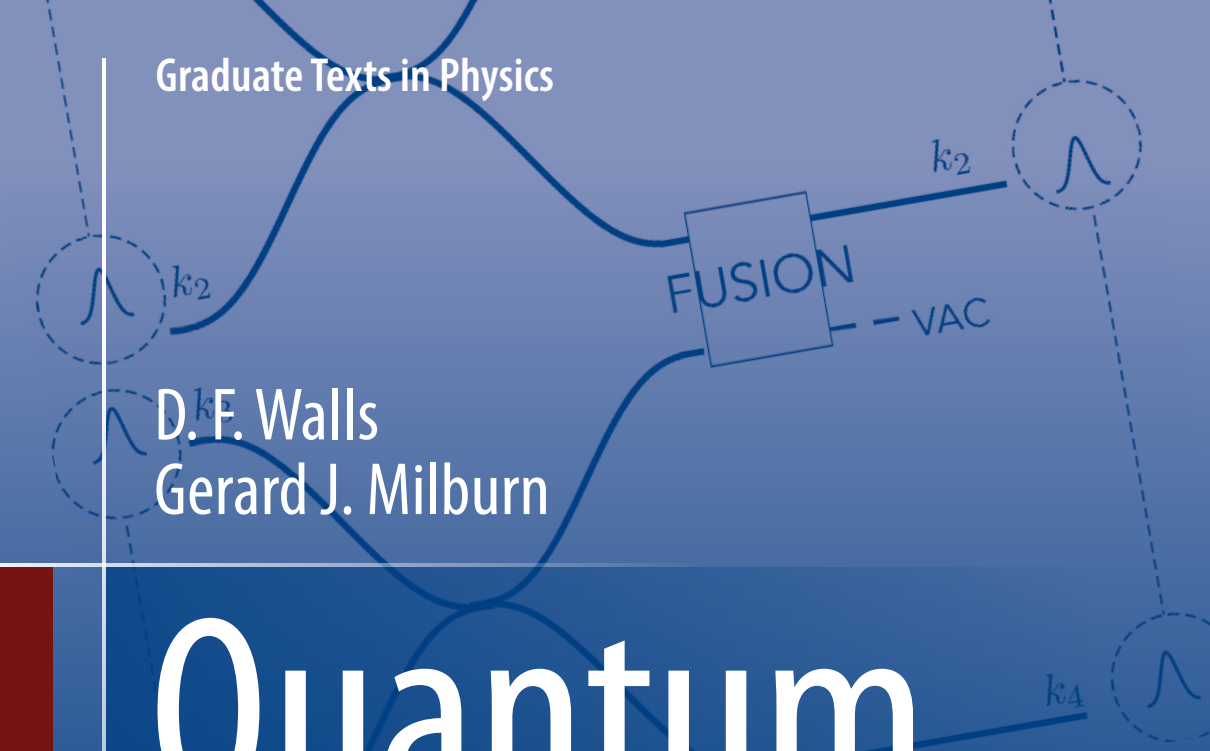

D. F. Walls
Gerard J. Milburn

Quantum Optics

Third Edition

Springer

Graduate Texts in Physics

Graduate Texts in Physics publishes core learning/teaching material for graduate- and advanced-level undergraduate courses on topics of current and emerging fields within physics, both pure and applied. These textbooks serve students at the MS- or PhD-level and their instructors as comprehensive sources of principles, definitions, derivations, experiments and applications (as relevant) for their mastery and teaching, respectively. International in scope and relevance, the textbooks correspond to course syllabi sufficiently to serve as required reading. Their didactic style, comprehensiveness and coverage of fundamental material also make them suitable as introductions or references for scientists entering, or requiring timely knowledge of, a research field.

D. F. Walls · Gerard J. Milburn

Quantum Optics

Third Edition

Springer

D. F. Walls
Auckland, New Zealand

Gerard J. Milburn
School of Mathematical and Physical Sciences
The University of Sussex
Falmer, UK

ISSN 1868-4513 ISSN 1868-4521 (electronic)
Graduate Texts in Physics
ISBN 978-3-031-84176-7 ISBN 978-3-031-84177-4 (eBook)
https://doi.org/10.1007/978-3-031-84177-4

This Springer imprint is published by the registered company Springer Nature Switzerland AG
The registered company address is: Gewerbestrasse 11, 6330 Cham, Switzerland

To memory of D. F. Walls (1942–1999)

Preface

It has been almost four decades since Dan Walls and I commenced the first edition of this book in Hamilton, New Zealand. In that time, quantum optics has spread over a large domain of theory and applications. Quantum computing, little more than a curious footnote to quantum foundations when I started, has grown into a multi billion dollar industry. The parallel fields of quantum communication and quantum sensors are impacting the wealth and security of nations. I have been unable to include recent advances in quantum machine learning in optical technologies for practical reasons. The field is new and changing very fast. I am quite sure that this will figure prominently in a future edition.

In four decades, I have accumulated a considerable debt of gratitude to a legion of teachers, collaborators, students and friends in the field of quantum optics, and theoretical physics more broadly, and the list grows steadily. There are far too many to name here. This work would not have been possible without your help.

Lewes, East Sussex, UK
October 2024

Gerard J. Milburn

Contents

Quantisation of the Electromagnetic Field

1

Abstract

The study of the quantum features of light requires the quantisation of the electromagnetic field. In this chapter we quantise the field and introduce a number of quantum states of light, including, number states, coherent states, squeezed states, cat states and GKP states. The properties of these states are discussed.

1.1 Field Quantisation

Quantum optics is a branch of quantum electrodynamics (QED) for low energy scales of light and matter. Typically this means optical frequencies for the light and electrons bound to atoms for the matter. It is concerned with the uniquely quantum-mechanical properties of the electromagnetic field, which are not present in a classical treatment of optics. We will begin by quantizing the electromagnetic field and return to the quantised matter field in later chapters. We shall make use of an expansion of the vector potential for the electromagnetic (EM) field in terms of free-field global modes. The bosonic nature of the EM field implies that quantization reduces to the quantization of the harmonic oscillator corresponding to each individual global free-field mode. The state of each mode lies in a separate Hillbert space.

We shall also introduce states of the electromagnetic field appropriate to the description of optical fields. The first set of states we introduce are the number states corresponding to their being a definite number of photons in each mode. It has become possible to experimentally prepare number states of the field with small number of photons. A more typical optical field will involve a superposition of number states, for example, the coherent state which has the minimum uncertainty in field amplitude and phase allowed by the uncertainty principle, and hence is the closest possible quantum mechanical state to a classical field. It also possesses a high degree of optical coherence as will be discussed in Chap. 3, hence the name coherent state. The coherent state plays a fundamental role in quantum optics and

D. F. Walls and G. J. Milburn, *Quantum Optics*, Graduate Texts in Physics,
https://doi.org/10.1007/978-3-031-84177-4_1

has a practical significance in that a highly stabilized laser operating well above threshold generates a coherent state.

Squeezed states are also minimum-uncertainty states but unlike the coherent states the quantum noise is not uniformly distributed in phase. Squeezed states may have less noise in one quadrature than the vacuum. As a consequence the noise in the other quadrature is increased. We introduce the basic properties of squeezed states in this chapter. In Chap. 8 we describe ways to generate squeezed states and their applications.

While states of definite photon number are readily defined as eigenstates of the number operator a corresponding description of states of definite phase is more difficult. This is due to the problems involved in constructing a Hermitian phase operator to describe a bounded physical quantity like phase. How this problem may be resolved together with the properties of phase states is discussed in the final section of this chapter.

A convenient starting point for the quantisation of the electromagnetic field are the classical field equations. The free electromagnetic field obeys the source free Maxwell equations.

$$\nabla \cdot \mathbf{B} = 0, \tag{1.1}$$

$$\nabla \times \mathbf{E}. = -\frac{\partial \mathbf{B}}{\partial t}\,, \tag{1.2}$$

$$\nabla \cdot \mathbf{D}. = 0, \tag{1.3}$$

$$\nabla \times \mathbf{H}. = \frac{\partial \mathbf{D}}{\partial t}\,, \tag{1.4}$$

where $\mathbf{B} = \mu_0 \mathbf{H}$, $\mathbf{D} = \varepsilon_0 \mathbf{E}$, μ_0, ε_0 being the magnetic permeability and electric permittivity of free space and $\mu_0 \varepsilon_0 = c^{-2}$ with c designating the speed of light. Maxwell's equations are gauge invariant when no sources are present. A convenient choice of gauge for problems in quantum optics is the Coulomb gauge. In the Coulomb gauge both $\mathbf{B}$ and $\mathbf{E}$ may be determined from a vector potential $\mathbf{A}(r, t)$ by

$$\mathbf{B} = \nabla \times \mathbf{A}, \tag{1.5}$$

$$\mathbf{E} = -\frac{\partial \mathbf{A}}{\partial t}\,, \tag{1.6}$$

with the Coulomb gauge condition

$$\nabla \cdot \mathbf{A} = 0\,, \tag{1.7}$$

We then find that $\mathbf{A}(r, t)$ satisfies the wave equation

$$\nabla^2 \mathbf{A}(r, t) = \frac{1}{c^2} \frac{\partial^2 \mathbf{A}}{\partial t^2}\,, \tag{1.8}$$

We separate the vector potential into positive and negative frequency components

$$\mathbf{A}(r, t) = \mathbf{A}^{(+}(r, t) + \mathbf{A}^{(-)}(r, t)\,, \tag{1.9}$$

where $\mathbf{A}^{(+)}(r,t)$ contains a superposition of terms that vary as $e^{-i\omega t}$ and $\mathbf{A}^{(-)}(r,t) = \left[\mathbf{A}^{(-)}(r,t)\right]^{\dagger}$ so that $\mathbf{A}^{(-)}(r,t)$ contains terms that vary as $e^{i\omega t}$ with $\omega > 0$.

For convenience we begin with a discrete set of global mode functions. This implicitly assumes that the field is confined to a finite volume, V, of space. We expand the positive frequency component of the field in terms of a complete set of orthonormal spatial mode functions

$$\mathbf{A}^{(+)}(\mathbf{r},t) = \sum_k c_k \mathbf{u}_k(\mathbf{r}) e^{-i\omega_k t} \ . \tag{1.10}$$

where the Fourier coefficients, c_k, are time independent for the free field. The vector-valued mode functions $\mathbf{u}_k(\mathbf{r})$ then satisfy the wave equation

$$\left(\nabla^2 + \frac{\omega_k}{c^2}\right)\mathbf{u}_k(\mathbf{r}) = 0 \ , \tag{1.11}$$

in a volume V that contains no refractive material. The mode functions are also required to satisfy the transversality condition following from the Coulomb gauge,

$$\nabla \cdot \mathbf{u}_k(\mathbf{r}) = 0 \ . \tag{1.12}$$

The mode functions satisfy the conditions for orthonormality,

$$\int_V \mathbf{u}_k^*(\mathbf{r})\mathbf{u}_l(\mathbf{r})d\mathbf{r} = \delta_{kl} \ . \tag{1.13}$$

The mode functions depend on the boundary conditions of the physical volume under consideration, e.g., periodic boundary conditions corresponding to travelling wave modes or conditions appropriate to reflecting walls which lead to standing waves. For example, the plane wave mode functions appropriate to a cubical volume of side length L may be written as

$$\mathbf{u}_l(\mathbf{r}) = L^{-3/2}\hat{\boldsymbol{\epsilon}}^{(\lambda)} e^{i\mathbf{k}.\mathbf{r}} \ , \tag{1.14}$$

where $\hat{\boldsymbol{\epsilon}}^{(\lambda)}$ is the unit polarisation vector. The mode index k represents several discrete indices: the polarisation index, $\lambda = 1, 2$, and the three cartesian components of the wave vector $\mathbf{k}$,

$$k_\alpha = \frac{2\pi n_\alpha}{L} \ . \tag{1.15}$$

where $\alpha \in \{x, y, z\}$ and $n_\alpha = 0, \pm 1, \pm 2, \ldots$. The polarization vector $\hat{\boldsymbol{\epsilon}}^{(\lambda)}$ is required to be perpendicular to $\mathbf{k}$ by the transversality condition (1.12).

The vector potential may now be written in the form

$$\mathbf{A}(r,t) = \sum_k \left(\frac{\hbar}{2\omega_k \epsilon_0}\right)^{1/2} \left[a_k \mathbf{u}_k(\mathbf{r}) e^{-i\omega_k t} + a_k^\dagger \mathbf{u}_k^*(\mathbf{r}) e^{i\omega_k t}\right] \ . \tag{1.16}$$

The corresponding form for the electric field is

$$\mathbf{E}(r,t) = i\sum_k \left(\frac{\hbar\omega_k}{2\epsilon_0}\right)^{1/2}\left[a_k\mathbf{u}_k(\mathbf{r})e^{-i\omega_k t} - a_k^\dagger\mathbf{u}_k^*(\mathbf{r})e^{i\omega_k t}\right] . \tag{1.17}$$

The normalization factors have been chosen such that the amplitudes a_k and $a_k^\dagger$ are dimensionless.

In classical electromagnetic theory these Fourier amplitudes are complex numbers. Quantisation of the electromagnetic field is accomplished by choosing a_k and $a_k^\dagger$ and to be mutually adjoint operators. Since photons are bosons the appropriate commutation relations to choose for the operators a_k and $a_k^\dagger$ are the boson canonical commutation relations

$$[a_k, a_l] = [a_k^\dagger, a_l^\dagger] = 0, \quad [a_k, a_l^\dagger] = \delta_{kl} . \tag{1.18}$$

The dynamical behaviour of the electric-field amplitudes may then be described by an ensemble of independent harmonic oscillators obeying the above commutation relations. The quantum states of each mode is a vector, $|\psi_k\rangle$, in independent Hilbert spaces. The states of the entire field are then defined in the tensor product space of the Hilbert spaces for all of the modes.

The Hamiltonian for the electromagnetic field is given by

$$H = \frac{1}{2}\int_V d\mathbf{r}\,(\epsilon_0\mathbf{E}^2 + \mu_0\mathbf{H}^2) . \tag{1.19}$$

Substituting (1.17) for E and the equivalent expression for H and making use of the conditions (1.12) and (1.13), the Hamiltonian may be reduced to the form

$$H = \sum_k \hbar\omega_k\left(a_k^\dagger a_k + \frac{1}{2}\right) . \tag{1.20}$$

The corresponding classical description of the EM field can be given using exactly the same mode decomposition because the classical field satisfies a classical wave equation. In that case, the operators, $a, a^\dagger$ are simply complex variables $\alpha, \alpha^* \in \mathbb{C}$. If the field is deterministic these take definite values fore each mode. If the field is stochastic these become complex valued random variables with some probability density function $P(\alpha, \alpha^*)$ on $\mathbb{C}$ such that

$$\frac{1}{\pi}\int d^2\alpha\, P(\alpha,\alpha^*) = 1 \tag{1.21}$$

where $d^2\alpha = dxdy$ and $\alpha = x + iy$. In general no such description is possible in the quantum case. We discuss this in more detail in Chap. 3.

1.2 Number States

The Hamiltonian (1.20) has the eigenvalues $\hbar\omega_k(n_k + 1/2)$ where n_k is a positive integer integer ($n_k = 0, 1, 2, \ldots, \infty$). The eigenstates are written as $|n_k\rangle$ and are known as *number* or *Fock* states. They are eigenstates of the number operator $N_k = a_k^\dagger a_k$

$$a_k^\dagger a_k |n_k\rangle = n_k |n_k\rangle \, . \tag{1.22}$$

The ground state or vacuum state of the field mode is defined by

$$a_k |0\rangle = 0 \, . \tag{1.23}$$

Thus the average energy of the vacuum state is

$$\langle 0|H|0\rangle = \frac{1}{2}\sum_k \hbar\omega_k \, . \tag{1.24}$$

Since there is no upper bound to the frequencies in the sum over electromagnetic field modes, the energy of the ground state is infinite, a conceptual difficulty for quantum field theory. However, since practical experiments measure a change in the total energy of the electromagnetic field the infinite zero-point energy does not lead to any divergence in practice. The operators a_k, $a_k^\dagger$ are raising and lowering operators for the harmonic oscillator ladder of eigenstates. In terms of photons they represent the annihilation and creation of a photon with the wave vector k and a polarisation $\hat{\mathbf{e}}^{(\lambda)}$. Hence the terminology, annihilation and creation operators. Application of the creation and annihilation operators to the number states yield

$$a_k |n_k\rangle = \sqrt{n_k}|n_k - 1\rangle, \quad a_k^\dagger |n_k\rangle = \sqrt{n_k + 1}|n_k + 1\rangle \, . \tag{1.25}$$

The state vectors for the higher excited states may be obtained from the vacuum by successive application of the creation operator

$$|n_k\rangle = \frac{(a_k^\dagger)^{n_k}}{\sqrt{n_k!}}|0\rangle \quad n_k = 0, 1, 2, \ldots \, . \tag{1.26}$$

The number states are orthogonal

$$\langle n_k | n_l \rangle = \delta_{kl} \, , \tag{1.27}$$

and complete

$$\sum_{n_k=0}^{\infty} |n_k\rangle\langle n_k| = \mathbb{I} \, , \tag{1.28}$$

where $\mathbb{I}$ is the identity operator. Since the norm of these eigenvectors is finite, they form a complete set of basis vectors for a Hilbert space.

While the number states form a useful representation for high-energy photons, e.g. γ rays where the number of photons is very small, they are not the most suitable representation for optical fields where the total number of photons is large. Most optical fields are either a superposition of number states (pure state) or a mixture of number states (mixed state). However recent experiments have demonstrated a number of methods to generate number states directly. One of these will be discussed in Sect. 14.2.1.

1.3 Coherent States

A more appropriate basis for many optical fields are the coherent states [2]. The coherent states have an indefinite number of photons which allows them to have a more precisely defined phase than a number state for which the phase is completely random. The product of the uncertainty in amplitude and phase for a coherent state is the minimum allowed by the uncertainty principle. In this sense they are the closest quantum mechanical states to a classical description of the field.We shall outline the basic properties of the coherent states below. These states are defined in terms of the unitary displacement operator, for a single mode

$$D(\alpha) = e^{\alpha a^\dagger - \alpha^* a}\ , \tag{1.29}$$

where α is an arbitrary complex number. One easily verifies $D^\dagger(\alpha) = D^{-1}(\alpha) = D(-\alpha)$. The name 'displacement operator' follows from the relations

$$D^\dagger(\alpha) a D(\alpha) = a + \alpha, \quad D^\dagger(\alpha) a^\dagger D(\alpha) = a^\dagger + \alpha^* \tag{1.30}$$

Using the operator ordering theorem

$$e^{A+B} = e^A e^B e^{-[A,B]/2} \tag{1.31}$$

which holds when $[A, [A, B]] = [B, [A, B]] = 0$, we can write $D(\alpha)$ in *normally ordered form*,

$$D(\alpha) = e^{-|\alpha|^2/2} e^{\alpha a^\dagger} e^{-\alpha^* a}\ , \tag{1.32}$$

or in *anti-normally ordered form*,

$$D(\alpha) = e^{|\alpha|^2/2} e^{-\alpha^* a} e^{\alpha a^\dagger} \tag{1.33}$$

Using this expression we can prove that the number state matrix elements of the displacement operator are [10]

$$\langle n|D(\alpha)|m\rangle = \sqrt{\frac{m!}{n!}} e^{-|\alpha|^2/2} \alpha^{n-m} L_m^{n-m}(|\alpha|^2) \quad n \geq m \ , \tag{1.34}$$

where $L_q^p(x)$ is the associated Lageurre polynomial.

The coherent state $|\alpha\rangle$ is then defined by acting on the vacuum state

$$|\alpha\rangle = D(\alpha)|0\rangle \ . \tag{1.35}$$

It then follows that the coherent states are eigenstates of the annihilation operator a as

$$a|\alpha\rangle = \alpha|\alpha\rangle \ . \tag{1.36}$$

Note that as a is a non-Hermitian operator its eigenvalues are not real.

The displacement operator acting on a coherent state transforms it to another coherent state. To prove this we use (1.31)

$$D(\alpha + \beta) = D(\alpha)D(\beta)e^{-i\Im(\alpha\beta^*)} \ . \tag{1.37}$$

Then we see that

$$D(\beta)|\alpha\rangle = e^{i\Im(\alpha\beta^*)}|\alpha + \beta\rangle \ . \tag{1.38}$$

The coherent states contain an indefinite number of photons. This may be made apparent by considering an expansion of the coherent states in the number states basis. Taking the scalar product of both sides of (1.36) with $|n\rangle$, we find the recursion relation

$$\sqrt{n+1}\langle n|\alpha\rangle = \alpha\langle n|\alpha\rangle \ . \tag{1.39}$$

It follows that

$$\langle n|\alpha\rangle = \frac{\alpha^n}{\sqrt{n!}}\langle 0|\alpha\rangle \tag{1.40}$$

Expanding $|\alpha\rangle$ in the number basis

$$|\alpha\rangle = \sum_{n=0}^{\infty} |n\rangle\langle n|\alpha\rangle = \langle 0|\alpha\rangle \sum_{n=0}^{\infty} \frac{\alpha^n}{\sqrt{n!}} \ . \tag{1.41}$$

Using the displacement operator,

$$\langle 0|\alpha\rangle = \langle 0|D(\alpha)|0\rangle = e^{-|\alpha|^2/2} \ , \tag{1.42}$$

which ensures the normalisation of the coherent state. Thus

$$|\alpha\rangle = e^{-|\alpha|^2/2} \sum_{n=0}^{\infty} \frac{\alpha^n}{\sqrt{n!}}|n\rangle \ . \tag{1.43}$$

The probability distribution for photon number in a coherent state is

$$P(n) = \frac{|\alpha|^{2n}}{n!} e^{-|\alpha|^2} \tag{1.44}$$

The mean and variance of this distribution as given by $\bar{n} = |\alpha|^2$, $\Delta n^2 = \bar{n}$. The mean is equal to the variance. This is the defining characteristic of a *Poisson* distribution.

The coherent states are not orthogonal. To see this we first note that

$$\langle \beta | \alpha \rangle = \langle 0 | D^\dagger(\beta) D(\alpha) | 0 \rangle \tag{1.45}$$

Using (1.37) we see that

$$\langle \beta | \alpha \rangle = e^{-(|\alpha|^2 + |\beta|^2)/2 + \alpha\beta^*} \,. \tag{1.46}$$

Thus

$$|\langle \beta | \alpha \rangle|^2 = e^{-|\alpha - \beta|^2} \,. \tag{1.47}$$

Coherent states of different complex amplitudes thus become approximately orthogonal exponentially fast as the magnitude of the Euclidean distance between their complex amplitudes increases.

The coherent states, while not orthogonal, do provide a resolution of identity

$$\frac{1}{\pi} \int |\alpha\rangle\langle\alpha| d^2\alpha = \mathbb{I} \tag{1.48}$$

To see this we expand the coherent states in the number basis

$$\frac{1}{\pi} \int |\alpha\rangle\langle\alpha| d^2\alpha = \frac{1}{\pi} \sum_{n,m=0}^{\infty} \int d^2\, \alpha \alpha^{*\,m} \alpha^n e^{-|\alpha|^2} \tag{1.49}$$

Changing to circular polar coordinates to evaluate the integral

$$\int d^2\, \alpha \alpha^{*\,m} \alpha^n = \int_0^\infty dr\; r^{n+m+1} e^{-r^2} \int_0^{2\pi} d\theta\; e^{i(n-m)\theta} \tag{1.50}$$

Using

$$\int_0^{2\pi} d\theta\; e^{i(n-m)\theta} = 2\pi \delta_{nm} \tag{1.51}$$

and defining $\epsilon = r^2$ we have

$$\frac{1}{\pi} \int |\alpha\rangle\langle\alpha| d^2\alpha = \sum_{n=0}^{\infty} (n!)^{-1} |n\rangle\langle n| \int_0^\infty d\epsilon e^{-\epsilon} \epsilon^n \tag{1.52}$$

The integral over ϵ is the definition of the Gamma function and is thus equal to $n!$ and thus

$$\frac{1}{\pi}\int |\alpha\rangle\langle\alpha| d^2\alpha = \sum_{n=0}^{\infty} |n\rangle\langle n| = \mathbb{I} \tag{1.53}$$

Coherent states are also known as minimum-uncertainy states. Define the canonical operators X_1, X_2—the quadrature phase operators—as

$$X_1 = a + a^\dagger, \quad X_2 = -i(a - a^\dagger) \tag{1.54}$$

These obey the canonical commutation relations

$$[X_1, X_2] = 2i \tag{1.55}$$

These are equivalent to the canonical commutation relations for position q and momentum p and as in that case all physical states must satisfy the Heisenberg uncertainty relation

$$\Delta X_1 . \Delta X_2 \geq 1 \tag{1.56}$$

where $\Delta A^2 = \langle A^2\rangle - \langle A\rangle^2$ is the variance in A. The coherent states satisfy the equality with $\Delta X_1 = \Delta X_2 = 1$.

In the diagonal basis of X_1 defined by

$$X_1 = \int_{-\infty}^{\infty} dx\ x|x\rangle\langle x| \tag{1.57}$$

we have the following results

$$\langle x|n\rangle = (2\pi)^{-1/4}(2^n n!)^{-1/2} H_n\left(\frac{x}{\sqrt{2}}\right) e^{-x^2/4} \tag{1.58}$$

where $H_n(x)$ is the n'th order Hermite polynomial. These are simply the energy eigenstates of a simple harmonic oscillator for a suitably scaled definition of position. The corresponding X_1-representation for the coherent state $|\alpha\rangle$ is

$$\langle x|\alpha\rangle = (2\pi)^{-1/4} e^{i\Im(\alpha)x - (x - 2\Re(\alpha))^2/4} \tag{1.59}$$

where $\Re(\alpha)$, $\Im(\alpha)$ are the real and imaginary parts of α respectively.

The coherent states have a physical significance in that the field generated by a highly stabilized laser operating well above threshold can be described as a coherent state with slowly diffusing phase but fixed intensity (see Chap. 10). They form a useful basis for expanding the optical field in problems in laser physics and nonlinear optics. The coherence properties of light fields and the significance of the coherent states will be discussed in Chap. 2.

1.4 Squeezed States

A general class of minimum-uncertainty states are known as squeezed states. In general, a squeezed state may have less noise in one quadrature than a coherent state. To satisfy the requirements of a minimum-uncertainty state the noise in the other quadrature is greater than that of a coherent state. In the case of pure squeezed states we require

$$\Delta X_1 = \frac{1}{\Delta X_2} \tag{1.60}$$

The coherent states are a particular member of this more general class of minimum uncertainty states with equal noise in both quadratures.

There is a useful heuristic to picture minimum uncertainty states. We regard the non -zero values of the quadrature phase variances ΔX_j as indicative of intrinsic quantum fluctuations. In Chap. 3 we will see this is to be interpreted as fluctuations in the results of a class of measurements but for now we will simply imagine it in semi-classical terms. We picture a coherent state as a bivariate random variable x_1, x_2 corresponding to the two quadrature phase operators X_1, X_2. The mean is determined by the real and imaginary components of the complex amplitude and the noise by the standard deviation in the quadrature phase operators, $\Delta X_1, \Delta X_2$. We picture this as an uncertainty circle centred on the real and imaginary components of the complex amplitude and with radius equal to unity. This heuristic picture is illustrated in Fig. 1.1. In terms of this picture the squeezed states are seen as replacing the uncertainty circle with an uncertainty ellipse.

The squeezed vacuum states are defined by a unitary transformation of the vacuum $|0, \xi\rangle = S(\xi)|0\rangle$ where

$$S(\xi) = e^{(\xi^* a^2 - \xi a^{\dagger\,2})/2}\,, \tag{1.61}$$

where $\xi = re^{-2i\phi}$. More generally the squeezed states are defined as displaced squeezed vacuum states

$$|\alpha, \xi\rangle = D(\alpha)S(\xi)|0\rangle\,. \tag{1.62}$$

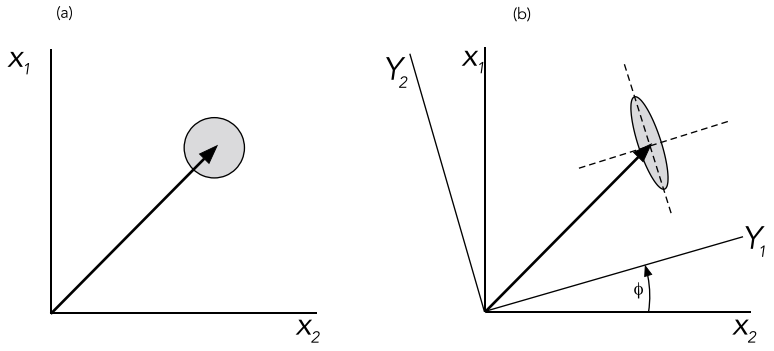

Fig. 1.1 A pictorial 'phase-space' heuristic to capture features of a minimum uncertainty state **a** coherent state **b** squeezed state

We can calculate the moments of the squeezed states using the following canonical transformation

$$S^{\dagger}(\xi)aS(\xi) = a\cosh r - a^{\dagger}e^{-2i\phi}\sinh r \tag{1.63}$$

This can be give a heuristic interpretation in phase space by first defining the rotated quadrature phase operators Y_1, Y_2

$$Y_1 + iY_2 = (X_1 + iX_2)e^{-i\phi}\ , \tag{1.64}$$

and then showing that

$$S^{\dagger}(\xi)(Y_1 + iY_2)S(\xi) = Y_1 e^{-r} + iY_2 e^{r}\ . \tag{1.65}$$

This is indicated in Fig. 1.1 with the inclusion of a displacement. Thus the squeezed state has unequal uncertainties in the rotated quadrature phase operators Y_1 and Y_2 as seen in the error ellipse shown in Fig. 1.1. The principal axes of the ellipse lie along the Y_1 and Y_2 axes, and the principal radii are ΔY_1 and. ΔY_2. A more rigorous definition of these error ellipses as contours of the Wigner function is given in Chap. 3.

The probability amplitude for the squeezed state $|\alpha, r\rangle$ (with $r \in \mathbb{R}$) in the diagonal basis of X_1 is defined by

$$\psi(x;\alpha,r) = \langle x|D(\alpha)S(r)|0\rangle \tag{1.66}$$

This may be evaluated by noting that

$$X_1 S(r)|x\rangle = xe^{-r}S(r)|x\rangle \tag{1.67}$$

The we find that

$$\psi(x;\alpha,r) = (2\pi)^{-1/4}e^{r/2}e^{i\Im(\alpha)x - e^{2r}(x-2\Re(\alpha))^2/4} \tag{1.68}$$

The photon number distribution for a squeezed state is given by $P(n;\alpha,r) = |\langle n|\alpha,r\rangle|^2$ where

$$\langle n|\alpha,r\rangle = \langle n|D(\alpha)S(r)|0\rangle \tag{1.69}$$

where for simplicity we have taken ξ as real. Let us first consider the squeezed vacuum state for which $\alpha = 0$

$$P(n;r) = |\langle n|S(r)|0\rangle|^2 \tag{1.70}$$

We first make use of the normally ordered disentangling of the squeezing operator,

$$S(r) = e^{-\tanh(r)\ a^{\dagger\ 2}/2}e^{-\ln(\cosh(r))(a^{\dagger}a+1/2)}e^{\tanh(r)a^2/2} \tag{1.71}$$

Thus

$$\langle n|S(r)|0\rangle = (\cosh r)^{-1/2}\langle n|e^{-\tanh(r)\ a^{\dagger\ 2}/2}|0\rangle \tag{1.72}$$

Clearly the probability of getting an odd photon number is zero, $Pr(n = odd) = 0$. Using (1.25) we see that

$$\langle n|S(r)|0\rangle = [\cosh(r)]^{-1/2}\frac{(-\tanh(r)/2)^{n/2}\sqrt{(n)!}}{(n/2)!} \tag{1.73}$$

and so

$$P(n;r) = \cosh(r)^{-1}\frac{(\tanh(r)/2)^n(n)!}{((n/2)!)^2} \quad n = 0, 2, 4, \ldots . \tag{1.74}$$

The amplitude $\langle\beta|0, r\rangle$ (which we call the Q-amplitude for reasons explained in Chap. 3) may be found by writing

$$\langle\beta|0, r\rangle = \sum_{n=0}^{\infty}\langle\beta|n\rangle\langle n|S(r)|0\rangle \tag{1.75}$$

using (1.73, 1.40). we see that this can be evaluated as

$$\langle\beta|0, r\rangle = \frac{1}{\sqrt{\cosh(r)}}\exp\left[-\frac{|\beta|^2}{2} - \frac{\tanh r\ \beta^{*\ 2}}{2}\right] \tag{1.76}$$

The photon amplitude for the displaced squeezed state can be found by using

$$\langle\beta|\alpha, r\rangle = \sum_{n=0}^{\infty}\langle\beta|n\rangle\langle n|\alpha, r\rangle = \sum_{n=0}^{\infty}\frac{\beta^n}{\sqrt{n!}}e^{-|\beta|^2/2}\langle n|\alpha, r\rangle \tag{1.77}$$

Using (1.76), the left hand side may be written

$$\langle\beta|\alpha, r\rangle = \frac{1}{\sqrt{\cosh r}}\exp\left[-i\Im(\alpha\beta^*) - |\beta-\alpha|^2/2 - \tanh r(\beta-\alpha)^2/2\right] \tag{1.78}$$

We may expand this in terms of $\beta^n e^{-|\beta|^2/2}$ by making use of the generating function for complex Hermite polynomials,

$$e^{2zt-t^2} = \sum_{n=0}^{\infty}\frac{H_n(z)}{n!}t^n \tag{1.79}$$

the result is

$$\langle n|\alpha, r\rangle = (n!\cosh r)^{-1/2}\lambda^{n/2}e^{-|\alpha|^2/2-\lambda\alpha^2}H_n(z) \tag{1.80}$$

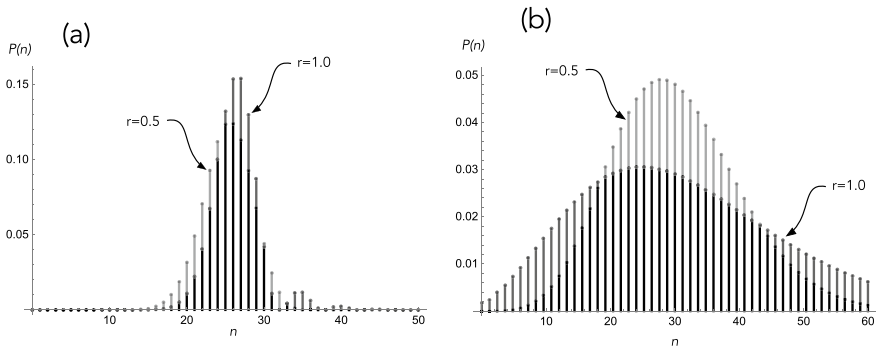

Fig. 1.2 Photon number distribution for a squeezed state $|\alpha, r\rangle$. **a** Amplitude squeezing case; $\alpha = 5.0$, $r = 0.5$ and $r = 1.0$. **b** Phase squeezing case $\alpha = 5.0$, $r = -0.5$ and $r = -1.0$

where

$$z = \sqrt{\lambda}\alpha + \frac{\alpha^*}{2\sqrt{\lambda}} \tag{1.81}$$

and $\lambda = \frac{1}{2}\tanh r$. Thus the photon number distribution for a squeezed state

$$P(n;\alpha, r) = \frac{|\lambda|^n}{n!\cosh r} e^{-|\alpha|^2 - \lambda(\alpha^2 + \alpha^{*\,2})} |H_n(z)|^2 \tag{1.82}$$

This is equivalent to the form given by Yuen [6] for a slightly different definition of a squeezed state known as the two-photon coherent state.

In Fig. 1.2 we plot the photon number distribution for a squeezed state $|\alpha, r\rangle$ with different coherent amplitudes, α and squeezing parameter, r. In viewing these distributions it is important to understand the relationship between the quadrature in phase with the coherent excitation and the squeezing of that quadrature. In the figures we always choose $r \in \mathbb{R}$ and vary the phase of the coherent excitation. If we choose $\alpha \in \mathbb{R}$ real, then $r > 0$ corresponds to amplitude-squeezing as the fluctuations in phase with the coherent amplitude quadrature are reduced, while $r < 0$ corresponds to phase-squeezing as the fluctuations in quadrature phase to the coherent amplitude are reduced. Note the oscillations in the distribution for the amplitude squeezed case. This is a particular example of a general feature known as interference in phase-space [8].

1.5 Two-Mode Squeezed States

Multimode squeezed states are important since several devices produce light which is correlated at the two frequencies ω_1 and ω_2. Usually these frequencies are symmetrically placed either side of a carrier frequency, ω_p so that $\omega_1 + \omega_2 = 2\omega_p$. The squeezing exists not in the quadrature operators associated with each mode but in a collective quadrature operator for the modes.

The two-mode squeezed vacuum state is defined by

$$|0,\xi\rangle = S_{12}(\xi)|0\rangle \tag{1.83}$$

where $|0\rangle = |0\rangle_1 \otimes |0\rangle_2$ is the joint vacuum state of the two modes and

$$S(\xi) = e^{\xi^* a_1 a_2 - \xi a_1^\dagger a_2^\dagger} \tag{1.84}$$

One then finds that

$$S^\dagger(\xi) a_1 S(\xi) = a_1 \cosh r - a_2^\dagger e^{i\theta} \sinh r \tag{1.85}$$

with $\xi = re^{i\theta}$. The coherenty excited two-mode squeezed states are then obtained by displacing both modes independently,

$$|\alpha_1, \alpha_2, \xi\rangle = D_1(\alpha_1) D_2(\alpha_2) S_{12}(\xi)|0\rangle \tag{1.86}$$

The following moments follow

$$\langle a_k \rangle = \alpha_k \tag{1.87}$$
$$\langle a_k^2 \rangle = \alpha_k^2 \tag{1.88}$$
$$\langle a_1 a_2 \rangle = \alpha_1 \alpha_2 - e^{i\theta} \sinh r \cosh r \tag{1.89}$$
$$\langle a_k^\dagger a_k \rangle = |\alpha_k|^2 + \sinh^2 r \tag{1.90}$$

the third of these equations implies that the two modes are correlated. As we are dealing with pure states this implies that the two modes are in *entangled* states, (see Chap. 14).

In the case of the two-mode squeezed vacuum state we find that the variances in each mode are given by

$$V(X_k) = V(Y_k) = 2\sinh^2 r + 1 \tag{1.91}$$

These are certainly not minimum uncertainty states. Define the collective quadrature phase operators

$$X_\pm = \frac{1}{\sqrt{2}}(X_1 \pm X_2) \tag{1.92}$$
$$Y_\pm = \frac{1}{\sqrt{2}}(Y_1 \pm Y_2) \tag{1.93}$$

This is a canonical transformation and thus $X_\pm, Y_\pm$ obey the standard canonical commutation relations $[X_+, Y_+] = [X_-, Y_-] = 2i$. We then find for the two-mode squeezed state that

$$\langle X_\pm^2 \rangle = e^{\mp 2r} \cos^2 \theta/2 + e^{\pm 2r} \sin^2 \theta/2 \tag{1.94}$$

$$\langle Y_\pm^2 \rangle = e^{\pm 2r} \cos^2 \theta/2 + e^{\mp 2r} \sin^2 \theta/2 \tag{1.95}$$

$$\langle X_+ X_- \rangle = 0 \tag{1.96}$$

$$\langle Y_+ Y_- \rangle = 0 \tag{1.97}$$

The last two equations tell us that the collective modes are uncorrelated and, as we are dealing with pure states, the joint modes are in separable states. Choosing θ we see that the separable states are squeezed minimum uncertainty states. Thus the local modes are entangled while the collective modes are separable squeezed states.

In the number basis the two-mode squeezed vacuum state can be found using the two-mode disentangling identity

$$e^{-r(a_1 a_2 - a_1^\dagger a_2^\dagger)} = e^{-\tanh r a_1^\dagger a_2^\dagger} e^{-\ln \cosh r (a_1^\dagger a_1 + a_2^\dagger a_2 + 1)} e^{\tanh r a_1 a_2} \tag{1.98}$$

Then

$$S(r)|0\rangle = (1 - \lambda^2)^{1/2} \sum_{n=0}^{\infty} (-\lambda)^n |n, n\rangle \tag{1.99}$$

where $\lambda = \tanh r$. Clearly this is an eigenstate of photon number difference $a_1^\dagger a_1 - a_2^\dagger a_2$. We will make use of this in Chap. 14 when we discuss quantum teleportation.

1.6 Phase Properties of the Field

The definition of an Hermitian phase operator corresponding to the physical phase of the field has long been a problem. Initial attempts by Dirac led to a non-Hermitian operator with incorrect commutation relations [11]. This difficulty was addressed in the work of Susskind and Glogower [12]. Pegg and Barnett [13] showed how to construct a Hermitian phase operator. We will first discuss the Susskind–Glogower (SG) phase operator.

Let $a, a^\dagger$ be the annihilation and creation operators for a single mode field. In analogy with the classical polar decomposition of a complex amplitude we define the SG phase operator,

$$\widehat{e^{i\phi}} = (aa^\dagger)^{-1/2} a \tag{1.100}$$

The operator $\widehat{e^{i\phi}}$ has the number state expansion

$$\widehat{e^{i\phi}} = \sum_{n=0}^{\infty} |n\rangle \langle n+1| \,. \tag{1.101}$$

This is a displacement operator in the number basis. The eigenstates of $\widehat{e^{i\phi}}$ are the (unormalisable) states

$$|e^{i\theta}\rangle = \sum_{n=0}^{\infty} e^{in\theta}|n\rangle \quad \text{for} -\pi < \theta \leq \pi \ , \tag{1.102}$$

with eigenvalue $e^{i\theta}$. Clearly these states are infinite energy states and, like position and momentum eginstates, do not lie in the Hilbert space of physical states.

It is easy to verify that $\widehat{e^{i\phi}}$ is not unitary. In fact

$$[\widehat{e^{i\phi}}, \widehat{e^{i\phi}}^{\dagger}] = |0\rangle\langle 0| \ . \tag{1.103}$$

An immediate consequence of this is that the SG phase eigenstates are not orthogonal

$$\langle e^{i\theta'}|e^{i\theta}\rangle = \frac{1}{1 - e^{i(\theta-\theta')}} \quad , \tag{1.104}$$

although $|\langle e^{i\theta'}|e^{i\theta}\rangle|^2$ is very sharply peaked on $\theta = \theta'$. Nonetheless these states do provide a resolution of identity,

$$\frac{1}{2\pi}\int_{\pi}^{-\pi} d\theta |e^{i\theta}\rangle\langle|e^{i\theta}| = 1 \tag{1.105}$$

This immediately implies that

$$P(\theta) = \text{tr}[|e^{i\theta}\rangle\langle e^{i\theta}|\rho] \tag{1.106}$$

is valid probability distribution on $-\pi < \theta \leq \pi$. In terms of quantum parameter estimation, the SG operator is optimal [14]. The fact that the SG phase operator is not Hermitian is an example of how non hermitian operators can describe certain kinds of quantum measurements (see Chap. 7). Pegg and Barnett [13] defined a Hermitian phase operator the measurement statistics of which converge, in an appropriate limit, to the phase distribution of the SG operator. The question arises; does this distribution correspond to the statistics of any physical phase measurement? Wiseman et al. [15] demonstrated an adaptive scheme that comes arbitrarily close.

1.7 Cat States

Advances in new quantum technologies now make it possible to create highly non classical states of the electromagntic field. A class of such states are known as cat state. These are defined as symmetric and anti-symmetric superpositions of coherent states;

$$|\alpha_{\pm}\rangle = \mathcal{N}_{\pm}(\alpha)[|\alpha\rangle \pm |-\alpha\rangle] \tag{1.107}$$

where the normalisation constant is

$$\mathcal{N}_{\pm}(\alpha) = \frac{1}{\sqrt{2\left(1 \pm e^{-2|\alpha|^2}\right)}} \tag{1.108}$$

It is easy to check that these states have opposite parity, that is to say, they are orthogonal eigenstates of the parity operator $\Pi = e^{i\pi a^\dagger a}$, so that the 'even' cat, $|\alpha_+\rangle$, only has even number states while the 'odd' cat, $|\alpha_-\rangle$ only has odd photon number. The two states are related by $a|\alpha_\pm\rangle = \alpha|\alpha_\mp\rangle$. Thus the cat states are degenerate eigenstates of a^2, with eigenvalues α^2. The cat states have zero average amplitude $\langle a\rangle = 0$ but $\langle a^2\rangle = \alpha^2$. The average photon number; $\langle a^\dagger a\rangle_\pm = |\alpha|^2(\tanh(|\alpha|^2)^{\pm 1}$. Cat states are used in certain quantum information schemes in quantum optics, see Chap. 15.

1.8 GKP States

In Chap. 15 we will discuss quantum computing based on a type of oscillator state invented by Gottesmann, Kitaev and Preskill known as GKP states [16]. As originally defined these are not physical states, but they are well approximated by superpositions of displaced squeezed states.

In terms of the continuous spectrum of the quadrature phase operators X_1, X_2 defined in (1.54), we define the translation operator $T_1(p) = e^{-ipX_1/2}$, $T_2(q) = e^{iqX_2/2}$ where q is a real number. These two operators are canonically conjugate in that

$$T_1(p)T_2(q) = T_2(q)T_1(p)e^{ipq/2} \tag{1.109}$$

Thus for $p = 2\sqrt{\pi}, q = 2\sqrt{\pi}$ these operators commute and can be simultaneously diagonalised. When $T_2(q)$ acts on a state $|\psi\rangle$ it displaces it in the X_1 representation (see (1.57)) as

$$\langle x|T_2(q)|\psi\rangle = \langle x + q|\psi\rangle = \psi(x + q) \tag{1.110}$$

The two orthogonal ideal GKP states as superpositions of two improper eigenstates of X_1

$$|0\rangle = \sum_{k=-\infty}^{\infty} T_2(2k\sqrt{\pi})|x = 0\rangle, \tag{1.111}$$

$$|1\rangle = \sum_{k=-\infty}^{\infty} T_2(2k\sqrt{\pi}))|x = \sqrt{\pi}\rangle \tag{1.112}$$

It is immediately apparent that these states are un-normalisable. Instead, the ideal encoding is approximated by a coherent superposition of Gaussian displaced squeezed vacuum states, Fig. 15.17.

$$|\tilde{0}\rangle = N_0 \sum_{k=-\infty}^{\infty} e^{-2\pi\tilde{\Delta}^2 k^2} D(k\sqrt{\pi})|r\rangle, \tag{1.113}$$

$$|\tilde{1}\rangle = N_1 \sum_{k=-\infty}^{\infty} e^{-2\pi\tilde{\Delta}^2 k^2} D((k+1/2)\sqrt{\pi})|r\rangle, \tag{1.114}$$

where $D(k\sqrt{\pi})$ is the displacement operator defined in (1.29) and $\Delta = e^{-2r}$. In terms of the diagonal representation of X_1 these can be written

$$\langle x|\tilde{0}\rangle = N_0 \sum_{k=-\infty}^{\infty} e^{-2\pi\tilde{\Delta}^2 k^2} (2\pi\Delta)^{-1/4} \exp\left[-\frac{(x-2k\sqrt{\pi})^2}{2\Delta}\right] \tag{1.115}$$

$$\langle x|\tilde{1}\rangle = N_1 \sum_{k=-\infty}^{\infty} e^{-2\pi\tilde{\Delta}^2 k^2} (2\pi\Delta)^{-1/4} \exp\left[-\frac{(x-(2k+1)\sqrt{\pi})^2}{2\Delta}\right] \tag{1.116}$$

where $\Delta = e^{-r}$. In cases of practical interest $\tilde{\Delta} = \Delta$. The X_2 representation, $\langle y|\tilde{s}\rangle$, is given by the Fourier transform of these functions. As this takes Gaussians to Gaussians we see that both functions are even functions of x, y. Note that these state are invariant under the parity transformation, $\hat{\Pi} = e^{-i2\pi a^\dagger a}$ that transforms $X_1 \to -X_1$, $X_2 \to -X_2$, these code states will always have an even number of photons.

Konno et al. [17] gave the first experimental demonstration of GKP states in a travelling wave optical system using conditional homodyne measurements and feed-forward. The GKP states are an important code for continuous variable optical quantum computation. See Chap. 15.

1.9 Multi-mode States of the Quantum Field

We are not restricted to sources that excite a single mode of the electromagnetic field. We will begin by discussing quantum states of the multi-mode field, with plane polarisation, in terms of the (dimensionless) positive frequency operator,

$$E^{(+)}(t, \mathbf{x}) = \int_0^\infty d\omega \tilde{a}(\omega) e^{-i(\omega t - \mathbf{k}.\mathbf{x})} \quad , \tag{1.117}$$

where $\tilde{a}(\omega), \tilde{a}^\dagger(\omega')$ are bosonic annihilation/creation operators satisfying

$$[\tilde{a}(\omega), \tilde{a}^\dagger(\omega')] = \delta(\omega - \omega'), \tag{1.118}$$

and $\omega = c|\mathbf{k}|$. The negative frequency components are defined by $E^{(-)}(t, \mathbf{x}) = (E^{(+)}(t, \mathbf{x}))^\dagger$.

We will assume that all modes are in the vacuum except for those propagating in the $+x$ direction with a carrier frequency centred on $\omega = \Omega$ and a frequency bandwidth B much less than the carrier frequency. In that case we can change the frequency variable to $\omega \to \omega - \Omega$ and extend the lower limit of integration over the displaced variable to $-\Omega \to -\infty$. We will refer to this set of approximations collectively as the 'quantum optics approximation'. We then only need consider those modes that contribute to the positive frequency operate defined as

$$a(t - x/c) = \int_{-\infty}^{\infty} d\omega\, \tilde{a}(\omega) e^{-i\omega(t-x/c)} \quad . \tag{1.119}$$

This operator represents the positive frequency components of the EM field in the quantum optics approximation. In this form the operators $a(t)$ and $\tilde{a}(\omega)$ appear as Fourier transform pairs. In our units $a(t)$ has units of $\mathrm{s}^{-1/2}$ which ensures that $\langle a^\dagger(t)a(t)\rangle$ has units of a rate. In what follows we will assume the detector is located at $x = 0$.

1.9.1 Coherent Pulses

Multimode coherent states are defined at $x, t = 0$ by quantum state functional of complex valued functions $\tilde{\alpha}(\omega)$,

$$|\tilde{\alpha}(\omega)\rangle = D(\tilde{\alpha}(\omega))|0\rangle \tag{1.120}$$

We then find that $\langle a(t)\rangle = \alpha(t)$ and $\langle a^\dagger(t)a(t)\rangle = |\alpha(t)|^2$ with

$$\alpha(t) = \int_{-\infty}^{\infty} d\omega \tilde{\alpha}(\omega) e^{-i\omega t} \quad , \tag{1.121}$$

The coherent amplitude of the state is determined by a Fourier transform. This is what one would expect for a transform limited classical field. In such cases there is no additional phase noise. Here we see that transform limited states are necessarily pure states. The state contains no more phase noise than required by the uncertainty principle.

1.9.2 Photon Number Pulses

We now define an N-photon (pure) state as a superposition of a single excitation over many frequencies [24],

$$|N_\xi\rangle = \frac{1}{\sqrt{N!}} \left[\int_{-\infty}^{\infty} d\omega\, \tilde{\xi}(\omega) \tilde{a}^\dagger(\omega) \right]^N |0\rangle \quad . \tag{1.122}$$

Here $\tilde{\xi}(\omega)$ is the probability amplitude that there is a single photon in a frequency band between ω and $\omega + d\omega$. Normalisation of the state requires that

$$\int_{-\infty}^{\infty} d\omega |\tilde{\xi}(\omega)|^2 = \int_{-\infty}^{\infty} dt |\xi(t)|^2 = 1 \tag{1.123}$$

where

$$\xi(t) = \int_{-\infty}^{\infty} d\omega \, e^{-i\omega t} \tilde{\xi}(\omega) \quad . \tag{1.124}$$

The average field amplitude of a single photon state is zero,

$$\langle 1|a(t)|1\rangle = 0 \quad . \tag{1.125}$$

We can interpret this result as an indication of the random optical phase of a photon number eigenstate. A phase dependent measurement on the single photon state, such as homodyne detection, would give a null signal on average. The quantum coherent nature of a single photon is revealed when we consider the probability per unit time to detect the photon on a photon counter.

In the case of the single photon state ($N = 1$) this becomes

$$n(t) = \langle a^{\dagger}(t)a(t)\rangle = |\xi(t)|^2 \quad , \tag{1.126}$$

The fact that $n(t)$ appears as the modulus square of a single, complex valued function in (1.126) is a reflection of the underlying purity of the single photon state. In optical terms we would say that the pulse is 'transform limited' although we need to bear in mind that this is highly non classical state with an average field amplitude of zero.

A single photon source is a highly non classical source of light as opposed to the typical semiclassical sources of a laser and thermal radiation. The key signature of a true pure-state single photon source is provided by Hong-Ou-Mandel (HOM) interference [22,23].

HOM interference is a fourth order interference effect. If two identical single photons arrive on a 50/50 beam-splitter the probability to detect a single photon at each of the two output ports—a coincidence—is zero. This is because there are two indistinguishable ways this event can occur: both photons are reflected or both photons are transmitted and the probability amplitudes for each of these paths cancel exactly in the ideal case. If we introduce a time delay between the two photon pulses, the probability to detect a coincidence drops from a value of 0.5 to near zero as the time delay is reduced to zero.

In Fig. 1.3, we show a HOM scheme with two input fields with positive frequency components $a_{in}(t)$, $b_{in}(t)$ and two output fields determined by the frequency space unitary transformation

$$\tilde{a}_{out}(\omega) = \frac{1}{\sqrt{2}}(\tilde{a}_{in}(\omega) + \tilde{b}_{in}(\omega)) \tag{1.127}$$

$$\tilde{a}_{out}(\omega)(t) = \frac{1}{\sqrt{2}}(\tilde{a}_{in}(\omega) - \tilde{b}_{in}(\omega)) \quad . \tag{1.128}$$

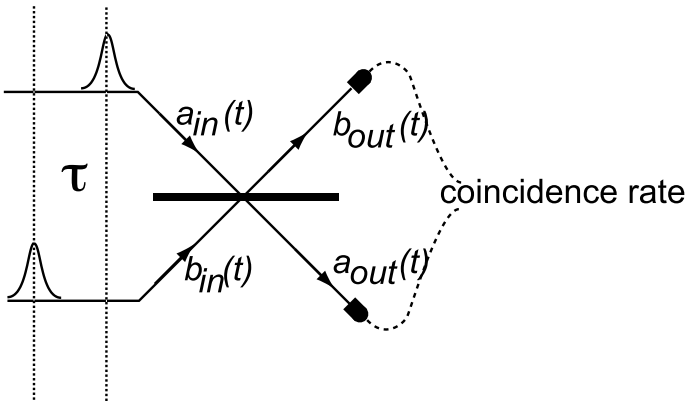

Fig. 1.3 A scheme for a Hong-Ou-Mandel interference experiment. A beam splitter couples two input field modes to two output field modes. The input field modes are prepared in identical single photon pulses and a variable time delay τ is introduced. Detectors placed in the path of the output field modes show a suppression of coincidence events when the delay time is zero

The change in sign of the second equation here is an indication of the time reversal invariance of an ideal beam splitter. Assume that at $t = 0$ the a-mode is prepared in the single photon state with amplitude function $\xi_a(t)$ while the b-mode is prepared in a single photon state at $t = \tau$ with amplitude function $\xi_b(t - \tau)$. To be specific we will choose,

$$\xi(t) = \begin{cases} \sqrt{\gamma} e^{-\gamma t/2} & t \geq 0 \\ 0 & t < 0 \end{cases} \quad . \tag{1.129}$$

The joint probability to count one photon in output mode-a and one photon in output mode-b is defined by

$$P_{ab} = \int_0^\infty \int_0^\infty \langle a^\dagger_{\text{out}}(t) b^\dagger_{\text{out}}(t') b_{\text{out}}(t') a_{\text{out}}(t) \rangle dt dt' \quad . \tag{1.130}$$

In this case we find that this is a function of τ and is given by

$$P_{ab}(\tau) = \frac{1}{2}\left(1 - e^{-\gamma|\tau|}\right) \quad . \tag{1.131}$$

A good example of a single photon source which exhibits both a suppression of second order correlation at zero time and good HOM interference visibility was demonstrated by the group of Rempe [19] in Garching and also by the group of Kuhn at Oxford [20]. This system is based on a Raman two photon transition in a three level system inside an optical cavity [21]. One transition is driven by a strong time dependent laser and the other is coupled to a cavity mode. A control pulse transforms the atomic system from the ground to an excited state while simultaneously exciting one photon in a cavity mode. The time taken to excite the cavity photon is determined primarily by the duration of the control pulse and can be short compared to the cavity

decay time. The photon is then emitted from the cavity via the usual process of cavity decay. Under these conditions a good approximation to the single photon amplitude function is the exponential in (1.129). The experiments of Rempe [19] and Kuhn [20] verified the temporal shape of their photon amplitudes and phases in detection-time resolved HOM and quantum homodyne experiments.

1.9.3 Pair Creation

Spontaneous parametric down conversion (see Chap. 8) is a multi-photon process that takes place in certain crystals with a significant second order optical non linearity. In this process a continuous wave or pulsed laser injects a coherent pump field into the non linear crystal. A single pump photon with wave vector $\mathbf{k}_p$ is absorbed at random times and a pair of photons called the signal (s) and idler (i) are created such that $\mathbf{k}_p = \mathbf{k}_s + \mathbf{k}_i$ and $\omega_p = \omega_i + \omega_s$. These ensure momentum and energy conservation.

We can write the two-photon state of the signal and idler as

$$|2\rangle_{si} = \int_{-\infty}^{\infty} d\omega_1 \int_{-\infty}^{\infty} d\omega_2 \tilde{f}(\omega_1, \omega_2) a_s^\dagger(\omega_1) a_i^\dagger(\omega_2)|0\rangle \tag{1.132}$$

Normalisation requires

$$\int_{-\infty}^{\infty} d\omega_1 d\omega_2 \, |\tilde{f}(\omega_1, \omega_2)|^2 = 1 \tag{1.133}$$

This state is entangled if $\tilde{f}(\omega_1, \omega_2) \neq \tilde{f}_1(\omega_1)\tilde{f}_2(\omega_2)$. The nature of entanglement can be seen using the Schmidt decomposition [24]

$$\tilde{f}(\omega_1, \omega_2) = \sum_j \sqrt{\lambda_j} \tilde{g}_j(\omega_1) \tilde{h}_j(\omega_2) \tag{1.134}$$

where $\tilde{g}_j, \tilde{h}_j$ are an orthonormal set of mode functions and $\sum_j \lambda_j = 1$.

The two-photon detection rate is

$$r(t, \tau) = \langle 2|a_s^\dagger(t) a_s(t) a_i^\dagger(t+\tau) a_i(t+\tau)|2\rangle = \left| \sum_j \sqrt{\lambda_j} g_j(t) h_j(t+\tau) \right|^2 \tag{1.135}$$

where $g(t), h(t)$ are the Fourier transforms of $\tilde{g}(\omega), \tilde{h}(\omega)$. In the temporal domain we see the entanglement is represented directly as correlations between pairs of temporal modes. In many experiments only a few temporal mode pairs may be required.

Problems

1.1 Derive the disentangling relation in (1.71). Hint: write

$$e^{r(a^2-a^{\dagger\,2})/2} = e^{f_+(r)a^{\dagger\,2}} e^{f_z(r)a^\dagger a} e^{f_-(r)a^2} \tag{1.136}$$

and differentiate both sides with respect to r to obtain differential equations for $f_\pm(r)$, $f_z(r)$.

1.2 Show that the mean and variance of a squeezed vacuum state are $\bar{n} = \sinh^2 r$ and $\mathbb{V}[n] = 2\cosh^2 r \sinh^2 r$.

1.3 Calculate the SG phase distribution for; number states, coherent states and squeezed states.

1.4 Calculate the mean and variance of the photon number in the two approximate GKP states, (1.115, 1.116) with $\tilde{\Delta} = \Delta$.

1.5 Derive the result in (1.135).

References

1. E.A. Power, *Introductory Quantum Electrodynamics* (Longmans, London, 1964)
2. R.J. Glauber, Phys. Rev. B **1**, 2766 (1963)
3. W.H. Louisell, *Statistical Properties of Radiation* (Wiley, New York, 1973)
4. D.F. Walls, Nature **324**, 210 (1986)
5. C.M. Caves, Phys. Rev. D **23**, 1693 (1981)
6. H.P. Yuen, Phys. Rev. A **13**, 2226 (1976)
7. R. Loudon, *Quantum Theory of Light* (Oxford University Press, Oxford, 1973)
8. W. Schleich, J.A. Wheeler, Nature **326**, 574 (1987)
9. C.M. Caves, B.L. Schumaker, Phys. Rev. A **31**, 3068 (1985)
10. K.E. Cahill, R.J. Glauber, Phys. Rev. **177**, 1857 (1969)
11. P.A.M. Dirac, Proc. R. Soc. Lond. **A11**, 4243–265 (1927)
12. L. Susskind, J. Glogower, Physics **1**, 49 (1964)
13. D.T. Pegg, S.M. Barnett, Phys. Rev. A **39**, 1665 (1989)
14. S.L. Braunstein , C.M. Caves and G.J. Milburn, Ann. Phys. **247**(1), 135–173 (1996)
15. H.M. Wiseman, D.W. Berry, S.D. Bartlett, B.L. Higgins, G.J. Pryde, IEEE J. Sel. Top. Quantum Electron. **15**(6), 1661–1672 (2009)
16. D. Gottesman, A. Kitaev, J. Preskill, Phys. Rev. A **64**, 012310 (2001)
17. S. Konno et al., Science **383**, 289 (2024)
18. M.G. Raymer, I.A. Walmsley, Phys. Scr. **95**, 064002 (2020)
19. H.P. Specht, J. Bochmann, M. Mücke, B. Weber, E. Figueroa, D.L. Moehring, G. Rempe, Nat. Photonics **3**, 469 (2009)

20. P.B.R. Nisbet-Jones, J. Dilley, D. Ljunggren, A. Kuhn, New J. Phys. **13**, 103036 (2011)
21. M. Keller, B. Lange, K. Hayasaka, W. Lange, H. Walther, Nature **431**, 1075 (2004)
22. C.K. Hong, Z.Y. Ou, L. Mandel, Phys. Rev. Lett. **59**, 2044 (1987)
23. F. Bouchard et al., Rep. Prog. Phys. **84**, 012402 (2021)
24. M.G. Raymer, I.A. Walmsley, Phys. Scr. **95**, 064002 (2020)

Quantum Theory of Optical Coherence

2

Abstract

In this chapter we introduce measurements via a simple model based on photoelectric detection. Ultimately, all experimental results can be expressed in terms of correlation functions evaluated at different spacetime points. We use this model to discuss how optical coherence is determined by quantum states of light and help us describe interference experiments.

2.1 Sources and Detectors

Non-relativistic quantum mechanics makes contact with reality through the Born rule, a mathematical specification for how quantum states determine the statistics of idealised measurement results. The same is true of quantum field theory where measurement takes place in detectors and states are prepared by sources. Quantum field theory, as usually presented, has little to say about sources and detectors, or measurement for that matter. In the case of high energy fields one is often concerned with sources that produce a few excitations and detectors that respond to small numbers of excitations. In quantum optics, we are concerned with the quantised electromagnetic field and sources and detectors that respond to very many excitations. In both cases, sources and detectors are comprised of quantised matter fields, a subject we will postpone to Chap. 9.

2.2 Photon Counting

The elementary measurement device in quantum optics involves the absorption of a photon. This has important consequences since this type of counter is insensitive to spontaneous emission. In such a device, measurement takes place by absorbing a photon and thus is sensitive to the positive frequency components field $E^{(+)}(\mathbf{r}, t)$ at the space-time point $(\mathbf{r}, t)$. This is nothing like the usual 'projection postulate'

D. F. Walls and G. J. Milburn, *Quantum Optics*, Graduate Texts in Physics,
https://doi.org/10.1007/978-3-031-84177-4_2

description of measurement, as when one photon is counted the only thing we can say for sure is that there is one photon less in the field. We follow the treatment of Glauber [1].

The transition probability per unit time (i.e. the detection rate) that the detector absorbs a photon at the position of the detector, $\mathbf{r}$, between t and $t + dt$ is proportional to

$$T_{fi} = \left| \langle f | E^{(+)}(\mathbf{r}, t) | i \rangle \right|^2 \tag{2.1}$$

where $|i\rangle$, $|f\rangle$ are the initial and final states of the field. We only care about the final state of the detector as it ultimately records the absorption. In order to obtain the total detection rate we sum over all states of the field which may be reached from the initial state by an absorption process. We can extend the sum over a complete set of final states since the states which cannot be reached (e.g., final states which differ from initial states by two or more photons) will not contribute to the result since they are orthogonal to the state with one photon less than the initial state. The total detection rate is

$$I(\mathbf{r}, t) = \sum_f \langle i | E^{(-)}(\mathbf{r}, t) | f \rangle \langle f | E^{(+)}(\mathbf{r}, t) | i \rangle \tag{2.2}$$

$$= \langle i | E^{(-)}(\mathbf{r}, t) E^{(+)}(\mathbf{r}, t) | i \rangle \tag{2.3}$$

where we have used the completeness relation $\sum_f |f\rangle\langle f| = 1$. From the photoelectric effect we expect the rate of absorption to be proportional to the intensity of the field, so we define $I(\mathbf{r}, t)$ as the measured intensity of the field at $(\mathbf{r}, t)$. If the field is in a mixed state, ρ the expression for $I(\mathbf{r}, t)$ becomes

$$I(x) = \mathrm{tr}\left[E^{(-)}(x) E^{(+)}(x) \rho \right] , \tag{2.4}$$

where we have defined the spacetime point $x = (\mathbf{r}, t)$. The normal ordering of the operators (that is, all annihilation operators are to the right of all creation operators) yields zero intensity for the vacuum state $\rho = |0\rangle\langle 0|$. This is a consequence of using a detector based on absorption. Had we chosen a detector working on a stimulated emission principle, problems would arise with vacuum fluctuations.

What would we expect the classical analogue of $I(x)$ to be? In Chap. 1, we saw that the quantum field resulted when we replaced the classical positive and negative frequency components of the field by operators. Thus we might expect that the measured intensity for a the classical field to be $I(x) = \mathcal{E}^{(-)}(x)\mathcal{E}^{(+)}(x) = |\mathcal{E}^{(+)}(x)|^2$. If the field was a single plane-wave mode this is a constant in time and space. Strictly speaking this assumes that the classical field is completely deterministic and not subject to amplitude and phase fluctuations. In that case we would replace $\mathcal{E}^{(\pm)}(x)$ by a stochastic process and average over the noise to get the measured intensity.

We can define a two-point correlation function for the field by generalising (2.4),

$$G^{(1)}(x, x') = \mathrm{tr}\left[E^{(-)}(x) E^{(+)}(x') \rho \right] . \tag{2.5}$$

This is a first-order correlation function. The physical interpretation of this in terms of a measurement will be treated in Chap. 7. It is based on measurements of the field amplitude rather than intensity as in direct photon counting. Field amplitude measurements are phase-dependent measurements unlike photon counting. As it is a measurement of the field amplitude it can be used to account for optical interference experiments. As we will see the first-order correlation function of the radiation field is sufficient to account for classical interference experiments.

The measurement of $g^{(2)}(t;\tau)$ by Hanbury Brown and Twiss in 1956 signalled the birth of quantum optics [2,3]. In this experiment an intensity, or photon number, correlation function for light was measured for the first time. To describe experiments involving intensity correlations, it is necessary to define higher-order correlation functions. The the n'th-order correlation function of the electromagnetic field is defined by

$$G^{(n)}(x_1,\ldots,x_n,x_{n+1},\ldots,x_{2n}) = \mathrm{tr}\left[\rho E^{(-)}(x_1)\ldots E^{(-)}(x_n) \times E^{(+)}(x_{n+1})\ldots E^{(+)}(2n)\right] \tag{2.6}$$

Such an expression follows from a consideration of an n-atom photon detector [1].

2.3 Correlation Functions

A number of interesting inequalities can be derived from the inequality

$$\mathrm{tr}\left[\rho A^{\dagger}A\right] \geq 0\,, \tag{2.7}$$

which follows from the non-negativity of $A^{\dagger}A$ for any operator A. Choosing $A = E^{(+)}(x)$ gives

$$G^{(1)}(x,x) \geq 0\,. \tag{2.8}$$

In general taking $A = E^{(+)}(x_n)\ldots E^{(+)}(x_1)$ yields

$$\sum_{ij}\lambda_i^*\lambda_j G^{(1)}(x_i,x_j) \geq 0\,. \tag{2.9}$$

Thus the set of correlation functions $G^{(1)}(x_i,x_j)$ forms a matrix of coefficients for a positive definite quadratic form. Such a matrix has a positive determinant, i.e.,

$$\det\left[G^{(1)}(x_i,x_j)\right] \geq 0\,. \tag{2.10}$$

For $n = 1$ this is (2.8). For $n = 2$ we find

$$G^{(1)}(x_1,x_1).G^{(1)}(x_2,x_2) \geq \left|G^{(1)}(x_1,x_2)\right|^2\,, \tag{2.11}$$

which is the Schwartz inequality. Choosing

$$A = \lambda_1 E^{(+)}(x_1) \dots E^{(+)}(x_n) + \lambda_2 E^{(+)}(x_{n+1}) \dots E^{(+)}(x_{2n}) \tag{2.12}$$

we find

$$G^{(n)}(x_1, \dots, x_n, x_n, \dots, x_1) \; . \; G^{(n)}(x_{n+1}, \dots, x_{2n}, x_{2n}, \dots, x_{n+1}) \geq \left| G^{(n)}(x_1, \dots, x_n, x_{n+1}, \dots, x_{2n}) \right|^2 \tag{2.13}$$

If we have two distinguishable fields (say, by direction of propagation) we take

$$A = \lambda_1 E_1^{(+)}(x) E_2^{(+)}(x') + \lambda_2 E_2^{(+)}(x) E_2^{(+)}(x') \tag{2.14}$$

with $x = (\mathbf{r}, 0)$ and $x' = (\mathbf{r}, t)$. Then

$$G_{11}^2(0) G_{22}^{(2)}(0) \geq \left| G_{12}^{(2)}(t) \right|^2 \; , \tag{2.15}$$

where

$$G_{12}^{(2)}(t) = \mathrm{tr} \left[\rho E_i^{(-)}(x) E_i^{(-)}(x') E_i^{(+)}(x') E_i^{(+)}(x) \right] \; . \tag{2.16}$$

Note that $G_{ii}^{(2)}$ is time independent.

An inequality closely related to (2.15) may be derived by choosing

$$A = \lambda_1 E_1^{(-)}(x) E_2^{(+)}(x) + \lambda_2 E_2^{(-)}(x) E_2^{(+)}(x) \; . \tag{2.17}$$

This leads to

$$\left| \langle E_1^{(-)}(x) E_1^{(+)}(x) E_2^{(+)}(x) E_2^{(-)}(x) | \right|^2 \leq \langle \left[E_1^{(-)}(x) E_1^{(+)}(x) \right]^2 \rangle \langle \left[E_2^{(-)}(x) E_2^{(+)}(x) | \right]^2 \rangle \; . \tag{2.18}$$

2.4 Correlation Functions and Optical Coherence

Classical optical interference experiments correspond to a measurement of the first order correlation function. We shall consider Young's interference experiment as a measurement of the first-order correlation function of the field and show how a definition of first-order optical coherence arises from considerations of the fringe visibility.

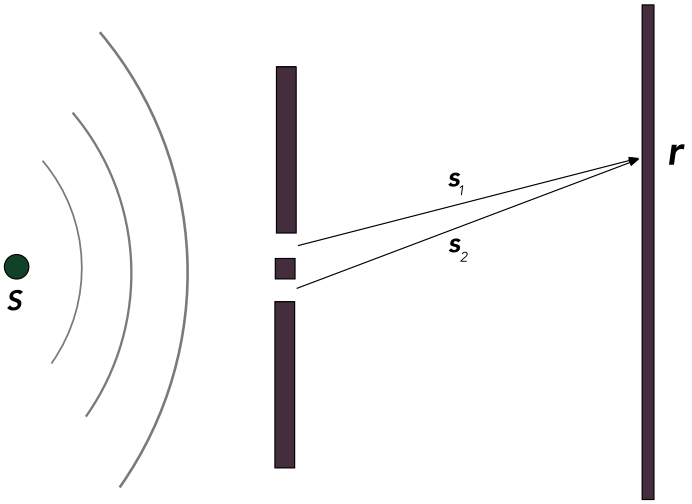

Fig. 2.1 Schematic representation of Young's interference experiment

A schematic sketch of Young's interference experiment is depicted in Fig. 2.1. The field incident on the screen at position r and time t is the superposition of the fields at the two pin holes,

$$E^{(+)}(\mathbf{r},t) = E_1^{(+)}(\mathbf{r}_i,t) + E_2^{(+)}(\mathbf{r},t)\ , \tag{2.19}$$

where $E_i^{(+)}(\mathbf{r},t)$ is the field produced by pinhole-i at the screen with

$$E_i^{(+)}(\mathbf{r},t) = E_i^{(+)}(\mathbf{r},t-s_i/c)\frac{e^{i(k-\omega/c)s_i}}{s_i}\ , \tag{2.20}$$

where $s_i = |\mathbf{r}_i - \mathbf{r}|$ and $E_i^{(+)}(\mathbf{r}_i,t-s_i/c)$ is the field at the i'th pinhole. For a spherical wave $k-\omega/c = 0$, thus (2.19) becomes

$$E^{(+)}(\mathbf{r},t) = \frac{E_1^{(+)}(\mathbf{r}_1,t-s_1/c)}{s_1} + \frac{E_2^{(+)}(\mathbf{r}_2,t-s_2/c)}{s_2}\ . \tag{2.21}$$

In the experiment we expect $s_1 \approx s_2 \approx R$, so

$$E^{(+)}(\mathbf{r},t) = \frac{1}{R}\left(E_1^{(+)}(x_1) + E_2^{(+)}(x_2)\right), \tag{2.22}$$

where

$$x_i = (\mathbf{r}_i, t-s_i/c)\ . \tag{2.23}$$

The intensity observed on the screen is proportional to

$$I(\mathbf{r},t) = \mathrm{tr}\left[\rho E^{(-)}(\mathbf{r},t)E^{(+)}(\mathbf{r},t)\right]\ . \tag{2.24}$$

Using (2.19) we find that

$$I(x_1, x_2) = G^{(1)}(x_1, x_1) + G^{(1)}(x_2, x_2) + 2\Re\left[G^{(1)}(x_1, x_2)\right] , \tag{2.25}$$

and the R^{-2} factor is absorbed into a normalisation constant. The first two terms on the right-hand side are the intensities from each pinhole in the absence of the other. The third term is the interference term. The correlation function for $x_1 \neq x_2$, in general takes on complex values. Writing this as

$$G^{(1)}(x_1, x_2) = \left|G^{(1)}(x_1, x_2)\right| e^{i\Psi(x_1, x_2)} , \tag{2.26}$$

we find

$$I(x_1, x_2) = G^{(1)}(x_1, x_1) + G^{(1)}(x_2, x_2) + 2\left|G^{(1)}(x_1, x_2)\right| \cos(\Psi(x_1, x_2)) , \tag{2.27}$$

The interference fringes arise from the oscillations of the cosine term. The envelope of the fringes is described by the correlation function $G^{(1)}(x_1, x_2)$.

2.5 First-Order Optical Coherence

The idea of coherence in optics was first associated with the possibility of producing interference fringes when two fields are superposed. The highest degree of optical coherence was associated with a field which exhibits fringes with maximum visibility. If $G^{(1)}(x_1, x_2)$ was zero there would be no fringes and the fields are then described as incoherent. Thus the larger is $G^{(1)}(x_1, x_2)$ the more coherent the field. The magnitude of $|G^{(1)}(x_1, x_2)|$ is limited by the relation

$$\left|G^{(1)}(x_1, x_2)\right| \leq \left[G^{(1)}(x_1, x_1)G^{(1)}(x_2, x_2)\right]^{1/2} . \tag{2.28}$$

The best possible fringe contrast is given by the equality sign. Thus the necessary condition for full coherence is

$$\left|G^{(1)}(x_1, x_2)\right| = \left[G^{(1)}(x_1, x_1)G^{(1)}(x_2, x_2)\right] . \tag{2.29}$$

Introducing the normalized first-order correlation function

$$g^{(1)}(x_1, x_2) = \frac{G^{(1)}(x_1, x_2)}{\left[G^{(1)}(x_1, x_1)G^{(1)}(x_2, x_2)\right]^{1/2}} \tag{2.30}$$

the condition for maximum fringe contrast is

$$g^{(1)}(x_1, x_2) = 1 , \tag{2.31}$$

or

$$g^{(1)}(x_1, x_2) = e^{i\Psi(x_1,x_2)} . \tag{2.32}$$

The *visibility* of the fringes is defined by

$$\mathcal{V} = \frac{I_{max} - I_{min}}{I_{max} + I_{min}} \tag{2.33}$$

This may be written as

$$\mathcal{V} = \left| g^{(1)} \right| \frac{2\sqrt{I_1 I_2}}{I_1 + I_2} . \tag{2.34}$$

If the fields incident on each pinhole have equal intensities the fringe visibility is equal to $|g^{(1)}|$. Thus the condition for first-order optical coherence $|g^{(1)}| = 1$ corresponds to the condition for maximum fringe visibility.

A more general definition of first-order coherence of the field E(x) is that the first-order correlation function factorizes

$$G^{(1)}(x_1, x_2) = \varepsilon^{(-)}(x_1)\varepsilon^{(+)}(x_2) \tag{2.35}$$

It is readily seen that this is equivalent to the condition for first-order optical coherence given by (2.31). It is clear that the coherent states are an example of such a field. It is this coherence property of the coherent states which gave them their name. in general, coherent states of the field lead to the factorisation

$$G^{(n)}(x_1, \ldots x_n, x_{n+1} \ldots, x_{2n}) = \varepsilon^{(-)}(x_1) \ldots \varepsilon^{(-)}(x_n)\varepsilon^{(+)}(x_{n+1}) \ldots \varepsilon^{(+)}(x_{2n}) \tag{2.36}$$

Photon interference experiments of the kind typified by Young's interference experiment and Michelson's interferometer played a central role in early discussions of the dual wave and particle nature of light. These experiments detect the interference pattern resulting from the superposition of two light beams. Classical theory based on the wave nature of light readily explained the observed interference pattern. The quantum-mechanical explanation is based on the interference of the probability amplitudes for the photon to take either of two paths. We shall demonstrate how interference occurs even for a one photon field. For full details of the classical theory and experimental arrangements the reader is referred to the classic text of Born and Wolf [7].

We consider an interference experiment of the type performed by Young which consists of light from a monochromatic point source S incident on a screen possessing two pinholes P_1 and P_2 which are equidistant from S (see Fig. 2.1). The pinholes act as secondary monochromatic point sources which are in phase and the beams from them are superimposed on a screen at position $\mathbf{r}$ and time t. In this region an interference pattern is formed. To avoid calculating the diffraction pattern for the pinhole, we assume their dimensions are of the order of the wavelength of light in which case they effectively act as sources for single modes of spherical radiation

in keeping with Huygen's principle. The appropriate mode functions for spherical radiation are

$$u_k(\mathbf{r}) = \sqrt{\frac{1}{4\pi L}} \frac{e^{i\mathbf{k}.\mathbf{r}}}{\mathbf{r}} \hat{e}_{\mathbf{k}} \ , \tag{2.37}$$

where L is the radius of the normalization volume, and $\hat{e}_{\mathbf{k}}$ is the unit polarization vector.

The field detected on the screen at position $\mathbf{r}$ and time t is then the sum of the two spherical modes emitted by the two pinholes,

$$E^{(+)}(\mathbf{r}, t) = f(\mathbf{r}, t)(a_1 e^{iks_1} + a_2 e^{iks_2}) \tag{2.38}$$

with

$$f(\mathbf{r}, t) = i\sqrt{\hbar\omega/2} \frac{\hat{e}_{\mathbf{k}}}{\sqrt{4\pi L R}} e^{-i\omega t} \ , \tag{2.39}$$

where s_1 and s_2 are the distances of the pinholes P_1 and P_2 to the point on the screen, and we have set $s_1 \approx s_2 = R$ in the denominator of the mode functions. The intensity on the screen is then given by

$$I(\mathbf{r}, t) = \eta \left(\mathrm{tr}(\rho a_1^\dagger a_1) + \mathrm{tr}(\rho a_2^\dagger a_2) + 2|\mathrm{tr}(\rho a_1^\dagger a_2)| \cos \Phi \right) \tag{2.40}$$

where

$$\begin{aligned} \mathrm{tr}(\rho a_1^\dagger a_2) &= \left| \mathrm{tr}(\rho a_1^\dagger a_2) \right| e^{i\Phi}, \\ \eta &= |f(\mathbf{r}, t)|^2, \\ \Phi &= k(s_1 - s_2) \ . \end{aligned}$$

This expression exhibits the typical interference fringes with the maximum of intensity occurring at $k(s_1 - s_2) = 2n\pi$ with n an integer. The maximum intensity of the fringes falls off as one moves the point of observation further from the central line by the R^{-2}.

We shall evaluate the intensity for fields which may be generated by a single mode excitation and hence have first-order coherence. A general representation of such a field is

$$|\psi\rangle = g(b^\dagger)|0\rangle \tag{2.41}$$

where $|0\rangle$ denotes the vacuum state of the field and $b^\dagger$ is the creation operator for a single mode. The operator $b^\dagger$ may be expressed as a linear combination of $a_1^\dagger$ and $a_2^\dagger$ as

$$b = \frac{1}{\sqrt{2}}(a_1 + a_2) \ , \tag{2.42}$$

where we have assumed equal intensities through each slit. We shall now consider as a special case the field with only one photon incident on the pinholes, i.e.,

$$|\psi\rangle = b^{\dagger}|0\rangle = \frac{1}{\sqrt{2}}(|1,0\rangle + |0,1\rangle) \tag{2.43}$$

where $|n_1, n_2\rangle$, means that there are n_1 photons in mode k_1 and n_2 photons in mode k_2. This state of the field reflects the fact that we don't know which pinhole the photon goes through. From (2.40) this yields the following expression for the mean intensity on the screen

$$I(\mathbf{r}, t) = \eta(1 + \cos\Phi) \tag{2.44}$$

It is clear from this equation that an interference pattern may be built up from a succession of one-photon interference fringes.

The quantum explanation for the interference pattern was first put forward by Dirac [8] in his classic text on quantum mechanics. There he argued that the observed intensity pattern results from interference between the probability amplitudes of a single photon to take either of two possible paths. The crux of the quantum mechanical explanation is that the wave function gives information about the probability of one photon being in a particular place and not the probable number of photons in that place. Dirac pointed out that the interference between the two beams does not arise because photons of one beam sometimes annihilate photons from the other, and sometimes combine to produce four photons. "This would contradict the conservation of energy. The new theory which connects the wave functions with probabilities for one photon gets over the difficulty by making each photon go partly into each of two components. Each photon then interferes only with itself. Interference between two different photons never occurs".

An early experiment to test if interference would result from a single photon was performed by Taylor [9] in 1905. In this experiment the intensity of a thermal source was so low that on average only one photon was incident on the slits at a time. The photons were detected on a photographic plate so that the detection time was very large. Interference fringes were observed in this experiment. This experiment did not definitively show that the interference fringes resulted from a single photon since the statistical distribution of photons meant that sometimes two photons could be incident on the slits. A definitive experiment was conducted by Grangier et al. [10] using a two-photon cascade as a source. A coincidence technique which detected one photon of the pair enabled them to prepare a one photon source.

Single photon interference in a two aperture device is the basis for various suggestions for a quantum version of a Michelson stellar interferometer first used to measure stellar diameters. The interference pattern is sensitive to source intensity variations on the scale of $\delta\theta \sim \lambda/B$ where λ is the wavelength and B is the separation between the sub-apertures. If one can combine the light collected by the separate telescopes along optical paths one can achieve a Young's double-slit experiment. However loss in the optical channels (typically fibres) dramatically limits the efficiency of this

so-called direct detection method. Nonetheless this approach outperforms heterodyne detection with classical communication for estimating the mutual coherence of bipartite thermal light when the average photon flux is low [11].

2.6 Coherent Field

We consider a coherent field as generated by an ideal laser incident on the pinholes. The state for this coherent field is a tensor product of two single mode coherent states,

$$|\alpha_1, \alpha_2\rangle = |\alpha_1\rangle \otimes |\alpha_2\rangle \,, \tag{2.45}$$

representing two independent light beams. Such a state is easily produced by illuminating the two-slit experiment with a coherent field so that

$$|\alpha_1, \alpha_2\rangle = e^{\alpha b^\dagger - \alpha^* b}|0\rangle = |\alpha/\sqrt{2}, \alpha/\sqrt{2}\rangle \tag{2.46}$$

where $b = \frac{1}{\sqrt{2}}(a_1 + a_2)$. The intensity pattern produced by this coherent field is

$$I(\mathbf{r}, t) = \eta^2(|\alpha|^2 + |\alpha|^2 \cos\Phi) \tag{2.47}$$

This example demonstrates the possibility of obtaining interference between independent light beams. Experimentally, this requires that the phase relation between the two beams be slowly varying or else the fringe pattern will be washed out. Such experiments were performed by Pfleegor and Mandel [17]. Interference between independent light beams is, however, only possible for certain states of the radiation field, for example, the coherent states as demonstrated above. Interference is not generally obtained from independent light beams. For example, it is easily verified that for two independent light beams prepared in Fock states, $|\psi\rangle = |n_1\rangle|n_2\rangle$, yields a zero first order correlation and there is no interference. The Fock states have completely random phase.

The analysis leading to (2.44) bears out Dirac's argument that the interference fringes may be produced by a series of one photon experiments. However, Young's interference fringes may perfectly well be explained by the interference of classical waves. Experiments of this kind which measure the first-order correlation functions of the electromagnetic field do not distinguish between the quantum and classical theories of light.

2.7 Photon Correlation Measurements

The first experiment performed outside the domain of first order coherence was the intensity correlation experiment of Hanbury-Brown and Twiss [2]. Although the original experiment involved the analogue correlation of photo-currents, later experiments used photon counters and digital correlations and were truly photon

correlation measurements. In essence these experiments measure the joint photocount probability of detecting the arrival of a photon at time t and another photon at time $t + \tau$ (regardless of how many are detected between these times). This may be written as an intensity or photon-number correlation function.

Using the quantum detection theory developed by Glauber, the measured quantity is proportional to $\langle E^{(-)}(t)E^{(-)}(t+\tau)E^{(+)}(t+\tau)E^{(+)}(t)\rangle$. In many cases the probability of this joint detection event is *stationary*, which means it is independent of the starting time t after initial transients in the source have died out. We then define the correlation function,

$$G^{(2)}(\tau) = \lim_{t\to\infty} \langle E^{(-)}(t)E^{(-)}(t+\tau)E^{(+)}(t+\tau)E^{(+)}(t)\rangle \tag{2.48}$$

where $\tau > 0$. The operator inside the average is in normal ordered form. The normalised second order correlation function is defined by

$$g^{(2)}(\tau) = \frac{G^{(2)}(\tau)}{\left|G^{(1)}(0)\right|^2} \tag{2.49}$$

In the case of a field prepared in a coherent state we find

$$G^{(2)}(\tau) = \varepsilon^*(0)\varepsilon^*(\tau)\varepsilon(0)\varepsilon(\tau) = \left|G^{(1)}(0)\right|^2 \tag{2.50}$$

where $\varepsilon(t)$ is the complex amplitude of the positive frequency components of the field

$$\varepsilon(t) = i\sqrt{\frac{\hbar\omega}{2\epsilon_0 V}}\ \varepsilon\ e^{-i\omega t} \tag{2.51}$$

For such a field $g^{(2)}(\tau) = 1$. Such a field is said to possess second order coherence. This is a classical field state.

If the classical field has fluctuating complex amplitudes, described by a probability density $P(\varepsilon)$, then

$$G^{(2)}(\tau) = \int d^2\varepsilon\, P(\varepsilon)\varepsilon^*(0)\varepsilon^*(\tau)\varepsilon(0)\varepsilon(\tau) \tag{2.52}$$

In the case of zero time delay $\tau = 0$, we see that

$$g^{(2)}(0) = \frac{\int d^2\varepsilon\, P(\varepsilon)\left(|\varepsilon|^2 - \overline{|\varepsilon|^2}\right)^2}{\left(\overline{|\varepsilon|^2}\right)^2} \tag{2.53}$$

where

$$\overline{|\varepsilon|^2} = \int d^2\varepsilon \; P(\varepsilon) \; |\varepsilon|^2 \tag{2.54}$$

and it is clear that $g^{(2)}(0) \geq 1$.

If the distribution $P(\varepsilon)$ is a Gaussian with zero mean amplitude we can use the factorisation properties of the moments to show that

$$g^{(2)}(\tau) = 1 + \left| g^{(1)}(\tau) \right|^2 \tag{2.55}$$

which is an example of the Siegert relation. There are two cases of particular physical interest. The noise power spectrum for a stochastically fluctuating amplitude is defined as [14]

$$S(\omega) = \int_{-\infty}^{\infty} d\tau e^{-i\omega\tau} G^{(1)}(\tau) \tag{2.56}$$

A field with a Lorentzian spectrum has

$$g^{(2)}(\tau) = 1 + e^{-\gamma|\tau|} \tag{2.57}$$

while a field with a Gaussian spectrum (thermal light) has

$$g^{(2)}(\tau) = 1 + e^{-\gamma|\tau|^2} \tag{2.58}$$

where γ is the *line-width*.

For a values of $\tau >> \tau_c = \gamma^{-1}$, the correlation time of the light, the correlation function factorizes and $g^{(2)}(\tau) \to 1$. The increased value of $g^{(2)}(\tau)$ for $\tau < \tau_c$ for Gaussian fluctuations (chaotic light) over coherent light is due to the increased intensity fluctuations in the chaotic light field. (Here "chaotic" is not necessarily "thermal", as chaotic light can be produced by many independent nonthermal sources.) There is a high probability that the photon which triggers the counter occurs during a high intensity fluctuation and hence a high probability that a second photon will be detected arbitrarily soon thereafter. This effect known as photon bunching was first detected by Hanbury-Brown and Twiss [2]. Later experiments [15] showed excellent agreement with the theoretical predictions for chaotic and coherent light. The preceding anlaysis does not rely on quantisation of the electromagnetic field but may be deduced from a purely classical analysis of the electromagnetic field with fluctuating amplitudes for the modes.

2.8 Quantum Mechanical Fields

The second-order correlation function can be used to characterise quantum mechanical fields. We shall restrict our attention to a single-mode and two-mode fields. There is a simple relation between $g^{(2)}(0)$ and the variance on the photon number for a

single mode field described in terms of the annihilation and creation operators, a, $a^\dagger$. It is

$$g^{(2)}(0) = \frac{\langle a^{\dagger\,2} a^2 \rangle}{\langle a^\dagger a \rangle^2} = 1 + \frac{V(n) - \bar{n}}{\bar{n}^2} \tag{2.59}$$

where $\bar{n} = \langle a^\dagger a \rangle$ is the mean photon number and $V(n) = \langle (a^\dagger a)^2 \rangle - \langle a^\dagger a \rangle^2$ is the variance n the photon number. In the case of a coherent state we find $g^{(2)}(0) = 1$ while for a number state, $|n\rangle$, we find $g^{(2)}(0) = 1 - 1/n$.

If $g^{(2)}(\tau) < g^{(2)}(0)$ there is a tendency for photons to arrive in pairs. This situation is referred to as photon bunching. The converse situation, $g^{(2)}(\tau) > g^{(2)}(0)$ is called anti-bunching. Equations (2.57, 2.58) indicate that $g^{(2)}(\tau) \to 1$ on a sufficiently long time scale. Thus a field for which $g^{(2)}(0) < 1$ will always exhibit anti-bunching on some time scale. A value of $g^{(2)}(0)$ less than unity could not have been predicted by a classical analysis. Equation (2.53) always predicts $g^{(2)}(0) \geq 1$. To obtain a $g^{(2)}(0) \leq 1$ would require the field to have elements of negative probability, which is forbidden for a true probability distribution. Photon anti-bunching is a feature peculiar to the quantum mechanical nature of the electromagnetic field.

A distinction should be maintained between photon anti-bunching and sub- Poissonian statistics, although the two phenomena are closely related. For Poisson statistics the variance of the photon number is equal to the mean. Thus a measure of sub-Poissonian statistics is provided by the quantity $V(n) < \overline{n}$. Certainly a field for which $g^{(2)}(\tau) < 1$ for all τ will exhibit sub-Poissonian statistics. However, it is possible to create fields for which $g^{(2)}(\tau) > g^{(2)}(0)$ but which exhibit super-Poissonian statistics over some time interval.

In the case of quantum fields the second oder correlation function is

$$G^{(2)}(t : \tau) = \langle a^\dagger(t) a^\dagger(t+\tau) a(t+\tau) a(t) \rangle \quad . \tag{2.60}$$

In the case of a stationary source, that is to say one in which all transients due to switch-on have died out, we can define the stationary second order correlation as

$$G^{(2)}(\tau) = \lim_{t \to \infty} G^{(2)}(t : \tau) \quad . \tag{2.61}$$

In the case of a stationary thermal source, if we detect a photon at time t it is very likely that we will detect another photon a short time later. Thus $G^{(2)}(\tau)$ has a peak at $\tau = 0$ and decays for increasing τ. This is known as photon bunching. In the case of a photon counting in the output of a laser, $G^{(2)}(\tau)$ is constant.

For photon number states discussed in Chap. 1, the photon counting statistics is certainly not stationary. However most single photon sources deliver periodic sequences of pulses for which each pulse is a single photon state. In that case we expect suppression of $G^{(2)}(0)$ and a peak at every period of the pulse sequence. The suppression is not surprising: if one conditions off a single count at $t = 0$ there are no more photons left to detect from that pulse and one must wait at least until the next single photon pulse comes along. Thus there are peaks at $\tau = T$, the period of the source.

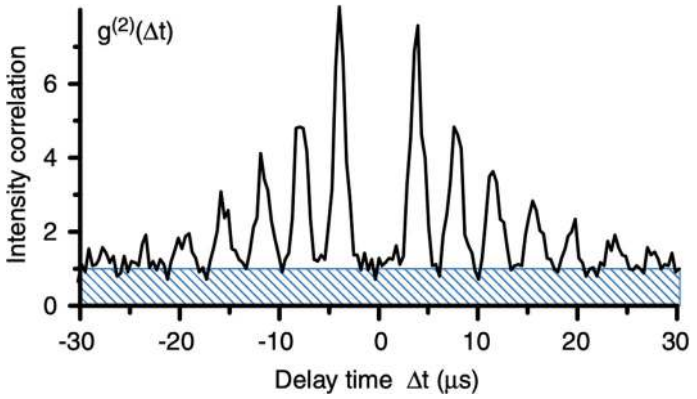

Fig. 2.2 The second order correlation function measured by Kuhn et al. using single photon source showing the suppression at zero delay expected for a single photon source. The hatched area represents correlations between photons and detector-noise counts. Reproduced, with permission, as Fig. 4 of [4]

An experiment to demonstrate this suppression using a single photon source was undertaken by Kuhn et al. [4]. In the experiment a sequence of single photon pulses is emitted on demand from a single three-level atom strongly coupled to a high-finesse optical cavity. The experimental results for $g^{(2)}(\tau)$ are shown in Fig. 2.2.

In the case of the two photon multi-mode state,

$$|2_\xi\rangle = \frac{1}{\sqrt{2}}\left[\int_{-\infty}^{\infty} d\omega\, \tilde{\xi}(\omega)\tilde{a}_{in}^{\dagger}(\omega)\right]^2 |0\rangle \quad . \tag{2.62}$$

the second order correlation function is given by

$$G^{(2)}(t;\tau) = 2|\xi(t)|^2|\xi(t+\tau)|^2 \tag{2.63}$$

This is the product for the rate of a detection of a single photon at time t *and* a second photon at time $t+\tau$. The pre factor of 2 is an indication of bosonic statistics, and is called *bunching* in quantum optics.

This effect may be observed in a two-photon version of the HBT experiment, Fig. 2.3. A two-photon state is directed towards a 50 : 50 beam splitter and a single photon detector is placed in each output mode. Let $b_1(t)$, $b_2(t)$ represent the positive frequency components of the field in each output. The second order correlation function for the output fields is

$$\langle b_1^{\dagger}(t)b_2^{\dagger}(t+\tau)b_2(t+\tau)b_1(t)\rangle = \frac{1}{4}\langle a_1^{\dagger}(t)a_1^{\dagger}(t+\tau)a_1(t+\tau)a_1(t)\rangle = \frac{1}{2}|\xi(t)|^2|\xi(t+\tau)|^2 \tag{2.64}$$

while

$$\langle b_i^{\dagger}(t)b_i(t)\rangle = \frac{1}{2}\langle a_i^{\dagger}(t)a_i(t)\rangle \tag{2.65}$$

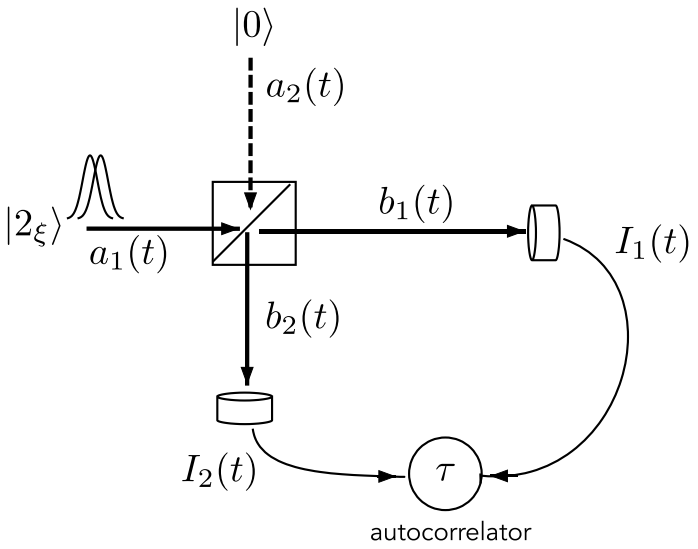

Fig. 2.3 A quantum Hanbury Brown Twiss (HBT) experiment with a two photon pulse. The input mode a_1 is prepared in the two photon state in (2.62). The input mode a_2 is in the vacuum state

The normalised second order correlation function is

$$g^{(2)}(t,\tau) = \frac{\langle b_1^\dagger(t) b_2^\dagger(t+\tau) b_2(t+\tau) b_2(t)\rangle}{\langle b_1^\dagger(t) b_1(t)\rangle \langle b_2^\dagger(t) b_2(t)\rangle} = 2\frac{|\xi(t+\tau)|^2}{|\xi(t)|^2} \tag{2.66}$$

Note that this is always equal to 2 at zero delay. This is similar to thermal light. In the case of thermal light however the functions $\xi(t)$ are complex amplitudes of a classical Gaussian process and an additional average must be made of these amplitudes as in (2.52). If $\xi(t)$ is given by (1.129) we find that this is independent of t,

$$g^{(2)}(\tau) = 2e^{-2\gamma\tau} \tag{2.67}$$

The peak of 2 at zero delay is the signature of photon bunching. An experimental demonstration was presented by Wolf et al. [5] using a two-photon source based on two trapped ions.

The original HBT experiment did not use two-photon states of this kind as the stellar sources are chaotic (Gaussian). In the case of Gaussian light we note that there is a simple relation between first order and second order correlation functions given by (2.55). The second order correlation function for thermal light is given by (2.58) and thus there is a connection between the first and second order correlation functions.

If the stellar sources are not thermal we need a more complicated intensity interferometer. A novel type of two-photon interferometer for astrometry, which uses photons from two separate sky sources was proposed by Gottesman, Jennewein and Croke [12] that goes beyond the HBT interferometer.

2.8.1 Squeezed State Photon Number Fluctuations

The variance of photon number for the squeezed state $|\alpha, r\rangle$, with $r \in \mathbb{R}$ and $\alpha = |\alpha|e^{i\theta}$ is

$$V(n) = 2\cosh^2 r \sinh^2 r + |\alpha|^2(\cosh 2r - \cos 2\theta . \sinh 2r) \tag{2.68}$$

In the case that the $\theta = 0$,

$$V(n) = 2\cosh^2 r \sinh^2 r + |\alpha|^2 e^{-2r} \qquad \theta = 0. \tag{2.69}$$

while for

$$V(n) = 2\cosh^2 r \sinh^2 r + |\alpha|^2 e^{2r} \qquad \theta = \pi/2. \tag{2.70}$$

The first case corresponds to the squeezed quadrature in the same quadrature as the coherent amplitude and the second case the squeezed quadrature is orthogonal to the phase of the coherent amplitude. We call the first case amplitude squeezed and the second case phase squeezed. These two situations are depicted in Fig. 2.4. It is clear that amplitude squeezed states can have reduced photon number fluctuations while phase squeezed states have enhanced photon number fluctuations.

2.8.2 Cat State Photon Number Fluctuations

Cat states, introduced in Chap. 1, are an interesting example of anti-bunched light. Consider the orthogonal states,

$$|\alpha_\pm\rangle = \mathcal{N}_\pm(\alpha)[|\alpha\rangle \pm |-\alpha\rangle] \tag{2.71}$$

with

$$\mathcal{N}_\pm(\alpha) = \frac{1}{\sqrt{2\left(1 \pm e^{-2|\alpha|^2}\right)}} \tag{2.72}$$

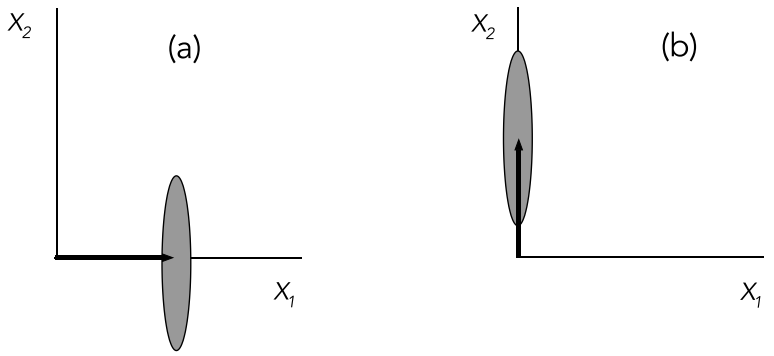

Fig. 2.4 In **a** we show an amplitude squeezed state. In **b** we show a phase squeezed state

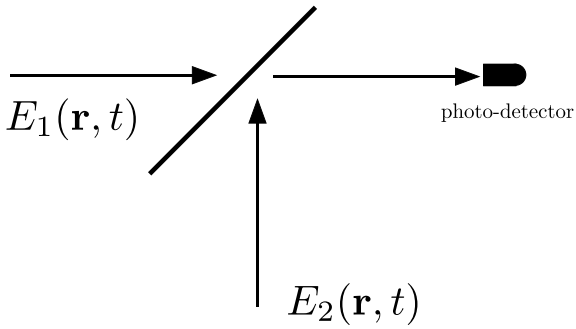

Fig. 2.5 Two fields are combined on a beam splitter with transmitivity as a first step to realise homodyne or heterodyne detection

The mean photon number is given by $\langle a^\dagger a\rangle_\pm = |\alpha|^2(\tanh(|\alpha|^2)^{\pm 1}$. It is easily verified that $\langle a^{\dagger\,2}a^2\rangle_\pm = |\alpha|^4$. Thus

$$g^{(2)}(0) = \begin{cases} \left[\tanh|\alpha|^2\right]^2 & \text{for } |\alpha_+\rangle \\ \left[\tanh|\alpha|^2\right]^{-2} & \text{for } |\alpha_-\rangle \end{cases} \tag{2.73}$$

These approach the same limit as $|\alpha|^2 \to \infty$ but have very different behaviour for small $|\alpha|$. This is because $|\alpha_+\rangle$ have only even photon numbers and thus the photon statistics are highly bunched, while the odd cat is anti-bunched as it contains mostly a one photon component. The second order correlation function for cat states were measured by Besse et al. [6] at microwave frequencies.

2.9 Phase-Dependent Correlation Functions

The even-ordered correlation functions such as the second-order correlation function $G^{(n,n)}(x)$ contain no phase information and are a measure of the fluctuations in the photon number. The odd-ordered correlation functions $G^{(n,m)}(x_1 \ldots x_n, x_{n+1} \ldots x_{n+m})$ with $n \neq m$ will contain information about the phase fluctuations of the electromagnetic field. The variances in the quadrature phases ΔX_1^2 and ΔX_2^2 are measurements of this type. These correspond to homodyne and heterodyne measurements (see Chap. 7). These schemes require a reference signal known as the local oscillator before photodetection. Homodyning with a reference signal of fixed phase gives the phase sensitivity necessary to yield the quadrature variances.

Consider two fields $E_1(\mathbf{r}, t)$ and $E_2(\mathbf{r}, t)$ of the same frequency, combined on a beam splitter with transmitivity η, as shown in Fig. 2.5. This is a phase dependent measurement as the intensity falling on the photo-detector depends on the relative phase and frequency of the two input fields.

We expand the two incident fields into the usual positive and negative frequency components

$$E_j(\mathbf{r}, t) = i\left(\frac{\hbar\omega}{2\epsilon_0 V}\right)^{1/2}(a_j e^{i(\mathbf{k}_j\cdot\mathbf{r}-\omega t)} - a_j^\dagger e^{-i(\mathbf{k}_j\cdot\mathbf{r}-\omega t)}) \tag{2.74}$$

The total field falling on the photo detector is given by

$$E_T(\mathbf{r},t) = i\left(\frac{\hbar\omega}{2\epsilon_0 V}\right)^{1/2}(ce^{i(\mathbf{k}_1\cdot\mathbf{r}-\omega t)} - c^\dagger e^{-i(\mathbf{k}_1\cdot\mathbf{r}-\omega t)}) \,, \tag{2.75}$$

where

$$c = \sqrt{\eta}a_1 + i\sqrt{1-\eta}a_2 \,. \tag{2.76}$$

We have included a 90° phase shift between the reflected and transmitted beams at the beam splitter required by time reversal invariance.

The photo-detector responds with a detection rate proportional to $\langle c^\dagger c\rangle$. This is given by

$$\langle c^\dagger c\rangle = \eta\langle a^\dagger a\rangle + (1-\eta)\langle b^\dagger b\rangle - i\sqrt{\eta(1-\eta)}(\langle a^\dagger b\rangle + \langle b^\dagger a\rangle) \,. \tag{2.77}$$

We will assume that the field $E_2(\mathbf{r},t)$ is in a coherent state with a large and controllable amplitude, $\beta = |\beta|e^{i\theta}$. We refer to this field as the *local oscillator* as it provides a phase and frequency reference, while we regard $E_1(\mathbf{r},t)$ as the signal field. In this case we have taken the carrier frequency of the signal field which is the condition for homodyne detection. To linear order in the field amplitude we see that

$$\langle c^\dagger c\rangle \approx (1-\eta)\langle|\beta|^2 - i|\beta|\sqrt{\eta(1-\eta)}\langle X_{\theta+\pi/2}\rangle \,. \tag{2.78}$$

where $X_{\theta+\pi/2} \equiv ae^{i\theta} + ae^{-i\theta}$. If the reflected intensity of the local oscillator field is subtracted, this is proportional to the mean of the quadrature phase of the signal field.

We now turn to a consideration of the fluctuations in the photo-current. The rms fluctuation current is determined by the variance of $c^\dagger c$. For an intense local oscillator in a coherent state this variance is

$$\langle\Delta(c^\dagger c)^2\rangle \approx |\beta|^2(1-\eta)^2 + |\beta|^2\eta(1-\eta)\langle\Delta X^2_{\theta+\pi/2}\rangle \tag{2.79}$$

The first term here represents reflected local oscillator intensity fluctuations. If this term is subtracted, the photo-current fluctuations are determined by the variance in $X_{\theta+\pi/2}$, the measured quadrature phase operator. To subtract out the contribution of the reflected local oscillator field balanced homodyne detection may be used. In that scheme the output from both ports of the beam splitter is directed to a photodetector and the resulting currents subtracted before subsequent analysis. Balanced homodyne detection realises a direct measurement of the signal field quadrature phase operators [16].

2.10 Photon Counting Measurements

2.10.1 Semi-classical Theory

The photo-electric effect was one of the key experiments that lead to the development of quantum theory. Einstein's explanation of the phenomenon introduced the idea of light quanta to explain photo-electron emission from a metal subjected to illumination. The energy of ejected electrons was determined by the frequency of the light falling on the metal while the number of electrons ejected per second was determined by the intensity of the light.

In a typical photo-counting experiment, the absorption of light in a material results in a photo-current. If the intensity of the light is low enough, the current is seen to be composed of individual current pulses resulting from individual photon absorption events. A simple integrator can count these events. The theory must describe the statistics of this current/count in terms of the quantum state of the light impinging on the detector. We will begin with a simpler semi-classical treatment in which the average photo-current current is proportional to the classical fluctuating intensity of the field.

As in all quantum measurement the actual observed phenomenon is a classical random variable. In the case of absorptive photo-detection measurements we postulate a *classical* random variable that corresponds to whether or not a photon is absorbed in a small time interval dt. We thus define a random variable, $dN(t) \in 0, 1$, that takes binary values. It follows that $dN(t)^2 = dN(t)$. The current resulting from this random variable is

$$J(t) = e \int_{-\infty}^{t} dN(t')h(t - t') \tag{2.80}$$

where e is the elementary charge and $h(t)$ is a causal response function for the entire measurement circuit, i.e $h(t) = 0$ for $t < 0$. Clearly the current is also a classical stochastic process. We can now say that the classical stochastic process $dN(t)$ is a conditional Poisson process conditioned on the quantum nature of the light.

The average current is determined by the average of $dN(t)$. This is simply the probability, $p_1(t)$, that a single photon is detected between t and $t + dt$. We expect that, for a classical field, the rate of detection is proportional to the field intensity, $I(t) = \mathcal{E}^{(-)}(t)\mathcal{E}^{(+)}(t)$, and so we set

$$p_1(t) = \mathbb{E}[dN(t)] = \eta\mathcal{E}^{(-)}(t)\mathcal{E}^{(+)}(t)dt = \eta I(t)dt \ . \tag{2.81}$$

where η is a device dependent constant. This defines an inhomogeneous Poisson process (a time dependent detection rate). Then

$$J(t) = e\eta \int_{-\infty}^{t} dt'h(t - t')I(t') \tag{2.82}$$

and α has units of (Watts . Ohms)$^{-1}$ and depends on the physical nature of the detector. We will assume for simplicity that the response function is a unit top-hat function a width of T. Then define

$$J(t;T) = e\eta \frac{1}{T}\int_t^{t+T} dt\, I(t) = e\eta \bar{I}(t;T) \tag{2.83}$$

and we have defined the time averaged intensity over a counting interval as

$$\bar{I}(t;T) = \frac{1}{T}\int_t^{t+T} dt\, I(t) \tag{2.84}$$

In the case of a single plane wave field, the intensity is a constant, so $\bar{I}(t;T) = I$, and $p_1(t) = \alpha I dt$. The probability for no counts to occur in the time interval $[t, t+T)$ may be found by dividing the time interval into N bins of size δt, or $\delta t = T/N$. The probability for no counts to occur in the time interval is

$$P_0(T+t,t) \approx (1 - \eta I T/N)^N \,, \tag{2.85}$$

In the limit of $N \to \infty$ with T fixed we see that

$$P_0(T+t,t) = e^{-\eta I T} \,, \tag{2.86}$$

In the case of a non constant intensity, the probability for no counts to occur in the time interval is

$$P_0(T+t,t) \approx \prod_{k=1}^{N} (1 - p_1(t_k)) \,, \tag{2.87}$$

where $t_k = k\delta t$. We can approximate $p_1(t_k) = \alpha I(t_k)\delta t$ and thus

$$1 - p_1(t_k) \approx e^{-\eta I(t_k)\delta t} \tag{2.88}$$

In the limit of $N \to \infty$ with T fixed, the probability for no counts in the time interval is

$$P_0(t;T) = \exp\left[-\eta \int_t^{t+T} dt'\, I(t')\right] = \exp\left[-\eta T \bar{I}(t:T)\right] \,. \tag{2.89}$$

where

$$\bar{I}(t:T) = \frac{1}{T}\int_t^{t+T} dt'\, I(t') \tag{2.90}$$

In the case of n counts in the interval t to $t+T$, we can specify a fine grained history of detection events $t_1, t_2, \ldots t_n$ where t_n means one count was observed between t_k and $t_k + dt$. The fine grained probability is given as a function of the history $P_n(t:T|t_1, t_2, \ldots t_n)$.

Suppose that $n = 1$ and this occurred at the end of the time interval. The probability for this history is

$$P_1(t; T|t_1 = t) = \eta I(T + t)dt \exp\left[-\eta \int_t^{t+T} dt'\ I(t')\right] . \tag{2.91}$$

If we know that only one cont has occurred, but do not know when during the counting interval it occurred, the probability for this even coarser-grained history is

$$P_1(t; T) = \eta \int_t^{t+T} dt_1\ I(t_1) \exp\left[-\eta \int_t^{t+T} dt'\ I(t')\right] \tag{2.92}$$

$$= \eta T \bar{I}(t; T) \exp\left[-\eta T \bar{I}(t; T)\right] . \tag{2.93}$$

Continuing this line of reasoning we encounter time ordered integrals of the form

$$\int_t^{t+T} dt_n \int_t^{t_n} dt_{n-1} \ldots \int_t^{t_2} dt_1 I(t_n) I(t_{n-1}) \ldots I(t_1) \tag{2.94}$$

which is equal to

$$f_n(t; T) = \frac{1}{n!} \left(\int_t^{t+T} dt'\ I(t') \right)^n \tag{2.95}$$

The probability to count n photons is thus

$$P_n(t; T) = \frac{1}{n!} \left(\eta T \bar{I}(t; T)\right)^n \exp\left[-\eta T \bar{I}(t; T)\right] . \tag{2.96}$$

This is a Poisson distribution with mean $\mathbb{E}[n] \equiv \bar{n} = \eta T \bar{I}(t; T)$.

In the simplest case of a constant intensity $I(t, T)$ is independent of t and T, hence

$$\bar{I}(t; T) = I \tag{2.97}$$

a constant. Thus

$$P_n(T) = \frac{\bar{n}^n}{n!} e^{-\bar{n}} \tag{2.98}$$

where the average count is $\bar{n} = \eta I T$.

In the case of a thermal source, $I = \overline{|\alpha|^2}$ where α is a gaussian random variable with mean zero, $\overline{\alpha} = 0$ and covariance $\overline{|\alpha|^2} = I_0$. The photon count distributions is then given by

$$P_n(T) = \frac{(\eta T)^n}{I_0 n!} \int \frac{d^2\alpha}{\pi} \frac{(|\alpha|^2)^n}{n!} e^{-\eta T|\alpha|^2} e^{-|\alpha|^2/I_0} \tag{2.99}$$

$$= \frac{1}{1 + \bar{n}} \left(\frac{\bar{n}}{1 + \bar{n}} \right)^n$$

where $\bar{n} = \eta T I_0$.

2.11 Quantum Mechanical Photon Count Distribution

In the quantum case, the detection rate is proportional to the average intensity $I(t) = \langle E^{(-)}(t)E^{(+)}(t)\rangle$. We now need to specify the quantum state of the field. Given that Galuber's theory assumes that detection corresponds to an absorption of a photon, detecting n photons should mean that, whatever state the field started in, it now has n photons *less* than when it started. The classical theory does not take this measurement 'back-action' into account. We will return to this question in Chap. 7 when we discuss measurement in more detail. Here we simply give the result first derived by Mandel [17] and usually referred to as the Mandel formula .

$$P_n(T) = \left\langle : \frac{[\eta \hat{I}(T)T]^n}{n!} \exp[-\eta \hat{I}(T)T] : \right\rangle \tag{2.100}$$

where

$$\hat{I}(T) = \frac{1}{T}\int_0^T dt\, a^\dagger(t)a(t) \tag{2.101}$$

where $a(t), a^\dagger(t)$ are given by (1.119) The notation $\langle : \ldots : \rangle$ denotes a normally ordered average over creation and annihilation operators. This means that between the colons we move all the creation operators to the left of the annihilation operators as if they commute.

For a single mode field we get

$$P_n(T) = \frac{(\eta T)^n}{n!}\sum_{m=0}^{\infty}\frac{(-\eta T)^m}{m!}\mathrm{tr}[\rho a^{\dagger\, n+m}a^{n+m}] \tag{2.102}$$

If the field is diagonal in the number basis $\rho = \sum_k p_k|k\rangle\langle k|$, we get

$$\begin{aligned} P_n(T) &= \sum_{k,m=0}^{\infty} p_k \frac{(-1)^m(\eta T)^{(n+m)}}{n!m!}\langle k|a^{\dagger\, n+m}a^{n+m}|k\rangle \\ &= \sum_{k=n}^{\infty} p_k \frac{(\eta T)^n}{n!}\sum_{m=0}^{k-n}\frac{(-\eta T)^m}{m!}\frac{k!}{(k-(n+m))!} \\ &= \sum_{k=n}^{\infty} p_k \binom{k}{n}(\eta T)^n \sum_{m=0}^{k-n}(-\eta T)^m \binom{k-n}{m} \\ &= \sum_{k=n}^{\infty} p_k \binom{k}{n}(\eta T)^n (1-\eta T)^{k-n} \end{aligned} \tag{2.103}$$

This is a Bernoulli deletion process where the probability of not counting a photon is $1 - \eta T$. We refer to ηT as the quantum efficiency. The photon number distributions

generated by a thermal light source in a single mode with frequency ω

$$p_n = (1 - \lambda_\beta) \sum_{n=0}^{\infty} \lambda_\beta^n \tag{2.104}$$

where $\lambda_\beta = e^{-\beta\hbar\omega}$. The resulting counting distribution is

$$P_n(T) = \frac{(\eta T \bar{n}_\beta)^n}{(1 + \eta T \bar{n}_\beta)^{n+1}} \tag{2.105}$$

with $\bar{n}_\beta = \lambda_\beta/(1 - \lambda_\beta)$. This is in the same for as the classical Gaussian result in (2.99).

If the field is in a coherent state $\rho = |\alpha_0\rangle\langle\alpha_0|$, the distribution is

$$P_n(T) = \frac{(\eta T \bar{n}_0)^n}{n!} e^{-\eta T \bar{n}_0} \tag{2.106}$$

where $\bar{n}_0 = |\alpha_0|^2$ is the mean photon number in the coherent state. This is a Poisson distribution with mean $\mathcal{E}[n] = \eta T \bar{n}_0$. This is the same as the classical result in (2.98) with $I = \bar{n}_0$.

The form of (2.100) is a special case of the general result

$$\hat{I}(t) = \int_{-\infty}^{t} dt' \; R(t, t') a_d^\dagger(t') a_d(t') \tag{2.107}$$

where $R(t, t')$ is a detector response function and $a_d(t)$ is a filtered temporal mode that is part of the definition of the detector [18],

$$a_d(t) = \int_{-\infty}^{\infty} d\tau G(t, \tau) a(\tau) \tag{2.108}$$

and G is the response function of the filter. In Sect. 14.2.2 we will discuss a non linear filter where

$$G(t, \tau) = \int_{-\infty}^{\infty} d\omega e^{-i\omega(t-\tau)} \tilde{\mu}^*(\omega) \tag{2.109}$$

that describes a Raman single photon detector (quantum memory).

2.11.1 Photo-Electron Current Fluctuations

The photoelectron current is given by the stochastic process in (2.80). For simplicity we will take the response function to be $h(t) = e^{-\gamma t}$ so that

$$J(t) = e \int_{-\infty}^{t} e^{-\gamma(t-t')} dN(t') \tag{2.110}$$

The mean current is

$$\mathbb{E}[J(t)] = e\eta \int_{-\infty}^{t} e^{-\gamma(t-t')} I(t') dt' \tag{2.111}$$

assuming that the intensity is a deterministic process. If this is not the case, and the intensity itself is a stochastic process, then we need to write

$$\mathbb{E}[J(t)] = e\eta \int_{-\infty}^{t} e^{-\gamma(t-t')} \mathbb{E}[I(t')] dt' \tag{2.112}$$

The mean squared current is

$$\mathbb{E}[J(t)J(t)] = e^2\eta^2 \int_{-\infty}^{t} \int_{-\infty}^{t} e^{-\gamma(2t-t'-t'')} \mathbb{E}[dN(t')dN(t'')] \tag{2.113}$$

This requires more care as $dN(t)^2 = dN(t)$. Discretising the integral gives

$$\mathbb{E}[J(t)J(t)] = e^2\eta^2 \int_{-\infty}^{t} dt' e^{-2\gamma t'} I(t') + 2 \int_{-\infty}^{t} dt' \int_{-\infty}^{t'} dt'' e^{\gamma(t'+t''-2t)} \mathbb{E}[I(t')I(t'')] \tag{2.114}$$

Thus the variance in the current is

$$\mathbb{E}[J(t), J(t)] = e^2\eta^2 \int_{-\infty}^{t} dt' e^{-2\gamma t'} I(t') + 2 \int_{-\infty}^{t} dt' \int_{-\infty}^{t'} dt'' e^{\gamma(t'+t''-2t)} \mathbb{E}[I(t'), I(t'')] \tag{2.115}$$

In the case of constant intensity this becomes

$$\mathbb{E}[J(t), J(t)] = \frac{e^2\eta^2}{2\gamma} I \tag{2.116}$$

This is called the shot-noise. We will discuss the quantum case in Chap. 7.

Problems

2.1 A beam splitter transforms incoming mode operators a_i, b_i to the outgoing operators a_o, b_o where

$$a_o = \sqrt{\eta}a_i - i\sqrt{1-\eta}b_i, \qquad b_0 = \sqrt{\eta}b_i - i\sqrt{1-\eta}a_i$$

(a) Show that such a transformation may be generated by the unitary operator

$$U = e^{-i\theta(a^\dagger b + ab^\dagger)} \qquad \eta = \cos^2\theta$$

(b) Thus show that if the incoming state is a coherent state $|\alpha_i\rangle \otimes |\beta_i\rangle$, the outgoing state is also a coherent state with

$$\alpha_o = \sqrt{\eta}\alpha_i - i\sqrt{1-\eta}\beta_i, \qquad \beta_0 = \sqrt{\eta}\beta_i - i\sqrt{1-\eta}\alpha_i$$

(c) Show that, if the incoming state is the product number state $|1\rangle \otimes |1\rangle$, the outgoing state is

$$(2\eta - 1)|1\rangle \otimes |1\rangle + i\sqrt{\eta(1-\eta)}(|2\rangle \otimes |0\rangle + |0\rangle \otimes |2\rangle)$$

Note that when $\eta = 1/2$ the 'coincidence' term $|1\rangle \otimes |1\rangle$ does not appear, a result known as Hong-Ou-Mandel interference [19]

2.2 In the experimental scheme of Fig. 2.3, light enters both input ports a_1, a_2. The incoming state is the two-mode mixed state

$$\rho = \frac{1}{2}|2_\mu, 0\rangle\langle 2_\mu, 0| + \frac{1}{2}|0, 2_\mu\rangle\langle 0, 2_\mu| + \frac{1}{\sqrt{2}}|1_\mu, 1_\mu\rangle\langle 1_\mu, 1_\mu| \tag{2.117}$$

where $|n_\mu\rangle$ is an n-photon state of a single mode with temporal mode function $\mu(t)$ (see (1.122)). Calculate the second order correlation function for the output field, $\langle b_1^\dagger(t)b_2^\dagger(t+\tau)b_2(t+\tau)b_1(t)\rangle$.

2.3 Show that, for sufficiently long T

$$\langle 1_\mu|\hat{I}(T)|1_\mu\rangle = 1 \tag{2.118}$$

for the single photon pulse $|1_\mu\rangle$ given in (1.122).

References

1. R.J. Glauber, Phys. Rev. **130**, 2529 (1963)
2. R. Hanbury-Brown, R.W. Twiss, Nature **177**, 27 (1956)
3. A. Aspect, Chapter 12 in the Proc. Les Houches Summer School 1996 : *Current Trends in Atomic Physics*, ed. by A. Browaeys, T. Porto, C.S. Adams, M. Weidemuller, L.F. Cugliandolo (Oxford University Press, 2019)
4. A. Kuhn, M. Hennrich, G. Rempe, Phys. Rev. Lett. **89**, 067901–1 (2002)
5. S. Wolf, S. Richter, J. von Zanthier, F. Schmidt-Kaler, Phys. Rev. Lett. **124**, 063603 (2020)
6. J.-C. Besse, S. Gasparinetti, M.C. Collodo, T. Walter, A. Remm, J. Krause, C. Eichler, A. Wallraff, Phys. Rev. X **10**, 011046 (2020)
7. M. Born, E. Wolf, *Principles of Optics*, 3rd edn. (Pergamon, London, 1965)
8. P.A.M. Dirac, *The Principles of Quantum Mechanics*, 3rd edn. (Clarendon, London, 1947)
9. G.I. Taylor, Proc. Cam. Phil. Soc. Math. Phys. Sci. **15**, 114 (1909)
10. P. Grangier, G. Roger, A. Aspect, Europhys. Lett. **1**, 173 (1986)
11. M. Tsang, Phys. Rev. Lett. **107**, 270402 (2011)
12. D. Gottesman, T. Jennewein, S. Croke, Phys. Rev. Lett. **109**, 070503 (2012)
13. R.F. Pfleegor, L. Mandel, Phys. Rev. **159**, 1084 (1967)
14. C.W. Gardiner, *A Handbook of Stochastic Processes for Physics, Chemistry and the Natural Sciences* (Springer, Berlin, 2009)
15. F.T. Arecchi, E. Gatti, A. Sona, Phys. Rev. Lett. **20**, 27 (1966); F.T. Arecchi, Phys. Lett. **16**, 32 (1966)
16. H.P. Yuen, J.H. Shapiro, IEEE Trans. IT **26**, 78 (1980)
17. L. Mandel, Fluctuations of light beams, *Progress in Optics*, vol. 2 (1963)
18. M.G. Raymer, I.A. Walmsley, Phys. Scr. **95**, 064002 (2020)
19. F. Bouchard et al., Rep. Prog. Phys. **84**, 012402 (2021)

Representations of the Electromagnetic Field

3

Abstract

A full description of the electromagnetic field requires a quantum statistical treatment. The electromagnetic field has an infinite number of modes and each mode requires a statistical description in terms of its allowed quantum states. Each mode is described by an independent Hilbert space. In this chapter we introduce a number of functional representations for the density operator of the electromagnetic field: the P-function, the Wigner function and the Q-function.

3.1 Classical Phase-Space Distributions

We saw in Chap. 1 that the classical electromagnetic field can be described in terms of a probability distribution $\mathcal{P}(\alpha, \alpha^*)$, over the complex amplitudes $\alpha \in \mathbb{C}$ for each mode. A similar description can be given for a classical simple harmonic oscillator by writing $\alpha = x + iy$ and treating x, y as the dimensionless canonical coordinates in the classical phase space. Classical states are specified by giving the distribution $\mathcal{P}(\alpha, \alpha^*)$ and observables are real valued, infinitely differentiable, functions $f(\alpha, \alpha^*) \in \mathbb{R}$ on phase-space. The average of a classical observable for a state $\mathcal{P}(\alpha, \alpha^*)$ is

$$\mathbb{E}[f(\alpha, \alpha^*)] = \int \frac{d^2\alpha}{\pi} f(\alpha, \alpha^*)\mathcal{P}(\alpha, \alpha^*) \tag{3.1}$$

States of maximal knowledge would correspond to $\mathcal{P}(\alpha, \alpha^*) = \delta^2(\alpha - \alpha_0)$, for which an observable takes the deterministic value $f(\alpha_0, \alpha_0^*)$.

Quantum states are specified in terms of the density operator ρ and have no natural phase space representation. However a number of phase-space representations have been invented as a means for computing operator averages. We might expect that deterministic distributions in terms of delta functions would be problematic due to the uncertainty principle and this is indeed the case.

D. F. Walls and G. J. Milburn, *Quantum Optics*, Graduate Texts in Physics,
https://doi.org/10.1007/978-3-031-84177-4_3

3.2 The P-Representation

The coherent states $|\alpha\rangle$ (see Sect. 1.3) form a complete set of states, in fact, an over-complete set of states. They may therefore be used as a basis set despite the fact that they are non-orthogonal. The following diagonal representation in terms of coherent states was introduced independently by Glauber [1] and Sudarshan [2]

$$\rho = \int d^2\alpha\, P_\rho(\alpha, \alpha^*)|\alpha\rangle\langle\alpha| \,. \tag{3.2}$$

This is clearly a statistical mixture of coherent states provided $P(\alpha, \alpha^*)$ is a true probability density on phase space. However it is easy to see that there are many quantum states for which such a distribution does not exist. The simplest example is a number state, $\rho = |N\rangle\langle N|$. Taking matrix elements with a coherent state $|\beta\rangle$, this requires that there exists a distribution $P_N(\alpha, \alpha^*)$ such that

$$e^{-|\beta|^2}\frac{|\beta|^{2N}}{N!} = \int d^2\alpha\, P_N(\alpha, \alpha^*)e^{-|\alpha-\beta|^2} \quad \forall N \,. \tag{3.3}$$

Evaluating the left hand side at $\beta = 0$ implies that $P_N(\alpha, \alpha^*)$ must be negative on some region in the complex plane. This is not possible for a true probability distribution. In the exercises we treat the case of a squeezed vacuum for which no Glauber-Sudarshan representation exists.

Nonetheless there are many physical states that do have a valid P-representation. It is obvious that the P-representation of the coherent state $|\alpha_0\rangle$ is

$$P(\alpha|\alpha_0) = \delta^{(2)}(\alpha - \alpha_0) \,. \tag{3.4}$$

where $\delta^{(2)}(x + iy) = \delta(x)\delta(y)$. A thermal state also has a P-representation. In that case

$$P_T(\alpha, \alpha^*) = \frac{1}{\pi\bar{n}}e^{-|\alpha|^2/\bar{n}} \tag{3.5}$$

where $\bar{n}$ is given by

$$\bar{n} = \frac{1}{e^{\hbar\omega/k_BT} - 1} \,. \tag{3.6}$$

Using this we can evaluate the photon number distribution for a thermal state (see exercises).

The P-representation assumes a central role in quantum optics as it gives normally ordered moments of the field by treating α as a random variable and integrating over the complex plane,

$$\langle a^{\dagger\,n}a^m\rangle = \mathrm{tr}[a^\dagger a\rho] = \int d^2\alpha\, P(\alpha, \alpha^*)\alpha^{*\,n}\alpha^m \,. \tag{3.7}$$

The P-representation does not give the marginal distributions for the quadrature phase operators directly. The probability distribution for $X_1 = a + a^\dagger$ for a system prepared in the state ρ is given by

$$P(x) = \langle x|\rho|x\rangle \tag{3.8}$$

with $X_1|x\rangle = x|x\rangle$. If ρ has a Glauber-Sudarshan P-representation,

$$P(x) = \int d^2\alpha\, P(\alpha)|\langle\alpha|x\rangle|^2\,, \tag{3.9}$$

where $\langle\alpha|x\rangle$ is given in (1.59). On the other hand the marginal distribution of $P(\alpha)$ for the real part of α is simply

$$p(x) = \int_{-\infty}^{\infty} dy\, P(x+iy)\,, \tag{3.10}$$

which is clearly not the same. This is reflected in the moments. While

$$\langle X_1\rangle = \int d^2\alpha\, P(\alpha)(\alpha+\alpha^*) \tag{3.11}$$

we find the second order moment is given by

$$\langle X_1^2\rangle = 1 + \int d^2\alpha\, P(\alpha)(\alpha+\alpha^*)^2\,. \tag{3.12}$$

as the P-function only gives normally ordered moments by direct integration. This is another reason why we cannot regard the P function as a true probability density in a classical phase space.

In classical stochastic processes an important role is played by the characteristic function as a moment generating function. Let $\mathcal{P}(\alpha,\alpha^*)$ be such a classical distribution function for a system with a single degree of freedom. The characteristic function is defined by the complex valued moment

$$\chi(\eta,\eta^*) = \int d^2\alpha\, \mathcal{P}(\alpha,\alpha^*)e^{\eta\alpha^*-\eta^*\alpha} = \mathbb{E}[e^{\eta\alpha^*-\eta^*\alpha}]\,. \tag{3.13}$$

It then follows that

$$\mathbb{E}[\alpha^n\alpha^{*\,m}] = \frac{\partial^n}{\partial\eta^{*\,n}}\frac{\partial^m}{\partial\eta^m}\chi(\eta,\eta^*)\bigg|_{\eta=0}\,. \tag{3.14}$$

Analogously the characteristic function for a state with a Glauber-Sudarshan P function is defined by

$$\chi_N(\eta,\eta^*) = \int d^2\alpha\, P(\alpha,\alpha^*)e^{\eta\alpha^*-\eta^*\alpha} = \langle e^{\eta a^\dagger}e^{-\eta^* a}\rangle \tag{3.15}$$

This determines normally ordered moments using (3.14), thus the subscript. Inverting the Fourier transform we see that

$$P(\alpha) = \frac{1}{\pi^2} \int d^2\eta \chi_N(\eta, \eta^*) e^{\eta^*\alpha - \eta\alpha^*} \tag{3.16}$$

3.2.1 Wigner's Phase-Space Density

The first quasi-probability distribution was introduced into quantum mechanics by Wigner [4]. It differs from the P function in that the marginal distributions correspond to the correct quantum distributions as given by the Born rule. The Wigner function may be defined as the Fourier transform of the symmetrically ordered characteristic function

$$\chi_S(\eta) = \langle e^{\eta a^\dagger - \eta^* a} \rangle = \mathrm{tr}[\rho e^{\eta a^\dagger - \eta^* a}] \tag{3.17}$$

Thus

$$W(\alpha) = \frac{1}{\pi^2} \int d^2\eta \chi_S(\eta) e^{\eta^*\alpha - \eta\alpha^*} \tag{3.18}$$

The Wigner function is a Gaussian convolution of the Glauber-Sudarshan P function,

$$W(\alpha) = \frac{2}{\pi} \int d^2\beta P(\beta) e^{-2|\alpha-\beta|^2} \tag{3.19}$$

While the Wigner function does give the quantum marginal distributions, it is not necessarily positive and thus cannot be a true phase-space probability density. For example, the symmetrically ordered characteristic function for a number state $|n\rangle$ is given by the average value of the displacement operator,

$$\chi_S(\eta) = \langle n|D(\eta)|n\rangle \ . \tag{3.20}$$

This may be calculated by first finding the matrix elements of the displacement operator in the number basis,

$$\langle m|D(\eta)|n\rangle = \sqrt{\frac{n!}{m!}} e^{-|\eta|^2/2} (\eta)^{m-n} L_n^{m-n}(|\eta|^2) \quad m \geq n \tag{3.21}$$

where $L_p^q(z)$ are associated Laguerre polynomials. Taking the Fourier transform we find that the Wigner function for a number state $|n\rangle$ is

$$W_n(\alpha) = \frac{(-1)^n}{\pi} e^{-2|\alpha|^2} L_n(4|\alpha|^2) \tag{3.22}$$

which is clearly negative for n odd.

The Wigner function for coherent squeezed states, $|\alpha, r\rangle$, are Gaussian (and positive). Writing $\bar{x}_1 = \alpha + \alpha^*$ and $\bar{x}_2 = -i(\alpha - \alpha^*)$ we find that

$$W_{\alpha,r}(x_1, x_2) = \frac{1}{2\pi} \exp[-\frac{e^{2r}}{2}(x_1 - \bar{x}_1)^2 - \frac{e^{-2r}}{2}(x_2 - \bar{x}_2)^2] \tag{3.23}$$

The Wigner function can be experimentally determined using the equality [5]

$$W(\alpha) = \frac{2}{\pi}\text{tr}[D(\alpha)\Pi D^\dagger(\alpha)\rho] \tag{3.24}$$

where $\Pi = e^{i\pi a^\dagger a}$ is the parity operator. A simple procedure was implemented by Banaszek et al. [6] based on photon counting. A simple example is the Schrödinger cat state of the form

$$|\chi\rangle = \frac{1}{\sqrt{2}}(e^{i\pi/4}|\alpha_0\rangle + e^{-i\pi/4}|-\alpha_0\rangle) \tag{3.25}$$

This is not a parity cat but can be generated by a Kerr non linearity (see Chap. 4). The Wigner function is given by

$$W(\alpha, 1/2) = \frac{1}{\pi}\left[W_+(\alpha) + W_-(\alpha) + 2\sqrt{W_+(\alpha)W_-(\alpha)}\sin(2\alpha_0\Im(\alpha))\right] \tag{3.26}$$

where

$$W_\pm(\alpha) = e^{-2|\alpha\pm\alpha_0|^2} \tag{3.27}$$

A contour plot of the Wigner function is shown in Fig. 3.1. The Wigner function for parity optical cat states was reported by Ourjoumtsev et al. [7]. They were generated by subtracting a single photon from a squeezed vacuum state (See chapter).

Hofheinz et al. [8] measured the Wigner functions for the Fock state superpositions, $|0\rangle + |N\rangle$, of a microwave field in a superconducting resonator (see Chap. 11). The results are shown in Fig. 3.2.

3.2.2 Q Function

The Q-function (or Husimi function) is defined as the diagonal matrix elements of the density operator in the coherent state basis,

$$Q(\alpha) = \langle\alpha|\rho|\alpha\rangle \tag{3.28}$$

Clearly the Q-function is positive and bounded by one. Using (1.48) we see that the normalisation integral is

$$\frac{1}{\pi}\int d^2\alpha Q(\alpha) = 1 \tag{3.29}$$

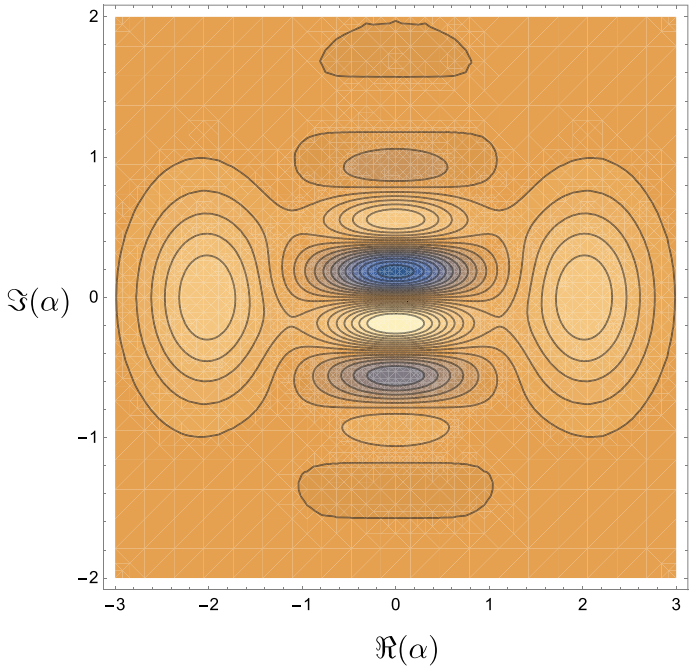

Fig. 3.1 The Wigner function contours for the cat state $|\chi\rangle$ with $\alpha_0 = 2$. Blue indicates regions of negativity

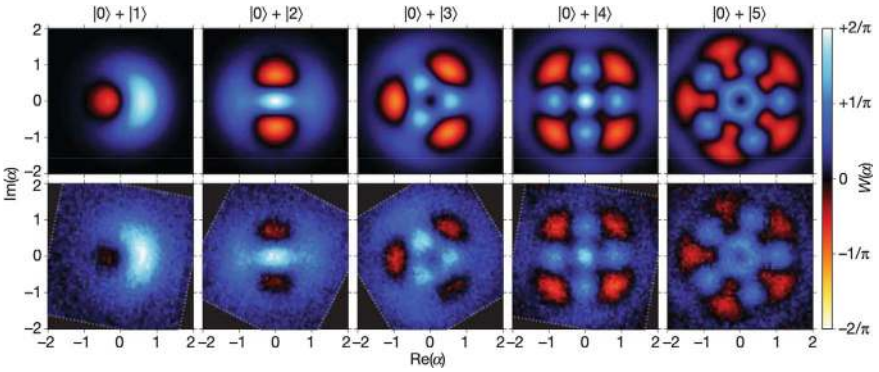

Fig. 3.2 A comparison of the predicted and measured Wigner representation of Fock state superpositions $|0\rangle + |N\rangle$ in a superconducting microwave resonantor. [Reproduced with permission from [8]]

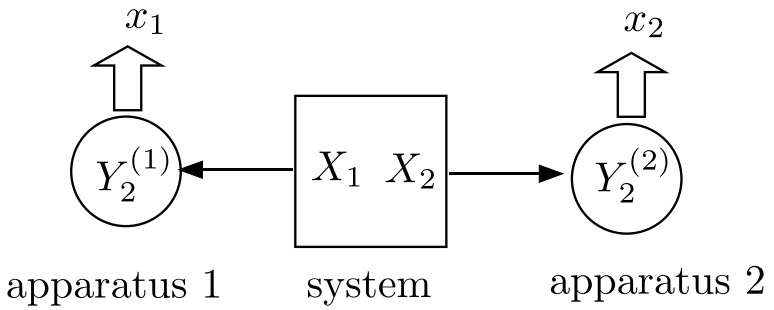

Fig. 3.3 A schematic representation of the Arthurs and Kelly scheme [9] for the simultaneous measurement of the two non commuting system operators X_1, X_2 by coupling them, respectively, to the commuting quadrature phase operator $Y_2^{(1)}$ and $Y_2^{(2)}$ of two distinct bosonic modes. The coupling is taken as impulsive as is the simultaneous projective measurement of the two apparatus observables resulting in the real values x_1, x_2

The Q-function is a true probability density for a special class of measurements. Suppose we set out to simultaneously measure the quadrature phase operators X_1, X_2 as defined in (1.54). As these operators do not commute the allowed physical states are constrained by the Heisenberg uncertainty principle (HUP), (1.55). However this does not prevent us from making simultaneous measurements of the quadrature operators so long as sufficient noise in added by the measurement so as to ensure the resulting conditional state does not violate the HUP. In other words, they can be measured simultaneous, but not arbitrarily accurately. The construction of such a measurement scheme was first given by Arthurs and Kelly [9]. We follow the presentation of [10].

We couple each quadrature phase operator of a field mode to two distinct readout modes and simultaneously readout a quadrature phase operator on each those two field modes, see Fig. 3.3. The impulsive interaction between the system and two distinct apparatus operators $Y_2^{(1)}$ and $Y_2^{(2)}$ is described by the unitary 'scattering' operator

$$U_{int} = \exp[-\frac{i}{2}(X_1 Y_2^{(1)} + X_2 Y_2^{(2)})] \tag{3.30}$$

where the apparatus operators are part of a canonically conjugate pair $[Y_1^{(j)}, Y_2^{(j)}] = 2i$. The input state of the three systems before the interaction is $|\psi\rangle_s|0\rangle_1|0\rangle_2$ where $|\psi\rangle$ is an arbitrary system state and $|0\rangle_j$ are oscillator ground states (vacuum states). After the interaction the output state is

$$|\Psi\rangle_{out} = U_{int}|\psi\rangle_s|0\rangle_1|0\rangle_2 \tag{3.31}$$

In the Heisenberg picture this interaction displaces the conjugate apparatus operators by X_1, X_2 respectively as

$$Y_1^{(j)} \to U_{int}^\dagger Y_1^{(j)} U_{int}^\dagger = Y_1^{(j)} + X_j \tag{3.32}$$

the first detector recording the system observable X_1 and the second detector recording the system observable X_2. To read out the results, we projectively measure the apparatus observables $Y_1^{(j)}$ immediately after the interaction with the result x_j for $j = 1, 2$. The joint probability density operator for these two results is given by Q-function of the arbitrary system state $|\psi\rangle$ with $\alpha = x_1 + ix_2$. It follows from (3.32) that the uncertainty of the apparatus operators after the measurement is given by

$$\langle (\Delta Y_1^{(j)})^2 \rangle_{out} = 1 + \langle \psi | \Delta X_j^2 | \psi \rangle \tag{3.33}$$

This shows that each measurement apparatus is adding a small amount of noise for each system quadrature operator. This is the price paid for a simultaneous measurement of these two non commuting operators. The noise added by the measurement enforces the moments of the Q-function to correspond to anti-normally ordered moments of the system annihilation and creation operators

$$\frac{1}{\pi} \int d^2\alpha \; \alpha^{*\,n} \alpha^m = \langle \psi | a^m a^{\dagger\,n} | \psi \rangle \tag{3.34}$$

The preceding discussion might appear a little abstract. In Chap. 7 we will see that the Q-function describes heterodyne detection of a cavity field mode.

The Q-functions for displaced squeezed states $|\alpha, r\rangle$ are easily seen to be Gaussian. See (1.77). The Q-function for a number state, $|n\rangle$ is given by

$$Q_n(\alpha) = \frac{|\alpha|^{2n}}{n!} e^{-|\alpha|^2} \tag{3.35}$$

While this is positive, it has zeros—a very unusual feature for a putative phase-space probability density. This is a general feature of the Q-function of highly non classical states and parallels the negativity of the Wigner functions of non classical states. The zeros of the Q-function can be considered a defining feature of non classical states. In fact, the Q-function is a holomorphic function and is determined by a Gaussian envelope and zeros in the complex plane. The number of zeros can characterise the non classicality of the state. This is known as the stellar rank [11].

3.2.3 Generalised P Representations

An expansion in non diagonal coherent state projection operators was suggested by Drummond and Gardiner [12] and is called the generalised P-representation,

$$P(\alpha, \beta) = \int d\mu(\alpha, \beta) P(\alpha, \beta) \Lambda(\alpha, \beta) \tag{3.36}$$

where $\mu(\alpha, \beta)$ is an integration measure chosen to ensure normalisability,

$$\int_D d\mu(\alpha, \beta) P(\alpha, \beta) = 1 \tag{3.37}$$

and

$$\Lambda(\alpha, \beta) = \frac{|\alpha\rangle\langle\beta^*|}{\langle\beta^*|\alpha\rangle} \tag{3.38}$$

This representation is not necessarily positive, in fact it is complex in general. Nonetheless it can used as an effective way to compute normally ordered moments for any state. In Chap. 8 we will see it can be used to give a powerful stochastic description of quantum dynamics in the doubled complex plane.

The definition given by (3.36) leads to different representations depending on the integration measure. The Glauber-Sudarshan representation corresponds to

$$d\mu(\alpha, \beta) = \delta^{(2)}(\alpha^* - \beta)d^2\alpha d^2\beta \tag{3.39}$$

3.2.4 The Complex P Representation

The complex P Representation is defined by $d\mu(\alpha, \beta) = d\alpha d\beta$, where (α, β) are treated as complex variables which are to be integrated on individual contours C and C'. The conditions for the existence of this representation are discussed in [12]. This representation may take on complex values so in no sense can it have any physical interpretation as a probability distribution. However, as we shall see it is an extremely useful representation giving exact results for certain problems and physical observables such as all the single time correlation functions.

Consider a density operator, expanded as

$$\rho = \frac{1}{\pi^2}\int_D\int_{D'}\langle\alpha|\rho|\beta^*\rangle|\alpha\rangle\langle\beta^*|d^2\alpha d^2\beta \tag{3.40}$$

Using the residue theorem we write this as

$$\rho = \frac{1}{\pi^2}\int_D\int_{D'}\langle\alpha|\rho|\beta^*\rangle\langle\beta^*|\alpha\rangle\left[\oint_C\oint_{C'}\frac{\Lambda(\alpha', \beta')}{(\alpha - \alpha')(\beta - \beta')}\right]|\alpha\rangle\langle\beta^*|d^2\alpha d^2\beta \tag{3.41}$$

Exchanging the order of integration we see the complex P function is

$$P(\alpha, \beta) = -\frac{1}{4\pi^2}\int_D\int_{D'}\langle\alpha'|\rho|\beta^{'\,*}\rangle\langle\beta^{'\,*}|\alpha'\rangle\frac{d^2\alpha' d^2\beta'}{(\alpha - \alpha')(\beta - \beta')} \tag{3.42}$$

The complex P representation of a coherent state $|z\rangle$ is

$$P_z(\alpha, \beta) = -\frac{1}{4\pi^2}(\alpha - z)^{-1}(\beta - z*)^{-1} \tag{3.43}$$

In the case of the number state $|n\rangle$ we find

$$P_n(\alpha, \beta) = -\frac{1}{4\pi^2}e^{\alpha\beta}\frac{n!}{(\alpha\beta)^{n+1}} \tag{3.44}$$

To see this, use (1.41, 1.46) and write

$$\rho = \oint d\alpha d\beta P(\alpha, \beta) \sum_{n,m=0}^{\infty} \frac{|n'\rangle\langle m'|}{\sqrt{n'!m'!}} e^{-\alpha\beta} \alpha^{n'} \beta^{m'} \tag{3.45}$$

Substituting (3.44),

$$\rho = -\frac{1}{4\pi^2} \sum_{n,m=0}^{\infty} \frac{(n!)^2}{\sqrt{n'!m'!}} \oint d\alpha d\beta \, \alpha^{-(n+1-n')} \beta^{-(n+1-m')} |n'\rangle\langle m'| \tag{3.46}$$

Choosing any contour of integration encircling the origin and using Cauchy's theorem,

$$\frac{1}{2\pi i} \oint dz \, z^n = 0 \text{ if } n \geq 0, \tag{3.47}$$

$$= 1 \text{ if } n \geq -1, \tag{3.48}$$

$$= 0 \text{ if } n < -1 \tag{3.49}$$

we find $\rho = |n\rangle\langle n|$ as required.

In the case of the squeezed state $|z, r\rangle$ the complex P representation is

$$P_{z,r}(\alpha, \beta) = \mathcal{N} e^{(\alpha - z)(\beta - z^*) + \coth r[(\alpha - z)^2 + (\beta - z^*)^2]} \tag{3.50}$$

The normalisation constant $\mathcal{N}$ is found by integrating along the imaginary axis for r real. The resulting normalisation for this choice of contour is

$$\mathcal{N} = -\frac{1}{2\pi \sinh r} \tag{3.51}$$

As an example of the use of the complex P representation we shall consider the photon counting formula given by (2.100). Using the diagonal coherent-state representation for ρ we may write the photon counting probability $P_m(T)$ as

$$P_m(T) = \int d^2 z P(z) \frac{(|z|^2 \mu(T))^m}{m!} \exp[-|z|^2 \mu(T)] \tag{3.52}$$

An appealing feature of this equation is that $P_m(T)$ is given by an averaged Poisson distribution with $P(z)$ in the role of a probability distribution over the complex field amplitude. It is a close analogue of the classical expression (2.99). We know however that $P(z)$ is not a true probability distribution and may take on negative values. In such cases we may consider a generalisation by way of the complex P representation for ρ. The photocount probability is then given by

$$P_m(T) = \oint_{CC'} dz dz' P(z, z') \frac{(zz' \mu(T))^m}{m!} \exp[-zz' \mu(T)] \, . \tag{3.53}$$

We shall demonstrate the use of this formula to calculate $P_m(T)$ for states for which no well behaved diagonal P distribution exists.

For a number state with density operator $\rho = |n\rangle\langle n|$ we have

$$P(z, z') = -\frac{1}{4\pi^2} e^{zz'} n!(zz')^{-(n+1)} \tag{3.54}$$

and the contours C and C' enclose the origin. Substituting into (3.53) for $m > n$ the integrand contains no poles and $P_m(T) = 0$ while for $m < n$ poles of order $n - m + 1$ contribute in each integration and we obtain

$$P_m(T) = \sum_{n=m}^{\infty} \binom{n}{m} \mu(T)^m (1 - \mu(T))^{n-m} \tag{3.55}$$

as obtained previously.

For a squeezed state with density operator $\rho = |\alpha, r\rangle\langle\alpha, r|$, where α and r are assumed real, we have

$$P(z, z') = -\frac{1}{2\pi} (\sinh r)^{-1} \exp[(z - \alpha)(z' - \alpha) + \coth r[(z - \alpha)^2 + (z' - \alpha)^2]] \tag{3.56}$$

and the contours are chosen along the imaginary axis in z, z'. The integral then gives

$$P_m(T) = \sum_{n=m}^{\infty} \binom{n}{m} \mu(T)^m (1 - \mu(T))^{n-m} P_n \tag{3.57}$$

with the photon number distribution given by (1.82).

3.2.5 Positive P Representation

The integration measure is chosen as $d\mu(\alpha, \beta) = d^2\alpha d^2\beta$ corresponds to the positive P representation $P(\alpha, \beta)$. In this case the phase space has doubled. It can be proved that $P(\alpha, \beta)$ always exists and is positive for any density operator.

For this reason we call it the positive P representation and it has all the mathematical properties of a genuine probability. It also has an interpretation as a probability distribution [13]. By using four apparatus instead of the two used in the Q function model, we can get a positive distribution that nonetheless gives normally ordered moments by direct integration. The positive P representation is useful in representing quantum irreversible dynamics as a stochastic process in the doubled phase space variables.

Problems

3.1 The Glauber-Sudarshan representation for a thermal state is given in (3.5) as

$$P_T(\alpha, \alpha^*) = \frac{1}{\pi \bar{n}} e^{-|\alpha|^2/\bar{n}} \tag{3.58}$$

Show that the photon number distribution is given by

$$p_n = \langle n|\rho_T|n\rangle = \frac{\bar{n}^n}{(1+\bar{n})^{n+1}} \tag{3.59}$$

3.2 Prove that the Wigner function is a Gaussian convolution of the Glauber-Sudarshan P function, (3.19).

3.3 Find the Q function and the Wigner function for the cat states in (1.107).

References

1. R.J. Glauber, Phys. Rev. **131**, 2766 (1963)
2. E.C.G. Sudarshan, Phys. Rev. Lett. **10**, 277 (1963)
3. J.R. Klauder, E.C.G. Sudarshan, *Fundamentals of Quantum Optics* (Benjamin, New York, 1968)
4. E.P. Wigner, Phys. Rev. **40**, 749 (1932)
5. A. Royer, Phys. Rev. A. **15**, 449 (1977)
6. K. Banaszek, C. Radzewicz, K. Wódkiewicz, J.S. Krasiński, Phys. Rev. A **60**, 674 (1999)
7. A. Ourjoumtsev, H. Jeong, R. Tualle-Brouri et al., Nature **448**, 784–786 (2007)
8. M. Hofheinz, H. Wang, M. Ansmann et al., Nature **459**, 546 (2009)
9. E. Arthurs, J.L. Kelly Jr., Bell Syst. Tech. J. **44**, 725 (1965)
10. S.L. Braunstein, C.M. Caves, G.J. Milburn, Phys. Rev. A **43**, 1153 (1991)
11. U. Chabaud, D. Markham, F. Grosshans, Phys. Rev. Lett. **124**, 063605 (2020)
12. P.D. Drummond, C.W. Gardiner, J. Phys. A **13**, 2353 (1980)
13. S.L. Braunstein, C.M. Caves, G.J. Milburn, Phys. Rev. A **43**, 1153 (1991)

Quantum Dynamics in Simple Nonlinear Optical Systems

4

Abstract

In this chapter we will analyse some simple processes in nonlinear optics where analytic solutions are possible. This will serve to illustrate how the formalism developed in the preceding chapters may be applied. In addition, the simple examples chosen illustrate many of the quantum phenomena studied in more complex systems in later chapters. This chapter will serve as an introduction to how quantum phenomena such as photon antibunching, squeezing and violation of certain classical inequalities may occur in nonlinear optical systems. In addition, we include an introduction to quantum limits to amplification.

4.1 Single-Mode Quantum Dynamics

A single-mode field is the simplest example of a quantum field and suffices to illustrate a number of quantum features such as photon antibunching and squeezing. To illustrate these phenomena we consider the degenerate parametric amplifier.

4.1.1 Degenerate Parametric Amplifier

One of the simplest interactions in nonlinear optics is where a photon of frequency 2ω is absorbed and converted into two photons each with frequency ω. This process known as parametric down conversion may occur in a medium with a second-order nonlinear susceptibility $\chi^{(2)}$ [1]. A more detailed discussion on nonlinear optical interactions is given in Chap. 8.

We begin with the simplified interaction Hamiltonian for a single cavity mode in degenerate parametric interaction

$$H = \hbar\omega a^\dagger a - i\frac{\hbar\chi}{2}\left(E^* a^2 e^{2i\omega t} - E a^{\dagger\,2} e^{-2i\omega t}\right) \tag{4.1}$$

D. F. Walls and G. J. Milburn, *Quantum Optics*, Graduate Texts in Physics,
https://doi.org/10.1007/978-3-031-84177-4_4

where χ is the second order nonlinear susceptibility and E is the complex amplitude of the pump field treated as a classical undepleted coherent state at a carrier frequency twice that of the quantum mode. If we work in the interaction picture we have the time independent Hamiltonian

$$H_I = -i\frac{\hbar g}{2}(a^2 - a^{\dagger\,2}) \,, \tag{4.2}$$

where we have chosen the phase of the pump such that $g = \chi E$ is real. The Heisenberg equations of motion are

$$\frac{da}{dt} = ga^\dagger, \qquad \frac{da^\dagger}{dt} = ga \,. \tag{4.3}$$

The solution is

$$a(t) = a(0)\cosh gt + a^\dagger(0)\sinh gt \tag{4.4}$$

which has the form of the squeezing transformation, see (1.63). As such, we expect the light produced by parametric amplification to be squeezed. This can immediately be seen by introducing the two quadrature phase amplitudes

$$X_1 = a + a^\dagger, \quad X_2 = -i(a - a^\dagger) \tag{4.5}$$

which satisfy the Heisenberg equations of motion

$$\frac{dX_1}{dt} = gX_2, \qquad \frac{dX_2}{dt} = -gX_1 \,. \tag{4.6}$$

The solution is

$$X_1(t) = X_1(0)e^{gt}, \quad X_2(t) = X_2(0)e^{-gt} \tag{4.7}$$

These equations demonstrate that the parametric amplifier is a phase-sensitive amplifier which amplifies one quadrature and attenuates the other. The variances are given by

$$\mathbb{V}[X_1(t)] = \mathbb{V}[X_1(0)]e^{2gt}, \quad \mathbb{V}[X_2(t)] = \mathbb{V}[X_2(0)]e^{-2gt} \tag{4.8}$$

In the case of a coherent state or vacuum state, $\mathbb{V}[X_1(0)] = \mathbb{V}[X_2(0)] = 1$, the product of the variances satisfies the minimum uncertainty relation. Thus the de-amplified quadrature has less quantum noise than the vacuum level. The amount of squeezing or noise reduction is proportional to the strength of the nonlinearity, the amplitude of the pump and the interaction time.

We shall next consider the photon statistics of the light produced by the parametric amplifier. First we analyse the light produced from an initial vacuum state. The intensity correlation function $g^{(2)}(0)$ in this case is

$$g^{(2)}(0) = 1 + \frac{\cosh 2gt}{\sinh^2 gt} \tag{4.9}$$

This indicates that the squeezed light generated from an initial vacuum exhibits photon bunching $g^{(2)}(0) > 1$. This is expected for a squeezed vacuum for which photon pairs are generated simultaneously.

4.1.2 Wigner and Q Function

The full photon statistics of the light generated in parametric amplification may be calculated via a quasi-probability distribution. The P function becomes singular due to the quantum correlations which build up during the amplification process. However the Wigner distribution and the Q-function remain positive and Gaussian.

The Wigner function describing the state of the parametric oscillator at any time, t, may now be calculated via the symmetrically ordered characteristic function,

$$\chi(\eta, t) = \mathrm{tr}[\rho(0) e^{\eta a^\dagger(t) - \eta^* a(t)}] \tag{4.10}$$

Using (4.4) we find that for an initial coherent state, $|\alpha\rangle$,

$$\chi(\eta, t) = \exp[\eta\alpha^*(t) - \eta^*\alpha(t) - \frac{|\eta|^2}{2}\cosh 2\chi t + \frac{1}{4}(\eta^2 + \eta^{*\,2})\sinh 2\chi t] \tag{4.11}$$

where $\alpha(t) = \alpha\cosh\chi t + \alpha^*\sinh\chi t$. This may be written as

$$\chi(\eta, t) = e^{\boldsymbol{\eta}^T\cdot\boldsymbol{\alpha}(t) + \frac{1}{2}\boldsymbol{\eta}^T\Lambda\boldsymbol{\eta}} \tag{4.12}$$

where $\boldsymbol{\eta}^T = (\eta, -\eta^*)$ and $\boldsymbol{\alpha}(t) = (\alpha(t), \alpha^*(t))$ with

$$\Lambda = \frac{1}{2}\begin{pmatrix} \sinh 2\chi t & \cosh 2\chi t \\ \cosh 2\chi t & \sinh 2\chi t \end{pmatrix} \tag{4.13}$$

The Wigner function is then given by the Fourier transform of $\chi(\eta, t)$ we find that

$$W(\alpha, t) = \frac{2}{\pi}\exp\left[-\frac{1}{2}(\boldsymbol{\alpha} - \boldsymbol{\alpha}(t))^T C^{-1}(\boldsymbol{\alpha} - \boldsymbol{\alpha}(t))\right] \tag{4.14}$$

where $\boldsymbol{\alpha}^T = (\alpha, \alpha^*)$. This is a bivariate Gaussian distribution with mean $\alpha(t)$ and covariance matrix $C = \Lambda$. In terms of the real variables $x_1 = \alpha + \alpha^*$ and $x_2 = -i(\alpha - \alpha^*)$, the Wigner function takes the form

$$W(\alpha, t) = \frac{1}{2\pi}\exp\left[-\frac{1}{2}(\mathbf{x} - \mathbf{x}(t))^T R^{-1}(\mathbf{x} - \mathbf{x}(t))\right] \tag{4.15}$$

where

$$R = \frac{1}{2}\begin{pmatrix} e^{2\chi t} & 0 \\ 0 & e^{-2\chi t} \end{pmatrix} \tag{4.16}$$

As the Q function is a Gaussian convolution of the Wigner function, the Q function itself must be Gaussian. In this case it is given by

$$Q(\alpha, t) = \frac{1}{\pi \cosh gt} \exp\left[-\frac{1}{2}(\boldsymbol{\alpha} - \boldsymbol{\alpha}(t))^T A^{-1}(\boldsymbol{\alpha} - \boldsymbol{\alpha}(t))\right] \tag{4.17}$$

where

$$A = \Lambda + \frac{1}{2}\begin{pmatrix} 0 & 1 \\ 1 & 0 \end{pmatrix}. \tag{4.18}$$

4.2 Two-Mode Quantum Dynamics

4.2.1 Non-degenerate Parametric Amplifier

The non-degenerate parametric amplifier is a generalization of the degenerate parametric amplifier considered in the previous section. In this case the classical pump mode at frequency ω_p interacts in a nonlinear optical medium with two modes at frequency ω_1 and ω_2 . These frequencies sum to the pump frequency, $\omega_p = \omega_1 + \omega_2$. It is conventional to designate one mode as the signal and the other as the idler.

The Hamiltonian describing this system is

$$H = \hbar\omega_1 a_1^\dagger a_1 + \hbar\omega_2 a_2^\dagger a_2 + i\hbar g\left(a_1^\dagger a_2^\dagger e^{-i\omega_p t} - a_1 a_2 e^{-i\omega_p t}\right), \tag{4.19}$$

where $a_1(a_2)$ is the annihilation operator for the signal (idler) mode. The coupling constant g is proportional to the second-order susceptibility of the medium and to the amplitude of the pump field.

The Heisenberg equations of motion in the interaction picture are

$$\frac{da_1}{dt} = g a_2^\dagger \tag{4.20}$$

$$\frac{da_2^\dagger}{dt} = g a_1 \tag{4.21}$$

The solutions to these equations are

$$a_1(t) = a_1(0)\cosh gt + a_2^\dagger(0)\sinh gt\ , \tag{4.22}$$

$$a_2(t) = a_2(0)\cosh gt + a_1^\dagger(0)\sinh gt\ . \tag{4.23}$$

If the system starts in an initial coherent state $|\alpha_1\rangle \otimes |\alpha_2\rangle$, the mean photon number in mode one at time t is

$$\bar{n}_1(t) = \langle a_1^\dagger(t) a_1(t)\rangle = |\alpha_1 \cosh gt + \alpha_2^* \sinh gt|^2 + \sinh^2 gt \tag{4.24}$$

The last term in this equation represents the amplification of vacuum fluctuations since if the system initially starts in the vacuum ($\alpha_1 = \alpha_2 = 0$) the mean number of photons is given by $\sinh^2 gt$.

The intensity correlation functions of this system exhibit interesting quantum features. With a two-mode system we may consider cross correlations between the two modes. We shall show that quantum correlations may exist which violate classical inequalities.

Consider the moment $\langle a_1^\dagger a_1 a_2^\dagger a_2\rangle$. We may express this moment in terms of the Glauber–Sudarshan P function as follows:

$$\langle a_1^\dagger a_1 a_2^\dagger a_2\rangle = \int d^2\alpha_1 \int d^2\alpha_2 |\alpha_1|^2 |\alpha_2|^2 P(\alpha_1, \alpha_2)\ . \tag{4.25}$$

If a positive P function exists the right-hand side of this equation is the classical intensity correlation function for two fields with the fluctuating complex amplitudes α_1, α_2. It follows from the Hölder inequality that

$$\begin{aligned}\int d^2\alpha_1 d^2\alpha_2 |\alpha_1|^2 |\alpha_2|^2 P(\alpha_1, \alpha_2) &\\ \leq \left[\int d^2\alpha_1 d^2\alpha_2 |\alpha_1|^4 P(\alpha_1, \alpha_2)\right]^{1/2} &\\ \times \left[\int d^2\alpha_1 d^2\alpha_2 |\alpha_2|^4 P(\alpha_1, \alpha_2)\right]^{1/2}\ .&\end{aligned} \tag{4.26}$$

This may be written in terms of an inequality for the operator moments

$$\langle a_1^\dagger a_1 a_2^\dagger a_2\rangle \leq \left[\langle {a_1^\dagger}^2 a_1^2\rangle \langle {a_2^\dagger}^2 a_2^2\rangle\right]^{1/2}\ , \tag{4.27}$$

a result known as the *Cauchy-Schwarz inequality*. If the two modes are symmetric, as for the non-degenerate parametric amplifier, this inequality implies

$$\langle a_1^\dagger a_1 a_2^\dagger a_2\rangle \leq \langle {a_1^\dagger}^2 a_1^2\rangle\ . \tag{4.28}$$

Because we have assumed a positive Glauber-Sudarshan P function, this is a weak inequality and there exists certain quantum fields which will violate it. It is more usual to express the Cauchy–Schwarz inequality in terms of the second-order intensity correlation functions defined for a single-mode field,

$$\left[g_{12}^{(0)}\right]^2 \leq g_1^{(2)}(0) g_2^{(2)}(0) \tag{4.29}$$

where

$$g_k^{(2)}(0) = \frac{\langle a_k^\dagger a_k^\dagger a_k a_k\rangle}{\langle a_k^\dagger a_k\rangle^2} \tag{4.30}$$

and

$$g_{12}^{(2)}(0) = \frac{\langle a_1^\dagger a_2^\dagger a_1 a_2\rangle}{\langle a_1^\dagger a_1\rangle\langle a_2^\dagger a_2\rangle} \tag{4.31}$$

A stronger inequality may be derived for quantum fields when a Glauber–Sudarshan P representation does not exist. Using (4.27),

$$\langle a_1^\dagger a_1 a_2^\dagger a_2\rangle^2 \leq \langle (a_1^\dagger a_1)^2\rangle\langle (a_2^\dagger a_2)^2\rangle \ . \tag{4.32}$$

and symmetry, this implies

$$\langle a_1^\dagger a_1 a_2^\dagger a_2\rangle \leq \langle ({a_1^\dagger}^2 a_1^2)\rangle + \langle a_1^\dagger a_1\rangle \ . \tag{4.33}$$

or

$$g_{12}^{(2)}(0) \leq g_1^{(2)}(0) + \frac{1}{\langle a_1^\dagger a_1\rangle} \ . \tag{4.34}$$

We now show that the non-degenerate parametric amplifier if initially in the ground state leads to a maximum violation of the Cauchy–Schwarz inequality (4.29), as is consistent with the inequality (4.34). That is, the correlations built up in the parametric amplifier are the maximum allowed by quantum mechanics.

In the degenerate parametric amplifier model In this system the following conservation law is easily seen to hold,

$$n_1(t) - n_2(t) = n_1(0) - n_2(0) \ , \tag{4.35}$$

where $n_k(t) = a_k^\dagger(t)a(t)$. Using this relation the intensity correlation function may be written

$$\langle n_1(t)n_2(t)\rangle = \langle n_1(t)^2\rangle + \langle n_1(t)(n_2(0) - n_1(0))\rangle \ . \tag{4.36}$$

If the system is initially in the vacuum state the last term is zero, thus

$$\langle n_1(t)n_2(t)\rangle = \langle a_1^\dagger(t)a_1^\dagger(t)a_1(t)a_1(t)\rangle + \langle a_1^\dagger(t)a_1(t)\rangle \ , \tag{4.37}$$

which corresponds to the maximum violation of the Cauchy–Schwarz inequality allowed by quantum mechanics. Thus the non-degenerate parametric amplifier exhibits quantum mechanical correlations which violate certain classical inequalities. These quantum correlations may be further exploited to give squeezing and states similar to those discussed in the EPR paradox (see Chap. 13).

In the interaction picture, the unitary operator for time evolution of the non degenerate parametric amplifier is

$$U(t) = e^{gt(a_1^\dagger a_2^\dagger - a_1 a_2)} \tag{4.38}$$

Comparison with (1.84) shows that $U(t)$ is the unitary two-mode squeezing operator with $r = -gt$. It is thus clear that the individual signal and idler modes are correlated

but not squeezed. In fact they have a reduced state that is equivalent to a thermal state with mean photon number $\sinh^2 gt$.

In order to see squeezing in a multi-mode system like this we need to be more careful in how we define the quadrature phase amplitudes that can be measured. This is done using homodyne detection as we describe in Chap. 7, and explicitly requires a frequency and phase coherent reference field that we call the *local oscillator*. We will define the squeezing with respect to the quadrature phase amplitudes of the field at the local oscillator frequency $\omega_{LO} = \omega_p/2$ and phase reference θ[2].

The total field, given by the sum of the signal and idler modes, has positive frequency components in the laboratory frame given by

$$E^{(-)}(t) = a_1(t)e^{-i\omega_1 t} + a_2(t)e^{-i\omega_2 t} \tag{4.39}$$

where $a_k(t)$ are given in (4.20) and $\omega_1 + \omega_2 = \omega_p/2$. Now define $\omega_1 = \omega_p/2 - \epsilon$, $\omega_2 = \omega_p/2 + \epsilon$. These are sidebands at half the pump frequency. The total field may now be written as

$$E(t) = (a_1(t)e^{i\epsilon t} + a_2(t)e^{-i\epsilon t})e^{-i\omega_p t/2} + (a_1^\dagger(t)e^{-i\epsilon t} + a_2^\dagger(t)e^{i\epsilon t})e^{i\omega_p t/2} \tag{4.40}$$

We are thus led to write this in terms of the quadrature phase amplitude operators defined by the carrier frequency $\omega_p/2$ and phase reference θ, (see Chap. 7 for a discussion of homodyne detection).

$$E(t) = X_\theta(t,\epsilon)\cos(\omega_p t/2 + \theta) - X_{\theta+\pi/2}(t,\epsilon)\sin(\omega_p t/2 + \theta) \tag{4.41}$$

where

$$X_\theta(t,\epsilon) = \frac{1}{\sqrt{2}}\left[\left((a_1(t)e^{i\theta} + a_2^\dagger(t)e^{-i\theta}\right)e^{i\epsilon t} + \text{h.c.}\right], \tag{4.42}$$

$$X_{\theta+\pi/2}(t,\epsilon) = \frac{i}{\sqrt{2}}\left[\left(a_1(t)e^{i\theta} - a_2^\dagger(t)e^{-i\theta}\right)e^{i\epsilon t} + \text{h.c.}\right]. \tag{4.43}$$

If the system starts in the vacuum state, the homodyne detection signal at frequency $\epsilon = 0$ will have a variance given by

$$X_\theta(t,\epsilon = 0) = \cosh 2gt + \cos 2\theta \sinh 2gt\ . \tag{4.44}$$

Thus for $\theta = 0$ we find

$$\mathbb{V}[X_0(t,\epsilon = 0)] = e^{2gt}\ , \tag{4.45}$$

$$\mathbb{V}[X_{\pi/2}(t,\epsilon = 0)] = e^{-2gt}\ . \tag{4.46}$$

Changing the phase of the local oscillator by $\pi/2$ enables one to move from enhanced to diminished noise in the homodyne signal.

The full quantum correlations present in the parametric amplifier may be represented using a quasi-probability distribution. If both modes of the amplifier are

initially in the vacuum state, no Glauber P function for the total system exists at any time. However, a positive Gaussian Wigner function may be obtained.

We may define a two mode characteristic function by a simple generalization of the single-mode definition. For both modes initially in the vacuum state this may be expressed as

$$\begin{aligned}\chi(\eta_1,\eta_2,t) &= \langle 0|e^{\eta_1 a_1^\dagger(t)-\eta_1^* a_1(t)}e^{\eta_2 a_2^\dagger(t)-\eta_2^* a_2(t)}|0\rangle \\ &= e^{-\frac{1}{2}(|\eta_1(t)|^2+|\eta_2(t)|^2)}\end{aligned} \tag{4.47}$$

where

$$\eta_1(t) = \eta_1\cosh gt - \eta_2^*\sinh gt \tag{4.48}$$

$$\eta_2(t) = \eta_2\cosh gt - \eta_2^*\sinh gt\ . \tag{4.49}$$

Performing the Fourier transform, the Wigner function is then given by,

$$W(\alpha_1,\alpha_2,t) = \frac{4}{\pi^2}\exp\left[-2|\alpha_1\cosh gt - \alpha_2^*\sinh gt|^2 - 2|\alpha_2\cosh gt - \alpha_1\sinh gt|^2\right] \tag{4.50}$$

Making the change of variable $\beta_1 = \alpha_1 + \alpha_2^*$ and $\beta_2 = \alpha_2 + \alpha_1^*$ we see that

$$W(\alpha_1,\alpha_2,t) = \frac{4}{\pi^2}\exp\left[-\frac{1}{2}\left(\frac{|\beta_1|^2}{e^{2gt}} + \frac{|\beta_2|^2}{e^{-2gt}}\right)\right] \tag{4.51}$$

in which form it is particularly easy to see that squeezing occurs in a linear combination of the two modes.

The photon number representation of the signal and idler modes, starting in a vacuum state, follows from the two-mode squeezing operator (see (1.99)). It is

$$|\psi(t)\rangle = \frac{1}{\cosh gt}\sum_{n=0}^{\infty}(\tanh gt)^n|n\rangle_1\otimes|n\rangle_2 \tag{4.52}$$

In this form it is easy to see how the non-degenerate parametric amplifier is a zero energy eigenstate of the photon number difference between the two modes.

The non-degenerate parametric amplifier exemplifies many features of general linear amplification. One such feature is the limit placed on the amplifier gain if the output is to be squeezed. To see how this limit arises, and to see how it might be overcome, we write the solutions (4.22) in the form

$$a_1^{out} = G^{1/2}a_1^{in} + (G-1)^{1/2}a_2^{in} \tag{4.53}$$

where $G = \cosh^2 gt$ is the gain and we now regard the initial operator as the input operators and the final operators as the output operators. It is clear that if the input state to mode-1 is an arbitrary state and the input to mode-2 is the vacuum that,

$$\langle n_1^{out}\rangle = G\langle n_1^{in}\rangle + (G-1) \tag{4.54}$$

where $n_1 = a_1^\dagger a_1$. The first term shows that the output photon number is G times the input photon number in mode-1. This suggests we regard G as the energy gain of the system. The second term arises from the vacuum in mode-2. This is the necessary noise that must accompany amplification in the quantum domain [3]. The noise of amplification means that we cannot amplify a squeezed state in mode-1 without decreasing the squeezing.

4.2.2 Cubic Quantum Dynamics

In cavity opto mechanics the radiation pressure force couples mechanical motion to optical field modes. The force on a mirror is proportional to photon number inside the cavity. Consider an optical cavity with one mirror harmonically confined by an elastic spring. The centre of mass motion of the mirror is described by a simple Harmonic oscillator. The Hamiltonian is

$$H_m = \frac{p^2}{2m} + m\omega_m^2 q^2 \tag{4.55}$$

where m is the effective mass of the bound mirror and ω_m is the resonant frequency. We introduce ladder operators, $b, b^\dagger$ as

$$q = \sqrt{\frac{\hbar}{2m\omega_m}}(b + b^\dagger) \tag{4.56}$$

$$p = -i\sqrt{\frac{m\hbar\omega_m}{2}}(b - b^\dagger) \tag{4.57}$$

As $[q, p] = i\hbar$ we see that $[b, b^\dagger] = 1$. The Hamiltonian for the cavity mode is given as usual by $H_c = \hbar\omega_c a^\dagger a$, where $a, a^\dagger$ are the annihilation and creation operators for the cavity field mode.

The interaction energy between the mechanical and optical degree of freedom is

$$H_i = fqa^\dagger a \tag{4.58}$$

where f is the force per photon. we write this in terms of the ladder operators as

$$H_I = \hbar g_0(b + b^\dagger)a^\dagger a \tag{4.59}$$

where

$$g_0 = \frac{f}{\sqrt{2\hbar m\omega_m}} \tag{4.60}$$

is the opto-mechanical coupling constant in units of frequency. The interaction Hamiltonian is of cubic order in the raising and lowering operators.

The full Hamiltonian is

$$H = \hbar\omega_m b^\dagger b + \hbar\omega_c a^\dagger a + \hbar g_0 (b + b^\dagger) a^\dagger a \, . \tag{4.61}$$

If we move to an interaction picture, we get the transformed hamiltonian

$$H_I = \hbar g_0 (b e^{-i\omega_m t} + b^\dagger e^{i\omega_m t}) a^\dagger a \tag{4.62}$$

The Heisenberg equations of motion are

$$\frac{db}{dt} = -i g_0 e^{i\omega_m t} a^\dagger a \tag{4.63}$$

$$\frac{da}{dt} = -i g_0 (b + b^\dagger) a \tag{4.64}$$

As $a^\dagger a$ is a constant of motion we can solve for $b(t)$

$$b(t) = b(0) - \frac{g_0 a^\dagger a}{\omega_m} (e^{i\omega_m t} - 1) \tag{4.65}$$

Substituting this into the equation of motion for a we see that

$$\frac{da}{dt} = -i g_0 (b(0) + b^\dagger(0)) a - i \frac{g_0^2}{\omega_m} a^\dagger a \, a \tag{4.66}$$

The second term here appears like a photon number dependent phase shift of the field. This is called a Kerr non linearity, and is discussed in the next section. It is expected here for the following reason. The radiation pressure force changes the momentum of the mechanical system. This causes the position of the mirror to change due to the harmonic motion of the mirror. However a changing position causes a detuning of the cavity. We thus see that the radiation pressure force will couple back to produce an intensity dependent detuning of the cavity.

There is another way to see this induced Kerr effect. Clearly $a^\dagger a$ is a constant of motion. Using the canonical transformation

$$b \to b + \frac{g_0}{\omega_m} a^\dagger a \tag{4.67}$$

the full Hamiltonian can be written

$$H = \hbar\omega_m \left(b^\dagger + \frac{g_0}{\omega_m} a^\dagger a \right) \left(b + \frac{g_0}{\omega_m} a^\dagger a \right) - \hbar\chi (a^\dagger a)^2 \tag{4.68}$$

where $\chi = g_0^2/\omega_m$. The term proportional to χ is called a self-Kerr interaction and is quartic in the annihilation and creation opertators for the field.

4.2.3 Kerr Quantum Dynamics

We will consider the self-Kerr interaction in more detail and generalise it to a cross Kerr interaction between two field modes. Consider the Hamiltoninan for a single mode field

$$H = \hbar\omega a^\dagger a + \hbar\chi (a^\dagger a)^2 \tag{4.69}$$

In the interaction picture, the Hamiltonian is

$$H_I = \hbar\chi (a^\dagger a)^2 \tag{4.70}$$

The Heisenberg equations of motion are

$$\frac{da}{dt} = -i\chi a - 2i\chi a^\dagger a \tag{4.71}$$

As $a^\dagger a$ is a constant of motion the solution is

$$a(t) = a(0)e^{-2i\chi t(a^\dagger a+1/2)} \tag{4.72}$$

If the system starts in a coherent state $|\alpha\rangle$, the mean value of the amplitude at time $t > 0$ is given by

$$\langle a(t)\rangle = \alpha e^{-i\chi t}\langle\alpha|e^{-2i\chi t a^\dagger a}|\alpha\rangle \tag{4.73}$$

Using $e^{-i\theta a^\dagger a}|\alpha\rangle = |\alpha e^{-i\theta}\rangle$ we see that

$$\langle a(t)\rangle = \alpha e^{-i\chi t}\langle\alpha|\alpha e^{-2i\chi t}\rangle = \alpha e^{-i\chi t-|\alpha|^2(1-e^{-2i\chi t})} \tag{4.74}$$

where we used (1.46). This function is clearly periodic with a period given by $T = \chi/2\pi$. However at times such that $\chi t = \pi$, the mean value is π out of phase with the initial amplitude.

We can get a better idea of what is happening by looking at the dynamics in the Schrödinger picture. Define the nonlinear transformation of a single mode coherent state, $|\alpha\rangle$, as

$$|\alpha, \theta\rangle = e^{-i\theta(a^\dagger a)^2}|\alpha\rangle \tag{4.75}$$

Using the number state expansion of coherent sates we see that

$$|\alpha, \theta\rangle = e^{-|\alpha|^2/2}\sum_{n=0}^{\infty}\frac{\alpha^n}{\sqrt{n!}}e^{-i\theta n^2}|n\rangle \tag{4.76}$$

If we set $\theta = \chi t$ we get the Schrödinger picture dynamics due to the Kerr self-interaction. Setting $\theta = 2\pi$ we see that the state is simply the initial state, $|\alpha\rangle$. Setting $\theta = \pi$ we get $|-\alpha\rangle$, the same as the initial state with a π phase shift.

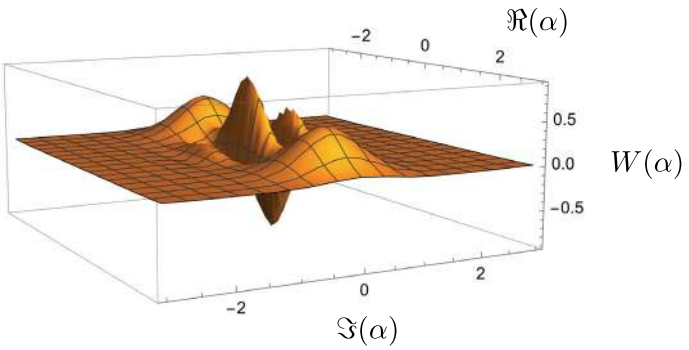

Fig. 4.1 The Wigner function (multiplied by $\pi/2$) for a Kerr cat-state with $\alpha = 2, \theta = \pi/2$ versus hte real and imaginary parts of α. Note the negative values between the two peaks

Something more interesting happens at rational fractions of π. Setting $\theta = \pi/2$ we see that

$$e^{-in^2\pi/2} = \begin{cases} 1 & n \text{ even} \\ -i & n \text{ odd} \end{cases} \tag{4.77}$$

so

$$|\alpha, \pi/2\rangle = \mathcal{N}_\alpha(e^{-i\pi/4}|\alpha\rangle + e^{i\pi/4}|-\alpha\rangle) \tag{4.78}$$

where $\mathcal{N}_\alpha$ is a normalisation constant. These superposition of coherent staters have come to be called cat states as they are superpositions of distinguishable semi-classical states reminiscent of Schrödinger's famous gendanken experiment on the quantum control of feline metabolism. Note that these states are *not* parity eigen-states. This is a direct result of the Kerr nonlinearity commuting with the photon number operator. The Wigner function for this state is shown in Fig. 4.1. Cat states were first investigated in [4,5]. In fact we can get more general single mode cat states using $\theta = 2\pi/K$. Then $n^2/K = n(n/K)$ so we only need to find n mod K to get the periodicity of the cat state. This is an effective measurement of photon number mod K. We plot the Q-functions for some examples in Fig. 4.2. Such states are known as fractional revivals and are common in integrable non linear quantum dynamics. We use the Q-function for this purpose as the fractional revivals are easy to see.

4.3 Universal Bosonic Dynamics

We saw above that a cubic non linearity can be transformed to a quartic self interaction. Kerr interactions generate states with negative Wigner functions. It is easy to see that Hamiltonians that are linear and quadratic in the annihilation and creation operators cannot generate states with a negative Wigner function (see Sect. 3.2.1). The Wigner function is given in terms of the displacement operator and the parity operator $\Pi = e^{-i\pi a^\dagger a}$ as

$$W(\alpha) = \frac{2}{\pi}\text{tr}(D(\alpha)\Pi D^\dagger(\alpha)\rho) \tag{4.79}$$

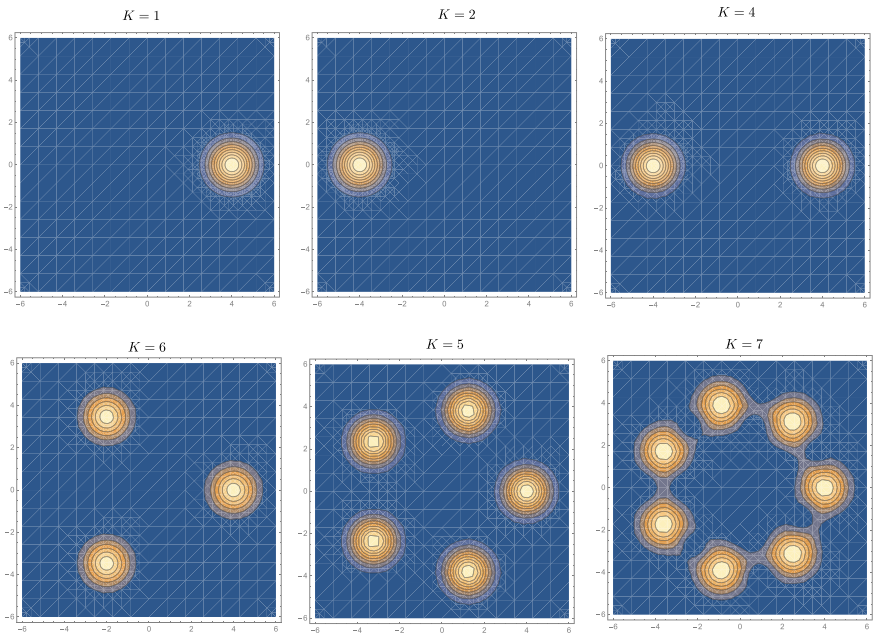

Fig. 4.2 The Q-function contours in the complex plane for a Kerr cat states with $\alpha = 4, \theta = 2\pi/K$

As Π has eigenvalues ± 1, it is clear that

$$|\mathrm{tr}(D(\alpha)\Pi D^{\dagger}(\alpha)\rho)| \leq 1 \tag{4.80}$$

What is the class of states that explore significant regions of negativity?

The answer is provided by a result of Lloyd and Braunstein [7]. They proved that universal simulation of a single bosonic mode is possible if the Hamiltonian includes operators that are at least cubic in the creation and annihilation operators, for example

$$\{a, a^{\dagger}, a^2, a^{\dagger\,2}, (a^{\dagger}a)^2\}\,, \tag{4.81}$$

is universal. The first two operators generate displacements (Heisenberg-Weyl group) the next two quadratic operators generate the squeezing transformations (SU(1,1)). The quartic operator is the Kerr nonlinearity. Starting from the vacuum state, all states in the Hilbert space can be reached by time dependent Hamiltonians involving the four operators. The first four generate only positive Wigner functions. Adding the Kerr non linearity gives us the entire state space including access to states with negative Wigner functions.

Problems

4.1 Verify (4.17).

4.2 Frequency conversion is another process that can occur in a material with a second order non linear susceptibility. When pumped by a coherent classical field with frequency ω_p it converts a photon at frequency ω_1 to a frequency ω_2 (and conversely) with $\omega_p = \omega_2 - \omega_1 > 0$. The Hamiltonian for frequency conversion is

$$H = \hbar\omega_1 a_1^\dagger a_1 + \hbar\omega_2 a_2^\dagger a_2 + \hbar g(a_1^\dagger a_2 e^{i\omega_p t} + a_1 a_2^\dagger e^{-i\omega_p t}) \tag{4.82}$$

Show that the photon number sum of the signal and idler modes is a constant of motion.

4.3 Show that a non degenerate parametric amplifier with a squeezed state at the input to the signal mode (labelled 1) and a vacuum state in the input to the idler mode (labelled 2) will decrease the squeezing at the output. Show that the maximum gain before squeezing is lost is

$$G_{max} = \frac{2}{\mathbb{V}[X_1^{in}] + \mathbb{V}[X_2^{in}]} \tag{4.83}$$

4.4 Let the initial state of the mechanical system be a coherent state $|\beta_0\rangle_m$ so that $b|\beta_0\rangle_m = \beta_0|\beta_0\rangle_m$ and the cavity field state be arbitrary with number state expansion $|\psi\rangle = \sum_n z_n|n\rangle$. Show that the the state at time $t > 0$ is

$$|\Psi(t)\rangle_{cm} = \sum_{n=0}^{\infty} z_n e^{-in\omega_c t}|n\rangle_c \otimes e^{i\Im(\beta_0^*\beta(t))}|\beta_n(t)\rangle_m \tag{4.84}$$

with the displacement

$$\beta_n(t) = \beta_0 e^{-i\omega_m t} - \frac{g_0 n}{\omega_m}(1 - e^{-i\omega_m t}) \tag{4.85}$$

If the cavity is prepared in a coherent state $|\alpha_0\rangle$ and the mechanical system is prepared in a thermal state

$$\rho_m = \frac{1}{\pi\bar{n}} \int d^2\beta e^{-|\beta|^2/\bar{n}}|\beta\rangle\langle\beta| \tag{4.86}$$

where $\bar{n}$ is the average number of phonons in the mechanical oscillator

$$\bar{n} = (e^{\beta\hbar\omega_m} - 1)^{-1} \tag{4.87}$$

where $\beta = (k_B T)^{-1}$ is the usual Boltzmann inverse temperature, show that the state of the total system at time $t > 0$ is then given by

$$\rho(t) = e^{-|\alpha|^2} \frac{1}{\pi \bar{n}} \int d^2\beta e^{-|\beta|^2/\bar{n}} \sum_{n,m=0}^{\infty} \frac{\alpha_n \alpha_m^* e^{-i\chi t(n^2-m^2)}}{\sqrt{n!m!}} |\beta_n\rangle\langle\beta_n| \otimes |n\rangle\langle m| \tag{4.88}$$

References

1. B.R. Mollow, R.J. Glauber, Phys. Rev. **160**, 1097 (1967); ibid. **162**, 1256 (1967)
2. B.L. Schumaker, C.M. Caves, Phys. Rev. A **31**, 3093 (1985)
3. C.M. Caves, Phys. Rev. D **26**, 1817 (1982)
4. G.J. Milburn, Phys. Rev. A **33**, 674 (1985)
5. B. Yurke, D. Stoler, Phys. Rev. Lett. **57**, 13 (1985)
6. M. Kitagawa, Y. Yamamoto, Phys. Rev. A **34**, 345 (1986)
7. S. Lloyd, S.L. Braunstein, Phys. Rev. Lett. **82**, 1784 (1999)

Open Quantum Systems

5

Abstract

No quantum system is ever completely isolated. At the very least, it must be coupled to the outside world when we make measurements. In this chapter we discuss techniques to treat open quantum systems. We consider the system of interest as weakly coupled to an environment which remains close to a steady state. We first derive a master equation for the density operator of the open system in the Schrödinger or interaction picture. Using the quasi-probability representations for the density operator, the master equation may be converted to a c-number Fokker–Planck equation. We describe an alternative formulation in terms of quantum stochastic differential equations, replacing the Heisenberg equations of motion for closed quantum systems.

5.1 Master Equation

An optical cavity, say a Fabry-Perot cavity, is open to the external world through photon loss out of the end mirrors. The cavity mode is the system of interest and evanescent coupling of the cavity field to the many mode field outside the cavity is responsible for this loss. Moreover, we can drive the cavity using external sources through the same coupling mechanism. We will refer to the external field as the environment and the cavity field as the system. We make measurements of the external field in order to infer the state of the cavity field.

We consider a system described by the Hamiltonian H_s coupled to an environment described by the Hamiltonian H_e, modelled as a large number of harmonic oscillators, for example, the modes of the external electromagnetic field. There is a weak interaction between the system and its environment given by an interaction Hamiltonian V. The total total Hamiltonian can be written $H = H_s + H_e + V$. The dynamics of the total system plus environment, ρ_T, is given in the interaction picture

D. F. Walls and G. J. Milburn, *Quantum Optics*, Graduate Texts in Physics,
https://doi.org/10.1007/978-3-031-84177-4_5

by

$$\frac{d\rho_T}{dt} = -\frac{i}{\hbar}[V(t), \rho_T]\,. \tag{5.1}$$

The reduced density operator for the system is defined by the partial trace $\rho(t) = \mathrm{tr}_e[\rho_T]$. We let the state of the environment be a time-independent steady state ρ_e typically a thermal equilibrium state. If we assume that, by some intervention, we can initialise the system state as $\rho(0)$, the total initial state is then

$$\rho_T(0) = \rho(0)\rho_e \tag{5.2}$$

This is a considerable idealisation as an open quantum system is usually always coupled to its environment but we will assume that this can be changed by a suitable preparation procedure acting at time $t = 0$. As we will see in the next chapter, this is typically a measurement.

The solution to (5.1) can be written in terms of the time ordered integral

$$\begin{aligned}\rho_T(t) = \rho_T(0) + \sum_{n=0}^{\infty}\left(\frac{-i}{\hbar}\right)^n \int_0^t dt_1 \int_0^{t_1} dt_2 \ldots \\ \times \int_0^{t_{n-1}} dt_n [V(t_1), [V(t_2), \ldots [V(t_n), \rho_T(t_n)]]]\end{aligned} \tag{5.3}$$

Taking the partial trace over the environment we see that

$$\begin{aligned}\rho(t) = \rho(0) + \sum_{n=0}^{\infty}\left(\frac{-i}{\hbar}\right)^n \int_0^t dt_1 \int_0^{t_1} dt_2 \ldots \\ \times \int_0^{t_{n-1}} dt_n \mathrm{tr}_e[V(t_1), [V(t_2), \ldots [V(t_n), \rho_T(t_n)]]]\end{aligned} \tag{5.4}$$

The ability to make sense of the partition into system plus environment implicitly assumes that the interaction between them is weak. If this is not the case, we need to find a new partition so that all components of the system are much more strongly interacting with each other than each component is interacting with the environment. If we can find such a partition then we can use second order perturbation theory to write

$$\begin{aligned}\rho(t) \approx \rho(0) - \frac{i}{\hbar}\int_0^t dt_1 \mathrm{tr}_e[V(t_1), \rho_e\rho(t_1)] \\ - \frac{1}{2\hbar^2}\int_0^t dt_1 \int_0^{t_1} dt_2 \mathrm{tr}_e[V(t_1), [V(t_2), \rho_e\rho(t_2)]]\end{aligned} \tag{5.5}$$

Note that we have also taken $\rho_T(t) \approx \rho_e\rho(t)$. This is consistent with a second order perturbation approximation. It implicitly assumes that the environment relaxes back to its steady state much faster than the system state is changing. We will need to

check the consistency of this assumption with second order perturbation theory. We now see that

$$\frac{d\rho(t)}{dt} \approx -\frac{i}{\hbar}\mathrm{tr}_e[V(t), \rho_e\rho(t)] - \frac{1}{2\hbar^2}\int_0^t dt_1 \mathrm{tr}_e[V(t), [V(t_1), \rho_e\rho(t_1)]] \tag{5.6}$$

We will assume that the interaction, $V(t)$, is not diagonal in the basis that diagonalises ρ_e. In that case the first term is zero. For example, in the case of a damped bosonic mode we take

$$V(t) = \hbar(a^\dagger\Gamma(t)e^{i\omega_0 t} + a\Gamma^\dagger(t)e^{-i\omega_0 t}) \tag{5.7}$$

where

$$\Gamma(t) = \sum_k g_k b_k e^{-i\omega_k t} \tag{5.8}$$

where $b_k, b_k^\dagger$ are annihilation and creation operators for bosonic modes in the environment. They could represent the many-mode field external to a cavity field or quantised elastic waves (phonons) coupled to an isolated nano-mechanical oscillator. The physical difference between these two cases appears in the choice of g_k as a function of k. Substituting into (5.6), we find that the following integrals are required,

$$I_1(t) = \int_0^t dt_1 \langle\Gamma(t)\Gamma(t_1)\rangle e^{i\omega_0(t+t_1)} \tag{5.9}$$

$$I_2(t) = \int_0^t dt_1 \langle\Gamma^\dagger(t)\Gamma^\dagger(t_1)\rangle e^{-i\omega_0(t+t_1)} \tag{5.10}$$

$$I_3(t) = \int_0^t dt_1 \langle\Gamma(t)\Gamma^\dagger(t_1)\rangle e^{i\omega_0(t-t_1)} \tag{5.11}$$

$$I_4(t) = \int_0^t dt_1 \langle\Gamma^\dagger(t)\Gamma(t_1)\rangle e^{-i\omega_0(t-t_1)} \tag{5.12}$$

The integrals can be evaluated once we have calculated the four two-time correlation functions

$$c_1(t,t_1) = \langle\Gamma(t)\Gamma(t_1)\rangle = \sum_{k,k'} g_k g_{k'} \langle b_k b_{k'}\rangle e^{-i(\omega t+\omega' t_1)} \tag{5.13}$$

$$c_2(t,t_1) = \langle\Gamma^\dagger(t)\Gamma^\dagger(t_1)\rangle = c_2^*(t_1,t) \tag{5.14}$$

$$c_3(t,t_1) = \langle\Gamma(t)\Gamma^\dagger(t_1)\rangle = \sum_{k,k'} g_k g_{k'}^* \langle b_k b_{k'}^\dagger\rangle e^{-i(\omega t-\omega' t_1)} \tag{5.15}$$

$$c_4(t,t_1) = \langle\Gamma^\dagger(t)\Gamma(t_1)\rangle = \sum_{k,k'} g_k^* g_{k'} \langle b_k^\dagger b_{k'}\rangle e^{i(\omega t-\omega' t_1)} \tag{5.16}$$

where ω, ω' are the frequencies associated to the modes labelled with wave numbers k, k'. In the case of electromagnetism the dispersion relation is $\omega = ck$. In the physical cases of interest in quantum optics, these will turn out to be functions of the time difference $t - t_1$ a situation we refer to as *stationary correlations*.

5.1.1 Thermal Environment

We need to specify the moments $\langle b_k b_{k'} \rangle$, $\langle b_k b_{k'}^\dagger \rangle$, $\langle b_k^\dagger b_{k'} \rangle$ which depend on the state of the environment. For an environment in thermal equilibrium at temperature T we set $\langle b_k b_{k'} \rangle = \langle b_k^\dagger b_{k'}^\dagger \rangle = 0$ and

$$\langle b_k b_{k'}^\dagger \rangle = (\bar{n}(\omega) + 1)\delta_{k,k'} \tag{5.17}$$

$$\langle b_k^\dagger b_{k'} \rangle = \bar{n}(\omega)\delta_{k,k'} \tag{5.18}$$

where the mean thermal excitation of mode k is

$$\bar{n}(\omega) = \frac{1}{e^{\beta\hbar\omega} - 1} \tag{5.19}$$

and $\beta = (k_B T)^{-1}$ where k_B is Boltzmann's constant. We then find that the only non zero correlation functions are

$$c_3(t, t_1) = \sum_k |g_k|^2 (\bar{n}(\omega) + 1) e^{-i\omega(t - t_1)} \tag{5.20}$$

$$c_4(t, t_1) = \sum_k |g_k|^2 \bar{n}(\omega) e^{-i\omega(t - t_1)} \tag{5.21}$$

which are functions only of the time difference reflecting the stationary statistics of a thermal field. We convert the sums to integrals using a density of states function $\rho(\omega)$,

$$c_3(t, t_1) = \int_0^\infty d\omega \rho(\omega) |g(\omega)|^2 (\bar{n}(\omega) + 1) e^{-i\omega(t - t_1)} \tag{5.22}$$

$$c_4(t, t_1) = \int_0^\infty d\omega \rho(\omega) |g(\omega)|^2 \bar{n}(\omega) e^{-i\omega(t - t_1)} \tag{5.23}$$

In quantum optics, at optical frequencies, the functions $\rho(\omega), |g(\omega)|^2, \bar{n}(\omega)$ are slowly varying over a bandwidth B around $\omega = \omega_0$ with $\omega_0 \gg B$. We then make a change of variable $\epsilon = \omega - \omega_0, t' = t - t_1$ and write

$$I_4(t) = \int_0^t dt' \int_{-\omega_0}^{\infty} d\omega \rho(\epsilon+\omega_0)|g(\epsilon+\omega_0)|^2 \bar{n}(\epsilon+\omega_0) e^{-i\epsilon t'} \tag{5.24}$$

$$\approx \int_{-\infty}^{\infty} d\omega\ \rho(\epsilon+\omega_0)|g(\epsilon+\omega_0)|^2 \bar{n}(\epsilon+\omega_0) \int_0^t dt' e^{-i\epsilon t'} \tag{5.25}$$

$$\approx \int_{-\infty}^{\infty} d\omega\ \rho(\epsilon+\omega_0)|g(\epsilon+\omega_0)|^2 \bar{n}(\epsilon+\omega_0) \int_0^{\infty} dt' e^{-i\epsilon t'} \tag{5.26}$$

where we have anticipated that the integral over ϵ is expected to lead to a rapidly decaying function of time and extended the upper limit of the time integral to infinity. Using

$$\int_0^{\infty} dt\ e^{-i\epsilon t} = \pi\delta(\epsilon) \pm PV[\frac{1}{\epsilon}] \tag{5.27}$$

where PV denotes the Cauchy principal value part. If we now define the damping rate as

$$\gamma = \rho^2(\omega_0) g^2(\omega_0) \tag{5.28}$$

and

$$\Delta = PV\left[\int_{-\infty}^{\infty} \frac{d\epsilon}{2\pi} \frac{1}{\epsilon} \rho(\epsilon+\omega_0)|g(\epsilon+\omega_0)|^2 \bar{n}(\epsilon+\omega_0)\right] \tag{5.29}$$

then

$$I_4 = \gamma \bar{n}(\omega_0) - i\Delta \tag{5.30}$$

In a similar way we can find

$$I_3 = \gamma(\bar{n}(\omega_0)+1) - i\Delta' \tag{5.31}$$

The imaginary parts constitute small frequency shifts and we will ignore them. The resulting equation of motion for the system is the master equation

$$\frac{d\rho}{dt} = \gamma(\bar{n}+1)\mathcal{D}[a]\rho + \gamma\bar{n}\mathcal{D}[a^\dagger]\rho \tag{5.32}$$

where we have set $\bar{n} = \bar{n}(\omega_0)$ and defined the super-operator

$$\mathcal{D}[A]\rho = A\rho A^\dagger - \frac{1}{2}A^\dagger A\rho - \frac{1}{2}\rho A^\dagger A \tag{5.33}$$

Equations of motion for the expectation values of system operators may be directly derived from the master equation, (5.32). For example, the mean amplitude of the simple harmonic oscillator is given by

$$\frac{d\langle a\rangle}{dt} = \mathrm{tr}\left[a\frac{d\rho}{dt}\right] = -\frac{\gamma}{2}\langle a\rangle\ . \tag{5.34}$$

with the solution

$$\langle a(t)\rangle = \langle a(0)\rangle e^{-\gamma t/2} . \tag{5.35}$$

This is in the interaction picture. In the Schrödinger picture it is

$$\langle a(t)\rangle = \langle a(0)\rangle e^{-i\omega_0 t-\gamma t/2} . \tag{5.36}$$

The mean amplitude decays towards zero. On the other hand the equation of motion for the mean photon number is

$$\frac{d\langle a^\dagger a\rangle}{dt} = -\gamma\langle a^\dagger a\rangle + \gamma\bar{n} , \tag{5.37}$$

with the solution

$$\langle a^\dagger(t)a(t)\rangle = \langle a^\dagger(0)a(0)\rangle e^{-\gamma t} + \bar{n}(1-e^{-\gamma t}) . \tag{5.38}$$

In the steady state this approaches $\bar{n}$ and indicates thermal equilibrium with the environment.

The photon number distribution defined by $p_n(t) = \mathrm{tr}[\rho(t)|n\rangle\langle n|]$ obeys the Markov master equation

$$\frac{dp_n(t)}{dt} = t_+(n-1)p_{n-1} + t_-(n+1)p_{n+1} - (t_+(n)+t_-(n))p_n \tag{5.39}$$

where the transition rates are given by

$$t_+(n) = \gamma\bar{n}(n+1) \tag{5.40}$$

$$t_-(n) = \gamma(\bar{n}+1)n \tag{5.41}$$

In the steady state the detailed balance condition holds,

$$t_-(n)p_{ss,n} = t_+(n-1)p_{ss,n-1} \tag{5.42}$$

and the steady state solution is found by iteration

$$p_{ss,n} = p_{ss,0}\prod_{k=1}^{n}\frac{t_+(k-1)}{t_-(k)} \tag{5.43}$$

After normalisation we get

$$p_{ss,n} = \frac{1}{\bar{n}+1}\left(\frac{\bar{n}}{\bar{n}+1}\right)^n = \frac{1}{\bar{n}+1}e^{-n\beta\hbar\omega_0} \tag{5.44}$$

At optical frequencies there are very few thermally excited photons at laboratory temperature $\bar{n}(\omega_0) \ll 1$. It is for this reason that most tests of quantum foundations have been done at optical frequencies (see Chap. 13). In this regime we can approximate the irreversible dynamics by the zero temperature master equation in the Schrödinger picture,

$$\frac{d\rho}{dt} = -i\omega_0[a^\dagger a, \rho] + \gamma \mathcal{D}[a]\rho \tag{5.45}$$

The solution to this equation can be written in terms of time ordered integrals [2]

$$\rho(t) = \sum_{n=0}^{\infty} \mathcal{N}_n(t)\rho(0) \tag{5.46}$$

where the super-operators $\mathcal{N}_n(t)$ are given by

$$\mathcal{N}_n(t) = \int_0^t dt_m \int_0^{t_m} dt_{m-1} \ldots \int_0^{t_2} dt_1 \mathcal{S}(t - t_m)\mathcal{J}\mathcal{S}(t_m - t_{m-1}) \ldots \mathcal{J}\mathcal{S}(t_1) \tag{5.47}$$

with

$$\mathcal{J}\rho = \gamma a \rho a^\dagger \tag{5.48}$$

$$\mathcal{S}(t)\rho = e^{-i(\omega_0 - i\gamma/2)ta^\dagger a}\rho e^{i(\omega_0 + i\gamma/2)ta^\dagger a} \tag{5.49}$$

$$\mathcal{N}_0(t)\rho = \mathcal{S}(t)\rho \tag{5.50}$$

We will refer to the super-operators $\mathcal{J}$ as the jump operations. Their action on a photon number eigenstate is

$$\mathcal{J}|n\rangle\langle n| = \gamma n |n-1\rangle\langle n-1| \tag{5.51}$$

The operations $\mathcal{S}(t)$ are called the no-jump operations as

$$\mathcal{S}(t)|n\rangle\langle n| = e^{-\gamma n t}|n\rangle\langle n| \,. \tag{5.52}$$

5.1.2 Squeezed Environment

As we have seen an environment in thermal equilibrium leads to stationary two-time correlation functions. There is another important situation in which this is true. It is the case of a pure squeezed environment in which modes at different frequencies are entangled.

In this case the phase dependent moments are non zero [1]

$$\langle b_k b_{k'} \rangle = M(\omega)\delta(2\omega_0 - \omega - \omega') \tag{5.53}$$

where $\langle b_k^\dagger b_{k'}^\dagger \rangle = \langle b_k b_{k'} \rangle^*$. If we make the change of variables $\omega = \omega_0 - \epsilon, \omega' = \omega_0 + \epsilon'$ we see that this can be written as

$$\langle b_k b_{k'} \rangle = M(\omega_0 - \epsilon)\delta(\epsilon + \epsilon') \tag{5.54}$$

This indicates that modes symmetrically displaced around ω_0 by ϵ are correlated. In the interaction picture we only need the function $M(\epsilon)$ and we assume this is symmetric and slowly varying around zero. The moments for the phase independent terms are

$$\langle b_k b_{k'}^\dagger \rangle = (N(\omega) + 1)\delta(\omega - \omega') \tag{5.55}$$

$$\langle b_k b_{k'}^\dagger \rangle = N(\omega)\delta(\omega - \omega') \tag{5.56}$$

where $|M(\omega)|^2 = N(\omega)(N(\omega) + 1)$.

Following the derivation of the thermal master equation using similar approximations we find that the master equation for a squeezed environment takes the form

$$\begin{aligned} \frac{d\rho}{dt} &= \gamma(N+1)\mathcal{D}[a]\rho + \gamma N \mathcal{D}[a^\dagger]\rho \\ &\quad + \frac{\gamma}{2}M(2a^\dagger \rho a^\dagger - a^{\dagger\,2}\rho - \rho a^{\dagger\,2}) + \frac{\gamma}{2}M^*(2a\rho a - a^2\rho - \rho a^2) \end{aligned} \tag{5.57}$$

where $M = M(\omega_0)$ and $N = N(\omega_0)$ with $|M|^2 = N(N+1)$.

5.2 The Fock State Master Equation

The previous examples have assumed that the external cavity fields are gaussian; vacuum, coherent or squeezed. A rather more interesting case is to consider the response of a cavity to a single photon input. In these cases an elegant master equation method has been developed by Combes and coworkers [5].

Let $\hat{X}$ be a *system* operator. First define the Heisenberg operator

$$j_t(\hat{X}) = U^\dagger(t)\left(\hat{X} \otimes \mathbb{I}_f\right)U(t) \tag{5.58}$$

where $\mathbb{I}_f$ is the identity operator acting on the field. Note that because $U(t)$ describes an interaction between the system and the field, $j_t(\hat{X})$ is, generally, a joint system-field operator. A typical example of relevance to us would be $\hat{X} = a^\dagger a$.

The objective is to find the moments of such time evolved operator. For example, if the initial state of the system is $|\eta\rangle$ and the initial state of the field is the one photon state $|1_\xi\rangle$. Then define the joint initial state as $|\eta\, 1_\xi\rangle = |\eta\rangle \otimes |1_\xi\rangle$ the moment of $j_t(\hat{X})$ is defined by

$$\varpi_t^{11}(\hat{X}) = \langle \eta, 1_\xi | j_t(\hat{X}) | \eta, 1_\xi \rangle \tag{5.59}$$

For example, if $\hat{X} = a^\dagger a$ then $\varpi_t^{11}(a^\dagger a) \equiv \langle \hat{n}(t) \rangle$ is simply the mean photon number inside the cavity at time t.

The next step is to write down an equation of motion for the arbitrary moment $\varpi_t^{11}(\hat{X})$. We then discover that this couples to other diagonal and off diagonal moments. As an example, consider the equations for the case of the number operator, $\hat{n} = a^\dagger a$. A word of caution, the operation $\mathcal{D}_L[A]$ is not the same as what appears in the master equation. It is defined as

$$\mathcal{D}_L[A] = L^\dagger A L - \frac{1}{2}(L^\dagger L A + A L^\dagger L) \tag{5.60}$$

a form that is sometimes called the adjoint Linbladian. We want the case in which $L \to \sqrt{\kappa} a$, so the first term here is the opposite way around from what appears in the master equation. This results from using the cyclic property of trace in the moments. We then find that

$$\frac{d\varpi_t^{11}(\hat{n})}{dt} = -\kappa \varpi_t^{11}(\hat{n}) - \sqrt{\kappa}(\varpi_t^{01}(a)\xi^*(t) + \varpi_t^{10}(a^\dagger)\xi(t)) \tag{5.61}$$

We thus find that we need the equations for $\varpi_t^{01}(a)$ and $\varpi_t^{10}(a)$. These are easily found using (19) in Gough et al. [5].

$$\frac{d\varpi_t^{01}(a)}{dt} = -\frac{\kappa}{2}\varpi_t^{01}(a) - \sqrt{\kappa}\xi(t) \tag{5.62}$$

$$\frac{d\varpi_t^{10}(a)}{dt} = -\frac{\kappa}{2}\varpi_t^{10}(a) - \sqrt{\kappa}\xi^*(t) \tag{5.63}$$

The initial conditions are

$$\varpi_0^{11}(\hat{n}) = \langle \eta | a^\dagger a | \eta \rangle \tag{5.64}$$

$$\varpi_0^{00}(\hat{n}) = \langle \eta | a^\dagger a | \eta \rangle \tag{5.65}$$

$$\varpi_0^{10}(a) = 0 \tag{5.66}$$

$$\varpi_0^{01}(a) = 0 \tag{5.67}$$

Solving the off-diagonal equations we find

$$\varpi_t^{01}(a) = -\sqrt{\kappa} e^{-\kappa t/2} \int_0^t dt' \xi(t') e^{\kappa t'/2} \tag{5.68}$$

$$\varpi_t^{10}(a^\dagger) = -\sqrt{\kappa} e^{-\kappa t/2} \int_0^t dt' \xi^*(t') e^{\kappa t'/2} \tag{5.69}$$

Thus

$$\frac{d\varpi_t^{11}(\hat{n})}{dt} = -\kappa \varpi_t^{11}(\hat{n}) + \kappa e^{-\kappa t/2} \int_0^t dt' (\xi(t')\xi(t) + \xi^*(t')\xi(t)) e^{\kappa t'/2} \tag{5.70}$$

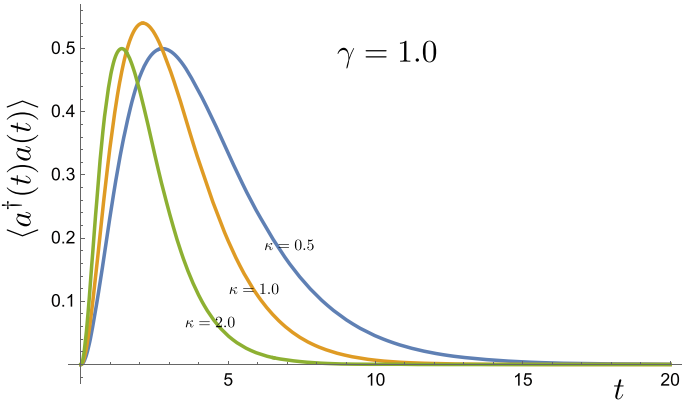

Fig. 5.1 The mean photon number in a one sided cavity driven by a single photon input at $t = 0$

In this case $\varpi_t^{11}(\hat{n})$ is the *unconditional* intracavity photon number $\langle a^\dagger(t)a(t)\rangle$.

With the choice

$$\xi(t) = \begin{cases} \sqrt{\gamma}e^{-\gamma t/2} & t \geq 0 \\ 0 & t < 0 \end{cases} \quad . \tag{5.71}$$

we find the solution

$$\langle a^\dagger a\rangle = \frac{4\gamma\kappa}{(\gamma-\kappa)^2}e^{-\kappa t}\left(1 - e^{-(\gamma-\kappa)t/2}\right)^2 \quad . \tag{5.72}$$

This is plotted in Fig. 5.1.

5.3 P Representation

An operator master equation may be transformed to a c-number equation using the Glauber–Sudarshan representation for ρ. It is necessary to first establish the rules for converting operators to an equivalent c-number form. We know the relation $a|\alpha\rangle = \alpha|\alpha\rangle$. What is $a^\dagger|\alpha\rangle$?

To answer this question it is convenient to use the Bargmann state $||\alpha\rangle$ defined by

$$||\alpha\rangle = e^{|\alpha|^2/2}|\alpha\rangle \tag{5.73}$$

Using (1.32) we see that

$$||\alpha\rangle = e^{\alpha a^\dagger}|0\rangle \tag{5.74}$$

It follows that

$$a^\dagger||\alpha\rangle = \frac{\partial}{\partial\alpha}||\alpha\rangle \tag{5.75}$$

If we write the Glauber-Sudarshan P-representation in terms of the Bargman states we get

$$\rho = \int d^2\alpha P(\alpha) e^{-|\alpha|^2} ||\alpha\rangle\langle\alpha|| \tag{5.76}$$

Then

$$a^\dagger \rho = \int d^2\alpha P(\alpha) e^{-|\alpha|^2} \frac{\partial}{\partial\alpha} ||\alpha\rangle\langle\alpha|| \tag{5.77}$$

We integrate this by parts to get

$$\begin{aligned} a^\dagger \rho &= \int d^2\alpha ||\alpha\rangle\langle\alpha|| \left(-\frac{\partial}{\partial\alpha} P(\alpha) e^{-|\alpha|^2} \right) \\ &= \int d^2\alpha |\alpha\rangle\langle\alpha| \left(\alpha^* - \frac{\partial}{\partial\alpha} P(\alpha) \right) \end{aligned} \tag{5.78}$$

We can use this relation to represent the term $a^\dagger\rho$ that appears in the master equation in terms of a differential operation on $P(\alpha)$. We are thus led to the following replacement rules

$$a\rho \to \alpha P(\alpha) \tag{5.79}$$

$$\rho a^\dagger \to \alpha^* P(\alpha) \tag{5.80}$$

$$a^\dagger \rho \to \left(\alpha^* - \frac{\partial}{\partial\alpha} \right) P(\alpha) \tag{5.81}$$

$$\rho a \to \left(\alpha - \frac{\partial}{\partial\alpha^*} \right) P(\alpha) \tag{5.82}$$

Similarly we can see that

$$a^\dagger a\rho \to \left(\alpha^* - \frac{\partial}{\partial\alpha} \right) \alpha P(\alpha) \tag{5.83}$$

$$\rho a^\dagger a \to \left(\alpha - \frac{\partial}{\partial\alpha^*} \right) \alpha^* P(\alpha) \tag{5.84}$$

Using these rules the equivalent P representation for the master equation (5.57) is

$$\frac{\partial P(\alpha)}{\partial t} = \left[\frac{\gamma}{2} \left(\frac{\partial}{\partial\alpha}\alpha + \frac{\partial}{\partial\alpha^*}\alpha^* \right) + \frac{\gamma}{2} \left(M^* \frac{\partial^2}{\partial\alpha^{*2}} + M \frac{\partial^2}{\partial\alpha^2} \right) + \gamma N \frac{\partial^2}{\partial\alpha\partial\alpha^*} \right] P(\alpha) \tag{5.85}$$

When $|M| > N$ this equation has "non positive-definite" diffusion, hence the P representation is unable to describe the system in terms of a classical stochastic process. Alternative representations will be discussed later in this chapter. When $M \leq N$ the equation has the form of a Fokker–Planck equation. We shall discuss some useful properties of Fokker–Planck equations below.

A general Fokker-Planck equation in n variables may be written in the form

$$\frac{\partial P(\boldsymbol{x})}{\partial t} = \left[-\frac{\partial}{\partial x_j} A_j(\boldsymbol{x}) + \frac{1}{2} \frac{\partial}{\partial x_i} \frac{\partial}{\partial x_j} D_{ij}(\boldsymbol{x}) \right] P(\boldsymbol{x}) \tag{5.86}$$

(There is an implicit sum over repeated indices). The first derivative term determines the mean, or deterministic, motion and is called the drift term, while the second derivative term, provided D_{ij} is positive definite, will cause a broadening or diffusion of $P(\boldsymbol{x}, t)$ and is called the diffusion term. The drift vector $\boldsymbol{A}$ has components A_j and the diffusion matrix is $\boldsymbol{D}$ has components D_{ij}. The different role of each of these terms may be seen in the equations for the first and second oder moments,

$$\frac{d\langle x_k \rangle}{dt} = \langle A_k(\boldsymbol{x}) \rangle \tag{5.87}$$

$$\frac{d\langle x_k x_l \rangle}{dt} = \langle x_k A_l(\boldsymbol{x}) \rangle + \langle x_l A_k(\boldsymbol{x}) \rangle + \frac{1}{2} \langle D_{kl}(\boldsymbol{x}) + D_{lk}(\boldsymbol{x}) \rangle \tag{5.88}$$

We see that A_k determines the motion of the mean amplitude whereas D_{lk} enters into the equation for correlations.

In the case of the damped harmonic oscillator interacting with a thermal bath, (5.85), with $M = 0,\ N = \bar{n}$,

$$\frac{d\langle \alpha \rangle}{dt} = -\frac{\gamma}{2} \langle \alpha \rangle \ , \tag{5.89}$$

$$\frac{d\langle \alpha^* \alpha \rangle}{dt} = -\gamma \langle \alpha^* \alpha \rangle + \gamma \bar{n} \ . \tag{5.90}$$

where the average $\langle ... \rangle$ refers to an integral over $P(\alpha)$,

$$\langle \alpha^{*\,m} \alpha^n \rangle = \int d^2\, \alpha \alpha^{*\,m} \alpha^n P(\alpha) \ . \tag{5.91}$$

Noting that the P-representation gives normally ordered moments, these equations are equivalent to (5.34, 5.37). In the case of a squeezed bath, the role of the terms multiplied by M can be seen in the phase-dependent second order moment,

$$\frac{d\langle \alpha^2 \rangle}{dt} = -\gamma \langle \alpha^2 \rangle + \gamma M \tag{5.92}$$

For many problems in nonlinear optics it is sufficient to know the steady state solution. That is the solution after all transients have died out. We shall therefore seek a steady state solution to (5.86). The steady state is given by the solution to

$$\left[-\frac{\partial}{\partial x_j} A_j(\boldsymbol{x}) + \frac{1}{2} \frac{\partial}{\partial x_i} \frac{\partial}{\partial x_j} D_{ij}(\boldsymbol{x}) \right] P_{ss}(\boldsymbol{x}) = 0 \tag{5.93}$$

If we define the probability current with components

$$J_i(\boldsymbol{x},t) = A_i(\boldsymbol{x})P(\boldsymbol{x},t) - \frac{1}{2}\frac{\partial}{\partial x_j}[D_{ij}(\boldsymbol{x})P(\boldsymbol{x},t)] \tag{5.94}$$

at steady state we have $\boldsymbol{J}_{ss}(\boldsymbol{x}) = 0$, which implies

$$D_{ij}(\boldsymbol{x})\frac{\partial \ln P_{ss}}{\partial x_j} = 2A_i(\boldsymbol{x}) - \frac{\partial}{\partial x_j}[D_{ij}(\boldsymbol{x})] \tag{5.95}$$

Writing $P_{ss}(\boldsymbol{x}) = \exp[-\phi(\boldsymbol{x})]$ we need to solve

$$-\frac{\partial \phi(\boldsymbol{x})}{\partial x_i} = 2(D^{-1})_{ij}\left[A_j - \frac{1}{2}\frac{\partial D_{jk}}{\partial x_k}\right] \equiv F_i(\boldsymbol{x}) \tag{5.96}$$

(implicit summation over repeated indices). The form of this suggests we regard $F_j(\boldsymbol{x})$ as a generalized force, and $\phi(\boldsymbol{x})$ the corresponding potential. The system of equations (5.96) can be solved by integration if the so called potential conditions are satisfied

$$-\frac{\partial^2 \phi}{\partial x_i \partial x_j} = \frac{\partial F_j}{\partial x_i} = \frac{\partial F_i}{\partial x_j} = -\frac{\partial^2 \phi}{\partial x_j \partial x_i} \tag{5.97}$$

so that the function $\phi(\boldsymbol{x})$ is well behaved and the multivariate integration is independent of the path of integration. This is always true in one dimension. Given the potential conditions, the steady state solution is

$$P_{ss}(\boldsymbol{x}) = \mathcal{N}e^{-\phi(\boldsymbol{x})} \tag{5.98}$$

with

$$\phi(\boldsymbol{x}) = \int dx_i \; 2[D^{-1}]_{ij}\left[-A_{ij} + \frac{1}{2}\frac{\partial D_{jk}}{\partial x_k}\right]dx_i \tag{5.99}$$

(There is a sum over repeated indices.). For further discussion of the steady state solution in multivariate Fokker-Planck equations see [3].

In systems where the diffusion matrix is diagonal and constant $D_{ij}(\boldsymbol{x}) = \sigma\delta_{ij}$ the potential conditions become

$$-\frac{\partial \phi(\boldsymbol{x})}{\partial x_i} = \frac{2A_i(\boldsymbol{x})}{\sigma} \tag{5.100}$$

Hence the turning points of the potential correspond exactly to the steady state solutions, that is the steady state solutions to the first-order moment equations.

Turning to the time dependent solutions, in the case where the drift term is linear in the variables and the diffusion coefficient is a constant, a solution to the

Fokker–Planck equation may be found using the method of Wang and Uhlenbeck [4]. Consider the Fokker–Planck equation

$$\frac{\partial P(\boldsymbol{x})}{\partial t} = -a_i \frac{\partial}{\partial x_i}\left(x_i P(\boldsymbol{x})\right) + \frac{1}{2} d_{ij} \frac{\partial^2}{\partial x_i \partial x_j} P(\boldsymbol{x}) \tag{5.101}$$

The Green's function solution to this equation given by the initial condition

$$P(\boldsymbol{x}, 0) = \delta^N(\boldsymbol{x} - \boldsymbol{x}_0) \tag{5.102}$$

is

$$P(\boldsymbol{x}, t) = \left[\pi^n \det[\Sigma(t)]\right]^{-1/2} \exp\left[-(\boldsymbol{x} - \bar{\boldsymbol{x}}(t))^T \cdot \Sigma^{-1} \cdot (\boldsymbol{x} - \bar{\boldsymbol{x}}(t))\right] \tag{5.103}$$

where

$$\bar{x}_j(t) = x_{j0} e^{a_j t} \tag{5.104}$$

and

$$\Sigma_{ij} = -\frac{d_{ij}}{a_i + a_j}[1 - e^{(a_i + a_j)t}] \tag{5.105}$$

The solution for a damped harmonic oscillator initially in a coherent state with $P(\alpha, 0) = \delta^2(\alpha - \alpha_0)$ is

$$P(\alpha, t) = [\pi \bar{n}(1 - e^{-\gamma t}]^{-1} \exp\left[-\frac{|\alpha - \alpha_0 e^{-\gamma t/2}|^2}{\bar{n}(1 - e^{-\gamma t})}\right] \tag{5.106}$$

This represents an initial coherent state undergoing relaxation with a heat bath. Its coherent amplitude decays, and fluctuations from the heat bath cause its P-function to assume a Gaussian form characteristic of thermal noise. The width of the distribution grows with time until the oscillator reaches equilibrium with the heat bath. The steady state solution is the same as that given in (3.5).

5.4 Q Representation

The Q-function is defined by $Q(\alpha) = \langle \alpha | \rho | \alpha \rangle$. We can covert a master equation to an equation of motion for the Q-function by first normally ordering all operator products. Let $f(a, a^\dagger)$ be a function that can be expanded in a power series of a and $a^\dagger$ then

$$[a, f(a, a^\dagger)\,] = \frac{\partial f}{\partial a^\dagger}\,, \tag{5.107}$$

$$[a^\dagger, f(a, a^\dagger)\,] = -\frac{\partial f}{\partial a}\,. \tag{5.108}$$

Noting that

$$\rho a^\dagger a = a^\dagger \rho a - [a^\dagger, \rho]a \, . \tag{5.109}$$

we use the results in above to write

$$\rho a^\dagger a = a^\dagger \rho a + \frac{\partial \rho}{\partial a} a \, . \tag{5.110}$$

Then

$$\langle \alpha | \rho a^\dagger a | \alpha \rangle = \alpha \langle \alpha | a^\dagger \rho + \frac{\partial \rho}{\partial a} | \alpha \rangle \tag{5.111}$$

$$= \left(|\alpha|^2 + \alpha \frac{\partial}{\partial \alpha} \right) Q(\alpha) \tag{5.112}$$

Following this procedure we may convert the master equation in (5.57) into an equation for the Q function,

$$\frac{\partial Q}{\partial t} = \frac{\gamma}{2} \left(\frac{\partial}{\partial \alpha} \alpha + \frac{\partial}{\partial \alpha^*} \alpha^* \right) Q + \frac{\gamma}{2} \left[M^* \frac{\partial^2}{\partial {\alpha^*}^2} + M \frac{\partial^2}{\partial \alpha^2} + 2(N+1) \frac{\partial^2}{\partial \alpha \partial \alpha^*} \right] Q \tag{5.113}$$

This differs from the corresponding equation of motion for the P function only through the phase independent diffusion coefficient which is $N + 1$ rather than N. This is sufficient to give a positive definite diffusion matrix when the bath is in an ideal squeezed state, reflecting the fact that the Q function is always positive.

As the diffusion matrix is positive definite we can immediately apply the method of Wang and Uhlenbeck to obtain the solution for an initial coherent state. The result is

$$Q(\alpha, t) = (4\pi^2 \det \Sigma(t))^{-1/2} \exp[-\frac{1}{2} \boldsymbol{u}(t)^T \Sigma^{-1} \boldsymbol{u}(t)] \tag{5.114}$$

where

$$\boldsymbol{u}(t) = \begin{pmatrix} \alpha - \alpha_0 e^{-\gamma t/2} \\ \alpha^* - \alpha_0^* e^{-\gamma t/2} \end{pmatrix} e^{-\gamma t/2} \tag{5.115}$$

and

$$\Sigma(t) = \frac{1}{2} \begin{pmatrix} -\sinh 2r & \cosh 2r + 1 \\ \cosh 2r + 1 & -\sinh 2r \end{pmatrix} e^{-\gamma t} + \begin{pmatrix} M & N+1 \\ N+1 & M^* \end{pmatrix} (1 - e^{-\gamma t}) \tag{5.116}$$

The variances for the quadrature phase operators for the oscillator are then easily found to be

$$\mathbb{V}(X_1) = (e^{-2r} - 1) e^{-\gamma t} + 2(N + \Re(M))(1 - e^{-\gamma t}) + 1 \tag{5.117}$$

$$\mathbb{V}(X_2) = (e^{-2r} + 1) e^{-\gamma t} + 2(N - \Re(M))(1 - e^{-\gamma t}) + 1 \tag{5.118}$$

Note that the steady state variances are squeezed.

5.5 Wigner Representation

We can convert the operator master equation into an equation of motion for the Wigner function. This is best accomplished by deriving an equation for the characteristic function,

$$\chi(\beta) = \mathrm{tr}[D(\alpha)\rho] \tag{5.119}$$

where $D(\alpha)$ is the displacement operator (see Chap. 1). Thus

$$\frac{\partial \chi(\beta)}{\partial t} = \mathrm{tr}\left[D(\alpha)\frac{d\rho}{dt}\right] \tag{5.120}$$

To illustrate the technique we shall derive the equation of motion for the Wigner function of a damped harmonic oscillator. Writing D in normal order (see (1.32)) we get

$$a^\dagger D = \left(\frac{\beta^*}{2} + \frac{\partial}{\partial \beta}\right) D \tag{5.121}$$

$$Da = -\left(\frac{\beta}{2} + \frac{\partial}{\partial \beta^*}\right) D \tag{5.122}$$

While writing D in anti normal order (see (1.33)) we get

$$Da^\dagger = \left(-\frac{\beta^*}{2} + \frac{\partial}{\partial \beta}\right) D \tag{5.123}$$

$$aD = \left(\frac{\beta}{2} - \frac{\partial}{\partial \beta^*}\right) D \tag{5.124}$$

Then using these rules the master equation (5.57) yields the following equation for the characteristic function

$$\frac{\partial \chi(\beta)}{\partial t} = -\frac{\gamma}{2}\left(|\beta|^2 + \beta^*\frac{\partial}{\partial \beta^*} + \beta\frac{\partial}{\partial \beta}\right)\chi(\beta) - \gamma N|\beta|^2\chi(\beta) \tag{5.125}$$

$$= -\frac{\gamma M}{2}\beta^{*\,2}\chi(\beta) - \frac{\gamma M^*}{2}\beta^2\chi(\beta) \tag{5.126}$$

The equation for the Wigner function is obtained by taking the Fourier transform of this equation as

$$W(\alpha) = \int d^2\beta\, e^{\beta^*\alpha - \beta\alpha^*}\chi(\beta) \tag{5.127}$$

Using constructions like

$$\int d^2\beta\, e^{\beta^*\alpha - \beta\alpha^*}\beta^*\beta\chi(\beta) = -\frac{\partial}{\partial\alpha\partial\alpha^*}W(\alpha) \tag{5.128}$$

we find that

$$\frac{\partial W}{\partial t} = \frac{\gamma}{2}\left(\frac{\partial}{\partial \alpha}\alpha + \frac{\partial}{\partial \alpha^*}\alpha^*\right) Q + \frac{\gamma}{2}\left[M^* \frac{\partial^2}{\partial \alpha^{*\,2}} + M\frac{\partial^2}{\partial \alpha^2} + 2(N + \frac{1}{2})\frac{\partial^2}{\partial \alpha \partial \alpha^*}\right] Q \tag{5.129}$$

A comparison of the three equations of motion for the P, Q and Wigner functions show that they differ only in the coefficient of the diffusion term being $\gamma N, \gamma(N+1)$ and $\gamma(N+1/2)$ respectively. However, the additional $+\gamma$ and $+\gamma/2$ in the equations for the Q and Wigner function are sufficient to ensure that these equations have positive definite diffusion. We conclude that the Q and Wigner function must always be positive and Gaussian for the solutions to the master equation (5.57) if we start from a coherent state.

5.6 Generalized P Representation

In our study of nonlinear problems we shall find systems which either do not give Fokker–Planck equations in the Q and Wigner representations or no steady state solution may readily be found. For some systems a steady state solution in terms of a Glauber–Sudarshan P representation does not exist. For such systems the complex P representation is sometimes useful in deriving a steady state solution to Fokker–Planck equations. The positive P representation is useful when it is desirable to have a Fokker–Planck equation with a positive definite diffusion term, as is necessary in order to deduce the corresponding stochastic differential equations.

Master equations may be converted to a c-number representation using the complex P representation by an analogous set of operator rules used for the diagonal P representation. The state may be written as

$$\rho = \int_D \Lambda(\alpha, \beta) P(\alpha, \beta) d\mu(\alpha, \beta) \tag{5.130}$$

(see Chap. 3). The non-diagonal coherent state projection operator is defined as,

$$\Lambda(\alpha, \beta) = \frac{|\alpha\rangle\langle\beta^*|}{\langle\beta^*|\alpha\rangle} \tag{5.131}$$

The following identities hold

$$a\Lambda(\alpha, \beta) = \alpha\Lambda(\alpha, \beta), \qquad a^\dagger \Lambda(\alpha, \beta) = \left(\beta + \frac{\partial}{\partial \alpha}\right) \tag{5.132}$$

$$\Lambda(\alpha, \beta)a^\dagger = \beta\Lambda(\alpha, \beta) \qquad \Lambda(\alpha, \beta)a = \left(\alpha + \frac{\partial}{\partial \beta}\right) \tag{5.133}$$

By substituting the above identities into (5.130), defining the generalized P representation, and using partial integration (providing the boundary terms vanish) these

identities can be used to generate operations on the P function depending on the representation.

In the case of the complex P representation

$$a\rho \leftrightarrow \alpha P(\alpha,\beta)\,, \qquad a^{\dagger}\rho \leftrightarrow \left(\beta - \frac{\partial}{\partial\alpha}\right) P(\alpha,\beta) \tag{5.134}$$

$$\rho a^{\dagger} \leftrightarrow \beta P(\alpha,\beta)\,, \qquad \rho a \leftrightarrow \left(\alpha - \frac{\partial}{\partial\beta}\right) P(\alpha,\beta) \tag{5.135}$$

This procedure yields a very similar equation to that for the Glauber–Sudarshan P function. We assume that, by appropriate reordering of the differential operators, we can reduce an operator master equation to an equivalent partial differential equation for $P(\alpha,\beta,t)$. Define the column vector $\boldsymbol{\alpha} = (\alpha,\beta)^T$. We need

$$\int_C\int_{C'} \Lambda(\alpha,\beta)\frac{\partial P(\alpha,\beta,t)}{\partial t}d\alpha d\beta = \tag{5.136}$$

$$= \int_C\int_{C'} \Lambda(\alpha,\beta)P(\alpha,\beta,t)\left[A_j(\boldsymbol{\alpha})\frac{\partial}{\partial\alpha_j} + \frac{1}{2}D_{ij}(\boldsymbol{\alpha})\frac{\partial}{\partial\alpha_i}\frac{\partial}{\partial\alpha_j}\right]\Lambda(\alpha,\beta)$$

We now integrate by parts and if we can neglect boundary terms, which may be made possible by an appropriate choice of contours, C, C', at least one solution is obtained by equating the coefficients of $\Lambda(\alpha,\beta)$,

$$\frac{\partial P(\alpha,\beta,t)}{\partial t} = \left[-A_j(\boldsymbol{\alpha})\frac{\partial}{\partial\alpha_j} + \frac{1}{2}\frac{\partial}{\partial\alpha_i}\frac{\partial}{\partial\alpha_j}D_{ij}(\boldsymbol{\alpha})\right]P(\alpha,\beta,t) \tag{5.137}$$

This equation is sufficient to imply (5.136) but is not a unique equation because the $\Lambda(\alpha,\beta)$ are not linearly independent. The Fokker–Planck equation has the same form as that derived using the diagonal P representation with α^* replaced by β . It should be noted that for the complex P representation, $A_j(\boldsymbol{\alpha})$ and $D_{ij}(\boldsymbol{\alpha})$ are always analytic in $\boldsymbol{\alpha}$, hence if $P(\alpha,\beta,t)$ is initially analytic (5.137) preserves this analyticity as time develops.

In the case of the positive P representation, the differential representation rules remain the same. In addition, using the analyticity of $\Lambda(\alpha,\beta)$ and noting that if $\alpha = \alpha_x + i\alpha_y,\ \beta = \beta_x + i\beta_y$ then

$$\frac{\partial}{\partial\alpha}\Lambda(\alpha,\beta) = \frac{\partial}{\partial\alpha_x}\Lambda(\alpha,\beta) = -i\frac{\partial}{\partial\alpha_y}\Lambda(\alpha,\beta) \tag{5.138}$$

$$\frac{\partial}{\partial\beta}\Lambda(\alpha,\beta) = \frac{\partial}{\partial\beta_x}\Lambda(\alpha,\beta) = -i\frac{\partial}{\partial\beta_y}\Lambda(\alpha,\beta) \tag{5.139}$$

Thus we also have

$$a^{\dagger}\rho \leftrightarrow \left(\beta - \frac{\partial}{\partial \alpha_x}\right) P(\alpha, \beta) \leftrightarrow \left(\beta + i\frac{\partial}{\partial \alpha}\right) P(\alpha, \beta) \tag{5.140}$$

$$\rho a \leftrightarrow \left(\alpha - \frac{\partial}{\partial \beta_x}\right) P(\alpha, \beta) \leftrightarrow \left(\alpha + i\frac{\partial}{\partial \beta_y}\right) P(\alpha, \beta) \tag{5.141}$$

The positive P representation may be used to give a Fokker–Planck equation with a positive definite diffusion matrix. We shall demonstrate this in the following.

We assume that the same (5.137) is being considered but with a positive P representation. The symmetric diffusion matrix can always be factorized in the form

$$\boldsymbol{D}(\boldsymbol{\alpha}) = \boldsymbol{B}(\boldsymbol{\alpha})\boldsymbol{B}(\boldsymbol{\alpha})^T \tag{5.142}$$

We now write

$$\boldsymbol{A}(\boldsymbol{\alpha}) = \boldsymbol{A}_x(\boldsymbol{\alpha}) + i\boldsymbol{A}_y(\boldsymbol{\alpha}) \tag{5.143}$$

$$\boldsymbol{B}(\boldsymbol{\alpha}) = \boldsymbol{B}_x(\boldsymbol{\alpha}) + i\boldsymbol{B}_y(\boldsymbol{\alpha}) \tag{5.144}$$

where $\boldsymbol{A}_x$, $\boldsymbol{A}_y$, $\boldsymbol{B}_x$, $\boldsymbol{B}_y$ are real. We then find that the master equation yields

$$\begin{aligned}\frac{\partial P(\alpha, \beta, t)}{\partial t} = \Bigg\{ &-\partial_j^x A_x^j(\boldsymbol{\alpha}) - \partial_j^y A_y^j(\boldsymbol{\alpha}) + \frac{1}{2}\Big[\partial_i^x \partial_j^x B_x^{ik}(\boldsymbol{\alpha}) B_x^{jk}(\boldsymbol{\alpha}) \\ &+2\frac{1}{2}\partial_i^x \partial_j^y B_x^{ik}(\boldsymbol{\alpha}) B_y^{jk}(\boldsymbol{\alpha}) + \frac{1}{2}\partial_i^y \partial_j^y B_y^{ik}(\boldsymbol{\alpha}) B_y^{jk}(\boldsymbol{\alpha})\Big]\Bigg\} P(\alpha, \beta, t)\end{aligned} \tag{5.145}$$

Again, this is not a unique time-development equation. However, the Fokker–Planck equation now possesses a positive semidefinite diffusion matrix, in a four-dimensional space, with vectors

$$\boldsymbol{\alpha} = (\alpha_x, \alpha_y, \beta_x, \beta_y)\ . \tag{5.146}$$

Problems

5.1 Use the squeezed ME to calculate the equations for the quadrature phase amplitudes.

5.2 The photon number distribution for a laser may be shown to obey the master equation

$$\frac{dp_n}{dt} = \frac{An}{1 + n/n_s} p_{n-1} - \frac{A(n+1)}{1 + (n+1)/n_s} p_n - \gamma n p_n + \gamma(n+1) p_{n+1} \tag{5.147}$$

where A is related to the gain, n_s is the saturation photon number and γ is the cavity loss rate. Use detailed balance to show that the steady state solution is

$$p_{ss,n} = \mathcal{N}\frac{(An_s/\gamma)^n}{(n+n_s)!} \tag{5.148}$$

where $\mathcal{N}$ is a normalisation constant.

5.3 The interaction picture master equation for a damped harmonic oscillator, driven by a resonant linear force, is

$$\frac{d\rho}{dt} = i\mathcal{E}[a+a^\dagger, \rho] + \gamma\mathcal{D}[a]\rho \tag{5.149}$$

Show that the steady state is a coherent state and find the amplitude.

5.4 A model for phase diffusion of a simple harmonic oscillator is provided by the master equation

$$\frac{d\rho}{dt} = -\Gamma[a^\dagger a, [a^\dagger a, \rho]] \tag{5.150}$$

Show that the Q function obeys the Fokker–Planck equation

$$\frac{\partial Q}{\partial t} = \frac{\Gamma}{2}\left(\frac{\partial}{\partial\alpha}\alpha + \frac{\partial}{\partial\alpha^*}\alpha^* + 2\frac{\partial}{\partial\alpha}\frac{\partial}{\partial\alpha^*}|\alpha|^2 - \frac{\partial^2}{\partial\alpha^2}\alpha^2 - \frac{\partial^2}{\partial\alpha^{*\,2}}\alpha^{*\,2}\right)Q \tag{5.151}$$

Thus show that while the mean amplitude decays the energy remains constant. Using polar coordinates, $\alpha = re^{i\phi}$, show that the model implies a diffusion process for the phase.

5.5 Show that in terms of the quadrature operators $X_1 = a + a^\dagger$, $X_2 = -i(a - a^\dagger)$ the master equation (5.57) may be written

$$\frac{d\rho}{dt} = i\frac{\gamma}{8}[X_2, \{X_1, \rho\}] - i\frac{\gamma}{8}[X_1, \{X_2, \rho\}] \tag{5.152}$$

$$-\frac{\gamma}{8}e^{2r}[X_1, [X_1, \rho]] - \frac{\gamma}{8}e^{-2r}[X_2, [X_2, \rho]] \tag{5.153}$$

where $\{,\}$ is an anticommutator and we have taken $N = \sinh 2r$, $M = \sinh r \cosh r$ for an ideal squeezed bath. Show that the first and second terms describe damping in X_1 and X_2 respectively, while the third and fourth terms describe diffusion in each quadrature phase amplitude.

References

1. C.W. Gardiner, P. Zoller, *Quantum Noise* (Springer, 2004)
2. E.B. Davies, *Quantum Theory of Open Systems* (Academic Press, 1976)
3. C.W. Gardiner, *Handbook of Stochastic Processes for Physics, Chemistry and the Natural Sciences*, 4th edn. (Springer, 2009)
4. M.C. Wang, G.E. Uhlenbeck, Rev. Mod. Phys. **17**, 323 (1945)
5. J.E. Gough, M.R. James, H.I. Nurdin, J. Combes, Phys. Rev. A **86**, 043819 (2012)
6. B. Baragiola, R. Cook, A. Branczyk, J. Combes, Phys. Rev. A **86**, 013811 (2012)

Classical and Quantum Langevin Equations

6

Abstract

In this chapter we give an alternative, but equivalent description of open quantum systems using a stochastic extension of Heisenberg's equations of motion. This is analogous to Langevin's description of Brownian motion. However care must be taken in the quantum case to ensure that the commutation relations of the system observables obey equal time commutation relations. This requirement is satisfied by using operator noise terms rather than classical fluctuating forces. We show how this provides a useful way to compute correlation functions for the field emitted by an open system, a source, into its environment via the input-output relations for fields scattered from the source.

6.1 Stochastic Differential Equations

The quantum master equation approach to open quantum systems is analogous to the classical description of Brownian motion given by Einstein. His description of diffusion focusses on the time dependance of a classical probability density, while the quantum master equation focusses on the dynamics of the density operator. Langevin gave an alternative description which added fluctuating forces to Hamilton's equations of motion for the Brownian particle. In this chapter we seek a quantum version of this approach.

Consider the first order differential equation

$$\frac{dX}{dt} = \alpha(X) + \beta(X)\xi(t) \tag{6.1}$$

where $\xi(t)$ is a rapidly fluctuating stationary noise source. Stationary means that the two-time correlation function $E[\xi(t)\xi(t+\tau)]$ is independent of t and we assume

$$\int_{-\infty}^{\infty} d\tau\, E[\xi(t)\xi(t+\tau)] = 1 \tag{6.2}$$

D. F. Walls and G. J. Milburn, *Quantum Optics*, Graduate Texts in Physics,
https://doi.org/10.1007/978-3-031-84177-4_6

This implies that the units are: $[\alpha] = [X]T^{-1}$ and $[\beta] = [X]T^{-1/2}$.

Langevin assumed that, on time scales relevant to the system dynamical time scales, we can approximate the fluctuating forces by

$$E[\xi(t)\xi(t')] = \delta(t - t') \tag{6.3}$$
$$E[\xi(t)] = 0 \tag{6.4}$$

This is a Markovian assumption for which correlation time of the noise is zero. The spectrum of the noise defined by

$$S(\omega) = \int_{-\infty}^{\infty} d\tau E[\xi(t)\xi(t+\tau)]e^{-i\omega\tau} \tag{6.5}$$

is independent of frequency. Clearly this is not physical as it would imply that the noise power is infinite. This entails a difficulty in interpreting (6.1) as a well defined physical description, mirrored as a mathematical difficulty. We have written a differential equation for $X(t)$ assuming that the trajectories are differentiable however the assumed nature of the force terms is inconsistent with this assumption.

One way to proceed is not to make the Markov assumption for the fluctuating forces by implementing a finite correlation time or a roll-off in the noise power spectrum. This leads to the Stratonovich approach to stochastic differential equations. While it is physically more reasonable, it makes calculations more difficult due to the non-zero correlation times for the noise. In particular it implies that the noise and the system state at equal time are correlated.

Gardiner [1] addresses the problem in a set of assumptions:

- The chain rule of standard calculus applies
- The infinitesimal increment of a quantity is equal to its rate of change times dt.
- The noise and the system state at equal time are independent.

Stratonovich rule takes the third assumption as false. The Ito rule takes the first assumption as false. We will follow the Ito approach.

We will summarise some of the rules required for Ito calculus. The Ito form corresponding to the Stratonovich form (6.1) is

$$dX = [\alpha(X) + \frac{1}{2}\beta(X)\beta'(X)]dt + \beta(X)dW(t) \tag{6.6}$$

where $dW(t)$ is defined by the *Wiener process*

$$W(t) = \int_{t_0}^{t} \xi(t')dt' \tag{6.7}$$

Following Gardiner [1], we can show that $W(t + \Delta t) - W(t)$ is independent of $W(s)$ for $s < t$ and

$$E[\Delta W(t)^2] = \Delta t \tag{6.8}$$
$$E[\Delta W(t)] = 0 \tag{6.9}$$

Consider the Ito form $dX = a(X)dt + b(X)dW(t)$. The noise is independent of the system so that $E[dX] = a(x)dt$. Now consider $dF(X)$ using a modified chain rule

$$df(X) = f'(X)dX + \frac{1}{2}f''(X)(dX)^2 \tag{6.10}$$

where the prime indicates differentiation with respect to X. Anticipating that $E[dW(t)^2] = dt$, we use the Ito form to write

$$df(X) = [f'(X)a(X) + \frac{1}{2}f''(X)b(X)^2]dt + f'(X)b(X)dW(t) \tag{6.11}$$

For example, if $f = X^2$, compute the increment in variance

$$E[dX(t)^2] - d(E[X(t)])^2 = b(X)^2dt \tag{6.12}$$

As an example, consider the Ito SDE, $dX = a(t) + b(t)dW$. The solution is

$$X(t) = X(0) + \int_0^t dsa(s) + \int_0^t b(s)dW(s) \tag{6.13}$$

Then the covariance is,

$$E[X(t_1), X(t_2)] \equiv E[X(t_1)X(t_2)] - E[X(t_1)]E[X(t_2)] \tag{6.14}$$

and

$$E[X(t_1), X(t_2)] = \int_0^{t_1}\int_0^{t_2} b(s))b(s')E[dW(s)dW(s')] \tag{6.15}$$

$$= \int_0^{min(t_1,t_2)} b(s)^2ds \tag{6.16}$$

6.2 Quantum Stochastic Differential Equations

We will consider a system-environment coupling in the rotating wave approximation and interaction picture of the form,

$$\hat{V}_{IP}(t) = i\hbar\int_0^\infty d\omega\,\kappa(\omega)(ab(\omega)^\dagger e^{i\delta t} - a^\dagger b(\omega)e^{-i\delta t})) \tag{6.17}$$

where $a, a^\dagger$ are system bosonic operators and $b(\omega), b(\omega)^\dagger$ are bosonic reservoir operators. $\delta = \omega - \Omega$. In Chap. 5 we saw that $\kappa(\omega)$ is slowly varying near the system frequency Ω and is only non-zero in some finite band around this frequency. We take $\kappa = \kappa(\Omega)$ and write

$$b(t) = \int_0^\infty d\omega b(\omega) e^{-i(\omega-\Omega)t} \tag{6.18}$$

with $[b(\omega), b^\dagger(\omega')] = \delta(\omega - \omega')$.

We now make a change of variable in the integration

$$\begin{aligned} b(t) &= \int_{-\Omega}^\infty d\omega' b(\omega' + \Omega) e^{-i\omega' t} \\ &= \int_{-\Omega}^\infty d\omega' \tilde{b}(\omega') e^{-i\omega' t} \end{aligned}$$

where $\tilde{b}(\omega') = b(\omega' + \Omega)$ which does not change commutation relations. If we assume that the bandwidth of the system-environment coupling is non-zero around the system frequency, Ω, and that this frequency is very large, we make the approximation

$$b(t) = \int_{-\infty}^\infty d\omega \tilde{b}(\omega) e^{-i\omega t} \tag{6.19}$$

Then, $[b(t), b^\dagger(t')] = \delta(t - t')$.

We now write the Hamiltonian in the interaction picture as

$$\hat{V}_{IP} = i\hbar\sqrt{\kappa}(ab^\dagger(t) - a^\dagger b(t)) \tag{6.20}$$

The unitary evolution operator for Schrödinger picture, $U(t)$, is

$$\frac{dU}{dt} = \sqrt{\kappa}(ab^\dagger(t) - a^\dagger b(t))U(t) \tag{6.21}$$

Now define

$$B(t) = \int_{-\infty}^t dt' b(t') \tag{6.22}$$

so that $dB(t) = b(t)dt$. We then see that

$$dU(t) = U(t + dt) - U(t) = \sqrt{\kappa}(adB^\dagger(t) - a^\dagger dB(t))U(t) \tag{6.23}$$

This is interpreted as a quantum Ito differential equation. Taking the trace over the environment we see that

$$\begin{aligned} \mathrm{tr}[dB^\dagger(t)dB(t)] &= \bar{n}dt \\ \mathrm{tr}[dB(t)dB^\dagger(t)] &= (\bar{n} + 1)dt \\ \mathrm{tr}[dB(t)dB(t)] &= 0 \end{aligned} \tag{6.24}$$

This looks a lot like what we would have if $dB(t)$ is treated as a complex valued Wiener increment. We can make the trace over the bath implicit by simply defining

$$\begin{aligned} dB^\dagger(t)dB(t) &= \bar{n}dt \\ dB(t)dB^\dagger(t) &= (\bar{n}+1)dt \\ dB(t)dB(t) &= 0 \end{aligned} \tag{6.25}$$

In particular for zero temperature we write $dB(t)dB^\dagger(t) = dt$. For a more complete discussion of the quantum Ito calculus see [3].

We can now check the consistency of this approach with the master equation method of Chap. 5. We compute the change in the total state of the system over a time increment

$$\begin{aligned} \rho(t+dt) &= U(t+dt)\rho(0)U^\dagger(t+dt) \\ &= (U(t)+dU(t))\rho(0)(U^\dagger(t)+dU^\dagger(t)) \\ &= [1+\sqrt{\kappa}(adB^\dagger(t)-a^\dagger dB(t)+\frac{\kappa}{2}(adB^\dagger(t)-a^\dagger dB(t))^2] \\ &\qquad \times\rho(t)\times \\ &\quad [1-\sqrt{\kappa}(adB^\dagger(t)-a^\dagger dB(t)+\frac{\kappa}{2}(adB^\dagger(t)-a^\dagger dB(t))^2] \end{aligned}$$

The system state at time $t+dt$ is then

$$\begin{aligned} \rho_S(t+dt) &= \mathrm{tr}_E(\rho(t+dt)) \\ &= \rho_S(t)+\sqrt{\kappa}\mathrm{tr}[(adB^\dagger(t)-a^\dagger dB(t))\rho(t)] \\ &\quad -\sqrt{\kappa}\mathrm{tr}[\rho(t)(adB^\dagger(t)-a^\dagger dB(t))] \\ &\quad +\frac{\kappa}{2}\mathrm{tr}[(adB^\dagger(t)-a^\dagger dB(t))^2\rho] \\ &\quad +\frac{\kappa}{2}\mathrm{tr}[\rho(adB^\dagger(t)-a^\dagger dB(t))^2] \\ &\quad -\kappa\mathrm{tr}[(adB^\dagger(t)-a^\dagger dB(t))\rho(t)(adB^\dagger(t)-a^\dagger dB(t))] \end{aligned}$$

This is the same form as derived in Chap. 5.

We are now in a position to define quantum stochastic differential equations for a damped bosonic mode. We define

$$\begin{aligned} a(t+dt) &= U^\dagger(t+dt)a(0)U(t+dt) \\ &= [1-\sqrt{\kappa}(adB^\dagger(t)-a^\dagger dB(t))+\frac{\kappa}{2}(adB^\dagger(t)-a^\dagger dB(t)^2] \\ &\qquad \times a(t)\times \\ &\quad [1+\sqrt{\kappa}(adB^\dagger(t)+a^\dagger dB(t)+\frac{\kappa}{2}(adB^\dagger(t)+a^\dagger dB(t)^2] \\ &= a(t)-\sqrt{\kappa}[(adB^\dagger(t)-a^\dagger dB(t)),a(t)] \\ &\quad +\frac{\kappa}{2}[(adB^\dagger(t)-a^\dagger dB(t)),[(adB^\dagger(t)-a^\dagger dB(t)),a(t)]] \\ &= a(t)-\sqrt{\kappa}dB(t)-\frac{\kappa}{2}a(t)dt \end{aligned}$$

We thus find that

$$da = -\frac{\kappa}{2}a(t)dt - \sqrt{\kappa}dB(t) \tag{6.26}$$

The solution is

$$a(t) = a(0)e^{-\kappa t/2} - \sqrt{\kappa}\int_0^t e^{-\kappa(t-t')/2}dB(t) \tag{6.27}$$

The mean photon number is

$$\langle a^\dagger(t)a(t)\rangle = \langle a^\dagger(0)a(0)\rangle e^{-\kappa t} + \kappa\int_0^t dt_1\int_0^t dt_2 e^{-\kappa(2t-t_1-t_2)/2}\langle dB^\dagger(t_1)dB(t_2)\rangle \tag{6.28}$$

Now use the Ito rules to evaluate integral over $\langle dB^\dagger(t_1)dB(t_2)\rangle = \delta(t_1 - t_2)$,

$$\int_0^t dt_1\int_0^{t'} dt_2 f(t_1)g(t_2)\langle dB^\dagger(t_1)dB(t_2)\rangle = \bar{n}\int_0^{min(t,t')} dt_1 f(t_1)g(t_1) \tag{6.29}$$

and

$$\langle a^\dagger(t)a(t)\rangle = \langle a^\dagger(0)a(0)\rangle e^{-\kappa t} + \kappa\bar{n}\int_0^t dt' e^{-\kappa(t-t')} \tag{6.30}$$

$$= \langle a^\dagger(0)a(0)\rangle e^{-\kappa t} + \bar{n}(1 - e^{-\kappa t}) \tag{6.31}$$

This agrees with (5.38).

6.3 Input-Output Relations

An apparently different approach to open quantum systems was introduced by Yurke and Denker [2] using infinite transmission lines for electronic circuits as illustrated in Fig. 6.1. This approach adopts a scattering theory perspective and we can adapt our approach to it by distinguishing input and output field operators in the environment. We regard the Heisenberg form of $dB(t)$ as the *output field*,

$$\begin{aligned} dB_{out} &= U^\dagger(dt)dB(t)U(dt) \\ &= [1 - \sqrt{\kappa}(adB^\dagger(t) - a^\dagger dB(t))]dB(t)[1 + \sqrt{\kappa}(adB^\dagger(t) - a^\dagger dB(t))] \\ &= dB(t) + \sqrt{\kappa}a(t)dt \end{aligned}$$

Writing $dB(t) = a_{in}(t)dt$, $dB_{out} = a_{out}(t)dt$, we see that

$$a_{out}(t) = \sqrt{\kappa}a(t) + a_{in}(t) \tag{6.32}$$

This is called the input-output relation in quantum optics.

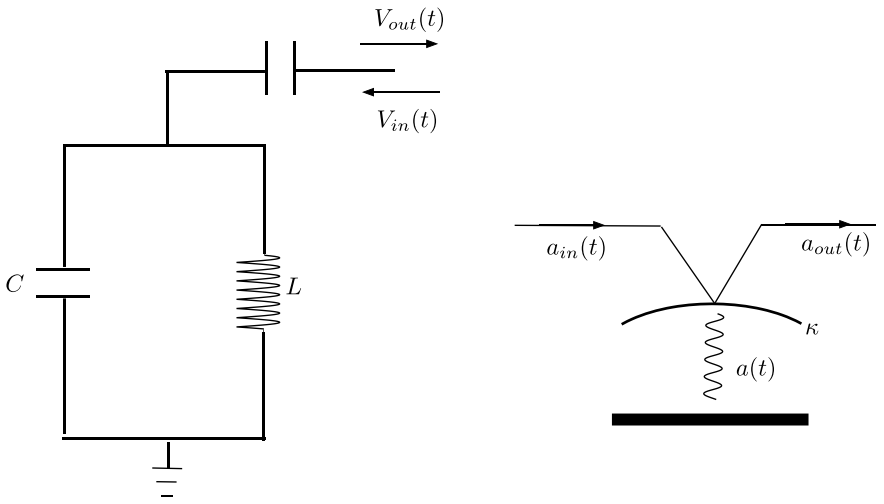

Fig. 6.1 Left: A transmission line model of dissipation in a LC oscillator. Then local system is capacitively coupled to input and output fields that propagate away from the system never to return. Right: the equivalent optical scheme is a single-sided cavity

The solution in (6.27), can now be written as

$$a(t) = a(0)e^{-\kappa t/2} - \sqrt{\kappa}\int_0^t dt' e^{-\kappa(t-t')/2} da_{in}(t') \tag{6.33}$$

We can check the equal-time canonical commutation relations using (6.27),

$$[a(t), a^\dagger(t)] = \ e^{-\kappa t} + \kappa \int_0^t dt_1 \int_0^t dt_2 e^{-(\kappa t - (t_1+t_2)/2)} [a_{in}(t_1), a_{in}^\dagger(t_2)] \tag{6.34}$$

Note that, without the quantum noise term, the right hand side decays to zero. The quantum noise term should be treated as if it was a quantum version of the Ito stochastic integral similar to (6.15) as $[a(t_1), a^\dagger(t_2)] = \delta(t_1 - t_2)$. We then implement the Ito rule to evaluate the upper limit of the integrals as

$$\int_0^t dt_1 \int_0^t dt_2 e^{-(\kappa t - (t_1+t_2)/2)} \delta(t_1 - t_2) = \int_0^t dt' e^{-\kappa(t-t')} \tag{6.35}$$

In which case we see that $[a_{in}(t), a_{in}^\dagger(t)] = 1$. It is easy to see that

$$[a(t), a_{in}(t)] = 0\,. \tag{6.36}$$

If we specify the initial condition in the remote past we may write the solution as

$$a(t) = -\sqrt{\kappa}\int_{-\infty}^t dt' e^{-\kappa(t-t')/2} a_{in}(t') \tag{6.37}$$

where we assume that the decay completely suppresses the dependance on the initial conditions. Recall that we are working in the interaction picture. Transforming back to the laboratory frame,

$$a(t) = -\sqrt{\kappa}\int_{-\infty}^{t} dt' e^{-(\kappa/2+i\Omega)(t-t')} a_{in}(t') \tag{6.38}$$

We now use the approximation of (6.19) to write $a(t)$, $a_{in}(t)$ as a Fourier transform we find that

$$\tilde{a}(\omega) = \frac{-\sqrt{\kappa}\tilde{a}_{in}(\omega)}{\kappa/2 + i(\Omega - \omega)} \tag{6.39}$$

Combining this with the Fourier transform of (6.32),

$$\tilde{a}_{out}(\omega) = \sqrt{\kappa}\tilde{a}(\omega) + \tilde{a}_{in}(\omega) \tag{6.40}$$

we get

$$\tilde{a}_{out}(\omega) = -\left[\frac{\kappa/2 - i(\Omega - \omega)}{\kappa/2 + i(\Omega - \omega)}\right]\tilde{a}_{in}(\omega) \tag{6.41}$$

This implies that there is a frequency dependent phase shift between the input and output field. The intensity does not change in the long time limit. Every incident photon is eventually reflected. The short time solution is discussed below.

6.3.1 Number State Input Fields

As an example of the use of the quantum stochastic differential calculus we consider the case where the input field is prepared in a single photon pulse of the form given in (1.122), with $N = 1$

$$|1_\xi\rangle = \int_{-\infty}^{\infty} d\omega\, \tilde{\xi}(\omega)\tilde{a}_{in}^\dagger(\omega)|0\rangle \quad . \tag{6.42}$$

we find that $\langle a_{in}^\dagger(t)a_{in}(t)\rangle = |\xi(t)|^2$. We will use as an example

$$\xi(t) = \begin{cases} \sqrt{\gamma}e^{-\gamma t/2} & t \geq 0 \\ 0 & t < 0 \end{cases} \quad . \tag{6.43}$$

This is similar to the output field from a single sided cavity when a single photon is injected into the cavity at $t = 0$.

After interacting with the cavity this state is transformed to

$$|\psi\rangle_{out} = \int_{-\infty}^{\infty} d\omega \tilde{\xi}(\omega)\tilde{a}_{out}^\dagger(\omega)|0\rangle \quad . \tag{6.44}$$

It is then easy to see that the probability per unit time to detect a single photon in the output field is

$$\langle a^\dagger_{out}(t)a_{out}(t)\rangle = \left|\int_{-\infty}^{\infty} d\omega \left(\frac{\frac{\kappa}{2} - i(\Omega-\omega)}{\frac{\kappa}{2} + i(\Omega-\omega)}\right)\tilde{\xi}(\omega)e^{-i\omega t}\right|^2 \quad , \tag{6.45}$$

In the time domain the output pulse is a convolution of the input pulse and the cavity response. Thus the temporal pulse is phase shifted by δt and broadened.

By ignoring transients in this calculation, we are effectively ignoring the possibility of reflection of photons reflected directly off the cavity from the source to detector. If the detector cannot distinguish these photons from those that enter the cavity to be re-emitted, an interference dip can occur in the overall detection rate as we now show.

Using input-output relation, $a_{out}(t) = a_{in}(t) + \sqrt{\kappa}a$ we see that

$$\langle a^\dagger_{out}(t)a_{out}(t)\rangle = \kappa\langle a^\dagger(t)a(t)\rangle + \langle a^\dagger_{in}(t)a_{in}(t)\rangle + \sqrt{\kappa}\langle a^\dagger_{in}(t)a(t) + a_{in}(t)a^\dagger(t)\rangle \tag{6.46}$$

The last term is an interference term between the two indistinguishable ways a photon can be detected: either it can be reflected directly from the input mirror into the detector or it can be absorbed by the cavity and remitted into the output field.

Using (6.33), the rate of detection in the output field is determined by

$$\langle a^\dagger_{out}(t)a_{out}(t)\rangle = \kappa\langle a^\dagger(t)a(t)\rangle + \gamma e^{-\gamma t} - \frac{4\kappa}{\gamma-\kappa}\left(e^{-(\kappa-\gamma)t/2} - 1\right)(\gamma e^{-\gamma t})$$

The first term is given by (5.72),

$$\langle a^\dagger a\rangle = \frac{4\gamma\kappa}{(\gamma-\kappa)^2}e^{-\kappa t}\left(1 - e^{-(\gamma-\kappa)t/2}\right)^2 \quad . \tag{6.47}$$

This is plotted in Fig. 6.2.

The output detection rate is zero at finite t. This is an interference effect due to the indistinguishablity of photons reflected from the cavity and transmitted by the cavity. In the long time limit we see that $\langle a^\dagger_{out}(t)a_{out}(t)\rangle = \langle a^\dagger_{in}(t)a_{in}(t)\rangle$ consistent with long time limit in (6.41).

6.3.2 Two Sided Cavity

The situation depicted in Fig. 6.3 is a two-sided cavity. In this case there are two sets of input and output fields. The stochastic differential equation is

$$\frac{da}{dt} = -i\Omega a - \frac{(\kappa_a + \kappa_b)}{2}a(t) - \sqrt{\kappa_a}a_{in}(t) - \sqrt{\kappa_b}b_{in}(t) \tag{6.48}$$

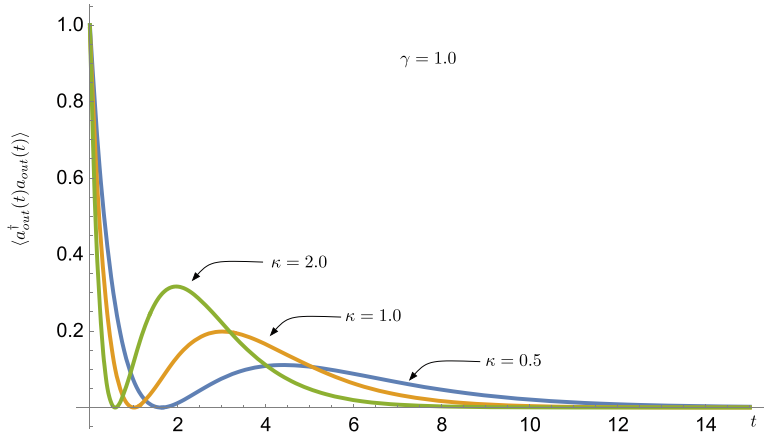

Fig. 6.2 The output intensity for a single photon input to a one sided cavity at $t = 0$. Note the interference point where the rate goes to zero

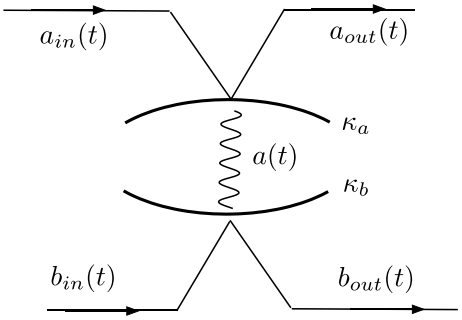

Fig. 6.3 A two-sided cavity with two sets of input and output fields. The total damping rate from the cavity is $\kappa = \kappa_a + \kappa_b$

The relationship between the external and internal fields is

$$\tilde{a}(\omega) = -\frac{(\sqrt{\kappa_a}\tilde{a}_{in}(\omega) + \sqrt{\kappa_b}\tilde{b}_{in}(\omega))}{\kappa/2 + i(\Omega - \omega)} \tag{6.49}$$

where the total decay rate is $\kappa = \kappa_a + \kappa_b$. The input-output relations are

$$a_{out}(t) = a_{in}(t) - \sqrt{\kappa_a}a(t) \tag{6.50}$$
$$b_{out}(t) = b_{in}(t) - \sqrt{\kappa_b}b(t) \tag{6.51}$$

Then

$$\tilde{a}_{out}(\omega) = -\frac{[\kappa_a - \kappa_b)/2 - i(\Omega - \omega)]\tilde{a}_{in}(\omega) + \sqrt{\kappa_a\kappa_b}\tilde{b}_{in}(\omega)}{(\kappa_a + \kappa_b)/2 + i(\Omega - \omega)} \tag{6.52}$$

For a symmetric cavity $\kappa_a = \kappa_b = \kappa$ this simplifies to

$$\tilde{a}_{out}(\omega) = \frac{i(\Omega - \omega)\tilde{a}_{in}(\omega) - \kappa\tilde{b}_{in}(\omega)}{\kappa + i(\Omega - \omega)} \tag{6.53}$$

6.4 Two-Time Correlation Functions

Let $c(t)$ be any system operator, then

$$[c(t), \sqrt{\kappa}a_{in}(t)] = \frac{\kappa}{2}[c(t), a(t)] \,. \tag{6.54}$$

Since $c(t)$ can only be a function of $a_{in}(t)$ for earlier times $t' < t$ and the input field operators must commute at different times we have

$$[c(t), a_{in}(t')] = 0 \quad t' > t \tag{6.55}$$

Similarly

$$[c(t), a_{out}(t')] = 0 \quad t' < t \tag{6.56}$$

We then see that in general

$$[c(t), \sqrt{\kappa}a_{in}(t')] = \kappa\theta(t - t')[c(t), a(t')] \tag{6.57}$$

where

$$\theta(t) = \begin{cases} 1 & t > 0 \\ \frac{1}{2} & t = 0 \\ 0 & t < 0 \end{cases} \tag{6.58}$$

The commutator for the output field may now be calculated to be

$$[a_{out}(t), a^{\dagger}_{out}(t')] = [a_{in}(t), a^{\dagger}_{in}(t')] \tag{6.59}$$

as expected.

For the case of a coherent or vacuum input it is now possible to express variances of the output field entirely in terms of those of the internal system. For an input field of this type all moments of the form $\langle a(t)a_{in}(t')\rangle$, $\langle a^{\dagger}(t)a_{in}(t')\rangle$, $\langle a^{\dagger}_{in}(t)a(t')\rangle$, $\langle a^{\dagger}_{in}(t)a^{\dagger}(t')\rangle$ will factorise. Then,

$$\langle a^{\dagger}_{out}(t), a_{out}(t)\rangle = \kappa\langle a^{\dagger}(t), a(t)\rangle \tag{6.60}$$

where we define $\langle A, B\rangle = \langle AB\rangle - \langle A\rangle\langle B\rangle$. In this case there is a direct relationship between the two time correlation of the output field and the internal field. Consider now the phase dependent two time correlation function

$$\begin{aligned} \langle a_{out}(t), a_{out}(t')\rangle &= \kappa\langle a(t), a(t')\rangle - \sqrt{\kappa}\langle [a_{in}(t'), a(t)]\rangle & (6.61)\\ &= \kappa\langle a(t), a(t')\rangle + \kappa\theta(t' - t)\langle [a(t'), a(t)]\rangle & (6.62)\\ &= \kappa\langle a(max(t, t')), a(min(t, t'))\rangle & (6.63) \end{aligned}$$

In this case the two time correlation functions of the output field are related to the time ordered two time correlation functions of the cavity field.

These results mean that the usual spectrum of the output field, as given by the Fourier transform of (6.60), will be identical to the spectrum of the cavity field. The photon statistics of the output field will also be the same as the intracavity field. A difference will arise in the phase-sensitive spectrum such as in squeezing experiments.

6.5 Parametric Oscillator

We now calculate the squeezing spectrum of the output of a parametric oscillator comprised of the degenerate parametric oscillator discussed in Sect. 4.1.1 inside an optical cavity. The system is stable so long as the amplifier gain is less than the damping rate. At some critical driving intensity, 'threshold', this breaks down. Below threshold the equations for the parametric oscillator are linear and hence we can directly apply the linear operator techniques. When the equations are nonlinear such as for the parametric oscillator above threshold, then linearization procedures must be used (see Chap. 8).

Below threshold the pump mode of the parametric oscillator may be treated classically. It can then be described by the interaction picture Hamiltonian

$$H = \hbar\Delta a^\dagger a + i\frac{\hbar}{2}(\varepsilon a^{\dagger\,2} - \varepsilon^* a^2) - i\hbar\sqrt{\kappa}[b(t)a^\dagger - b^\dagger(t)a] \tag{6.64}$$

where $a, a^\dagger$ are the bosonic operators for the cavity field, ε is proportional to the product of a coherent driving field and the nonlinear susceptibility of the medium, $b(t), b^\dagger(t)$ are reservoir operators introduced in (6.19). The detuning from the pump frequency is defined as $\Delta = \Omega - \omega_p/2$ where Ω is the cavity frequency. We consider here the case of a single ended cavity with loss rate κ.

The quantum SDEs are

$$\frac{d}{dt}\begin{pmatrix} a \\ a^\dagger \end{pmatrix} = \begin{pmatrix} -i\Delta - \frac{\kappa}{2} & \epsilon \\ \epsilon^* & i\Delta - \frac{\kappa}{2} \end{pmatrix}\begin{pmatrix} a \\ a^\dagger \end{pmatrix} - \sqrt{\kappa}\begin{pmatrix} a_{in} \\ a_{in}^\dagger \end{pmatrix} \tag{6.65}$$

The eigenvalues of the systematic part of this system are

$$\lambda_\pm = -\frac{\kappa}{2} \pm \sqrt{|\epsilon|^2 - 4\Delta^2} \tag{6.66}$$

The system has a stable fixed point at the origin if $|\epsilon| < 2\Delta$ and unstable if $|\epsilon|^2 > 4\Delta^2 + \kappa^2/4$. In the frequency domain

$$\begin{pmatrix} \tilde{a}(\omega) \\ \tilde{a}^\dagger(\omega) \end{pmatrix} = \sqrt{\kappa}\begin{pmatrix} -i(\Delta - \omega) - \frac{\kappa}{2} & \epsilon \\ \epsilon^* & i(\Delta - i\omega) - \frac{\kappa}{2} \end{pmatrix}^{-1}\begin{pmatrix} \tilde{a}_{in}(\omega) \\ \tilde{a}_{in}^\dagger(\omega) \end{pmatrix} \tag{6.67}$$

Combining this with the input-output relation in the frequency domain

$$\tilde{a}_{out}(\omega) = \tilde{a}_{in}(\omega) - \sqrt{\kappa}\tilde{a}(\omega) \tag{6.68}$$

we find that

$$\tilde{a}_{out}(\omega) = \mu(\omega)\tilde{a}_{in}(\omega) - \nu(\omega)\tilde{a}^{\dagger}_{in}(\omega) \tag{6.69}$$

where

$$\mu(\omega) = 1 - \frac{\kappa(\frac{\kappa}{2} + i(\omega - \Delta))}{\left|i(\Delta - \omega) + \frac{\kappa}{2}\right|^2 - |\epsilon|^2} \tag{6.70}$$

$$\nu(\omega) = \frac{\kappa\epsilon}{\left|i(\Delta - \omega) + \frac{\kappa}{2}\right|^2 - |\epsilon|^2} \tag{6.71}$$

Notice that

$$|\mu(\omega)|^2 - |\nu(\omega)|^2 = 1 \tag{6.72}$$

so that the linear transformation is a frequency dependent squeezing transformation.

Suppose the output field is directed towards a balanced homodyne detection (see Sect. 7.3) that measures, in the lab frame, the quadrature amplitude

$$X_\theta(t) = A_{out}(t)e^{-i(\theta - \Omega_{LO}t)} + A^{\dagger}_{out}(t)e^{i(\theta - \Omega_{LO}t)} \tag{6.73}$$

where $A_{out}(t)$, $A^{\dagger}_{out}(t)$ are the positive and negative frequency components of the output field in the lab frame and where θ, Ω_{LO} are the phase-shift and frequency of the local oscillator with respect to the output field. This definition is equivalent to moving to an interaction picture at the frequency of Ω_{LO}. Setting $\Omega_{LO} = \omega_p/2$ the detuning becomes $\Delta = \Omega - \Omega_{LO}$. In terms of the the interaction picture operators we are measuring the output field

$$X_\theta(t) = a_{out}(t)e^{-i\theta} + a^{\dagger}_{out}(t)e^{i\theta} \tag{6.74}$$

We will assume the resonance condition $\Delta = 0$.

In Sect. 7.3.1 we show that the stationary noise power spectrum function of the homodyne current is given by

$$S_\theta(\omega) = \kappa \int_{-\infty}^{\infty} e^{-i\omega\tau} \langle : X_\theta(\tau)X_\theta(0) : \rangle_{ss} \tag{6.75}$$

where : : denotes time and normal ordering.

Choosing the phase of the local oscillator to optimise the noise reduction in S_2, we get the following results for the spectrum

$$S_2(\omega) = 1 - \frac{2\kappa|\epsilon|}{\left(\frac{\kappa}{2} + |\epsilon|\right)^2 + \omega^2} \tag{6.76}$$

Shifting this phase choice by $\pi/2$ we get

$$S_1(\omega) = 1 + \frac{2\kappa|\epsilon|}{\left(\frac{\kappa}{2} - |\epsilon|\right)^2 + \omega^2} \tag{6.77}$$

The maximum squeezing occurs at the threshold for parametric oscillation $|\epsilon| = \kappa/2$ where

$$S_1(\omega) = 1 + \left(\frac{\kappa}{\omega}\right)^2 \tag{6.78}$$

$$S_2(\omega) = 1 - \frac{\kappa^2}{\kappa^2 + \omega^2} \tag{6.79}$$

We see that the squeezing occurs in the quadrature which is $\pi/2$ out of phase with the pump. The fluctuations in the in-phase quadrature diverge at $\omega = 0$. This is characteristic of critical fluctuations which diverge at a critical point. As the fluctuations in one phase are reduced to zero the fluctuations in the other phase necessarily diverge. That would of course imply a divergence in the output energy, an unphysical result. This divergence is avoided by including pump depletion [4]. We will return to this problem in Chap. 8

Problems

6.1 A particle is moving in a quadratic potential and subject to viscous damping. The corresponding classical Ito stochastic differential equations are

$$dx = ydt \tag{6.80}$$

$$dy = -xdt - \Gamma y dt + \sigma dW(t) \tag{6.81}$$

where x, y are (dimensionless) canonical position and momentum variables, and Γ is a viscous damping rate, while where $\sigma^2 = 2m\Gamma k_B T$ and T is the ambient temperature. Define the kinetic energy as $E = p^2/2$. Use the Ito rule to show that the average kinetic energy, $\bar{E}$, obeys

$$\frac{d\bar{E}}{dt} = -\Gamma\overline{y^2} + \frac{\sigma^2}{2}\,. \tag{6.82}$$

Thus show that the steady state average kinetic energy obeys the equipartition theorem.

6.2 A simple model of a quantum memory for a single photon pulse uses a controllable coupling between two cavity modes, with one cavity otherwise uncoupled from the environment. The Hamiltonian is

$$H = -i\hbar\sqrt{\kappa_1}[b_1(t)a_1^\dagger - b_1^\dagger(t)a_1] - i\hbar g(t)[a_1 a_2^\dagger - a_1^\dagger a_2] \tag{6.83}$$

where

$$\int_{-\infty}^{\infty} |g(t)|^2 = I \tag{6.84}$$

Find the long-time probability *not* to store a single photon pulse in (6.43). This is the error probability. Show that it is a minimum when $g(t) = \xi(t)$.

6.3 A degenerate parametric oscillator in a double side cavity is described by the Hamiltonain

$$H = \hbar\Delta a^{\dagger}a + i\frac{\hbar}{2}(\varepsilon a^{\dagger\,2} - \varepsilon^{*}a^{2}) - i\hbar\sqrt{\kappa_1}[b_1(t)a^{\dagger} - b_1^{\dagger}(t)a] - i\hbar\sqrt{\kappa_2}[b_2(t)a^{\dagger} - b_2^{\dagger}(t)a]\,. \tag{6.85}$$

Calculate the optimum squeezing spectrum in this case.

References

1. C.W. Gardiner, *Handbook of Stochastic Processes for Physics Chemistry and the Natural Sciences* (Springer, 2009)
2. B. Yurke, J.S. Denker, Quantum network theory. Phys. Rev. A **29**, 1419 (1984)
3. C.W. Gardiner, P. Zoller, *Quantum Noise A Handbook of Markovian and Non-Markovian Quantum Stochastic Methods with Applications to Quantum Optics* (Springer, 2004)
4. G.J. Milburn, D.F. Walls, Optics Commun. **39**, 401 (1981)

Quantum Measurement

7

Abstract

In this chapter we will introduce the theoretical description of continuous measurements in quantum optics, including photon counting, homodyne and heterodyne measurement. Our objective is to show how the quantum theory of measurement provides a new perspective on irreversible quantum dynamics as we have treated it in the two preceding chapters.

All measurement results are classical random variables available to any observer co located with the measurement instruments, or remote provided there is a communication channel of some sort. Quantum theory, like all physical theories, must provide statistical predictions for these random variables and tell us of how to consistently predict future measurement results given a record of previous results. In this way all initial conditions presuppose a measurement to define them. In Chap. 2 we introduced the concept of a photon counting measurement and we return to this kind of experiment to begin.

7.1 Single Shot Measurements

All measurements are described by irreversible open systems. A simple model of a measurement can be given in terms of a system coupled to an apparatus. Initially the state of system+apparatus is separable. The state of the system is unknown but the state of the apparatus is given (and usually carefully prepared). The apparatus is coupled irreversibly to an environment. The result of a measurement is a classical random variable.

As simple example is shown in Fig. 7.1. The system and the apparatus are two distinct modes of the electromagnetic field with bosonic annihilation operators a, b respectively. In this simple example the interaction is a unitary transformation. The apparatus-mode is prepared in the same known pure state $|\phi_0\rangle$ for every trial. The

D. F. Walls and G. J. Milburn, *Quantum Optics*, Graduate Texts in Physics,
https://doi.org/10.1007/978-3-031-84177-4_7

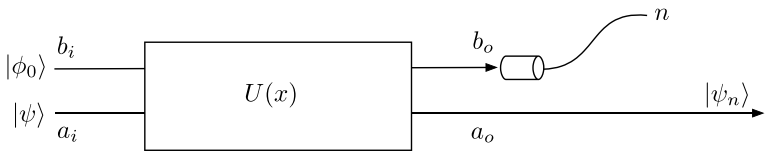

Fig. 7.1 A simple measurement scheme. One mode **a** is the system to be measured and another mode **b** is the apparatus

state of the system-mode is $|\psi\rangle$ for every trial. The interaction between the two modes is defined by a unitary operator, $U(x)$, parameterised by a single real number, x. Let us assume that in each trial the photon number is measured at the output of the apparatus mode and an integer n is recorded. It is a random variable that varies from one trial to the next. What is the probability distribution for n?

Rather than give a detailed description of the irreversible nature of the photon counting process (see below) we simply assume it is an irreversible 'event' at the spacetime location of the detector. According to the Born rule, the probability distribution of measurement results is given by

$$\mathrm{P}(n) = \langle n|\rho_{b,o}|n\rangle \,, \tag{7.1}$$

where the reduced state of mode-b is

$$\rho_{b,o} = \mathrm{tr}[U(x)|\phi_0\rangle\langle\phi_0| \otimes |\psi\rangle\langle\psi|U^\dagger(x)] \tag{7.2}$$

This may be written more compactly as

$$\mathrm{P}(n) = \mathrm{tr}_a[\hat{\Upsilon}_n^\dagger \hat{\Upsilon}_n |\psi\rangle\langle\psi|] \,, \tag{7.3}$$

where the operator acting on the state of mode-a is

$$\hat{\Upsilon}_n = \langle n|U(x)|\phi_0\rangle \,, \tag{7.4}$$

This will be referred to as a Krauss operator.

The *conditional state* of mode-a, given that the measurement result is n, is given by

$$|\psi_{|n}\rangle = [\mathrm{P}(n)]^{-1/2}\hat{\Upsilon}(n)|\psi\rangle \tag{7.5}$$

The unconditional state (the state averaged over all measurement results) is a mixed state,

$$\rho' = \sum_{n=0}^{\infty} \hat{\Upsilon}(n)|\psi\rangle\langle\psi|\hat{\Upsilon}^\dagger(n) \tag{7.6}$$

Let us now assume that $U(x) = e^{-ix\hat{G}}$ where $\hat{G}$ is an operator on the tensor product Hilbert space of both system and apparatus, and we assume that the apparatus

is prepared in the vacuum state $|\phi_0\rangle = |0\rangle$. As an example we consider, $G = a^\dagger b + ab^\dagger$, called the Stokes model. In this case

$$a_o = U^\dagger(x) a_i U(x) = \cos x\ a_i - i \sin x\ b_i \tag{7.7}$$
$$b_o = U^\dagger(x) a_i U(x) = \cos x\ b_i + i \sin x\ a_i\ . \tag{7.8}$$

This is equivalent to the beam spliter model in problem (2.1) with transmitivity $\eta = \cos^2 x$. Using these equations we see that

$$\langle b_0^\dagger b_0 \rangle = (1-\eta)\langle a_i^\dagger a_i \rangle \tag{7.9}$$
$$\langle (\Delta b_0^\dagger b_0)^2 \rangle = (1-\eta)^2 \langle (\Delta a_i^\dagger a_i)^2 \rangle \tag{7.10}$$

where $\Delta \hat{A} = \hat{A} - \langle \hat{A} \rangle$).

In order to construct the Krauss operator we need to specify the apparatus state $|\phi_0\rangle$. Let us assume it is a vacuum state so that

$$\hat{\Upsilon}(n) = \langle n | e^{-ix(a^\dagger b + ab^\dagger)} |0\rangle\ , \tag{7.11}$$

Using the disentangling identity

$$e^{-ix(a^\dagger b + ab^\dagger)} = e^{-i\mu a b^\dagger} e^{\nu(b^\dagger b - a^\dagger a)/2} e^{i\mu a^\dagger b} \tag{7.12}$$

where $\mu = \tan x$ and $\nu = -\ln(\cos x)$. Thus

$$\hat{\Upsilon}(n) = \frac{1}{\sqrt{n!}} (1-\eta)^{n/2} (\eta)^{a^\dagger a/2} a^n \tag{7.13}$$

with $\eta = \cos^2 x$. Thus

$$\mathrm{P}(n) = \sum_{m=0}^{\infty} \binom{m+n}{n} \eta^m (1-\eta)^n p_{m+n} \tag{7.14}$$

where $p_m = \langle m | \rho_{a,i} | m \rangle$ is the photon number distribution of the input state to mode-a. This is a Bernoulli deletion process in which the probability of deleting a single photon is $(1-\eta)$ and every photon deleted is counted. It then follows that the mean and variance of the measurement results are

$$\mathbb{E}[n] = (1-\eta)\langle a_i^\dagger a_i \rangle \tag{7.15}$$
$$\mathbb{V}[n] = (1-\eta)^2 \langle \Delta (a_i^\dagger a_i)^2 \rangle \tag{7.16}$$

as expected.

Let us look at the conditional states, heralded by a particular count on the probe. We can also interpret this method as a photon subtraction scheme as the probe mode is always in the vacuum state, any count other than zero must subtract photons from

the signal mode. This is easily seen when the signal state is a number state. In the case of an initial coherent state for the signal we find that the state is unchanged. This is a typical result for a Poisson distribution. Subtracting a single photon from a squeezed vacuum state creates a cat-state.

Another important case arises when the probe is prepared in a Fock state $|m\rangle$ and the readout is n [1]. This is the basis of linear optical quantum computing considered in Chap. 15. Define

$$\hat{\Upsilon}(n|m) = \langle n|e^{-i\theta(a^\dagger b + ab^\dagger)}|m\rangle \,, \tag{7.17}$$

Some examples are

$$\begin{aligned}
\hat{\Upsilon}(0|0) &= \sum_{n=0}^{\infty} \frac{(\cos\theta - 1)^n}{n!}(a_1^\dagger)^n a_1^n =: \; e^{-ln(\cos\theta)a_1^\dagger a_1} \; : \\
\hat{\Upsilon}(1|1) &= \cos\theta \hat{E}(0|0) - \sin^2\theta a_1^\dagger \hat{E}(0|0) a_1 \\
\hat{\Upsilon}(0|1) &= -a_1^\dagger \sin\theta \hat{E}(0|0) \\
\hat{\Upsilon}(1|0) &= \sin\theta \hat{E}(0|0) a_1
\end{aligned}$$

The Krauss operator $\hat{\Upsilon}(0|1)$ is called a photon addition process.

Another example is the two mode squeezing generator $\hat{G} = -i(a^\dagger b^\dagger - ab)$, sometimes called the anti-Stokes model, and again assume that the apparatus is prepared in the vacuum state $|\phi_0\rangle = |0\rangle$. We use the disentangling theorem

$$e^{-r(ab - a^\dagger b^\dagger)} = e^{-\tanh r a^\dagger b^\dagger} e^{-\ln\cosh r(a^\dagger a + b^\dagger b + 1)} e^{\tanh r ab} \tag{7.18}$$

to show that the Krauss operator for a count of n on mode-b is

$$\hat{\Upsilon}(n) = \frac{1}{\sqrt{n!}}(-\tanh r)^n a^{\dagger\, n/2} \mu^{aa^\dagger/2} \tag{7.19}$$

where $\mu = \mathrm{sech}^2 r$. The corresponding POVM for this measurement is

$$\hat{\Upsilon}^\dagger(n)\hat{\Upsilon}(n) = \frac{(\tanh r)^{2n}}{n!}(aa^\dagger)^n \mu^{aa^\dagger} \tag{7.20}$$

The probability for a measurement outcome n can be written as

$$\mathrm{P}(n) = \mathrm{tr}\left[\hat{\Upsilon}^\dagger(n)\hat{\Upsilon}(n)\rho\right] = \sum_{m=0}^{\infty} p(n|m)\, p_m \tag{7.21}$$

where $p_m = \langle m|\rho|m\rangle$ and the conditional probability is given by

$$p(n|m) = \binom{m+n}{m} \mu^{(m+1)}(1-\mu)^n \tag{7.22}$$

the mean and variance of the measurement outcomes are

$$\mathbb{E}[n] = \sinh^2 r \langle a_i a_i^\dagger \rangle \tag{7.23}$$

$$\mathbb{V}[n] = \sinh^4 r \mathbb{V}[a_i a_i^\dagger]_i + \mathbb{E}[n] \tag{7.24}$$

Then measurement statistics are responding to the anti-normally ordered number operator for the signal. The square of the signal-to-noise, in the limit of $r \to \infty$, is

$$SNR^2 = \frac{\langle a_i a_i^\dagger \rangle^2}{\mathbb{V}[a_i a_i^\dagger]} \tag{7.25}$$

7.2 Continuous Measurement: Photon Counting Measurement

Let us assume we have a single side cavity emitting radiation preferentially into one spatial output mode directed into a photon counter, see Fig. 7.2, and that every photon lost is counted. What is the conditional state of the cavity at time t, when $n(t)$ photons have been counted? It is clearly not projected into the state $|n\rangle$. Whatever state it started in, it must have n photons less.

At first sight, the master equation for the cavity field

$$\frac{d\rho}{dt} = \kappa(2a\rho a^\dagger - a^\dagger a\rho/2 - \rho a^\dagger a/2) \tag{7.26}$$

does not help us answer this question. However there is an interesting way to write solution to the master equation written in terms of the number of photon lost from the cavity [2,3]

$$\rho(t) = \sum_{n=0}^{\infty} \mathcal{N}_n(t)\rho(0) \tag{7.27}$$

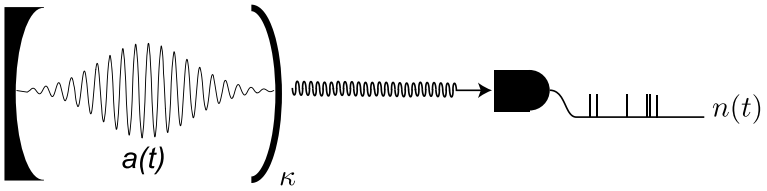

Fig. 7.2 A single sided cavity emitting photon directed towards a photon counter. The cavity decay rate is κ and $n(t)$ photons are counted in time t after an initial state $|\psi(0)\rangle$ was prepared in the cavity at $t = 0$

where the super-operator is defined by

$$\mathcal{N}_n(t)\rho = \int_0^t dt_n \int_0^{t_n} dt_{n-1} \ldots \int_0^{t_2} dt_1 \mathcal{S}(t-t_n)\mathcal{J}\mathcal{S}(t_n-t_{n-1}) \ldots \mathcal{S}(t_2-t_1)\mathcal{J}\mathcal{S}(t_1)\rho \tag{7.28}$$

where

$$\mathcal{J}\rho = \kappa a \rho a^\dagger \tag{7.29}$$

$$\mathcal{S}(t)\rho = e^{-\kappa t a^\dagger a/2}\rho e^{-\kappa t a^\dagger a/2} \tag{7.30}$$

The operation $\mathcal{J}$ is called the jump operation. This solution can be verified by differentiating with respect to time. We can confirm the interpretation of this form by considering the case $\rho(0) = |N\rangle\langle N|$. Substituting and performing the time ordered integrals we get

$$\rho(t) = \sum_{n=0}^{N} \binom{N}{n} \eta(t)^n (1-\eta(t))^{N-n} |N-n\rangle\langle N-n|. \tag{7.31}$$

where

$$\eta(t) = 1 - e^{-\kappa t} \tag{7.32}$$

We used the important result

$$\int_0^t dt_n \int_0^{t_n} dt_{n-1} \ldots \int_0^{t_2} dt_1 f(t_1) f(t_2) \ldots f(t_n) = \frac{1}{n!}\left(\int_0^t dt' f(t')\right)^n \tag{7.33}$$

This describes a Bernoulli deletion process in which n photons are lost in time, t leaving $N-n$ and the probability for each deletion is $\eta(t)$. As we assumed every photon lost is counted then the probability that m photons are counted is

$$p_n(t) = \binom{N}{n} \eta(t)^n (1-\eta(t))^{(N-n)} = \mathrm{tr}\,[\mathcal{N}_n(t)\rho] \tag{7.34}$$

We can interpret each term in (7.28) as the unnormalised conditional state of the cavity given that m photons are counted where the normalisation is just $p_n(t)$. Comparing this to (2.103) we see that when $\kappa t \ll 1$ we can interpret $\eta(t)$ as the quantum efficiency for the continuous photon counting process.

There is an alternative way to write the solution in (7.31),

$$\rho(t) = \sum_{k=0}^{\infty} \Upsilon_k(t)\rho(0)\Upsilon_k^\dagger(t) \tag{7.35}$$

where

$$\Upsilon_k(t) = \frac{1}{\sqrt{k!}}(\eta(t))^{k/2}(1-\eta(t))^{a^\dagger a/2}a^k \tag{7.36}$$

The conditional state, given a count k is

$$\rho(t|k) = [p_k(t)]^{-1}\Upsilon_k(t)\rho(0)\Upsilon_k^\dagger(t) \tag{7.37}$$

where

$$p_k(t) = \mathrm{tr}[\Upsilon_k^\dagger(t)\Upsilon_k(t)\rho(0)] \tag{7.38}$$

The form in (7.35) represents a general representation for measurement processes [4]. The operators Υ_k are called Krauss operators, labelled by the measurement result k. The Krauss form given in (7.35) is called the damping channel. It corresponds to the single shot measurement model discussed in the previous section.

The count as a function of time for the situation depicted in Fig. 7.2 is a classical stochastic process, a Poisson process [6]. In a time interval between t and $t+dt$, we either get no counts or a single count. This is a classical random variable $dN(t)$ such that $dN(t)^2 = dN(t)$. We now define the infinitesimal Krauss operators for these mutually exclusive outcomes

$$\begin{aligned}\hat{M}_1(dt) &= \sqrt{\kappa dt}\, a \\ \hat{M}_0(dt) &= \hat{1} - (\hat{R}/2 + i\hat{H}/\hbar)dt\end{aligned} \tag{7.39}$$

where $\hat{H}$ is the Hamiltonian and

$$\hat{R} = \kappa a^\dagger a \tag{7.40}$$

which implies that

$$\hat{M}_0^\dagger(dt)\hat{M}_0(dt) + \hat{M}_1^\dagger(dt)\hat{M}_1(dt) = \hat{1}. \tag{7.41}$$

to linear order in dt.

The probability for the result $dN(t) = 1$ is

$$p_1(dt) = \mathrm{Tr}[\mathcal{J}[\hat{M}_1(dt)]\rho] = \kappa dt\,\mathrm{tr}[a^\dagger a\rho], \tag{7.42}$$

while the probability for the result $dN(t) = 0$ is

$$p_0(dt) = \mathrm{Tr}[\mathcal{J}[\hat{M}_0(dt)]\rho] = 1 - \kappa dt\,\mathrm{tr}[a^\dagger a\rho], \tag{7.43}$$

For almost all infinitesimal time intervals, the measurement result is $dN(t) = 0$, a null result.

The state at time $t+dt$, averaging over all possible results, is

$$\rho(t+dt) = \sum_r \mathcal{J}[\hat{M}_r(dt)]\rho(t). \tag{7.44}$$

where

$$\mathcal{J}[\hat{A}]\rho = \hat{A}\rho\hat{A}^\dagger \tag{7.45}$$

When $dN(t) = 1$, the state vector changes to

$$|\psi_1(t+dt)\rangle = \frac{\hat{M}_1(dt)|\psi(t)\rangle}{\sqrt{\langle\hat{M}_1^\dagger(dt)\hat{M}_1(dt)\rangle}} = \frac{a|\psi(t)}{\sqrt{\langle a^\dagger a\rangle}} \tag{7.46}$$

If there is no detection, $dN(t) = 0$,

$$|\psi_0(t+dt)\rangle = \frac{\hat{M}_0(dt)|\psi(t)\rangle}{\sqrt{\langle\hat{M}_0^\dagger(dt)\hat{M}_0(dt)\rangle}} \tag{7.47}$$

$$= \left\{1 - dt\left[iH/\hbar + \frac{1}{2}\kappa a^\dagger\hat{a} - \frac{1}{2}\kappa\langle a^\dagger a\rangle\right]\right\}|\psi(t)\rangle, \tag{7.48}$$

where the denominator has been expanded to first order in dt to yield the term, $\langle a^\dagger a\rangle|\psi(t)\rangle = \langle\psi(t)|a^\dagger a|\psi(t)\rangle|\psi(t)\rangle$ which is non linear in the conditional state at time t.

We can write this in terms of $dN(t)$ as the stochastic evolution equation,

$$d|\psi(t)\rangle = \left[dN(t)\left(\frac{a}{\sqrt{\langle a^\dagger a\rangle}} - 1\right)\right. \tag{7.49}$$

$$\left. + dt\left(\frac{\kappa\langle a^\dagger a\rangle}{2} - \frac{\kappa a^\dagger a}{2} - i\hat{H}/\hbar\right)\right]|\psi(t)\rangle. \tag{7.50}$$

As this preserves the purity of the state we refer to it as a *stochastic Schrödinger equation* (SSE). Purity is preserved as we have complete information about the measurement record in terms of $dN(t)$. If the system started as a mixed state, we would not be able to write this as a stochastic equation for a pure state but a stochastic master equation. It takes the form

$$d\rho_c(t) = -\frac{i}{\hbar}[H, \rho_c(t)]dt + dN(t)\mathcal{G}[a]\rho_c(t) - \frac{1}{2}\kappa dt\mathcal{H}[a^\dagger a]\rho_c(t) \tag{7.51}$$

where we define the super operators

$$\mathcal{G}[A]\rho = \frac{A\rho A^\dagger}{\mathrm{tr}[A\rho A^\dagger]} - \rho \tag{7.52}$$

$$\mathcal{H}[A]\rho = A\rho + \rho A^\dagger - \mathrm{tr}[A\rho + A^\dagger\rho]\rho \tag{7.53}$$

In the interaction picture, without coherent driving, the stochastic differential equation for the conditional photon number distribution $p_{c,n} = \langle n|\rho_c|n\rangle$ is given by

$$dp_{c,n} = dN(t)\left(\frac{(n+1)p_{c,n+1}}{\bar{n}_c} - p_{c,n}\right) - \kappa dt(n - \bar{n}_c)p_{c,n} \tag{7.54}$$

where

$$\bar{n}_c = \sum_{n=0}^{\infty} n p_{c,n} \tag{7.55}$$

is the conditional mean of the photon number. Averaging over the noise gives the unconditional master equation

$$\frac{dp_n}{dt} = \kappa(n+1)p_{n+1} - \kappa n p_n \tag{7.56}$$

The conditional mean photon number then obeys the stochastic differential equation

$$d\bar{n}_c = dN(t)\left(\frac{\mathbb{V}_c[n]}{\bar{n}_c} - 1\right) - \kappa dt \mathbb{V}_c[n] \tag{7.57}$$

this becomes deterministic if the conditional distribution is Poissonian. Then, if the system starts in a Poisson distribution (e.g., a coherent state), it remains in a coherent state. If the system starts in a number state, the variance is zero and the conditional dynamics is entirely stochastic

$$d\bar{n}_c = -dN(t) \tag{7.58}$$

indicating that the conditional photon number decreases by one every time a photon is counted.

7.2.1 Output Correlations Functions for Photon Counting

The output current from direct detection is given by

$$I(t) = r\int_{-\infty}^{t} e^{-r(t-t')}dN(t') \tag{7.59}$$

where r is an inverse response time determined by the circuit in which the photoelectron counter is embedded and we have set the electric charge $e = 1$. This measures the current in units of photoelectrons per second. This is stochastic process with mean current given by

$$\mathbb{E}[I(t)] = r\kappa\int_{-\infty}^{t} e^{-r(t-t')}\langle a^{\dagger}(t')a(t')\rangle dt' \tag{7.60}$$

In the limit of of fast response $r \gg \kappa$ this is approximated by

$$\mathbb{E}[I(t)] = \kappa \langle a^\dagger(t) a(t) \rangle \tag{7.61}$$

We now define the stationary two-time correlation function as the average current at time $\tau > t$ given a photon was counted at time t. This is a conditional average and is given by [4],

$$\mathbb{E}[I(t+\tau)I(t) = \mathrm{tr}[a^\dagger a e^{\mathcal{L}\tau} a\rho(t)a^\dagger] + \mathrm{tr}[a^\dagger a \rho(t)]\delta(\tau) \tag{7.62}$$

The first term has the following interpretation. At time t the system state is $\rho(t)$ at which point one photon was counted. The unnormalised conditional state given this event is $a\rho(t)a^\dagger$. We then evolve the state forward under the dissipative dynamics, ignoring all counts, and ask for the rate of detecting a photon at time $t+\tau$. The last term arises as, at $\tau = 0, dN(t)^2 = dN(t)$ and corresponds to the shot noise term. At finite response rate r, the delta-function becomes bounded function. Finally, if there is a stationary state, we can substitute $\rho(t) \to \rho_{ss}$ where $\mathcal{L}\rho_{ss} = 0$.

7.3 Continuous Measurement: Homodyne and Heterodyne Detection

Continuous photon counting is a measurement of the intensity of the field emitted by the source. We can also make direct measurements of the electric field emitted by a source. This requires a phase and frequency reference called the *local oscillator*. We will agin consider the source to be a single side cavity.

Phase-dependent measurement is based on optical interference as discussed in Sect. 2.9. A signal field, with carrier frequency Ω_s is mixed with a strong coherent field—the local oscillator (LO)—with carrier frequency Ω_{LO} on a 50/50 beam splitter. A relative phase shift is introduced between the signal and LO. If $\Omega_s = \Omega_{LO}$ we have homodyne detection. If the signal and LO carrier are detuned, we have heterodyne detection. The output from the beam splitter are directed onto photo-detectors and the resulting signal currents are combined on a signal processor that outputs a difference current; the measurement signal. The scheme is depicted in Fig. 7.3.

We will assume that the source of the signal is a single-sided cavity with linewidth κ. The corresponding conditional master equation for homodyne detection is [4]

$$d\rho_c(t) = -\frac{i}{\hbar}[H, \rho_c]dt + \kappa \mathcal{D}[a]\rho_c(t)dt + \sqrt{\kappa} dW(t) \mathcal{H}[a e^{-i\phi}]\rho_c(t) \tag{7.63}$$

where $dW(t)$ is the Weiner increment, the phase-shift between the signal and the LO is ϕ, and the super operators are defined in (7.53). The corresponding homodyne current satisfies the Ito stochastic equation

$$J(t)dt = \kappa \langle a e^{-i\phi} + a^\dagger e^{i\phi} \rangle_c dt + \sqrt{\kappa} dW(t) \tag{7.64}$$

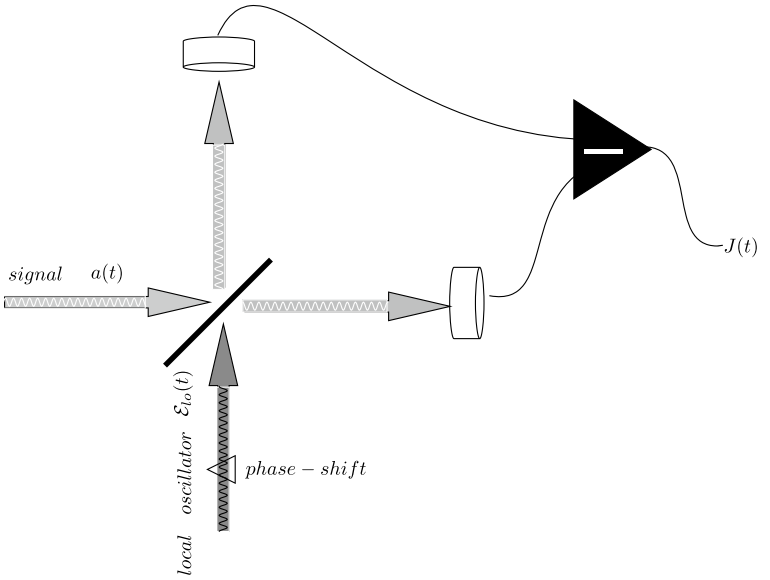

Fig. 7.3 A balanced homodyne or heterodyne detection scheme for making phase-dependent measurements on a signal field $a(t)$ using a strong coherent field called the local oscillator, $\mathcal{E}_{LO}(t)$

depends on the conditional average of the quadrature amplitude operator $ae^{-i\phi} + a^{\dagger}e^{i\phi}$ for the cavity field.

In the case of the difference current is modulated at the detuning frequency $\Delta = \Omega_s - \Omega_{LO}$. We then form the Fourier components in the signal processing

$$J_x(t) = \frac{1}{\delta t}\int_t^{t+\delta t} 2\cos(\Delta s)J(s)ds \tag{7.65}$$

$$J_y(t) = -\frac{1}{\delta t}\int_t^{t+\delta t} 2\sin(\Delta s)J(s)ds \tag{7.66}$$

To lowest order in the averaging time δt these are given by

$$J_x(t)dt = \kappa\langle a + a^{\dagger}\rangle dt + \sqrt{2\kappa}dW_x(t) \tag{7.67}$$

$$J_y(t)dt = -i\kappa\langle a - a^{\dagger}\rangle dt + \sqrt{2\kappa}dW_y(t) \tag{7.68}$$

where $dW_x(t), dW_y(t)$ are independent Weiner increments. It is conventional to combine these into a single complex measurement current

$$J_{het}dt = \frac{1}{2}(J_x(t) + iJ_y(t))dt = \kappa\langle a\rangle dt + \sqrt{\kappa}dZ(t) \tag{7.69}$$

where we define the complex Weiner increment,

$$dZ(t) = \frac{1}{\sqrt{2}}(dW_x(t) + idW_y(t)) \tag{7.70}$$

The corresponding conditional master equation is

$$d\rho_c(t) = -\frac{i}{\hbar}[H, \rho_c]dt + \kappa\mathcal{D}[a]\rho_c dt + \sqrt{\kappa}\mathcal{H}[dZ^*(t)a]\rho_c \tag{7.71}$$

7.3.1 Squeezing Spectrum

In the laboratory the noise power spectrum of the homodyne and heterodyne current give important information on the quantum noise in the output field and enable us to define the squeezing spectra calculated in Sect. 6.5. We first define the two-time correlation function for the homodyne current in the case of a photo-detector with very fast response time. As in the case of direct photo currents this is effectively a conditional average. It is given by [4]

$$\mathbb{E}[J_{hom}(t+\tau)J_{hom}(t)] = \kappa^2 \mathrm{tr}\left[\hat{X}_\theta e^{\mathcal{L}\tau}\left(a\rho(t)e^{i\theta} + \rho(t)a^\dagger e^{-i\theta}\right)\right] + \kappa\delta(\tau) \tag{7.72}$$

where

$$\hat{X}_\theta = ae^{i\theta} + a^\dagger e^{-i\theta} \tag{7.73}$$

The stationary two-time correlation function is obtained by $\rho(t) \to \rho_{ss}$ where $\mathcal{L}\rho_{ss} = 0$. The corresponding stationary spectrum is defined by

$$S_{hom}(\omega)/\kappa = \lim_{t\to\infty}\int_{-\infty}^{\infty} d\tau e^{-i\omega\tau}\mathbb{E}[J_{hom}(t+\tau)J_{hom}(t)] \tag{7.74}$$

$$= 1 + \int_{-\infty}^{\infty} d\tau e^{-i\omega\tau}\,\mathrm{tr}\left[\hat{X}_\theta e^{\mathcal{L}\tau}\left(a\rho_{ss}e^{i\theta} + \rho_{ss}a^\dagger e^{-i\theta}\right)\right] \tag{7.75}$$

This is known as the squeezing spectrum.

In the case of heterodyne detection, the stationary two-time correlation function is [4]

$$\mathbb{E}[J_{het}(\tau)^* J_{het}(0)] = \kappa\mathrm{tr}[a^\dagger e^{\mathcal{L}\tau}a\rho_{ss}] + \kappa\delta(\tau) \tag{7.76}$$

the first term is Glauber's first-order coherence function $G^{(1)}(\tau)$ in the steady state. The stationary power spectrum is

$$P(\omega) = \frac{\kappa}{2\pi}\int_{-\infty}^{\infty} d\tau e^{-i\omega\tau}\mathrm{tr}[a^\dagger e^{\mathcal{L}\tau}a\rho_{ss}] \tag{7.77}$$

Integrating this over all frequencies gives the total flux as $P = \kappa\langle a^\dagger a\rangle_{ss}$.

7.4 Continuous Measurement: Non-absorbing Photon Detection

We can use the homodyne detection process to design a non absorbing photon detector. The first step is to couple the signal cavity to a probe cavity via the cross-Kerr interaction

$$H_K = \hbar\chi a^\dagger a b^\dagger b \tag{7.78}$$

where a, b are the annihilation operators for the signal and probe cavity modes respectively. This describes a mutual phase shift of each mode proportional to the photon number in the other mode. The interaction Hamiltonian commutes with the free Hamiltonian for each mode. In order to configure the probe mode as a measurement apparatus we need to add a coherent driving term that is detuned by $\Delta = \omega_b - \omega_d$ from the probe cavity frequency. The total interaction Hamiltonian then takes the form.

$$H_I = \hbar\Delta b^\dagger b + \hbar\epsilon(b + b^\dagger) + \hbar\chi a^\dagger a b^\dagger b \tag{7.79}$$

Including dissipation the master equation for the signal-probe, the total master equation is

$$\frac{d\rho}{dt} = -\frac{i}{\hbar}[H_I, \rho] + \kappa_a \mathcal{D}[a]\rho + \kappa_b \mathcal{D}[b]\rho \tag{7.80}$$

The corresponding quantum Langevin equations are

$$\frac{da}{dt} = -i(\Delta + \chi b^\dagger b)a - \frac{\kappa_a}{2}a + \sqrt{\kappa_a}a_{in} \tag{7.81}$$

$$\frac{db}{dt} = -i\chi a^\dagger a b - i\epsilon - \frac{\kappa_b}{2}b + \sqrt{\kappa_b}b_{in} \tag{7.82}$$

We assume that the probe cavity is strongly damped, $\kappa_b \gg \kappa_a, \chi$, and thus the probe dynamics is slaved to the signal mode. This enables us to use adiabatic elimination of the probe mode from the dynamics. In the absence of the cross Kerr coupling the probe mode relaxes to a coherent state with amplitude

$$\beta_0 = -\frac{2i\epsilon}{\kappa_b} \tag{7.83}$$

To lowest order in χ this leads to a shift in the detuning of the signal mode

$$\Delta \to \Delta + \chi|\beta_0|^2. \tag{7.84}$$

There is also a fluctuating component contribution to the detuning due to number fluctuations in the probe mode number. As this is approximated by a coherent state with amplitude β_0, these fluctuations are Poisson distributed. This means the frequency of the signal mode is fluctuating and should be described by the phase diffusion model (10.32).

We can incorporate both the systematic and noise contributions by the replacement

$$b \to \beta_0(1 - \frac{2i\chi}{\kappa_b}a^\dagger a) \tag{7.85}$$

This makes it clear that the signal number implements a phase shift on the probe mode. We can then use homodyne detection on the probe output to effect a signal number measurement that is not based on absorption.

To lowest order in χ the stochastic master equation for the probe takes the form,

$$\frac{d\rho}{dt} = -\frac{i}{\hbar}[H_a, \rho] + \kappa_a \mathcal{D}[a]\rho + \Gamma \mathcal{D}[a^\dagger a]\rho + \sqrt{\Gamma} dW \mathcal{H}[a^\dagger a]\rho \tag{7.86}$$

where

$$\Gamma = \frac{4\chi^2|\beta_0|^2}{\kappa_b} \tag{7.87}$$

and we have made an appropriate change of phase for the LO phase shift. The corresponding homodyne current is

$$J(t)dt = \sqrt{\kappa_b \Gamma}\left(\bar{n}_c(t)dt + \sqrt{\frac{1}{\Gamma}}dW(t)\right) \tag{7.88}$$

where

$$\bar{n}_c(t) = \mathrm{tr}\langle a^\dagger a\rangle_c \tag{7.89}$$

is the conditional mean number. This makes it clear that the signal-to noise-ratio improves as Γ increases.

The Lindbald term proportional to Γ diagonalises the density operator in the eigenstates of the probe number, the measured operator, at the rate $\Gamma/2$. This is what one expects for a continuous measurement of photon number. As a large signal to noise ratio corresponds to large Γ we see that the better the measurement the faster the diagonalisation. The stochastic dynamics tends to force the system into an eigenstate of photon number. To see this we can use the stochastic master equation to write a stochastic Markov process for the conditional number distribution of the signal mode $p_{c,n} = \langle n|\rho|n\rangle$. Ignoring the free dynamics, we find that

$$dp_{c,n} = \kappa_a(n+1)p_{c,n+1} - \kappa n p_{c,n} + \sqrt{\Gamma}(n - \bar{n}_c)p_{c,n}dW(t) \tag{7.90}$$

The conditional mean thus obeys the stochastic differential equation

$$d\bar{n}_c(t) = -\kappa_a \bar{n}_c(t)dt + \sqrt{\Gamma}\mathbb{V}_c[n]dW \tag{7.91}$$

where $\mathbb{V}_c[n]$ is the conditional variance in the population number. If the system ends up in a number state, this equation becomes deterministic. If we can approximate the conditional state by a Poisson distribution the resulting stochastic differential equation corresponds to geometric Brownian motion, a key equation in financial mathematics. The conditional mean is entirely deterministic, a defining idea in the definition of a quantum non demolition measurement (QND).

7.5 Quantum Non Demolition Measurements (QND)

The concept of quantum nondemolition measurements was introduced in the context of detection of gravitational waves [8]. Gravitational waves interact so weakly with terrestrial detectors that a displacement of the order of 10^{-19} cm is expected. This requires the detection of very weak forces, below the level of quantum noise in the detector.

The basic requirement of a QND measurement is the availability of a variable which may be measured repeatedly giving predictable results in the absence of external forces. Clearly this requires that the act of measurement itself does not degrade the predictability of subsequent measurements. Then, in a sufficiently long sequence of measurements, the output becomes predictable. This requirement is satisfied if for an observable $A^I(t)$ (in the interaction picture)

$$[A^I(t), A^I(t')] = 0 \tag{7.92}$$

The condition ensures that if the system is in an eigenstate of $A^I(t_0)$ it remains in this eigenstate for all subsequent times although the eigenvalues may change. Such observables are called QND observables. Clearly constants of motion will be QND observables.The continuous, non absorbing number measurement discussed in Sect. 7.4 is an example.

Having first determined the QND variables of the detector it is necessary to couple the detector to a readout system or meter. It is essential that the coupling to the meter does not feed back fluctuations into the QND variable of the detector. In order to avoid this it is sufficient if the QND variable A commutes with the Hamiltonian coupling the system and the apparatus

$$[A, H_{SA}] = 0 \tag{7.93}$$

This is known as the back action evasion criterion. In this chapter we are primarily concerned with QND measurements on optical systems. This requires a slight change in nomenclature. We will refer to the field with respect to which the QND variable is defined as the 'signal' rather than the system, and the field upon which measurements are ultimately made as the 'probe' rather than the apparatus.

In the case of a harmonic oscillator, we can define two canonically conjugate operators that are explicitly time dependent in the Schrödinger picture,

$$X_1(t) = \; ae^{i\Omega t} + a^\dagger e^{-i\Omega t} \tag{7.94}$$

$$X_2(t) = \; -i(ae^{i\Omega t} + a^\dagger e^{-i\Omega t}) \tag{7.95}$$

These are constants of motion as

$$\frac{dX_j(t)}{dt} = -i\Omega[a^\dagger a, X_j(t)] + \frac{\partial X_j(t)}{\partial t} = 0 \tag{7.96}$$

7.6 Criteria for a QND Measurement

We need to clearly define the objectives of a quantum nondemolition measurement in an optical context. These objectives may differ depending on the situation of the measurement. For example, in a transmission with a series of receivers, the goal may be to tap information from the signal, without degrading the signal transmitted to the next receiver. In a system used to measure the magnitude of an external force the goal of the measurement may be state preparation. That is an initial measurement prepares the system in a known quantum state. The presence of the perturbing force will be detected by a subsequent measurement on the system. In order to evaluate the merits of a measurement scheme we shall define a set of criteria for a good measurement. We begin by considering the general measurement scheme depicted in Fig. 7.4 where an observable X_{in} of the input signal is determined by a measurement of an observable Y_{out} of the output probe.

The measurement may be characterised by the following criteria:

1. How good is the measurement scheme?
   This is determined by the level of correlation between the probe field measured by a detector and the signal field incident on the apparatus. The appropriate correlation function is,

$$\mathbb{C}[X_{in}, Y_{out}] = \frac{|\langle X_{in} Y_{out}\rangle_S - \langle X_{in}\rangle\langle Y_{out}\rangle|^2}{\mathbb{V}[X_{in}]\mathbb{V}[Y_{out}]} \tag{7.97}$$

   where $\langle AB\rangle_S \equiv \langle AB + BA\rangle/2$ and $\mathbb{V}[A] = \langle A^2\rangle - \langle A\rangle^2$ is the variance of A. For a perfect measurement device the phase quadrature of the probe output is equal to the amplitude quadrature of the signal input multiplied by the QND gain, plus the input probe phase quadrature. In this case the correlation coefficient defined above is unity, for large gain.
2. How much does the scheme degrade the signal?
   The quantity of interest here is the correlation between the signal input field and the signal output field:

$$\mathbb{C}[X_{in}, X_{out}] = \frac{|\langle X_{in} X_{out}\rangle_S - \langle X_{in}\rangle\langle X_{out}\rangle|^2}{\mathbb{V}[X_{in}]\mathbb{V}[X_{out}]} \tag{7.98}$$

   This is a measure of the back action evasion, that is the ability of the scheme to isolate quantum noise introduced by the measurement process from the observable

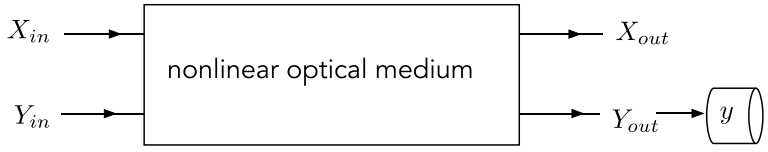

Fig. 7.4 General scheme for a QND measurement in an optical context. The actual observed value on the probe output is y, a random variable

of interest. For an ideal QND scheme we require this correlation to be unity. Thus, for a perfect QND scheme we have

$$\mathbb{C}[X_{in}, Y_{out}] + \mathbb{C}[X_{in}, X_{out}] = 2 \tag{7.99}$$

3. How good is the scheme as a state preparation device?
If we have a perfect measurement device that does not degrade the signal at all, we satisfy the two previous criteria exactly. These criteria can be calculated regardless of the actual measurement result. They refer to the unconditional moments of the output state. The ideal for a QND measurement is that given a measurement result we should be able to predict the conditional result of future measurements. We need to determine the conditional states after the measurements conditioned on the measurement result, say y, to answer this question. The ideal case would see the conditional state of the signal become an eigenstate of the measured quantity. This may be impossible, for example in the case of the QND observables $X_1(t)$, $X_2(t)$. Thus as a measure of how well the scheme prepares eigenstates at the output we need to consider the conditional variance $\mathbb{V}[X_{out}|y]$. In Sect. 7.1 we saw that the conditional state of the signal is given in terms of the Krauss operator $\hat{\Upsilon}(y)$

$$\rho_{S,out}^{(y)} = \frac{\hat{\Upsilon}(y)\rho_{S,in}\hat{\Upsilon}^{\dagger}(y)}{P(y)} \tag{7.100}$$

where the distribution of measurement results is

$$P(y) = \mathrm{tr}[\hat{\Upsilon}^{\dagger}(y)\hat{\Upsilon}(y))\rho_{S,in}] \tag{7.101}$$

The conditional variance is then given by

$$\mathbb{V}[X_{out}|y] = \mathrm{tr}[\rho_{S,out}^{(y)}X^2] - \mathbb{E}[X_{out}|y]^2 \tag{7.102}$$

where the conditional mean is given by

$$\mathbb{E}[X_{out}|y] = \mathrm{tr}[\rho_{S,out}^{(y)}X] \tag{7.103}$$

In many cases of interest we are dealing with Gaussian states and one can show (see Exercise 7.5) that the conditional variance does not depend on the measurement result, then

$$\mathbb{V}[X_{out}|y] = \mathbb{V}[X_{out}](1 - \mathbb{C}[X_{out}, Y_{out}]) \tag{7.104}$$

where

$$\mathbb{C}[X_{out}, Y_{out}] = \frac{|\langle X_{out}Y_{out}\rangle_S - \langle X_{out}\rangle\langle Y_{out}\rangle|^2}{\mathbb{V}[X_{out}]\mathbb{V}[Y_{out}]} \tag{7.105}$$

Thus, the condition for a perfect state reduction in these cases is

$$\mathbb{C}[X_{out}, Y_{out}] \to 1 \tag{7.106}$$

As an example we consider a perfect QND measurement of the quadrature phase of a single mode field.We shall assume that the amplitude quadratures of each mode are coupled with the interaction Hamiltonian

$$H_I = \hbar\chi(a + a^\dagger)(b + b^\dagger) = \hbar\chi X_a X_b \tag{7.107}$$

where a/b is the annihilation operator for the signal/probe, and $X_a = a + a^\dagger,\ X_b = b + b^\dagger$ are the signal and probe quadratures respectively. Clearly X_a is a constant of the motion and a QND variable. The interaction is also back action evading. Solving the Heisenberg equations of motion over a time T we get

$$X_{a,out} = X_{a,in} \tag{7.108}$$

$$Y_{b,out} = Y_{b,in} + GX_{a,in} \tag{7.109}$$

where $Y_b = -i(b - b^\dagger)$ is canonically conjugate to X_b and the gain is $G = 2\chi T$. We will refer to X_a as the signal quadrature and assume it has a non zero mean. We will treat Y_b as the probe quadrature and assume it has zero mean.

Clearly $\mathbb{C}[X_{a,in}, X_{a,out}] = 1$ and the signal quadrature is unaffected by the measurement. The correlation

$$\mathbb{C}[X_{in}, Y_{out}] = \frac{G^2\mathbb{V}[X_{a,in}]}{G^2\mathbb{V}[X_{a,in}] + \mathbb{V}[Y_{b,in}]} \tag{7.110}$$

If the gain is very large $\mathbb{C}[X_{in}, Y_{out}] \to 1$. The conditional variance of the output, given a result y of a perfectly accurate measurement of $Y_{b,out}$ is independent of y and given by

$$\mathbb{V}[X_{out}|y] = \mathbb{V}[X_{a,in}]\left(1 - \frac{G^2\mathbb{V}[X_{a,in}]}{G^2\mathbb{V}[X_{a,in}] + \mathbb{V}[Y_{b,in}]}\right) \tag{7.111}$$

$$\sim \frac{\mathbb{V}[Y_{b,in}]}{G^2} \tag{7.112}$$

For large $G \gg 1$ this goes to a very small number. In the limit of high QND gain this device operates as a good state preparation device.

Finally, the performance of the measurement is the signal-to-noise ratio squared of the probe output

$$SNR^2 = \frac{\langle Y_{b,out}\rangle^2}{\mathbb{V}[Y_{b,out}]} \tag{7.113}$$

$$= \frac{G^2\langle X_{a,in}\rangle^2}{G^2\mathbb{V}[X_{a,in}] + \mathbb{V}[Y_{b,in}]} \tag{7.114}$$

$$\to \frac{\langle X_{a,in}\rangle^2}{\mathbb{V}[X_{a,in}]} \quad G \gg 1 \tag{7.115}$$

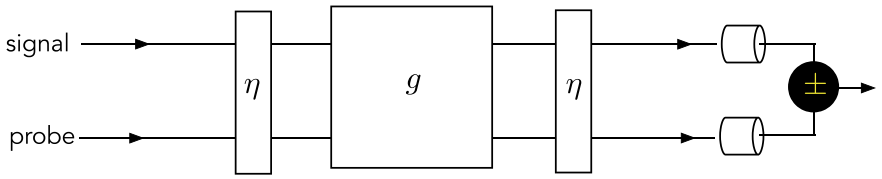

Fig. 7.5 Schematic representation of a perfect QND scheme based on a parametric interaction

In the limit of large QND gain the signal-to-noise ratio of the output probe is equal to that of the signal input.

It is possible to achieve a QND coupling of this form using beam splitters

$$a \to \sqrt{\eta}a + i\sqrt{1-\eta^2}\, b\,, \tag{7.116}$$

and parametric amplification $g = e^r$, see Fig. 7.5. When the beam splitter parameters can be matched to the gain by

$$\eta = \frac{(g+1)^2}{2(g^2+1)} \tag{7.117}$$

the transformations are given by the ideal case in (7.108)

$$G = (g - g^{-1}) \tag{7.118}$$

This experiment was first performed by LaPorta et al. [9].

7.7 Single-Shot QND Measurements of Photon Number

We return to the case of QND number measurements. The number operator is a constant of motion for a harmonic oscillator and thus a QND observable. The objective is to estimate the number of photons in a single cavity in fixed time interval without absorbing or exciting photons in the cavity. This requires that the interaction between the cavity and a probe is back action evading. See the experiment of Besse et al. [10].

Problems

7.1 If the cavity starts in a coherent state $|\alpha\rangle$ use (7.35) to show that it remains in a coherent state but the amplitude decays as $e^{-\kappa t/2}\alpha$.

7.2 Use (7.35) to consider the conditional states produced when the signal is prepared in a

a A coherent state
b A squeezed vacuum state,
c A thermal state.

7.3 Use (7.19) to consider the conditional states produced when the signal is prepared in a

a A coherent state
b A squeezed vacuum state,
c A thermal state.

7.4 Show that if the single-side is empty up to time $t = 0$ at which point one photon is injected into the cavity, the mean current is

$$\mathbb{E}[I(t)] = \kappa \frac{(e^{-\kappa t} - e^{-rt})}{1 - \kappa/r} \tag{7.119}$$

In the limit of infinite response rate this is simply $\kappa e^{-\kappa t}$ for $t > 0$.

7.5 Let the Krauss operator for the QND measurement in Sect. 7.6 be given by

$$\hat{\Upsilon}(y) = (2\pi\Delta)^{-1/4} e^{-(\hat{X}-y)^2/4\Delta} \tag{7.120}$$

and the input state be diagonal in X_{in} so that $P_{S,in}(x) = \langle x|\rho_{S,in}|x\rangle$ where $X_{in}|x\rangle = x|x\rangle$. Find $\mathbb{V}[X_{out}|y]$ and show that it is independent of y. Further show that

$$\mathbb{C}[X_{out}, Y_{out}] = \frac{\sigma}{\Delta + \sigma} \tag{7.121}$$

which goes to unity when the $\Delta \ll \sigma$. This means that the noise added by the probe is negligible.

References

1. G.J. Milburn, J. Opt. Soc. Am. B **24**, 167–170 (2007)
2. E.B. Davies, *Quantum Theory of Open Systems* (Academic Press, 1976)
3. M.D. Srinivas, E.B. Davies, J. Mod. Opt. **28**, 981 (1981)
4. H.M. Wiseman, G.J. Milburn, *Quantum Measurement and Control* (Cambridge University Press, 2010)
5. C.W. Gardiner, P. Zoller, *Quantum Noise* (Springer, 2004)
6. C.W. Gardiner, *Handbook of Stochastic Processes for Physics, Chemistry and the Natural Sciences*, 4th edn. (Springer, 2009)
7. M.C. Wang, G.E. Uhlenbeck, Rev. Mod. Phys. **17**, 323 (1945)

8. C.M. Caves, K.S. Thorne, R.W.P. Drever, V.P. Sandberg, M. Zimmerman, Rev. Mod. Phys. **52**, 341 (1980)
9. A. La Porta, R.E. Slusher, B. Yurke, Phys. Rev. Lett. **62**, 28 (1989)
10. J.-C. Besse, S. Gasparinetti, M.C. Collodo, T. Walter, P. Kurpiers, M. Pechal, C. Eichler, A. Wallraff, Phys. Rev. X **8**, 021003 (2018)

Nonlinear Quantum Dissipative Systems

8

Abstract

In this chapter we go beyond the linear quantum stochastic differential equations to treat non linear intracavity interactions. It is not possible, in general, to find exact solutions to the nonlinear quantum equations which arise in nonlinear optical interactions. It has, however, been possible to find solutions to some specific systems using the complex P representation. These solutions provide a test of the region of validity of the linearised solutions especially in the region of an instability. Furthermore they allow us to consider the situation where the quantum noise is large and may no longer be treated as a perturbation. In this case, manifestly quantum mechanical states may be produced in a nonlinear dissipative system.

8.1 Parametric Oscillator with Pump Depletion

We can give a quantum treatment of the parametric oscillator with a quantised pump mode using the generalised P representation. This is an interaction between the cavity field at frequency ω and a pump mode at frequency 2ω. It is often referred to as sub/second harmonic generation. We shall first solve for the steady state of the cavity mode (the sub-harmonic mode) using the complex P function when the pump mode can be adiabatically eliminated when it undergoes rapid damping. Then we show, using the positive P function, that the steady state sub-harmonic field is in a superposition state. We go on to calculate the tunnelling time between the two states in the superposition.

We consider the degenerate parametric oscillator with quantised pump described Drummond et al. [1]. The Hamiltonian is

$$\begin{aligned} H = \; & \hbar\omega a_1^\dagger a_1 + 2\hbar\omega a_2^\dagger a_2 + i\hbar\frac{\kappa}{2}(a_1^{\dagger\,2} a_2 - a_1^2 a_2^\dagger) \\ & + i\hbar(\epsilon a_2^\dagger e^{-2i\omega t} - \epsilon^* a_2 e^{2i\omega t}) \\ & + a_1\Gamma_1^\dagger + a_2\Gamma_2^\dagger + a_1^\dagger\Gamma_1 + a_2^\dagger\Gamma_2 \end{aligned} \tag{8.1}$$

D. F. Walls and G. J. Milburn, *Quantum Optics*, Graduate Texts in Physics,
https://doi.org/10.1007/978-3-031-84177-4_8

where a_1 and a_2 are the annihilation operators for two cavity modes of frequency ω and 2ω, respectively. The coupling constant for the nonlinear coupling between the modes is κ. The cavity is driven externally by a coherent driving field with frequency 2ω and amplitude ε_2. The bosonic bath operators describing the cavity damping of the two modes are Γ_1, Γ_2. The quantum Langevin equations in the interaction picture are

$$\frac{da_1}{dt} = \kappa a_1^\dagger a_2 - \gamma_1 a_1 + \sqrt{2\gamma_1}a_{1,in} \tag{8.2}$$

$$\frac{da_2}{dt} = -\frac{\kappa}{2}a_1^{\dagger\,2} - \gamma_2 a_2 + \epsilon + \sqrt{2\gamma_2}a_{2,in} \tag{8.3}$$

(Note that we have changed the convention for damping rates so that the line width of the cavity is $2\gamma_1$. This is the convention used in [1]). The corresponding master equation is

$$\frac{d\rho}{dt} = -\frac{i}{\hbar}[H, \rho] + 2\gamma_1 \mathcal{D}[a_1]\rho + 2\gamma_2 \mathcal{D}[a_2]\rho \tag{8.4}$$

The equation of evolution in the generalised P representation is

$$\begin{aligned}\frac{\partial P(\alpha)}{\partial t} = \Bigg\{ & \frac{\partial}{\partial \alpha_1}(\gamma_1\alpha_1 - \kappa\beta_1\alpha_2) + \frac{\partial}{\partial \beta_1}(\gamma_1\beta_1 - \kappa\alpha_1\beta_2) \\ & + \frac{\partial}{\partial \alpha_2}(\gamma_2\alpha_2 - \epsilon\alpha_1 - \kappa\alpha_1\beta_2) + \frac{\partial}{\partial \beta_2}(\gamma_2\beta_2 - \epsilon^*\alpha_1 + \frac{\kappa}{2}\beta_1^2) \\ & + \frac{1}{2}\left(\frac{\partial^2}{\partial \alpha_1^2}(\kappa\alpha_2) + \frac{\partial^2}{\partial \beta_1^2}(\kappa\beta_2)\right)\Bigg\} P(\alpha)\end{aligned} \tag{8.5}$$

The semiclassical deterministic equations of motion are

$$\frac{d\alpha_1}{dt} = \kappa\alpha_1^*\alpha_2 - \gamma_1\alpha_1 \tag{8.6}$$

$$\frac{d\alpha_2}{dt} = -\frac{\kappa}{2}\alpha_1^{*2} - \gamma_2\alpha_2 + \epsilon \tag{8.7}$$

there are two stable steady state solutions depending on whether the driving field amplitude is above or below the threshold amplitude $\varepsilon_c = \gamma_1\gamma_2/\kappa$. In particular, the steady states for the low frequency mode α_1 are

$$\alpha_1 = 0 \quad \epsilon < \epsilon_c \tag{8.8}$$

$$\alpha_1 = \pm\left[\frac{2}{\kappa}(\epsilon - \epsilon_c)\right]^{1/2} \tag{8.9}$$

The Fokker-Planck equation does not satisfy the potential conditions so we cannot easily find the steady state. However if we adiabatically eliminate the pump mode (the mode at frequency 2ω) we get a Fokker-Planck equation that does satisfy the potential conditions. We proceed by adiabatically eliminating the high-frequency mode. This

may be accomplished best in the Langevin equations equivalent to Fokker-Planck equation. These are

$$\frac{d}{dt}\begin{pmatrix}\alpha_1\\ \beta_1\end{pmatrix} = \begin{pmatrix}\kappa\beta_1\alpha_2 - \gamma_1\alpha_1 + \sqrt{\kappa\alpha_2}\eta_1(t)\\ \kappa\alpha_1\beta_2 - \gamma_1\beta_1 + \sqrt{\kappa\beta_2}\eta_2(t)\end{pmatrix}$$
$$\frac{d}{dt}\begin{pmatrix}\alpha_2\\ \beta_2\end{pmatrix} = \begin{pmatrix}\epsilon_2 - \frac{\kappa}{2}\alpha_1^2 - \gamma_2\alpha_2\\ \epsilon_2^* - \frac{\kappa}{2}\beta_2^2 - \gamma_2\beta_2\end{pmatrix}$$

where $\eta_1(t)$, $\eta_2(t)$ are noise terms that satisfy

$$\langle\eta_1(t)\rangle = \langle\eta_2(t)\rangle = \langle\eta_1(t)\eta_1(t')\rangle = \langle\eta_2(t)\eta_2(t')\rangle = 0, \quad \langle\eta_1(t)\eta_2(t')\rangle = \delta(t-t').$$

Under the conditions $\gamma_2 \gg \gamma_1$ we can adiabatically eliminate α_2, β_2 which gives the resultant Langevin equation for the cavity mode alone,

$$\frac{d}{d\tau}\begin{pmatrix}\alpha\\ \beta\end{pmatrix} = \begin{pmatrix}-\alpha - \beta(\lambda-\alpha^2)\\ -\beta - \alpha(\lambda-\beta^2)\end{pmatrix} + \begin{pmatrix}g\sqrt{(\lambda-\alpha^2)} & \eta_1(t)\\ g\sqrt{(\lambda-\beta^2)} & \eta_2(t)\end{pmatrix} \tag{8.10}$$

where we have changed variables $\tau = \gamma_1 t$, $\alpha = g\alpha_1$, $\beta = g\beta_1$ with

$$g = \frac{\kappa}{\sqrt{2\gamma_1\gamma_2}} \equiv \frac{1}{\mu} \tag{8.11}$$

The Fokker–Planck equation corresponding to these equations is

$$\frac{\partial P(\alpha,\beta)}{\partial\tau} = \left\{\frac{\partial}{\partial\alpha}\left[\alpha + \beta(\lambda-\alpha^2)\right] + \frac{\partial}{\partial\beta}\left[\beta + \alpha(\lambda-\beta^2)\right]\right. \tag{8.12}$$
$$\left. + \frac{g^2}{2}\frac{\partial^2}{\partial\alpha^2}\left[(\lambda-\alpha^2)\right] + \frac{g^2}{2}\frac{\partial^2}{\partial\beta^2}\left[(\lambda-\beta^2)\right]\right\} P(\alpha,\beta)$$

As the potential conditions are satisfied the steady state solution is then given by

$$P_{ss}(\alpha,\beta) = \mathcal{N}\left[(\lambda-\alpha^2)(\lambda-\beta^2)\right]^{1/g^2-1} e^{2\alpha\beta/g^2} \tag{8.13}$$

It is clear that this function diverges for the usual integration domain of the complex plane with $\beta_1 = \alpha_1^*$. The moments may, however, be obtained by use of the complex P representation and complex contour integration. The calculations are described in [2].

The semi-classical solution for the intensity exhibits a threshold behaviour at $\epsilon = \epsilon_c = \gamma_1\gamma_2/\kappa$. This is compared in Fig. 8.1 with the mean intensity $I = \mathbb{E}[\beta\alpha]$ calculated from the solution (8.13). The quantum calculation shows a feature never observed in a classical system where the mean intensity actually drops below the semi-classical intensity. This deviation from the semi-classical behaviour is most significant for small threshold photon numbers. As the parameter $\epsilon_c = \gamma_1\gamma_2/\kappa$ is increased the quantum mean approaches the semi-classical value.

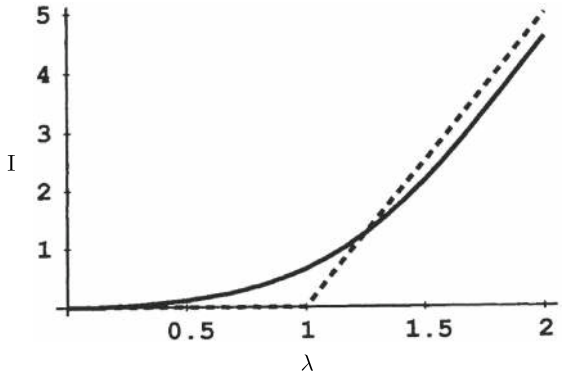

Fig. 8.1 Plot of the mean intensity for the degenerate parametric oscillator versus the scaled driving field $\lambda = \epsilon/\epsilon_c$. The dashed curve represents the semi-classical intensity, the solid curve is the exact quantum result. In both cases $2\epsilon_c/\kappa = 100$. Note that above threshold the exact quantum result is less than the semi-classical prediction

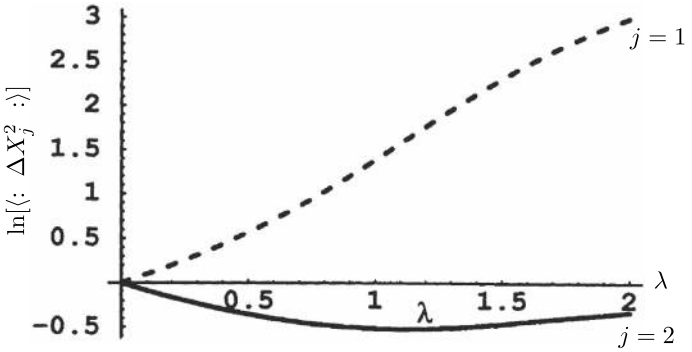

Fig. 8.2 The log of the normally ordered variance of the squeezed (solid) and unsqueezed (dashed) quadrature in a degenerate parametric amplifier versus the scaled driving field with $2\epsilon_c/\kappa = 5.0$. See [3]

The normally ordered variance of fluctuations in the quadratures $X_1 = a + a^\dagger$ and $X_2 = -i(a - a^\dagger)$ are given by the integration of the steady state P function, again using contour integration, for the variables $(\alpha + \beta)/2$ and $-i(\alpha - \beta)/2$. The variance in the quadratures is plotted in Fig. 8.2 versus the scaled driving field $\lambda = \epsilon/\epsilon_c$. The variance in the phase quadrature, X_2 reaches a minimum at threshold. This minimum approaches $1/2$ as the threshold intensity is increased [3]. The value of one half in the variance of the intracavity field corresponds to zero fluctuations found at the resonance frequency in the external field. The fluctuations in the amplitude quadrature X_1 increase dramatically as the threshold is approached.However, unlike the calculation in section (6.5), where the pump is treated classically, the fluctuations do not diverge. This is because (8.13) is an exact solution to the nonlinear interaction including pump depletion. As the threshold value increases and therefore the number of pump photons required to reach threshold increases, the fluctuations become

larger. In the limit $\gamma_1\gamma_2/\kappa^2 \to \infty$ the fluctuations diverge, as this corresponds to the classical pump (infinite energy). The variance in the amplitude quadrature above threshold continues to increase as the distribution is then double-peaked (see (8.8)) at the two stable output amplitudes.

This solution demonstrates the usefulness of the complex P representation. Although the solution obtained for the steady state distribution has no interpretation in terms of a probability distribution, the moments calculated by integrating the distribution on a suitable manifold correspond to the physical moments. We have demonstrated how exact moments of a quantized intracavity field undergoing a nonlinear interaction may be calculated. To calculate the moments of the external field however, we must resort to linearization techniques.

8.1.1 Cat State Formation in the Parametric Oscillator

The two π out of phase solutions to the semiclassical steady states, (8.8), suggests that the quantum steady state may exhibit cat state characteristics. This is indeed the case and can be shown using the positive P representation. Following the treatment of Wolinsky and Carmichael [4], we can obtain an analytic solution for the steady state positive P function. This solution is a function of two phase space variables; one variable is the classical field amplitude, the other is a non-classical variable needed to represent superpositions of coherent states. A three-dimensional plot of the positive P function allows one to distinguish between the limiting regions of essentially classical behaviour and predominantly quantum behaviour.

The Langevin equations are the same as (8.10) but the domain of the variables α, β is different and describe trajectories in a four-dimensional phase space. The region of phase space satisfying the conjugacy condition $\beta = \alpha^*$ is called the classical subspace. Two extra non-classical dimensions are required by the quantum noise. If we neglect the noise the deterministic equations have the stable steady states as we saw. In the new variables these become (i) $\alpha = \beta = 0$ below threshold, ($\lambda < 1$), and $\alpha = \beta = \pm(\lambda - 1)^{1/2}$ above threshold ($\lambda > 1$). In the full phase space there are additional steady states which do not satisfy the conjugacy condition: two steady states $\alpha = \beta = \pm i(1 - \lambda)^{1/2}$ below threshold and two steady states $\alpha = -\beta = \pm(\lambda + 1)^{1/2}$ both below and above threshold.

The variables α and β are restricted to a bounded manifold $\alpha = x,\ \beta = y$ with x, y both real, and $|x|, |y| \leq \sqrt{\lambda}$. Denote this manifold by $\Lambda(x, y)$. Trajectories are confined within this manifold by reflecting boundary conditions. If a trajectory starts within this manifold, then it is clear that the drift and noise terms remain real, so a trajectory will remain on the real plane. Furthermore, at the boundary, the trajectory must follow the deterministic flow inwards, as the transverse noise component vanishes. If the initial quantum state is the vacuum state, the entire subsequent evolution will be confined to this manifold.

The manifold $\Lambda(x, y)$ is alternatively denoted by $\Lambda(u, v)$with $u = (x + y)/2$ and $v = (x - y)/2$. The line $v = 0$ is a one-dimensional classical subspace, the subspace preserving $\alpha = \beta$. The variable v denotes a transverse, non-classical dimension used

by the noise to construct manifestly non-classical states. We may now construct a pictorial representation of these states which dramatically distinguishes between the quantum and classical regimes.

With $\alpha = x$ and $\beta = y$, both real, the solution to the Fokker-Planck equation is of the form given by (8.13), with $|x|, |y| \leq \sqrt{\lambda}$,

$$P_{ss}(x, y) = \mathcal{N}\left[(\lambda - x^2)(\lambda - y^2)\right]^{1/g^2 - 1} e^{2xy/g^2} \tag{8.14}$$

For weak noise ($g \ll 1$) we illustrate $P_{ss}(x, y)$ in Fig. 8.3 threshold ($\lambda < 1$), $P_{ss}(u, v)$ may be written

$$P_{ss}(u, v) = \frac{(1 - \lambda^2)^{1/2}}{\pi \lambda g/2} \exp\left[-\frac{(1 - \lambda)u^2 + (1 + \lambda)v^2}{\lambda g^2/2}\right] \tag{8.15}$$

The normally ordered variance of fluctuations in the quadratures $X_1 = a + a^\dagger$ and $X_2 = -i(a - a^\dagger)$ are given by the integration of the steady state P function to compute the variances $\mathbb{V}[(\alpha + \beta)/2]$ and $\mathbb{V}[-i(\alpha - \beta)/2]$. As $u = (\alpha + \beta)/2$ and $v = (\alpha - \beta)/2$, on the manifold $\Lambda(u, v)$, the quadrature variances are given by

$$\langle: \Delta X_1^2 :\rangle = \mathbb{V}[u]/g^2 \tag{8.16}$$

$$\langle: \Delta X_2^2 :\rangle = -\mathbb{V}[v]/g^2 \tag{8.17}$$

indicating squeezing as we have already seen. It is interesting that a non zero variance for the non classical variable, v, is necessary for squeezing.

The threshold distribution ($g \ll 1,\ \lambda = 1$) is given by

$$P_{ss}(u, v) = \sqrt{16\pi g^3}\, \Gamma(1/4) e^{-(u^4 + 4v^2)/g^2} \tag{8.18}$$

Above threshold the distribution splits into two peaks.We note that in the low-noise regime $P_{ss}(x, y)$ is a slightly broadened version of the classical steady state with only a small excursion into the nonclassical space.

Figure 8.4 shows $P_{ss}(x, y)$ for the same values of λ as Fig. 8.3 but for the noise strength $g = 1$. The quantum noise has become sufficiently strong to explore thoroughly the non-classical dimension of the phase space and is strongly influenced by the boundary $\Lambda(x, y)$.

As the noise strength g is increased beyond 1, the characteristic threshold behaviour of the parametric oscillator disappears and squeezing is significantly reduced (Fig. 8.5). In the large-g limit the stochastic trajectories are all driven to the boundary of $\Lambda(x, y)$, and then along this boundary to the corners, where both noise terms vanish and $P_{ss}(x, y)$ approaches a sum of δ functions. When $4\lambda/g^2 \ll 1$ all δ functions carry equal weight and the state of the subharmonic field is the coherent pure state superposition of coherent states—cat states of the form

$$\frac{1}{\sqrt{2}}\left[|\sqrt{\lambda}/g\rangle + |-\sqrt{\lambda}/g\rangle\right] \tag{8.19}$$

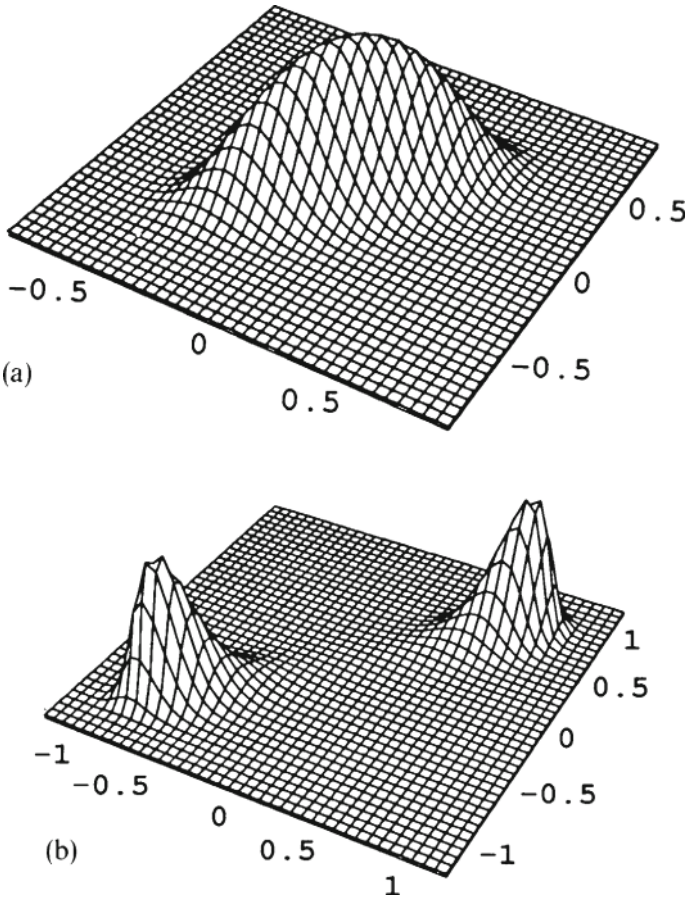

Fig. 8.3 A plot of the positive P representation of the steady state of the degenerate parametric amplifier, below and above threshold: **a** $\lambda = 0.8$ **b** $\lambda = 1.5$. In both cases $g = 0.25$

As λ increases, this superposition state is replaced by a classical mixture of coherent states $\{|\sqrt{\lambda}/g\rangle, |-\sqrt{\lambda}/g\rangle\}$ for $4\lambda/g^2 \gg 1$. This is a consequence of the competition between the creation of quantum coherence by the parametric process and the destruction of this coherence by dissipation.

8.1.2 Dissipative Quantum Tunnelling

In the classical theory of stochastic processes in double well potentials, similar multi-peaked distributions arise in the steady state. However when such a system is continuously monitored we see a sequence of stochastic jumps between the wells with the dwell times in each well determined by the switching rates between wells [5]. The switching rates are given by Kramer's rule. The stochastic switching

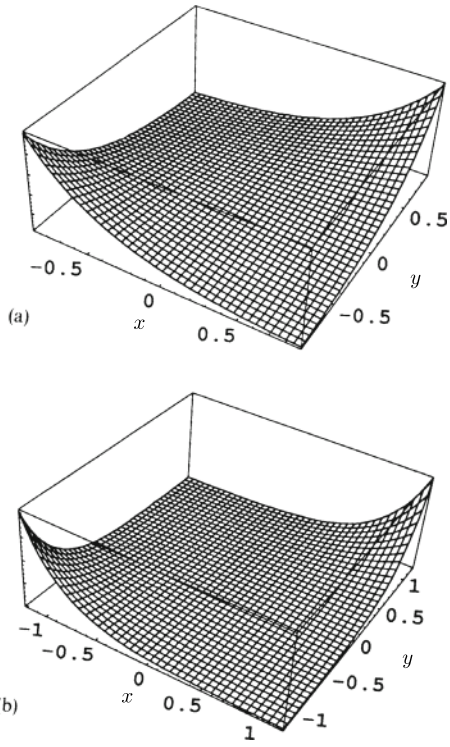

Fig. 8.4 As in Fig. 8.3 but with quantum noise parameter $g = 1.0$. **a** $\lambda = 0.8$ **b** $\lambda = 1.5$

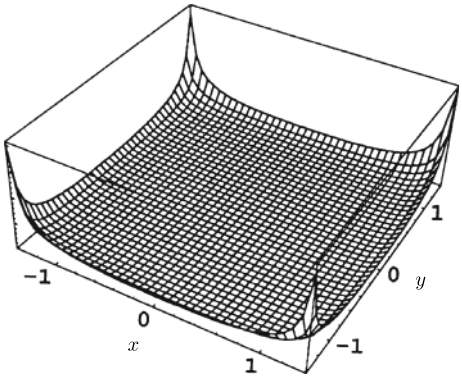

Fig. 8.5 As in Fig. 9.3 but with $\lambda = 1.5$ and $g = 10$

is in the classical case determined by thermal noise The stochastic switching turns out to be critical to understanding the stochastic thermodynamics of such systems.

Similar considerations apply to the quantum case but now the switching is entirely due to quantum noise at zero temperature. This is called dissipative quantum tunnelling. In order to see this in the lab, one needs to make continuous measurements of the emitted field amplitudes via homodyne or heterodyne detection when the system has reached the steady state. Rather than pursue this approach here we adopt a

method due to Kinsler and Drummond [6] that adapts the method used in the classical approach to first passage times.

In order to calculate the quantum tunnelling rate, we shall transform the variables α, β to give constant diffusion, or additive stochastic noise,

$$u = \sin^{-1}\left(\frac{g\alpha}{\sqrt{\lambda}}\right) + \sin^{-1}\left(\frac{g\beta}{\sqrt{\lambda}}\right), \tag{8.20}$$

$$v = \sin^{-1}\left(\frac{g\alpha}{\sqrt{\lambda}}\right) - \sin^{-1}\left(\frac{g\beta}{\sqrt{\lambda}}\right). \tag{8.21}$$

These new variables are constrained to have a range such that $|u| + |v| \leq \pi$. Referring back to the variables α and β, it can be seen that the u axis represents the classical subspace of the phase space where $\alpha = \beta$. Thus the variable v is a non-classical dimension which allows for the creation of quantum features. The stochastic equations corresponding to these variables are

$$du = \left\{\lambda \sin(u) - \sigma\left[\tan\left(\frac{u+v}{2}\right) + \tan\left(\frac{u-v}{2}\right)\right]\right\} d\tau + \sqrt{2g}dW_u, \tag{8.22}$$

$$dv = \left\{-\lambda \sin(v) - \sigma\left[\tan\left(\frac{u+v}{2}\right) - \tan\left(\frac{u-v}{2}\right)\right]\right\} d\tau + \sqrt{2g}dW_v. \tag{8.23}$$

Here $\sigma = 1 - g^2/2$, dW_u, dW_v are Wiener processes.

These Ito equations have a corresponding Fokker-Planck equation and a probability distribution in the limit as $\tau \to \infty$ of

$$P(u, v) = N \exp[-V(u, v)/g^2] \tag{8.24}$$

where the potential $V(u, v)$ is

$$V(u, v) = -2\sigma \ln|\cos u + \cos v| + \lambda \cos u - \lambda \cos v. \tag{8.25}$$

Above threshold the potential has two minima corresponding to the stable states of the oscillator. These minima have equal intensities and amplitudes of opposite sign, and are at classical locations with $\alpha = \alpha^*$

$$(u_0, v_0) = \left(\pm 2 \sin^{-1}[(\lambda - \sigma)^{1/2}/\sqrt{\lambda}], 0\right) \tag{8.26}$$

or

$$g\alpha_0 = \pm(\lambda - 1 + g^2)^{1/2}. \tag{8.27}$$

There is also a saddle point at $(u_s, v_s) = (0, 0)$.

Along the u axis the second derivative of the potential in the v direction is always positive. The classical subspace ($v = 0$) is therefore at a minimum of the potential with respect to variations in the non-classical variable v. This valley along the u axis between the two potential wells is the most probable path for a stochastic trajectory in switching from one well to the other. The switching rate between them will be dominated by the rate due to trajectories along this route. Using an extension of Kramer's method, developed by Landauer and Swanson [7], the mean time taken for the oscillator to switch from one state to the other in the limit of $g^2 \ll 1$ is

$$T_p = \frac{\pi}{\gamma_1}\left(\frac{\lambda+\sigma}{\lambda(\lambda-\sigma)^2}\right)^{1/2} \exp\left\{\frac{2}{g^2}\left[\lambda-\sigma-\sigma\ln\left(\frac{\lambda}{\sigma}\right)\right]\right\}. \tag{8.28}$$

The switching time is increased as the pump amplitude λ is increased or the nonlinearity g^2 is reduced.

Previous attempts to compute the tunnelling time for this problem have used the Wigner function [8]. Unfortunately the time-evolution equation for the Wigner function contains third-order derivative terms and is thus not a Fokker–Planck equation. In the case of linear fluctuations around a steady state truncating the evolution equation at second-order derivatives is often a good approximation. However, it is not clear that this procedure will give quantum tunnelling times correctly.

In the limit of large damping in the fundamental mode the truncated Wigner function of the sub-harmonic mode obeys with $\tau = \gamma_1 t$

$$\frac{d}{d\tau}W(\beta,t) = \left\{\frac{\partial}{\partial\beta}[\beta-\beta^*(\lambda-g^2\beta^2)] + \frac{\partial}{\partial\beta^*}[\beta^*-\beta(\lambda-g^2\beta^{*2})] + \frac{\partial^2}{\partial\beta\partial\beta^*}(1+2g^2\beta\beta^*)\right\}W(\beta,\tau). \tag{8.29}$$

This truncated Wigner function equation does not have potential solutions, however an approximate potential solution can be obtained that is valid near threshold. Here, the noise contribution $2g^2\beta\beta^*$ is small and is neglected leaving only subharmonic noise. Writing $\beta = x + ip$, the solution in the near threshold approximation is

$$W_{NT} = N_{NT}\exp[-V_{NT}(x,p)] \tag{8.30}$$

where

$$V_{NT}(x,p) = \frac{2}{g^2}\left[g^2x^2+g^2p^2+\frac{1}{2}(g^2x^2+g^2p^2)^2-\lambda(g^2x^2-g^2p^2)\right] \tag{8.31}$$

and N_{NT} is the normalisation constant.

Above threshold this potential has two minima, at $gx = \pm(\lambda-1)^{1/2}$. In the limit of large-threshold photon numbers, these minima are very close to those obtained

in (8.27). The tunneling time has been calculated from the Wigner distribution by Graham [8], with the result

$$T_w = \frac{\pi}{\gamma_1}\left(\frac{\lambda+1}{\lambda(\lambda-1)^2}\right)^{1/2}\exp\left[\frac{1}{g}(\lambda-1)^2\right]. \tag{8.32}$$

This result is compared with the expression derived using the P function in Fig. 8.6 which shows the variation in the logarithm of the tunnelling rate with the pump amplitude λ. The Wigner function result predicts a slower switching time above threshold. The difference in the two predictions can be many orders of magnitude. The calculations from the exact positive P Fokker–Planck equation represent a true quantum tunnelling rate. Whereas the truncation of the Wigner function equation involves dropping higher order derivatives dependent on the interaction strength g.

Thus nonlinear terms in the quantum noise are neglected and the only quantum noise terms included are due to the vacuum fluctuations from the cavity losses. These give a diffusion term in the truncated Wigner Fokker–Planck equation which is identical to classical thermal noise, with an occupation number of half a photon per mode. Also indicated in Fig. 8.6 are the tunnelling times computed by direct numerical simulation of the stochastic differential equations resulting from either the positive P representation (Fig. 8.6a, b) or the Wigner representation (Fig. 8.6c, d) and by directly solving the master equation in the number basis.

The differences between the two rates obtained reflect the difference between classical thermal activation and true quantum tunnelling. Classical thermal-activation rates are slower than quantum tunnelling rates far above threshold where the former are large since the thermal trajectory must go over the barrier. A quantum process, on the other hand, can short cut this by tunnelling.

8.2 Dispersive Optical Bistability

We consider a single mode model for dispersive optical bistability [9]. An optical cavity is driven off resonance with a coherent field. The intracavity medium has an intensity dependent refractive index. As the intensity of the driving field is increased the cavity is tuned to resonance and becomes highly transmissive.

We shall model the intracavity medium as a Kerr type $\chi^{(3)}$ nonlinear susceptibility treated in the rotating wave approximation. The Hamiltonian is given by (5.79). The Fokker–Planck equation is

$$\begin{aligned}\frac{\partial P}{\partial t} = &\left[\frac{\partial}{\partial\alpha}(\kappa\alpha + 2i\chi\alpha^2\beta - E_0) - i\chi\frac{\partial^2}{\partial\alpha^2}\alpha^2\right. \\ &\left. + \frac{\partial}{\partial\beta}(\kappa^*\beta - 2i\chi\beta^2\alpha - E_0) + i\chi\frac{\partial^2}{\partial\beta^2}\beta^2\right]P(\alpha,\beta)\end{aligned} \tag{8.33}$$

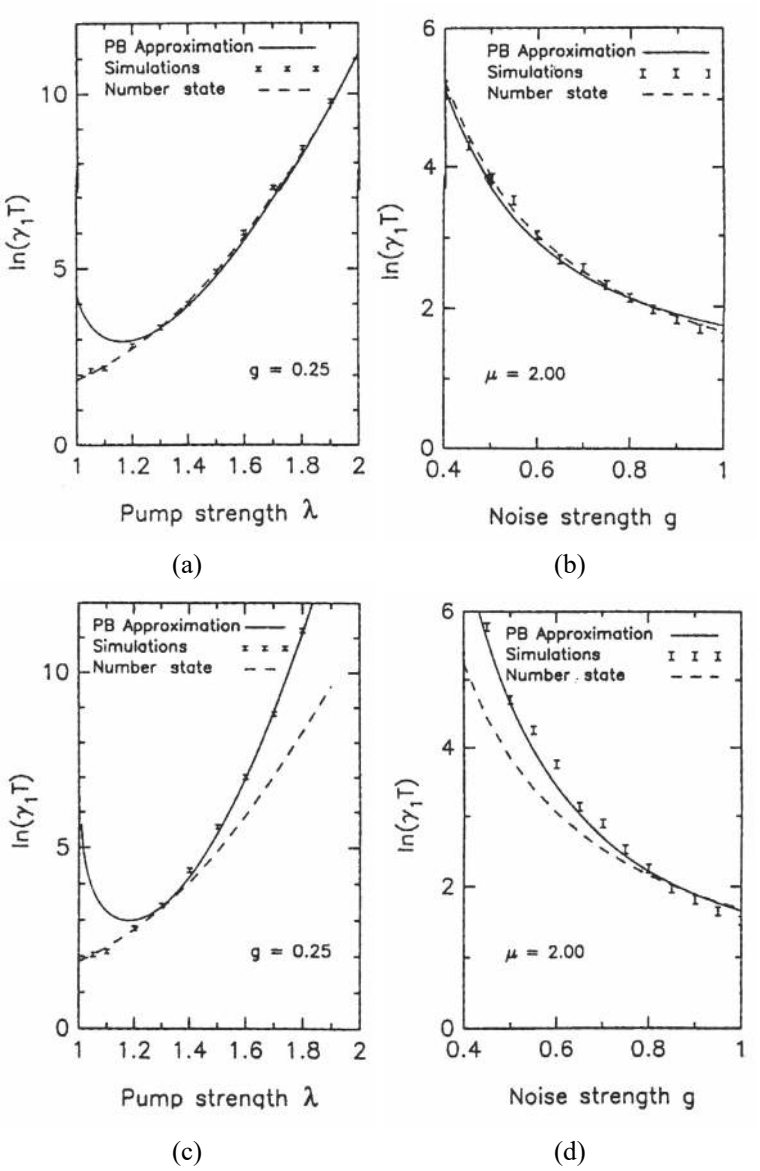

Fig. 8.6 A plot of the log of the tunnelling time for the degenerate parametric amplifier above threshold, versus pump strength or noise strength. In **a** and **b** we show the results computed by the positive P Representation (PB approximation) while in **c** and **d** we give the results for the truncated Wigner function model. In all cases we contrast the results obtained by potential methods with the results obtained by direct simulation of the corresponding stochastic differential equations and number state solution of the master equation (dashed line) [6]

where we choose the phase of the driving field such that E_0 is real and $\kappa = \gamma + i\delta$. We shall seek a steady state solution using the potential conditions (6.72). The calculation of F gives

$$F_1 = -\left(\frac{i}{\chi}\right)\left(\frac{\bar{\kappa}}{\alpha} + 2\chi\beta - \frac{E_0}{\alpha^2}\right), \quad F_2 = \left(\frac{i}{\chi^*}\right)\left(\frac{\bar{\kappa}^*}{\alpha} - 2\chi^*\beta - \frac{E_0}{\beta^2}\right), \tag{8.34}$$

where we have defined $\bar{\kappa} = \kappa - 2i\chi$. The cross derivatives

$$\partial_\alpha F_2 = \partial_\beta F_1 = 1 \tag{8.35}$$

so that the potential conditions are satisfied.

The steady state distribution is given by

$$P_{ss}(\alpha, \beta) = \exp\left[\int_\alpha^{\alpha'} F_p(\alpha')d\alpha'\right] \tag{8.36}$$

$$= \exp\left[\int_\alpha^{\alpha'}\left(\frac{1}{i\chi}\left(\frac{\bar{\kappa}}{\alpha_1} + 2i\chi\beta_1 - \frac{E_0}{\alpha_1^2}\right)d\alpha_1 - \frac{1}{i\chi}\left(\frac{\bar{\kappa}^*}{\beta_1} - 2i\chi\alpha_1 - \frac{E_0}{\beta_1^2}\right)d\beta_1\right)\right] \tag{8.37}$$

$$= \alpha^c\beta^{-2}\exp\left[\left(\frac{E_0}{i\chi}\right)\left(\frac{1}{\alpha} + \frac{1}{\beta}\right) + 4\alpha\beta\right] \tag{8.38}$$

where $c = \frac{\bar{\kappa}}{i\chi}$, $d = \left(\frac{\bar{\kappa}}{i\chi}\right)^*$.

It can be seen immediately that the usual integration domain of the complex plane with $\alpha^* = \beta$ is not possible since the potential diverges for $\alpha\beta \to \infty$. However, the moments may be calculated using the complex P representation. The results for the mean amplitude $\langle\alpha\rangle$ and correlation function $g^{(2)}(0)$ are plotted in Fig. 8.7 where they are compared with the semi-classical value for the amplitude α_{ss}.

It is seen that, whereas the semi-classical equation predicts a bistability or hysteresis, the exact steady state equation which includes quantum fluctuations does not exhibit bistability or hysteresis. The extent to which bistability is observed in practice will depend on the fluctuations, which in turn determine the time for random switching from one branch to the other. The driving field must be ramped in time intervals shorter than this random switching time in order for bistability to be observed.

The variance of the fluctuations as displayed by $g^{(2)}(0)$ show an increase as the fluctuations are enhanced near the transition point. The dip in the steady state mean at the transition point is due to out-of-phase fluctuations between the upper and lower branches.

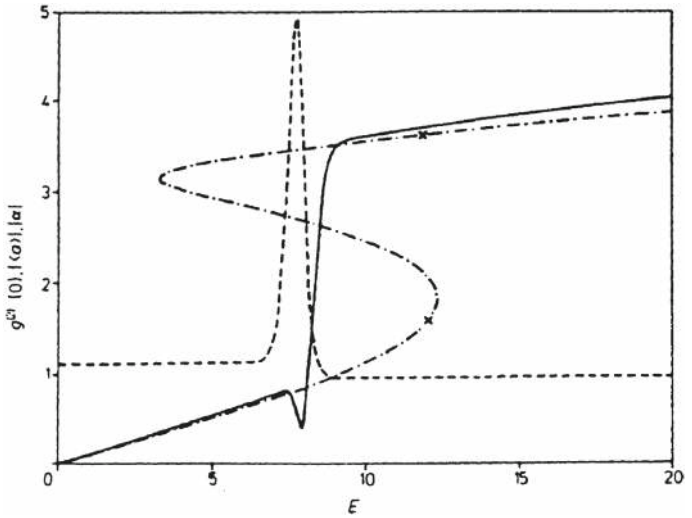

Fig. 8.7 The steady state amplitude, and second-order correlation function for optical bistability versus the pump amplitude. The chain curve gives the semi-classical steady state amplitude. The full curve gives the exact steady state amplitude. The broken curve presents the second-order correlation function $g^{(2)}(0)$. The detuning is chosen so that $\Delta\omega\chi < 0$ with $\Delta\omega = -10$ and $\chi = 0.5$

8.2.1 Comment on the Use of the Q and Wigner Representations

We will compare the above solution we have obtained with the generalised P representation with the equation obtained using the Q and Wigner representations. With the Q representation we obtain the following equation

$$\frac{\partial Q(\alpha^*,\alpha)}{\partial t} = \left[\frac{\partial}{\partial\alpha}(-E_0 + \bar{\kappa}\alpha + 2i\chi\alpha^2\alpha^*) + i\chi\frac{\partial^2}{\partial\alpha^2}\alpha^2 + \left(\frac{\bar{\kappa}}{2}\right)\frac{\partial^2}{\partial\alpha\partial\alpha^*} + \text{c.c.}\right] Q(\alpha^*,\alpha) \tag{8.39}$$

where $\bar{\kappa} = \kappa - 4i\gamma + i\Delta\omega$.

This equation has a non-positive definite diffusion matrix. Furthermore, it does not satisfy the potential conditions, hence its steady-state solution is not readily obtained.

The equation for the Wigner function is,

$$\begin{aligned}\frac{\partial W(\alpha^*,\alpha)}{\partial t} = \Bigg(&E_0\frac{\partial}{\partial\alpha} + \kappa\frac{\partial}{\partial\alpha} + \frac{\kappa}{2}\frac{\partial^2}{\partial\alpha^*\partial\alpha} - 2i\gamma\frac{\partial}{\partial\alpha} - i\chi\frac{1}{2}\frac{\partial^2}{\partial\alpha^*\alpha} \\ &+2i\chi\frac{\partial^3}{\partial\alpha^3}\alpha^*\alpha^2 + \text{c.c.}\Bigg) W(\alpha^*,\alpha).\end{aligned} \tag{8.40}$$

This equation is not of a Fokker–Planck form since it contains third-order derivatives. Again a steady-state solution is not readily obtainable. It is clear that for this problem the use of the complex P representation is preferable to the other two representations.

Problems

8.1 Derive the Fokker–Planck equation for $P(\alpha_1, \alpha_2, t)$ for the non-degenerate parametric oscillator after adiabatically eliminating the pump mode. Solve for the potential solution and derive the moments.

8.2 Derive the evolution equations for the Q and Wigner functions for the degenerate parametric oscillator described by (8.1).

8.3 Derive the equation of motion for the Q function for optical bistability. Show that with zero detuning and zero driving the solution for an initial coherent state is

$$Q(\alpha, t) = \sum_{q,p=0}^{\infty} (q!p!)^{-1} (\alpha\alpha_0^*)^q (\alpha^*\alpha_0)^p (f(t))^{(p+q)/2} \exp\left[-|\alpha|^2 - |\alpha_0|^2 \left(\frac{f(t) + i\delta}{1 + i\delta}\right)\right]$$

where

$$\delta = \frac{(p-q)}{\kappa}, \quad f(t) = \exp\left[-\kappa\nu - i\nu(p-q)\right], \quad \nu = 2\mu t, \quad \kappa = \frac{\gamma}{2\mu}.$$

References

1. P.D. Drummond, K.J. McNeil, D.F. Walls, Optica Acta **27**, 321 (1980)
2. P.D. Drummond, K.J. McNeil, D.F. Walls, Optica Acta **28**, 1 (1981)
3. G.J. Milburn, D.F. Walls, Optics Commun. **39**, 401 (1981)
4. M. Wolinsky, H.J. Carmichael, Phys. Rev. Lett. **60**, 1836 (1988)
5. C.W. Gardiner, *Handbook of Stochastic Processes for Physics Chemistry and the Natural Sciences* (Springer, 2009)
6. P. Kinsler, P.D. Drummond, Phys. Rev. A **43**, 6194 (1991)
7. R. Landauer, S. Swanson, Phys. Rev. **121**, 1668 (1961)
8. R. Graham, F. Haake, *Quantum Statistics in Optics and Solid State Physics*, Springer Tracts in Modern Physics, vol. 66 (Springer, Berlin, Heidelberg, 1973)
9. P.D. Drummond, D.F. Walls, J. Phys. A **13**, 725 (1980)

Interaction of Radiation with Atoms

9

Abstract

The preceding chapters have been concerned with the properties of the radiation field alone. In this chapter we turn to the interaction between radiation and matter. This is of course the domain of quantum electrodynamics, however in quantum optics we are usually only concerned with low energy systems of bound electrons which simplifies matters considerably. We will use the occupation number representation for bound many-electron systems to quantize the electronic degrees of freedom, following the approach of Haken (Waves, Photons and Atoms. North Holland, Amsterdam, vols. 1 and 2, 1981, [1]) and also Cohen-Tannoudji (Photons and Atoms: Introduction to Quantum Electrodynamics. Wiley-Interscience, 1997, [2]).

9.1 Quantization of the Many-Electron System

In the full theory of QED, the interaction between the electromagnetic field and charged matter is described by coupling between the vector potential and the Dirac spinor field. In quantum optics we only need the low energy (non relativistic) limit of this interaction. This is given by the minimal coupling Hamiltonian [3]

$$H = \frac{1}{2m}(\mathbf{p} - e\mathbf{A})^2 + eV(\mathbf{x}) + H_{\text{rad}} \tag{9.1}$$

where $\mathbf{p}$ is the momentum operator for a particle of charge e moving in a Coulomb potential $V(\mathbf{x})$. The vector potential is quantised in a box of volume V as

$$\mathbf{A}(\mathbf{x}, t) = \sum_{n,\nu} \sqrt{\frac{\hbar}{2\epsilon_0 \omega_n V}} \mathbf{e}_{n,\nu} \left[e^{i(\mathbf{k}_n \cdot \mathbf{x} - \omega_n t)} a_{n,\nu} + e^{-i(\mathbf{k}_n \cdot \mathbf{x} - \omega_n t)} a^\dagger_{n,\nu} \right] \tag{9.2}$$

where $\mathbf{e}_{n,\nu}$ are two orthonormal polarisation vectors ($\nu = 1, 2$) which satisfy $\mathbf{k}_n \cdot \mathbf{e}_{n,\nu} = 0$, as required for a transverse field, and the frequency is given by the dis-

D. F. Walls and G. J. Milburn, *Quantum Optics*, Graduate Texts in Physics,
https://doi.org/10.1007/978-3-031-84177-4_9

persion relation $\omega_n = c|\mathbf{k}_n|$. The positive and negative frequency Fourier operators, respectively $a_{n,\nu}$ and $a^\dagger_{n,\nu}$, satisfy

$$[a_{n,\nu}, a^\dagger_{m,\nu'}] = \delta_{nm}\delta_{\nu\nu'} \tag{9.3}$$

The last term, H_{rad} is the Hamiltonian of the free radiation field given by

$$H_{\text{rad}} = \sum_k \hbar\omega_k a^\dagger_k a_k \tag{9.4}$$

where we have subsumed polarisation and wave vectors labels into the single subscript k.

We now use an occupation number representation in the antisymmetric sector of the many body Hilbert space for the electronic system based on a set of single particle states $|\phi_j\rangle$, with position probability amplitudes, $\phi_j(\mathbf{x})$, which we take as the bound energy eigenstates of the electronic system without radiation. They could for example be the stationary states of an atom, the quasi bound states of a single Cooper pair on a mesoscopic super-conducting metal island, or the bound exciton states of semiconductor quantum dot. We then define the electronic field operators

$$\hat{\Psi}(\mathbf{x}) = \sum_j c_j \phi_j(\mathbf{x}) \tag{9.5}$$

where the appropriate commutations relations for the antisymmetric sector are the fermionic forms

$$c_k c^\dagger_l + c^\dagger_l c_k = \delta_{kl} \tag{9.6}$$

$$c_k c_l + c_l c_k = c^\dagger_k c^\dagger_l + c^\dagger_l c^\dagger_k = 0 \tag{9.7}$$

In the occupation number representation the Hamiltonian may be written as the sum of three terms, $H = H_{\text{el}} + H_I + H_{\text{rad}}$ where the electronic part is given by

$$H_{\text{el}} = \int d^3x \hat{\Psi}^\dagger(\mathbf{x}) \left[-\frac{\hbar^2}{2m}\nabla^2 + eV(\mathbf{x}) \right] \hat{\Psi}(\mathbf{x}) = \sum_j E_j c^\dagger_j c_j \tag{9.8}$$

The interaction part may be written as the sum of two terms $H_I = H_{I,1} + H_{I,2}$ where

$$H_{I,1} = \int d^3x \hat{\Psi}^\dagger(\mathbf{x}) \left(-\frac{e}{2m}(\mathbf{A}(\mathbf{x}) \cdot \mathbf{p} + \mathbf{p} \cdot \mathbf{A}(\mathbf{x})) \right) \hat{\Psi}(\mathbf{x}) \tag{9.9}$$

$$H_{I,2} = \int d^3x \hat{\Psi}^\dagger(\mathbf{x}) \left(\frac{e^2}{2m}(\mathbf{A}(\mathbf{x})^2) \right) \hat{\Psi}(\mathbf{x}) \tag{9.10}$$

Unless we are dealing with very intense fields for which multi-photon processes are important, the second term $H_{I,2}$ may be neglected. The dominant interaction energy may then be written as

$$H_I = \hbar \sum_{k,\mu,m} g_{k,\mu,m}(b_k + b_k^\dagger)c_n^\dagger c_m \tag{9.11}$$

The interaction coupling constant is

$$g_{k,n,m} = -\frac{e}{m}\left(\frac{1}{2\epsilon_0 \hbar \omega_k V}\right)^{1/2} \int d^3x \phi_n^*(\mathbf{x})\left(e^{i\mathbf{k}\cdot\mathbf{x}}\mathbf{p}\right)\phi_m(\mathbf{x}) \tag{9.12}$$

We now proceed by making the dipole approximation. The factor $e^{i\mathbf{k}\cdot\mathbf{x}}$ varies on a spatial scale determined by the dominant wavelength scale, λ_0, of the field state. At optical frequencies, $\lambda_0 \approx 10^{-6}$ m. However the atomic wave functions, $\phi_n(\mathbf{x})$ vary on a scale determined by the Bohr radius, $a_0 \approx 10^{-11}$ m. Thus we may remove the oscillatory exponential from the integral and evaluate it at the position of the atom $\mathbf{x} = \mathbf{x}_0$. Using the result

$$[\mathbf{p}^2, \mathbf{x}] = -i2\hbar\mathbf{p} \tag{9.13}$$

we can write the interaction in terms of the atomic dipole moments

$$\int d^3x \phi_n^*(\mathbf{x})\left(e^{i\mathbf{k}\cdot\mathbf{x}}\mathbf{p}\right)\phi_m(\mathbf{x}) = i\frac{m}{e}\omega_{nm}e^{i\mathbf{k}\cdot\mathbf{x}_0}\int d^3x \phi_n^*(\mathbf{x})(\mathbf{e}\cdot\mathbf{k})\phi_m(\mathbf{x}) \tag{9.14}$$

where $\omega_{nm} = (E_n - E_m)/\hbar$.

In the interaction picture the interaction Hamiltonian becomes explicitly time dependent,

$$\hat{H}_I(t) = \hbar \sum_{k,n,m} g_{k,n,m}\left(b_k e^{-i\omega_k t} + b_k^\dagger e^{i\omega_k t}\right)c_n^\dagger c_m e^{i\omega_{nm}t} \tag{9.15}$$

where the tilde indicates that we are in the interaction picture. If the field is in state for which the dominant frequency is such that $\omega(\mathbf{k}_0) \approx \omega_{nm}$, the field is resonant with a particular atomic transition and we may neglect terms rotating at the very high frequency $\omega(\mathbf{k}) + \omega_{nm}$. This is known as the rotating wave approximation. This assumes that the field strength is not too large and further that the state of the field does not vary rapidly on a time scale of ω_{nm}^{-1}, i.e. we ignore fields of very fast strong pulses. As a special case we assume the field is resonant (or near-resonant) with a single pair of levels with $E_2 > E_1$. The interaction picture Hamiltonian in the dipole and rotating wave approximation is then given by

$$\hat{H}_I = \hbar \sum_{\mathbf{k}} \left(c_1^\dagger c_2 b_{\mathbf{k}}^\dagger g_{\mathbf{k}} e^{-i(\omega(\mathbf{k})-\omega_{21})t} + \text{h.c.}\right) \tag{9.16}$$

where

$$g_{\mathbf{k}} = -i\,(2\hbar\epsilon_0\omega(\mathbf{k})V)^{-1/2}\,\omega_a\mu_{21}e^{i\mathbf{k}\cdot\mathbf{x}_0} \tag{9.17}$$

and

$$\mu_{21} = \langle\phi_n|\mathbf{e}\cdot\mathbf{x}|\phi_m\rangle \tag{9.18}$$

with $\omega_a = \omega_2 - \omega_1$.

It is conventional to describe the operator algebra of a two-level system in terms of pseudo-spin representation by noting that the Pauli operators may be defined as

$$\sigma_z = c_2^\dagger c_2 - c_1^\dagger c_1 \tag{9.19}$$

$$\sigma_x = c_2^\dagger c_1 + c_1^\dagger c_2 \tag{9.20}$$

$$\sigma_y = -i(c_2^\dagger c_1 - c_1^\dagger c_2) \tag{9.21}$$

$$\sigma_+ = \sigma_-^\dagger = c_2^\dagger c_1 \tag{9.22}$$

The operators $s_\alpha = \sigma_\alpha/2$ (with $\alpha = x, y, z$) then obey the $su(2)$ algebra for a spin half system. In terms of these operators we may write the total Hamiltonian for the system of field plus atom in the dipole and rotating wave approximation as

$$H = \sum_{\mathbf{k}} \hbar\omega(\mathbf{k})b_{\mathbf{k}}^\dagger b_{\mathbf{k}} + \frac{\hbar\omega_a}{2}\sigma_z + \hbar\sum_{\mathbf{k}}(g_{\mathbf{k}}b_{\mathbf{k}}\sigma_+ + \text{h.c.}) \tag{9.23}$$

The free Hamiltonian for the two-level electronic system is

$$H_{\text{el}} = \frac{\hbar\omega_a}{2}\sigma_z \tag{9.24}$$

Denoting the ground and excited states as $|1\rangle$ and $|2\rangle$ respectively, we see that

$$H_{\text{el}}|s\rangle = (-1)^s\frac{\hbar\omega_a}{2}|s\rangle \quad s = 1, 2 \tag{9.25}$$

The action of the raising and lowering operators on the energy eigenstates is: $\sigma_+|1\rangle = |2\rangle$ and $\sigma_-|2\rangle = |1\rangle$, while $\sigma_\pm^2 = 0$. We now relabel the ground state and excited state respectively as $|1\rangle \equiv |g\rangle$, $|2\rangle \equiv |e\rangle$. If the state of the system at time t is ρ, the probability to find the electronic system in the excited state and ground state are, respectively,

$$p_e(t) = \langle 2|\rho|2\rangle = \langle\sigma_+\sigma_-\rangle \tag{9.26}$$

$$p_g(t) = \langle 1|\rho|1\rangle = \langle\sigma_-\sigma_+\rangle \tag{9.27}$$

The *atomic inversion* is defined as the difference between these two probabilities and is given by

$$p_e(t) - p_g(t) = \langle\sigma_z\rangle \tag{9.28}$$

While the *atomic coherences* are defined by

$$\rho_{12} \equiv \langle 1|\rho|2\rangle = \langle \sigma_+ \rangle \tag{9.29}$$

with $\rho_{21} = \rho_{12}^*$.

9.1.1 Interaction of a Single Two-Level Atom with a Single Mode Field

If we further restrict the state of the field to include only a single mode, with frequency ω_0 (perhaps using a high Q optical resonator), we arrive at the Jaynes-Cummings Hamiltonian,

$$H = \hbar\omega_0 b^\dagger b + \frac{\hbar\omega_a}{2}\sigma_z + \hbar(gb\sigma_+ + g^* b^\dagger \sigma_-) \tag{9.30}$$

coupling a single harmonic oscillator degree of freedom to a two-level system. The coupling constant g can vary from a few kHz to many MHz. An example is provided by the experiment of Aoki et al. [5] in which a cesium atom interacts with the toroidal whispering gallery mode of a micro-resonator as it falls under the action of gravity from a magneto-optical trap. The atomic resonance is at the $6S_{1/2}$; $F = 4 \rightarrow 6P_{3/2}$; $F' = 5$ transition in cesium. A coupling constant as large as $g/2\pi = 50$ MHz was achieved.

On resonance, $\omega_a = \omega_c = \omega$, we see that the interaction Hamiltonian $H_I = \hbar g(b\sigma_+ + b^\dagger\sigma_-)$ (with g chosen as real), commutes with the free Hamiltonian, $H_0 = \hbar(b^\dagger b + \frac{1}{2}\sigma_z)$, so that the eigenstates of the full Hamiltonian can be written as a linear combination of the degenerate eigenstates of H_0. Defining $|n, s\rangle = |n\rangle|s\rangle$, where $b^\dagger b|n\rangle = n|n\rangle$, the degenerate eigenstates of the free Hamiltonian are $|n, 2\rangle$, $|n+1, 1\rangle$. Within this degenerate subspace, the state at time t may be written $|\psi_n(t)\rangle = c_{n,2}(t)|n, 2\rangle + c_{n+1,1}(t)|n+1, 1\rangle$, and the Schrödinger equation in the interaction picture is

$$\begin{pmatrix} \dot{c}_{n,2} \\ \dot{c}_{n+1,1} \end{pmatrix} = -i\Omega_n \sigma_x \begin{pmatrix} c_{n,2} \\ c_{n+1,1} \end{pmatrix} \tag{9.31}$$

where $\Omega_n = g\sqrt{n+1}$. The eigenvalues of this system of linear equations are $\pm i\Omega_n$ corresponding to the eigenstates of H_I

$$|n, \pm\rangle = \frac{1}{\sqrt{2}}\left(|n, 2\rangle \pm |n+1, 1\rangle\right) \tag{9.32}$$

which are often referred to as the dressed states. The splitting of the degeneracy is depicted in Fig. 9.1.

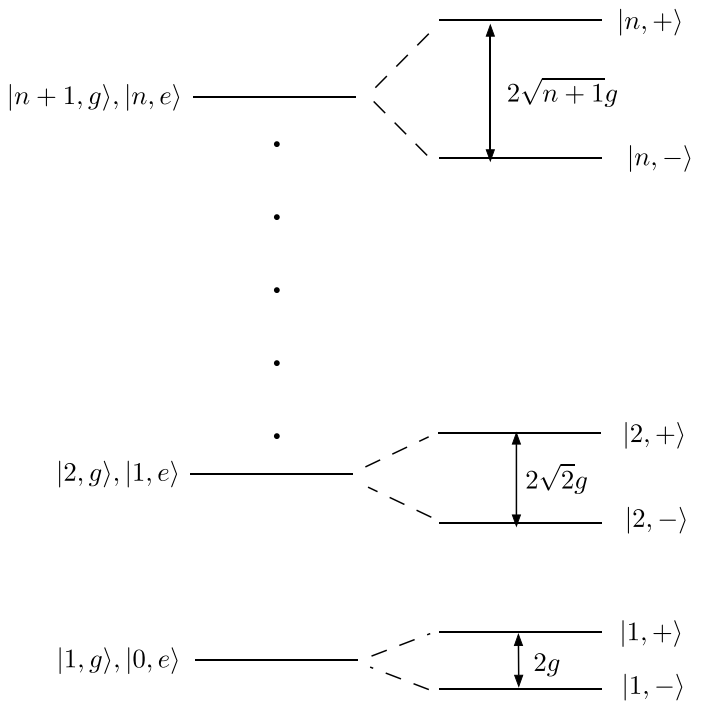

Fig. 9.1 The dressed states for the energy eigenstates of the Jaynes–Cummings interaction. On the left are show the degenerate states for zero interaction. When the interaction is turned on the degeneracies are lifted

Thus the general solution is

$$c_{n,2}(t) = c_{n,2}(0)\cos\Omega_n t - ic_{n+1,1}(0)\sin\Omega_n t \tag{9.33}$$

$$c_{n+1,1}(t) = c_{n+1,1}(0)\cos\Omega_n t - ic_{n,2}(0)\sin\Omega_n t \tag{9.34}$$

If the atom is initially in the excited state and the cavity field has exactly n photons, the probability for finding the atom in the same state at time $t > 0$ is

$$p_e(t) = |\langle n, 2|\psi_n(t)\rangle|^2 = \frac{1}{2}(1 + \cos 2\Omega_n t) \tag{9.35}$$

The excitation oscillates backward and forth between the cavity and the electronic system with frequency Ω_n, the Rabi frequency. Note that for $n = 0$ the separation of these eigenvalues is $2g$, which is known as the *vacuum Rabi splitting*. If the field is in an arbitrary pure state, $|\phi\rangle = \sum_n f_n|n\rangle$ and the atom is initially excited, the probability to find the atom in the excited state at time $t > 0$ may be written

$$p_e(t) = \frac{1}{2}\left[1 + \sum_{n=0}^{\infty} |f_n|^2 \cos(2g\sqrt{n+1}t)\right] \tag{9.36}$$

This is a discrete superposition of harmonic oscillations with incommensurate frequencies. Thus it must exhibit quasiperiodic behaviour. If the initial photon number distribution $|f_n|^2$ has narrow support on n, only a few frequencies are involved and there is a beating between these different frequencies leading to what are known as collapses and revivals. The collapse refers to the decay of oscillations at short times due to beating between the incommensurate frequencies. The revival refers to partial re-phasing of the oscillations at later times. In the case of the field initially in a coherent state, $|\alpha\rangle$, the initial number distribution is Poissonian with standard deviation in number given by the root mean, $\bar{n}^{1/2}|\alpha|$. An approximate evaluation of the sum valid for times such that $gt < \bar{n}^{1/2}$ gives [6]

$$p_e(t) = \frac{1}{2}\left[1 + e^{-\frac{g^2t^2}{2(\bar{n}+1)}}\cos(2g\sqrt{\bar{n}+1}t)\right] \tag{9.37}$$

There is an average Rabi oscillation frequency under a Gaussian envelope. The characteristic time for the collapse of the oscillation is thus

$$t_{col} \sim \frac{1}{g} \tag{9.38}$$

A more accurate evaluation using the Laplace summation formulae shows that the oscillations first revival at a time

$$t_{\text{rev}} \sim \frac{2\pi\bar{n}^{1/2}}{g} \tag{9.39}$$

Thus a quasi periodic burst of Rabi oscillations occurs every $\bar{n}$ Rabi periods. The collapse and revival has been seen experimentally using an atom excited to a Rydberg ground state interacting with the microwave field in a superconducting cavity [6]. The results of the experiment are shown in Fig. 9.2.

9.1.2 Spontaneous Emission from a Two-Level Atom

Spontaneous emission can also be treated using a master equation. In this case the system is a two-level electronic system, with ground state $|g\rangle$ of energy $\hbar\omega_1$ and excited state $|e\rangle$ with energy $\hbar\omega_2$, representing an electric dipole transition, coupled to the many modes of the radiation field in the dipole and rotating wave approximation. The master equation is

$$\frac{d\rho}{dt} = -\frac{i}{\hbar}[H, \rho] + \gamma(\bar{n}+1)\mathcal{D}[\sigma_-]\rho + \gamma\bar{n}\mathcal{D}[\sigma_+]\rho \tag{9.40}$$

where $\bar{n}$ is the thermal occupation of the radiation field mode at the atomic resonance frequency $\omega_a = \omega_2 - \omega_1$. We have neglected a small term which gives rise to a shift in the atomic transition frequency and which contributes to the Lamb shift. At optical

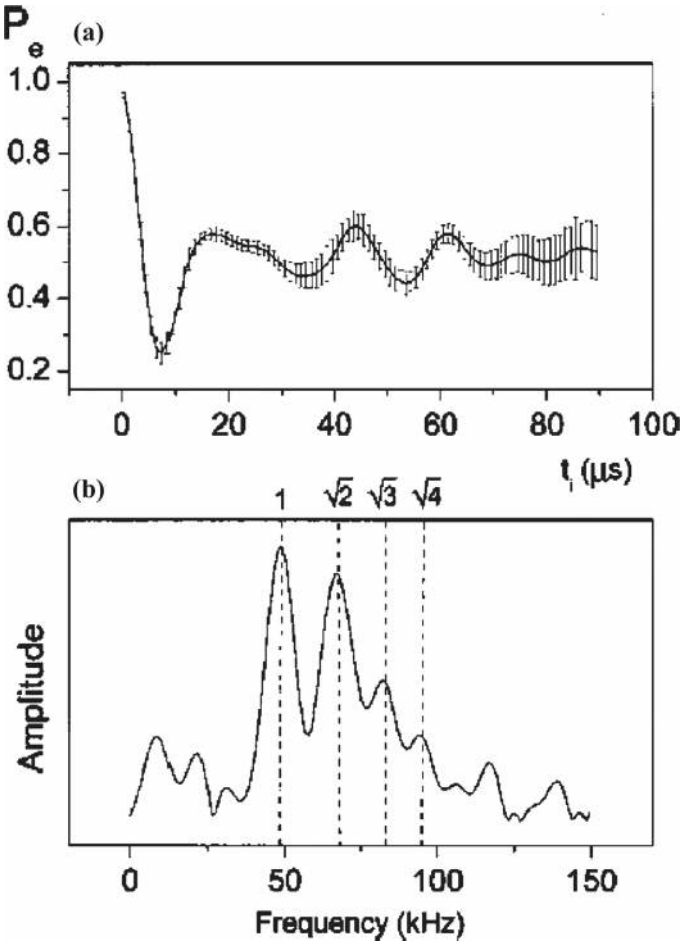

Fig. 9.2 **a** The experimental observation of collapse and revival of the oscillations in the occupation of the excited state of a two-level atom interacting with a microwave field initially in a coherent state with mean photon number $\bar{n} = 0.85$. In **b** is the Fourier transform of the oscillations with the Rabi frequencies Ω_n, $n = 0, 1, 2, 3$ marked (from [7])

frequencies, $\bar{n} \approx 0$. In the case of a free two-level atom, $H = \frac{\hbar\omega_a}{2}\sigma_z$, the probability to find the atom in the excited state, $p_e(t) = \langle e|\rho|e\rangle$ satisfies the equation

$$\frac{dp_e}{dt} = -\gamma p_e(t) \tag{9.41}$$

with the solution $p_e(t) = p_e(0)e^{-\gamma t}$, which describes spontaneous emission. The dipole polarisation is proportional to the atomic coherence, $\langle e|\rho|g\rangle = \langle\sigma_-\rangle$ which obeys

$$\frac{d\langle\sigma_-\rangle}{dt} = -\left(i\omega_a + \frac{\gamma}{2}\right)\langle\sigma_-\rangle \tag{9.42}$$

with the solution

$$\langle \sigma_-(t) \rangle = \langle \sigma_-(0) \rangle e^{-(\gamma/2 + i\omega_a)t} \tag{9.43}$$

The dipole oscillates at the transition frequency and decays, as it radiates.

The radiated field is related to the input field and the local source through an input/output relation in analogy with the case of a cavity discussed above. The positive frequency components of the field operator takes the form

$$E^{(+)}(\mathbf{x}, t) = E_i^{(+)}(\mathbf{x}, t) - \frac{\omega_a^2}{4\pi\epsilon_0 c^2 r} \left(\boldsymbol{\mu} \times \frac{\mathbf{x}}{r} \right) \times \frac{\mathbf{x}}{r} \sigma_-(t - r/c) \tag{9.44}$$

where $r = |\mathbf{x}|$ is the distance from the source to the point $\mathbf{x}$ and $\boldsymbol{\mu}$ is the atomic dipole moment.

9.1.3 Phase Decay in a Two-Level System

Spontaneous emission is not the only irreversible process involved in the absorption and emission of light. In an atomic vapour, atomic collisions are also a source of decoherence and cause a decay of the atomic polarisation, $\sigma_x + i\sigma_y$, without changing the decay of the inversion, σ_z. We can model this process by a coupling between the inversion and a high temperature heat bath,

$$H_{col} = \sigma_z \Gamma_c(t) \tag{9.45}$$

where $\Gamma_c(t)$ is a bath operator describing the collisions. This Hamiltonian commutes with σ_z and thus does not contribute to the decay of the inversion. It appears like a fluctuating detuning in the Bloch equations and thus will affect the atomic polarisation. The corresponding master equation, in the interaction picture and including spontaneous emission, is

$$\frac{d\rho}{dt} = \frac{\gamma}{2}(2\sigma_-\rho\sigma_+ - \sigma_+\sigma_-\rho - \rho\sigma_+\sigma_-) - \gamma_p[\sigma_z, [\sigma_z, \rho]] \tag{9.46}$$

The Bloch equations now become

$$\frac{d\langle \sigma_z \rangle}{dt} = -\gamma(\langle \sigma_z \rangle + 1) \tag{9.47}$$

$$\frac{d\langle \sigma_x \rangle}{dt} = -\left(\frac{\gamma}{2} + \gamma_p \right) \langle \sigma_x \rangle \tag{9.48}$$

$$\frac{d\langle \sigma_y \rangle}{dt} = -\left(\frac{\gamma}{2} + \gamma_p \right) \langle \sigma_y \rangle \tag{9.49}$$

In the presence of collisions the decay time for the polarisation, $T_2 = (\gamma/2 + \gamma_p)^{-1}$, is no longer given by twice the decay time for the inversion, $T_1 = \gamma^{-1}$, but rather $T_2 < 2T_1$.

9.2 Resonance Fluorescence

If the atom is driven by a classical radiation field, the Hamiltonian is given by (9.30) and replace $b \to \beta$

$$H = \frac{\hbar\omega_0}{2}\sigma_z + \Omega(\sigma_+ e^{-i\omega_L t} + \sigma_- e^{i\omega_L t}) \tag{9.50}$$

where $\Omega = g\beta$ is the Rabi frequency and ω_L is the carrier frequency of the driving field. The master equation in an interaction picture at the frequency ω_L is

$$\frac{d\rho}{dt} = -i\frac{\Delta}{2}[\sigma_z, \rho] - i\Omega[\sigma_+ + \sigma_-, \rho] + \gamma\mathcal{D}[\sigma_-]\rho \tag{9.51}$$

where the detuning is $\Delta = \omega_a - \omega_L$. The resulting Bloch equations for the atomic moments are linear

$$\frac{d\langle\sigma_-\rangle}{dt} = -\left(\frac{\gamma}{2} + i\Delta\right)\langle\sigma_-\rangle + i\Omega\langle\sigma_z\rangle \tag{9.52}$$

$$\frac{d\langle\sigma_z\rangle}{dt} = -\gamma(\langle\sigma_z\rangle + 1) - 2i\Omega(\langle\sigma_+\rangle - \langle\sigma_-\rangle) \tag{9.53}$$

These inhomogeneous equations can be written as homogeneous equations as

$$\frac{d}{dt}(\langle\boldsymbol{\sigma}(t)\rangle - \langle\boldsymbol{\sigma}\rangle_{ss}) = A((\langle\boldsymbol{\sigma}(t)\rangle - \langle\boldsymbol{\sigma}\rangle_{ss})) \tag{9.54}$$

The steady state solution is

$$\langle\sigma_x\rangle_{ss} = \frac{4\Delta\Omega}{\gamma^2 + 4\Delta^2 + 8\Omega^2} \tag{9.55}$$

$$\langle\sigma_y\rangle_{ss} = \frac{2\gamma\Omega}{\gamma^2 + 4\Delta^2 + 8\Omega^2} \tag{9.56}$$

$$\langle\sigma_z\rangle_{ss} = -\frac{\gamma^2 + 4\Delta^2}{\gamma^2 + 4\Delta^2 + 8\Omega^2} \tag{9.57}$$

The solutions for resonance ($\Delta = 0$), with the atom initially in the ground state, are [8]

$$\langle\sigma_z(t)\rangle = \frac{1}{1+Y^2}\left[1 + Y^2 e^{-3\gamma t/4}\left(\cosh\delta t + \frac{3\gamma}{4\delta}\sinh\delta t\right)\right] \tag{9.58}$$

$$\langle\sigma_\pm(t)\rangle = \pm i\frac{1}{\sqrt{2}}\frac{Y}{1+Y^2}\left[1 - Y^2 e^{-3\gamma t/4}\left(\cosh\delta t + \frac{3\gamma}{4\delta}\sinh\delta t\right)\right] \tag{9.59}$$

$$\pm i\sqrt{2}Y e^{-3\gamma t/4}\left(\frac{\gamma}{4\delta}\right)\sinh(\delta t)\ . \tag{9.60}$$

where

$$Y = \frac{2\sqrt{2}\Omega}{\gamma} \tag{9.61}$$

and

$$\delta = \frac{1}{2}\sqrt{\frac{\gamma^2}{4} - 16\Omega^2} \tag{9.62}$$

bear in mind that this is in the interaction picture. Transforming back to the Schrödinger picture we meed to multiply the solution for $\langle\sigma_\pm(t)\rangle$ by $e^{-i\omega t}$.

Clearly there is a threshold at $\Omega = \gamma/8$ below which the solutions monotonically approach the steady state and above which they are oscillating. A similar threshold occurs in the solutions for the two-time correlation function $\langle\sigma_+(t)\sigma_-(t+\tau)\rangle_{t\to\infty}$, which determines the spectrum of the scattered light. The stationary spectrum, as measured by a monochromatic detector at the point $\mathbf{x}$ is defined by [9].

$$S(\mathbf{x},\omega) = \lim_{t\to\infty}\frac{1}{2\pi}\int_{-\infty}^{\infty}\langle E^{(-)}(\mathbf{x},t)E^{(+)}(\mathbf{x},t+\tau)\rangle d\tau\,, \tag{9.63}$$

the Fourier transform of the stationary two-time correlation function $\langle E^{(-)}(t)E^{(+)}(t+\tau)\rangle$ which using (9.44) is given by

$$S(\mathbf{x},\omega) = \frac{I_0(\mathbf{x})}{2\pi}\int_{-\infty}^{\infty} d\tau e^{-i\omega\tau}G(\tau) \tag{9.64}$$

where

$$I_0(\mathbf{x}) = \left|\frac{\omega_0^2}{4\pi\epsilon_0 c^2 r}\left(\boldsymbol{\mu}\times\frac{\mathbf{x}}{r}\right)\times\frac{\mathbf{x}}{r}\right|^2 \tag{9.65}$$

and

$$G(\tau) = \lim_{t\to\infty}\langle\sigma_+(t)\sigma_-(t+\tau)\rangle \equiv \langle\sigma_+(t)\sigma_-(\tau)\rangle_{ss} \tag{9.66}$$

with

$$\langle\sigma_+(t)\sigma_-(t+\tau)\rangle = \mathrm{tr}\left[\sigma_- e^{\mathcal{L}\tau}[\rho(t)\sigma_+]\right] \tag{9.67}$$

and

$$\langle\sigma_+(t)\sigma_-(\tau)\rangle_{ss} = \mathrm{tr}\left[\sigma_- e^{\mathcal{L}\tau}[\rho_{ss}\sigma_+]\right] \tag{9.68}$$

Here $e^{\mathcal{L}\tau}[A]$ is the solution to the master equation starting with the initial condition $\rho(0) = A$.

The equation of motion for $G(\tau)$ couples in many other moments. If we define the correlation matrix

$$\mathcal{G}(\tau) = \begin{pmatrix} \langle\sigma_+\sigma_+(\tau)\rangle_{ss} & \langle\sigma_-\sigma_+(\tau)\rangle_{ss} & \langle\sigma_z\sigma_+(\tau)\rangle_{ss} \\ \langle\sigma_+\sigma_-(\tau)\rangle_{ss} & \langle\sigma_-\sigma_-(\tau)\rangle_{ss} & \langle\sigma_z\sigma_-(\tau)\rangle_{ss} \\ \langle\sigma_+\sigma_z(\tau)\rangle_{ss} & \langle\sigma_-\sigma_z(\tau)\rangle_{ss} & \langle\sigma_z\sigma_z(\tau)\rangle_{ss} \end{pmatrix} \tag{9.69}$$

It is easy to verify that $\mathcal{G}(\tau)$ as a function of τ obeys the same equations of motion as $\langle \boldsymbol{\sigma}(\tau)\rangle - \langle \boldsymbol{\sigma}\rangle_{ss}$,

$$\frac{d\mathcal{G}(\tau)}{d\tau} = A\mathcal{G}(\tau) \tag{9.70}$$

This is the quantum regression theorem. The initial conditions are simplified due to the algebra of the Pauli matrices, for example $\sigma_+\sigma_- = (\sigma_z + 1)/2$ and $\sigma_\pm^2 = 0$, and may thus be written in terms of the stationary solutions in (9.55–9.57). On resonance we find that in the interaction picture at Ω_a,

$$G(\tau) = \frac{1}{4}\frac{Y^2}{1+Y^2}e^{-\gamma\tau/2} \tag{9.71}$$

$$-\frac{1}{8}\frac{Y^2}{(1+Y^2)^2}\left[1 - Y^2 + (1-5Y^2)\frac{\gamma}{4\delta}\right]e^{-(3\gamma/4-\delta)\tau} \tag{9.72}$$

$$+\frac{1}{8}\frac{Y^2}{(1+Y^2)^2}\left[1 - Y^2 - (1-5Y^2)\frac{\gamma}{4\delta}\right]e^{-(3\gamma/4+\delta)\tau} \tag{9.73}$$

where Y and δ are given in (9.61, 9.62).

The corresponding spectrum has a single Lorentzian peak for weak driving fields, $4\Omega^2 \ll \gamma^2/16$, In the Schrödinger picture the peak is at $\omega = \omega_a$, so this is elastic scattering. For very strong driving fields, $\Omega \gg \gamma$ we find that the spectrum acquires three Lorentzian peaks at $\omega = \omega_a$ and $\omega = \omega_a \pm 2\Omega$. This is the inelastic scattering limit and the three peak structure is know as the Mollow triplet [10]. Note that the weight of the central peak is twice as large as the side peaks.

The light scattered by a two-level atom also exhibits photon anti-bunching. Consider the conditional probability that given a photon is counted at time t another photon will be counted a time τ later. This is proportional to the second-order correlation function

$$G^{(2)}(t,\tau) = \langle a^\dagger(t)a^\dagger(t+\tau)a(t+\tau)a(t)\rangle \tag{9.74}$$

Usually we are interested in a stationary source so we let $t \to \infty$ and we normalize this by the intensity squared to define

$$g^{(2)}(\tau) = \lim_{t\to\infty}\frac{G^{(2)}(t,\tau)}{\langle a^\dagger(t)a(t)\rangle^2} \tag{9.75}$$

Using the result in (9.44) we can express this directly in terms of correlation functions for the atomic polarization. As the equations of motion for the atomic variables are linear, the stationary correlation function $\langle\sigma_+(t)\sigma_-(t+\tau)\rangle_{t\to\infty}$ is given by the quantum regression theorem. We then find that

$$g^{(2)}(\tau) = 1 - e^{-3\gamma\tau/4}\left(\cosh\delta\tau + \frac{3\gamma}{4\delta}\sinh\delta\tau\right) \tag{9.76}$$

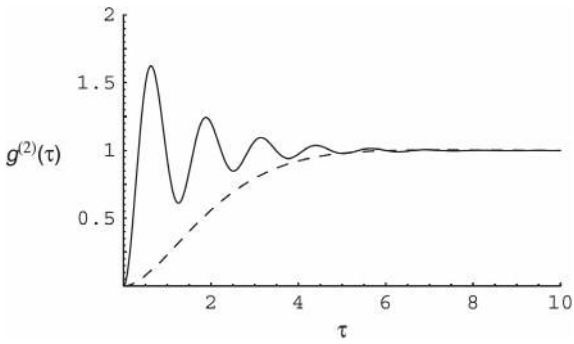

Fig. 9.3 The second order correlation function of the fluorescent light, given by (10.74) versus delay time τ. The *solid line* corresponds to $\Omega = 2.5$, while the *dashed line* corresponds to $\Omega = 0.25$. In both cases $\gamma = 1.0$

The result $g^{(2)}(\tau = 0) = 0$ indicates photon anti-bunching, as the probability to count a second photon, immediately after a first one has been counted, vanishes. This is a direct result of the emission process of the source. Photons are emitted when an excited atom relaxes back to the ground state. If a photon is counted, the atom is likely to be in the ground state and thus a finite time must elapse before it is re-excited and capable of emitting another one. The probability to find the atom in the excited state at time τ given that it starts in the ground state at $\tau = 0$ is

$$P_e(\tau) = \frac{4\Omega^2}{\gamma^2 + 8\Omega^2}\left[1 - e^{-3\gamma\tau/4}\left(\cosh\delta\tau + \frac{3\gamma}{4\delta}\sinh\delta\tau\right)\right] \tag{9.77}$$

Comparison with Fig. 9.3 indicates this interpretation is correct. This prediction, first made by Carmichael and Walls [11], was one of the earliest examples of how quantum optics would differ from a semiclassical description of light. In Fig. 9.3 we plot $g^{(2)}(\tau)$ for two values of the Rabi frequency.

The first observation of photon anti-bunching was made by Kimble et al. in 1977 on atomic beams [12]. They saw a positive slope for $g^{(2)}(\tau)$ which is consistent with the predictions of the theory, however fluctuations from atomic numbers in the beam made a detailed comparison with the single atom result impossible. Ion traps (see Chap. 12) provided a means to observe photon antibunching from a single atom. In Fig. 9.4 we show the results of a measurement of the second order correlation function performed on a single trapped mercury ion [14].

9.3 Cavity QED

We will now consider the case of a two-level atom interacting with the radiation field in an optical cavity. The study of this system is often known as cavity quantum electrodynamics (cavity QED). We are typically interested in the strong coupling regime in which the single photon Rabi frequency, g (the coupling constant in the Jaynes–Cummings model) is lager than both the spontaneous decay rate, γ, of the two-level emitter and the rate, κ , at which photons are lost from the cavity.

The primary difficulty we face in cavity QED is finding a way to localise a single two-level atom in the cavity mode for long time intervals. One approach, pioneered

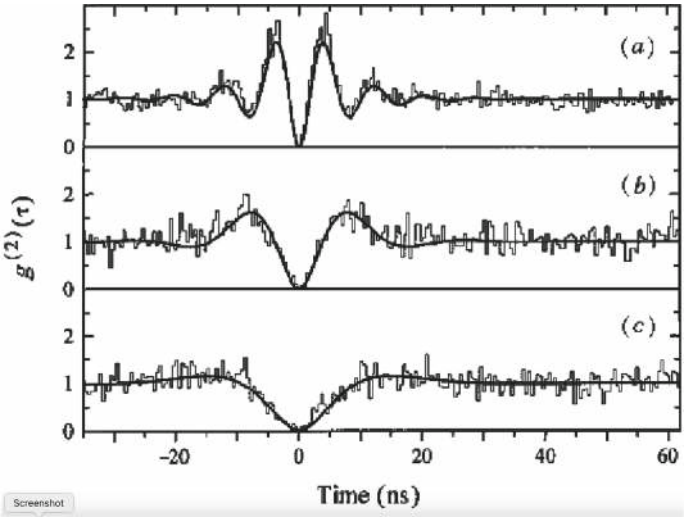

Fig. 9.4 The second order correlation function of the fluorescent light from a single mercury ion in a trap versus delay, τ. **a** $\Delta = -2.3\gamma$, $\Omega = 2.8\gamma$. **b** $\Delta = -1.1\gamma$, $\Omega = \gamma$. **c** $\Delta = -0.5\gamma$, $\Omega = 0.6\gamma$ (from [14])

by Kimble [15], is to first trap and cool two-level atoms in a magneto-optical trap (MOT) and then let them fall into a high finesse cavity placed directly below the MOT. If the geometry is correctly arranged then at most one atom will slowly fall through the cavity at a time.

The group of Haroche pioneered an approach using Rydberg atoms passing transversely through a microwave cavity [16]. The success of this approach resulted in Haroche being a joint recipient of the Nobel prize in physics in 2012. Other approaches use constraining forces to trap a single atom in the optical cavity. This can be done using the light shift forces of a far off resonant laser field on a two-level atom [17,18], or it can be done using an ion trap scheme (see Chap. 12).

Consider the scheme in Fig. 9.5. The interaction Hamiltonian between a single two-level atom at the point $\mathbf{x}$ in a Fabry-Perot cavity is given by

$$H_I = g(\mathbf{x})a^\dagger\sigma_- + g^*(\mathbf{x})a\sigma_+ \tag{9.78}$$

where

$$g(\mathbf{x}) = \left(\frac{\mu^2\omega_c}{2\hbar\epsilon_0 V}\right)^{1/2} U(\mathbf{x}) \equiv g_0 U(\mathbf{x}) \tag{9.79}$$

This is obtained from (9.17) with the traveling wave mode function replaced by a cavity standing wave mode function, $U(\mathbf{x})$. Here μ is the dipole moment for the two-level system and V is the cavity mode volume defined by $V = \int \sin[U(\mathbf{x})]^2 d^3x$.

Let us consider the interaction between a single cavity mode and a two-level system. For the present we neglect the spatial dependance of $g(\mathbf{x})$. The master equation,

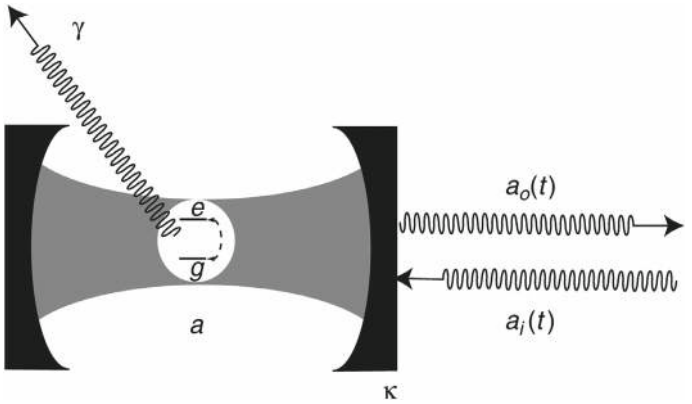

Fig. 9.5 A cavity QED scheme: a single two-level dipole emitter is fixed at a particular location inside a Fabry-Perot cavity. The dipole is strongly coupled to a single cavity mode, a, but can emit photons at rate γ into external modes. Photons are emitted from the end mirror of the cavity at rate κ

in the interaction picture, for a single two-level atom interacting with a single cavity mode, at optical frequencies, is

$$\frac{dp}{dt} = -i\delta[a^\dagger a, \rho] - i\frac{\Delta}{2}[\sigma_z, \rho] - i[\epsilon^* a + \epsilon a^\dagger, \rho] - ig[a\sigma_+ + a^\dagger\sigma_-, \rho] + \frac{\kappa}{2}(2a\rho a^\dagger - a^\dagger a\rho - \rho a^\dagger a) + \frac{\gamma}{2}(2\sigma_-\rho\sigma_+ - \sigma_+\sigma_-\rho - \rho\sigma_+\sigma_-) \quad (9.80)$$

where ϵ represents a classical coherent laser field driving the cavity mode at frequency ω_L, the detuning between the cavity field and the driving field is $\delta = \omega_c - \omega_L$, and $\Delta = \omega_a - \omega_L$ is the detuning between the two-level system and the driving field. From this equation we can derive equations for first order field/atom moments;

$$\frac{d\langle a\rangle}{dt} = -\left(\frac{\kappa}{2} + i\delta\right)\langle a\rangle - i\epsilon - ig\langle\sigma_-\rangle \quad (9.81)$$

$$\frac{d\langle\sigma_-\rangle}{dt} = -\left(\frac{\gamma}{2} + i\Delta\right)\langle\sigma_-\rangle + ig\langle a\sigma_z\rangle \quad (9.82)$$

$$\frac{d\langle\sigma_z\rangle}{dt} = -\frac{\gamma}{2}(\langle\sigma_z\rangle + 1) - ig\left(\langle a\sigma_+\rangle - \langle a^\dagger\sigma_-\rangle\right) \quad (9.83)$$

Looking at these equations we see that we do not get a closed set of equations for the first order moments, for example the equation for $\langle\sigma_-\rangle$ is coupled to $\langle a\sigma_z\rangle$. A number of procedures have been developed to deal with this. If there are many atoms interacting with a single mode field, an expansion in the inverse atomic number can be undertaken and we will describe this approach below. However a good idea of the behaviour expected can be obtained simply by factorising all higher order moments. This of course neglects quantum correlations and is thus not expected to be able to give correct expressions for, say, the noise power spectrum of light emitted from

the cavity. Nonetheless it is often a good place to start as it captures the underlying dynamical structure of the problem. We thus define the semiclassical equations as

$$\dot{\alpha} = -\frac{\tilde{\kappa}}{2}\alpha - i\epsilon - ig\nu \tag{9.84}$$

$$\dot{\nu} = -\frac{\tilde{\gamma}}{2}\nu + ig\alpha z \tag{9.85}$$

$$\dot{z} = ig\left(\alpha^*\nu - \alpha\nu^*\right) - \frac{\gamma}{2}(z+1) \tag{9.86}$$

where the dot signifies differentiation with respect to time and

$$\tilde{\kappa} = \kappa + 2i\delta \tag{9.87}$$

$$\tilde{\gamma} = \gamma + 2i\Delta \tag{9.88}$$

The first thing to consider is the steady state solutions, α_s, z_s, ν_s which are given implicitly by

$$z_s = -\left[1 + \frac{n}{n_0\left(1+\Delta_1^2\right)}\right]^{-1} \tag{9.89}$$

$$\alpha_s = -\frac{2i\epsilon}{\tilde{\kappa}}\left[1 + \frac{2C\,(1+i\phi)^{-1}\,(1+i\Delta_1)^{-1}}{1+\frac{n}{n_0(1+\Delta_1^2)}}\right]^{-1} \tag{9.90}$$

$$\nu_s = \frac{2ig}{\tilde{\gamma}}\alpha_s z_s \tag{9.91}$$

where

$$n = |\alpha_s|^2 \tag{9.92}$$

is the steady state intra-cavity intensity and

$$\phi = \frac{2\delta}{\kappa} \tag{9.93}$$

$$\Delta_1 = \frac{2\Delta}{\gamma} \tag{9.94}$$

$$n_0 = \frac{\gamma^2}{8g^2} \tag{9.95}$$

$$C = \frac{2g^2}{\kappa\gamma} \tag{9.96}$$

The parameter n_0 sets the scale for the intracavity intensity to saturate the atomic inversion and is known as the critical photon number. The parameter C is sometimes defined in terms of the critical atomic number, N_0, as $C = N_0^{-1}$.

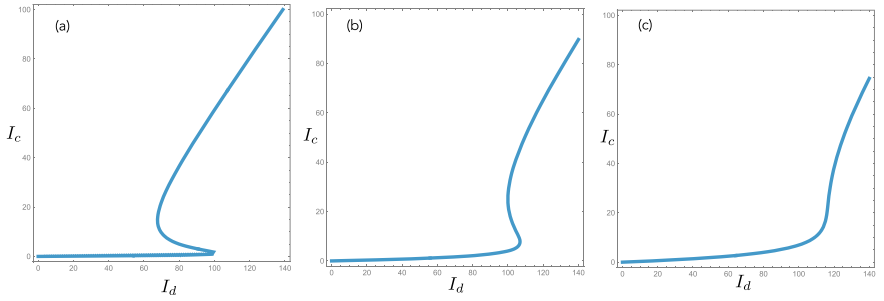

Fig. 9.6 The intracavity intensity versus the driving intensity, as given implicitly by (9.99), for various values of the detuning between the atom and the driving field. In all cases we assume the driving is on resonance with the cavity so that $\phi = 0$ and $C = 9$. **a** $\Delta_1 = 0$, **b** $\Delta_1 = 2$, **c** $\Delta_1 = 3$

We can now determine how the steady state intracavity intensity depends on the driving intensity. We first define the scaled driving intensity and intra-cavity intensity by

$$I_d = \frac{4\epsilon^2}{\kappa^2 n_0} \tag{9.97}$$

$$I_c = \frac{n}{n_0} \tag{9.98}$$

The driving intensity and the intracavity intensity are then related by

$$I_d = I_c \left[\left(1 + \frac{2C}{1 + \Delta_1^2 + I_c} \right)^2 + \left(\phi - \frac{2C\Delta_1}{1 + \Delta_1^2 + I_c} \right)^2 \right] \tag{9.99}$$

The phase θ_s of the steady state cavity field is shifted from the phase of the driving field (here taken as real) where

$$\tan\theta_s = \frac{\phi - 2\Delta_1 C/\left(1 + \Delta_1^2 + I_c\right)}{1 + 2C/\left(1 + \Delta_1^2 + I_c\right)} \tag{9.100}$$

Equation (9.99) is known as the bistability state equation, a name that makes sense when we plot the intracavity intensity versus the driving intensity, see Fig. 9.6. It can be shown that the steady state corresponding to those parts of the curve with negative slope are unstable. Clearly there are regions for which two stable steady states coexist for a given driving intensity.

Cavity QED requires that we are in the strong coupling limit in which $g_0 > \gamma, \kappa$. Furthermore a necessary condition for strong coupling is that $(n_0, N_0) \ll 1$. In this limit a single photon in the cavity can lead to significant dynamics. One way to make g_0 large is to use a very small mode volume V and a large dipole moment. Thompson et al. [20] trapped a single rubidium atom in a photonic crystal waveguide cavity. They achieved a Rabi frequency of several gigahertz. Typical parameters

are $2g = 2\pi \times 0.6$ Ghz, $\kappa = 2\pi \times 840$ GHz and $\gamma = 2\pi \times 0.006$ GHz. If the Rabi frequency begins to approach the atomic frequency we enter what is called the ultra-strong coupling regime wherein the rotating wave approximation begins to fail and the Jaynes-Cummings model breaks down [21].

9.3.1 Vacuum Rabi Splitting

With the ability to trap a single atom in the cavity and cool it to very low kinetic energies, it becomes possible to measure the vacuum Rabi splitting. This is the splitting energy, induced by the interaction in (9.30), of the degenerate states $|n = 0\rangle|e\rangle$, $|n = 1\rangle|g\rangle$ where $a^\dagger a|n\rangle = n|n\rangle$ is a photon number eigenstate for the intracavity field. As we saw in Sect. 9.1.1 these states are split in energy by $2g$. If g is large enough an excited atom is likely to emit a single photon into the cavity mode and periodically reabsorb and remit before the excitation is lost.

Boca et al. [19] observed the vacuum Rabi splitting using a single Cs atom trapped inside an optical Fabry-Perot cavity using a far off-resonance optical dipole trap. An important breakthrough that enabled this experiment was the ability to cool the atom using a Raman cooling scheme for motion of the atom along the cavity axis. The inferred uncertainties in the axial and transverse position of the atom in the trap were $\Delta z_{ax} \approx 33$ nm and $\Delta z_{trans} \approx 5.5\,\mu$m. The two electronic levels used were the $6S_{1/2}$, $F = 4 \rightarrow 6P_{3/2}$, $F' = 5$ transition of the $D2$ with a maximum single photon Rabi frequency of $2g_0/2\pi = 68$ MHz. The transverse atomic decay rate is $\gamma/2\pi = 1.3$ MHz and the cavity decay rate is $\kappa/2\pi = 2.05$ MHz. Clearly this is in the strong coupling regime.

A weak probe laser beam is incident on the cavity with a frequency ω_p that can be tuned through the atomic resonance frequency. The transmitted light is detected at a photodetector and thus the transmission coefficient can be measured. The results for six cases in which one atom was present in the cavity are shown in Fig. 9.7. Also shown as a solid line is the theoretical prediction based on the steady state solution to the master equation. The asymmetry of the peaks is due to the different Stark shifts for the Zeeman sub-levels of the excited state and optical pumping.

Problems

9.1 In the Jaynes-Cummings model, show that if the atom begins in the ground state and the field begins in the state, $|\phi\rangle = \sum_n f_n|n\rangle$, the probability to find the atom in the excited state at time $t > 0$ is given by

$$p_e(t) = \sum_{n=1}^{\infty} |f_n|^2 \sin^2(\Omega_{n-1}t) \tag{9.101}$$

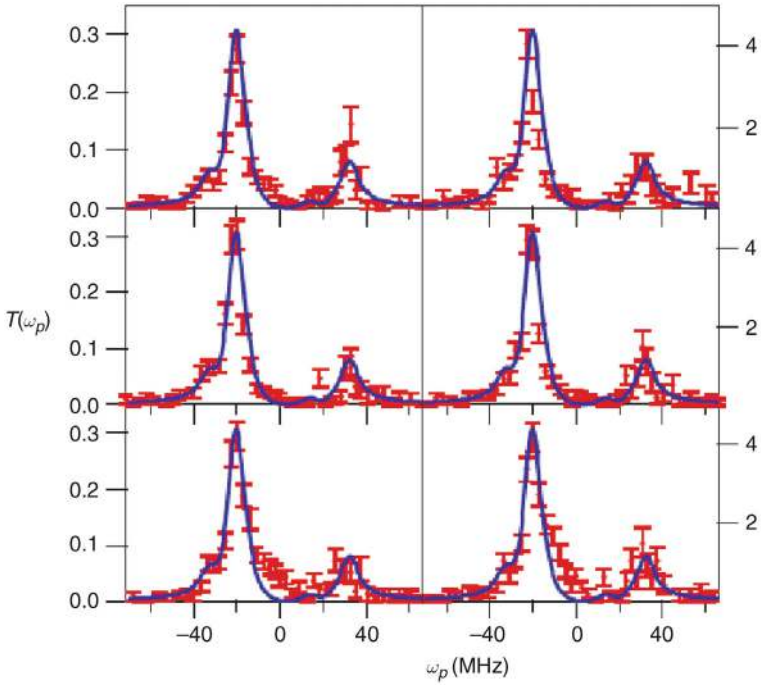

Fig. 9.7 The results of a measurement of the vacuum Rabi splitting performed by the Caltech group. Transmission spectrum for six randomly drawn atoms. Six different studies are shown, together with a comparison to theory (solid line). The error bars reflect the statistical uncertainties in the number of photocounts. From [19]

9.2 In the Jaynes–Cummings model, show that if the atom begins in the ground state and the field starts in an arbitrary state, $|\phi\rangle = \sum_n f_n|n\rangle$, the state at time $t > 0$ is the entangled state

$$|\Psi(t)\rangle = |\phi_g(t)\rangle|g\rangle + |\phi_e(t)\rangle|e\rangle \tag{9.102}$$

where

$$|\phi_g(t)\rangle = \sum_n f_n \cos(\Omega_{n-1}t)\ , \quad |\phi_e(t)\rangle = \sum_n f_n \sin(\Omega_{n-1}t)\ |\phi_e(t)\rangle$$

In the case of the field initially in a coherent state, plot the Q-functions for $|\phi_g(t)\rangle$, $|\phi_e(t)\rangle$ at times equal to half way to the first revival and at the first revival.

9.3 In the Jaynes-Cummings model suppose we prepare the two-level system in the state $|g\rangle$ and that the interaction with the field mode proceeds for a time τ at which point we make an arbitrarily accurate measurement of the atomic state. The resulting conditional (un-normalized) state for the field mode is $|\tilde{\psi}^{(x)}\rangle = E(x)|\psi(0)\rangle_a$ where $x = g, e$ and $E(x) = \langle x|e^{-i\theta(a\sigma_+ + a^\dagger\sigma_-)}|g\rangle$. Show that

$$E(g) = \cos(\theta\sqrt{aa^\dagger})\ , \quad E(e) = -ia^\dagger(aa^\dagger)^{-1/2}\sin(\theta\sqrt{aa^\dagger})\ . \tag{9.103}$$

If the field starts in a coherent state $|\alpha\rangle$ show that the conditional states can approximate cat-states.

9.4 A two-level atom driven by a thermal radiation field satisfies the master equation (9.40). Show that the steady state of the atom is a thermal state with steady state probabilities satisfying

$$\frac{p_e}{p_g} = e^{-\hbar\omega_a/k_BT} \tag{9.104}$$

9.5 A two-level atom resonantly coupled to a cavity field via the Jaynes-Cummings interaction, at zero temperature, is described by the master equation

$$\begin{aligned}\frac{dp}{dt} =& -i[\epsilon^* a + \epsilon a^\dagger, \rho] - ig[a\sigma_+ + a^\dagger\sigma_-, \rho] \\ &+ \frac{\kappa}{2}(2a\rho a^\dagger - a^\dagger a\rho - \rho a^\dagger a) + \frac{\gamma}{2}(2\sigma_-\rho\sigma_+ - \sigma_+\sigma_-\rho - \rho\sigma_+\sigma_-)\end{aligned} \tag{9.105}$$

Show that, in the limit that the cavity damping rate is much greater than the spontaneous emission rate, the effective master equation for the atom is

$$\frac{d\rho}{dt} = -ig[\alpha_0\sigma_+ + \alpha_0^*\sigma_-, \rho] + \frac{\Gamma}{2}(2\sigma_-\rho\sigma_+ - \sigma_+\sigma_-\rho - \rho\sigma_+^\dagger\sigma_-) \tag{9.106}$$

where $\alpha = -2i\epsilon/\kappa$ and $\Gamma = \gamma + 4g^2/\kappa$.

References

1. H. Haken, *Waves, Photons and Atoms*, vols. 1 and 2 (North Holland, Amsterdam, 1981)
2. C. Cohen-Tannoudji, J. Dupont-Roc, G. Grynberg, *Photons and Atoms: Introduction to Quantum Electrodynamics* (Wiley-Interscience, 1997)
3. R. Loudon, *Quantum Theory of Light* (Oxford University Press, Oxford, 1973)
4. B.W. Shore, P.L. Knight, The Jaynes–Cummings model. J. Mod. Opt. **40**, 1195–1238 (1993)
5. T. Aoki, B. Dayan, E. Wilcut, W.P. Bowen, A.S. Parkins, T.J. Kippenberg, K.J. Vahala, H.J. Kimble, Nature **443**, 671 (2006)
6. S. Haroche, in *New Trends in Atomic Physics*, ed. by G. Grynberg, R. Stora, Les Houche Session XXXVIII (Elsevier, Amsterdam 1984)
7. J.M. Raimond, M. Brune, S. Haroche, Rev. Mod. Phys. **73**, 565–582 (2001)
8. H.J. Carmichael, *Statistical Methods in Quantum Optics-I* (Springer, 1999)
9. R.J. Glauber, Phys. Rev. **131**, 2766 (1963)
10. B.R. Mollow, Phys. Rev. **188**, 1969 (1969)
11. H.J. Carmichael, D.F. Walls, Proposal for the measurement of the resonant stark effect by photon correlation techniques. J. Phys. B **9**, L43 (1976)
12. H.J. Kimble, M. Degenais, L. Mandel, Phys. Rev. Lett. **39**, 691 (1977)
13. F. Diedrich, H. Walther, Phys. Rev. Lett. **58**, 203 (1987)
14. H. Walther, Proc. R. Soc. Lond. A **454**, 431 (1998)
15. T. Aoki, B. Dayan, E. Wilcut, W.P. Bowen, A.S. Parkins, H.J. Kimble, Nature **443**, 671 (2006)

16. S. Haroche, J.-M. Raimond, *Exploring the Quantum: Atoms, Cavities and Photons* (Oxford University Press, 2006)
17. J. Ye, D.W. Vernooy, H.J. Kimble, Phys. Rev. Lett. **83**, 4987 (1999)
18. T. Puppe, I. Schuster, A. Grothe, A. Kubanek, K. Murr, P.W.H. Pinske, G. Rempe: quantph/072162 (2007)
19. A. Boca, R. Miller, K.M. Birnbaum, A.D. Boozer, J. McKeever, H.J. Kimble, Phys. Rev. Lett. **93**, 233603 (2004)
20. J.D. Thompson et al., Science **340**, 1202 (2013)
21. P. Forn-Diaz, L. Lamata, E. Rico, J. Kono, E. Solano, Rev. Mod. Phys. **91**, 025005 (2019)

Quantum Theory of the Laser

10

Abstract

The quantum theory of the laser was developed in the 1960s principally by the groups associated with H. Haken, W.E. Lamb and M. Lax. Haken and Lax independently developed sophisticated techniques to convert operator master equations into c-number Fokker–Planck equations or equivalent Langevin equations. In this chapter we shall follow the approach of Scully and Lamb to compute photon statistics and the linewidth of the laser. In the Scully–Lamb treatment the pumping is modelled by the injection of a sequence of inverted atoms into the laser cavity. In a usual laser, with a thermal pumping mechanism, a Poisson distributed sequence of inverted atoms is assumed. Introduction of a Bernoulli distribution enables a more general class of pumping mechanisms to be considered, including the case of the regularly pumped laser.

10.1 Master Equation

A single mode cavity field is excited by a sequence of atoms injected into the cavity. Let t_i be the arrival time of the atom i in the cavity and τ the time spent by each atom in the cavity. The change in the density operator for the field due to the interaction with the ith atom may be represented by

$$\rho(t_i + \tau) = \mathcal{P}(\tau)\rho(t_i). \tag{10.1}$$

The explicit form of $\mathcal{P}(\tau)$ depends on the particular atomic system used in the excitation process. The model we will employ is indicated in Fig. 10.1.

Of the four levels, only levels $|1\rangle$ and $|2\rangle$ are coupled to the intracavity field, which thus are referred to as the lasing levels. Each of these levels may then decay. Level $|1\rangle$ decays to level $|3\rangle$ at a rate γ_1 while level $|2\rangle$ decays to level $|4\rangle$ at a rate γ_2.

We will assume that these decay rates are very much greater than the spontaneous decay rate of level $|2\rangle$ to level $|1\rangle$, and thus we neglect spontaneous emission in the lasing levels. Each atom is prepared in the excited state $|2\rangle$ prior to interaction with

D. F. Walls and G. J. Milburn, *Quantum Optics*, Graduate Texts in Physics,
https://doi.org/10.1007/978-3-031-84177-4_10

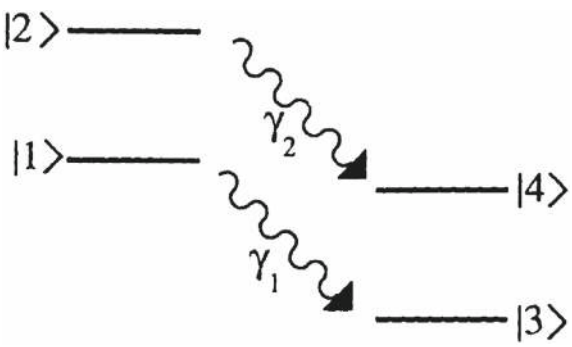

Fig. 10.1 Schematic representation of the four-level atomic model of a laser. Only levels 1 and 2 are coupled to the laser field

the cavity field. In the usual laser system the lifetimes γ_1^{-1} and γ_2^{-1} are much shorter than the time τ spent by each atom in the cavity. This means that each atom rapidly attains a steady state in passing through the cavity and the pump operation $\mathcal{P}(\tau)$ is effectively independent of the time τ. The effect of a single atom on the state of the field may then be written as

$$\rho' = \mathcal{P}\rho, \tag{10.2}$$

where we have dropped the time dependence in ρ for simplicity, the prime serving to indicate the state of the field after the passage of a single atom through the cavity. We may represent the initial state of the field quite generally as

$$\rho = \sum_{n,m=0}^{\infty} \rho_{n,m}(0)|n\rangle\langle m|. \tag{10.3}$$

In Appendix A.10, we solve the master equation for the system over the time τ under the assumptions discussed above. The result is

$$\rho' = \sum_{n,m=0}^{\infty} \rho_{n,m}(0)\left(A_{nm}|n\rangle\langle m| + B_{nm}|n+1\rangle\langle m+1|\right), \tag{10.4}$$

where the explicit expressions for A_{nm}, B_{nm} are given in the appendix.

We now assume that each atom contributes independently to the field. (This assumption remains valid even if there is more than one atom in the cavity at any time, provided that they are sufficiently dilute.) Thus, if k atoms are passed through the cavity from time 0 to time t the field density operator at time t is given by

$$\rho(t) = \mathcal{P}^k\rho(0). \tag{10.5}$$

More generally, however, not all atoms entering the cavity are prepared in the excited state. Let the probability for an excited atom to enter the cavity between t and $t + \Delta t$ be $r\Delta t$, r being the average injection rate. This defines a Poisson

excitation process. Thus the field at time $t + \Delta t$ is made up of a mixture of states corresponding to atomic excitation and no atomic excitation, thus

$$\rho(t + \Delta t) = r\Delta t \mathcal{P}\rho(t) + (1 - r\Delta t)\rho(t). \tag{10.6}$$

In the limit $\Delta t \to 0$ we have

$$\frac{d\rho(t)}{dt} = r\mathcal{U}\rho(t) \tag{10.7}$$

where

$$\mathcal{U} = \mathcal{P} - 1. \tag{10.8}$$

We must now include the decay of the cavity field through the end mirrors. This is modelled in the usual way by coupling the field to a zero temperature heat bath. Thus the total master equation for the field density operator is

$$\frac{d\rho}{dt} = r\mathcal{U}\rho + \frac{\kappa}{2}(2a\rho a^\dagger - a^\dagger a\rho - \rho a^\dagger a), \tag{10.9}$$

where κ is the cavity decay rate. This is the Scully–Lamb laser master equation [3].

In the special case that $\gamma_1 = \gamma_2 = \gamma$ the matrix elements of $\mathcal{U}$ in the number basis are greatly simplified. In this case the master equation in the number basis may be written as

$$\begin{aligned}\frac{d\rho_{nm}}{dt} =& G\left(\frac{\sqrt{nm}}{1 + (n+m)/2n_s}\rho_{n-1,m-1}\right. \\ &\left. - \frac{(m+n+2)/2 + (m-n)^2/8n_s}{1 + (n+m+2)/2n_s}\rho_{nm}\right) \\ &+ \frac{\kappa}{2}[2\sqrt{(n+1)(m+1)}\rho_{n+1,m+1} - (n+m)\rho_{nm}],\end{aligned} \tag{10.10}$$

where

$$G = \frac{r}{2n_s} \tag{10.11}$$

and

$$n_s = \frac{\gamma^2}{4g^2}. \tag{10.12}$$

where g is the coupling strength between the cavity and the levels 1 and 2. We have neglected terms $\propto n_s^{-2}$ in the denominators of the first two coefficients.

The master equation (10.10) can be written in the form [4]

$$\dot{\rho} = Gn_s\mathcal{D}[a^\dagger]\left(\mathcal{A}[a^\dagger] + n_s\right)^{-1}\rho + \kappa\mathcal{D}[a]\rho \tag{10.13}$$

where the super-operators are defined by

$$\mathcal{D}[B]\rho = B\rho B^\dagger - \frac{1}{2}(A^\dagger A\rho + \rho A^\dagger A) \tag{10.14}$$

$$\mathcal{A}[B]\rho = \frac{1}{2}(B^\dagger B\rho + \rho B^\dagger B) \tag{10.15}$$

and G is the small signal gain, n_s is the saturation photon number and κ is the cavity decay rate. The inverse superoperator can be represented as

$$\left(\mathcal{A}[a^\dagger] + n_s\right)^{-1} = \int_0^\infty d\beta e^{-\beta(aa^\dagger + n_s)/2}\rho e^{-\beta(aa^\dagger + n_s)/2} \tag{10.16}$$

which describes the incoherent pumping process that leads to saturation of the amplification. The first term in (10.13) represents gain, that is to say, the injection of energy into the cavity field, while the second term represents photon loss through the cavity mirrors. We have also assumed operation at optical frequencies to ignore thermal photons entering the cavity. Any noise necessarily arises from quantum fluctuations not thermal fluctuations.

The photon number distribution obeys the equation

$$\frac{dp_n}{dt} = -G\left(\frac{n+1}{1+(n+1)/n_s}p_n - \frac{n}{1+(n/n_s)}p_{n-1}\right) + \kappa(n+1)p_{n+1} - \kappa n p_n. \tag{10.17}$$

If we expand the denominators in (10.17) to first-order an approximate equation for the mean photon number may be obtained, namely

$$\frac{d\bar{n}}{dt} = (G-\kappa)\bar{n} - \frac{G}{n_s}(\bar{n}^2 + 2\bar{n} + 1) + G. \tag{10.18}$$

If $G > \kappa$ there will be an initial exponential increase in the mean photon number. Thus $G = \kappa$ is the threshold condition for the laser.

The steady state photon number distribution may be deduced directly from (10.17), using the condition of detailed balance. It may be written in the form

$$P_n^{ss} = \mathcal{N}\frac{(Gn_s/\kappa)^{n+n_s}}{(n+n_s)!}, \tag{10.19}$$

where $\mathcal{N}$ is a normalisation constant. Below threshold ($G < \kappa$) this distribution may be approximated by a chaotic (thermal) distribution with the mean $\bar{n} = G/(\kappa - G)$ (Exercise 10.1). Above threshold ($G > \kappa$) the mean and variance are given, to a good approximation, by (Exercise 10.2),

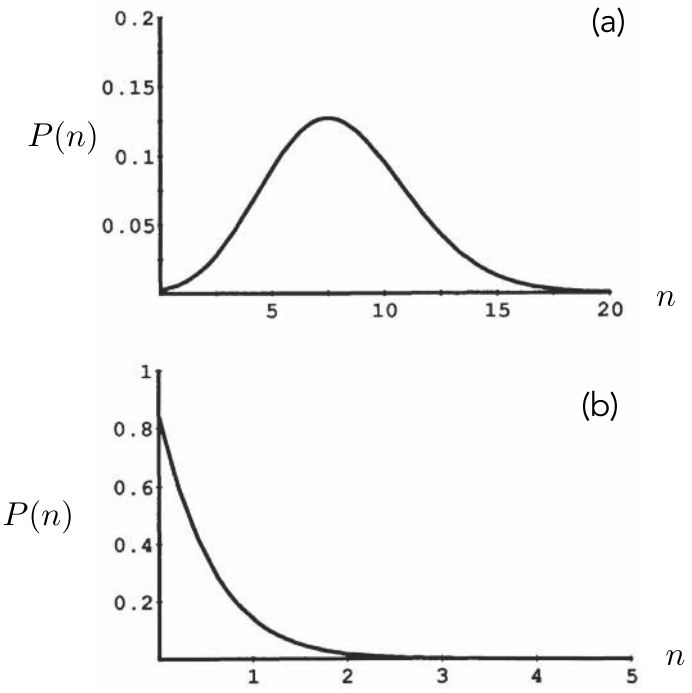

Fig. 10.2 The steady state photon number distribution of a laser operating above and below threshold. In **a** $G/\kappa = 5.0$, in **b** $G/\kappa = 0.25$. In both cases $n_s = 2$

$$\bar{n} = n_s \left(\frac{G}{\kappa} - 1 \right), \tag{10.20}$$

$$V(n) = \bar{n} + n_s. \tag{10.21}$$

Well above threshold $\bar{n} \gg n_s$ and thus $V(n) \approx \bar{n}$, indicating an approach to Poisson statistics. We can write the steady state density operator as

$$\rho_{ss} = \sum_{n=0}^{\infty} \frac{\bar{n}^n}{n!} e^{-\bar{n}} |n\rangle\langle n| = \int_0^{2\pi} \frac{d\phi}{2\pi} |\sqrt{\bar{n}} e^{i\phi}\rangle\langle\sqrt{\bar{n}} e^{i\phi}| \tag{10.22}$$

In Fig. 10.2 we show the exact photon number distribution for below and above threshold. The transition from power law to the Poisson distribution is quite evident.

Photon counting experiments by Arecchi [6], Johnson et al. [7], and Morgan and Mandel [10], demonstrated that the photon statistics of a laser well above threshold, approaches a Poisson distribution. In Fig. 10.3 we present the results of photon counting measurements by Arecchi on both thermal and laser light. A comparison of the experimental data with the thermal and Poisson distributions is also shown.

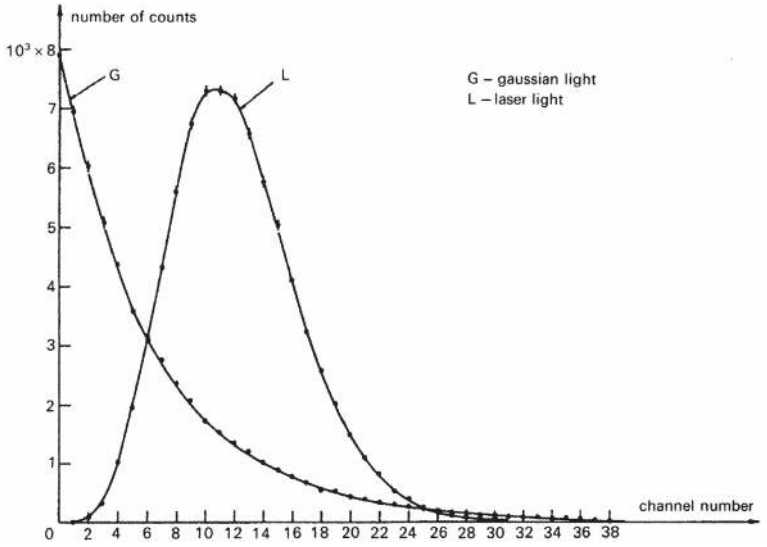

Fig. 10.3 Experimental results for the steady state photon number distribution for a thermal (i.e., Gaussian) light source and a laser operator above threshold. The laser exhibits Poissonian photon number statistics [5]

10.1.1 Laser Linewidth

First we will consider an equivalent classical model. This can be found by computing the dynamics of the average field $\alpha(t) = \mathrm{tr}(a\rho(t))$. Substituting this into the master equation and factorising moments (equivalent to neglecting quantum noise) the semiclassical dynamics (in the lab frame) is given by

$$\dot{\alpha} = -i\omega\alpha - \frac{\kappa\alpha}{2}\left(1 - \frac{Gn_s}{\kappa(|\alpha|^2 + n_s)}\right) \tag{10.23}$$

Well above threshold this is similar to the van der Pol oscillator in a rotating frame. There are two fixed points $\alpha_0 = 0$ and $|\alpha_0|^2 = (G-1)n_s/\kappa \equiv \mu$. The second solution is the above threshold limit-cycle solution with a frequency of ω.

In oder to include the quantum noise we can convert the interaction picture master equation to an equivalent Fokker-Planck equation in the P representation [8] from which we can deduce the Ito stochastic differential equations (in the interaction picture). The Fokker-Planck equation is

$$\frac{\partial P}{\partial t} = \frac{1}{2}\frac{\partial}{\partial\alpha}\left[\kappa\alpha\left(1 - \frac{G/\kappa}{1 + |\alpha|^2/n_s}\right) + c.c\right]P + G\frac{\partial^2}{\partial\alpha\partial\alpha^*}P \tag{10.24}$$

$$\dot{\alpha} = -\frac{\kappa\alpha}{2}\left(1 - \frac{Gn_s}{\kappa(|\alpha|^2 + n_s)}\right) + \Gamma(t) \tag{10.25}$$

where the Weiner noise term is

$$d\Gamma(t)^2 = d\Gamma^*(t)^2 = 0 \tag{10.26}$$

$$d\Gamma(t)d\Gamma^*(t) = Gdt \tag{10.27}$$

and N is the number of atoms.

Define $\alpha = re^{i\phi}$. Using the Ito rules we then find that these obey the stochastic differential equations

$$dr = -\frac{\kappa r}{2}\left(1 - \frac{Gn_s}{\kappa(r^2 + n_s)} + \frac{G}{4r}\right)dt + d\Gamma_r(t) \tag{10.28}$$

$$d\phi = \frac{1}{r}d\Gamma_\phi(t) \tag{10.29}$$

where

$$d\Gamma_r(t)^2 = d\Gamma_\phi(t)^2 = \frac{G}{2}dt \tag{10.30}$$

$$d\Gamma_r(t)d\Gamma_\phi(t) = 0 \tag{10.31}$$

Note that the noise in the phase variable is inversely proportional to the size of the limit cycle. This is typical of how noise enters limit cycles [9]. We can linearise the phase noise by evaluating it on the limit cycle $r_0^2 = \bar{n}$.

$$d\phi = -i\omega dt + 2\sqrt{\Gamma}dW \tag{10.32}$$

where

$$\Gamma = \frac{G}{8\bar{n}} \tag{10.33}$$

We see that the phase diffusion rate decreases as the mean photon number increases. As the rate of energy dissipated from the laser cavity is $\kappa\bar{n}$ we conclude that the phase diffusion rate decreases as the rate of energy dissipation increases. This has important consequences for clock design.

The phase diffusion means that the period (T) on the limit cycle is a random variable, where T is defined as the time taken for the phase to change by 2π. This is a first passage time problem as each period is an independent random variable. The distribution of periods is given by the inverse Gaussian distribution [9]

$$W(T, \alpha, \lambda) = \sqrt{\frac{\lambda}{2\pi}}T^{-3/2}\exp\left[-\frac{\lambda}{2\alpha^2 T}(T-\alpha)^2\right] \quad t \geq 0. \tag{10.34}$$

where α, λ are positive real parameters (λ is called the spread parameter). The mean and variance are

$$\overline{T} = \alpha \tag{10.35}$$

$$\overline{\Delta T^2} = \frac{\alpha^3}{\lambda} \tag{10.36}$$

In the laser we find that

$$\overline{T} = \frac{2\pi}{\omega} \tag{10.37}$$

$$\overline{\Delta T^2} = \frac{8\pi}{\Gamma\omega^3} \tag{10.38}$$

Clearly the laser above threshold is a noisy clock. A quality measure of this clock can be defined as

$$N = \frac{\overline{T}^2}{\overline{\Delta T^2}} \tag{10.39}$$

In this case we see that

$$N = \pi\omega/(2\Gamma) \tag{10.40}$$

The performance of the clock gets better as the line width gets smaller, that is to say, the further the laser is above threshold. It also indicates that the clock gets better the more power is dissipated.

Well above threshold the laser produces Poisson photon statistics. A coherent state has the same photon statistics, and this suggests that well above threshold the laser might be producing a coherent state. This is not the case. While the intensity of the laser is stabilized with a Poissonian distribution the phase of the laser undergoes a diffusion process. We previously saw that the coherent amplitude undergoes phase diffusion at a rate that decreases as the limit cycle increases. Can we see this directly from the master equation?

We first consider the dynamics of the mean amplitude $\langle a(t)\rangle$ for a laser well above threshold. Care must be take as there are two different time scales involved; relaxation onto the limit cycle and a slower phase diffusion on the limit cycle.

The effect of this phase diffusion is to cause a decay in the mean amplitude of the laser field, as the phase becomes uniformly distributed over 2π. The mean amplitude is defined by

$$\langle a(t)\rangle = \sum_{n=0}^{\infty} n^{1/2}\rho_{n,n-1}(t). \tag{10.41}$$

Using (10.13) we find

$$\frac{d\langle a\rangle}{dt} = -\frac{G}{2}\sum_{n=0}^{\infty}\frac{1/4n_s + 1}{1 + (2n+1)/2n_s}\sqrt{n}\rho_{n,n-1} - \frac{\kappa}{2}\langle a\rangle \tag{10.42}$$

Assuming the laser operates well above threshold we can replace n by $\bar{n}$ in the denominator of each coefficient. Then as $\bar{n} \gg n_s$

$$\frac{d\langle a\rangle}{dt} = -\frac{G}{8\bar{n}}\langle a\rangle. \tag{10.43}$$

The rate of amplitude decay Γ is thus a direct measure of the phase diffusion rate. We now show that Γ is the measured laser linewidth. In oder to do this we consider heterodyne detection of the field emitted from the laser cavity.

We now turn to the noise power spectrum. The key quantity is the two-time correlation function

$$G^{(1)}(\tau) = \kappa \mathrm{tr}[a^\dagger e^{\mathcal{L}\tau} a \rho_{ss}] \tag{10.44}$$

Using the quantum regression theorem we expect that

$$G^{(1)}(\tau) = \kappa \bar{n} e^{-\gamma|\tau|} \tag{10.45}$$

where $\gamma = \frac{G}{8\bar{n}}$.

The noise power spectrum is the Fourier transform of this

$$P(\Omega) = \frac{\kappa \bar{n}}{2\pi} \frac{\gamma}{\gamma^2 + (\omega - \Omega)^2} \tag{10.46}$$

where the line width is

$$\gamma = \frac{G}{8\bar{n}} \tag{10.47}$$

a Lorentzian. Thus the line width of the laser, well above threshold, is inversely proportional to the intensity of the laser and gets smaller as the power dissipation increases.

Problems

10.1 The van der Pol (VdP) oscillator model was introduced to explain limit cycles (sometimes called relaxation oscillations) in electronic circuits. The equations of motion are

$$\begin{aligned} \dot{x} &= y \,, \\ \dot{y} &= \epsilon(1 - x^2)y - x + a \,. \end{aligned}$$

The original model set $a = 0$. If $a \neq 0$ it is called the driven VdP oscillator. when $\epsilon = 0$ this describes an undamped harmonic oscillator. When $\epsilon \neq 0$ it describes non linear damping for $x^2 > 1$ and non linear gain when $x^2 < 1$.

Use a coding environment of your choice to simulate the dynamics of this system and investigate the fixed points and limit cycles as a function of ϵ, a.

10.2 This problem refers to the photon number statistics of the laser, see (10.17)

(a) Show that the steady state solution is

$$p_n^{ss} = \mathcal{N} \frac{(Gn_s/\kappa)^{n+n_s}}{(n + n_s)!}$$

(b) Below threshold $G < \kappa$ show that this can be approximated by

$$p_n^{ss} \approx \frac{1}{1+\bar{n}} \left(\frac{\bar{n}}{\bar{n}+1} \right)^n \qquad G < \kappa$$

(c) Show that this is analogous to a thermal distribution with mean photon number given by

$$\bar{n} = \frac{G}{\kappa - G}$$

(d) Show that well above threshold, $G \gg \kappa$, the steady state distribution is Poisson with mean $\bar{n} = G n_s / \kappa$

10.3 A semiclassical model for a laser is given in terms of the complex amplitude of the field in the rotating frame. $\alpha(t)$

$$\dot{\alpha} = -\frac{\kappa \alpha}{2} \left(1 - \frac{G n_s}{\kappa (|\alpha|^2 + n_s)} \right)$$

Show that are two fixed points $\alpha_0 = 0$ and $|\alpha_0|^2 = G(n_s - 1)/\kappa$ and investigate their stability. This is done by using a linear approximation for the dynamics near each fixed point and calculating the eigenvalues of the corresponding matrix. The second solution is the above threshold limit-cycle solution.

Appendix 10.1: Derivation of the Single-Atom Increment

Consider a single multilevel atom (Fig. 10.1) prepared in the state $|2\rangle$. Level $|1\rangle$ is damped at the rate γ_1 to level $|3\rangle$ and level $|2\rangle$ is damped at the rate γ_2 to level $|4\rangle$. Only levels $|1\rangle$ and $|2\rangle$ interact with the cavity field. The master equation describing the dynamics of this system is

$$\begin{aligned} \frac{d\rho}{dt} &= ig \left[a^\dagger \sigma_{12}^- + a \sigma_{12}^+, \rho \right] \\ &\quad + \frac{\gamma_1}{2} \left(2\sigma_{13}^- \rho \sigma_{13}^+ - \sigma_{13}^+ \sigma_{13}^- \rho - \rho \sigma_{13}^+ \sigma_{13}^- \right) \\ &\quad + \frac{\gamma_2}{2} \left(2\sigma_{24}^- \rho \sigma_{24}^+ - \sigma_{24}^+ \sigma_{24}^- \rho - \rho \sigma_{24}^+ \sigma_{24}^- \right). \end{aligned} \tag{10.48}$$

Define the operation

$$J\rho = \gamma_1 \sigma_{13}^- \rho \sigma_{13}^+ + \gamma_2 \sigma_{24}^- \rho \sigma_{24}^+, \tag{10.49}$$

and the rate operator

$$\begin{aligned} R &= \gamma_1 \sigma_{13}^+ \sigma_{13}^- + \gamma_2 \sigma_{24}^+ \sigma_{24}^- \\ &= \gamma_1 |1\rangle \langle 1| + \gamma_2 |2\rangle \langle 2|. \end{aligned} \tag{10.50}$$

The formal solution to the master equation is

$$\rho(t) = S(t)\rho(0) + \int_0^t dt_1\, S(t-t_1) J S(t_1)\rho(0) + \int_0^t dt_1 \int_0^{t_1} dt_2\, S(t-t_1) J S(t_1-t_2) J S(t_2)\rho(0) + \cdots, \tag{10.51}$$

where

$$S(t)\rho = B(t)\rho B^\dagger(t), \tag{10.52}$$

with

$$B(t) = \exp\left[-ig(a^\dagger \sigma_{12}^- + a\sigma_{12}^+) - \gamma_1 t\, |1\rangle\langle 1| - \gamma_2 t\, |2\rangle\langle 2|\right]. \tag{10.53}$$

Assume the initial state

$$\rho(0) = |2\rangle\langle 2| \otimes \rho_F(0) = \sum_{n,m=0}^{\infty} \rho_{nm}(0)\, |n,2\rangle\langle m,2|, \tag{10.54}$$

where

$$|n,2\rangle = |n\rangle_F \otimes |2\rangle. \tag{10.55}$$

After the action of J, the atom is in a mixture of the states $|3\rangle$ and $|4\rangle$ and is decoupled from the field. The series truncates at first order.

Use the eigenstates of the free Hamiltonian:

$$|n,+\rangle = \frac{1}{\sqrt{2}}(|n,2\rangle + |n+1,1\rangle), \tag{10.56}$$

$$|n,-\rangle = \frac{1}{\sqrt{2}}(|n,2\rangle - |n+1,1\rangle), \tag{10.57}$$

to show

$$S(t)(|n,2\rangle\langle m,2|) = \left(c_n^+(t)\,|n,+\rangle + c_n^-(t)\,|n,-\rangle\right)\left(\langle m,+|\, c_m^{+*}(t) + \langle m,-|\, c_m^{-*}(t)\right), \tag{10.58}$$

where

$$c_n^+(t) = \frac{-ie^{-\gamma_+ t/2}}{2\sqrt{2\Delta\Omega(n)}}\left\{\left[-i\Omega(n)(1-\Delta) + \frac{\gamma_-}{2}\right]e^{i\Delta\Omega(n)t} + \left[i\Omega(n)(1+\Delta) - \frac{\gamma_-}{2}\right]e^{-i\Delta\Omega(n)t}\right\}, \tag{10.59}$$

$$c_n^-(t) = \frac{-ie^{-\gamma_+ t/2}}{2\sqrt{2\Delta\Omega(n)}}\left\{\left[i\Omega(n)(1+\Delta) + \frac{\gamma_-}{2}\right]e^{i\Delta\Omega(n)t} + \left[-i\Omega(n)(1-\Delta) - \frac{\gamma_-}{2}\right]e^{-i\Delta\Omega(n)t}\right\}, \tag{10.60}$$

with

$$\gamma_{\pm} = \frac{1}{2}(\gamma_1 \pm \gamma_2), \tag{10.61}$$

$$\Delta = \left(1 - \frac{\gamma_2^2}{4\Omega(n)^2}\right)^{1/2}, \tag{10.62}$$

$$\Omega(n) = g\sqrt{n+1}. \tag{10.63}$$

Assume $\gamma_{1,2}t \gg 1$ so that the first term in the expansion can be neglected. Then trace over atomic states:

$$\begin{aligned}\mathrm{Tr}_A\left(JS(t)\left|n,2\right\rangle\left\langle m,2\right|\right) = \frac{\gamma_2}{2}\left|n\right\rangle\left\langle m\right|\left[c_n^+(t)+c_n^-(t)\right]\left[c_m^+(t)^*+c_m^-(t)^*\right] \\ + \frac{\gamma_1}{2}\left|n+1\right\rangle\left\langle m+1\right|\left[c_n^+(t)-c_n^-(t)\right]\left[c_m^+(t)^*-c_m^-(t)^*\right].\end{aligned} \tag{10.64}$$

Thus, in steady state, the single-atom increment is

$$\rho' = \sum_{n,m=0}^{\infty} \rho_{nm}(0)\left(A_{nm}\left|n\right\rangle\left\langle m\right| + B_{nm}\left|n+1\right\rangle\left\langle m+1\right|\right), \tag{10.65}$$

with

$$A_{nm} = \frac{\gamma_2}{2}\int_0^{\infty} dt\left[c_n^+(t)+c_n^-(t)\right]\left[c_m^+(t)^*+c_m^-(t)^*\right], \tag{10.66}$$

$$B_{nm} = \frac{\gamma_1}{2}\int_0^{\infty} dt\left[c_n^+(t)-c_n^-(t)\right]\left[c_m^+(t)^*-c_m^-(t)^*\right]. \tag{10.67}$$

We require $\mathrm{Tr}(\rho) = 1$, so $A_{nn} + B_{nn} = 1$. Diagonal elements are

$$A_{nn} = \left(\frac{\gamma_2}{2\gamma_+}\right)\frac{4\Omega(n)^2 + 2\gamma_1\gamma_+}{4\Omega(n)^2 + \gamma_1\gamma_2}, \tag{10.68}$$

$$B_{nn} = 1 - A_{nn} = \left(\frac{\gamma_2}{2\gamma_+}\right)\frac{4\Omega(n)^2}{4\Omega(n)^2 + \gamma_1\gamma_2}. \tag{10.69}$$

To compute the change in the state, write

$$\rho' = (1+U)\rho = P\rho. \tag{10.70}$$

The diagonal elements of $U\rho$ are

$$\left\langle n\right|U\rho\left|n\right\rangle = -a_{n+1}p_n + a_n p_{n+1}, \tag{10.71}$$

where

$$a_{n+1} = A_{n-1}. \tag{10.72}$$

References

1. H. Haken, *Laser Theory, Reproduction from Handbuch der Physik* (Springer, Berlin, Heidelberg, 1984)
2. M. Sargent III, M.O. Scully, W.E. Lamb, *Laser Physics* (Addison Wesley, 1974)
3. M.O. Scully, W.E. Lamb, Phys. Rev. **159**, 208 (1967)
4. H.M. Wisemanm, Phys. Rev. A **60**, 4083 (1999)
5. M. Lax, W.H. Louisell, Phys. Rev. **185**, 568 (1969)
6. F.T. Arecchi, Phys. Rev. Lett. **15**, 912 (1965)
7. E.A. Johnson, R. Jones, T.P. McLean, E.R. Pike, Phys. Rev. Lett. **16**, 589 (1966)
8. C.W. Gardiner, P. Zoller, *Quantum Noise* (Springer, 2004)
9. Z. Aminzare , P. Holmes, V. Srivastava, *EEE 58th Conference on Decision and Control (CDC)*, vol. 4717 (2019)
10. B.L. Morgan, L. Mandel, Phys. Rev. Lett. **16**, 1012 (1966)

Quantum Optics at Microwave Frequencies

11

Abstract

In this chapter we discuss cavity quantum electrodynamics for microwave photons. As there is a significant population of thermal photons at microwave frequencies, these experiments require significant cooling. We describe two approaches; (a) using Rydberg atoms in high finesse three dimensional microwave cavities and (b) superconducting circuits. The latter approach is called circuit quantum electrodynamics.

11.1 Microwave Quantum Optics Using Rydberg Atoms

Haroche pioneered an approach to cavity QED using circular Rydberg atoms with dipole transitions in the microwave regime (∼51 GHz) coupled to superconducting microwave Fabry–Perot cavities [1]. A circular Rydberg atom is an atom in an excited state with a high principal quantum number (typically $n \sim 50$). The Bohr radius of such an excited state is very large with a diameter of 0.25 μm. These states have very long lifetimes (∼30 ms). Likewise the cavity has a very narrow line-width ($\kappa^{-1} \sim 130$ ms). The atoms are not trapped inside the cavity, but enter the cavity one at a time from a laser-cooled atomic beam. Typically, the vacuum Rabi frequency is $\Omega/2\pi = 50$ kHz. The scheme is shown in Fig. 11.1.

Unlike trapped atom experiments, in these experiments the atom sees a time dependent electric field as it samples the spatial mode function of a single cavity mode. In effect the interaction is turned on and off when the atom enters and exits the cavity. If the two-level transition frequency is close to the cavity frequency we can use an interaction Hamiltonian of the Jaynes-Cummings form,

$$H(t) = \hbar\omega_c a^\dagger a + \frac{\hbar\omega_a}{2}\sigma_z - i\frac{\hbar g(t)}{2}(\sigma_+ a - \sigma_- a^\dagger) \tag{11.1}$$

where

$$g(t) = g_0 e^{-\mu(vt)^2/w^2} \tag{11.2}$$

D. F. Walls and G. J. Milburn, *Quantum Optics*, Graduate Texts in Physics,
https://doi.org/10.1007/978-3-031-84177-4_11

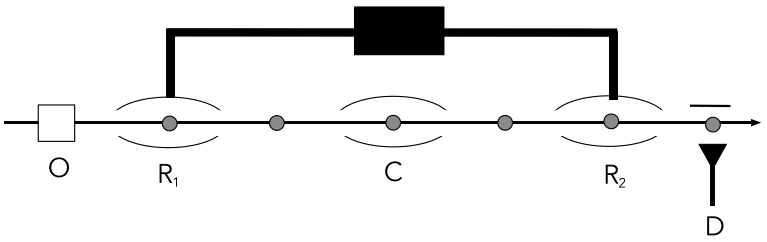

Fig. 11.1 The Rubidium atoms, with pre-selected velocities, are prepared in the circular level with principal quantum number 50 by excitation in O. This is the ground state. The atomic internal state is subject to a resonant classical microwave (Ramsey) pulse in R_1 inducing the transition $|g\rangle \rightarrow |e\rangle$ where $|e\rangle$ is a Rydberg state with $n = 51$. This dipole then interacts with the microwave field in C. A second Ramsey pulse is applied at R_2 and the atom is measured by state-selective field-ionization at D

where x is a transverse displacement from the cavity axis at $x = 0$ and the atomic velocity is v, w determines the beam waist and μ is a numerical factor.

If the atom and cavity are on resonance $\omega_c = \omega_a$ the dynamics are given by the unitary transformation

$$U(t_i) = e^{-\frac{\Omega t_i}{2}(\sigma_+ a - \sigma_- a^\dagger)} \tag{11.3}$$

where the effective Rabi frequency is

$$\Omega = \frac{1}{t_i}\int_0^{t_i} g(t')dt' \tag{11.4}$$

If the atom starts in the ground state and the cavity is in the vacuum state we find the total state at time t is

$$|\Psi_e(t_i)\rangle = \cos(\Omega t_i/2)|e,0\rangle + \sin(\Omega t_i/2)|g,1\rangle \tag{11.5}$$

We can thus interpret Ω as the vacuum Rabi frequency. This can be measured by making an atomic state measurement on the atom after it leaves the cavity. The probability to find the atom in the excited state is $\frac{1}{2}(1 + \cos\Omega t_i)$ and this can be sampled for various interaction times to determine Ω. In a typical experiment $\Omega/2\pi = 47$ kHz, see Fig. 11.2. The form of (11.5) indicates that the atom is entangled with the state of the field in the cavity. This lasts as long as the photon remains in the cavity, around 5 μms [2].

In the case that $\Omega t_i = \pi/2$—known as a $\pi/2$ Rabi pulse—the state at the end of the pulse is

$$|\Psi_e(\pi/2)\rangle = \frac{1}{\sqrt{2}}(|e,0\rangle + |g,1\rangle) \tag{11.6}$$

This is the $+$ eigenstate of the Pauli operator σ_x. This is a pure entangled state between atom and field. If we trace out the field state, the atom is in the totally mixed state. In the case that $\Omega t_i = \pi$ the state at the end of the pulse is

$$|\Psi_e(\pi)\rangle = |g,1\rangle \tag{11.7}$$

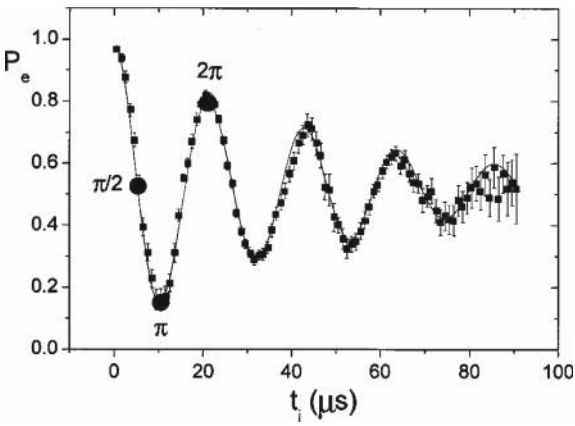

Fig. 11.2 From [2] Reviews of Modern Physics, Volume 73, July 2001

The atom has prepared the cavity in a single photon state. If the atom was prepared in an arbitrary superposition state, $c_g|g\rangle + c_e|e\rangle$, after a π pulse we see that the field is prepared in the pure state $\phi\rangle = c_g|0\rangle + c_e|1\rangle$. This is not a Fock state. In fact, it has a weak coherent amplitude as $\langle\phi|a|\phi\rangle = c_e c_g^*$.

In order to treat arbitrary cavity field states we can use the dressed states to diagonalise the Hamiltonian (see Sect. 9.1.1). Foe example if the field is in a weak coherent state and the atom is prepared in the excited state, the probability to find the atom in the excited state at time t is

$$\mathrm{P}_e = \frac{1}{2}e^{-|\alpha_0|^2}\sum_{n=0}^{\infty}\frac{|\alpha_0|^2}{n!}(1+\cos\Omega\sqrt{n+1}T_i) \tag{11.8}$$

11.1.1 Dispersive Interaction

The Jaynes-Cummings interaction results in the exchange of energy between the atom and the cavity. Another kind of important interaction, the dispersive interaction, does not result in energy exchange. This can arise if the atom and cavity frequencies are far from resonance. The starting point is the interaction Hamiltonian in the interaction picture

$$H = -i\frac{\hbar g(t)}{2}(\sigma_+ a e^{-i\Delta t} - \sigma_- a^\dagger e^{i\Delta t}) \tag{11.9}$$

where $\Delta = \omega_c - \omega_a$. The unitary time evolution operator satisfies

$$\dot{U}(t) = \frac{g(t)}{2}(\sigma_+ a e^{-i\Delta t} - \sigma_- a^\dagger e^{i\Delta t})U(t) \tag{11.10}$$

The solution can be written in a recursive form

$$U(t) = 1 + \int_0^t dt' \frac{g(t')}{2}(\sigma_+ a e^{-i\Delta t'} - \sigma_- a^\dagger e^{i\Delta t'})U(t') \tag{11.11}$$

Nesting the function and truncating to second order we find that

$$U(t_i) = 1 + \int_0^{t_i} dt' \frac{g(t')}{2}(\sigma_+ a e^{-i\Delta t'} - \sigma_- a^\dagger e^{i\Delta t'}) \tag{11.12}$$
$$+ \int_0^{t_i} dt' \int_0^{t'} dt'' \frac{g(t')}{2}(\sigma_+ a e^{-i\Delta t'} - \sigma_- a^\dagger e^{i\Delta t'})$$
$$\times \frac{g(t'')}{2}(\sigma_+ a e^{-i\Delta t''} - \sigma_- a^\dagger e^{i\Delta t''})$$

We now assume that $\Delta \gg \Omega$ as defined in (11.4). Then we can neglect the first term. Intuitively we expect the oscillations to be fast compared to the variation of g that this term averages to zero on the time scale of interest. The second term is dominated by

$$\frac{1}{4}\int_0^{t_i} dt' \int_0^{t'} dt'' g(t')g(t'')(\sigma_+\sigma_- a a^\dagger e^{-i\Delta(t'-t'')} - \sigma_-\sigma_+ a^\dagger a e^{-i\Delta(t'-t'')})$$

This is approximately $-i\chi(\sigma_+\sigma_- a a^\dagger - \sigma_-\sigma_+ a^\dagger a)$ where

$$\chi = \frac{1}{4\Delta}\int_0^{t_i} dt' g(t')^2 \approx \frac{\Omega^2}{4\Delta} \tag{11.13}$$

Then the effective Hamiltonian is

$$H_{dis} = \hbar\chi\sigma_z a^\dagger a \tag{11.14}$$

where we have neglected a small atomic frequency shift $\sim \chi$. We call this the dispersive interaction Hamiltonian. Clearly this does not result in energy exchange between the field and the atom.

The dispersive interaction can be used to implement Ramsey interferometry [3]. In this case we inject weak coherent fields into resonant cavities R_1, R_2 in Fig. 11.1 to implement a $\pi/2$ rotation about the $y-$axis on the Bloch sphere. An atom entering in the ground state entering in the ground state from O is prepared in the $+$ eigenstate of σ_x. After the atom interacts dispersively with the central cavity it then again undergoes a resonant $-\pi/2$ pulse prior to being read out in the energy basis. This is the inverse of the first $\pi/2$ transformation. The overall effect on an atom entering in the ground state is equivalent to the unitary generated by the effective Hamiltonian

$$H_{eff} = -\hbar\chi\sigma_x a^\dagger a \tag{11.15}$$

Using this technique cat states of the microwave field can be created. If the central cavity si prepared in a weak coherent state and an atom enters from O in the ground state, the output state after R_2 is the state

$$|\Psi\rangle = e^{i\chi t_i \sigma_x a^\dagger a}|g\rangle|\alpha\rangle = \frac{1}{\sqrt{2}}(|+\rangle|\alpha e^{i\chi t_i}\rangle + |-\rangle|\alpha e^{-i\chi t_i}\rangle \tag{11.16}$$

where $|\pm\rangle = (|g\rangle \pm |g\rangle)/\sqrt{2}$. If the atom is measured and found to be in state $|g\rangle$ the conditional state of the field is

$$|\phi\rangle = \frac{1}{\sqrt{2}}(|\alpha e^{i\chi t_i}\rangle + |\alpha e^{-i\chi t_i}\rangle \tag{11.17}$$

If $\chi t_i = \pi$ this is an even parity cat state (see Sect. 1.7). If the atom is found in the excited state, the conditional state of the field is the odd cat state.

11.2 Circuit QED

A very different approach to microwave quantum optics is based on superconducting coplanar microwave cavities [4]. The dipole emitter in this case is a single superconducting metallic island separated by tunnel junctions from a Cooper pair reservoir. Under appropriate conditions it is possible for the charge on the island to be restricted to at most a single Cooper pair. This Cooper pair tunnelling on and off the island constitutes a single large electric dipole system. A possible experimental implementation is shown in Fig. 11.3.

In the figure, an oscillating current in the central conductor produces an oscillating electric field between the central conductor and two ground planes on either side. The magnetic field lines wrap around the central conductor. The gaps at the end of the central conductor define a microwave resonator and act as an effective capacitive coupling between the resonator and the transmission lines on either side. The quantisation of this system is done using collective circuit variables describing an equivalent circuit [4]. See Fig. 11.3. The transmission lines act as dissipative reservoirs for the microwave resonator [5].

The Hamiltonian for this circuit is

$$H = \frac{1}{2L}\hat{\Phi}^2 + \frac{1}{2C_E}\hat{Q}^2 + \frac{1}{2C_J}(\hat{Q} - \hat{Q}_J)^2 - E_J \cos\left(\frac{2e}{\hbar}\hat{\Phi}_J\right) \tag{11.18}$$

where $E_J = \frac{\hbar I_o}{2e}$ and I_0 is the critical junction current, and $L = L_1 + L_2$,

$$\frac{1}{C_E} = \frac{1}{C_1 + C_{in}} + \frac{1}{C_2 + C_{out}}\,. \tag{11.19}$$

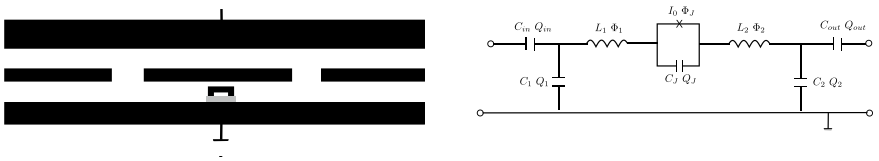

Fig. 11.3 Left: A co-planar microwave resonator is coupled to a Cooper pair box electric dipole. Right: equivalent circuit

The collective quantum degrees of freedom are: $\hat{Q}$, $\hat{Q}_J$ are defined by

$$\hat{Q} = C_E \frac{d\hat{\Phi}}{dt} + C_E \frac{d\hat{\Phi}_J}{dt} \tag{11.20}$$

$$\hat{Q}_J = C_E \frac{d\hat{\Phi}}{dt} + (C_E + C_J) \frac{d\hat{\Phi}_J}{dt} \tag{11.21}$$

with $\hat{\Phi} = \hat{\Phi}_1 + \hat{\Phi}_2$. The canonical commutation relations are

$$[\hat{\Phi}, \hat{Q}\,] = i\hbar \tag{11.22}$$

$$[\hat{\Phi}_J, \hat{Q}_J\,] = i\hbar \tag{11.23}$$

The term proportional to $(\hat{Q} - \hat{Q}_J)^2$ is the quadratic coupling between the two degrees of freedom.

We introduce a charge basis via the number operator $\hat{N}$ defined by $\hat{N} = e\hat{Q}_J$ that describes the number of excess Cooper pairs on the Cooper pair island,

$$\hat{N} = \sum_{n=-\infty}^{\infty} N|N\rangle\langle N| \tag{11.24}$$

The canonical commutation relations then imply

$$\cos\left(\frac{2e}{\hbar}\hat{\Phi}_J\right) = \frac{1}{2}\sum_{n=0}^{\infty} |N\rangle\langle N-1| + |N-1\rangle\langle N| \tag{11.25}$$

To begin with we will assume that there is a classical DC bias gate acting on the junction and ignore the circuit degrees of freedom in the resonator. The Hamiltonian for the junction is

$$H_g = 4E_c(N_g - \hat{N})^2 - \frac{E_J}{2}\sum_N |N\rangle\langle N-1| + |N-1\rangle\langle N| \tag{11.26}$$

where $E_c = \frac{e^2}{2(C_J+C_g)}$, the bias voltage on the junction is $V_g = 2eN_g/C_g$ and C_g is the total capacitance of the junction with respect to ground. The energy levels can be changed by changing N_g. When $N_g = N + 1/2$ the levels with $n = N, n = N + 1$ are degenerate (with energy E_C) when $E_J = 0$. This value of N_g is called the degeneracy point. When $E_J \neq 0$ this degeneracy is lifted. In Fig. 11.4 we plot the lowest few energy eigenvalues (11.26) for $N_g = 5/2$. Note that the two-lowest levels are well separated from the next excited state. If field in the microwave resonator has a frequency close to the splitting of the two lowest levels we can approximate the dipole with only these two levels: a kind of engineered artificial atom.

We can then write H_g as

$$H_g = 2E_c\bar{\sigma}_z - \frac{E_J}{2}\bar{\sigma}_x \tag{11.27}$$

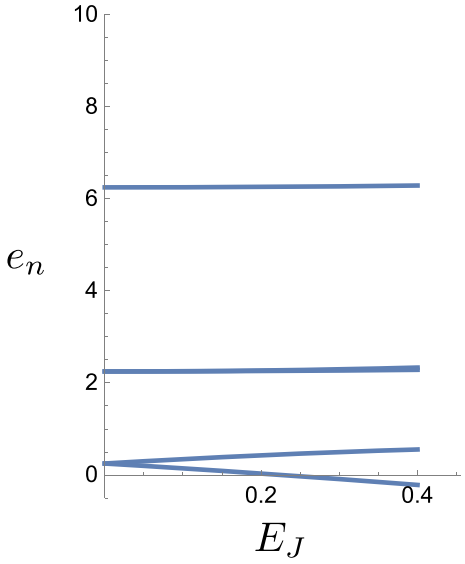

Fig. 11.4 The four lowest energy levels of a superconducting junction for $N_g = 3/2$, $E_c = 0.25$ and **a** $E_J = 0.0$, **b** $E_J = 0.1$

where in the number basis $\bar{\sigma_z} = |N+1\rangle\langle N+1| - |N\rangle\langle N|$, $\bar{\sigma_x} = |N+1\rangle\langle N| + |N\rangle\langle N+1|$.

We introduce annihilation and creation operators as follows.

$$\hat{\Phi} = i\sqrt{\frac{\hbar\omega_c L}{2}}(a - a^\dagger) \tag{11.28}$$

$$\hat{Q} = \sqrt{\frac{\hbar\omega_c C_E}{2}}(a + a^\dagger) \tag{11.29}$$

where $\omega_c = (LC_E)^{-1/2}$. In a typical experiment this is $\omega_c/2\pi \sim 8$ Ghz. The zero point rms electric field is $\sqrt{\frac{\hbar\omega_c}{2C_E}}$. In a typical experiment this is about $\sim 1\,\mu$V [4]. Superconducting circuits necessarily use low temperature systems to reach the superconducting transition. However it is important to understand that much colder temperatures are required. This is because the thermal occupation of microwave field modes at room temperature is very high. In order to reach a quantum optical regime we need $\hbar\omega_c > k_B T$. At Ghz frequencies this requires temperatures in the tens to hundreds of millikelvin; dilution fridge temperatures.

Using the two-level approximation for the junction, the full circuit Hamiltonian in (11.18) can be written in the charge basis as

$$H = \hbar\omega_c a^\dagger a + H_g - \hbar\bar{g}(a + a^\dagger)\bar{\sigma_z} \tag{11.30}$$

where

$$\bar{g} = \frac{e}{2C_J}\sqrt{\frac{\hbar\omega_c C_E}{2}} \tag{11.31}$$

We next make a change of basis to the two eigenstates of H_g, using $\sigma_\alpha = U^\dagger \bar{\sigma}_\alpha U$ for each Pauli matrix. This is a rotation around the y axis on the Bloch sphere, Then

$$H = \hbar\omega_c a^\dagger a + \frac{\hbar\omega_J}{2}\sigma_z - \hbar\bar{g}(a + a^\dagger)(\mu\sigma_z + \nu\sigma_x) \tag{11.32}$$

where

$$\omega_J = 2E_C\sqrt{1 + \frac{E_J^2}{16E_C^2}} \tag{11.33}$$

where μ, ν are direction cosines. In the case of a transmon device E_J/E_C is large adn we can approximate the Hamiltonian as

$$H = \hbar\omega_c a^\dagger a + \frac{\hbar\omega_J}{2}\sigma_z - \frac{\hbar\bar{g}}{2}(a + a^\dagger)\sigma_x \tag{11.34}$$

If we are in the weak coupling regime g is much less than the line-width of the resonator, and the spontaneous emission rate of the two level system, we can make the rotating wave approximation and use the Jaynes-Cummings Hamiltonian. The Rabi frequency is then $\Omega = \bar{g}$. In typical experiments in this coupling regime $\Omega/2\pi \sim 200$ MHz. However it is quite possible to engineer devices to be in a ultra-strong coupling regime for which $g \sim \omega_J$. This is very difficult to achieve in atom physics.

The form of the interaction in (11.34) suggests a Jahn-Teller model [7]. The interaction has a parity symmetry with respect to the unitary transformation $U = \exp[i\pi(a^\dagger a + \sigma_z)]$. It exhibits a kind of quantum phase transition as the parameter $\lambda = \frac{\bar{g}^2}{\omega_J\omega_c}$is varied. At $\lambda = 1/\sqrt{3}$. Above this threshold the energy eigenstates are entangled. The ground state, and first excited state, can be approximated by

$$|\epsilon_0\rangle = \frac{1}{\sqrt{2}}\left[|+\rangle \otimes |\phi_+\rangle + |-\rangle \otimes |\phi_-\rangle\right] \tag{11.35}$$

$$|\epsilon_1\rangle = \frac{1}{\sqrt{2}}\left[|+\rangle \otimes |\phi_+\rangle - |-\rangle \otimes |\phi_-\rangle\right] \tag{11.36}$$

where $\sigma_x|\pm\rangle = \pm|\pm\rangle$ and $|\phi_\pm\rangle$ are oscillator coherent states given by the displacement operator as,

$$|\phi_\pm\rangle = D\left(\pm\frac{\bar{g}}{2\omega_c}\right)|0\rangle\ . \tag{11.37}$$

11.2.1 Measurement in Circuit QED

We now turn to the role of quantum measurement noise in superconducting quantum circuits using a dispersive coupling [8]. The experiment we describe is based on a

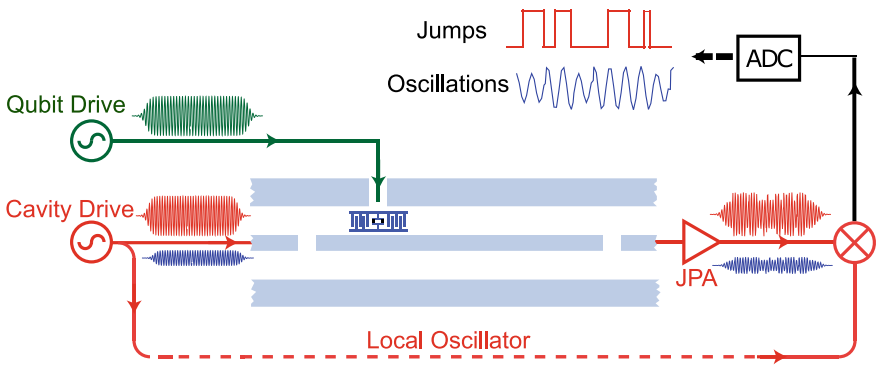

Fig. 11.5 The experimental dispersive scheme for a transmon quantum oscillator by [8]. A transmon two level system is dispersively coupled to a superconducting microwave cavity, and the cavity and qubit are driven coherently. The output field is directed to a heterodyne detector (Josephson parametric amplifier) that produces the clock signal for counting

superconducting quantum circuit driven by a microwave source containing a transmon TLS, see Fig. 11.5. We will describe a measurement of the state of the TLS in the energy basis. This is done by dispersively coupling the transmon to a superconducting microwave cavity. When the cavity and qubit are driven coherently the phase of the coherent field is periodically modulated and this modulation may be monitored by subjecting the output field of the resonator to a heterodyne measurement.

In this case the stochastic master equation is

$$\begin{aligned} d\rho_c &= -iE[a+a^\dagger, \rho_c]dt - i\Omega[\sigma_x, \rho_c]dt \\ &\quad -i\chi[a^\dagger a\sigma_z, \rho_c]dt + \gamma\mathcal{D}[\sigma_-]\rho_c + \kappa\mathcal{D}[a]\rho_c dt + \sqrt{\eta\kappa}\mathcal{H}[a]\rho_c dW(t). \end{aligned} \tag{11.38}$$

where χ is the dispersive coupling, γ is qubit spontaneous decay rate, κ is the cavity damping rate, and η is the homodyne detector efficiency efficiency. The final term proportional to the Wiener noise increment reflects the state updating required for conditional dynamics. We will assume that the readout cavity is rapidly damped so that it responds quickly to the dynamics of the TLS. This means it can be adiabatically eliminated. The conditional master equation for the reduced state of the qubit (ρ_σ) becomes,

$$d\rho_\sigma = -i[H_\sigma, \rho_\sigma]dt + \gamma\mathcal{D}[\sigma_-]\rho_\sigma dt + \Gamma\mathcal{D}[\sigma_z]\rho_\sigma dt - \sqrt{\Gamma}\mathcal{H}[\sigma_z]\rho_\sigma dW(t). \tag{11.39}$$

Here $H_\sigma = \Omega\sigma_x + \Delta\sigma_z$ and

$$\frac{\Gamma}{\kappa} = 4\left(\frac{\chi}{\kappa}\right)^2 n_0 \quad \text{measurement dephasing rate} \tag{11.40}$$

$$\frac{\Delta}{\kappa} = \left(\frac{\chi}{\kappa}\right) n_0 \quad \text{effective Stark shift} \tag{11.41}$$

$n = |\alpha_0|^2 = 4|E|^2/\kappa$. Note that Γ can be changed by varying E.

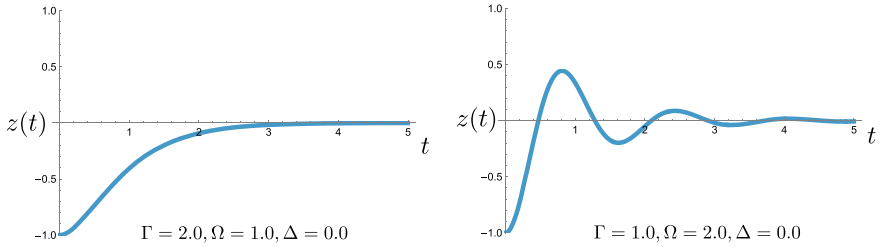

Fig. 11.6 The unconditional dynamics for $\langle\sigma_z\rangle$ for over-damped (left) and under-damped (right)

As we are dealing with a two level system the dynamics can be described in terms of the Bloch sphere conditional dynamics.

$$
\begin{aligned}
dX &= -2\Delta Y dt - \gamma_2 X dt \\
dY &= 2\Delta X dt - 2\Omega Z dt - \gamma_2 Y dt \\
dZ &= 2\Omega Y dt - \gamma(1+Z)dt - 2\sqrt{\Gamma}(1-Z^2)dW
\end{aligned}
$$

where $X = \langle\sigma_x\rangle_c$ etc, and $\gamma_2 = \gamma/2 + 2\Gamma$ is the transverse decay rate of the conditional polarization. In the experiment the spontaneous emission rate, $\gamma \ll 1$, so $\gamma_2 \approx 2\Gamma$.

The unconditional dynamics is obtained by averaging over the noise. $\overline{dW} = 0$. There are two regimes, under-damped for which $\Omega > \Gamma/2$ and over-damped for which $\Omega < \Gamma/2$. The unconditional average for Z is shown in Fig. 11.6. The conditional dynamics corresponding to each of these regimes are shown in Fig. 11.7. In both cases, the noise is quantum not thermal. It arises from measurement back-action itself. There is a transition from a diffusive under-damped conditional dynamics to a jump conditional dynamics in the over-damped regime. This is a partical manifestation of the quantum Zeno effect. It occurs when the rate of information extracted by the measurement is so strong that it overwhelms the coherent periodic dynamics. In Fig. 11.8 we show the homodyne signal in the quantum jumps regime for the experiment of [8].

11.3 Circuit Non Linear Optics

There are many experiments that exploit the highly non linear microwave susceptibility of a supercodncuting device in a resonator. Much large Kerr non linearities are possible then one can achieve in non liner optics. For example, in experiments at Chalmers [9], a quarter wave coplanar microwave cavity was grounded at one end via a superconducting quantum interference devices (SQUIDs) that can be modelled as a large Kerr non linearity. By modulating the flux through the loop, the cavity frequency can be modulated. If the flux is varied at twice the cavity frequency this implements a parametric driving of the cavity field. The cavity field also exhibits a large effective nonlinear susceptibility that can be modelled as an intensity dependent phase shift.

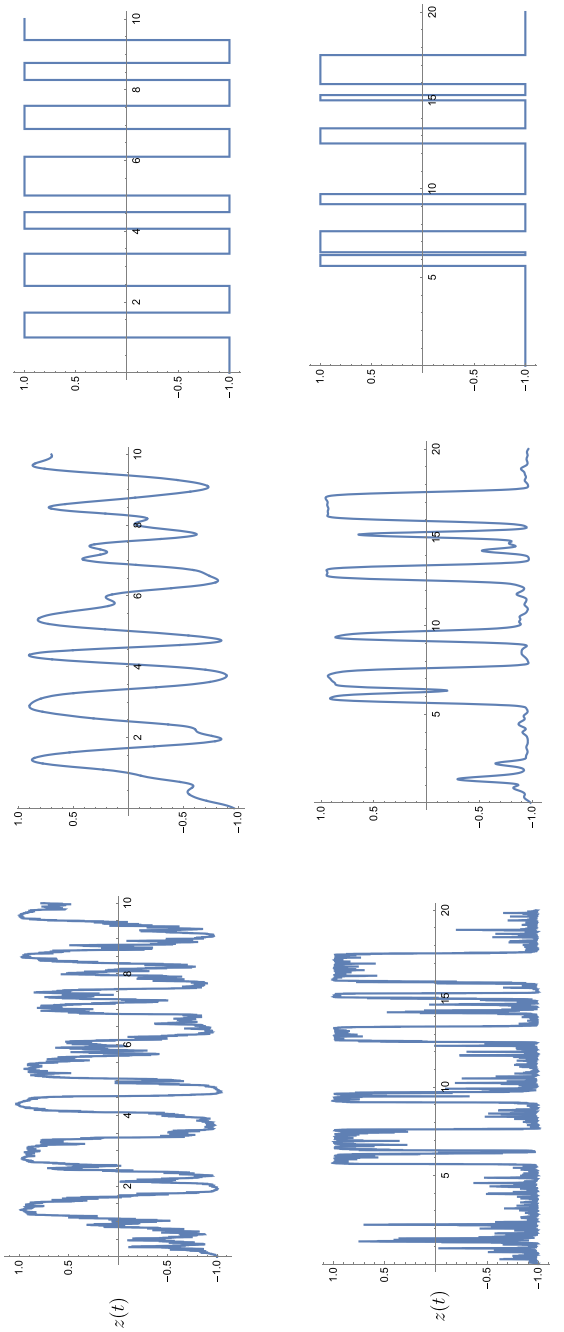

Fig. 11.7 The conditional dynamics for $\langle \sigma_z \rangle$. Top line: under-damped, $\Omega > \Gamma/2$. Bottom line: over-damped: $\Omega < \Gamma/2$. In each row the first graph is the simulated conditional mean, the second graph is a low-pass filtered version and the third is a plot of the sign of the low-pass version that is used as a clock signal for counting. Time is in dimensionless units

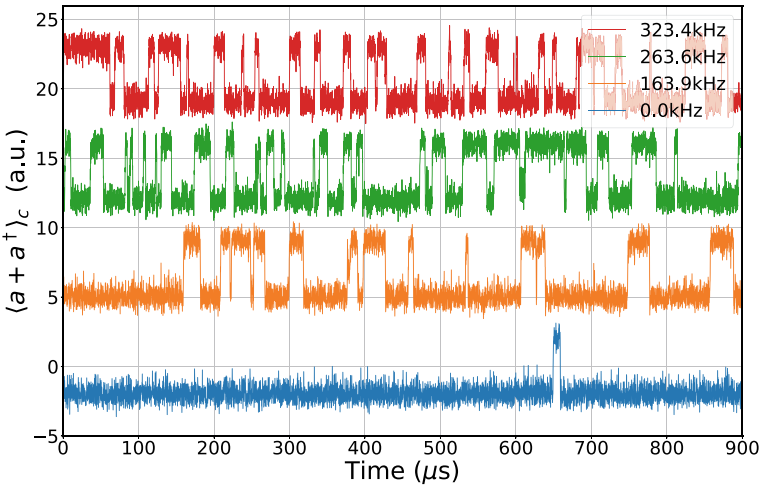

Fig. 11.8 Observed quantum jumps in the strong measurement regime. Sample of the time traces indicating quantum jumps (between ground and excited states) with different qubit drive amplitudes (Ω, shown as different colours with different vertical offsets). In each curve, a low signal indicates the ground state, and a high signal indicates the excited state. Thermal noise yields a small excited state population when using zero qubit drive. As the qubit drive amplitude increases, the qubit approaches an equal amount of time spent in the ground and excited states

We will discuss the model of [10] in which a microwave resonator containing a large Kerr non linear cavity is simultaneously parametrically driven and linearally driven. The Hamiltonian in the interaction picture is

$$\mathcal{H} = \hbar\Delta\hat{a}^\dagger\hat{a} + \hbar\left(\epsilon^*\hat{a} + \epsilon\hat{a}^\dagger\right) + \hbar\chi\hat{a}^{\dagger 2}\hat{a}^2 + \frac{\hbar}{2}\left(\kappa^*\hat{a}^{\dagger 2} + \kappa\hat{a}^2\right), \tag{11.42}$$

We assume that the dissipation is described by the usual master equation

$$\dot{\rho} = -\frac{i}{\hbar}[\mathcal{H}, \rho] + \gamma\mathcal{D}[a]\rho \tag{11.43}$$

This model has an exact steady solution. Using the positive P representation we find the system obeys the Ito stochastic differential equations

$$\begin{aligned} d\alpha &= -(\gamma + i\Delta)\alpha\, dt - i\epsilon\, dt - i(\chi\alpha^2 + \kappa)\beta\, dt \\ &\quad + \left[-i(\kappa + \chi\alpha^2)\right]^{1/2} dz_1, \\ d\beta &= -(\gamma - i\Delta)\beta\, dt + i\epsilon^*\, dt + i(\chi\beta^2 + \kappa^*)\alpha\, dt \\ &\quad + \left[i(\kappa^* + \chi\beta^2)\right]^{1/2} dz_2. \end{aligned} \tag{11.44}$$

On the sub manifold $\beta = \alpha^*$ the semiclassical equations can be found as

$$\frac{d\alpha}{dt} = -(\gamma + i\Delta + i\chi|\alpha|^2)\alpha - i\epsilon - i\kappa\alpha^*, \tag{11.45}$$

The fixed points of this equation have a rich bifurcation structure [10].

The Fokker-Planck for the complex P representation satisfies potential conditions and this there is an exact steady state in the form

$$P_s(\alpha, \beta) = \mathcal{N} e^{-V(\alpha,\beta)}, \tag{11.46}$$

with

$$P_s(\alpha, \beta) = \mathcal{N} \left(\frac{\alpha_0 - \alpha}{\alpha_0 + \alpha}\right)^{\mu} \left(\frac{\alpha_0^* - \beta}{\alpha_0^* + \beta}\right)^{\mu^*} \left((\chi\alpha^2 + \kappa)\right)^{\lambda} \left((\chi\beta^2 + \kappa)\right)^{\lambda^*} e^{2\alpha\beta}, \tag{11.47}$$

with $\lambda = -1 + \Delta/\chi - i\gamma/\chi$ and $\mu = i\epsilon/\sqrt{\kappa\chi}$. Systems of this kind can be configured as a superconducting parametric amplifier [11].

References

1. S. Haroche, M. Brune, J.M. Raimond, Nat. Phys. **16**, 243–246 (2020)
2. J.M. Raimond, M. Brune, S. Haroche, Rev. Mod. Phys. **73**, 565 (2001)
3. N.F. Ramsey, Chapter 1 Magnetic resonance contributions to other sciences, *Advances in Quantum Chemistry*, vol. 53, ed. by S. Salomonson, E. Lindroth (Academic Press, 2008)
4. A. Blais, A.L. Grimsmo, S.M. Girvin, A. Wallraff, Rev. Mod. Phys. **93**, 025005 (2021)
5. C. Meaney, *Quantum Mechatornics*, PhD thesis https://espace.library.uq.edu.au/view/UQ:273756
6. B. Yurke, J.S. Denker, Phys. Rev. A **29**, 1419 (1984)
7. A.P. Hines, C.M. Dawson, R.H. McKenzie, G.J. Milburn, Phys. Rev. A **70**, 022303 (2004)
8. X. He, P. Pakkiam, A.A. Gangat, M.J. Kewming, G.J. Milburn, A. Fedorov, Phys. Rev. Appl. **20**, 034038 (2023)
9. M. Sandberg, C.M. Wilson, F. Persson, T. Bauch, G. Johansson, V. Shumeiko, T. Duty, P. Delsing, Appl. Phys. Lett. **42**, 203501 (2008)
10. C.P. Meaney, H. Nha, T. Duty, G.J. Milburn, EPJ Quantum Technol. **1** , 7 (2014)
11. S.V. Uchaikin, J. Kim, J. Kim, C. Kutlu, et al., Front. Phys., Sec. High-Energy and Astro Particle, Physics **12** (2024)

Ion Traps

12

Abstract

The ability to trap an individual ion and cool it close to the ground state of vibrational motion has enabled precise quantum control to be achieved together with very high efficiency measurement. The technology originated over four decades ago in the effort to develop ultra high precision spectroscopy with particular application to frequency standards. In optical ion traps, external lasers are used to couple the internal electronic motion of trapped ions to the vibrational degrees of freedom. This enables a plethora of quantum control protocols, including an implementation of quantum computation, and many analogue quantum simulations of few body quantum systems.

12.1 Introduction

One of the keys to the success of ion traps is the ability to detect the electronic state of a single ion with high efficiency. This is done by laser induced fluorescence on a dipole allowed transition, scattering millions of photons per second. The idea goes back to a proposal of Dehmelt in 1975 [2] and appears in various applications such as electron shelving, cycling transitions and quantum jumps [3]. Another key to the success of ion traps is the invention of sub Doppler cooling techniques, particularly resolved side band cooling [4]. This makes it possible to prepare a single ion in a state with very few quanta of vibrational excitation, even so few as to reach the vibrational ground state. A single trapped ion is well approximated by a particle moving in a three dimensional harmonic potential. It is possible to stochastically remove vibrational energy by laser induced Raman transitions coupling electronic and vibrational degrees of freedom. In effect, heat is removed from the vibrational motion of of the ion and pumped into the very low temperature heat bath associated with the much higher frequency of the fluorescent radiation.

D. F. Walls and G. J. Milburn, *Quantum Optics*, Graduate Texts in Physics,
https://doi.org/10.1007/978-3-031-84177-4_12

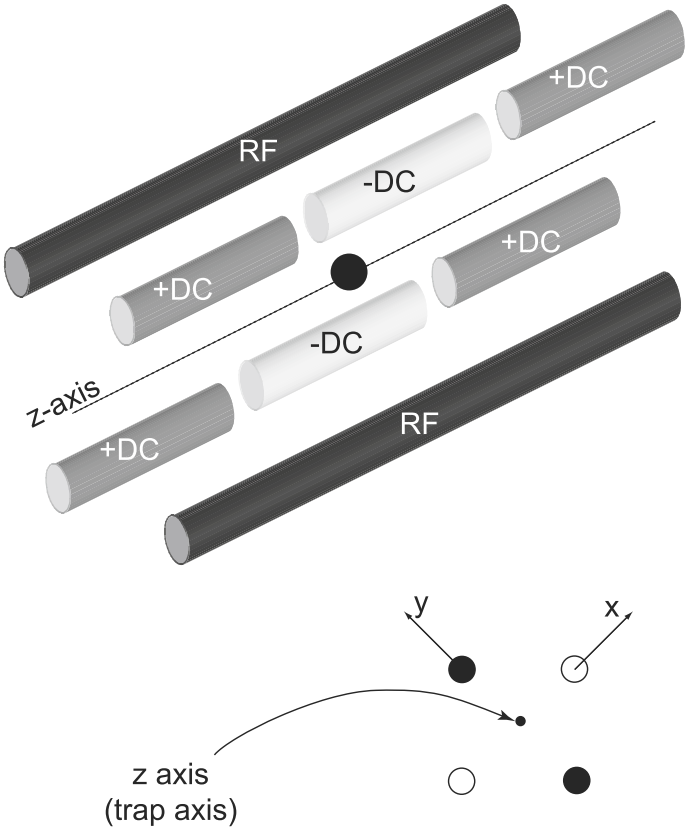

Fig. 12.1 A schematic representation of a linear radio frequency ion trap (after [4])

12.2 Trapping and Cooling

It is not possible to trap a charged particle in a static potential. This is because Laplaces equation implies there is always one unstable (not trapped) direction in the electrostatic potential. However a time dependent electric potential can produce an effective harmonic potential for a charge particle. In Fig. 12.1 we show a possible configuration of electrodes.

The time dependent potential seen by the ion can be written

$$V(x, y, z, t) = \frac{\bar{V}}{2}(k_x x^2 + k_y y^2 + k_z z^2) + \frac{1}{2} V \cos(\omega_{rf} t)(k'_x x^2 + k'_y y^2) \quad (12.1)$$

where ω_{rf} is the frequency of the time dependent potential and the effective spring constants must satisfy Laplace's equation which implies, $k_x + k_y + k_z = 0$, $k'_x + k'_y = 0$. If we assume the following conditions [4]

$$a_x = \frac{4Z|e|\bar{V}k_x}{m\omega_{rf}^2} \ll 1$$
$$q_x = \frac{2Z|e|Vk'_x}{m\omega_{rf}^2} \ll 1$$

then the motion in the x-direction is approximately harmonic. Similarly for the motion in the y-direction. We assume isotropy in the $x-y$ plane, so that $k_x = k_y,\ k'_x = k'_y$ and the motion is harmonic with the secular frequency

$$\nu = \left(a_x + q_x^2/2\right)^{1/2} \omega_{rf}/2 \tag{12.2}$$

There is a smaller amplitude oscillatory motion at frequency ω_{rf} superimposed on the secular motion, called the micromotion, which we neglect. In a recent experiment with $^9Be^+$, the axial frequency was about 3 MHz while the transverse frequency was about 8 MHz. The static potential due to end caps gives harmonic confinement along the trap axis (z-direction) and micromotion is absent. If this is kept weak, multiple ions can be trapped in a line along the z-direction. In summary, an ion is trapped in a harmonic potential in all three dimensions and we assume that one direction, the axial direction, has a lower frequency than motion in the other two orthogonal directions, the transverse directions. Typically the transverse frequencies are three to four times more than the axial.

The quantum description of the centre of mass motion of the ion is given in terms of the eigenstates of the Hamiltonian

$$H = \hbar\nu a_z^\dagger a_z + \hbar\nu_t (a_x^\dagger a_x + a_y^\dagger a_y) \tag{12.3}$$

The motion is thus separable into axial and transverse motion and, to be specific, we now concentrate on the axial motion alone, although much of the discussion can be applied to the transverse motion as well. Henceforth, as we neglect the transverse motion, we will drop the subscript on $a_z, a_z^\dagger$.

Many different kinds of ions can be trapped, but availability of lasers limits the kinds of ions that can be easily laser cooled. For example, the Wineland group at NIST Colorado uses $^9Be^+$ while the Blatt group in Innsbruck uses $^{40}Ca^+$. When the ion is first trapped it is in a highly excited state of its vibrational motion, corresponding to a temperature of the order of 10^4 K. Cooling typically proceeds in two stages. The first stage is based on Doppler cooling and is very efficient, the second stage is based on resolved sideband cooling (see section below).

Ion traps are a remarkably versatile quantum devices for a number of reasons. Firstly, it is possible to coherently couple the vibrational motion and the internal electronic state using an external laser. Secondly, resolved sideband cooling enables the vibrational motion to be prepared in its ground state with probability approaching unity. This is done using an external laser to induce Raman transitions between the ground and excited internal electronic state which absorb one photon and one phonon of vibrational per excitation cycle. Finally, the method of fluorescence shelving

enables the internal electronic state of a single trapped ion to be measured with efficiency approaching unity. In order to understand these three features we need to begin with a description of how an external laser can couple the vibrational and electronic degrees of freedom.

We will assume that the external laser can couple two internal electronic states, the ground state $|g\rangle$ and the excited state $|e\rangle$. This might involve a direct electric dipole transition. However for quantum information applications it typically involves a Raman two photon transition connecting the ground state to an excited meta-stable state. In either case the Hamiltonian describing the system is (see (9.16)),

$$H = \hbar\nu a^\dagger a + \hbar\omega_A \sigma_z + \frac{\hbar\Omega}{2}\left(\sigma_- e^{i(\omega_L t - k_L \hat{q})} + \sigma_+ e^{-i(\omega_L t - k_L \hat{q})}\right) \tag{12.4}$$

where $\hat{q}$ is the operator for the displacement of the ion from its equilibrium position in the trap, ν is the trap (secular) frequency, Ω is the Rabi frequency for the two level transition, ω_A is the atomic transition frequency, and ω_L, k_L are the laser frequency and wave number. The sigma matrices are defined in Sect. 9.1. There are three frequencies in the problem: ν, ω_A and ω_L. A wide variety of processes can be made dominant by carefully choosing relationships between these three frequencies. Note that the phase of the laser field as seen by the ion is dependent upon the position of the ion. As the ion moves harmonically in the trap the phase is modulated at the trap frequency. As we shall see, this leads to sidebands in the absorption spectrum for the two level system.

The ion position operator, in terms of the vibrational raising and lowering operators, is

$$\hat{q} = \left(\frac{\hbar}{2m\nu}\right)^{1/2}(a + a^\dagger) \tag{12.5}$$

We now define the Lamb-Dicke parameter, η

$$\eta = k_L \left(\frac{\hbar}{2m\nu}\right)^{1/2} = 2\pi\,\Delta x_{rms}/\lambda_L \tag{12.6}$$

where the r.m.s position fluctuations in the oscillator ground state is Δx_{rms}. Then moving to an interaction picture via the unitary transformation

$$U_0(t) = \exp[-i\nu a^\dagger a t - i\omega_A \sigma_z t] \tag{12.7}$$

the interaction Hamiltonian can be written as

$$H_I(t) = \frac{\hbar\Omega}{2}\left(\sigma_- \exp[-i\eta(a e^{-i\nu t} + a^\dagger e^{i\nu t})]\exp[-i(\omega_A - \omega_L)t] + \text{h.c}\right) \tag{12.8}$$

The exponential of exponentials make this a complicated hamiltonian system. However in most ion trap experiments the ion is confined to a spatial region that is significantly smaller than the wavelength of the exciting laser so that we may assume that

the Lamb-Dicke parameter is small $\eta < 1$ (typically $\eta \approx 0.01 - 0.1$). Expanding the interaction to second order in the Lamb-Dicke parameter gives

$$\begin{aligned} H_I(t) = & \frac{\hbar\Omega}{2}[1 - \eta^2 a^\dagger a]\left(\sigma_- e^{-i\delta t} + \sigma_+ e^{i\delta t}\right) \\ & -i\,\frac{\hbar\Omega\eta}{2}\left(a e^{-i\nu t} + a^\dagger e^{i\nu t}\right) e^{-i\delta t}\sigma_- + i\,\frac{\hbar\Omega\eta}{2}\left(a e^{-i\nu t} + a^\dagger e^{i\nu t}\right) e^{i\delta t}\sigma_+ \\ & -\frac{\hbar\Omega\eta^2}{4}\left(a^2 e^{-2i\nu t} + (a^\dagger)^2 e^{2i\nu t}\right)\left(e^{-i\delta t}\sigma_- + e^{i\delta t}\sigma_+\right) \end{aligned}$$

where the detuning of the laser from the atomic frequency is $\delta = \omega - \omega_L$.

By carefully selecting δ to be positive or negative integer multiples of the trap frequency, various resonant terms may be extracted and all time dependent terms neglected. In the first case, known as the carrier excitation, $\delta = 0$, and the resonant terms are

$$H_c = \hbar\Omega(1 - \eta^2 a^\dagger a)\sigma_x \qquad \text{carrier excitation} \tag{12.9}$$

where $\sigma_x = (\sigma_- + \sigma_+)/2$. If we choose $\delta = \nu$ so that the laser frequency is detuned below (to the red of) the carrier frequency by one unit of trap frequency, $\omega_L = \omega_A - \nu$, the resonant terms are

$$H_r = i\,\frac{\hbar\eta\Omega}{2}\left(a\sigma_+ - a^\dagger\sigma_-\right) \qquad \text{first red sideband excitation} \tag{12.10}$$

This is just the Jaynes-Cummings Hamiltonian except that it involves the absorption of a trap *phonon* as well as one laser photon. On the other hand we can choose $\delta = -\nu$ so that $\omega_L = \omega_A + \nu$ and the laser is detuned one unit of vibrational frequency to the blue of the carrier, the resonant interaction Hamiltonian is

$$H_b = i\,\frac{\hbar\eta\Omega}{2}\left(a^\dagger\sigma_+ - a\sigma_-\right) \qquad \text{first blue sideband excitation} \tag{12.11}$$

This describes an excitation process that absorbs one photon from the laser and *emits* one trap phonon. Continuing in this way we can define the second red sideband excitation $\delta = 2\nu$ and second blue sideband excitation $\delta = -2\nu$, and so on. In Fig. 12.2 we give an energy level diagram that represents the carrier, red and blue sideband excitations.

If two laser fields are used to simultaneously drive the red and blue sideband we can combine the two Hamiltonians to get

$$H_{rb} = -\frac{\hbar\eta\Omega}{2}(a + a^\dagger)\sigma_y \tag{12.12}$$

where $\sigma_y = -i(\sigma_+ - \sigma_-)$.

Once excited to $|e\rangle$ the ion can spontaneously decay to the ground state. For a dipole allowed transition this can be quite fast, thus enabling another excitation process to occur. In the case of red sideband excitation the net result is to remove

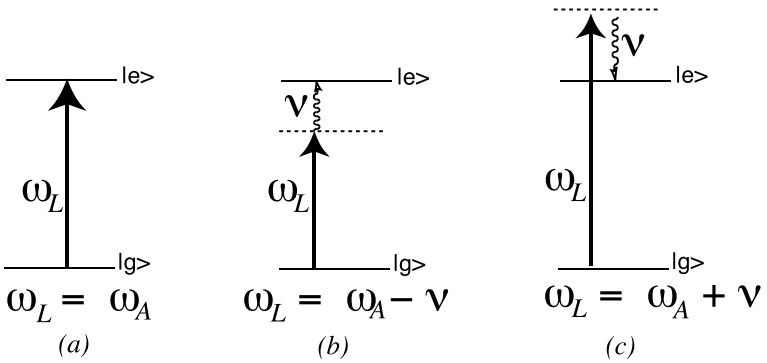

Fig. 12.2 Energy level diagram for **a** carrier **b** first red sideband and **c** first blue sideband excitation

one phonon per excitation cycle. This is the basis of sideband cooling. In effect the external laser has coupled the vibrational motion to a very low temperature heat bath: the vacuum radiation field at frequency ω_A. Of course it is only possible to address the sidebands if the laser can be accurately tuned to each. As each transition is homogeneously broadened by a width equal to the spontaneous emission rate, γ, we require that $\nu > \gamma$ for resolved sideband cooling. An explicit expression for the spectrum of resonance fluorescence for a single trapped ion follows from the methods given in Chap. 9. A detailed calculation in the low intensity limit ($\Omega < \gamma$) for a traveling wave field, by Cirac et al. [5] shows that the spectrum of the motional sidebands exhibits the following features

- the first red side band is centred on $\omega_L = \omega_A - \nu$ and the first blue sideband is centred on $\omega_L = \omega_A + \nu$ with line-widths determined by

$$\gamma_s = \eta^2 \left(\frac{\Omega}{2}\right)^2 [P(\nu + \delta) - P(\nu - \delta)] \tag{12.13}$$

  where $P(\delta) = \gamma/(\gamma^2 + \delta^2)$ and $\delta = \omega_L - \omega_A$ and γ is the spontaneous emission rate.
- the ratio of the peak height of the red sideband to the blue side band is $(\bar{n} + 1)/\bar{n}$ where $\bar{n}$ is the steady state mean photon number of vibrational excitation.

Note that the heights of the peaks are different reflecting the fact that the red transition involves the absorption of a phonon while the blue involves the emission of a phonon.

Resolved sideband cooling requires that the exciting laser be tuned one unit of trap frequency below the atomic transition frequency. The atom is then excited by the absorption of one laser photon and one trap phonon. In the Lamb-Dicke limit relaxation is dominated by spontaneous emission into the spectral peak at the carrier frequency ($\omega = \omega_A$). Thus on each excitation cycle one unit of vibrational energy is removed on average. A simple rate equation method suffices to understand this

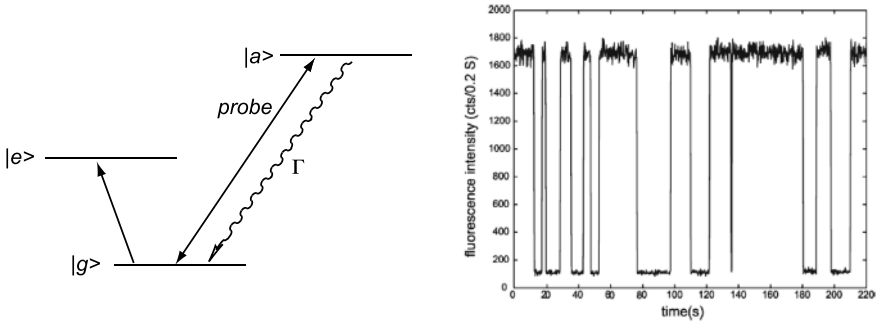

Fig. 12.3 Energy level diagram showing fluorescence readout of the ground atomic state. A strong probe laser drives a dipole allowed transition between the ground state $|g\rangle$ and an auxiliary state $|a\rangle$ which decays back to the ground state at a rate Γ scattering many many photons. Also show is fluorescent signal on the probe transition when a weak laser couples the ground and excited state (reproduced, with permission, from Leibfried et al. [4])

phenomenon. In Exercise 12.1, we find that the rate of change of the average phonon number is given by

$$\frac{d\bar{n}}{dt} = -\gamma \left(\frac{\eta^2 \Omega^2 \bar{n}}{2\eta^2 \Omega^2 \bar{n} + \gamma^2} \right) \tag{12.14}$$

Note that as the cooling proceeds, the rate decreases until the vibrational ground state is a steady state. In a more careful treatment we need to consider heating mechanisms, for example off-resonant excitation of the blue sideband [4], and the probability of populating the vibrational ground state in the steady state is less than unity. Despite this, resolved sideband cooling can prepare an ion in the vibrational ground state with a probability greater than 99%. Ground state cooling in all three dimensions was first achieved by the NIST group in Boulder [6]. Other heating mechanisms due to experimental artifacts are often important. For example, fluctuating charge distributions on the trap electrodes lead to a stochastic displacement of the centre of the trap. In Exercise 12.2 we consider this example in more detail. The experimental technique for determining the probability of occupying the ground state will be discussed after we consider the fluorescence technique for determining the ion electronic state.

In order to readout the state of the ion, an additional auxiliary level can be coupled by a strong laser to one or the other of the ground or excited states, to be specific let us say the ground state (see Fig. 12.3). If the ion is in the ground state when the probe laser is turned on, fluorescent photons are scattered in all directions and can easily be detected. On the other hand if the ion is in the excited state, it is not resonant with the probe laser and no photons are scattered: the ion remains dark.

If we now apply a weak laser to couple the ground and excited states, incoherent transitions occur $|g\rangle \leftrightarrow |e\rangle$. These transitions are incoherent as the strong coupling to the $|a\rangle$ state destroys coherence between the ground and excited states, see [7]. The net result is that the fluorescent signal due to the probe laser blinks on and off in fashion of a random telegraph process. A typical signal is shown in Fig. 12.3. In so far as fluorescence indicates that the ion is in the ground state, the random switching

of the fluorescence is a direct indicator of quantum jumps between the ground and excited states. These jumps were first reported in a number of laboratories [3].

The efficiency of the readout is a function of the integration time of the fluorescence signal, that is to say, how long we need to monitor the fluorescence to be sure that we are in period of high intensity. This time must be at least of the order of the average time between photon emission events. In an experiment however there are other sources of error, such as dark counts in the detector and typically the minimum time to distinguish ground and excited states is of the order of 2 ms. We capture the quality of the readout in an overall efficiency, η, which is the conditional probability for the ion to be detected in the ground state given that it was prepared in the ground state before the probe laser was turned on.

We now return to the experimental determination of the efficiency of sideband cooling. The objective is to determine the state of vibrational motion by coupling it to the internal state of the ion and then using the fluorescent readout technique described above. At the end of a cooling stage, the electronic state of the ion is first coupled to its vibrational motion for a time T using the first red and blue sideband transitions. If we write the probability for the atom to found in the excited state after time T as $P_e^R(T)$ and $P_e^B(T)$ for red and blue sideband excitation respectively it can be shown (see Exercise 12.3) that the mean phonon number $\bar{n}$ is given by $\bar{n}/(1+\bar{n}) = P_e^R(T)/P_e^B(T)$. Thus measurement of the ratio of excitation probability on the first red and blue sideband yields $\bar{n}$ directly, and the temperature of vibrational motion inferred.

12.3 Novel Quantum States

The ability to carefully control the coupling between internal electronic state of the ion and its vibrational motion in the trap enables us to carefully engineer novel quantum states of the vibrational degree of freedom. Lloyd and Braunstein [8] show that universal simulation of a single bosonic mode is possible if the Hamiltonian includes operators that are at least cubic in the creation and annihilation operators, for example $\{a, a^\dagger, a^2, a^{\dagger\,2}, (a^\dagger a)^2\}$, is universal. We could drop the quartic term and replace it with the cubic term $(a + a^\dagger)^3$, an important case we will consider in Chap. 15. The first two operators generate displacements (Heisenberg-Weyl group) the next two quadratic operators generate the squeezing transformations (SU(1,1)). The quartic operator is the Kerr nonlinearity. Starting from the vacuum state, all states in the Hilbert space can be reached by time-dependent Hamiltonians involving the four operators. The first four generate only positive Wigner functions. Adding the Kerr non linearity gives us the entire state space including access to states with negative Wigner functions.

Suppose that over some time interval we implement the Hamiltonian

$$H_T = \hbar\omega_0 a^\dagger a + \frac{\hbar g}{2}(a + a^\dagger)\sigma_z + \frac{\hbar\Omega_x}{2}\sigma_x \tag{12.15}$$

It is easy to see that we can write the Hamiltonian in (12.15) as

$$H_T = \hbar\omega_0(a^\dagger + \mu\sigma_z)(a + \mu\sigma_z) + \frac{\hbar\Omega_x}{2}\sigma_x \tag{12.16}$$

up to an additive constant with $\mu = \frac{g}{2\omega_0}$ a dimensionless parameter. This looks like it is a simple displacement transformation acting on the oscillator and can be removed using the unitary transformation

$$U_p(\mu) = e^{\mu\sigma_z(a-a^\dagger)} = \cosh(\mu(a - a^\dagger))\mathbb{I} + \sinh(\mu(a - a^\dagger))\sigma_z \tag{12.17}$$

as

$$U_p^\dagger(\mu) a U_p(\mu) = a - \mu\sigma_z \tag{12.18}$$

This is the *polaron transformation* as it mixes the Hilbert space of oscillator and qubit. The transformed Hamiltonian is

$$\begin{aligned} U_p^\dagger(\mu) H_T U_p(\mu) = \hbar\omega_0 a^\dagger a \\ + \frac{\hbar\Omega_x}{2}\left(\cosh(2\mu(a - a^\dagger))\sigma_x - i\sinh(2\mu(a - a^\dagger))\sigma_y\right) \end{aligned} \tag{12.19}$$

Clearly this satisfies the Lloyd-Braunstein condition for universal control of the oscillator Hilbert space if we do not truncate the hyperbolic functions below cubic. You can use this approach to generate the cubic phase gate (see (15.98)) on the vibrational degree of freedom. This is a universal gate for continuous variable (CV) quantum computation, see Chap. 15. In other words, an ion trap quantum computer can also implement universal quantum computation using only the vibrational degrees of freedom of multiple trapped ions.

As another example we will here consider the preparation of a 'cat state': a pure quantum state in which the two internal electronic states are correlated with different coherent states of the oscillator. There are a number of ways to prepare the vibrational motion in a coherent state, $|\alpha\rangle$. The ion is first cooled to the vibrational ground state. A classical uniform driving force oscillating at the secular frequency, ν, can then be applied by changing the bias conditions on the trap electrode. Alternatively a non adiabatic displacement of the trap centre can be made again by changing the bias conditions. Finally a spatially varying Stark shift can be applied by using the moving standing wave that results from two laser beams with frequency difference $\Delta\omega = \nu$ to resonantly drive the motion of the ion in the trap. If the laser polarisation is carefully chosen this will result in a force that depends on the internal electronic state. From the point of view of the electronic and vibrational states, this is a two photon Raman process depicted in Fig. 12.4 that Stark shifts the excited state $|e\rangle$. We will refer to this choice of Raman pulses as the Raman displacement pulse. If we detune the Raman lasers by a frequency $\Delta\omega = \omega_A$ we can drive a carrier transition that coherently superposes the ground and excited states. We will refer to this choice of Raman pulses as the carrier pulse.

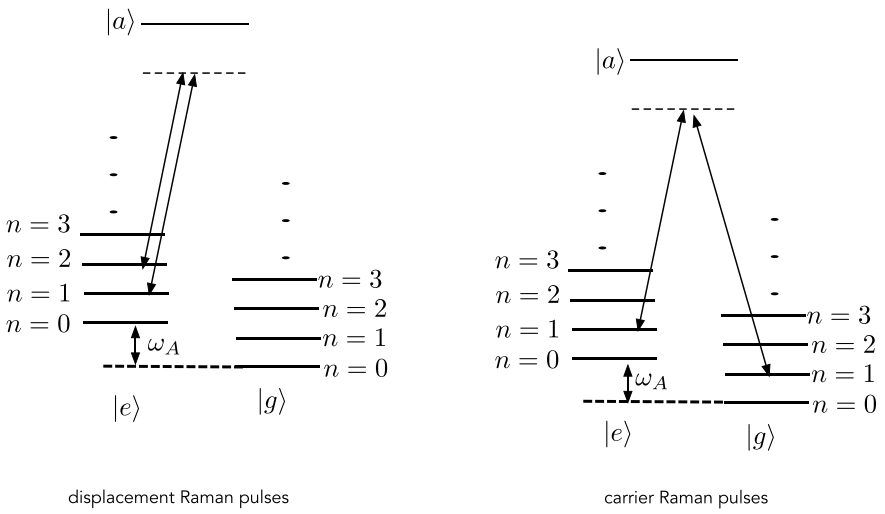

Fig. 12.4 A schematic indication of the optical transitions required to prepare a single ion in a linear superposition of displaced ground states (coherent states). On the left is the Raman pulse excitation scheme for applying a force to the ion conditional on it being prepared in the excited electronic state. On the right is the carrier pulse excitation scheme for producing coherent excitations of the internal electronic state leaving the vibrational motion unaffected. The vibrational frequency is ν while the atomic transition frequency is ω_A

The state-dependent displacement is described by the interaction picture Hamiltonian

$$H_d = \hbar\chi(t)(a + a^\dagger)|e\rangle\langle e| + \hbar\Omega(t)\sigma_x \tag{12.20}$$

the coupling constants χ and Ω are shown as time dependent as they can be turned on and off with the external Raman displacement pulse (χ) or the external carrier pulse (Ω).

Assume that initially the electronic system and vibrational motional are in the ground state, $|\psi(0)\rangle = |0 \otimes |g\rangle$. In the first step, we apply a carrier pulse (so $\chi = 0$) for a time, T, such that $\omega T = \pi/2$. This gives the state transformation

$$|0\rangle \otimes |g\rangle \stackrel{\pi/2}{\Longrightarrow} |0\rangle \otimes \frac{1}{\sqrt{2}}(|g\rangle + |e\rangle) \tag{12.21}$$

In the second step we turn off the carrier pulse and turn on the displacement Raman pulse for a time τ. Only the $|e\rangle$ component sees the displacement, according to (12.20), so the state is transformed as

$$\frac{1}{\sqrt{2}}(|0\rangle \otimes |g\rangle + |0\rangle \otimes |e\rangle) \stackrel{\text{displace}}{\Longrightarrow} \frac{1}{\sqrt{2}}(|0\rangle \otimes |g\rangle + |\alpha\rangle \otimes |e\rangle) \tag{12.22}$$

In the third step we apply a $\pi = \Omega T$ carrier pulse that flips the electronic states and inserts a π phase shift

$$\frac{1}{\sqrt{2}}(|0\rangle \otimes |g\rangle + |\alpha\rangle \otimes |e\rangle) \stackrel{\pi}{\Longrightarrow} \frac{1}{\sqrt{2}}(|\alpha\rangle \otimes |g\rangle - |0\rangle \otimes |e\rangle) \tag{12.23}$$

In the fourth step we apply another state selective displacement with a relative phase ϕ,

$$\frac{1}{\sqrt{2}}(|\alpha\rangle \otimes |g\rangle - |0\rangle \otimes |e\rangle) \stackrel{\text{displace}}{\Longrightarrow} \frac{1}{\sqrt{2}}(|\alpha\rangle \otimes |g\rangle - |\alpha e^{i\phi}\rangle \otimes |e\rangle) \tag{12.24}$$

In the fifth and final step, we apply another $\pi/2$ pulse to give

$$\begin{aligned}\frac{1}{\sqrt{2}}(|\alpha\rangle \otimes |g\rangle - |\alpha e^{i\phi}\rangle \otimes |e\rangle) \stackrel{\pi/2}{\Longrightarrow} &\left(\frac{|\alpha\rangle - |\alpha e^{i\phi}\rangle}{2}\right) \otimes |g\rangle + \left(\frac{|\alpha\rangle + |\alpha e^{i\phi}\rangle}{2}\right) \otimes |e\rangle \\ &\equiv |\alpha_-\rangle \otimes |g\rangle + |\alpha_+\rangle \otimes |e\rangle\end{aligned}$$

If we now readout the state of the ion, the conditional states are highly non classical superpositions of two different coherent states of vibrational motion, $|\alpha_\pm\rangle$ known in quantum optics as *cat states*.

We thus have correlated different motional states with each of the electronic states. This kind of entangled state is reminiscent of Schrödinger's famous thought experiment in which two different metabolic (and thus macroscopic) states of a cat are correlated with a two level system in just this way. Indeed if we stopped after the second step the cat state analogy could be sustained with the identification $|\alpha\rangle \rightarrow |\text{alive}\rangle$ and $|0\rangle \rightarrow |\text{dead}\rangle$. However pursuing the analogy to the final state at the end of step 5 produces the rather disturbing prospect (for the cat at least) of correlating different superposition of metabolic states with the internal electronic states.

In the experiment of Monroe at al. [9], the presence of an entangled state of different coherent states was demonstrated by measuring the electronic state at the end of step 5. Repeated measurements enabled a sampling of the distribution $P_g(\phi)$, for different values of ϕ. This is given by

$$\begin{aligned}P_g(\phi) &= \langle \alpha_- | \alpha_- \rangle \\ &= \frac{1}{2}\left[1 - e^{-|\alpha|^2(1-\cos\phi)} \cos\left(|\alpha|^2 \sin\phi\right)\right]\end{aligned} \tag{12.25}$$

In Fig. 12.5 we reproduce the results from Monroe et al. [9] comparing the experiment with the theoretical prediction. The agreement is remarkable. It is worth pausing to reflect on just what has been demonstrated in this experiment. The experiment shows that a single massive particle can be prepared in a superposition of a position on the left and the right of the equilibrium position, and travelling in opposite directions in each case.

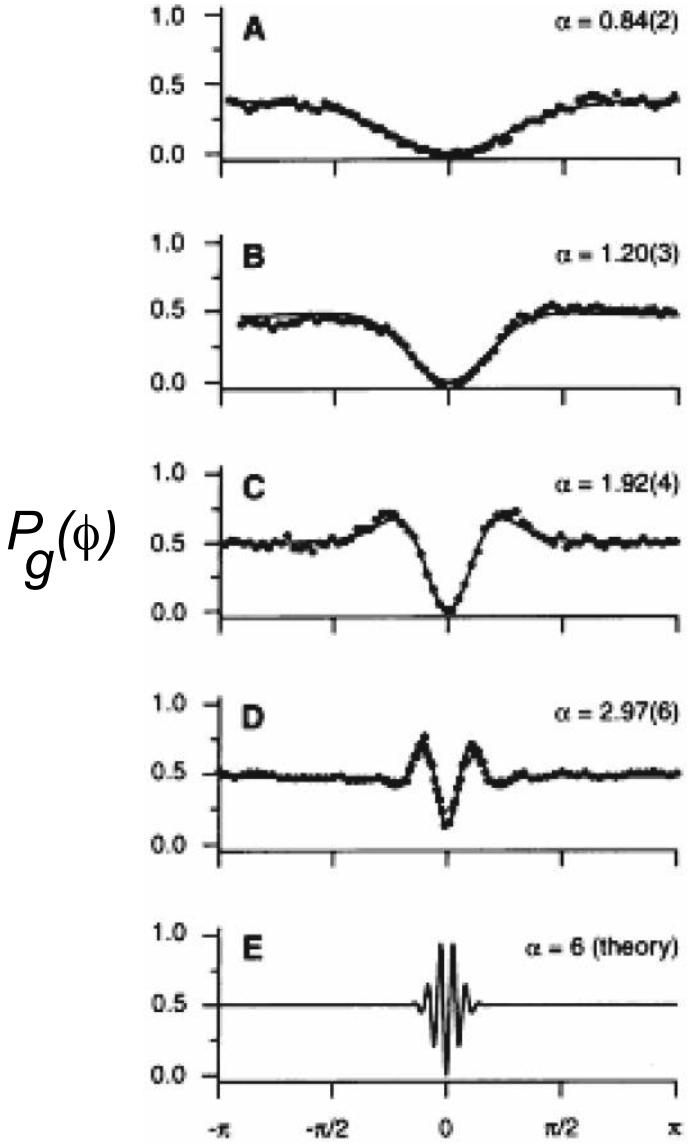

Fig. 12.5 The probability of finding the ion in the ground electronic state as a function of the phase difference, after Fig. 4 [9]

12.4 Trapping Multiple Ions

In a linear ion trap such as depicted in Fig. 12.1, multiple ions may be trapped and cooled to the collective ground states of vibrational motion. Each ion has an equilibrium position, $\bar{x}_i$, corresponding to a minimum in the total potential comprising the trap plus Coulomb potential for each ion. These equilibrium points are analogous to the atomic ions at the lattice points of a crystal, however unlike a crystal they are not equally spaced. In terms of a natural length scale given by the Coulomb potential for each ion,

$$l = \left(\frac{Z^2 e^2}{4\pi \epsilon_0 M \nu^2} \right)^{1/3}, \tag{12.26}$$

and a coordinate system in which $z = 0$ is in the middle of the trapped ions, James [10] has computed the equilibrium positions for different numbers of ions in a trap, see Table 12.1.

If we expand the overall potential to second order in the small oscillations, $q_n(t)$ (in dimensionless units), around the equilibrium points we obtain a simple coupled oscillator Hamiltonian of the form,

$$H = \frac{1}{2M} \sum_{n=1}^{N} p_m^2 + \frac{M\nu^2}{2} \sum_{n,m=1}^{N} A_{nm} q_n q_m \tag{12.27}$$

where p_n is the canonical momentum to q_n. Explicit expressions for the coefficients A_{nm} are given in [10]. This hamiltonian represents a linear array of N simple harmonic oscillators with quadratic coupling. We can now make a change of variable to normal-mode coordinates (sometimes called collective or global coordinates).

Table 12.1 Scaled equilibrium positions as a function of the number of trapped ions, from [10]

N	Scaled equilibrium positions
2	–0.62996, 0.62996
3	–1.0772, 1.0772
4	–1.4368, –0.45438, 0.45438, 1.4368
5	–1.7429, –0.8221, 0.8221, 1.7429
6	–2.0123, –1.1361, –0.36992, 0.36992, 1.1361, 2.0123
7	–2.2545, –14129, –0.68694, 0.68694, 1.4129, 2.2545
8	–2.4758, –1.6621, –0.96701, –0.31802, 0.31802, 0.96701, 1.6621, 2.4758
9	–2.6803, –1.8897, –1.2195, –0.59958, 0.59958, 1.2195, 1.8897, 2.6803
10	–2.8708, –2.10003, –1.4504, –0.85378, –0.2821, 0.2821, 0.85378, 1.4504, 2.10003, 2.8708

The transformation is chosen to diagonalise the real symmetric $N \times N$ matrix with entries A_{nm}. The eigenvalue equation is

$$\sum_{n=1}^{N} A_{nm}\beta_n^{(p)} = \mu_p \beta_m^{(p)} \quad (p = 1, \ldots, N) \tag{12.28}$$

where the eigenvalues are $\mu_p > 0$ and the eigenvectors $\boldsymbol{\beta}^{(p)}$ are assumed to be numbered in order of increasing eigenvalue and are normalised so that

$$\sum_{p=1}^{N} \beta_n^{(p)} \beta_m^{(p)} = \delta_{nm}$$
$$\sum_{n=1}^{N} \beta_n^{(p)} \beta_n^{(q)} = \delta_{pq}$$

For example, when $N = 3$ the eigenvalues are $\mu_1 = 1, \mu_2 = 3, \mu_3 = 29/5$. The normal modes are then given in terms of the small oscillations as

$$Q_p(t) = \sum_{m=1}^{N} \beta_m^{(p)} q_m(t) \tag{12.29}$$

Note the number of normal modes is equal to the number of ions. Of course we can equally well write the *local coordinates* q_n as

$$q_m(t) = \sum_{p=1}^{N} \beta_m^{(p)} Q_p(t) \tag{12.30}$$

The first normal mode, Q_1 represents the centre of mass mode in which all the ions oscillate as if they were train wagons linked together. The second mode Q_2 represents a breathing mode in which each ion oscillates with an amplitude proportional to is displacement form the trap centre. In terms of the normal mode coordinates, Q_P and conjugate momenta P_p, the hamiltonian is

$$H = \frac{1}{2M} \sum_{p=1}^{N} P_p^2 + \frac{M}{2} \sum_{p=1}^{N} \nu_p^2 Q_p^2 \tag{12.31}$$

where the frequencies of each of the normal modes is given by

$$\nu_p = \nu \sqrt{\mu_p} \tag{12.32}$$

This is the Hamiltonian of N independent simple harmonic oscillators. Thus we introduce raising and lowering operators for each normal mode as

$$Q_p = \sqrt{\frac{\hbar}{2M\nu_p}}(b_p + b_p^\dagger) \tag{12.33}$$

$$P_p = -i\sqrt{\frac{\hbar M\nu_p}{2}}(b_p - b_p^\dagger) \tag{12.34}$$

with $[b_p, b_q^\dagger] = \delta_{pq}$.

Let us now assume that each ion in the trap can be addressed with a separate laser beam. For example in a linear ion trap for $^{40}Ca^+$ built in Innsbruck, the average spacing for 4 ions was greater than 5 μm, which is above the diffraction limit for the laser beams. This spacing is also sufficient for the fluorescence (at readout) of each ion to be separately imaged.

The interaction picture Hamiltonian describing how the i'th ion is coupled to small oscillations around equilibrium is given by an obvious generalisation of (12.4)

$$H_I^{(i)} = \hbar\frac{\Omega_i}{2}\left(\sigma_-^{(i)} e^{-ik_L q_i(t)} e^{-i(\omega_A-\omega_L)t} + \text{h.c}\right) \tag{12.35}$$

where we have taken the Rabi frequency for the i'th ion to be Ω_i and $\sigma_\pm^{(i)}$ are the Pauli raising and lowering operators for the i'th ion, while $q_i(t)$ are local coordinates of the i'th ion. If we now again assume that the Lamb-Dicke parameter for each ion is small, the interaction between the electronic and vibrational degree of freedom is

$$H_I^{(i)} = -i\hbar\frac{k_L\Omega_i}{2}\left(\sigma_-^{(i)} q_i(t) e^{-i(\omega_A-\omega_L)t} - \text{h.c}\right) \tag{12.36}$$

This may be written in terms of the global modes as

$$H_I^{(I)} = -i\hbar\frac{\eta\Omega_i}{2\sqrt{N}}\sum_{p=1}^{N} s_i^{(p)}\left(b_p e^{-i\nu_p t} + b_p^\dagger e^{i\nu_p t}\right) e^{-i(\omega_A-\omega_L)t}\sigma_-^{(i)} - \text{h.c} \tag{12.37}$$

where $s_p^{(i)} = \sqrt{N}\mu_p^{-1/4}\beta_i^{(p)}$.

We now assume that we can tune the external laser to address only a single global vibrational mode (a particular normal mode), say the centre of mass mode at frequency, $\mu_1 = \nu$ and $s_i^{(1)} = 1$ with $\omega_A - \omega_L = \nu$. Then we can ignore all the other modes and approximate the Hamiltonian as

$$H_I^{(i)} = -i\hbar\frac{\eta\Omega_i}{2\sqrt{N}}\left(\sigma_+^{(i)} b_1 + \sigma_-^{(i)} b_1^\dagger\right) \tag{12.38}$$

This is the Cirac-Zoller Hamiltonian [1] and enables a scheme for quantum computing using trapped ions. If there are many ions in the trap this may not be a good

approximation. In that case there are many normal modes and it is difficult to resolve individual normal mode frequencies as they become very closely spaced. To some extent this may be mitigated by cooling all the normal modes to their ground states. Further discussion of the validity of this approximation may be found in [10] and also [11].

12.5 Ion Trap Quantum Information Processing

In 1995 Cirac and Zoller [1] proposed the first scheme for implementing quantum logic gates for trapped ions. In a quantum computer (see Chap. 15) information is stored in the states of a collection of two level systems, generically referred to as qubits. In the Cirac-Zoller (CZ) scheme, the qubits are the two-level electronic states of the trapped ions. Arbitrary transformations of the state of a single qubit are easily implemented by external laser fields. For universal computation we also need to have access to two qubit interactions. However the electronic states of different ions do not interact. CZ proposed to overcome this by using the collective vibrational mode of the ions to implement a virtual interaction between the qubits. The Cirac-Zoller scheme was first implemented by the Innsbruck group led by Blatt in 2003 [12]. They used two $^{40}Ca^{+}$ ions held in a linear trap and individually addressed by focussed laser beams.

Other schemes have been proposed for implementing quantum gates in ion traps. Sørenson and Mølmer [13] developed a scheme which mitigates to some extent the deleterious effects of noise entering via the vibrational degree of freedom (eg patch potential heating) and implemented by the Wineland group in NIST [14]. A related scheme [15] uses far off-resonance optical dipole forces to implement a geometric phase gate, also first implemented by the NIST group [16].

The Mølmer-Sørenson gate uses a bichromatic laser field. The resulting Hamiltonian for two ions (see (12.12))

$$H_{ms}(t) = \frac{\hbar\eta\Omega}{2}(be^{i\delta t} + b^{\dagger}e^{-i\delta t})(\sigma_y^{(1)} + \sigma_y^{(2)}) \tag{12.39}$$

where we have included an additional symmetric detuning δ from the relevant normal mode frequency where $\omega_{L1} - \omega_{L2} = 2(\nu + \delta)$ is the difference between the frequencies of the two laser driving fields. This Hamiltonian is explicitly time dependent in the interaction picture. In a time interval $0 < t < T$ we can write the unitary time evolution operator as a Dyson expansion

$$\begin{aligned}\mathcal{U}(T) = 1 + \sum_{n=1}^{\infty}\left(\frac{-i}{\hbar}\right)^n \int_0^T dt_n \int_0^{t_n} dt_{n-1} \\ \ldots \int_0^{t_2} dt_1 H_{ms}(t_n)\ldots H_{ms}(t_2)H_{ms}(t_1)\end{aligned} \tag{12.40}$$

If we assume that $\delta T \gg 1$ (dispersive regime) we can approximate this to lowest order in T as

$$\mathcal{U}(T) = e^{-\frac{i}{\hbar} H_{eff} T} \tag{12.41}$$

where the effective Hamiltonian is

$$H_{eff} = \hbar \frac{(\eta\Omega)^2}{2\delta} \sigma_y^{(1)} \sigma_y^{(2)} \tag{12.42}$$

up to an additive constant. This is an effective interaction between the internal states of the ions and will suffice to entangle these state given carrier frequency control of the state of each ion independently.

There is a fundamental operation underlying the MS gate related to the idea of a geometric phase [15]. Suppose we use two consecutive fast pulses so that one ion at a time is driven bichromatically by very fast pulses. If the phase is adjusted from one pulse to the next we can implement

$$\begin{aligned} U_1 &= e^{-i\kappa_p (b+b^\dagger)\sigma_y^{(1)}} \\ U_2 &= e^{-i\kappa_x (b-b^\dagger)\sigma_y^{(2)}} \end{aligned} \tag{12.43}$$

These give conditional phase space displacements of the vibrational degree of freedom. If we use the commutation relation $[b, b^\dagger] = 1$ we can show that

$$U_2(\kappa_p) U_1(-\kappa_x) U_2(-\kappa_p) U_1(\kappa_x) = e^{i\kappa_x \kappa_p \sigma_y^{(1)} \sigma_y^{(2)}} \tag{12.44}$$

The basic idea of a geometric phase gate is to use a sequence of such laser pulse sequences, applied to two ions, that move the vibrational degree of freedom of the ion through a loop in phase space that depends on the internal states of the two ions. Up to a single ion rotation unitary, this is an Ising-like unitary interaction between the two qubits. Note that there is no dependance on the vibrational degree of freedom at all. Inspection of the various phase space orbits that result for each choice of the joint eigenstates of $\sigma_y^{(1)} \sigma_y^{(2)}$ indicates why this is called a geometric phase gate. The effective conditional phase between the two qubits is proportional to the area of the rectangle, $\chi = \kappa_x \kappa_p$ and the sign is given by the sense of rotation. It is clear that the actual shape of the closed orbit in phase space does not matter: only the area and sense of rotation matter. Effectively the Sørenson and Mølmer gate implements the phase space rotations by a time varying driving fields.

Problems

12.1 A laser is tuned to the first read sideband transition for a single two level transition, $|g\rangle \leftrightarrow |e\rangle$, with a spontaneous emission rate of γ. Ignoring all but the spontaneous emission decay channel, the master equation (in the interaction picture) describing this system is

$$\frac{d\rho}{dt} = \frac{\eta\Omega}{2}[a\sigma_+ - a^\dagger\sigma_-, \rho] + \gamma\mathcal{D}[\sigma_-]\rho \tag{12.45}$$

where η is the Lamb-Dicke parameter, Ω is the Rabi frequency for the transition and $a, a^\dagger$ are the lowering and raising operators for the vibrational motion of the ion in the trap. Obtain equations of motion for $\bar{n} = \langle a^\dagger a\rangle$, $\langle a\rangle$, $\langle\sigma_\pm\rangle$, $\langle\sigma_z\rangle$ by factorising all higher order moments in the equations of motion. Assuming that the spontaneous emission rate is large enough so that the average polarisation $\langle\sigma_\pm\rangle$ is stationary and the vibrational motion is slaved to the atomic motion, show that the rate of change of $\bar{n}$ is given by (12.14).

12.2 A simple model for the heating of a trapped ion due to fluctuation potentials may be given in terms of the Hamiltonian

$$H(t) = \hbar\nu a^\dagger a + \hbar\epsilon(t)(a + a^\dagger) \tag{12.46}$$

where $\epsilon(t)$ is fluctuating force term with the following classical moments

$$\bar{\epsilon} = \mathcal{E}(\epsilon(t)) = 0$$
$$G(\tau) = \mathcal{E}(\epsilon(t)\epsilon(t+\tau)) = \frac{D}{2\gamma}e^{-\gamma|\tau|}$$

Show that the heating rate is given by

$$\frac{d\langle a^\dagger a\rangle}{dt} = \frac{\pi}{2}S(\nu) \tag{12.47}$$

where the noise power spectrum for the fluctuating force is defined by

$$S(\omega) = \frac{1}{2\pi}\int_{-\infty}^{\infty} e^{-i\omega t}G(\tau) \tag{12.48}$$

12.3 Show that if a harmonic oscillator in its ground state is subjected to a sequence of displacements in phase space that form a closed loop, the state is returned to the ground state up to an overall phase proportional to the area of the loop.

References

1. J.I. Cirac, P. Zoller, Phys. Rev. Lett. **74**, 4091 (1995)
2. H.G. Dehmelt, Bull. Am. Phys. Soc. **20**, 60 (1975)
3. J.C. Bergquist, R.G. Hulet, W.M. Itano, D.J. Wineland, Phys. Rev. Lett. **57**, 1699 (1986): W. Nagourney, J. Sandberg, H.G. Dehmelt, Phys. Rev. Lett. **56**, 2797 (1986): T. Sauter, W. Neuhauser, R. Blatt, P.E. Toschek, Phys. Rev. Lett. **57**, 1696 (1986)
4. D. Leibfried, R. Blatt, C. Monroe, D. Wineland, Rev. Mod Phys. **75**, 281 (2003)
5. J.I. Cirac, R. Blatt, P. Zoller, W.D. Philips, Phys. Rev. A **46**, 2668 (1992)
6. C. Monroe, D.M. Meekhof, B.E. King, S.R. Jefferts, W.M. Itano, D.J. Wineland, P.L. Gould, Phys. Rev. Lett. **75**, 4011 (1995)
7. M.J. Gagen, G.J. Milburn, Phys. Rev. A **45**, 5228 (1992)
8. S. Lloyd, S. Braunstein, Phys. Rev. Lett. **82**, 1784 (1999)
9. C. Monroe, D.M. Meekhof, B.E. King, D.J. Wineland, Science **272**, 1131 (1996)
10. D.F.V. James, Appl. Phys. B **66**, 181 (1998)
11. D.J. Wineland, C. Monroe, W.M. Itano, D. Liebfried, B.E. King, D.M. Meekhof, J. Res. Natl. Stand. Technol. **103**, 259 (1998)
12. F. Schmidt-Kaler, H. Häffner, M. Riebe, S. Gulde, G.P.T. Lancaster, T. Deuschle, C. Becher, C.F. Roos, J. Eschner, R. Blatt, Nature **422**, 408 (2003)
13. A. Sørensen, K. Mølmer, Phys. Rev. A **62**, 022311 (2000)
14. C.A. Sackett, D. Kielpinski, B.E. King, C. Langer, V. Meyer, C.J. Myatt, M. Rowe, Q.A. Turchette, W.M. Itano, D.J. Wineland, C. Monroe, Nature **404**, 256 (2000)
15. G.J. Milburn, S. Schneider, D.F.V. James, Fortschritte der Physik **48**, 801 (2000)
16. D. Leibfried, B. De Marco, V. Meyer, D. Lucas, M. Barrett, J. Britton, W.M. Itano, B. Jelenkovic, C. Langer, T. Rosenband, D.J. Wineland, Nature **422**, 412 (2003)

Quantum Optics and Quantum Foundations

13

Abstract

The early days of quantum mechanics were characterised by debates over the applicability of established classical concepts, such as position and momentum, to the new formulation of mechanics. The issues became quite distinct in the protracted exchange between A. Einstein and N. Bohr, culminating in the paper of Einstein, Podolsky and Rosen (EPR) in 1935 (Einstein et al. in Phys. Rev. 47:777, 1935, [1]). Thus the matter rested until 1964 when J.S. Bell (Physics 1:105, 1964; Rev. Mod. Phys. 38:447, 1966, [4]) opened up the possibility of directly testing the consequences of the EPR premises. We will discuss the EPR argument and the analysis of Bell in the context of correlated photon states.

13.1 The Einstein-Podolsky-Rosen (EPR) Argument

The essential step in the EPR argument is to introduce entangled pure states of two degrees of freedom. In the original EPR argument these degrees of freedom were the mechanical states of two interacting particles but, following Reid [3], we will consider two interacting field modes, a, b with canonical quadrature phase operators $\hat{X}_\mu, \hat{Y}_\nu$ with $\mu, \nu = \{a, b\}$ that satisfy the canonical commutation relations

$$[\hat{X}_\mu, \hat{Y}_\nu] = 2i\delta_{\mu\nu} \tag{13.1}$$

We will consider the state defined by

$$|\Psi\rangle = e^{-i\hat{Y}_a\hat{X}_b/2}|X = X_0\rangle_a|Y = Y_0\rangle_b \tag{13.2}$$

where $|X = X_0\rangle_a$ is an eigenstate of $\hat{X}_a$ with eigenvalue X_0 while $|Y = Y_0\rangle_b$ is an eigenstate of $\hat{Y}_b$ with eigenvalue Y_0. Note that this cannot be a physical state as it is a unitary transformation of a non normalisable eigenstate of the quadrature phase operators. We will consider a more physical version of this state later.

D. F. Walls and G. J. Milburn, *Quantum Optics*, Graduate Texts in Physics,
https://doi.org/10.1007/978-3-031-84177-4_13

The state in (13.2) is in fact a simultaneous eigenstate of the operators $\hat{X}_a - \hat{X}_b$ and $\hat{Y}_a + \hat{Y}_b$ with eigenvalues X_0 and Y_0 respectively. Suppose one makes perfectly accurate measurements of $\hat{X}_a$ and $\hat{X}_b$, using say homodyne detection. The measurement results are random variables x_a, x_b constrained so that in each and every trial $x_a - x_b = X_0$. Likewise, one can make perfectly accurate measurements of $\hat{Y}_a$ and $\hat{Y}_b$, giving random variables y_a, y_b constrained so that in each trial $y_a + y_b = Y_0$. In the case that we set $X_0 = Y_0 = 0$ then we have that in each trial $x_a = x_b$ and $y_a = -y_b$, a perfect correlation and anti correlation.

The EPR argument rests on the correlations that result when homodyne measurements are made on each of the two modes, a and b, using local detectors far from the source that produced the entangled state. The detectors may even be space like separated. In that case a measurement of $\hat{X}_a$, with result x, enables that observer to predict that the result of the measurement of $\hat{X}_b$ at the other detector, no matter how distant, will give the result x. Similar statements apply for measurements of the Y-quadratures. Thus, without in anyway interacting with the distant detector at b, the observer at a can predict with certainty the result of measurements at the distant detector, b. This result is of course symmetric under interchange of the labels a and b. Note that there is no possibility of using this correlation to signal as the results of the measurements at each detector are completely random: you only see the perfect correlation when the results are brought together.

EPR now make the following claim [1]:

> if without in any way disturbing the system, we can predict with certainty the value of a physical quantity, then there exists an element of physical reality corresponding to this quantity.

EPR assume that there can be “no action at a distance” or special relativistic causal structure, so that, in the case that the two detectors are space-like separated, there can be no way for the action of measurements at one detector to influence the results of measurements at the other detector. The notion of "an element of physical reality” is a way of stating the classical ideal that systems have physical properties that take values independent of observers even if those values happen to be unknown due to ignorance.

Should the observer at a choose to measure the X quadrature, they can predict with certainty the results of a measurement of the X quadrature at the distant detector, b. So there is an element of physical reality associated with this predicted result. The observer at a could equally well have chosen to measure the Y quadrature in which case they can predict, with certainty, the result of a Y quadrature measurement at b. We are forced to conclude that the values of two physical quantities, represented by non committing operators $(\hat{X}_b, \hat{Y}_b)$, take objective values even if they are not measured at b. This appears to be in conflict with the uncertainty principle. EPR then concluded that quantum mechanics gives an incomplete description of the state of the field at the detectors as the quantum state of the two particles *before* the measurements are made does not determine the results of complementary quadrature phase measurements.

Bohr's response can be anticipated when we admit that, in a single trial, we can chose to measure either the X_a quadrature or the Y_a quadrature but not both simultaneously. We can; (i) chose to measure the X_a quadrature and predict with certainly the results of an X_b quadrature measurement or (ii) we can chose to measure the Y_a quadrature and predict with certainly the results of an Y_b quadrature measurement. But (i) and (ii) are two *different* experiments or, as Bohr might say, complementary experiments. While this is undoubtedly true, it does little to mitigate the discomfort forced on us by the EPR argument.

We will postpone further discussion of the quadrature phase operator version of the EPR argument to later in this chapter. We now turn to Bell's contribution [4] which provides a sharp and unambiguous quantitative statement of the difference between classical and quantum correlations. Bell noted that, if as EPR claim, quantum mechanics is incomplete how would the predictions change if the theory were supplemented by additional variables in order to restore the classical ideal of causality and locality? Using a precise mathematical formulation of local hidden variables, Bell showed that the predictions would then be incompatible with the predictions of quantum mechanics.

13.2 Bell Inequalities and the Aspect Experiment

Bell used a spin-half example of EPR-like correlations first presented by Bohm and Aharonov [5]. The first optical tests was performed by Freedman and Clauser [6] and Aspect, Dalibard and Roger [7,8]. These experiments uses the polarisation degree of freedom of pairs of photons. Aspect et al. used a two-photon emission cascade between electronic states $(J = 0) \rightarrow (J = 1) \rightarrow (J = 0)$ in calcium-40. The two photons are emitted in opposite directions (by conservation of linear momentum) with correlated polarisation states (by conservation of angular momentum). Each photon passes through separate polarisation analysers, emerging in either the horizontal $(+)$ channel, or the vertical channel $(-)$ of each analyser. Initially, assume that the horizontal polarisation is chosen to be orthogonal to the plane of the experiment and that both analysers are so aligned. However, we are free to rotate the polarisers in the plane orthogonal to the propagation direction of the photons.

The Aspect experiment introduced the key features of many subsequent tests of Bell inequalities in quantum optics. There have since been hundreds of experiments and there is no doubt that quantum correlations violate the various forms of Bell-like inequalities that have been tested. Aspect, together with John Clauser and Anton Zeilinger were jointly awarded the Nobel prize in physics in 2022 for their pioneering work in these experiments. The basic experimental arrangement for these experiments in shown in Fig. 13.1.

In an ideal experiment we use single-photon excitations of polarised spatio-temporal modes. In most experiments this is done by post-selection but we postpone the discussion of this aspect of the experiments for now. A two photon state is generated, in a correlated, but distinguishable, spatio-temporal modes k_a, k_b. The photons are entangled in their polarisation degree of freedom. For example the source could prepare, in every trial, the two-photon state,

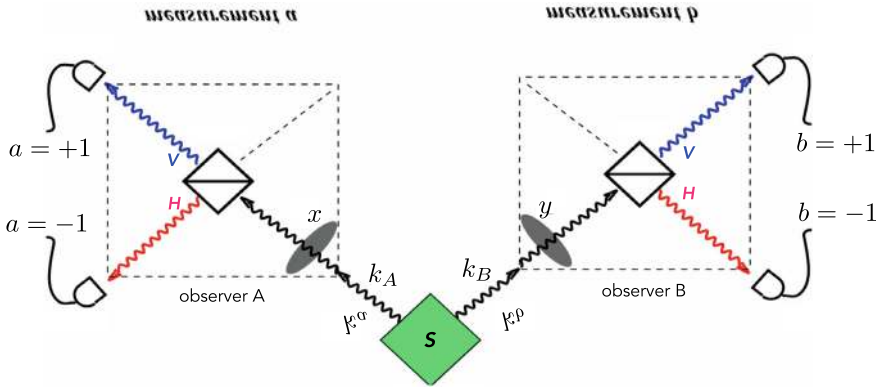

Fig. 13.1 A typical photonic test of a Bell inequality using polarisation entangled photons. S is a source of two photons in a polarisation entangled state. They are directed towards two detectors, space-like separated from each other. Label each detector A, B. Each detector requires a choice be made for the polarisation settings, labelled x at A and y at B. and has two output channels labelled $a = \pm 1$ at A and $b = \pm 1$ at B. These are the reflected and transmitted outputs of a polararising beam splitter

$$|\Psi^-\rangle = \frac{1}{\sqrt{2}}(|HV\rangle - |VH\rangle) \tag{13.3}$$

where $|HV\rangle = |1\rangle_{k_A,H} \otimes |1\rangle_{k_B,V}$ and the subscripts label spatio-temporal modes with wave vectors k_A, k_B and corresponding polarisation. The state $|\Psi^-\rangle$ is one of the four orthogonal Bells states traditionally designated as

$$|\Psi^\pm\rangle = \frac{1}{\sqrt{2}}(|HV\rangle \pm |VH\rangle) \tag{13.4}$$

$$|\Phi^\pm\rangle = \frac{1}{\sqrt{2}}(|HH\rangle \pm |VV\rangle) \tag{13.5}$$

A single trial corresponds to emitting a two-photon state and counting two photons; one at observer-a and one at observer-b. If for some reason two photons are not detected, that trial is discarded. As no detector is perfect this is likely to happen quite often. Let the measurement settings be chosen from a set of discrete rotations $x \in \{\theta_{A,1}, \theta_{A,2}, \ldots \theta_{A,n}\}$ and $y \in \{\theta_{B,1}, \theta_{B,2}, \ldots \theta_{B,n}\}$. Suppose the detector settings are the same, $x = y$, that is to say, the same angle is chosen. We can rotate both angles jointly until we see a perfect anti-correlation at each output. When the photon at A is detected at $a = 1$ channel the photon at B is detected at $b = -1$ channel, and vice versa. However from trail to trial the local measurement outcomes are a random binary numbers ± 1.

There is an important elision in the previous paragraph. In order to see the correlation an observer must have access to both outcomes in each trial. In the lab this is obvious, as the experimentalist collects all the data from both detectors in each trial. However we should make this step explicit as we have assumed that each detector

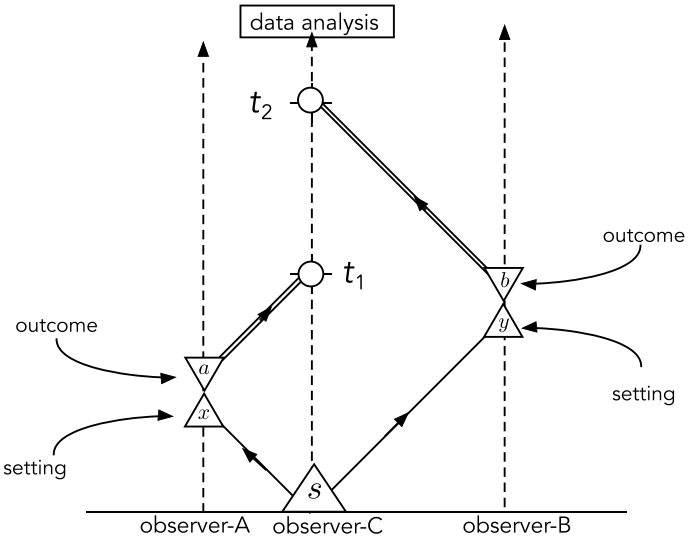

Fig. 13.2 A two-party Bell experiment with entangled photons. A source at the origin produces entangled photons pairs. The photons are in oppositely directed spatial modes. One goes to detector-A and the other goes to detector-B. Both observers are space-lie separated. After each measurement the setting and the outcome are sent, over classical channels (double lines), to a checker, observer-c, who stores the data for each trial and constructs the appropriate correlation function to check a Bell inequality

is space-like separated. This can easily be resolved by introducing a 'checker'—labelled c—that receives the data (setting and outcome at each detector) from each observer in a trial in the future light cone of the detection events. For convenience we will suppose the verifier is at the same place as the source. Note that the verifier is getting results of experiments and this is purely classical information. A space-time diagram for the experiment is shown in Fig. 13.2. Note that observer-c is at rest in the frame of the source and thus can easily synchronise emission and detection events to ensure that data is collected from each trial.

So far there is nothing unusual in this experiment. We can easily arrange for a classical source to produce perfect correlations of this kind. The real quantum surprise is only found when observer-A and observer-B make different choices for the measurement settings x, y. This was Bell's insight. It remains the case that the outcome at each observer is random, but now c will find a non classical statistical feature.

The protocol is as follows.

- All observers agree that only two measurement settings will be used $a, b \in \{\theta_1, \theta_2\}$.
- In each trial, observers a and b each toss a coin to determine which measurement setting to use.

- Data analysis: when the checker gets the classical information about the setting and the result from each observer they compute the product $x_{a,i} \times x_{b,j}$ $(i, j \in \{1, 2\})$ for every trial and then average over all trials to get $E(i, j) \equiv \mathbb{E}[x_{a,i} \times x_{b,j}]$.
- Given enough trials, and measurement settings, the checker calculates the correlation function.

$$S = |E(1, 1) + E(1, 2) + E(2, 1) - E(2, 2)|$$

This correlation is the CHSH correlation function.

If we make some assumptions on how the measurement outcomes should be correlated we can prove the CHSH theorem. The assumptions capture EPR's concept of local realism.

Realism—measurement outcomes are determined by properties of the particles that exist prior to and independent of the experimental situation.

Locality—measurement outcomes obtained at one location are independent of any measurements, or actions, performed at a space-like separation.

Freedom of Choice—Any process that leads to the choice of measurements made by observers A and B, is completely independent of other processes in the experiment.

The assumption of realism and locality can be expressed in terms of a unknown classical quantity λ, possibly unknown with probability distribution $p(\lambda)$. We assume that

$$\mathrm{P}(a, b|x, y) = \int_{\lambda} p(\lambda)\mathrm{P}(a|x, \lambda)\mathrm{P}(b|y, \lambda) \tag{13.6}$$

This is often glossed as; correlations must be explained by local common causes. We stress that there are no spacetime labels included in this condition. It is meant to capture our intuition about causes in such situations but it is far more general.

Given these assumptions, correlation function $E(A_i, B_j)$, $i, j = 1, 2$ between Alice and Bob's measurement outcomes, labelled respectively as A_i and B_j, satisfies the following inequality,

$$S = |E(A_1, B_1) + E(A_1, B_2) + E(A_2, B_1) - E(A_2, B_2)| \leq 2. \tag{13.7}$$

The quantum theory predicts a very different result. The joint probability of measurement outcomes $\mathrm{P}(a, b|x, y)$ is determined by a joint POVM

$$\mathrm{P}(a, b|x, y) = \mathrm{tr}[\rho \hat{E}_x(a) \otimes \hat{E}_y(b)] \tag{13.8}$$

where ρ is the joint state prepared by the source. The basic POVM for polarisation is

$$\hat{E}_x(a)] = \frac{1}{2}\left(1 + a\boldsymbol{x} \cdot \hat{\boldsymbol{\sigma}}\right) \quad a = \pm 1 \tag{13.9}$$

where $U(x)$ is an arbitrary unitary in the two dimensional Hilbert space of polarisation. The probability distribution for a single mode is

$$\mathrm{P}(a|x) = \mathrm{tr}[\hat{E}_x(a)\rho] = \frac{1}{2}\left(1 + a\mathrm{tr}[\boldsymbol{x}\cdot\hat{\boldsymbol{\sigma}}\,\rho]\right) \tag{13.10}$$

where $\boldsymbol{n}$ is a unit vector and $\hat{\boldsymbol{\sigma}} = (\sigma_x, \sigma_y, \sigma_z)$ with the Pauli matrices defined

$$\sigma_z = |H\rangle\langle H - |V\rangle\langle V| \,, \sigma_y = -i(|H\rangle\langle V| - |V\rangle\langle H|) \,, \sigma_x = |H\rangle\langle V + |V\rangle\langle H| \,. \tag{13.11}$$

Then the average is

$$E[j] = \mathrm{P}(1|x_j) - \mathrm{P}(-1|x_j) = \mathrm{tr}[\boldsymbol{x}_j\cdot\hat{\boldsymbol{\sigma}}\,\rho] \tag{13.12}$$

We can show that for the state in (13.3)

$$E(i,j) = -\boldsymbol{x}_i\cdot\boldsymbol{y}_j = -\cos\theta_{ij} \tag{13.13}$$

where θ_{ij} is the angle between $\boldsymbol{x}_i$ and $\boldsymbol{y}_i$. There exists choices for directions $\boldsymbol{x}_i$ and $\boldsymbol{y}_i$ such that $S = 2\sqrt{2}$, violating the Bell inequality. This is the maximum violation possible in quantum mechanics [9].

13.3 Description of the Aspect Experiment

We can use the generalised P function methods to describe the Apsect polarisation test of the Bell inequality. We follow the treatment of Reid and Walls [10]. Let $a_i(b_i)$ be the annihilation operator for the horizontally ($i = +$) or vertically ($i = -$) polarised mode for the field travelling to analyser A or analyser B. The measurements are made using photo-detection. As there are two spatial modes each of which has two polarisation modes, we need a four mode description.

The state of the two photons may be written as

$$|\Psi^-\rangle = \frac{1}{\sqrt{2}}(a_+^\dagger b_-^\dagger - a_-^\dagger b_+^\dagger)|0\rangle, \tag{13.14}$$

where $|0\rangle$ is the vacuum state. Using the notation $|n_1, n_2, n_3, n_4\rangle$ to denote n_1 photons in mode a_+, n_2 photons in mode a_-, n_3 photons in mode b_+, and n_4 photons in mode b_-, the state may be expressed as

$$|\Psi\rangle = \frac{1}{\sqrt{2}}(|1,0,0,1\rangle - |0,1,1,0\rangle). \tag{13.15}$$

If the photon in analyser A is detected in the $(+)$ channel, the state of the photon detected in analyser B must be polarised in the $(-)$ direction. We are free to measure the polarisation in any direction by rotating the analysers through angles θ_1 and θ_2,

for detector A and B, respectively. The mode detected in this case are orthogonal transformations of the modes a_i and b_i:

$$c_i = a_i \cos\theta_i + b_i \sin\theta_i, \tag{13.16}$$

$$d_i = -a_i \sin\theta_i + b_i \cos\theta_i, \tag{13.17}$$

$$c_j = a_j \cos\theta_j + b_j \sin\theta_j, \tag{13.18}$$

$$d_j = -a_j \sin\theta_j + b_j \cos\theta_j. \tag{13.19}$$

The detectors placed after the polarisers measure the intensities $\langle I_1^{\pm}\rangle$ and $\langle I_2^{\pm}\rangle$ while the correlators measure $\langle I_1^{\pm} I_2^{\pm}\rangle$, etc. Clearly these moments depend on θ and θ_2. Let us further suppose that in a complete theory these functions also depend on the variable λ which remains hidden from direct determination and for which only a statistical description is available. This variable is distributed according to some density $\rho(\lambda)$. In general, we may then write

$$\langle I_1^{\pm} I_2^{\pm}\rangle_{\theta_1\theta_2} = \int \rho(\lambda) I_1^{\pm}(\lambda, \theta_1, \theta_2) I_2^{\pm}(\lambda, \theta_1, \theta_2) d\lambda, \tag{13.20}$$

where I_j^+ denotes the expected intensity at detector j given a value for λ, namely

$$I_j^+(\lambda, \theta_j, \theta_2) = \int I_j^+(\lambda, \theta_1, \theta_2)\rho(\lambda) d\lambda. \tag{13.21}$$

It is reasonable to assume, as in Bell's approach, that for a given value of λ the results at 1 cannot depend on the angle θ chosen at 2 (and conversely). This is the 'locality assumption', it is formally represented by

$$I_1^{\pm}(\lambda, \theta_1, \theta_2) = I_1^{\pm}(\lambda, \theta_1), \tag{13.22}$$

$$I_2^{\pm}(\lambda, \theta_1, \theta_2) = I_2^{\pm}(\lambda, \theta_2). \tag{13.23}$$

Consider the following correlation functions:

$$E(\theta_1, \theta_2) = \frac{\langle (I_1^+ - I_1^-)(I_2^+ - I_2^-)\rangle}{\langle (I_1^+ + I_1^-)(I_2^+ + I_2^-)\rangle}. \tag{13.24}$$

In terms of the detected mode operators this may be written in the form

$$E(\theta_1, \theta_2) = \frac{\langle : (c_+^\dagger c_+ - c_-^\dagger c_-)(d_+^\dagger d_+ - d_-^\dagger d_-) : \rangle}{\langle : (c_+^\dagger c_+ + c_-^\dagger c_-)(d_+^\dagger d_+ + d_-^\dagger d_-) : \rangle} \tag{13.25}$$

where : denotes normal ordering. Assuming a local hidden variable theory we may write

$$E(\theta_1, \theta_2) = N^{-1} \int f(\lambda) S_1(\lambda, \theta_1) S_2(\lambda, \theta_2) d\lambda, \tag{13.26}$$

where

$$S_1(\lambda, \theta_1) = \frac{I_1^+(\lambda, \theta_1) - I_1^-(\lambda, \theta_1)}{I_1(\lambda)}, \tag{13.27}$$

$$S_2(\lambda, \theta_2) = \frac{I_2^+(\lambda, \theta_2) - I_2^-(\lambda, \theta_2)}{I_2(\lambda)}. \tag{13.28}$$

with

$$f(\lambda) = \rho(\lambda) I_1(\lambda) I_2(\lambda), \tag{13.29}$$

$$I_1(\lambda) = I_1^+(\lambda, \theta_1) + I_1^-(\lambda, \theta_1), \tag{13.30}$$

$$I_2(\lambda) = I_2^+(\lambda, \theta_2) + I_2^-(\lambda, \theta_2). \tag{13.31}$$

Equations (13.30, 13.31) correspond to the intensity of light measured at A or B with the polarisers removed. The normalisation N is

$$N = \int f(\lambda) d\lambda. \tag{13.32}$$

The functions $S_1(\lambda, \theta_1)$ and $S_2(\lambda, \theta_2)$ are bounded by unity:

$$|S_1(\lambda, \theta_1)| \leq 1, \tag{13.33}$$

$$|S_2(\lambda, \theta_2)| \leq 1. \tag{13.34}$$

To obtain a testable statistical quantity we need to consider how $E(\theta_1, \theta_2)$ changes as the orientation of the polarisers are changed. With this in mind, consider $E(\theta_1, \theta_2) - E(\theta_1, \theta_2')$. This quantity may be expressed as

$$E(\theta_1, \theta_2) - E(\theta_1, \theta_2') = N^{-1} \int f(\lambda) [S_1(\lambda, \theta_1) S_2(\lambda, \theta_2) - S_1(\lambda, \theta_1) S_2(\lambda, \theta_2')] d\lambda. \tag{13.35}$$

Then using (13.17), (13.18)

$$|E(\theta_1, \theta_2) - E(\theta_1, \theta_2')| \leq N^{-1} \int f(\lambda) |S_1(\lambda, \theta_1)| |S_2(\lambda, \theta_2) - S_2(\lambda, \theta_2')| d\lambda \tag{13.36}$$

$$= N^{-1} \int f(\lambda) [1 \cdot |S_2(\lambda, \theta_2) - S_2(\lambda, \theta_2')|] d\lambda \tag{13.37}$$

$$= 2 + [E(\theta_1, \theta_2) + E(\theta_1', \theta_2)]. \tag{13.38}$$

Finally, we obtain the Bell inequality

$$|E(\theta_1, \theta_2) + E(\theta_1', \theta_2) + E(\theta_1, \theta_2') - E(\theta_1', \theta_2')| \leq 2, \tag{13.39}$$

This is the same Clauser-Horne-Shimony-Holt (CHSH) inequality in (13.7). We know the two-photon entangled state will violate the inequality. The existence of a Glauber-Sudarshan P function excludes a violation.

13.4 Closing the Loop Holes

Did the original Aspect experiment rule out local hidden variables? A positive response is open to two objections. Firstly, the two measurements on each of a pair of correlated photons were not space-like separated, the "locality loop-hole". Secondly a very large number of trials do not yield a result due to detector inefficiencies, the "detection loop-hole". In that case one could imagine that the events that are registered do not give a fair-sampling of the entangled states; somehow the measurement settings might influence which events are recorded. The second Aspect experiment [8] went some way to closing the first loop hole.

Closing both the detection and locality loopholes was achieved using a very different kind of source based on NV diamond single photon emitters. In addition to using very efficient single photon detectors, the experiment used a novel 'heralded' source of entanglement of pairs of electron spins in physically distinct diamond crystals. This is closer to the original Bohm-Aharonov-Bell formulation of EPR correlations. We will describe this experiment in some detail.

Nitrogen vacancy centres in diamond exhibit good single photon emission depending on the electron spin of the vacancy at low temperatures [14]. The level structure and optical transitions are depicted in Fig. 13.3. The ground state is a spin-triplet split by a crystal field into spin states $m_s = 0$ and a degenerate doublet $m_s = \pm 1$ separated by 2.88 GHz. If necessary, a Zeeman field can be included to lift the degeneracy of the $m_s = \pm 1$ ground states.

There are two optical transitions, one labelled E_x between the $m = 0$ ground state and an $m_s = 0$ excited state and another labelled A_1 between $m_s = \pm 1$ and a mostly $m = \pm 1$ excited state. When one of these transitions is resonantly driven, the fluorescence decays due to weak transitions into the ground state of the opposite excitation path. This mechanism enables optical pumping of either the $m_s = 0$ ground state or the $m_s = \pm 1$ ground state. This feature enables high fidelity electron spin initialisation. The spin dependent transitions A_1, E_x also enable 'single-shot' spin-dependent optical readout of the triplet ground state through observation of the strong spin-resolved fluorescence on these transitions. In Robledo et al. [15] the fidelity of preparation plus readout of the $m_s = 0$ state was 99.7% while for the $m_s = \pm 1$ states it was 99.2%.

The key feature of the Hanson experiment is the preparation of an initial entangled state of two NV centres in distinct diamond samples, separated by 1280 m, using

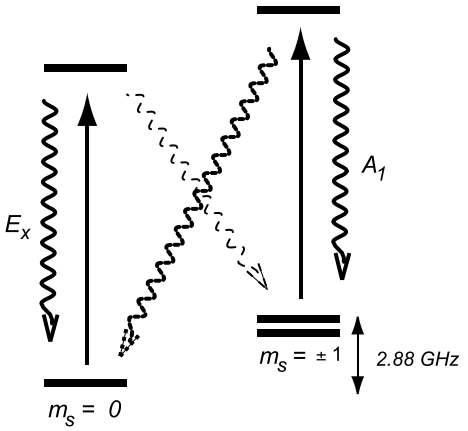

Fig. 13.3 The level structure of the electronic states of a nitrogen vacancy centre in diamond and the associated optical transitions

a variation [16] of the scheme of Barrett and Kok [17]. This is based on a non-deterministic but heralded detection of single single photons emitted by one or the other of the NV centres. The basic idea is depicted in Fig. 13.4. A single photon is emitted from one of two sources located at *A* and *B*, following an optical excitation pulse, and is detected at *C* after passing though a beam splitter that erases information on which source it came from. In the experiment, the NV centre is located in a surface fabricated confocal microscope so that the emission can be effectively coupled into multi mode fibres. The fibres coming from *A* and *B* are directed towards a fibre beam splitter (FBS). The photons in the output ports of the FBS are detected and recorded.

The electronic spin state of each NV centre is controlled using microwave pulses applied to on-chip wires. In this way we can prepare the spin state of each NV centre independently. This is essential as it is possible only to readout the spin state directly in the Z-basis. However we can readout in other bases by first unitary rotating the spin state with microwave pulses. In this way we can implement the two rotation angles at each emitter prior to a spin readout in the Z-basis.

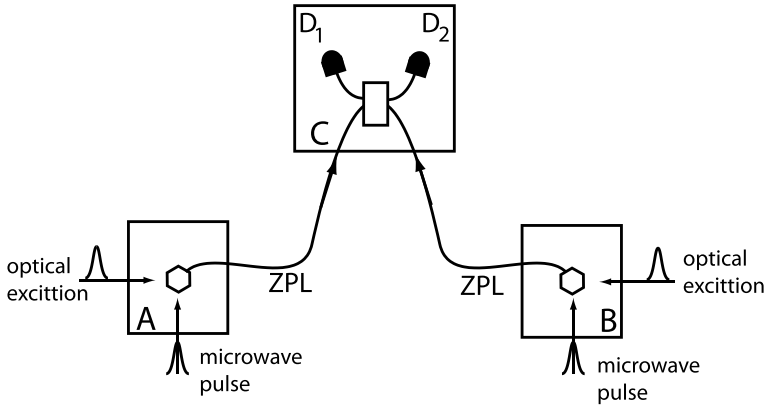

Fig. 13.4 The Barrett-Kok scheme for entangling two distant spins

We first describe the state preparation step. Label the spin states in each emitter as $|m_s = 0\rangle = |\uparrow\rangle$ and $|m_s = -1\rangle = |\downarrow\rangle$. Assume that, at $t = 0$, each of the emitters is prepared in the superposition state $|+\rangle = (|\uparrow\rangle + |\downarrow\rangle)/\sqrt{2}$ by optical pumping into $m_s = 0$ followed by a microwave pulse on the $0 \leftrightarrow -1$ transition. Each NV centre is now excited on the E_x transition by a short laser pulse. Spontaneous emission on this transition rapidly produces the entangled state $(|\uparrow, 1\rangle + |\downarrow, 0\rangle)/\sqrt{2}$ as the spin state $|\downarrow\rangle$ is not coupled to this transition. This neglects a very small amplitude that the state has a component in the excited states of the E_x transition but this is exponentially small. Given that we ultimately post-select on the basis of counting a single photon this amplitude does not contribute in any case. The state of both emitters a short time after excitation can then be written as.

$$|\Psi\rangle = \frac{1}{2}(|\uparrow, 1\rangle_A \otimes |\uparrow, 1\rangle_B + |\downarrow, 0\rangle_A \otimes |\uparrow, 1\rangle_B + |\uparrow, 1\rangle_A \otimes |\downarrow, 0\rangle_B + |\downarrow, 0\rangle_A \otimes |\downarrow, 0\rangle_B) \tag{13.40}$$

We now direct the emitted photons into optical fibres and through a fibre beam-splitter. If the photons emitted from each NV centre are identical this will erase information on which source emitted a single photon. If we now ask for the conditional state of the emitters give that we detect one and only one photon after the beam-splitter, the conditional state is of the form

$$|\Psi^{(1)}\rangle = \frac{1}{\sqrt{2}}(|\uparrow\rangle_A \otimes |\downarrow\rangle_B \pm e^{i\phi}|\downarrow\rangle_A \otimes |\uparrow\rangle_B) \tag{13.41}$$

and the phase ϕ depends on optical path lengths in the detection pathways.

This makes the unreasonable assumption that the detectors are perfect and no photon is missed. In the case of imperfect detection a single photon detection could also result from an amplitude for the $|\uparrow, 1\rangle_A \otimes |\uparrow, 1\rangle_B$ state. To fix this Bernien et al. [16] used an ingenious scheme in which, after a single detection event, the states $|\uparrow\rangle, |\downarrow\rangle$, are flipped with microwave pulses and each NV optically excited for a second time. This induces $|\uparrow\rangle_A \otimes |\uparrow\rangle_B \rightarrow |\downarrow\rangle_A \otimes |\downarrow\rangle_B$ which is now decoupled from the optical transition and subsequent excitation cannot result in a spontaneous emitted photon. However the components $|\uparrow\rangle_A \otimes |\downarrow\rangle_B, |\downarrow\rangle_A \otimes |\uparrow\rangle_B$ do emit a photon. If we detect a single photon in both excitation rounds (and the emitted photons are again identical) the conditional state is

$$|\Psi^{(1,1)}\rangle = \frac{1}{\sqrt{2}}(|\uparrow\rangle_A \otimes |\downarrow\rangle_B \pm |\downarrow\rangle_A \otimes |\uparrow\rangle_B) \tag{13.42}$$

The relative phase ϕ is converted into a global phase by the second round of excitation. The sign in this superposition depends on whether the same detector or different detectors recorded an event in the both rounds. At the end of the protocol we have an entangled spin state in NV centres separated by a large distance. Of course this is a non deterministic protocol. The probability for a success in each trial preparation is

of the order of 10^{-9} corresponding to one heralded entangled state generation every hour.

The test of the Bell inequality can now begin. The local spin readout is done using resonant driving on a spin-dependent cycling transition (similar to the readout of the electronic state of a trapped ion discussed in Sect. 12.2). The NV emits many photons when it is in the $m_s = 0$ state and emits no photons when it is in the $m_s = -1$ state. Photon emission is labelled as a $+1$ result while no photon mission is labelled as a -1 result. This is a Z basis measurement. In order to readout in a rotated basis we use the ability to rotate the spin states using microwave pulses followed by a Z-basis measurement. The rotated basis measurements are chosen using fast random number generation. It takes roughy 490 ns to chose the basis and ready for readout which takes a further 37 μs. As the NV samples are separated by 1280 m space-like separation of events at A and B allow a time window of 4.27 μs. This leaves 90ns for any additional uncertainties. The fidelity of preparation and readout is as good as 97%.

The experiment took 245 trials during a total measurement time of 220 h in a period of 18 days to yield the CHSH correlation $S = 2.42 \pm 0.20$. This is a clear violation of the CHSH Bell inequality with both the detection loophole and locality loophole confidently closed.

13.5 EPR Correlations

We return now to a discussion of experiments to test the original EPR scheme and the related idea of *steering*. As we noted above, the original EPR state is not a physical state. Instead we use a physical state that can approach the ideal state in a suitable limit. Reid [18] proposed to use the quadrature phase correlations in the two modes of non degenerate parametric down conversion.

In Chap. 4 we discussed to what extent parametric down conversion can produce a two mode squeezed state. In the photon number basis this is an entangled state of the form

$$|\Psi\rangle_{ab} = \sqrt{1-\lambda^2}\sum_{n=0}^{\infty}\lambda^n|n\rangle_a \otimes |n\rangle_b \tag{13.43}$$

It can be written as a unitary transformation of the two-mode vacuum state $|\Psi\rangle_{ab} = e^{r(a^\dagger b^\dagger - ab)}|0\rangle$ with $\lambda = \tanh r$. In the limit this approaches the EPR state. To see this we write the state in the basis of the quadrature phase operators $\hat{X}_a$, $\hat{X}_b$;

$$\Psi(x_a, x_b) = (2\pi)^{-1/2}\exp\left[-\frac{e^{2r}(x_a - x_b)^2}{8} - \frac{e^{-2r}(x_a + x_b)^2}{8}\right] \tag{13.44}$$

Using the Fourier transform, the state in the basis of the quadrature phase operators $\hat{Y}_a$, $\hat{Y}_b$ is

$$\Psi(y_a, y_b) = (2\pi)^{-1/2}\exp\left[-\frac{e^{2r}(y_a + y_b)^2}{8} - \frac{e^{-2r}(y_a - y_b)^2}{8}\right] \tag{13.45}$$

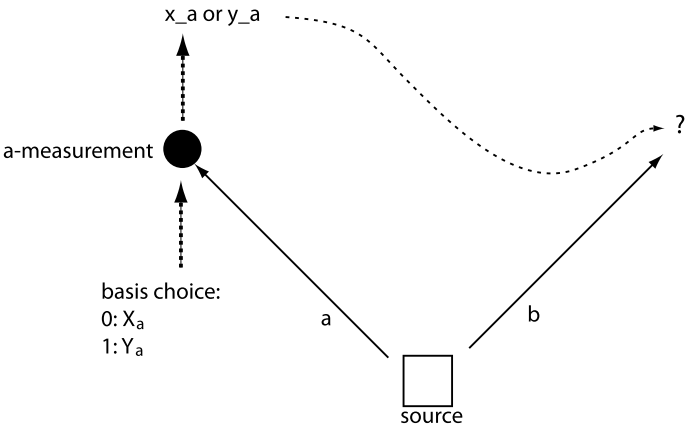

Fig. 13.5 A scheme for testing the EPR proposal using non ideal quadrature phase measurements on one mode of a two-mode squeezed state. A random binary number determines the choice of which quadrature phase amplitude is measured at a. What state does the observer at a assign for b, conditional on the results x_a or y_a?

This state thus gives the joint quadrature phase operator variances

$$\mathrm{Var}(\hat{X}_a - \hat{X}_b) = \mathrm{Var}(\hat{Y}_a + \hat{Y}_b) = 2e^{-2r} \tag{13.46}$$

In the limit $r \to \infty$ this approaches the perfect correlation of the EPR state. The state in (13.44) is clearly Gaussian in both quadrature amplitudes $\hat{X}_\alpha$ and $\hat{Y}_\alpha$ so we only need to give the means and co-variance matrix of the state to completely characterise it. (Strictly speaking there is also a global phase factor but this will play no role in what follows.)

We now consider an experiment, depicted in Fig. 13.5, in which a non ideal measurement of a quadrature phase operator is made on one mode of the two mode state, say mode-a. By non ideal we mean that this measurement is not perfectly accurate. In reality this corresponds to a homodyne measurement. We allow for some measurement accuracy to provide greater flexibility in describing an experiment. The question we wish to answer is: what conditional state does the observer at a assign to the state at b conditioned on the results of the measurement? We use a random binary number to choose which of the two canonically conjugate quadrature phase amplitudes to measure at a.

To answer this question we need to be able to calculate the conditional reduced state of mode-b given particular measurement results at a. We will first treat the case of an $\hat{X}_a$ quadrature amplitude measurement of mode-a. The measurement is completely described by the measurement operator

$$\hat{\Upsilon}_\Delta(x_a) = (2\pi\Delta)^{-1/4} \exp[-(\hat{X}_a - x_a)^2/(4\Delta)] \tag{13.47}$$

The statistics of measurement outcomes is

$$P(x_a) = \mathrm{Tr}_{ab}\left[\hat{\Upsilon}^\dagger_\Delta(x_a)\hat{\Upsilon}_\Delta(x_a)|\Psi\rangle_{ab}\langle\Psi|\right] \tag{13.48}$$

The conditional state of mode-b, given the result x_a for the measurement on mode-a, is

$$\rho_b^{(x_a)} = [P(x_a)]^{-1}\mathrm{Tr}_a\left[\hat{\Upsilon}_\Delta(x_a)|\Psi\rangle_{ab}\langle\Psi|\hat{\Upsilon}_\Delta^\dagger(x_a)\right] \tag{13.49}$$

The conditional marginal distribution for the $\hat{X}_b$ quadrature amplitude is defined as

$$P(x_b|x_a) = \langle x_b|\rho_b^{(x_a)}|x_b\rangle \tag{13.50}$$

In Exercise 13.3 you can show that the distribution of measurement outcomes, $P(x_a)$ is a gaussian with variance with mean and variance given by

$$\mathrm{E}(x_a) = 0 \tag{13.51}$$
$$\mathrm{Var}(x_a) = \Delta + \cosh 2r \tag{13.52}$$

Thus the mean of the measurement outcomes is zero and so equal to the mean of x_a in the prior quantum state, while the variance in the measurement outcome is the sum of the error in the measurement and the prior variance in variable x_a. In the limit of perfectly accurate measurements, $\Delta \to 0$, we see that the statistics of measurement outcomes mirrors the marginal quantum statistics of ideal measurements of $\hat{X}_a$ on the state $|\Psi\rangle_{ab}$.

In Exercise 13.3 you can show that the conditional distribution $P(x_b|x_a)$ is also a gaussian with conditional mean and conditional variance give by

$$\mathrm{E}(x_b|x_a) = x_a \tanh 2r(\sigma/\Delta) \tag{13.53}$$
$$\mathrm{Var}(x_b|x_a) = \delta \tag{13.54}$$

where

$$\sigma = \left(\frac{1}{\Delta} + \frac{1}{\cosh 2r}\right)^{-1} \tag{13.55}$$
$$\delta = \frac{1 + \Delta\cosh 2r}{\Delta + \cosh 2r}. \tag{13.56}$$

Note that, while the conditional mean of the state at mode-b is a random variable, the conditional variance is deterministic. In the limit of perfect correlations, $r \to \infty$ we see that $\sigma = \Delta$ and the conditional mean of mode-b is equal to x_a while $\delta = \Delta$ in which case the variance for the unmeasured quadrature at mode-b is reduced to zero in the limit of perfectly accurate measurements on mode-a. This is the expected perfect correlation of the EPR state. In general the observer at a can now define an *inferred* value for the $\hat{X}_b$ quarter amplitude with uncertainty given by

$$\Delta_{inf}^2(x_b) = \delta \tag{13.57}$$

A similar calculation can be done for the case that we choose to measure the $\hat{Y}_a$ quadrature amplitude measurement of mode-a. This requires a *different* measurement set up to that used to measure the $\hat{X}_a$ quadrature amplitude. We will assume that is is described by the measurement operator

$$\hat{\Phi}_\Delta(y_a) = (2\pi\Delta)^{-1/4} \exp[-(\hat{Y}_a - y_a)^2/(4\Delta)] \tag{13.58}$$

Note that $\hat{\Upsilon}_\Delta(x_a)$ and $\hat{\Phi}_\Delta(y_a)$ do not commute, a reflection of the fact that these describe different and complimentary measurements. We could have chosen the uncertainty in the Y quadrature measurements to be different for that for the X quadrature measurements but this does not make a fundamental change to the argument.

In this case the conditional mean and variance of the mode-b state is given by

$$\mathrm{E}(y_b|y_a) = -y \tanh 2r(\sigma/\Delta) \tag{13.59}$$

$$\mathrm{Var}(y_b|y_a) = \delta \tag{13.60}$$

Note the anti-correlation expected for the conditional mean in the limit of perfect correlations and ideal measurements. In general the observer at a can now define an *inferred* value for the $\hat{Y}_b$ quarter amplitude with uncertainty given by

$$\Delta^2_{inf}(y_b) = \delta \tag{13.61}$$

Following the logic of the EPR argument we now note that

$$\Delta_{inf}(x_b)\Delta_{inf}(y_b) = \delta \tag{13.62}$$

The right hand side will be less than unity for any non zero correlation provided $\delta < 1$, that is to say, when the measurement accuracy is better than the vacuum state uncertainly in the relevant quadrature amplitude. This looks like a violation of the uncertainty principle and EPR concluded that this result indicates the incompleteness of quantum mechanics. Bohr's response might be simply to point out that the two factors in the right hand side of (13.62) are obtained under distinct and complimentary experimental arrangements. The quantum uncertainty principle has nothing to say about such a product as each factor refers to a *different* conditional quantum state. Despite this we can define the EPR criterion as

$$\Delta_{inf}(x_b)\Delta_{inf}(y_b) < 1 \tag{13.63}$$

The previous analysis assumes that the conditional state is pure. In an actual experiment based on homodyne detection one needs to account for the non unit quantum efficiency of the photo-current detectors at mode-a. This requires us to consider non pure conditional states. Nonetheless, the resulting homodyne distributions remain Gaussian. Reid et al. [19] show that for this case,

$$\Delta_{inf}(x_b)\Delta_{inf}(y_b) = \frac{1 + \cosh 2r\ ((1-\eta_a)/\eta_a)}{\cosh 2r + ((1-\eta_a)/\eta_a)} \tag{13.64}$$

This has the same form as the pure state analysis with a measurement uncertainty $\Delta = ((1 - \eta_a)/\eta_a)$. We thus see that the EPR criterion will be satisfied when $\eta_a > 0.5$.

The two-mode squeezed state is a pure state and is entangled for any value of r. In an experiment the state produced is never pure and we need to consider the relationship between the degree of squeezing, purity and entanglement. It is possible for a mixed Gaussian bi partite state to exhibit entanglement without satisfying the EPR criterion. The EPR criterion is a stronger test of non locality than entanglement itself [19].

The first experiment to test the EPR criterion was performed by Ou et al. in 1992 [20]. The two-mode squeezed states were produced using a non degenerate optical parametric oscillator. Bowen et al. [21] used two independent optical parametric amplifiers produced single mode squeeze states that were mixed with a $\pi/2$ phase difference on a 50/50 beam splitter to produce a two-mode squeezed state (see Sect. 1.5). The two output beams from the beam splitter were then directed towards two separate homodyne detection devices with the ability to change the detected quadrature amplitude independently at each device. A polarising beam splitter is introduced into each arm to enable the loss in each mode of the bi partite entangled state to be varied. In this way both the inseparability and EPR criterion can be investigated. The optimum value for the EPR criterion was achieved when the product of the inferred variances reached 0.58 ± 0.02.

13.6 Quantum Steering

In 1935 Schrödinger introduced a new aspect to the EPR argument which has come to be known as quantum steering [22]. The concept again relies on the way in which different measurements on one component of a bipartite entangled state can lead to different conditional quantum states for the other component. It appears as if one can steer the conditional state at a remote location by making different choices for the measurements. Wiseman, Jones and Doherty (WJD) [23] introduced a quantitative formulation of quantum steering by defining it as a quantum information task capable of experimental tests, for example [26]. WJD showed that quantum steering is a distinct nonlocal property of some bipartite quantum states that differs from Bell nonlocality and nonseparability.

The quantum information task introduced by WJD is an asymmetric communication task involving two parties, Alice (a) and Bob (b). Alice has control over an optical source and can send quantum states to Bob over a quantum channel (e.g. a single mode optical fibre) as well as classical information over a classical channel. Alice's source might produce two-mode entangled states, one mode of which is directed through the quantum channel to Bob's detectors, and the classical information she can send could be the results of local measurements, just as in the standard Bell correlation experiments.

Alice however may not have a genuine source of entangled two-mode states but is trying to convince Bob she does by sending one component of a separable state to Bob

together with limited classical information about that state, for example, it may be classical information masquerading as the result of a local homodyne measurement result. Putting it another way, can Bob verify Alice's honesty by computing correlations between the classical information sent to him by Alice and the results of local measurements at his detectors? Can Bob discover that the states he receives are simply unknown (or hidden) separable states correlated with Alice's results or genuine bi-partite entangled states? WJD derived an inequality that Bob can construct from his data and the data sent to him by Alice that enables him to determine the answer to this question and verify that Alice is indeed sending him a non-separable state. What is surprising is that the class of such steerable states are a subset of all possible non-separable states but not all steerable states violate a Bell inequality. This introduces a hierarchy of entangled states: steerability is stronger than nonseparability and weaker than Bell nonlocality.

The significance of quantum steering for other quantum communication protocols arises from Bob's ability to verify Alice's claim even with a complete lack of trust in anything that happens in Alice's laboratory. It is particularly relevant for device independent protocols.

The first experimental test of steering using qubit states was performed by Saunders et al. [27]. Using polarisation photonic qubits to implement Werner states, they demonstrated that steerable states were a strict superset of the set of states that could violate a Bell inequality. A key feature of the steering communication protocol is its asymmetry; either Alice or Bob can be untrusted but not both. A fully asymmetric steering protocol was first demonstrated by Wollmann et al. [25]. This experiment used polarization photonic Bell states generated using a heralding method via spontaneous parametric down-conversion (SPDC) source. This closes the detection loophole. These states were then used to prepare Werner states. By introducing loss into one arm, say Bob's, Wollmann et al. were able to demonstrate the asymmetry of the protocol. The resulting loss of information in Bob' s arm makes him unable to steer the state for Alice.

Problems

13.1 A two qubit system is prepared in the pure state

$$|\Psi^-\rangle = \frac{1}{\sqrt{2}}(|01\rangle - |10\rangle)$$

A CHSH experiment is performed with two settings for each party. Alice measures $A_1 = \sigma_z$ and $A_2 = \sigma_x$. Bob measures $B_1 = -(\cos\theta\sigma_z + \sin\theta\sigma_x)$ and $B_2 = \cos\theta\sigma_z - \sin\theta\sigma_x)$. Calculate the correlation function

$$C = |\langle A_1 B_1\rangle + \langle A_2 B_1\rangle + \langle A_2 B_2\rangle - \langle A_1 B_2\rangle|$$

as a function of θ. At what value of θ is there a maximal violation of the CHSH inequality?

13.2 An experiment attempts to make the $|\Psi^-\rangle$ maximally entanged state of two qubits. However, due to imperfections in the experiment, it produces that state with probability ϵ and otherwise produces one of the four Bell states at random.

(a) Show that this state may be written as

$$\epsilon|\Psi^-\rangle\langle\Psi^-| + (1-\epsilon)\frac{\mathbb{I}}{4}$$

where $\mathbb{I}$ is the 4×4 identity matrix.

(b) Show that this state is entangled for $\epsilon > 1/3$.

13.3 A two-mode system is prepared in the squeezed state

$$|\Psi\rangle_{ab} = \sqrt{1-\lambda^2}\sum_{n=0}^{\infty}\lambda^n|n\rangle_a \otimes |n\rangle_b \tag{13.65}$$

and a measurement of the $\hat{X}_a$ quadrature is made described by the Krauss operator

$$\hat{\Upsilon}_\Delta(x_a) = (2\pi\Delta)^{-1/4}\exp[-(\hat{X}_a - x_a)^2/(4\Delta)] \tag{13.66}$$

where x_a is the measured result. Calculate the conditional and unconditional state and the corresponding mean and variance of $\hat{X}_a$.

References

1. A. Einstein, B. Podolsky, N. Rosen, Phys. Rev. **47**, 777 (1935)
2. N. Bohr, Phys. Rev. **48**, 696 (1935)
3. M.D. Reid, Phys. Rev. A **140**, 913 (1989)
4. J.S. Bell, Physics **1**, 105 (1964); Rev. Mod. Phys. **38**, 447 (1966)
5. D. Bohm, A. Aharonov, Phys. Rev. **108**, 1070 (1952)
6. S.J. Freedman, J.F. Clauser, Phys. Rev. Lett. **28**, 938 (972)
7. A. Aspect, P. Grangier, G. Roger, Phys. Rev. Lett. **49**, 91 (1982)
8. A. Aspect, J. Dalibard, G. Roger, Phys. Rev. Lett. **49**, 1804 (1982)
9. B.S. Cirel'son, Lett. Math. Phys. **4**, 93–100 (1980)
10. M.D. Reid, D.F. Walls, Phys. Rev. A **34**, 1260 (1986)
11. G. Weihs, T. Jennewein, C. Simon, H. Weinfurter, A. Zeilinger, Phys. Rev. Lett. **81**, 5039 (1998)
12. Z.Y. Ou, L. Mandel, Phys. Rev. Lett. **61**, 50 (1988)
13. Y.H. Shih, C. Alley, Phys. Rev. Lett. **61**, 2921 (1988)
14. P. Kok, B.W. Lovett, *Introduction to Optical Quantum Information Processing* (Cambridge University Press, 2010)
15. L. Robledo, L. Childress, H. Bernien, B. Hensen, P.F.A. Alkemade, R. Hanson, Nature **477**, 547 (2011)
16. H. Bernien, B. Hensen, W. Pfaff, G. Koolstra, M.S. Blok, L. Robledo, T.H. Taminiau, M. Markham, D.J. Twitchen, L. Childress, R. Hanson, Nature **497**, 86 (2013)
17. S.D. Barrett, P. Kok, Phys. Rev. A **71**, 060310 (2005)
18. M.D. Reid, Phys. Rev. A **40**, 913 (1989)

19. M.D. Reid, P.D. Drummond, W.P. Bowen, E.G. Cavalcanti, P.K. Lam, H.A. Bachor, U.L. Andersen, G. Leuchs, Rev. Mod. Phys. **81**, 1727 (2009)
20. Z.Y. Ou, S.F. Pereira, H.J. Kimble, K.C. Peng, Phys. Rev. Lett. **68**, 3663 (1992)
21. W.P. Bowen, R. Schnabel, P.K. Lam, T.C. Ralphs, Phys. Rev. Lett. **90**, 043601 (2003)
22. E. Schrödinger, Proc. Cambridge Philos. Soc. **31**, 553 (1935); **32**, 446 (1936)
23. H.M. Wiseman, S.J. Jones, A.C. Doherty, Phys. Rev. Lett. **98**, 140402 (2007)
24. M. Fuwa, S. Takeda, M. Zwierz, H.M. Wiseman, A. Furusawa, Nat. Commun. 10.1038/ncomms7665 (2015)
25. S. Wollmann, N. Walk, A.J. Bennet, H.M. Wiseman, G.J. Pryde, Phys. Rev. Lett. **116**, 160403 (2016)
26. T. Guerreiro, F. Monteiro, A. Martin, J.B. Brask, T. Vrtesi, B. Korzh, M. Caloz, F. Bussires, V.B. Verma, A.E. Lita, R.P. Mirin, S.W. Nam, F. Marsilli, M.D. Shaw, N. Gisin, N. Brunner, H. Zbinden, R.T. Thew, Phys. Rev. Lett. **117**, 070404 (2016)
27. D.J. Saunders, S.J. Jones, H.M. Wiseman, G.J. Pryde, Nat. Phys. **6**, 845 (2010). Phys. Rev. A **92**, 032107 (2015)

Quantum Optical Communication

14

Abstract

Quantum information theory is the study of communication and information processing tasks using physical systems that obey the rules of quantum theory. Information theory was largely the creation of Claude Shannon working at Bell laboratories over fifty years ago. Shannon produced an elegant mathematical theory for information encoding, transmission and decoding in the presence of noise. In the early 1980's a number of pioneers including, Holevo, Schumachor, Brassard, Ekert and Bennett, began to re-consider these issues in the light of quantum noise. In this chapter we will consider some of these developments including quantum cryptography and quantum teleportation.

14.1 Introduction

In classical information theory, the elementary unit of communication and information processing is the binary digit, or bit, which can take the mutually exclusive values 0 or 1. All communication and information processing can be reduced to operations on strings of binary digits. In 1946 Shannon [1] established a number of theorems for such operations and founded the subject of information theory [2]. Somewhat paradoxically, the key for this development lay in asking how much information is gained when the result of a random binary choice is known. Consider, for example, a fair coin toss. If we encode a head as 1 and a tail as 0, it is clear that to record the result of a single coin toss we require one binary digit. When the result is known we have gained one bit of information. If we toss N coins there are 2^N possible outcomes, yet to record a single outcome requires only N bits. It would appear from this that an intuitive definition for a numerical measure of information is the logarithm of the number of possible alternative ways a given outcome can be realised. If all outcomes are equally likely, as in the case of a fair coin toss of N coins, the probability of each outcome is 2^{-N}. The information content of a the i 'th outcome is then $H = -\log_2\ p_i$ where $p_i = 2^{-N}$is the probability of the outcome. The depen-

D. F. Walls and G. J. Milburn, *Quantum Optics*, Graduate Texts in Physics,
https://doi.org/10.1007/978-3-031-84177-4_14

dence of the information measure on the logarithm of the probability ensures that information is additive as our intuition with coin tosses would suggest. In general all outcomes are not equally likely. In that case we are led to define the average information of an outcome as $H = -\sum_i p_i \log_2 p_i$ We choose to define our logarithms base two as this leads to a measure of information in bits, which appears more natural in this context.

14.1.1 The Qubit

Quantum mechanics indicates that, at its most fundamental level, the physical world is irreducibly random. Given complete knowledge of the state of a physical system (that is a pure state) there is at least one measurement the results of which are completely random. The simplest example is provided by a two-state system such as a spin-half particle, a polarised photon, or a two-level atom. An elementary optical two-state system is a beam splitter, Fig. 14.1. A single photon pulse (see Sect. 1.9.2) is directed towards a 50/50 beam splitter will be reflected or transmitted with equal probability (we assume an ideal device that does not absorb the photon). If we place a perfect photon detector in both output ports of the beam splitter we will get a count at one or the other detector with equal probability. At first sight it would appear that a single two-state system such as this is a perfect quantum coin toss, but the reality is more subtle.

To understand why this is so consider the example depicted in Fig. 14.2 in which we try to toss the quantum coin twice in succession by redirecting the photon towards another identical beam splitter. In a real coin toss the outcome is no less uncertain than the first coin toss. Such is not the case for this 'quantum coin toss'. In Fig. 14.2 we illustrate a possible way to make the photon choose twice in succession whether to be reflected or transmitted, and immediately recognise the form of a Mach-Zehnder interferometer. Clearly we can set up this device so that the photon will be detected

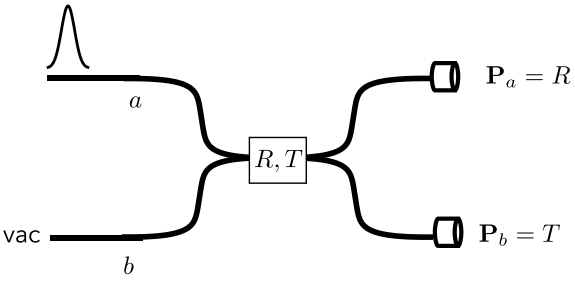

Fig. 14.1 A single photon pulse travelling in a single-mode fibre is mixed with another single-mode fibre at an R/T beam splitter can be reflected with probability $\mathbf{P}_a = R$ or transmitted with probability $\mathbf{P}_b = T$. In the case of a 50/50 beam splitter $R = T = 0.5$ and a perfect photon detector in both output ports of the beam splitter, will register a count at one or the other detector with equal probability

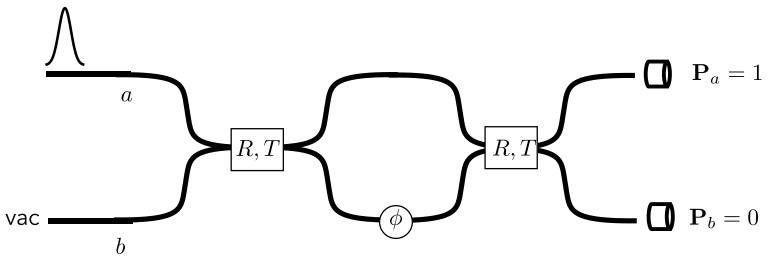

Fig. 14.2 Tossing a quantum coin twice using a Mach-Zhender inteferometer. After the first beam splitter (fibre-mixer) in Fig. 14.1, a single photon is redirected, using optical fibres, towards an identical beam splitter with $R = T = 0.5$. The device is now a Mach-Zehnder interferometer and can be adjusted using a phase shift so that the photon emerges with certainty in the upper output mode

with certainty in say the upper photon detector. This is very different from tossing two coins in succession.

The explanation of this phenomenon takes us to the heart of why quantum information theory will necessarily be different from classical information theory. Immediately after the first beam splitter the photon is in a quantum superposition of two distinct spatial modes of the field;

$$|\psi\rangle = \frac{1}{\sqrt{2}}(|1\rangle_a \otimes |0\rangle_b + |0\rangle_a \otimes |1\rangle_b \tag{14.1}$$

If we place a photon detector in both output modes after the first fibre coupler it is easy to see that we will count a photon in each mode with equal probability. However the state is not a truly random state. In fact it is a pure state, the entropy of which is zero. The beam-splitter has unitarily transformed the initial pure state $|1\rangle_a \otimes |0\rangle_b$. If the system is caused to pass through another beam splitter a further unitary transformation takes place which, for an appropriate phase shift, will produce the state $|1\rangle_a \otimes |0\rangle_b$ at the output and the photon will be detected with certainty in the upper detector.

We need to distinguish a true coin toss from a 'quantum' coin toss. The key distinguishing feature is the ability of the quantum system to be prepared in a coherent superposition of the two mutually exclusive alternatives. While it is true that the result of an arbitrary Pauli measurement on a single two state system will give one bit of information in general, the system state is not like a classical coin toss, as the single photon example illustrates.

To distinguish a true one bit classical probabilistic system from a quantum one bit probabilistic system we will refer to the quantum case as a *qubit*. A qubit is then a quantum system which can yield at most one bit of information upon measurement, but which can be in a coherent quantum superposition of the two mutually exclusive outcomes prior to measurement. In the example of Fig. 14.2 the state inside the

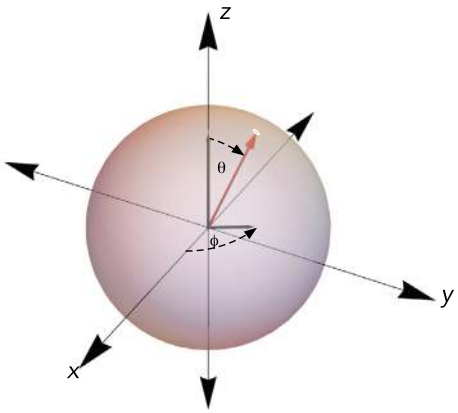

Fig. 14.3 The parametrisation of a single qubit state is one-to-one correspondence with a point on the unit sphere, called the Bloch sphere. here the point is labelled by spherical polar coordinates for a unit radius

interferometer can be written as a superposition of the two possible paths, reflected (R) or transmitted (T) after the first fibre mixer as

$$|\psi\rangle = \cos\theta|\mathbf{0}\rangle + e^{-i\phi}\sin\theta|\mathbf{1}\rangle \tag{14.2}$$

where $R = \cos^2\theta$, $T = \sin^2\theta$ and ϕ accounts for phase difference due to unequal path lengths, and we define the qubit basis states as $|\mathbf{0}\rangle = |1\rangle_a \otimes |0\rangle_b$, $|\mathbf{1}\rangle = |0\rangle_a \otimes |1\rangle_b$. This is called dual rail encoding . The states of a single qubit are in one to one correspondance with the points on a unit sphere if we identify θ, ϕ as spherical polar coordinates, Fig. 14.3. There are an uncountable infinity of such states, yet when photon number measurements are made at the output of the device we obtain a single bit of information with probability distribution $P(\mathbf{0}) = \cos^2\theta = 1 - P(\mathbf{1})$. It is easy to see that photon number measurements are equivalent to a σ_z measurement. In contrast a probabilistic description of a true coin toss is defined by a single real number p.

It is conventional to define the Pauli matrices so that σ_z is diagonal in the qubit basis. In this basis the Pauli matrices are

$$\sigma_z = |\mathbf{1}\rangle\langle|\mathbf{1}| - |\mathbf{0}\rangle\langle|\mathbf{0}| \tag{14.3}$$
$$\sigma_y = -i(|\mathbf{1}\rangle\langle|\mathbf{0}| - |\mathbf{0}\rangle\langle|\mathbf{1}|) \tag{14.4}$$
$$\sigma_x = |\mathbf{1}\rangle\langle|\mathbf{0}| + |\mathbf{0}\rangle\langle|\mathbf{1}| \tag{14.5}$$

The input state in Fig. 14.2 can be written in the qubit code as $|\psi\rangle_{in} = |\mathbf{0}\rangle$ and the state transformation from input to output is $|\mathbf{0}\rangle \rightarrow \cos\theta|\mathbf{0}\rangle + e^{-i\phi}\sin\theta|\mathbf{1}\rangle$. If we had injected the single photon pulse into mode-b we would have $|\mathbf{1}\rangle \rightarrow \cos\theta|\mathbf{1}\rangle - e^{i\phi}\sin\theta|\mathbf{0}\rangle$. This is called a single qubit gate. In summary, the single qubit gate implements the unitary transformation

$$|\mathbf{0}\rangle \rightarrow \cos\theta|\mathbf{0}\rangle + e^{-i\phi}\sin\theta|\mathbf{1}\rangle \tag{14.6}$$
$$|\mathbf{1}\rangle. \rightarrow \cos\theta|\mathbf{1}\rangle - e^{i\phi}\sin\theta|\mathbf{0}\rangle \tag{14.7}$$

In the case of 2 qubits the system can exist in a superposition of all 4 possible product states of each individual qubit. This requires 6 real numbers, in general, to parameterise and there is no simple visualisation of the topology of the parameter space as in the case of the Bloch sphere. A recent attempt can be found in [3]. In contrast the case of two classical bits (two coins) requires three real numbers, and the space of parameters is a simple tetrahedron. In the case of N qubits the topology becomes very complex affording an extraordinary level of control compared to the case of N bits. It is this complex level of control over probability distributions for measurement outcomes, compared to that for classical distributions, that give quantum communication and computation their power. We discuss below an example of how even a single qubit can be harnessed to do things that a classical one bit system never could; secure key distribution.

14.2 Single Photon Sources and Detectors

The technology of the internet is based entirely on coherent pulses propagating in optical fibres. Huge advances in the ability to produce and control coherent optical pulses has made this possible [4]. Key components are: laser diodes, optical filters, couplers, switches, amplifiers, electro-optic modulators, photon counting detection. Integrated optical systems using waveguides in bulk materials have added new ways of processing optical signals.

Quantum communication in fibre optical networks, and integrated optical systems, use quantum states of light, possibly encoding qubits, at transmitters and receivers We will concentrate on using single photon sources and single photon detectors capable of resolving the number of photons counted.

Good single photon sources has been developed over the past couple of decades. From an optical communication perspective, it must be possible to produce transform limited single photon pulses with arbitrary temporal modulation. It is relatively easy to do this with coherent pulses but single photon pulse requires more sophisticated methods. One approach that can be used for both is based on Raman stimulated emission.

14.2.1 A Raman Single Photon Source

As an example of a single photon source we discuss a Raman model based on a three-level Λ atomic system placed inside a single-sided cavity, see Fig. 14.4. Two long-lived states $|g\rangle$ and $|e\rangle$ are coupled by a third radiative state $|b\rangle$. A strong classical electromagnetic control pulse $E(t)$ is applied to the ground state $|g\rangle$ at frequency Ω. The pulse is detuned from the atomic transition $|g\rangle \to |b\rangle$, ensuring that the radiative state is never significantly populated. The resonance condition is $\Omega - \omega_a = \omega_{ge}$, where ω_{ge} is the energy difference between $|g\rangle$ and $|e\rangle$. The transition $|g\rangle \to |e\rangle$ is mediated by the emission of a photon at frequency ω_a.

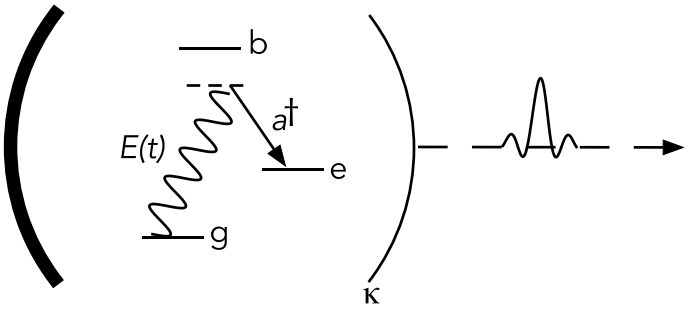

Fig. 14.4 An intracavity Raman single photon source. The atomic system is prepared in the ground state. A classical control field pulse $E(t)$ has a carrier frequency ω_c. The cavity resonant frequency is ω_a. The Raman resonance condition is $\omega_c - \omega_a = \omega_{ge}$ where $\hbar\omega_{ge}$ is the energy difference between states $|g\rangle$ and $|e\rangle$. Both the control and cavity field are detuned from the auxiliary state $|b\rangle$. When the control pulse is applied, the atom makes a two photon transition $g \rightarrow e$ emitting a cavity field photon in the process. If the cavity id rapidly damped this photon is emitted very rapidly from the cavity. The temporal shape of the emitted photon is determined by the cavity response function and the temporal shape of the control field pulse

In the interaction picture under the rotating wave approximation, the Hamiltonian describing this interaction is

$$H_{\rm a} = \hbar E(t) a^\dagger \sigma_+ + \hbar E^*(t)\sigma_- a\,, \tag{14.8}$$

where $a^\dagger$ and a are the internal cavity mode creation and annihilation operators, and σ_+ and σ_- are the raising and lowering operators in the subspace formed $|g\rangle$ and $|e\rangle$. At a finite temperature, the evolution of the cavity-atomic joint state is governed by the master equation (ME)

$$\frac{d\rho}{dt} = -i\,[H_{\rm a},\,\rho] \tag{14.9}$$

$$+\kappa\,(\bar{n}+1)\,\mathcal{D}[a]\rho + \kappa\bar{n}\mathcal{D}[a^\dagger]\rho\,, \tag{14.10}$$

where κ is the decay rate of the cavity mode into the environment, $\bar{n} = (e^{\mu_a} - 1)^{-1}$ is the mean photon number in the environment with Boltzmann factors $\mu_i = \hbar\omega_i/k_B T$, and $\mathcal{D}[a]\rho = a\rho a^\dagger - \{a^\dagger a,\,\rho\}/2$ is the Lindblad dissipator. We have neglected decay between $|e\rangle \rightarrow |g\rangle$ with the assumption that the atomic decay rate is much slower than the intra-cavity mode κ. We further assume the atom-cavity system is initially in thermal equilibrium with the environment, and thus it is in a separable Gibbs state, $\rho_{\rm sys} = \bar{\rho}_a \otimes \bar{\rho}_\sigma$. Thermal equilibrium ensures $\mu_a = \mu_\sigma$.

A reliable single photon source requires sufficient control over the mean photon number $\langle a_o^\dagger(t) a_o(t)\rangle$ and optical coherence of the pulse. The quantum Langevin equations describing the stochastic evolution of the intracavity field $a(t)$ is

$$\frac{da}{dt} = -i\,E(t)\sigma_+ - \frac{\kappa}{2}a + \sqrt{\kappa}a_i\,. \tag{14.11}$$

The initial condition is $\langle a(0)\rangle = \langle a_i(0)\rangle = 0$. The input-output relation $a_i(t) + a_o(t) = \sqrt{\kappa}a(t)$, shows that the output field is the convolution of the cavity response and the product of the control field amplitude and atomic polarization

$$\langle a_0(t)\rangle = -i\sqrt{\kappa}\int_0^t dt' \exp(\kappa(t'-t)/2)E(t')\langle\sigma_+(t')\rangle\,. \tag{14.12}$$

Controlling the shape of the classical drive $E(t)$ shapes the overall single photon pulse.

The intensity of the emitted pulse is

$$\langle a_o^\dagger a_o\rangle = \kappa\langle a^\dagger a\rangle - \sqrt{\kappa}\langle a^\dagger a_i + a_i^\dagger a\rangle + \langle a_i^\dagger a_i\rangle\,, \tag{14.13}$$

where $\langle a_i^\dagger a_i\rangle = \bar{n}$ is the mean photon number of the external field. A reliable single photon source will operate in the limit of a large cavity decay rate κ and thus preferentially emit into the environment rather than be coherently absorbed by the atom. In this limit, we can adiabatically eliminate the cavity dynamics,

$$a(t) \to -\frac{2iE(t)}{\kappa}\sigma_+ + \frac{2}{\sqrt{\kappa}}a_i\,. \tag{14.14}$$

After adiabatic elimination , the cavity dynamics, the output intensity is

$$\langle a_o^\dagger(t)a_o(t)\rangle = \bar{n} + \frac{2i}{\sqrt{\kappa}}\langle E(t)a_i^\dagger\sigma_+ - E^*(t)\sigma_- a_i\rangle\,. \tag{14.15}$$

To find the second term, we start by rewriting the master equation (14.9) for the atomic system by replacing a in the adiabatic limit

$$\mathcal{L}\rho^{(\sigma)} = \frac{4(\bar{n}+1)I(t)}{\kappa}\mathcal{D}[\sigma_+]\rho^{(\sigma)} + \frac{4\bar{n}I(t)}{\kappa}\mathcal{D}[\sigma_-]\rho^{(\sigma)}\,, \tag{14.16}$$

where $\rho^{(\sigma)}$ describes the quantum state of the atom alone and $I(t) = |E(t)|^2$. The dynamics of the atom appear to spontaneously absorb and emit photons according to the mean-photon number of the environment $\bar{n}$ and the intensity of the control pulse $I(t)$.

We derive the quantum Langevin equation for σ_+ using the input mode a_i, which yields the general solution to $\sigma_+(t)$

$$\sigma_+(t) = -\frac{2i}{\sqrt{\kappa}}\int_0^t dt' e^{\frac{\kappa}{2}(t-t')}\sigma_z(t')a_i(t')E^*(t') \tag{14.17}$$

Multiplying this expression by $a_i^\dagger$ from the right and making use of the commutation relation $[a_i(t), a_i^\dagger(t')]=\delta(t-t')$ and the integral identity $\int_0^t \delta(t-t')g(t')dt' = g(t)/2$, we find the general solution

$$\frac{2i}{\sqrt{\kappa}}\langle E(t)a_i^\dagger\sigma_+ - E^*(t)\sigma_- a_i\rangle = \frac{4I(t)}{\kappa}\langle\sigma_z(t)\rangle\,. \tag{14.18}$$

Rewriting (14.15), we obtain the expression for the mean photon number in the output mode

$$\langle a_o^\dagger(t)a_o(t)\rangle = \bar{n} + \frac{4I(t)}{\kappa}\langle\sigma_z(t)\rangle\,. \tag{14.19}$$

Finally we can find the behavior of $\langle\sigma_z(t)\rangle$. Making use of the fact that $\sigma_z = 1 - 2P_g(t)$, we can find the evolution of σ_z by computing the probability of measuring a photon in the ground state $P_g(t)$. Thus, in the Heisenberg picture $P_g(t)$ evolves according to (14.16), resulting in

$$\frac{dP_g(t)}{dt} = -\frac{4I(t)}{\kappa}(2\bar{n}+1)P_g(t) + \frac{4I(t)\bar{n}}{\kappa} \tag{14.20}$$

which has the following general solution—given the initial condition $P_g(0)=(1+e^{-\mu_\sigma})^{-1}$:

$$P_g(t) = \frac{e^{-\tau}(1+\bar{n})+\bar{n}}{2\bar{n}+1} - \frac{e^{-\tau}}{1+e^{\mu_\sigma}}\,. \tag{14.21}$$

Here $\tau = (4/(2\bar{n}+1)\kappa)\int_0^t dt' I(t')$ and approaches 0 in the long-time limit at zero temperature, corresponding to a perfect emission. In the long-time limit where $t \gg 0$, the inversion of the atom $\langle\sigma_z(t)\rangle$ becomes constant

$$\langle\sigma_z(t)\rangle = \frac{1}{2\bar{n}+1} = \tanh\left(\frac{\hbar\omega}{2k_BT}\right), \tag{14.22}$$

which describes the mean atomic polarization of a two-level atom in a thermal bath as expected. The mean intensity emitted in the long-time limit is

$$\langle a_o^\dagger(t)a_o(t)\rangle = \bar{n} + \frac{4I(t)}{\kappa}\tanh\left(\frac{\hbar\omega}{2k_BT}\right). \tag{14.23}$$

As the temperature goes to zero we find that

$$\langle a_o^\dagger(t)a_o(t)\rangle = \frac{4|E(t)|^2}{\kappa}\,. \tag{14.24}$$

The Raman single photon source emits a pulse with temporal shape determined by the classical drive $E(t)$. See Sect. 1.9.

14.2.2 Single Photon Detectors

A single photon detector is a measurement device that can reliably count a single event from a single photon pulse with high efficiency. Currently superconducting nanowire detectors (SNSPD) are the best choice [5]. They consists of a thin film (typically 5–10 nm thick) of superconducting material patterned as a meandering nanowire (50–100 nm wide). In such a device the superconducitng wire undergoes a highly

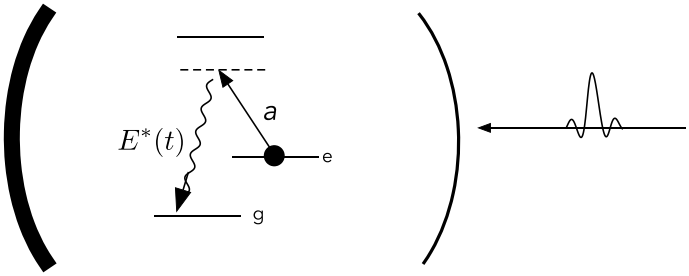

Fig. 14.5 An intracavity Raman single photon detector. The atomic system is prepared in the excited (e) state. A classical control field pulse $E(t)$ has a carrier frequency ω_c. The cavity resonant frequency is ω_a. The Raman resonance condition is $\omega_c - \omega_a = \omega_{ge}$ where $\hbar\omega_{ge}$ is the energy difference between states $|g\rangle$ and $|e\rangle$. Both the control and cavity field are detuned from the auxiliary state $|b\rangle$. When the control pulse is applied, a synchronous single photon pulse will be absorbed with probability p_a (or reflected with probability $1 - p_a$) and the atom makes a two photon transition $e \rightarrow g$. The probability p_a is maximised when the temporal shape of the control field matches the temporal shape of the single photon pulse. If the atom is found in the ground state, or a reflected photon is counted, the photon has been absorbed. This detector functions as a time-resolved single photon detector

localised transition form superconducting state to a resistive state due to photon absorption. This causes a rapid spike in resistance and a consequent voltage spike as the superconductor rapidly relaxes back to the superconducting state. SNSPDs offer near-unity detection efficiencies over a wide spectral range.combined with a low dark count rate. They have a very fast response with short dead times and fine timing resolution.

Another approach to a single photon detector is based on a "time reversed" version of a Raman single photon source, see Fig. 14.5.

The absorption probability for a rapidly damped cavity can be calculated using the Fock state master equation method described in Sect. 5.2. The result to lowest order in κ^{-1} is [6]

$$p_a = \frac{4}{\kappa}\left|\int dt' E^*(t')\nu(t')\right|^2 \tag{14.25}$$

where $\nu(t)$ is the temporal mode shape for the single photon input and κ is the cavity linewidth. Using (1.123) this is a maximum when $E(t) = E_0\nu(t)$. Note that we must ensure that $|E_0|^2 < \kappa$ for the approximation to be valid.

The Raman single photon detection scheme can be formalised as a time resolved photon detection measurement. We first define a projection operator valued measure as

$$\Pi_\mu = a_d^\dagger(t)|0\rangle\langle 0|a_d(t) \tag{14.26}$$

where

$$a_d(t) = \int_{-\infty}^{\infty} d\omega e^{-i\omega t}\tilde{\mu}^*(\omega)a(\omega) \tag{14.27}$$

Note that this operator does not obey the free field commutation relations. The detector is addressable in so far as the experimentalist has control over the function $\mu(\omega)$. The probability to count a single photon pulse, prepared in the state $|\nu\rangle$, is

$$p = \mathrm{tr}[\Pi_\mu |\nu\rangle\langle\nu|] = \left| \int_{-\infty}^{\infty} dt \mu^*(t)\nu(t) \right|^2 \tag{14.28}$$

14.3 Entanglement

Quantum entanglement refers to correlations between the results of measurements made on distinct subsystems of a composite system that cannot be explained in terms of standard statistical correlations between classical properties inherent in each subsystem. An example is provided by the violation of the Bell inequality for two distinct two-state quantum systems (see Chap. 13). If the subsystems are space like separated, quantum entanglement implies non-locality. Non-locality means that measurements on distinct subsystems, local measurements, are incapable of determining the joint state of the composite system. While quantum entanglement and non-locality are related they are not the same.

In quantum optics the simplest source of entanglement is provided by the non-degenerate squeezed vacuum state produced by spontaneous parametric down conversion (see Sect. 1.5),

$$|\mathcal{E}\rangle = (1 - \lambda^2)^{1/2} \sum_{n=0}^{\infty} \lambda^n |n\rangle_a \otimes |n\rangle_b \tag{14.29}$$

where $\lambda = \tanh r$ with r the squeezing parameter. Note that this state is a zero eigenstate of the photon number difference operator, $\hat{n}_a - \hat{n}_b$, between the two modes. The entanglement here results from a superposition of the infinite number of indistinguishable ways we can distribute equal numbers of photons in each mode. The reduced state of each subsystem (modes a and b) is in fact a thermal state (see Sect. 1.5). This is the maximum entropy state for a mode with a fixed average energy. Thus while the total state is a pure state with zero entropy, the state of each subsystem is as uncertain as it can be given the constraint on the average energy.

Measurements on the component sub-systems of entangled states are insufficient to completely determine the joint state of the system. In some cases local measurements may give no information at all about the joint state and the entropy of the subsystem reduced states are maximal. Such states are called maximally entangled. An example is provided by the following eigenstates of total photon number,

$$|\psi_N\rangle = \frac{1}{\sqrt{N+1}} \sum_{n=0}^{N} |n\rangle_a \otimes |N-n\rangle_b \tag{14.30}$$

Local measurements on either mode, say a, are described by the reduced density operator

$$\rho_a = \mathrm{Tr}_b(\rho) \tag{14.31}$$

where Tr_b refers to the partial trace over mode b. In this case the resulting reduced density operator for each mode is the identity matrix in $N+1$ dimensions. The entropy of such a state is

$$S_{a,b} = -\mathrm{Tr}\rho_{a,b} \ln \rho_{a,b} = \ln(N+1) \tag{14.32}$$

which, given the constraint on total photon number, is maximal. In general the entropy of each subsystem satisfy an important inequality, the Araki-Lieb inequality,

$$|S_a - S_b| \leq S \leq S_a + S_b \tag{14.33}$$

where S is the entropy of the state of the joint system. In the case of a pure entangled state this implies that $S_a = S_b$.

Entangled states do not necessarily need to be pure states. Furthermore there can be non-entangled states that still exhibit classical correlations between the subsystems. If an entangled state interacts with an environment entanglement can be reduced to zero while classical correlations remain. An example is provided by a two-mode squeezed vacuum state undergoing phase diffusion in each mode. The steady state density operator describing such a system is

$$\rho = (1-\lambda^2)\sum_{n=0}^{\infty} \lambda^{2n} |n\rangle_a\langle n| \otimes |n\rangle_b\langle n| \tag{14.34}$$

which still retains a perfect classical correlation between the photon numbers in each mode. However as the sate is a convex sum of states which factorise, the state in (14.34) is not entangled and in fact is defined as separable.

It seems reasonable to suggest that between pure entangled states and totally separable mixed states there is a gradation of entanglement. To quantify this we require a measure of entanglement, and a number of such measures for finite dimensional Hilbert spaces have been proposed. The situation for infinite dimensional Hilbert spaces, which is the case for much of quantum optics, is complicated except for a special class of states known as Gaussian states. Such states have a gaussian Wigner function. The two mode squeezed state is an example (see Chap. 3).

When a pure state, $|\psi\rangle$ interacts with an environment it undergoes decoherence and generally becomes a mixed state, ρ. We can then ask for the probability of finding the initial state, ψ in the ensemble represented by ρ. This probability is given by

$$F = \mathrm{Tr}(\rho|\psi\rangle\langle\psi|) \tag{14.35}$$

which is called the fidelity. Fidelity has a deeper significance in terms of the statistical distinguishability of quantum states.

14.4 Quantum Key Distribution

For millennia, communicating parties have devised schemes whereby messages can be authenticated (the signature) and secured from unauthorised access (cryptography). Modern methods (symmetrical crypto-systems) for secure electronic communication involve the prior exchange of a random number which is called the key. If the communicating parties share this number with each other and no one else, messages can be securely encrypted and decoded. The method however is vulnerable to a third party acquiring access to the key. In this section we will describe how quantum mechanics enables two communicating parties to arrive at a shared secure key via Quantum Key Distribution (QKD).

The idea that quantum mechanics might enable more secure communication was hinted at in the work of Wiesner [9] and made explicit in the pioneering work of Bennett and Brassard [10], in which the first QKD protocol, BB84, was presented. It uses a set of four qubit states to encode one bit. The first experimental demonstration of QKD was made by Bennett, Brassard and co-workers in 1989 [11]. A thorough review can be found in [12].

The key idea behind QKD is the Heisenberg uncertainty principle which ensures that any attempt to measure a quantum state will change it, and thus eavesdropping can in principle be detected. This is related to a powerful theorem in quantum information theory, the 'no-cloning' theorem: an unknown quantum state cannot be duplicated [13]. Thus experimental QKD offers important new insights into the nature of quantum physics. Let us now follow a classical protocol to establish a shared random key between two communicating parties, called Alice (A) and Bob(B).

Alice and Bob are assumed to have a means to generate completely random binary numbers. Alice generates a random binary number and sends it to Bob, and Bob generates a random binary number and compares it to the binary number received from Alice. If it is the same he tells Alice publicly that this is the case, but does *not* reveal what the value actually was. If it was the same, Alice and Bob keep this binary number, otherwise they discard it. Alice and Bob then repeat the procedure for another binary number and continue in this way until they share a binary string that is a subset of the total binary string that Alice sent to Bob. If for some reason Alice's binary number fails to get to Bob in a particular run, it makes no difference to the final shared binary string (although it does reduce the rate of communication for the shared binary string). The big problem with this method is that classically it is possible for an eavesdropper, Eve, to copy Alice's transmitted binary number without disturbing it. Then Eve can listen to the public channel and hear Bob telling Alice that this number was the same as his binary number. QKD avoids this problem by making it impossible for Eve to measure (or copy) an unknown quantum state without also disturbing it in general. If Alice and Bob chose carefully the quantum state encoding their binary numbers an eavesdropper can be detected by Alice and Bob.

Alice and Bob will communicate with polarised single photon pulses. These are defined in the same way as in Sect. 1.9 but now the modes are indexed by a polarization vector as well as wave vector. They first need to agree on how to physically implement

the encoding. Suppose Alice decides to transmit only vertically (V) and $+45°$ (D—for diagonal) photons. She will send a V-photon when a previously generated random binary number is a 0 and a D-photon when the random binary number is a 1.

$$A: \quad V \leftrightarrow 0; \quad D \leftrightarrow 1 \tag{14.36}$$

Bob and Alice also agree that Bob can make a polarisation *measurements* of Alice's photon in only two directions; horizontally (H) or at $-45°$ (A—for anti-diagonal). These measurements project onto non-orthogonal polarisation states. Bob randomly decides which of his two allowed measurements he will make on any photon he receives from Alice. The choice of measurement is made by referring to a previously generated random bit according to the code,

$$B: \quad 0 \leftrightarrow A; \quad 1 \leftrightarrow H \tag{14.37}$$

When Bob measures the polarisation he records the result as a yes (Y) or a no (N) depending on whether the photon was indeed found to have that particular polarisation. Bob will never record a Y if his bit is different from Alice's (crossed polarisers), and he records a Y on 50% of runs in which their bits are the same. Thus Bob can only get a Y if his bit is the same as Alice's (although he may get a N in that case as well). Finally Bob sends a copy of his results to Alice, over a public channel, but he does not tell Alice what measurement he made on each bit. Now Alice and Bob retain only those bits for which Bob's result was "Y". This process is called sifting and A and B share the same key in principle but there may be errors.

If Eve, an eavesdropper, makes a QND polarisation measurement of Alice's transmitted photons in an attempt to learn what was sent, she will introduce a 25% error rate between Alice and Bob's shared key. This occurs because her measurement will project the transmitted state into the eigenstates corresponding to her measurement result and this state may be different from that sent by Alice. Alice and Bob can test for eavesdropping by agreeing to sacrifice part of their shared key to check the error rate in a process called reconciliation. If the error rate is 25% or higher they will suspect an eavesdropper and discard the entire shared key. In reality errors are inevitable, and Alice and Bob will need to agree on an acceptable error threshold less than 25%. The reconciliation algorithm uses parity and error correcting codes to reconcile errors without exposing the key values. A final essential step is privacy amplification to reduce any partial information acquired by an eavesdropper about the raw key to a negligible level. It is a hashing algorithm that compresses a longer, partially secure key into a shorter, more secure final key.

The performance of an experimental QKD system is stated in terms of the number of bits per second of a shared secret key (the distilled bit rate R_{dis}) and the distance between the communicating parties. It is usually easier to determine the raw bit rate (R_{raw}). This is determined by actual losses in the quantum channel, sources and detectors as well as possible intervention of an eavesdropper. From this the error rate in the sifted key (obtained after Alice and Bob perform a round of classical communication to reconcile their bases) is called the quantum bit error rate (QBER).

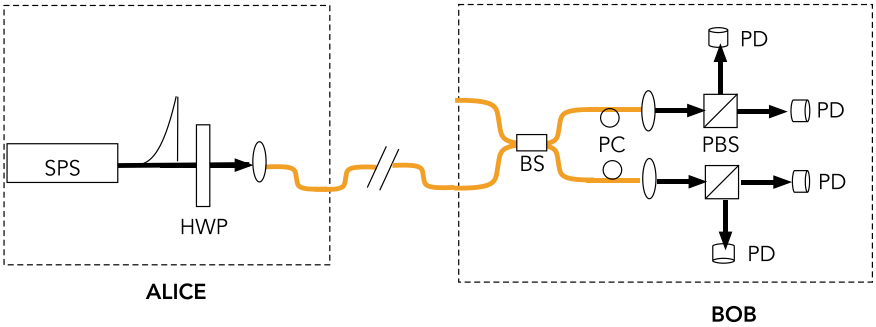

Fig. 14.6 A QKD BB84 implementation using a single photon source (SPS) [14]. Telecom single photon pulses are generated by Alice and passed through a half-wave plate (HWP). The polarised photons are coupled into a single-mode fibre connected to Bob. A 50/50 beam splitter (BS) fibre coupler makes a passive random choice for which basis Bob measures. Each of the two output channels pass through polarisation (PC) control elements towards polarising beam splitters (PBS) before photo-detection (PD)

The requirement that we use single photon states to code the bits of information places considerable demands on the physical resources required to implement BB84. Considerable progress has been made in single photon sources. Given such a source we also need to be able to reliably detect single photons, with a small dark count rate, and we need to propagate single photon pulses over possibly large distances with as little loss as possible. If the loss rate is too high very few counts will be available to Alice and Bob to construct their shared key and thus the data transmission rate could be unacceptably low. Finally, if we are to use standard optical fibres to transmit the photons, polarisation encoding is difficult owing to the birefringence of optical fibres. In practice this can be addressed using a polarisation compensation protocol to automatically follow the drift of polarisation and recover any polarisation changes.

An example of a QKD BB84 using single photon sources was presented by Morrison et al. [14]. A simplified scheme is shown in Fig. 14.6. The single photon source was a frequency doubled output from a InGaAs/GaAs quantum dot inside an oxide-apertured micropillar. The source repetition rate was 160.7 MHz. The quality of the single photon source is defined by how identical successive pulses are. This is measured by $g^{(2)}(0)$ which here is 0.036 (see Sect. 2.7). The four BB84 polarisation states are encoded using a motorised half-wave plate (HWP). A motorised half-wave plate combines a half-wave plate (HWP), which is a birefringent optical element, with a motorised mount that can rotate the plate to a desired orientation. Photons are transmitted through a quantum channel consisting of optical fibre spools with an average propagation loss of 0.1904 dB/km including connectors. The receiver at Bob consists of a 50/50 fibre beam-splitter (BS) followed by two polarising beam splitters and in-fibre polarisation controllers (PC) to project into the H/V and D/A basis respectively. Photons are detected with superconducting nanowire single-photon detectors (SNSPDs). The quantum bit error rate (QBER) at the maximum tolerable loss of $\sim$35 dB is $\sim$2% and is primarily limited by the quality of the single photon source.

14.5 Quantum Teleportation

Quantum teleportation is a key quantum communication scheme, with no classical analogue, and plays a key role in quantum networks and quantum computing. It permits the transfer of an unknown quantum state from a *client* system (C) provided to a *sender* (A), to a remote *receiver* (B). The sender and receiver share a maximally entangled state, and they can communicate via a classical channel. The original proposal of Bennett et al. [15] was posed in terms of systems with a two dimensional Hilbert space. Furasawa et al. [16], using a proposal of Braunstein and Kimble [17], demonstrated that the method can also be applied to entangled systems with an infinite dimensional Hilbert space (called continuous variable 'CV' teleportation), specifically for harmonic oscillator states. In that work, a coherent state was teleported using an entanglement resource that consisted of a two mode squeezed vacuum state. The joint measurements required for teleportation are joint quadrature phase on the client system and that part of the entangled resource shared by the receiver.

Teleportation of continuous variables is possible using a perfect quadrature phase QND (quantum nondemolition) measurement between two optical modes, A and B, to create the entanglement resource. The state that is produced is an optical analogue of the EPR state which had previously been shown by Vaidman [18] to enable teleportation of continuous observable. The EPR state is not a physical state because quadrature phase eigenstates are infinite energy states. However we can use arbitrary close approximations to these states in terms of a squeezed vacuum state, see Sect. 13.5. This is essential feature exploited in the scheme of Furasawa et al. [16].

Suppose that at some prior time a two mode squeezed vacuum state is generated and that one mode is available for local operations and measurements at the sender's location A by observer Alice, while the other mode is open to local operations and measurements in the receiver's location B, by observer Bob. Alice and Bob can communicate via a classical communication channel. Thus Alice and Bob each have access to one of the two entangled subsystems described by

$$|\mathcal{E}\rangle_{AB} = \sqrt{(1-\lambda^2)} \sum_{n=0}^{\infty} \lambda^n |n\rangle_A \otimes |n\rangle_B \tag{14.38}$$

This state is generated from the vacuum state by the Unitary transformation

$$U(r) = e^{r(a^\dagger b^\dagger - ab)} \tag{14.39}$$

where $\lambda = \tanh r$ and where a, b refer to the mode accessible to Alice and the mode accessible to Bob respectively (see Fig. 14.7).

The entanglement of this state can be viewed in two ways. Firstly as an entanglement between quadrature phases in the two modes (EPR entanglement) and secondly as an entanglement between number and phase in the two modes. We can easily show that this state approximates the entanglement of an EPR state in the limit $\lambda \to 1$ or

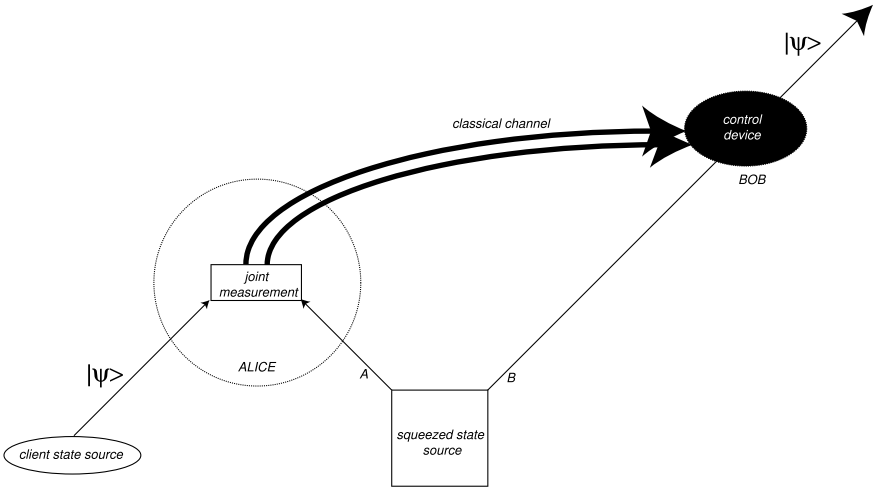

Fig. 14.7 A teleportation protocol. The sender, Alice, shares one mode A of a two-mode squeezed state, and another mode, the client, the state of which is unknown to her. Alice makes a measurement of the sum of the quadrature phase amplitudes of the client mode and mode A. The results of the measurement are sent via a classical channel to the receiver, Bob, who conditional on the information received, applies a unitary control to his share of the two-mode entangled state, mode B. The output of Bob's action is a mode now prepared in the same state as the client mode, but neither Alice or Bob learn what this state is

$r \to \infty$. The quadrature phase entanglement is easily seen by calculating the effect of the squeezing transformation (14.39) in the Heisenberg picture. We first define the quadrature phase operators for the two modes

$$\hat{X}_A = a + a^\dagger \tag{14.40}$$
$$\hat{Y}_A = -i(a - a^\dagger) \tag{14.41}$$
$$\hat{X}_B = b + b^\dagger \tag{14.42}$$
$$\hat{Y}_B = -i(b - b^\dagger) \tag{14.43}$$

Then

$$Var(\hat{X}_A - \hat{X}_B) = 2e^{-2r} \tag{14.44}$$
$$Var(\hat{Y}_A + \hat{Y}_B) = 2e^{-2r} \tag{14.45}$$

where $Var(A) = \langle A^2 \rangle - \langle A \rangle^2$ is the variance. Thus in the limit of $r \to \infty$ the state $|\mathcal{E}\rangle$ approaches a simultaneous eigenstates of $\hat{X}_A - \hat{X}_B$ and $\hat{Y}_A + \hat{Y}_B$. This is the analogue of the EPR state with position replaced by the real quadratures $\hat{X}$ and the momentum replaced by the imaginary quadratures, $\hat{Y}$.

The sender, Alice, has access to another quantum system, the client (C), in state $|\psi\rangle_C$. Perfect (projective) measurements are made of the joint quadrature phase quantities, $\hat{X}_C - \hat{X}_A$ and $\hat{Y}_C + \hat{Y}_A$ on the client mode and the Alice's part of the entangled mode, A, with the results X, Y respectively. The conditional state resulting

from this joint quadrature measurement is described by the projection onto the state $|X, Y\rangle_{CA}$ where

$$|X, Y\rangle_{CA} = e^{-\frac{i}{2}\hat{X}_A\hat{Y}_C}|X\rangle_C \otimes |Y\rangle_A \tag{14.46}$$

The (unnormalised) conditional state of total system after the measurement is then seen to be given by

$$|\tilde{\Psi}^{(X,Y)}\rangle_{out} = {}_{CA}\langle X, Y|\psi\rangle_C|\mathcal{E}\rangle_{AB} \otimes |X, Y\rangle_{CA} \tag{14.47}$$

The state of mode B at the receiver, denoted as Bob, is the pure state

$$|\phi^{(X,Y)}(r)\rangle_B = [P(X, Y)]^{-1/2}\,{}_{CA}\langle X, Y|\psi\rangle_C \otimes |\mathcal{E}\rangle_{AB} \tag{14.48}$$

with the wave function (in the $\hat{X}_B$ representation),

$$\phi_B^{(X,Y)}(x) = \int_{-\infty}^{\infty} dx' e^{-\frac{i}{2}x'Y}\mathcal{E}(x, x')\psi(X + x') \tag{14.49}$$

where $\psi(x) = {}_C\langle x|\psi\rangle_C$ is the wavefunction for the client state we seek to teleport. The kernel is simply the wave function for the two mode squeezed state resource.

The state in (14.49) is clearly not the same as the state we sought to teleport. However in the limit of infinite squeezing, $r \to \infty$, we find that $\mathcal{G}(x_1, x_2; r) \to \delta(x_1 + x_2)$ and the state of mode B approaches

$$|\phi_{XY}(r)\rangle_B \to e^{-\frac{i}{2}Y\hat{X}_B}e^{\frac{i}{2}X\hat{Y}_B}|\psi\rangle_B \tag{14.50}$$

which, up to the expected unitary translations in phase-space, is the required teleported state.

For finite squeezing the state after Bob's conditional control is not an exact replica of the client state. We can quantify the fidelity of the reproduction by computing the probability that the state received by Bob, after displacement, is the same as the client state. This probability is called the *fidelity* and is given by

$$F = |\langle\psi|e^{\frac{i}{2}\mu\hat{X}_B}e^{-\frac{i}{2}\nu\hat{Y}_B}|\phi^{(X,Y)}\rangle|^2 \tag{14.51}$$

with $\mu = gY$, $\nu = gX$ which allows for some flexibility in the choice of displacements in the non ideal case. The quantity g is called the *gain*. In the limit of infinite squeezing we expect $g \to 1$.

In the experimental context, imperfections in the measurements, noise in the classical communication channel, degradation of the entanglement, and imperfections in the local unitary transformations, mean that Bob's state is not precisely the same as the state of the client, C. A final step in any teleportation protocol is to check to see to what extent the state is teleported. In other words we need to determine the probability that the teleported state is the one we want, that is we need the fidelity.

This of course requires knowledge of the actual state of the mode C. As the fidelity is a probability it must be adequately sampled, so the verification stage requires repeated measurements upon the output state of the teleportation scheme at mode B. The previously mentioned errors act independently from trial to trial which means we must describe the teleported state as a mixed state, ρ_B, in general. In this case the fidelity is given by

$$F = \langle\psi|\rho_B|\psi\rangle \tag{14.52}$$

We can also define an overall measure of performance in terms of the average fidelity $\bar{F}$ obtained by averaging the fidelity over all possible client states, $|\psi\rangle$, with some appropriate measure on the set of pure states. We first need to specify the class of client states and the ensemble from which they are drawn. In the case of client states drawn from an ensemble of coherent states we can obtain an explicit result. If A and B share no entanglement $\bar{F} = \frac{1}{2}$. This is the classical boundary for teleportation of a coherent state. A quantum protocol would need to give an average fidelity greater than 0.5.

In order to effect a joint measurement of the combined quadratures $\hat{X}_C - \hat{X}_A$, $\hat{Y}_C + \hat{Y}_A$, the experiment of [16] first combined the client and sender field amplitudes on a 50/50 beam splitter, followed by direct homodyne measurements of the output fields after the beam splitter. After the beam splitter we then make a homodyne measurement of X-quadrature on mode C and the Y-quadrature on mode A. In the case of homodyne detection, the actual measurement records are two photo-currents (I_X, I_P). For unit efficiency detectors, this is an optimal measurement of the corresponding quadratures $\hat{X}_C, \hat{Y}_A$. In reality however efficiency is not unity and some noise is added to the measurement results. We shall return to this point below.

The measured photo-currents are a classical stochastic processes and may be sent to the receiver, B, over a standard communication channel. On receipt of this information the receiver must apply the appropriate unitary operator, a displacement, to complete the protocol. Displacement operators are quite easy to apply in quantum optics. To displace a mode, say B, we first combine it with another mode, prepared in a coherent state with large amplitude, $\alpha \to \infty$, on a beam splitter with very high reflectivity, $R \to 1$, for mode B. If $|\phi\rangle_B$ is the state of B, then after the combination at the beam splitter the state of B is transformed by

$$|\phi\rangle_B \to D(\beta)|\phi\rangle_B \tag{14.53}$$

where $D(\beta) = \exp(\beta b^\dagger - \beta^* b)$ is the unitary displacement operator, and

$$\beta = \lim_{R\to 1}\lim_{\alpha\to\infty} \alpha\sqrt{1-R} \tag{14.54}$$

In terms of the quadrature operators for B the displacement operator can be written

$$D(x, y) = e^{iy\hat{X}_B + ix\hat{Y}_B} \tag{14.55}$$

with $\beta = x + iy$. A suitable choice of β will produce the required displacements to complete the teleportation protocol. This was achieved by using the measured photocurrents to control the real and imaginary components of the displacement field using electrically controlled modulators. As the measurement records, the photocurrents, are classical stochastic processes they can be scaled by a gain factor, g, to produce the required β.

The experiment included an additional step to verify to what extent the state received by Bob faithfully reproduced the state of the client field. In this experiment the state of the client was a coherent state. In essence another party, Victor, is verifying the fidelity of the teleportation using homodyne detection to monitor the quadrature variances of the teleported state.

The key feature that indicates success of the teleportation is a drop in the quadrature noise seen by Victor when Bob applies the appropriate unitary operator to his state. This is done by varying the gain g. If Bob simply does nothing to his state ($g = 0$), then Victor simply gets one half of a squeezed state. Such a state has a quadrature noise level well above the vacuum level of the coherent state. As Bob varies his gain, Victor finds the quadrature noise level fall until, at optimal gain, the teleportation is effected and the variance falls to the vacuum level of a coherent state. In reality of course extra sources of noise introduced in the detectors and control circuits limit the extent to which this can be achieved.

In a perfect implementation, the fidelity should be peaked at unit gain. However photon loss in the shared entanglement resource and detector inefficiencies reduce this. In the experiment, the average fidelity at unit gain was found to be $F = 0.58 \pm 0.002$. As discussed previously, this indicates that entanglement is an essential part of the protocol. Subsequent experiments have considerably improved on this, for example, Yukawa et al. [19] reported that a coherent state was teleported with a fidelity $F = 0.83 \pm 0.01$.

14.6 Entanglement Swapping

In developing quantum networks it is desirable to be able to entangle optical systems that are widely separated in space. Entanglement swapping [20] is one way to achieve this. Entanglement swapping is a 'five agent' scenario, see Fig. 14.8. Two agents, S_1 and S_2 prepare independent pairs of two-photon entangled states. A central observer C, located at the origin, performs a joint measurement on one mode of each of the independent entangled pairs that propagate towards the origin. Conditional on this result, the remaining modes of each entangled pair are entangled, despite the fact that they never locally interacted in their past. In order to verify this, A and B can perform a Bell test (an CHSH test) and send the measurement settings and results back to C who will use her measurement results to partition the data received from A and B in order to verify a Bell violation.

We will discuss an elegant entanglement swapping experiment reported by Halder et al. [21] as it illustrates some important aspects of temporal modes that parallels

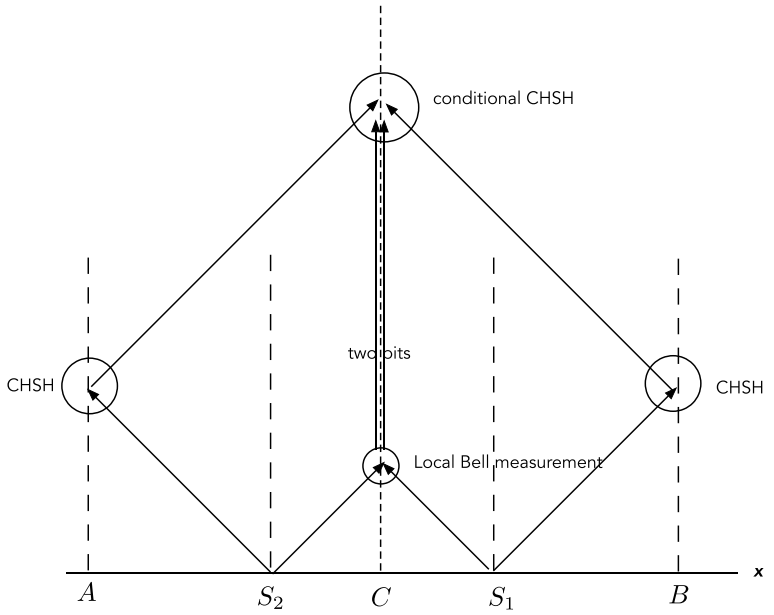

Fig. 14.8 A space-time diagram for entanglement swapping. Two independent agents, S_1 and S_2 each prepare a two-photon entangled state. One mode of each pair propagates to a central observer C, who performs a local Bell measurement, while the other modes of each pair propagate to observers A, B who each perform a Bell test (CHSH). Then A and B send the results to C who, conditioned on his results can verify that the photons received by A, B were entangled

optical time division multiplexing in classical optical communication schemes. The scheme is depicted in Fig. 14.9.

The experiment uses time-bin entangled photon pulses. To understand this, we first consider a classical time-bin coding scheme. In some counting interval $[0, t)$ we define N time bins each of duration T. Within each time bin a pulse can arrive early or late. A pulse arriving in the first half of a bin is a logical one while. pulse arriving in the second half of a bin is logical zero. This is depicted in Fig. 14.10.

The scheme in Fig. 14.9 works as follows. Two set of time-correlated photon pairs are created in each of the spontaneous parametric down convertors. Of the two pulses. the only way to get a coincidence count at the central detectors is if the incoming photon pulses do not overlap in time. Let us assume that we have good time resolution for these single photon detectors. In this case we do not know from which source the early or late photon originated. This means the undetected photon pairs are time bin entangled despite the fact that they originated in completely independent SPDC sources. In the experiment of [21] these two photons were subject to a correlation measurement to show that they are entangled, conditioned on the time-resolved single photon detection evens at the central detectors in the center.

If we use only linear optics we cannot make a complete Bell measurement however we can make a non deterministic Bell measurement that succeeds 50% of the time. See Exercise 14.3.

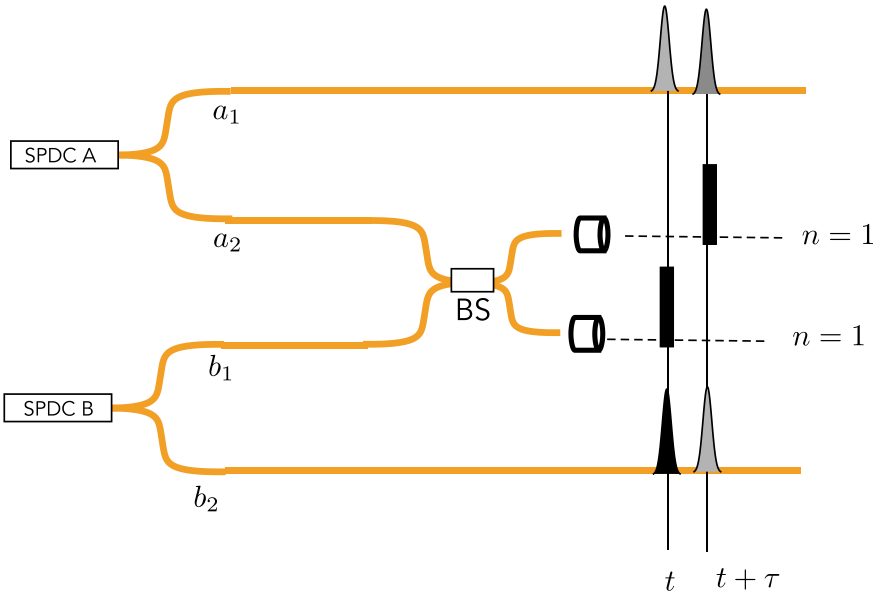

Fig. 14.9 A scheme for entanglement swapping with time-bin encode qubits [21]

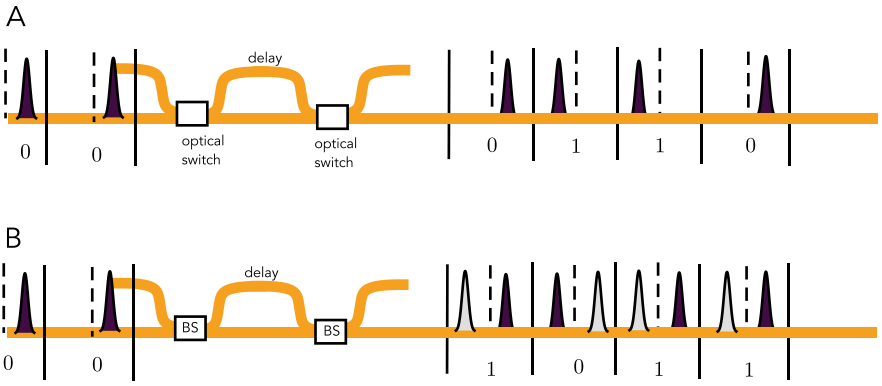

Fig. 14.10 **A** A classical optical circuit to encode a bit string into pulse time code. An incoming stream of equally spaced coherent pulses is optically switched onto a direct path or a delay path to encode bits as early or late pulses in each time bin. **B** A time-bin qubit encoder. A sequence of single photon pulses is input to an optical circuit using 50/50 fibre couplers to create an equal quantum superposition of logical bits. This is a time-bin encoded qubit. Note that the total photon number in each time bin is one

Problems

14.1 Show that the unitary transformation from input to output in Fig. 14.2 is given by

$$|\mathbf{0}\rangle \rightarrow \cos(\phi/2)|\mathbf{0}\rangle + i\sin(\phi/2)|\mathbf{1}\rangle \tag{14.56}$$

up to an overall phase.

14.2 In an entanglement swapping experiment, the two sources generate the polarisation entangled pairs

$$|\Psi\rangle = \frac{1}{2}\left(|HH\rangle_{12} + |VV\rangle_{12}\right)\left(|HH\rangle_{34} + |VV\rangle_{34}\right) \tag{14.57}$$

where $|xx\rangle_{jk} = a^\dagger_{x,j}a^\dagger_{x,k}|0\rangle$ and j, k label spatial plane wave modes and $x \in \{H, V\}$ labels polarisation of those modes. A Bell basis measurement on modes 2, 3 is a simultaneous measurement of the Pauli operators X_2X_3, Z_2Z_3 where

$$Z = |H\rangle\langle H| - |V\rangle\langle V|, \;\; X = |H\rangle\langle V| + |V\rangle\langle H|.$$

Show that the conditional state of modes 1, 4 are entangled conditional on the two binary outcomes of these measurements.

14.3 A partial Bell state measurement can be made on two dual-rail qubit states involving two photons in four modes using only beam splitters and number resolving detectors. In terms of dual-rail encoding, the polarisation Bell states in (13.4) can be written

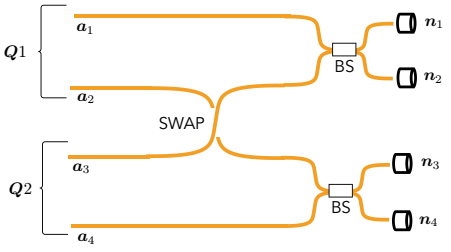

$$|\Psi^\pm\rangle = \frac{1}{\sqrt{2}}(|\mathbf{01}\rangle \pm |\mathbf{10}\rangle) \tag{14.58}$$

$$|\Phi^\pm\rangle = \frac{1}{\sqrt{2}}(|\mathbf{00}\rangle \pm |\mathbf{11}\rangle) \tag{14.59}$$

where $|\mathbf{00}\rangle = |1\rangle_1|0\rangle_2|1\rangle_3|0\rangle_4$, $|\mathbf{10}\rangle = |0\rangle_1|1\rangle_2|1\rangle_3|0\rangle_4$, $|\mathbf{01}\rangle = |1\rangle_1|0\rangle_2|0\rangle_3|1\rangle_4$, $|\mathbf{11}\rangle = |0\rangle_1|1\rangle_2|0\rangle_3|1\rangle_4$. We will refer to $|\Phi^\pm\rangle$ as even parity states while $|\Psi^\pm\rangle$ are odd parity states.

Using the HOM interference effect (see Sect. 1.9.2) show that this implements a partial Bell state measurement that distinguishes the states $|\Psi^+\rangle$ and $|\Psi^-\rangle$ but not the states $|\Phi^+\rangle$ and $|\Phi^-\rangle$, depending on the count pattern.

References

1. C.E. Shannon, Bell Syst. Tech. J., **27**, 379 (1948): Reprinted in, C.E. Shannon, W. Weaver, *The Mathematical Theory for Communication* (The University of Illinois Press, Urbana, 1949)
2. R.B. Ash, *Information Theory* (Dover, New York, 1965)
3. L.-H.H. Chang, S. Roccaforte, Z. Xu, P. Cadden-Zimansky, Am. J. Phys. **92**(7), 528–537 (2024). https://doi.org/10.1119/5.0137901
4. G. Keiser, *Fiber Optic Communications* (Springer, 2021)
5. I. Esmaeil Zadeh, J. Chang, J.W.N. Los, S. Gyger, A.W. Elshaari, S. Steinhauer, S.N. Dorenbos, V. Zwiller, Appl. Phys. Lett. **1118**, 190502 (2021)
6. K.J. Kewming, S. Shrapnel, G.J. Milburn, Phys. Rev. A **103**, 032411 (2021)
7. C.K. Hong, Z.Y. Ou, L. Mandel, Phys. Rev. Lett. **59**, 2044 (1987)
8. M.B. Plenio, V. Vedral, Contp. Phys. **39**, 431 (1998)
9. S. Wiesner, Conjugate coding. SIGACT News **15**, 78 (1983)
10. C.H. Bennett, G. Brassard, Quantum cryptography: public key distribution and coin tossing, in *Proceedings of IEEE International Conference on Computers, Systems and Signal Processing*, Bangalore (New York, IEEE, 1984)
11. C.H. Bennett, G. Brassard, The dawn of a new era for quantum cryptography: the experimental prototype is working. SIGACT NEWS **20**(4), 78 (1989); C.H. Bennett et al., Experimental quantum cryptography. J. Crypto. **5**, 3 (1992)
12. N. Gisin, G. Ribordy, W. Tittel, H. Zbinden, Rev. Mod. Phys. **74**, 145–195 (2002)
13. W.K. Wootters, W.H. Zurek, Nature **299**, 802 (1982): D. Dieks, Phys. Lett. A **92**, 271 (1982)
14. C.L. Morrison, R.G. Pousa, F. Graffitti et al., Nat. Commun. **14**, 3573 (2023)
15. C.H. Bennett, G. Brassard, C. Crepeau, R. Jozsa, A. Peres, W.K. Wooters, Phys. Rev. Lett. **70**, 1895 (1993)
16. A. Furasawa, J.L. Sørensen, S.L. Braunstein, C.A. Fuchs, H.J. Kimble, E.S. Polzik, Science **282**, 706 (1998)
17. S.L. Braunstein, H.J. Kimble, Phys. Rev. Lett. **80**, 869 (1998)
18. L. Vaidman, Phys. Rev. A **49**, 1473 (1994)
19. M. Yukawa, H. Benichi, A. Furusawa, Phys. Rev. A **77**, 022314 (2008)
20. M. Zukowski, A. Zeilinger, M.A. Horne, A.K. Ekert, Phys. Rev. Lett. **71**, 4287 (1993)
21. M. Halder, A. Beveratos, N. Gisin et al., Nat. Phys. **3**, 692–695 (2007)

Quantum Optical Computation

15

Abstract

In 1982 Richard Feynman (Int J Theor Phys 21:467, 1982, [1]) suggested there were certain problems that would be difficult to preform on a computer running according to classical mechanics but which would be easy to do on a computer running according to quantum principles. The reason why this is so is easy to see. A quantum system consisting of N interacting spins requires a simulation using vectors of 2^N dimensions in general. This exponential growth of the basis size is what makes classical simulations of complex quantum problems so difficult. On the other hand if we built a system with N interacting spins and allowed it to evolve unitarily, no such difficulty would be encountered. It would appear that a computer executing unitary evolution on a system of two level systems could significantly outperform a classical computer set to solve the equivalent problem. In this chapter we introduce the idea of universal quantum computation and discuss various quantum optical schemes for implementing it.

15.1 Introduction

In 1985 David Deutsch [2] gave examples of problems that might be solved more efficiently on such a machine when compared to a classical machine. The promise of quantum computation suggested by Feynman and elaborated by Deutsch was made very apparent in the factoring algorithm of Shor in 1994 [3]. Shor gave a quantum algorithm by which a large integer could be factored into its prime components with high probability, more efficiently than any known algorithm for a classical computer. As the supposed difficulty of factoring large integers is used in modern encryption schemes, Shor's algorithm indicated that such schemes would be open to attack by anyone with a quantum computer.

To build a computer we need to build a cascaded array of irreversible switches, synchronised by a clock signal, so that the change in state of one switch can act as a control for another. In a modern silicon computer the basic controllable switches

D. F. Walls and G. J. Milburn, *Quantum Optics*, Graduate Texts in Physics,
https://doi.org/10.1007/978-3-031-84177-4_15

are transistors and signals are voltages. It is a very large array (trillions) of cascaded switches. We do not use optical switches for computer chips as the resulting device would be too large, however they are used extensively for optical communication systems. Optical switches use pulses of classical light generated by a laser.

Quantum computers are as constrained as classical computers in the kinds of functions they can evaluate (so called computable functions) however a quantum computer can potentially solve a problem more efficiently than a classical computer.

A quantum computer is a cascaded array of *reversible* (unitary) quantum switches—usually we call them gates—synchronised by a clock signal. The overall device is reversible (in a perfect device) right up until the output is readout. That step is necessarily irreversible. Once a measurement is made a quantum switch cannot be reversed. This is a fundamental feature of measurement in quantum theory (see Chap. 7). Thermodynamics again ensures that no measurement can be perfect so some measurements make mistakes and accidental measurements are also irreversible.

The efficiency of an algorithm is related to how many computational steps (number of switches) are required to solve the problem as the 'size' of the problem increases. The size of a problem can often be expressed by the number of bits in a single number, for example in the case of the factoring problem, the size of the problem is just the number of bits required to store the number to be factored. If the number of steps required to implement an algorithm grows exponentially with the size of the problem, the algorithm is not efficient. If however the number of steps grows only as a polynomial power of the size of the problem, the algorithm is efficient. Shor's algorithm is an efficient factoring algorithm for a quantum computer, while all known algorithms for factoring on a classical computer require an exponentially increasing number of steps as the size of the integer to be factored increases.

How does a quantum computer achieve this enormous increase in efficiency? The answer lies in the quantum superposition principle. Suppose we wish to evaluate a function f on some binary input string x to produce a binary output string, $f(x)$. We can code the input and output binary string as the product state of N qubits. The output qubits however are preset to zero. Now we set up a machine so that under unitary quantum evolution the state transforms as

$$|x\rangle|0\rangle \rightarrow |x\rangle|f(x)\rangle \tag{15.1}$$

Why do we demand that the transformation be unitary? Consider what happens when we prepare the input qubits in a uniform superposition of all possible input states;

$$\sum_x |x\rangle|0\rangle \rightarrow \sum_x |x\rangle|f(x)\rangle \tag{15.2}$$

If the dynamics is unitary the linearity of quantum mechanics ensures that (15.1) implies (15.2). It would appear that in a single run of the machine we have evaluated all possible values of the function.

This is not quite as interesting as it seems. If we measure the output qubits we will get one value at random. That does not seem very useful. To see why it is useful

to do this let us ask; when would we ever want to evaluate every value of a particular function? The answer is, when we are not so much interested in a particular value of the function as a *property* of the function. The power of quantum computation arises in what we do next, after the transformation in (15.2). In the next step we continue to unitarily process the output register to extract, in one go, a property of the function, while simultaneously giving up information on the output of any particular evaluation. In all of this we emphasise the need to perform perfect unitary transformations of the qubits. Moreover the unitary transformations necessarily entangle many qubit degrees of freedom. A quantum computer must produce highly entangled states of many qubits without suffering any decoherence. It is this requirement that makes a physical realisation of a quantum computer so difficult to achieve as we shall see below.

How can we use the superposition state in (15.2) to determine properties of functions? To see this consider a function f which maps the binary numbers $\{0, 1\}$ to $\{0, 1\}$. There must be four such functions, two of which are constant functions with $f(0) = f(1)$, and two have $f(0) \neq f(1)$, so called balanced functions. Suppose now the problem involves determining if a function is balanced or constant. On a classical computer to answer this we need to make two evaluations of the function, $f(0)$, $f(1)$. We would then need to run the computer twice. However a quantum computer can determine this property in only a single run.

Suppose we have two qubits. One qubit will be used to encode the input data and the other qubit, the output qubit, will contain the value of the function after the machine is run. The output qubit is initially set to 0. The machine might then run according to (15.1). However there is a problem with this expression. If f is a constant function we have two distinct input states unitarily transformed to the same output state. Clearly this is not a reversible transformation and thus cannot be implemented unitarily. The problem is easily fixed however by setting up the machine to evolve the states according to

$$|x\rangle|y\rangle \rightarrow |x\rangle|y \oplus f(x)\rangle \tag{15.3}$$

where the addition is defined modulo two and we have allowed all possible settings of both qubits. The unitary transformation which realises this operation is called the f-controlled NOT gate. The input qubit x is the control qubit while the output qubit y is the target. If the value of f on the control qubit is one, the bit on the target is flipped; thus the name. Every unitary transformation on qubits can be realised as suitable networks of simple one and two qubit gates using primitive gate operations.

The quantum algorithm that solves this problem is a version of a quantum algorithm first proposed by Deutsch. It proceeds as follows. In the first step we prepare the output qubit in the state $|0\rangle - |1\rangle$ (we ignore normalisation in what follows for simplicity). This can be done using a single qubit rotation $|1\rangle \rightarrow |0\rangle - |1\rangle$. Such a rotation is called a Hadamard transformation. In the second step the input qubit is prepared in the 0 state and is then subjected to a Hadamard gate as well, which immediately produces a superposition of the two possible inputs for the function f. In the third step we couple the input and output qubit via the f-controlled NOT gate. The transformation is

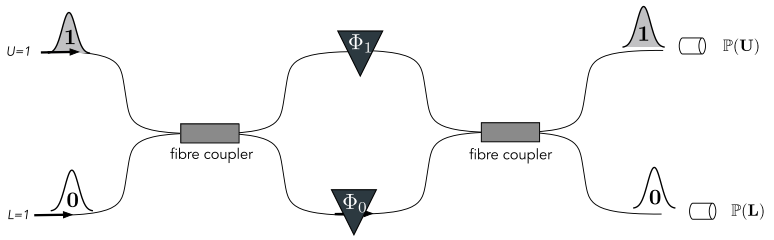

Fig. 15.1 An optical realisation of the Deutsch algorithm in terms of an optical fibre (or waveguide) Mach-Zehnder interferometer. The fibre couplers are symmetric (50/50). Synchronous transform-limited single photon pulses can be injected into either arm. In this case only the upper (U) arm is used. Single photon detectors sample the probability distributions for detection at the upper detector or lower detector. The phase shifts are chosen according to the values of a binary function f as $\phi_0 = f(0)\pi,\ \phi_1 = f(1)\pi$

$$(|0\rangle + |1\rangle)(|0\rangle - |1\rangle) \rightarrow ((-1)^{f(0)}|0\rangle + (-1)^{f(1)}|1\rangle)(|0\rangle - |1\rangle) \tag{15.4}$$

In the last step we apply a Hadamrd gate to the input qubit so that

$$((-1)^{f(0)}|0\rangle + (-1)^{f(1)}|1\rangle)(|0\rangle - |1\rangle) \rightarrow (-1)^{f(0)}|f(0) \oplus f(1)\rangle(|0\rangle - |1\rangle) \tag{15.5}$$

Thus the input qubit is in state 0 if f is constant and is in state 1 if f is balanced and measurement of the qubit will determine if the function is balanced or constant with certainty in a single run of the machine.

There is a simple quantum optical realisation of this algorithm based on a Mach-Zehnder interferometer, see Fig. 15.1. The interferometer couples two modes of the field, labeled upper (U) and lower (L). A single photon in the mode-U encodes logical 1 while a single photon in mode-L encodes logical 0. At the input a single photon in mode-U is transformed by the first beam splitter into a superposition state in which it is in either mode-1 or mode-0. If we encode our qubits so that a $|1\rangle$ corresponds to the photon in mode-1 and a $|0\rangle$ corresponds to a photon in mode-0, the first beam splitter performs a Hadamard transformation. Now we insert into each arm a phase shift ϕ_i which can only be set at 0 or π phase shift. We encode the value of the functions as $\phi_0 = f(0)\pi,\ \phi_1 = f(1)\pi$. Set the interferometer so that in the absence of the phase shift the photon emerges with certainty at the upper detector, which encodes a 1. The lower detector encodes a zero. It is then clear that if $f(0) = f(1)$ a single photon will emerge at the upper detector, while if $f(0) \neq f(1)$ the photon will be detected at the lower detector, that is the result is a 0. This device is a classically controlled all-optical switch.

The previous example illustrates the key features of a quantum algorithm. Firstly it involves unitary transformations of pure quantum states. Secondly we need both single qubit and two qubit interactions to produce entangled states. These were the Hadamard transformation (H-gate) and a controlled NOT transformation (CNOT-gate). It turns out that suitable networks of an arbitrary single qubit rotations, together with a controlled NOT gate, can perform any computation involving arbitrarily many

qubits. These features guide us in the search for a suitable physical implementation of a quantum computer. The requirement of unitarity is most severe. In general small imperfections in an actual machine will not enable perfect unitary evolution. The pure states are necessarily degraded by unwanted interactions with extraneous degrees of freedom, the environment. The necessity for at least two qubit interactions means we must necessarily seek interactions that entangle at least two quantum systems. Fortunately even in the presence of nonunitary transformations we can use quantum error correction methods to mitigate the deleterious effects of environment induced errors.

The difficulty for optical quantum computation is that photons at optical frequencies do not interact except when mediated by matter, and these interactions are weak at the single photon level. This problem can be circumvented using measurement based approaches that produce highly non classical states of light in a multimode system, conditioned on a measurement outcome (photon counting or homodyne detection) made on a subset of modes [4]. When this is combined with the ease of generating entangled photon pairs (Bell states) in down conversion, a powerful scheme for quantum computation was developed based on fusion gates [6]. A second difficulty is that photons are easily lost due to absorption or scattering. This leads to computational errors. Of course, all quantum computation schemes need to battle errors and powerful error correction codes have been developed for many schemes including photonic.

Photonic schemes are of two general kinds depending how a qubit is encoded in the physical states of an optical mode. This encoding needs to be adapted to the particular qubit measurement scheme. If the measurement is based on photon counting, the measurement results are integers (a count) and the scheme is called discrete. If the measurement is based on homodyne/heterodyne detection, the measurement results are real numbers. This is called continuous variable quantum computing. We will begin with the discrete case.

15.2 Photon Boson Sampling

The Hong-Ou-Mandel (HOM) two-photon interference discussed in Sect. 1.9 is a hint of the much deeper complexity at the core of multi-photon interference in linear optical interferometers. This was made explicit in the discovery of photonic boson sampling by Scott Aaronson and Alex Arkhipov in 2013 [7].

In Fig. 15.2 we show a general liner optical unitary transformation with an unknown product number state and known number states (ancilas) $|\boldsymbol{n}\rangle = |n_1\rangle|n_2\rangle \ldots |n_k\rangle$ at input. A photon counter records a count record $\boldsymbol{m} = (m_1, m_2, \ldots n_m)$ for the last k modes. The linear optical device performs a unitary transformation on all the input states. It may be described by a unitary transformation of the form

$$U(H) = \exp[-i\mathbf{a}^\dagger H\mathbf{a}] \tag{15.6}$$

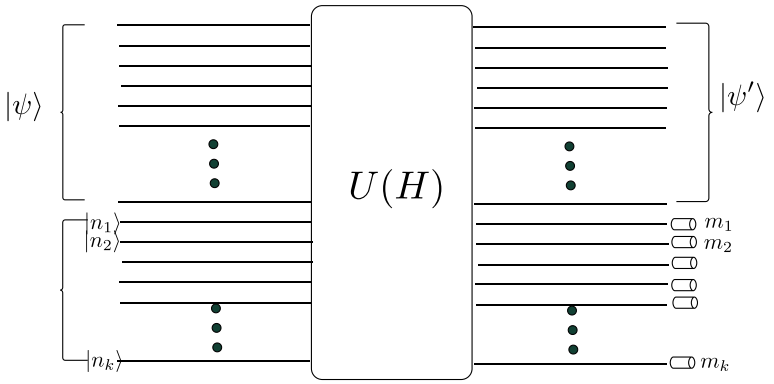

Fig. 15.2 A conditional linear optical gate

where

$$\mathbf{a} = \begin{pmatrix} a_1 \\ a_2 \\ \vdots \\ a_N \\ a_{N+1} \\ \vdots \\ a_{N+K} \end{pmatrix} \tag{15.7}$$

and H is a hermitian matrix. This transformation leaves the total photon number invariant,

$$U^\dagger(H)\mathbf{a}^\dagger \cdot \mathbf{a}U(H) = \mathbf{a}^\dagger \cdot \mathbf{a} \tag{15.8}$$

It also induces a linear unitary transformation on the vector $\mathbf{a}$ as

$$U^\dagger(H)\mathbf{a}U(H) = S(H)\mathbf{a} \tag{15.9}$$

One should not confuse the unitary transformation, $U(H)$, acting on states, with the induced unitary representation, $S(H)$, acting on the mode operators.

The *conditional state* of the signal modes, $|\psi'\rangle$ are then determined by

$$|\psi'\rangle_s = \frac{1}{\sqrt{p(\mathbf{m})}}\hat{E}(\mathbf{n}|\mathbf{m})|\psi\rangle_s \tag{15.10}$$

where the observed count is represented by the vector of values $\mathbf{m}$, and the probability for this event is $p(\mathbf{m})$. The measurement operator is

$$\hat{E}(\mathbf{n}|\mathbf{m}) = {}_{anc}\langle\mathbf{m}|U(H)|\mathbf{n}\rangle_{anc} \tag{15.11}$$

with

$$|\mathbf{m}\rangle_{anc} = |m_1\rangle_{N+1} \otimes |m_2\rangle_{N+2} \otimes \ldots \otimes |m_k\rangle_{N+K} \tag{15.12}$$

We will first calculate how coherent states transform under this process. Define

$$|\boldsymbol{\alpha}\rangle = |\alpha_1\rangle \otimes |\alpha_2\rangle \otimes \ldots |\alpha_{N+K}\rangle \tag{15.13}$$

where

$$\boldsymbol{\alpha} = \begin{pmatrix} \alpha_1 \\ \alpha_2 \\ \vdots \\ \alpha_N \\ \alpha_{N+1} \\ \vdots \\ \alpha_{N+K} \end{pmatrix} \tag{15.14}$$

Then

$$U(H)|\boldsymbol{\alpha}\rangle = |\boldsymbol{\alpha}(H)\rangle = |\alpha_1(H)\rangle \otimes |\alpha_2(H)\rangle \ldots |\alpha_{N+K}(H)\rangle \tag{15.15}$$

where $\boldsymbol{\alpha}(H) = S^{\dagger}(H)\boldsymbol{\alpha}$, reflecting the well known fact that coherent states do not become entangled through a linear optical transformation of the kind considered here. The matrix element,

$$\mathcal{U}_H(\boldsymbol{\alpha}) = \langle \boldsymbol{\alpha}|U(H)|\boldsymbol{\alpha}\rangle = \langle \boldsymbol{\alpha}||U(H)||\boldsymbol{\alpha}\rangle e^{-\boldsymbol{\alpha}^{\dagger}.\boldsymbol{\alpha}} \tag{15.16}$$

completely determines the operator $U(H)$, and the Bargmann coherent states are

$$||\boldsymbol{\alpha}\rangle = e^{\mathbf{a}^{\dagger}.\boldsymbol{\alpha}}|0\rangle \tag{15.17}$$

which are related to Glauber coherent states by $|\boldsymbol{\alpha}\rangle = \exp[-\boldsymbol{\alpha}^{\dagger}.\boldsymbol{\alpha}/2]||\boldsymbol{\alpha}\rangle$.

Consider two modes, a_1, a_2, coupled with

$$H = \begin{pmatrix} 0 & \theta \\ \theta & 0 \end{pmatrix} \tag{15.18}$$

then the transformation is parameterised by a single parameter, θ and

$$a_1(\theta) = \cos\theta a_1 - \sin\theta a_2 \tag{15.19}$$

$$a_2(\theta) = \cos\theta a_2 - \sin\theta a_1 \tag{15.20}$$

so that

$$S(H) = \begin{pmatrix} \cos\theta & \sin\theta \\ -\sin\theta & \cos\theta \end{pmatrix} \tag{15.21}$$

Then we see that

$$\mathcal{U}_H(\alpha_1, \alpha_2) = e^{-(|\alpha_1|^2+|\alpha_2|^2)} \exp[(|\alpha_1|^2 + |\alpha_2|^2)\cos\theta + (\alpha_2^*\alpha_1 - \alpha_1^*\alpha_2)\sin\theta] \tag{15.22}$$

Due to the over completeness of the coherent state basis, this diagonal matrix element suffices to completely determine the operator. We will call this diagonal matrix element the Q-symbol.

We now assume that photons are counted on mode a_2 and calculate the conditional state for mode a_1 for the four cases: $n = 0, 1$ and $m = 0, 1$. The conditional state of mode a_1 is given by,

$$|\psi^{(n,m)}\rangle_1 = \frac{1}{\sqrt{p(m|n)}}\hat{E}(n|m)|\psi\rangle_1 \tag{15.23}$$

where

$$p(m|n) = {}_1\langle\psi|\hat{E}^\dagger(n|m)\hat{E}(n|m)|\psi\rangle_1 \tag{15.24}$$

The Q-symbol for the operator $\hat{E}(n|m)$ is

$$\begin{aligned}\mathcal{E}(\alpha_1|n,m) = \; & e^{-(|\alpha_1|^2+|\alpha_2|^2)} \times \\ & \left(\frac{\partial}{\partial\alpha_2^*}\right)^m \left(\frac{\partial}{\partial\alpha_2}\right)^n \left[\exp[(|\alpha_1|^2+|\alpha_2|^2)\cos\theta \right. \\ & \left. +(\alpha_2^*\alpha_1 - \alpha_1^*\alpha_2)\sin\theta]\right]\Big|_{\alpha_2=0}\end{aligned} \tag{15.25}$$

The corresponding operators are

$$\begin{aligned}\hat{E}(0|0) &= \sum_{n=0}^{\infty}\frac{(\cos\theta-1)^n}{n!}(a_1^\dagger)^n a_1^n =: \; e^{-ln(\cos\theta)a_1^\dagger a_1} \; : \\ \hat{E}(1|1) &= \cos\theta\hat{E}(0|0) - \sin^2\theta a_1^\dagger\hat{E}(0|0)a_1 \\ \hat{E}(1|0) &= -a_1^\dagger\sin\theta\hat{E}(0|0) \\ \hat{E}(0|1) &= \sin\theta\hat{E}(0|0)a_1\end{aligned}$$

The generalisation to many modes is straightforward. It is easy to see that the Q-symbol for a general $U(H)$ is given by

$$\mathcal{U}_H(\boldsymbol{\alpha}) = \exp\left[-\boldsymbol{\alpha}^\dagger\cdot\boldsymbol{\alpha}\right]\exp[\boldsymbol{\alpha}^\dagger S^\dagger(H)\boldsymbol{\alpha}] \tag{15.26}$$

The Q-symbol for the measurement operator in (15.10) as

$$\mathcal{E}_H(\boldsymbol{\alpha}_s|\mathbf{n},\mathbf{m}) = {}_s\langle\boldsymbol{\alpha}_s|\hat{E}(\mathbf{n}|\mathbf{m})|\boldsymbol{\alpha}_s\rangle_s \tag{15.27}$$

where

$$\boldsymbol{\alpha}_s = \begin{pmatrix}\alpha_1\\ \alpha_2\\ \vdots\\ \alpha_n\end{pmatrix} \tag{15.28}$$

where the subscript s refers to the signal modes alone.

Noting that

$$|n\rangle = \frac{1}{\sqrt{n!}} \left(\frac{\partial}{\partial \alpha} \right)^n ||\alpha\rangle \Big|_{\alpha=0} \tag{15.29}$$

and that the partial derivatives commute with $U(H)$, we find

$$\begin{aligned} \mathcal{E}_H(\boldsymbol{\alpha}_s|\mathbf{n},\mathbf{m}) = \; & e^{-\boldsymbol{\alpha}_s^\dagger \cdot \boldsymbol{\alpha}_s} \left[m_{N+1}! \ldots m_{N+K}! n_{N+1}! \ldots n_{N+K}! \right]^{-1/2} \\ & \left[\left(\partial_{N+1}^* \right)^{m_{N+1}} \ldots \left(\partial_{N+K}^* \right)^{m_{N+K}} \right. \\ & \left. \times \left(\partial_{N+1} \right)^{n_{N+1}} \ldots \left(\partial_{N+K} \right)^{n_{N+K}} \exp[\boldsymbol{\alpha}^\dagger S^\dagger(H) \boldsymbol{\alpha}] \right] \Big|_{\alpha_{anc}=0} \end{aligned} \tag{15.30}$$

where

$$\boldsymbol{\alpha}_{anc} = \begin{pmatrix} \alpha_{N+1} \\ \alpha_{N+2} \\ \vdots \\ \alpha_{N+K} \end{pmatrix} \tag{15.31}$$

and

$$\begin{aligned} \partial_n^* &= \frac{\partial}{\partial \alpha_n^*} \\ \partial_n &= \frac{\partial}{\partial \alpha_n} \end{aligned}$$

This expression enables us to construct the relevant Q-symbol for the conditional state transformation by expanding the function $\mathcal{U}_H(\boldsymbol{\alpha})$ as a power series and reading off the relevant coefficient. This function thus plays the role of a Feynman propagator in ordinary quantum mechanics. If it is expanded as a Taylor series, each term describes the many ways in which a classical coherent amplitude can propagate through the linear optical network, keeping track of the manyfold coherent amplitudes for reflection and transmission.

The case of Boson sampling is a special case of this with the input state such that all signal modes have exactly one photon each and all ancilla modes are in the vacuum, see Fig. 15.3. The output state is

$$|\psi_{out}\rangle = \sum_C \gamma_C |\boldsymbol{n}^C\rangle \tag{15.32}$$

where C is a configuration of $|\boldsymbol{n}^C\rangle = |n_1^{(C)}, n_2^{(C)}, \ldots, n_m^{(C)}\rangle$. This is an m-fold partition of the integer n into partial sums

$$n = \sum_{j=1}^{m} n_j^{(C)} \tag{15.33}$$

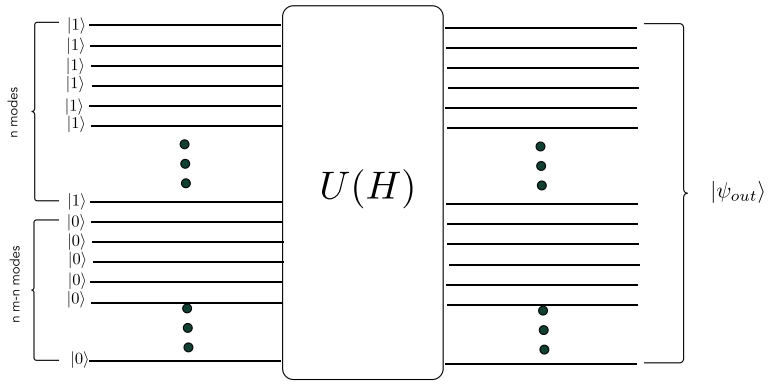

Fig. 15.3 A boson sampling configuration of a linear optical network

The probability for a particular configuration is $P_C = |\gamma_C|^2$. The connection to partitions can be used to show that

$$\gamma_C = \frac{\text{Per}(S)_C}{\sqrt{n_1^{(C)}! \ldots n_m^{(C)}!}} \tag{15.34}$$

where $\text{Per}(S)_C$ is the permanent of the $n \times n$ sub-matrix of $S(H)$. Unless you know some number theory, you may be surprised to learn that permanents, unlike determinants, are computationally hard. Calculating matrix permanents is $\#P$-complete. This is even more intractable than NP-complete problems. This suggests that the most efficient way to compute a permanent is to set up a linear optical analogue experiment.

In what sense is an analogue experiment like this a computation of a permanent? The permanent determines a probability. How many trials would we need to perform to sample a probability to estimate the permanent? Any experiment is finite and prone to errors. How sure can we be that an estimated probability in a finite experiment will actually be a good estimate of the permanent—by definition a known function of the corresponding matrix. The number of configurations C is

$$N[C] = \binom{n+m-1}{n} \tag{15.35}$$

This is super-exponential in n. In a finite experiment we cannot sample this efficiently except in special cases. The conclusion is that we cannot use boson sampling to calculate a permanent. Despite the apparent complexity of linear optical experiments of this kind , there is no known practical application of boson sampling.

15.3 Photon Number Quantum Computation

In the interferometric implementation of Deutsch algorithm we used a simple physical qubit based on a single photon pulse of one of a pair of spatio-temporal modes (pulses). This is know as a "dual rail" logic. Single photon pulses were described in Sect. 1.9,

$$|\xi_j\rangle = \int_{-\infty}^{\infty} d\omega\, \tilde{\xi}(\omega) a_j^\dagger(\omega)|0\rangle \tag{15.36}$$

where k_j labels a particular spatial mode. We will drop the explicit reference to $\tilde{\xi}(\omega)$ as we assume that all single photon pulses are prepared in the same temporal mode and write $|\xi_j\rangle = |1\rangle_j$. The relationship between logical states and the physical photon number state is

$$|\mathbf{0}\rangle_L = |1\rangle_1 \otimes |0\rangle_2 = \int_{-\infty}^{\infty} d\omega\, \tilde{\xi}(\omega) a_1^\dagger(\omega)|0\rangle \tag{15.37}$$

$$|\mathbf{1}\rangle_L = |0\rangle_1 \otimes |1\rangle_2 = \int_{-\infty}^{\infty} d\omega\, \tilde{\xi}(\omega) a_2^\dagger(\omega)|0\rangle \tag{15.38}$$

The modes could be two input modes to a beam splitter distinguished by the different directions of the wave vector, or they could be distinguished by polarisation. In the case of a beam splitter a single qubit gate is easily implemented by the linear transformation

$$a_i(\omega, \theta) = U(\theta)^\dagger a_i(\omega) U(\theta) \tag{15.39}$$

In order to simplify the notation we drop the explicit frequency dependance from now on but it must be kept in mind that these are defined in frequency space and have the delta function commutation relations for the free field. We write $U(\theta) = \exp\left[\theta(a_1 a_2^\dagger - a_1^\dagger a_2)\right]$. Thus

$$a_1(\theta) = \cos\theta a_1 - \sin\theta a_2 \tag{15.40}$$

$$a_2(\theta) = \cos\theta a_2 + \sin\theta a_1 \tag{15.41}$$

In the case of a pulse-mode fibre coupler, $a_i^\dagger$ creates a single-photon pulse in a single mode fibre labelled by subscript i, see Fig. 15.4. The description in the logical basis becomes,

$$|0\rangle_L \to \cos\theta_1 |0\rangle_L - \sin\theta_1 |1\rangle_L \tag{15.42}$$

$$|1\rangle_L \to \cos\theta_1 |1\rangle_L + \sin\theta_1 |0\rangle_L \tag{15.43}$$

While single qubit gates are readily implemented by linear optical devices such as beam splitters, quarter wave plates, phase shifters etc., two qubit gates are difficult. In order to implement the controlled phase gate (CSIGN) defined by

$$|x\rangle_L |y\rangle_L \to U_{CP}|x\rangle_L |y\rangle_L = (-1)^{x.y}|x\rangle_L |y\rangle_L \tag{15.44}$$

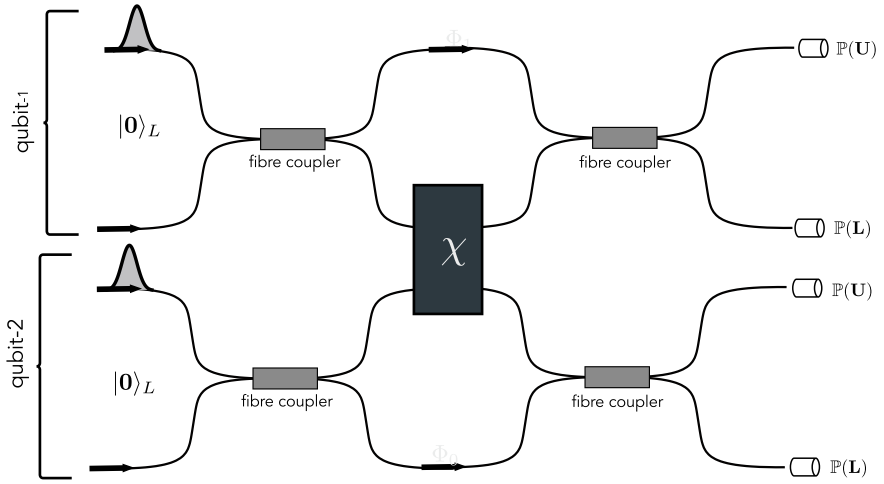

Fig. 15.4 An optical realisation of a CZ gate with dual rail photonic encoding. The final single photon counters make a measurement of the qubit in the computational basis as they determine which rail has a photon. In the case of a correctly running CZ gate, the probability to detect a photon in the upper arm at each output is 1

In a dual rail, single photon code, this can be implemented using a two mode Kerr nonlinearity. A simple nonlinear optical model of a Kerr nonlinearity was discussed in Chap. 8 in relation to optical bistability. The two mode generalisation is described by the Hamiltonian

$$H = \hbar\chi a_1^\dagger a_1 a_2^\dagger a_2 \tag{15.45}$$

At the level of single photons this Hamiltonian produces the transformation, $|x\rangle|y\rangle \rightarrow e^{-ixy\chi t}|x\rangle|y\rangle$ and it is a simple matter to implement the CSIGN gate in the logical basis for the dual rail single photon code. The optical circuit is illustrated in Fig. 15.4. While this gate does not change the total photon number in each pulse because the Kerr interaction is photon number conserving, it does change the temporal shape in each pulse due to quantum phase back-action.

There are at least two problems in pursuing this approach; (a) the difficulty of realising number states in the laboratory, (b) the difficulty of producing one photon phase shifts of the order of π. We will say more about the fist of these problems below. The second difficulty is very considerable. Third order optical nonlinearities are very small for a field with such a low intensity as a single photon. However experimental advances may eventually overcome this.

A quite different approach to achieve large single photon conditional phase shifts is based on the non-unitary transformation of a state that results when a measurement is made. Consider the situation shown in Fig. 15.5. Two modes of an optical field are coupled via a beam splitter. One mode is assumed to be in the vacuum state (a) or a one photon state (b), while the other mode is arbitrary. A single photon counter is placed in the output port of mode-2. What is the conditional state of mode-1 given a count of n photons?

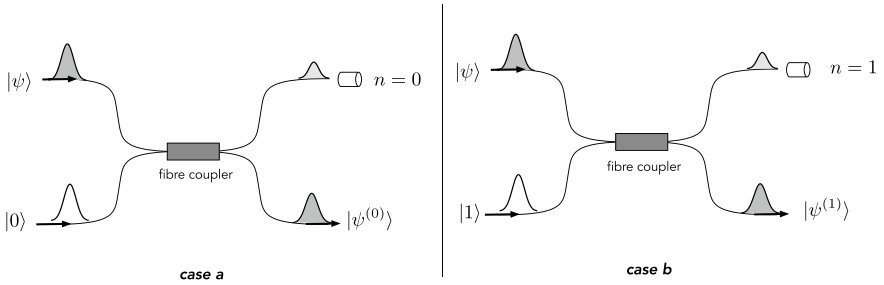

Fig. 15.5 A conditional state transformation conditioned on photon counting measurements. In case a an optical pulse in an arbitrary quantum state is injected into the top rail and vacuum is applied at the bottom rail. The conditional state of the bottom rail, given no photons are counted in the top rail is $|\psi^{(0)}\rangle$. In case b an optical pulse in an arbitrary quantum state is injected into the top rail and a single photon pulse (not a logical qubit state) is injected at the bottom rail. The conditional state of the bottom rail, given one photon is counted in the top rail is $|\psi^{(1)}\rangle$

Consider two modes, a_1, a_2, coupled with a beam splitter interaction, described by the unitary transformation given in (15.40, 15.41). We now assume that photons are counted on mode a_2 and calculate the conditional state for mode a_1 for two cases: no count and also for a single count at mode a_2. The conditional state of mode a_1 is given by (unnormalised),

$$|\tilde{\psi}^{(i)}\rangle_1 = \hat{\Upsilon}(i)|\psi\rangle_1 \tag{15.46}$$

where

$$\hat{\Upsilon}(i) = {}_2\langle i|U(\theta)|i\rangle_2 \tag{15.47}$$

with $i = 1, 0$. The probability to observe each event is given by

$$P(i) = \langle\psi|\Upsilon^\dagger(i)\hat{\Upsilon}(i)|\psi\rangle_1 \tag{15.48}$$

which fixes the normalisation of the state,

$$|\psi^{(i)}\rangle_1 = \frac{1}{\sqrt{P(i)}}|\tilde{\psi}^{(i)}\rangle_1 \tag{15.49}$$

In Exercise 15.4 we find that

$$\begin{aligned}\hat{\Upsilon}(0) &= \sum_{n=0}^{\infty}\frac{(\cos\theta-1)^n}{n!}(a_1^\dagger)^n a_1^n \\ \hat{\Upsilon}(1) &= \cos\hat{\Upsilon}^{(0)} - \sin^2\theta a_1^\dagger\hat{\Upsilon}^{(0)}a_1\end{aligned}$$

This can be written more succinctly using normal ordering,

$$\hat{\Upsilon}(0) =: e^{\ln(\cos\theta)} : \tag{15.50}$$

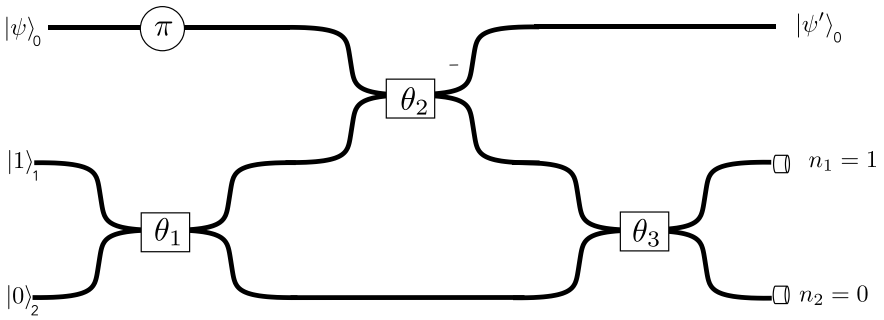

Fig. 15.6 A conditional state transformation on three optical modes, conditioned on photon counting measurements on the ancilla modes a_1, a_2. The signal mode, a_0 is subjected to a π phase shift

In order to see how we can use these kind of transformations to effect a CSIGN gate, consider the situation shown in Fig. 15.6. Three optical modes are mixed on a sequence of three beam splitters with beam splitter parameters θ_i. The *ancilla* modes, a_1, a_2 are restricted to be in the single photon states $|1\rangle_1, |0\rangle_2$ respectively. We will assume that the *signal* mode, a_0, is restricted to have *at most* two photons, thus

$$|\psi\rangle = \alpha|0\rangle_0 + \beta|1\rangle_0 + \gamma|2\rangle_0 \tag{15.51}$$

This captures the fact that in the dual rail encoding a general two qubit state can have at most two photons. The objective is to chose the beam splitter parameters so that when the two detectors at the output of modes 2, 3 detect 1, 0 photons respectively (that is detect no change in their occupation), the signal state is transformed as

$$|\psi\rangle \to |\psi'\rangle = \alpha|0\rangle + \beta|1\rangle - \gamma|2\rangle \tag{15.52}$$

with a probability that is *independent* of the input state $|\psi\rangle$. This last condition is essential as in a quantum computation, the input state to a general two qubit gate is completely unknown. We will call this transformation the NS (for nonlinear sign shift) gate. In Exercise 15.6 we find that this can be achieved using: $\theta_1 = -\theta_3 = 22.5$ deg and $\theta_2 = 65.53$ deg. The probability of the conditioning event $(n_2 = 1, n_3 = 0)$ is 1/4. Note that we can't be sure in a given trial if the correct transformation will be implemented. Such a gate is called a *nondeterministic* gate. However the key point is that success is heralded by the results on the photon counters (assuming ideal operation).

We can now proceed to a CZ gate in the dual rail basis. Consider the situation depicted in Fig. 15.7. We first take two dual rail qubits encoding for $|1\rangle_L|1\rangle_L$. The single photon components of each qubit are directed towards a 50/50 beam splitter where they overlap perfectly in space and time. This is precisely the case of the Hong-Ou-mandel interference discussed in Sect. 1.9, and produces a state of the form $|0\rangle_2|2\rangle_3 + |2\rangle_2|0\rangle_3$. We then insert an NS gate into each output arm of the HOM interference. When the conditional gates in each arm work, which occurs with

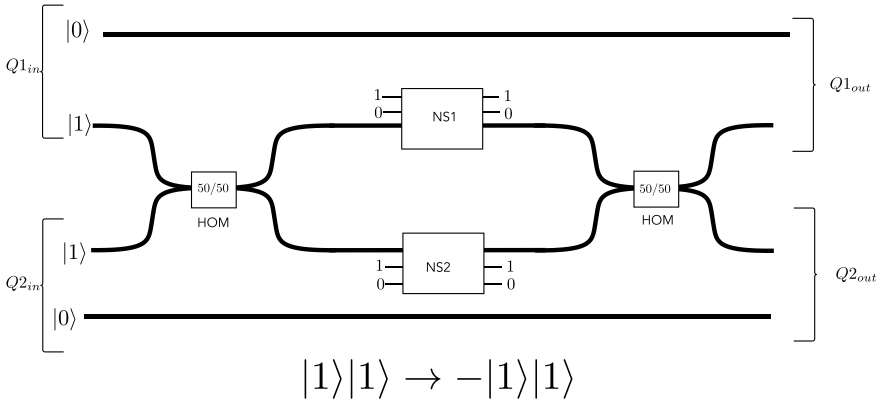

Fig. 15.7 A conditional state transformation conditioned on photon counting measurements. A CZ gate that works with probability of 1/16. It uses HOM interference and two NS gates

probability $1/16$, the state is multiplied by an overall minus sign. Finally we direct these modes towards another HOM interference. The output state is thus seen to be $-|1\rangle_L|1\rangle_L$. One easily checks the three other cases for the input logical states to see that this device implements the CZ gate with a probability of $1/16$ and successful operation is heralded. We call this the $\mathrm{CZ}_{1/16}$ gate.

Clearly a sequence of nondeterministic gates is not going to be much use: the probability of success after a few steps will be exponentially small. The key idea in using nondeterministic gates for quantum computation is based on the idea of gate teleportation of Gottesmann and Chuang [11]. We saw in Sect. 14.5 that in quantum teleportation an unknown quantum state can be transferred from A to B provided A and B first share an entangled state. Gottesmann and Chuang realised that it is possible to simultaneously teleport a two qubit quantum state and implement a two qubit gate in the process by first applying the gate to the entangled state that A and B share prior to teleportation.

We use a non deterministic NS gate to prepare the required entangled state, and only complete the teleportation when this stage is known to work. The teleportation step itself is non deterministic but, as we see below, by using the appropriate entangled resource the teleportation step can be made near deterministic. The near deterministic teleportation protocol requires only photon counting and fast feed-forward. We do not need to make measurements in a Bell basis which would require entangling operations that cannot be done using linear optics alone.

A nondeterministic teleportation measurement is shown in Fig. 15.8. The client state is a one photon state in mode-0 $\alpha|0\rangle_0 + \beta|1\rangle_0$ and we prepare the entangled ancilla state

$$|t_1\rangle_{12} = |01\rangle_{12} + |10\rangle_{12} \tag{15.53}$$

where mode-1 is held by the sender, A, and mode-2 is held by the receiver, B. For simplicity we omit normalisation constants wherever possible. This an ancilla state is easily generated from $|01\rangle_{12}$ by means of a beam splitter.

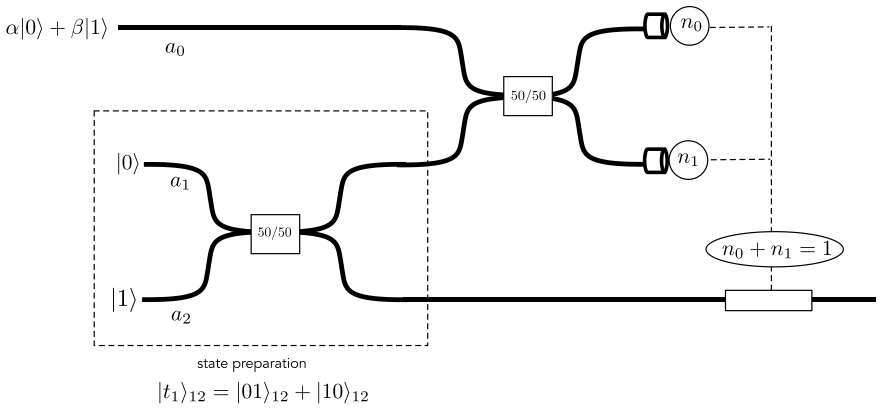

Fig. 15.8 A partial teleportation scheme ($\mathbf{T}_{1/2}$) for single photon states using linear optics

If the total count is $n_0 + n_1 = 0$ or $n_0 + n_1 = 2$, an effective measurement has been made on the client state and the teleportation has failed. However if $n_0 + n_1 = 1$, which occurs with probability 0.5, teleportation succeeds with the two possible conditional states being

$$\alpha|0\rangle_2 + \beta|1\rangle_2 \text{ if } n_0 = 1, n_1 = 0 \tag{15.54}$$

$$\alpha|0\rangle_2 - \beta|1\rangle_2 \text{ if } n_0 = 0, n_1 = 1 \tag{15.55}$$

This procedure implements a partial bell measurement and we will refer to it as a nondeterministic teleportation protocol, $\mathbf{T}_{1/2}$. Note that teleportation failure is detected and corresponds to a photon number measurement of the state of the client qubit. Detected number measurements are a very special kind of error and can be easily corrected by a suitable error correction protocol. For further details see [4].

The next step is to use $\mathbf{T}_{1/2}$ to effect a conditional sign flip $\text{csign}_{1/4}$ which succeeds with probability $1/4$. Note that to implement csign on two bosonic qubits in modes 1, 2 and 3, 4 respectively, we can first teleport the first modes of each qubit to two new modes (labelled 6 and 8) and then apply csign to the new modes. When using $\mathbf{T}_{1/2}$, we may need to apply a sign correction. Since this commutes with csign, there is nothing preventing us from applying csign to the prepared state before performing the measurements. The implementation is shown in Fig. 15.9 and now consists of first trying to prepare two copies of $|t_1\rangle$ with csign already applied, and then performing two partial Bell measurements. Given the prepared state, the probability of success is $(1/2)^2$. The state can be prepared using $\text{csign}_{1/16}$, which means that the preparation has to be retried an average of 16 times before it is possible to proceed.

To improve the probability of successful teleportation to $1 - 1/(n+1)$, we generalise the initial entanglement by defining

$$|t_n\rangle_{1\ldots 2n} = \sum_{j=0}^{n} |1\rangle^j |0\rangle^{n-j} |0\rangle^j |1\rangle^{n-j}. \tag{15.56}$$

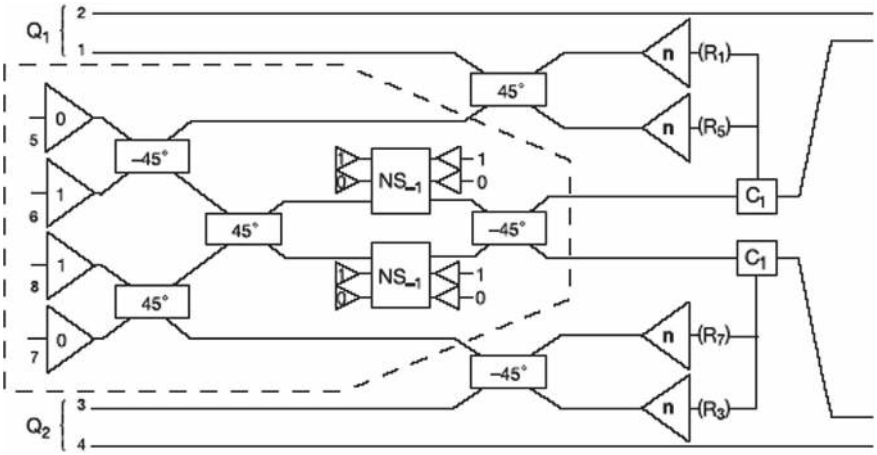

Fig. 15.9 A CZ two qubit gate with teleportation to increase success probability to 1/4. When using the basic teleportation protocol (T1), we may need to apply a sign correction. Since this commutes with CZ, it is possible to apply CZ to the prepared state before performing the measurements, reducing the implementation of CZ to a state-preparation (outlined) and two teleportations. The two teleportation measurements each succeed with probability 1/2, giving a net success probability of 1/4. The correction operations C1 consist of applying the phase shifter when required by the measurement outcomes

The notation $|a\rangle^j$ means $|a\rangle|a\rangle \ldots$, j times. The modes are labelled from 1 to $2n$, left to right. Note that the state exists in the space of n bosonic qubits, where the k'th qubit is encoded in modes $n+k$ and k (in this order).

To teleport the state $\alpha|0\rangle_0 + \alpha|1\rangle_0$ using $|t_n\rangle_{1\ldots 2n}$ we first couple the client mode to half of the ancilla modes by applying an $n+1$ point Fourier transform on modes 0 to n. This is defined by the mode transformation

$$a_k \to \frac{1}{\sqrt{n+1}} \sum_{l=0}^{n} \omega^{kl} a_l \tag{15.57}$$

where $\omega = e^{i2\pi/(n+1)}$ This transformation does not change the total photon number and is implementable with passive linear optics. After applying the Fourier transform, we measure the number of photons in each of the modes 0 to n. If the measurement detects k bosons altogether, it is possible to show [4] that if $0 < k < n+1$, then the teleported state appears in mode $n+k$ and only needs to be corrected by applying a phase shift. The modes $2n-l$ are in state 1 for $0 \le l < (n-k)$ and can be reused in future preparations requiring single bosons. The modes are in state 0 for $n-k < l < n$. If $k = 0$ or $k = n+1$ an effective measurement of the client is made, and the teleportation fails. The probability of these two events is $1/(n+1)$, regardless of the input. Note that again failure is detected and corresponds to measurements in the basis $|0\rangle, |1\rangle$ with the outcome known. Note that both the necessary correction and the receiving mode are unknown until after the measurement. The success probability of the teleported CZ gate can thus be boosted to $n^2/(n+1)^2$.

A number of LOQC protocols have been implemented in the laboratory. The first experiment was performed by Pittmann and Franson [15]. This used entangled ancillas that are readily produced as photon pairs in a spontaneous parametric down conversion process. This idea was subsequently used to develop fusion gates for optical QC discussed below.

A simplified version of the LOQC model was implemented by O'Brien et al. [16], based on a proposal of Ralph et al. [17] for a CNOT gate. The simplification requires only detecting photon coincidences at the output. This gate performs all the operations of a CNOT gate but requires only a two photon input. Detecting only coincidences means that the device must be configured so that correct operation leads to a coincidence detection of both photons at the output. The gate is non deterministic but gate failures are simply not detected at all. Successful operation is heralded by coincidence detection of both photons and success will occur with probability $1/9$. In the UQ experiment the two modes of each qubit are distinguished by orthogonal polarisations. The advantage in using a gate based on two photon coincidence detection is that spontaneous parametric down conversion (SPDC) may be used in place of true single photon sources. An SPDC produces a photon pair in two distinct spatio-temporal modes at random times. There is a small probability of producing more than two photons, but this can be neglected.

It is possible to do quantum computation with single photon pulses using heralded non unitary operations, the probabilistic nature of the process means that many trials need to be made. This leads to an explosion in the number of beam splitters and counters required to do even simple gates. One way to reduce the resource count was proposed by Neilsen using cluster states and measurement based quantum computation MBQC [12]. The cluster state model was developed by Raussendorf and Breigel [13] and is quite different from the circuit models that we have been using. In cluster state QC, an array of qubits is initially prepared in a special entangled state. The computation then proceeds by making a sequence of single qubit measurements. Each measurement is made in a basis that depends on prior measurement outcomes. Nielsen realised that the LOQC scheme discussed above could be used to efficiently assemble the cluster using the nondeterministic teleportation t_n. The failure mode of this gate constituted an accidental measurement of the qubit in the computational basis. Such an error does not destroy the entire assembled cluster but merely detaches one qubit from the cluster. This enables a protocol to be devised that produces a cluster that grows on average. The LOQC cluster state method dramatically reduces the number of optical elements required to implement the original LOQC scheme. For example, the KLM CZ gate with 95% success probability requires $\sim 10^{14}$ operations!

15.3.1 Fusion Gates

A breakthrough in simplifying linear optics quantum computation with single photons when Browne and Rudolph [6] combined cluster state measurement based quantum computation with the gate of Pitmann and Franson to build operations that can fuse small clusters into large ones. The first step is to consider a simple implemen-

tation of a different approach to quantum computation called measurement based quantum computation (MBQC) [8].

Consider a two-dimensional array of qubits shown below. Each qubit at a vertex is prepared in the *physical qubit/photon* state $|+\rangle = (|0\rangle + |1\rangle)/\sqrt{2}$. We then apply a CZ (CPHASE) gate between each vertex connected by an edge. For example

$$CZ_{12}CZ_{23}CZ_{34}|++++\rangle = \frac{1}{2}(|0+0+\rangle + |0-1-\rangle + |1-0+\rangle + |1+1-\rangle) \tag{15.58}$$

We have ordered the qubit states so that the corresponding label increases from left to right. We now regard each row of a cluster as one *logical qubit*. The notion CZ_{jk} means that the unitary operator $\exp[i\pi Z_j Z_k]$ is applied to the pair of qubits labelled jk. We have introduced a more compact notation for Pauli matrices so that $X = \sigma_x$, $Y = \sigma_y$, $Z = \sigma_z$ and Z is diagonal in the qubit basis.

When we make independent Pauli measurements on the physical qubits labelled 2, 3, there are four possible outcomes. Label the outcomes $s_2, s_3 \in \{0, 1\}$. These then label the conditional states of physical qubits 1, 4. As an example suppose we measure σ_x on physical qubits 2, 3 and further that $s_2 = 1, s_3 = 1$, corresponding to finding these two physical qubits both in state $+\rangle$. Inspection of (15.58) gives the corresponding conditional state of physical qubits 1, 4 as

$$|\psi\rangle_{24} = |0+\rangle + |1-\rangle \qquad s_2 = s_3 = 1 \tag{15.59}$$

(We are ignoring the normalisation to simplify the notation). The conditional transformation for the physical qubits on the right hand column from pre to post measurement state is

$$|++\rangle = (H \otimes \mathbb{I} + \mathbb{I} \otimes HZ)|++\rangle \tag{15.60}$$

Of course the measured qubits now factor out of the cluster state, and are no longer entangled with physical qubits 1, 4. Measured physical qubits are deleted from the cluster state.

We now adopt a more abstract notation that distinguishes physical qubits from logical qubits. We regard the physical qubits in each horizontal line as encoding a *logical qubit*. In this example, this gives two logical qubits initially prepared in the state $|++\rangle_L$. After the measurement there are only two physical qubits in each row of the cluster and the state in this example is given by (15.60) $(H \otimes \mathbb{I} + \mathbb{I} \otimes HZ)|++\rangle_L$. Thus the transformation of logical qubits, given these particular measurement outcomes, is

$$|++\rangle_L \rightarrow (H \otimes \mathbb{I} + \mathbb{I} \otimes HZ)|++\rangle_L \tag{15.61}$$

In this case the cluster has simulated a particular circuit on the two logical qubits. Working through the other three possible measurement outcomes we find that in general the circuit for logical qubits is shown in Fig. 15.11.

Using LOQC we need to be able to assemble cluster states non deterministically as we do not have a deterministic CZ gate. This can be done using the teleported non deterministic gate $CZ_{n^2/(n+1)^2}$ described previously. Nielsen [5] adapted this gate

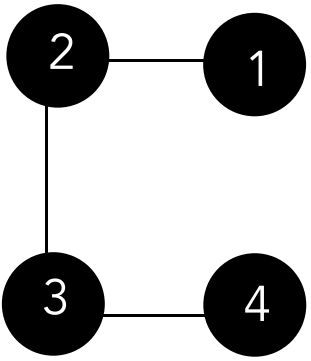

Fig. 15.10 A simple two dimensional cluster of entangled qubits. Vertices label qubits and edges show which pairs are entangled. We now regard each row of a cluster as one logical qubit

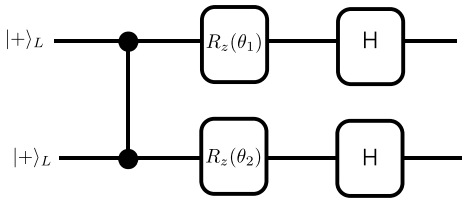

Fig. 15.11 The cluster state simulation using the graph in Fig. 15.10 of a simple gate for two logical qubits. The operators $R_z(\theta)$ represent rotations about the Z axis. The values used for θ_j depend on the outcomes for measurements on physical qubits 2, 3

to make cluster states non deterministically. In the case of a general two qubit CZ gate, he showed that each physical qubit in a cluster has at most one vertical edge. We connect another physical qubit by one horizontal and one vertical edge using requires two successful $CZ_{4/9}$ gates. He showed that for $n = 2$ this requires less than 70 beam splitters, 30 photodetectors, and 12 single-photon preparations.

Nielsen showed how to build the cluster non deterministically using two types of operation: add a qubit connected to the current cluster by a single bond, and attempting to add a qubit connected by a double bond. Any cluster can be built up by alternating these operations. Operations of the first kind can be done using the $CZ_{4/9}$. Two key features of the procedure are: failure does not change the rest of the cluster, and a cluster of size $S(n)$ can be grown with about $9S(n)$ attempts.

Browne and Rudolph (BR) [6] substantially improved Nielsen's scheme using the non deterministic gate of Pittman and Franson. In BR we code physical qubits as single photons in polarisation modes. ($H \to 0, V \to V$) and use polarisation rotations to measure qubits in arbitrary basis. Instead of CZ gates between clusters they use probabilistic fusion gates described by a fusion operation $|0\rangle\langle 00| + |1\rangle\langle 11|$. This replaces two qubits with a single qubit while retaining all cluster state bonds on each qubit. The important insight was that this would enable LOQC schemes to dispense with gate teleportation and use instead resource states of the form of photonic Bell pairs

$$|C_2\rangle = \frac{1}{2}\left[|H\rangle(|H\rangle + |V\rangle) + |V\rangle(|H\rangle - |V\rangle)\right] \tag{15.62}$$

These are two qubit clusters $|0+\rangle + |1-\rangle$ with polarisation mode encoding $|H\rangle \rightarrow |0\rangle, \quad |V\rangle \rightarrow |1\rangle$. These states can be generated by spontaneous parametric down conversion, see Sect. 4.2.

We use Fock state pulses of four distinct modes. Each spatio-temporal mode is labelled by wave vectors k_1, k_2 and two orthogonal polarisation vectors, H, V. Now define four pairs of annihilation and creation pairs $(a_1, a_1^\dagger)$, $(a_2, a_2^\dagger)$, $(\bar{a}_1, \bar{a}_1^\dagger)$, $(\bar{a}_2, \bar{a}_2^\dagger)$, such that

$$a_j^\dagger|\text{vac}\rangle = |H\rangle_j \tag{15.63}$$

$$\bar{a}_j^\dagger|\text{vac}\rangle = |V\rangle_j \tag{15.64}$$

where $|\text{vac}\rangle$ is the four mode vacuum state. In the experiments we will describe the spatio-temporal modes are Fock state pulses in waveguides labelled by j. (Recall that our notion explicitly assumes these are frequency space operators $a_j(\omega)$.) We do not specify the temporal pulse shape $\xi_j(t)$ for each wave guide as they are all the same. This is in fact defined by a suitably engineered single photon source. The cluster state in (15.62) can now be written as

$$|C_2\rangle = \frac{1}{2}\left[a_1^\dagger(a_2^\dagger + \bar{a}_2^\dagger) + \bar{a}_1^\dagger(a_2^\dagger - \bar{a}_2^\dagger)\right]|\text{vac}\rangle \tag{15.65}$$

We first discuss type-1 non deterministic fusion operation shown in Fig. 15.12 This uses a polarising beam splitter that enables us to direct orthogonally polarised photonic pulses in different directions. We will take the convention that vertically polarised photons are reflected and horizontally polarised photons are transmitted. The PBS thus implements the following unitary transformation in the Heisenberg picture

$$a_j \rightarrow a_j \tag{15.66}$$

$$\bar{a}_1 \rightarrow \bar{a}_2, \qquad \bar{a}_2 \rightarrow \bar{a}_1 \tag{15.67}$$

In Fig. 15.12, there is one photon in each input and so there are four possible output counts $(n_1, n_2) \in (1,1), (2,0), (0,2)$. The case $(1,1)$ can occur in two indistinguishable ways depending on the input state, $|HH\rangle$ or $|VV\rangle$. The last two cases correspond to the input states $|HV\rangle$ and $|VH\rangle$ respectively. A single count will occur 50% of the time. The count $n_2 = 0, 2$ is a heralded failure and is discarded. Thus the success probability is 50%. The transformation of the cluster state by the PBS is given by

$$|C_2\rangle \rightarrow \frac{1}{2}\left[a_1^\dagger a_2^\dagger - \bar{a}_1^\dagger \bar{a}_2^\dagger\right]|\text{vac}\rangle + \frac{1}{2}\left[a_1^\dagger \bar{a}_1^\dagger + a_2^\dagger \bar{a}_2^\dagger\right]|\text{vac}\rangle \tag{15.68}$$

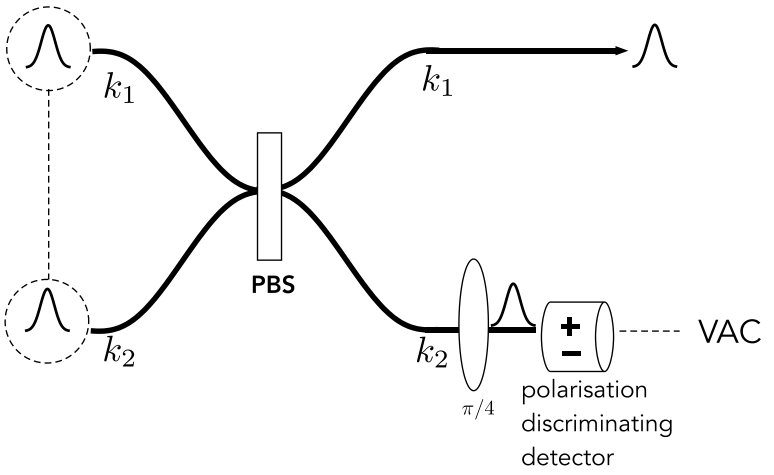

Fig. 15.12 A type-1 non deterministic fusion operation using single photon pulses at a polarising beam splitter (PBS) and conditioning on single photon detection events. We label spatial modes by wave vectors k_1 for top waveguide modes and k_2 for bottom waveguide modes. We label polarised two-photon states as an ordered symbol string, for example, $|HV\rangle = |1\rangle_{k_1,H} \otimes |1\rangle_{k_2,V}$. Prior to detection, an optical element rotates the polarisation by $\pi/4$

The second term is the component that leads to a total count of $n_2 = 2$ or $n_2 = 0$ at the detector. We therefore drop this term as we only condition from single photon detection events determined by the state

$$|\psi^{(1)}\rangle = \frac{1}{\sqrt{2}}\left[a_1^\dagger a_2^\dagger - \bar{a}_1^\dagger \bar{a}_2^\dagger\right]|\text{vac}\rangle \tag{15.69}$$

The counter has two output channels that discriminate orthogonal polarisations of the single photon counted. This occurs after the $\pi/4$ polarisation rotation that implements the unitary transformation on mode k_1 alone

$$a_1 \rightarrow \frac{1}{\sqrt{2}}(a_1 + \bar{a}_1) \tag{15.70}$$

$$\bar{a}_1 \rightarrow \frac{1}{\sqrt{2}}(a_1 - \bar{a}_1) \tag{15.71}$$

The state in the single photon sector is then transformed to

$$|\psi^{(1)}\rangle \rightarrow \frac{1}{2}\left[(a_1^\dagger + \bar{a}_1^\dagger)a_2^\dagger - (a_1^\dagger - \bar{a}_1^\dagger)\bar{a}_2^\dagger\right]|\text{vac}\rangle \tag{15.72}$$

$$= \frac{1}{2}\left[(|H\rangle + |V\rangle)|H\rangle - (|H\rangle - |V\rangle)|V\rangle\right] \tag{15.73}$$

If the single photon counter is engineered to discriminate between H/V polarisation, there are two conditional states are

$$|\phi^{(\pm)}\rangle = \frac{1}{\sqrt{2}}(|H\rangle \pm |V\rangle) \otimes |\text{vac}\rangle \tag{15.74}$$

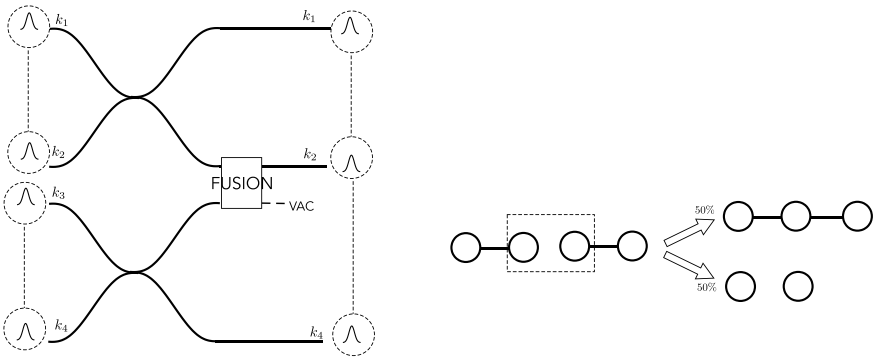

Fig. 15.13 A scheme for fusing two Bell pair clusters to produce a three node cluster. At the right we give a graphical representation of the process. When fusion fails it has the effect of measuring both input qubits in the σ_z basis

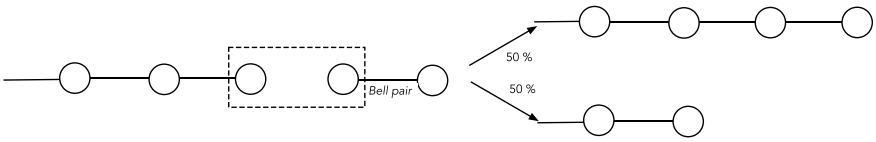

Fig. 15.14 Adding a polarisation entangled Bell pair to an existing polarisation encoded qubit cluster

depending on which polarisation channel registers the count. We treat the photon detection as an absorption event which returns mode k_2 to the vacuum state. It doesn't matter which of these we get as they differ by a local σ_z which can be included in the control protocol. If we have two Bell pairs, i.e. two qubit cluster states, we can use type-1 fusion to get a three qubit cluster state. Let us begin with the Bell pair $|C_2\rangle_{12} \otimes |C_2\rangle_{34}$ where there are now four polarised single photon pulses, see Fig. 15.13. As this operation is only 50% successful, we use four Bell pairs, on average, to create a three qubit cluster. We can use this operation to add a Bell pair to an existing linear cluster state, see Fig. 15.14. T On average, the length of cluster does not increase. On average cluster increases by half qubit. To add one qubit to the cluster need $2 \times 4 - 1 = 7$ Bell pairs. Thus, 6.5 Bell pairs per added qubit.

We also need to be able to grow two-dimensional clusters from linear clusters. We seem to be heading in the right direction however type-1 fusion is only 50% successful. Failure is equivalent to σ_z measurement and this breaks a bond. To get around this the type-II fusion gate can be used. These use a two Bell pairs for a resource state. This is depicted in Fig. 15.15. Successful operation is heralded by a single count at each photon counter. Failure is indicated if there are no photons detected at one of the counters. In order to understand how this can be used, BR introduced a photonic redundant encoding. This uses polarised multi-photon pulses to encode a qubit. For example,

$$|0\rangle_L = a_1^\dagger a_2^\dagger |0\rangle \equiv |H\rangle^{\otimes 2}, \qquad |1\rangle_L = \bar{a}_1^\dagger \bar{a}_2^\dagger |0\rangle \equiv |V\rangle^{\otimes 2} \tag{15.75}$$

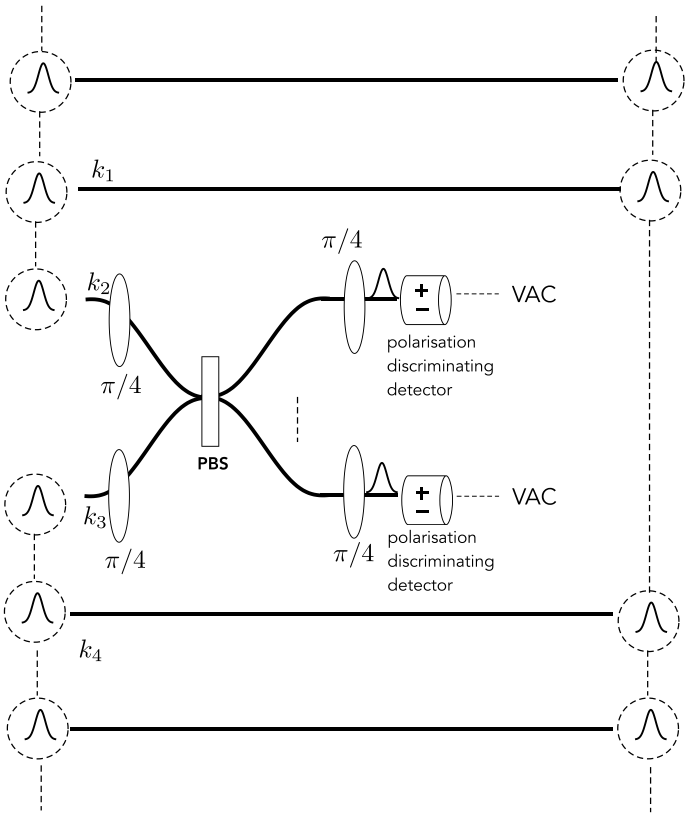

Fig. 15.15 A type-II fusion gate. Successful operation is heralded by a simultaneous single photon detection event at each photon counter

A single qubit in the cluster state may be represented by two photons and a generic cluster state by $|\phi\rangle_0 \otimes |0\rangle_L + |\phi\rangle_1 \otimes |1\rangle_L$ where we have singled out from the rest of the cluster the particular qubit which is redundantly encoded with two photons. If we measure the polarisation of the second photon in the $|H\rangle \pm |V\rangle$ basis, a σ_x measurement, of the redundant logical qubit, it simply removes this photon but does not destroy the cluster, up to a phase shift. Returning to the type-II fusion gate in Fig. 15.15, we see that failure corresponds to an accidental σ_x measurement on one of the photons in each of the redundantly encoded qubits at the input. Provided we start with enough photons in the redundant qubit we can try the gate many times until success.

If we want to 'knit' two linear clusters together to form a two-dimensional cluster, we ensure that somewhere in the chain of pulses in each chain there is a N photon pulse. We can then apply a type-II fusion gate between those redundantly encoded qubits. This is illustrated in Fig. 15.16.

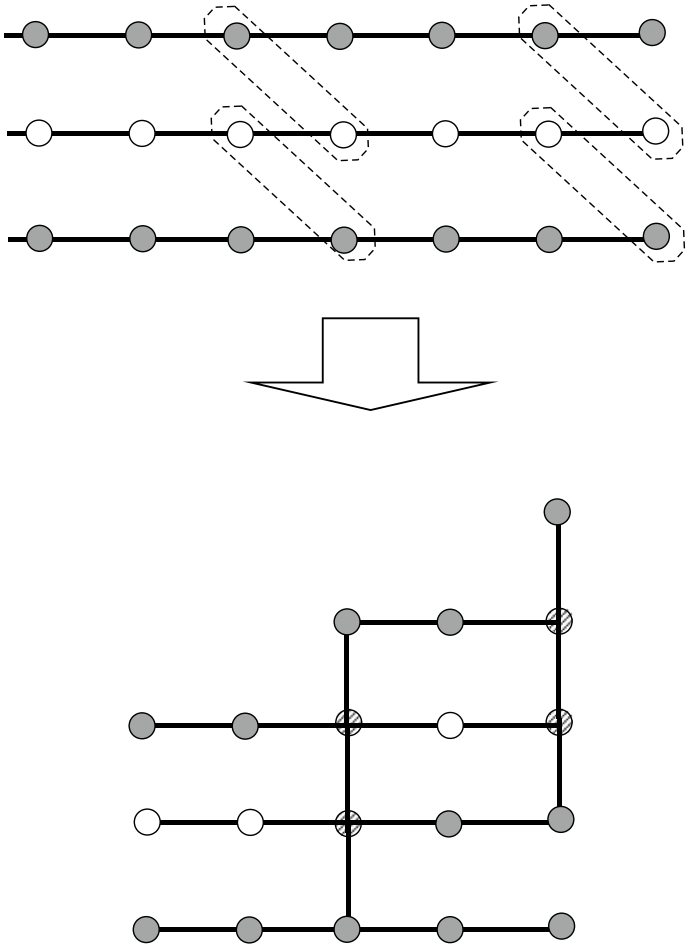

Fig. 15.16 An example of a two dimensional cluster state, with redundantly encoded qubits

15.4 Continuous Variable (CV) Optical Quantum Computation

Encoding a qubit in single-photon pulses is not the only way to use optical switching networks for quantum computation. We can use single pulses prepared in squeezed states, cat states or GKP states (see Sect. 1.8). An MBQC protocols can then be used with linear optics to do universal quantum computation.

An important theorem for CV quantum computation was presented by Braunstein and Lloyd [21]. What kinds of Hamiltonians are capable of generating an arbitrary state of a single optical mode? In terms of the corresponding unitaries we can ask the equivalent question about the generators of the unitary. In addition to displacements and squeezing unitaries it turns out that we need a unitary with a generator that is at least cubic in the annihilation and creation operators. The opto-mechanical

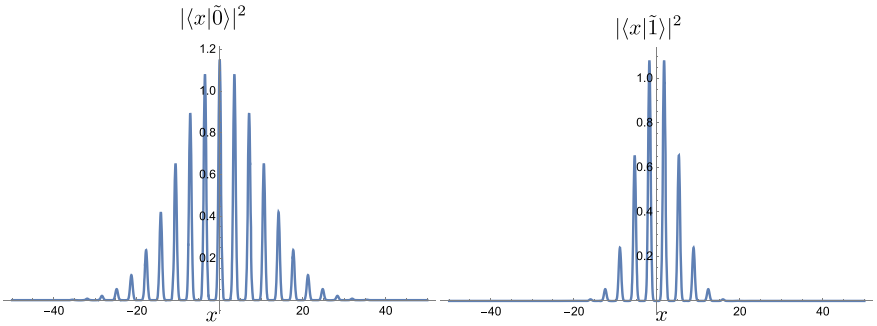

Fig. 15.17 The probability distribution for $|\tilde{0}\rangle$ (left) and $|\tilde{1}\rangle$ (right) in the diagonal representation of $X_1 = a + a^\dagger$ with $r = -1.2,\ \tilde{\Delta} = 0.01$

interaction in Chap. 7 is an example. Another is a Kerr nonlinearity in Sect. 4.2. These unitaries in suitable sequences can create an arbitrary single mode state. These states are typically non classical in so far as they do not have Glauber-Sudarshan P representations. Another way to pose the question is to ask for the class of unitaries that transform states with Gaussian wave functions for quadrature phase operators into each other.

The first CV encoding scheme in the context of encoding a qubit in the states of a harmonic oscillator, was proposed by Gottesmann, Kitaev and Preskill [22]. It is known as the GKP encoding. As each optical field mode is equivalent to a quantised harmonic oscillator, this scheme can be used for CV encoding of optical qubits. The ideal states are defined in Sect. 1.8. These are not physical states. Instead, the ideal encoding is approximated by a coherent superposition of Gaussian displaced squeezed vacuum states, Fig. 15.17.

$$|\tilde{0}\rangle = N_0 \sum_{k=-\infty}^{\infty} e^{-2\pi\tilde{\Delta}^2 k^2} D(k\sqrt{\pi})|r\rangle, \tag{15.76}$$

$$|\tilde{1}\rangle = N_1 \sum_{k=-\infty}^{\infty} e^{-2\pi\tilde{\Delta}^2 (2k+1)^2} D((k+1/2)\sqrt{\pi})|r\rangle, \tag{15.77}$$

where $D(k\sqrt{\pi})$ is the displacement operator defined in (1.29) and $\Delta = e^{-2r}$. In terms of the diagonal representation of X_1 these can be written

$$\langle x|\tilde{0}\rangle = N_0 \sum_{k=-\infty}^{\infty} e^{-2\pi\tilde{\Delta}^2 k^2} (2\pi\Delta)^{-1/4} \exp\left[-\frac{(x - 2k\sqrt{\pi})^2}{2\Delta}\right] \tag{15.78}$$

$$\langle x|\tilde{1}\rangle = N_1 \sum_{k=-\infty}^{\infty} e^{-2\pi\tilde{\Delta}^2 (2k+1)^2} (2\pi\Delta)^{-1/4} \exp\left[-\frac{(x - (2k+1)\sqrt{\pi})^2}{2\Delta}\right] \tag{15.79}$$

where $\Delta = e^{-r}$. In cases of practical interest $\tilde{\Delta} = \Delta$.

These states are produced as post selected (conditional) states in a measurement protocol. We will describe two schemes. The first makes use of the cubic interaction between a signal $(a, a^\dagger)$ and probe $(b, b^\dagger)$ field described by the 'optomechanical' Hamiltonian,

$$H = \hbar\chi(a^\dagger + a)b^\dagger b \tag{15.80}$$

where $a, a^\dagger$ are the annihilation and creation operators of the signal mode and $b, b^\dagger$ are the annihilation operators for the probe mode. The signal mode is prepared in a squeezed state

$$|\psi_{in}\rangle = S(r)|0\rangle \tag{15.81}$$

and the probe mode is prepared in a coherent state $|\beta\rangle$ with $\beta \in \mathbb{C}$. We choose a phase convention such that α is real and $r > 0$. This implies a phase squeezed state, that is to say, the quadrature phase amplitude in phase with the coherent displacement is anti-squeezed.

The probe mode is now prepared in a coherent state $|\beta\rangle$ with $\beta \in \mathbb{C}$. After a fixed interaction we project the probe mode into an eigenstate of $X_b = (b + b^\dagger)$. This is equivalent to homodyne detection with an integrated signal current [23]. Let the result of this measurement be $y \in \mathbb{R}$. The (unnormalised) conditional state of the signal mode is then given by

$$|\tilde{\psi}_{out}\rangle = \hat{\Upsilon}(y)|\psi_{in}\rangle \tag{15.82}$$

where the Krauss operator is given by

$$\hat{\Upsilon}(y) = {}_b\langle y|e^{-i\theta(a^\dagger + a)b^\dagger b}|\beta\rangle_b \tag{15.83}$$

where $\theta = \chi T$ for interaction time T. This operator is diagonal in $X = a + a^\dagger$. In this basis we define

$$\Upsilon(x|y) = \langle x|\hat{\Upsilon}(y)|x\rangle \tag{15.84}$$

We then find that

$$\Upsilon(x|y) = (2\pi)^{-1/4}\exp\left[iyr\sin(\theta x - \phi) - (y - 2r\cos(\theta x - \phi))^2/4\right] \tag{15.85}$$

is a conditional probability amplitude, and

$$|\Upsilon(x|y)|^2 = (2\pi)^{-1/2}\exp\left[-(y - 2r\cos(\theta x - \phi))^2\right] \tag{15.86}$$

is a conditional probability with $\beta = |\beta|e^{i\phi}$.

In Fig. 15.18 we plot the conditional probability $|\Upsilon(x|y)|^2$ versus x for various values of y. The peaks are centred at $\cos(\theta x - \phi) = y/2r$. For r sufficiently large the peaks are separated in displacement by by π/θ. The off-set between the peaks for $\phi = 0$ and $\phi = \pi/2$ is $\delta x = \pi/2\theta$ so choosing $\theta = \sqrt{\pi}/2$ gives the GKP qubit states.

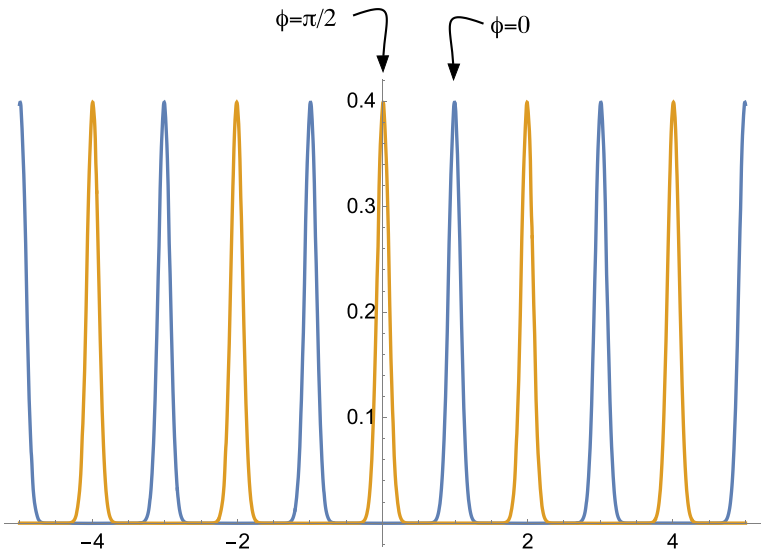

Fig. 15.18 A plot of the conditional probability versus x with $y = 0.1$, $r = 4$, $\theta = \pi/2$

The un-normalised conditional output state, conditioned on the measuremt result y, in the diagonal representation of X is

$$\tilde{\psi}^{(\phi)}(x|y) = \Upsilon(x|y)\psi_{in}(x) \tag{15.87}$$

Normalising the state we see that

$$\psi^{(\phi)}(x|y) = \frac{1}{\sqrt{\mathcal{P}(y)}}\Upsilon(x|y)\psi_{in}(x) \tag{15.88}$$

where

$$\mathcal{P}(y) = \int_{-\infty}^{\infty} dx \ |\Upsilon(x|y)|^2 \ |\psi_{in}(x)|^2 \tag{15.89}$$

is the probability distribution of the measurement outcomes. The mean and variance of this distribution are

$$\mathbb{E}(y) = \ 2r\langle\cos(\theta\hat{X} - \phi)\rangle \tag{15.90}$$

$$\mathbb{V}(y) = \ 1 + 4r^2(\langle\cos^2(\theta\hat{X} - \phi)\rangle - \langle\cos(\theta\hat{X} - \phi)\rangle^2) \tag{15.91}$$

Clearly $\langle\cos^2(\theta\hat{X} - \phi)\rangle \leq 1$ thus

$$\mathbb{V}(y) \leq 1 + 4r^2 \tag{15.92}$$

We now take two special cases $\phi = 0, \pi/2$ and define correspondingly

$$\hat{C} = \cos(\theta\hat{X}) \tag{15.93}$$

$$\hat{S} = \sin(\theta\hat{X}) \tag{15.94}$$

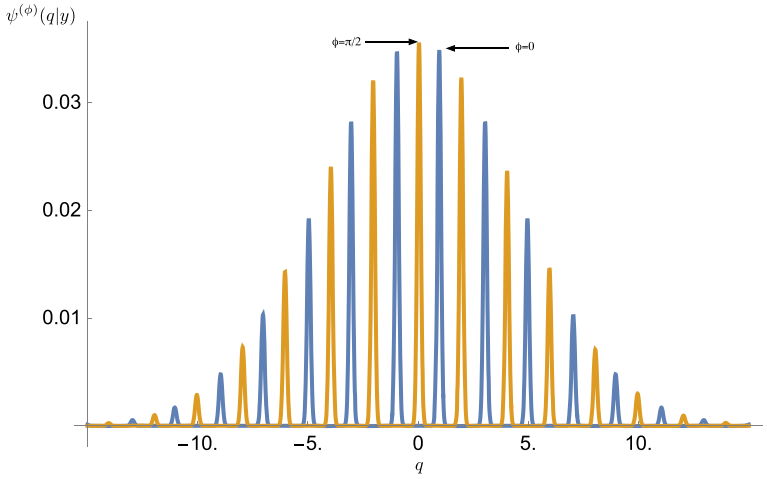

Fig. 15.19 The probability density of the conditional output state with $y = 0.5$, $\sigma = 20$, $\theta = \pi/2$

If we take the input state as a squeezed vacuum state,

$$\langle \hat{C} \rangle = e^{-\sigma\theta^2} \tag{15.95}$$

$$\langle \hat{S} \rangle = 0 \tag{15.96}$$

Thus in the case that $\phi = 0$ we have that

$$\mathbb{E}(y) = 2re^{-\sigma\theta^2} \tag{15.97}$$

Figure 15.19 we plot the position probability density of the output state.

Assuming that we can prepare a GKP encoded qubit, what is required for universal computation? It was shown in the original proposal [22] that if we can implement the unitary transformation

$$U_3(\gamma) = e^{i\gamma\hat{X}^3} = e^{i\gamma(a+a^\dagger)^3} \tag{15.98}$$

then we can implement universal QC using the GKP code. This is called the cubic phase gate.

The cubic phase gate is implicit in the unitary factor of the Krauss operator in (15.85). Expanding the trignometric functions to third order in x and setting $\theta = 0$, we find that

$$\Upsilon(x|y) = (2\pi)^{-1/4} \exp\left[iyr(\theta x - (\theta x)^3/6) - (y - 2r)^2/4\right] \tag{15.99}$$

The phase shift linear in x can be removed with a conditional displacement once y is recorded. The real factor drops out after normalisation as it does not depend on x. Many other approaches have been suggested for the cubic phase gate. A deterministic scheme to implement the cubic phase gate in a single microwave mode was

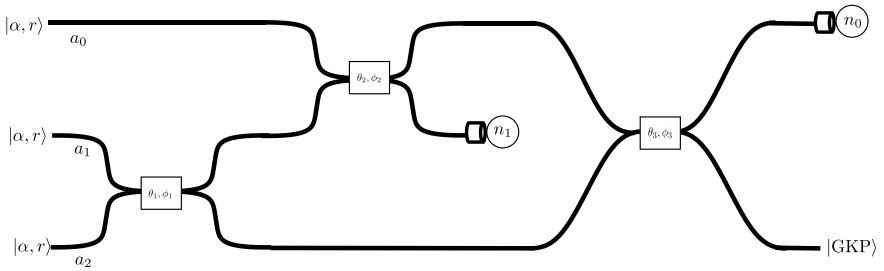

Fig. 15.20 An optical Gaussian Boson Sampling scheme for producing an approximation to a GPK state, conditioned on the correct count string (n_1, n_2). The inputs are single mode displaced squeezed vacuum states

demonstrated at Chalmers University using a non liner inductance and a microwave cavity [24].

15.4.1 GKP via Gaussian Boson Sampling

The qubit codes of GKP can also be generated by adapting the method of Gaussian boson sampling (GBS) [25]. This relies on the ability to prepare single mode squeezed states (with Gaussian probability amplitudes for the quadrature phase operators), entangled by Gaussian unitary transformations (an LOQC network), with number-resolving photon counting for post-selection. This approach was proposed in Bourassa et al. [26]. It can produce cluster states built from GKP states, thereby enabling measurement based QC that is fault tolerant in principle.

An example of this approach is shown in Fig. 15.20. The analysis of this GBS scheme is given in [27]. The heralded output state is a superposition of number states, with bounded total number (n_{max}), followed by a squeezing operation, parametrised by ξ and a displacement, parametrised by d,

$$|\psi\rangle_{out} = D(d)S(\xi)\sum_{n=0}^{n_{max}} c_n|n\rangle. \tag{15.100}$$

By carefully adjusting the parameters of each of the three beamsplitters, the output state can be made a good approximation to a GKP state with a Gaussian envelope for a particular count pattern.

15.5 Cat State Qubits

An early proposal using nondeterministic teleportation gates for cat state codes was given in [28]. Many more schemes have been proposed. Parity cat states are defined as

$$|\pm\rangle = \mathcal{N}_{\pm}(|\alpha\rangle \pm |-\alpha\rangle) \tag{15.101}$$

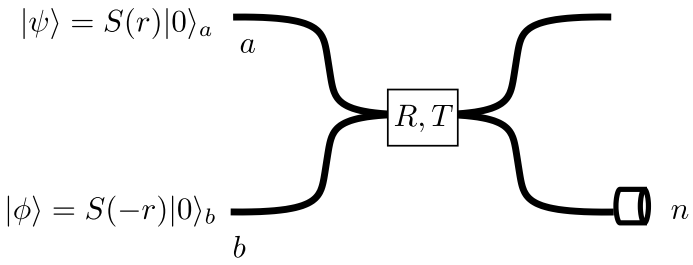

Fig. 15.21 A scheme first suggested by [29] for the non deterministic of cat states using a special two-mode GBS implementation of GBS equivalent to photon subtraction

where the normalisation constant is given by $\mathcal{N}_{\pm}^{-1/2} = \sqrt{2}\left(1 \pm e^{-2|\alpha|^2}\right)$. They are eigenstates of the parity operator $\Pi = e^{-i\pi a^\dagger a}$. The qubit code is then simply $|0\rangle = |+\rangle, |1\rangle = |-\rangle$. Cat states produced nondeterministically can easily be entangled on beamsplitters [28], thus entangling gates are easy. Single qubit gates are more difficult but can be done using weak displacements and teleportation.

Kerr nonlinearities can produce cat states with Poisson statistics. Such nonlinearities can be large in superconducting quantum circuits, but are too small for optical systems. In that case nondeterminsistic (measurement-based) protocols can be used. These only require single-mode squeezed states (a Gasussian resource) and number-resolving detection. This approach is promising for scalability.

An example is shown in Fig. 15.21 which is a variation on a simple two mode GBS scheme. Consider two optical modes with annihilation operators a, b. These are prepared in the product input state

$$|\Psi\rangle_{in} = |\psi\rangle_a \otimes |\phi\rangle_b \tag{15.102}$$

Each mode then interacts via a beam splitter described by the unitary transformation

$$U_{BS}^\dagger(\theta) a U_{BS}^\dagger(\theta) = \sqrt{R}a + \sqrt{T}b \tag{15.103}$$
$$U_{BS}^\dagger(\theta) b U_{BS}^\dagger(\theta) = \sqrt{R}b - \sqrt{T}a \tag{15.104}$$

where $\sqrt{R} = \cos\theta$, $\sqrt{T} = \sin\theta$ so that $R + T = 1$. Thus the joint output state is

$$|\Psi\rangle_{out} = U_{BS}^\dagger(\theta)|\Psi\rangle_{in} \tag{15.105}$$

Using the coherent state resolution of identity this may be written as

$$|\Psi\rangle_{out} = \int \frac{d^2\alpha}{\pi}\frac{d^2\beta}{\pi}\mathcal{A}(\alpha)\mathcal{B}(\beta)\, U_{BS}^\dagger(\theta)|\alpha\rangle_a \otimes |\beta\rangle_b \tag{15.106}$$

where $\mathcal{A}(\alpha) = \langle\alpha|\psi\rangle$ and $\mathcal{B}(\beta) = \langle\beta|\phi\rangle$. As coherent states are not entangled by the beam splitter interaction this becomes

$$|\Psi\rangle_{out} = \int \frac{d^2\alpha}{\pi}\frac{d^2\beta}{\pi}\mathcal{A}(\alpha)\mathcal{B}(\beta)|\sqrt{R}\alpha + \sqrt{T}\beta\rangle_a|\sqrt{R}\beta - \sqrt{T}\alpha\rangle_b \tag{15.107}$$

As the beam splitter transformation does not change phase space volume we can make a change of variable by the rotation,

$$\begin{pmatrix} \tilde{\alpha} \\ \tilde{\beta} \end{pmatrix} = \begin{pmatrix} \sqrt{R} & \sqrt{T} \\ -\sqrt{T} & \sqrt{R} \end{pmatrix} \begin{pmatrix} \alpha \\ \beta \end{pmatrix} \tag{15.108}$$

The output state then becomes

$$|\tilde{\Psi}\rangle_{out} = \int \frac{d^2\alpha}{\pi} \frac{d^2\beta}{\pi} \mathcal{A}(\sqrt{R}\alpha - \sqrt{T}\beta)\mathcal{B}(\sqrt{R}\beta + \sqrt{T}\alpha)\ |\alpha\rangle_a\ |\beta\rangle_b \tag{15.109}$$

where we have dropped the tildes.

Now suppose that the input states are squeezed vacuum states with equal and opposite squeezong

$$|\psi\rangle = S(r)|0\rangle_a \tag{15.110}$$
$$|\phi\rangle = S(-r)|0\rangle_b \tag{15.111}$$

Then

$$\mathcal{A}(\alpha) = \frac{1}{\sqrt{\cosh(r)}} \exp\left[-\frac{1}{2}(|\alpha|^2 + \tanh r\ \alpha^{*\,2})\right] \tag{15.112}$$
$$\mathcal{B}(\alpha) = \frac{1}{\sqrt{\cosh(r)}} \exp\left[-\frac{1}{2}(|\beta|^2 - \tanh r\ \beta^{*\,2})\right] \tag{15.113}$$

In this case we find that

$$\begin{aligned} &\mathcal{A}(\sqrt{R}\alpha - \sqrt{T}\beta)\ \ \mathcal{B}(\sqrt{R}\beta + \sqrt{T}\alpha) \\ &\quad = \exp\left[-\frac{1}{2}(|\alpha|^2 + |\beta|^2) - \frac{1}{2}\tanh r\left(\mu(\alpha^{*\,2} - \beta^{*\,2}) - 4\nu\alpha^*\beta^*\right)\right] \end{aligned} \tag{15.114}$$

with $\mu = R - T$ and $\nu = \sqrt{RT}$.

Suppose we make a measurement of the output photon number on mode-b with result n. The unnormalised conditional state of mode-a is then given by

$$|\tilde{\psi}_n\rangle = \int d^2\alpha\, \mathcal{P}_n(\alpha)|\alpha\rangle \tag{15.115}$$

with

$$\mathcal{P}_n(\alpha) = e^{-|\alpha|^2/2 - \mu \tanh r \alpha^{*\,2}/2} \int d^2\beta\ \frac{\beta^n}{\sqrt{n!}}\ e^{-|\beta|^2 - \frac{\tanh r}{2}\left(\mu\beta^{*\,2} + 4\nu\alpha^*\beta^*\right)} \tag{15.116}$$

The norm of $|\tilde{\psi}_n\rangle$ is the probability P_n to obtain the result n.

The β integral can be done using the generating function for complex Hermite polynomials. We first use

$$e^{-a\beta^2+2b\alpha\beta} = \sum_{m=0}^{\infty} \frac{(\sqrt{a}\beta)^m}{m!} H_m(b\alpha/\sqrt{a}) \tag{15.117}$$

with $a = (\mu/2)\tanh r$ and $b = -\nu \tanh r$. Then use

$$\int d^2\beta e^{-|\beta|^2} \beta^n \beta^{*\,m} = n! \tag{15.118}$$

We thus end up with

$$\int d^2\beta \, \frac{\beta^n}{\sqrt{n!}} \, e^{-|\beta|^2} e^{-a\beta^{*\,2}+2b\alpha^*\beta^*} = \frac{a^{n/2}}{\sqrt{n!}} H_n(b\alpha^*/\sqrt{a}) \tag{15.119}$$

The cat state structure is clearly evident. The unnormalised conditional output state is determined by the amplitude

$$\mathcal{P}_n(\alpha) = \frac{a^{n/2}}{\sqrt{n!}} H_n(b^*/\sqrt{a}) e^{-|\alpha|^2/2-a\alpha^{*\,2}} \tag{15.120}$$

with $a = (\mu/2)\tanh r$ and $b = -\nu\alpha \tanh r$ and $\mu = R - T$. The beamsplitter parameters μ, ν are related by

$$\nu^2 = 1 - \frac{\mu^2}{4} \tag{15.121}$$

In Fig. 15.22 we plot $|\mathcal{P}_n(\alpha)|^2$ in the complex pane for various values of n, μ.

Problems

15.1 Find an array of beam splitters and phase shifters that implements the three-port transformation.

$$\begin{aligned}
a_0 &\to \frac{1}{\sqrt{3}}(a_0 + a_1 + a_2) \\
a_1 &\to \frac{1}{\sqrt{3}}(a_0 + e^{-2\pi i/3} a_1 + e^{2\pi i/3} a_2) \\
a_2 &\to \frac{1}{\sqrt{3}}(a_0 + e^{2\pi i/3} a_1 + e^{-2\pi i/3} a_2)
\end{aligned}$$

15.2 It is not possible to do teleportation with duel rail encoded qubits using linear optics alone however a non deterministic scheme exists can be constructed for single photon states. Prove that the teleportation of the input state $\alpha|0\rangle + \beta|1\rangle$ works 50% of the time provided the total count at the top two detectors is one.

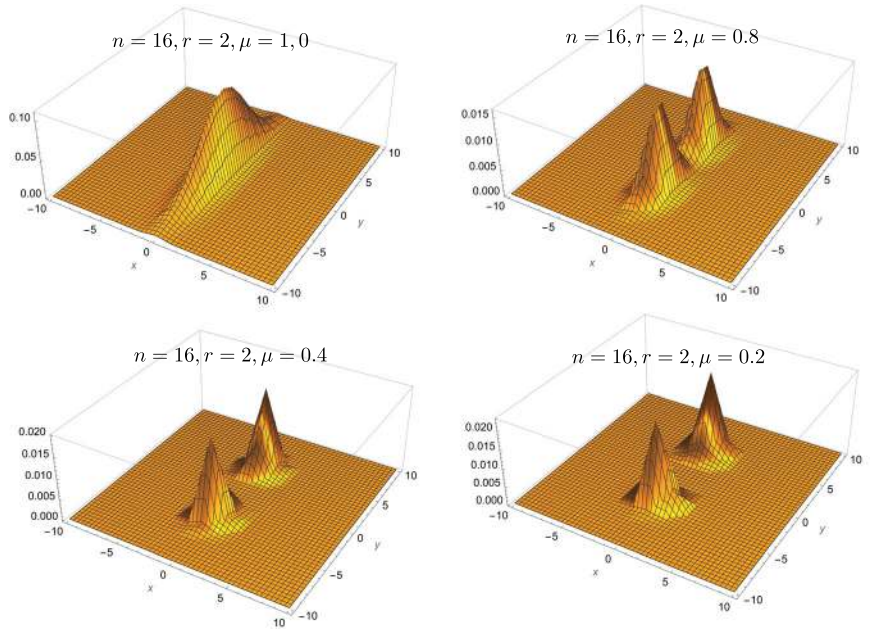

Fig. 15.22 The Q-function amplitudes for the conditional state achieved in Fig. 15.21 with a count of $n = 16$ and decreasing values of μ

15.3 A cluster state is to be created according to the graph shown below.

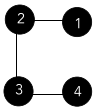

The first step is to prepare all the qubits in the state $|++++\rangle$ by single qubit H gates.

(a) Verify that

$$CZ_{12}CZ_{23}CZ_{34}|++++\rangle = \frac{1}{2}\left(|0+0+\rangle + |0-1-\rangle + |1-0+\rangle + |1+1-\rangle\right)$$

(b) If a z-measurement is made on qubit-1, show that this qubit is removed from the cluster but the rest of the cluster is unchanged. What happens if a z-measurement is made on qubit-2.?

(c) What happens of an x-measurement is made on the second qubit?

15.4 Consider the conditional experiment shown in Fig. 15.5. The fibre coupler implements the unitary transformation

$$\begin{aligned} a_1(\theta) &= \cos\theta a_1 - \sin\theta a_2 \\ a_2(\theta) &= \cos\theta a_2 - \sin\theta a_1 \end{aligned}$$

The conditional state at the output is determined by

$$|\psi'\rangle_s = \frac{1}{\sqrt{p(m)}}\hat{E}(n|m)|\psi\rangle_s$$

and $\hat{E}(n|m) = {}_{anc}\langle m|U(H)|n\rangle_{anc}$ where $n, m \in \{0, 1\}$. Show that

$$\begin{aligned}
\hat{E}(0|0) &= \sum_{n=0}^{\infty} \frac{(\cos\theta - 1)^n}{n!}(a_1^\dagger)^n a_1^n =: \; e^{\ln(\cos\theta)a_1^\dagger a_1} \; : \\
\hat{E}(1|1) &= \cos\theta\,\hat{E}(0|0) - \sin^2\theta a_1^\dagger \hat{E}(0|0)a_1 \\
\hat{E}(0|1) &= -a_1^\dagger \sin\theta\,\hat{E}(0|0) \\
\hat{E}(1|0) &= -\sin\theta\,\hat{E}(0|0)a_1
\end{aligned}$$

15.5 Show that a σ_x measurement on a qubit in a linear cluster combines the neighbouring qubits into a single logical qubit (redundantly encoded).

15.6 Derive (15.120).

References

1. R.P. Feynman, Simulating physics with computers. Int. J. Theor. Phys. **21**, 467 (1982)
2. D. Deutsch, Quantum-theory, the Church-Turing principle and the universal quantum computer. Proc. R. Soc. Lond. A **400**, 97–117 (1985)
3. P.W. Shor, Algorithms for quantum computation: discrete logarithms and factoring, in *Proceedings 35th annual symposium on foundations of computer science* (IEEE, 1994), pp. 124–134
4. E. Knill, R. Laflamme, G.J. Milburn, Nature **409**, 46 (2001)
5. M.A. Nielsen, Phys. Rev. Lett. **93**, 040503 (2004)
6. D.E. Browne, T. Rudolph, Phys. Rev. Lett. **95**, 010501 (2005)
7. S. Aaronson, A. Arkhipov, Theory Comput. **9**, 143 (2013)
8. R. Raussendorf, H.J. Briegel, Phys. Lett. **86**, 5188 (2001); H. Briegel, D. Browne, W. Dür, et al., Nat. Phys. **5**, 19–26 (2009). https://doi.org/10.1038/nphys1157
9. Q.A. Turchette, C.J. Hood, W. Lange, H. Mabuchi, H.J. Kimble, Phys. Rev. Letts. **75**,(1995)
10. K. Nemoto, W.J. Munro, Phys. Rev. Lett. **93**, 250502 (2004)
11. D. Gottesman, I.L. Chuang, Nature **402**, 390–393 (1999)
12. M.A. Nielsen, Phys. Rev. Lett. **93**, 040503 (2004)
13. R. Raussendorf, H.J. Briegel, Phys. Rev. Lett. **86**, 5188 (2001)
14. G.D. Hutchinson, G.J. Milburn, J. Mod. Opt. **51**, 1211–1222 (2004)
15. T.B. Pittman, B.C. Jacobs, J.D. Franson, Phys. Rev. A **64**, 062311 (2001)
16. J.L. O'Brien, G.J. Pryde, A.G. White, T.C. Ralph, D. Branning, Nature **426**, 264 (2003)
17. T.C. Ralph, N.K. Langford, T.B. Bell, A.G. White, Phys. Rev. A **65**, 062324 (2002)
18. D.F.W. James, P.G. Kwiat, W.G. Munro, A.G. White, Phys. Rev. A **64**, 052312 (2001)
19. K. Sanaka, T. Jennewein, J.-W. Pan, K. Resch, A. Zeilinger, Phys. Rev. Lett. **92**, 017902-1 (2004)
20. P. Walther, K.J. Resch, T. Rudolph, E. Schenck, H. Weinfurter, V. Vedral, M. Aspelmeyer, A. Zeilinger, Nature **434**, 169 (2005)
21. S. Lloyd, S.L. Braunstein, Phys. Rev. Lett. **82**, 1784 (1999)

22. D. Gottesman, A. Kitaev, J. Preskill, Phys. Rev. A **64**, 012310 (2001)
23. H.M. Wiseman, G.J. Milburn, *Quantum Measurement and Control* (Springer, 2009)
24. A.M. Eriksson, T. Sépulcre, M. Kervinen et al., Nat. Commun. **15**, 2512 (2024)
25. C.S. Hamilton et al., Phys. Rev. Lett. **119**, 170501 (2017)
26. J.E. Bourassa, R.N. Alexander, M. Vasmer, A. Patil, I. Tzitrin, T. Matsuura, D. Su, B.Q. Baragiola, S. Guha, G. Dauphinais, K.K. Sabapathy, N.C. Menicucci, I. Dhand, Blueprint for a scalable photonic fault-tolerant quantum computer. Quantum **5**, 392 (2021)
27. D. Su, C.R. Myers, K.K. Sabapathy, Phys. Rev. A **100**, 052301 (2019)
28. T.C. Ralph, A. Gilchrist, G.J. Milburn, W.J. Munro, S. Glancy, Quantum computation with optical coherent states. Phys. Rev. A **68**, 042319 (2003)
29. K. Takase, J. Yoshikawa, W. Asavanant, M. Endo, A. Furusawa, Phys. Rev. A **103**, 013710 (2021)

Quantum Optical Sensors

16

Abstract

The development of quantum sensors is a major component of emerging quantum technologies. As our understanding of measurement in quantum mechanics advanced it became clear that there would be new opportunities for quantum sensors that could out perform their classical counterparts. Optical sensors have long been a key sector of the precision sensor industry and quantum optical sensors are a natural extension of this, especially for remote sensing. The recent progress in machine learning has led to a new kind of smart-sensor and these ideas can be readily applied to quantum optical sensors.

16.1 Precision Sensing

Precision sensors are ubiquitous in modern technology. A sensor is a device that enables us to detect changes in one or more parameters in a physical process. The output signal is a result of some physical measurement, eg a voltage, a photo-current or a homodyne signal. The sensitivity of the sensor will determine how small a change in the parameter of interest can be detected in the measurement signal and this will depend on the noise added by the measurement process as well as intrinsic background noise sources, typically thermal.

In Fig. 16.1 we give an example of an optical accelerometer based on a Michelson interferometer. The parameter of interest is an acceleration in the horizontal direction. What is measured is the displacement of the proof mass due to this acceleration. The optical measurement scheme seeks to detect the change in the relative arm length and estimate the acceleration. We can treat the proof mass as a mirror with a linear restoring force in the horizontal direction. The spring constant is k and the mass is m_0. Let the displacement from equilibrium be x and thus the change in the relative path length for the interferometer is also x. The effect of the acceleration is to apply a time-dependent force $f(t) = m_0 a(t)$ to the oscillator. For simplicity, we will assume that the oscillator is heavily damped with damping rate η and that the temperature

D. F. Walls and G. J. Milburn, *Quantum Optics*, Graduate Texts in Physics,
https://doi.org/10.1007/978-3-031-84177-4_16

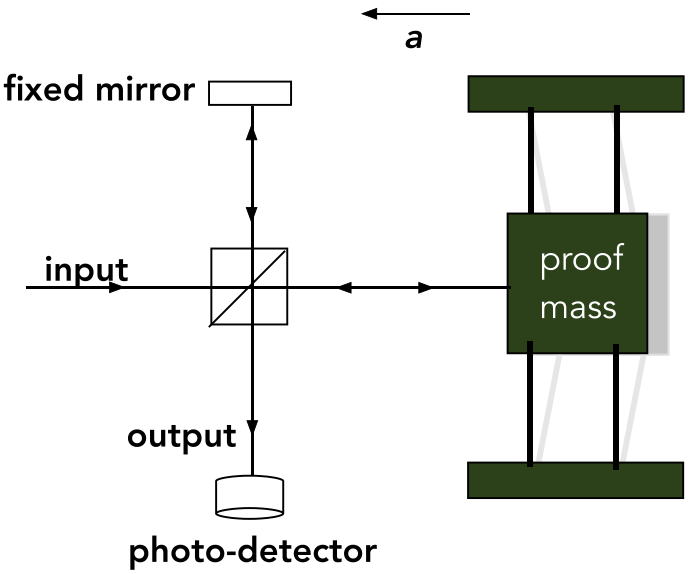

Fig. 16.1 A simple Michelson interferometer for an optical sensor for inertial acceleration

of the environment is T. In the classical case, the displacement obeys the classical Smolochowski process with stochastic differential equation [1]

$$dx = -\frac{\omega_0^2}{\gamma} x dt + (a/\gamma) dt + \sigma dW \tag{16.1}$$

where the fluctuation-dissipation theorem requires that $\sigma^2 = 2k_B T\gamma$. The stationary solution for the displacement is

$$\mathrm{P}(x|a) = e^{-(x-a/\omega_0^2)^2/2\Delta} \tag{16.2}$$

The mean and variance of the displacement is

$$\bar{x} = \frac{a}{\omega_0^2}, \quad \Delta = \frac{k_B T}{m_0 \omega_0^2} \tag{16.3}$$

This suggests that in order to estimate a we need to measure the displacement and form the empirical average

$$a_{est} = \omega_0^2 \frac{1}{N} \sum_{n=1}^{N} x_n \tag{16.4}$$

The deviation of the estimate from the parameter is $\delta a = a_{est} - a$. The precision of the estimation is the second moment of δa. This is bounded below by the Cramer-Rao lower bound [2]

$$\mathbb{E}[(\delta a)^2] \geq \frac{1}{NF(a)} \tag{16.5}$$

where $F(a)$ is the Fisher information defined by

$$F(a) \equiv \int dx \frac{1}{P(x|a)} \left(\frac{\partial P(x|a)}{\partial a} \right)^2 \tag{16.6}$$

In this case $F(a) = \Delta$ so the precision is bounded by

$$\mathbb{E}[(\delta a)^2] \geq \frac{k_B T}{N m_0 \omega_0^2} \tag{16.7}$$

This scheme constitutes a linear sensor as $\bar{x} \propto a$. The estimate can be improved by lowering the temperature, or increasing the mass or increasing the oscillator frequency. As we lower the temperature and increase the frequency we will need a quantum description of overdamped motion when $\hbar\omega_0 > k_B T$. We will not pursue this here. In stead we will consider a quantum optical version of this sensor after we have formulated the quantum parameter estimation problem.

16.1.1 Optical Accelerometer

It is straightforward to model the quantum limits to the accelerometer depicted in Fig. 16.1. To simplify the explanation we reconfigure the scheme so as to look like a Fabry-Perot interferometer, see Fig. 16.2. In this case the input-output methods in Chap. 6 give

$$a_{out}(\omega) = \frac{\frac{\kappa}{2} + i(\omega - \delta)}{\frac{\kappa}{2} - i(\omega - \delta)} a_{in}(\omega) \ . \tag{16.8}$$

where $\delta = \omega_c x/L$ where L is the length of the cavity and x is the displacement of the mirror from an exact cavity resonance. A coherent pulse at the cavity resonance $\omega = 0$ with amplitude α_0 experiences the phase shift $\phi(\delta)$ where

$$\tan(\phi(\delta)) = \frac{\kappa\delta}{\gamma^2/4 - \delta^2} \tag{16.9}$$

Integrating the quadrature-phase homodyne current current over a measurement time T gives a random variable is (see (7.64)),

$$z = \kappa T \alpha_0 \sin(\phi(\delta)) \approx \frac{4\alpha_0 \omega_c T}{L} x + \sqrt{\kappa} \int_0^T dW(t) \tag{16.10}$$

for small displacements. The mean signal is thus linear in the acceleration and we define the signal as $\mathbb{E}[z] = gTa$ where the gain is

$$g = \frac{4\alpha_0 \omega_c}{\omega_0^2 L} \tag{16.11}$$

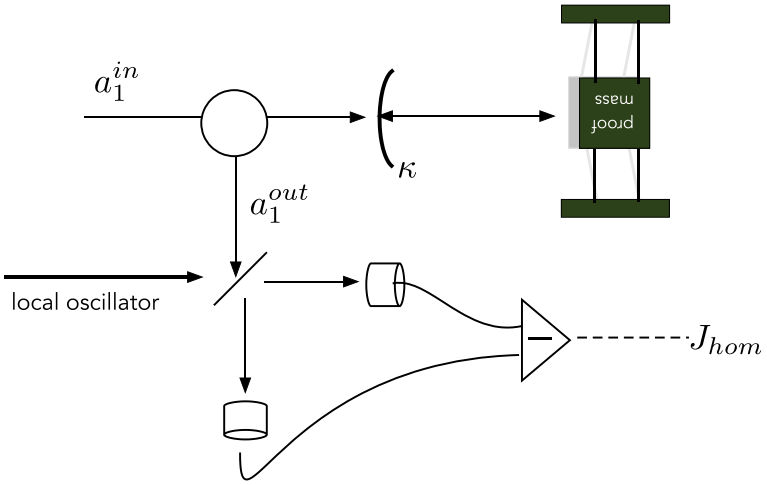

Fig. 16.2 xxx

The variance in z is $\mathbb{V}[z] = \kappa T$. The square of the signal-to-noise ratio is

$$SNR^2 = \frac{g^2 a^2 T}{\kappa} \tag{16.12}$$

In order for this to be greater than one, we need

$$a_{min} > \frac{\sqrt{\kappa}}{g\sqrt{T}} \tag{16.13}$$

As g^2 is proportional to the input power, we can make this small by using a more powerful laser input. As we will see in Sect. 16.6, there is a another limit that sets in while increasing the laser power. We can also make the sensor more sensitive by increasing the integration time, at the expense of making it slower.

16.2 Quantum Parameter Estimation

The general quantum parameter estimation, for a sequential scenario, is sketched in Fig. 16.3 An initial state, ρ_i, undergoes a dynamical transformation that depends on some real parameter θ to produce an output state $\rho_o(\theta)$. A measurement is made of some observable, described by a POVM $\hat{P}(\xi)$. After N repetitions, the sequence of outcomes is used to form an estimate $\tilde{\theta}$ of the parameter θ. The probability distribution of outcomes, conditioned on the parameter θ is

$$P(\xi|\theta) = \text{tr}[\hat{P}(\xi)\rho_o(\theta)] \tag{16.14}$$

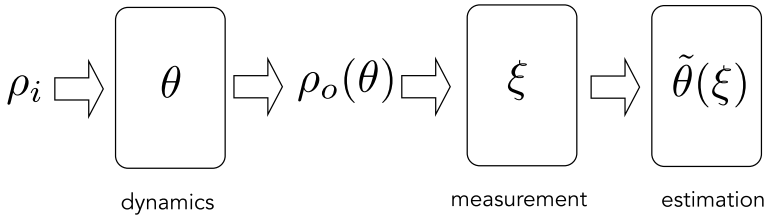

Fig. 16.3 A sequential scheme of parameter estimation

The estimate of the parameter is a function of the measurement results $\tilde{\theta} = \tilde{\theta}(\xi_1, \xi_2, \ldots, \xi_N)$, for example, the empirical mean

$$\tilde{\theta} = \frac{1}{N} \sum_{k=1}^{N} \xi_k \tag{16.15}$$

We form the deviation as

$$\delta\theta = \lambda\tilde{\theta} - \theta \tag{16.16}$$

where

$$\lambda^{-1} = \frac{d\tilde{\theta}}{d\theta} \tag{16.17}$$

removes the local difference in the "units" of the estimator and the parameter.

The quantum Cramer Rao lower bound is obtained by a further optimisation over all POVMs [2]

$$\mathbb{E}[\delta\theta^2] \geq \frac{1}{N(ds/d\theta)^2} \tag{16.18}$$

where the statistical distance is defined by

$$(ds/d\theta)^2 = \mathrm{tr}[\rho' \mathcal{L}_\rho(\rho')] \tag{16.19}$$

and $\rho = \rho_o(\theta),\ \rho' = \frac{d}{d\theta}\rho_o(\theta)$. The super-operator $\mathcal{L}_\rho$, in the basis that diagonalizes ρ , takes the form

$$\mathcal{L}_\rho(\hat{A}) = \sum_{\{j,k|p_j+p_k\neq 0\}} \frac{2}{p_j + p_k} A_{jk} |j\rangle\langle k| \tag{16.20}$$

and $A_{jk} = \langle j|\hat{A}|k\rangle$.

16.2.1 Single Parameter Unitary Transformations

As a simple example, suppose we want to estimate how much coordinate time has elapsed by making measurements of an arbitrary observable on the unitarily evolved state

$$\rho_o(T) = e^{-i\hat{H}T/\hbar}\rho_i e^{i\hat{H}T/\hbar} \tag{16.21}$$

where $\hat{H}$ is the system Hamiltonian. The quantum Cramer-Rao (QCR) bound gives

$$\mathbb{E}[\delta T^2] \geq \frac{\hbar^2}{N\langle \Delta\hat{H}^2\rangle_i} \tag{16.22}$$

where

$$\langle \Delta\hat{H}^2\rangle_i = \mathrm{tr}[\rho_i(\Delta\hat{H})^2] \tag{16.23}$$

with $\Delta\hat{H} = \hat{H} - \langle\hat{H}\rangle$. We see that we need to use an input state with as large a variance in the energy as possible.

It is important to note that the QCR bound does not tell us what POVM to use to saturate the bound. It might in fact be a very difficult measurement to make. For example, suppose the system is a single mode cavity field, $\hat{H} = \hbar\omega a^\dagger a$. Consider an input squeezed vacuum state $|r\rangle$ (see Sect. 1.4). The variance in the energy is

$$\langle r|(\Delta\hat{H})^2|r\rangle = \frac{1}{2}\hbar^2\omega^2\bar{n}(\bar{n}+1) \tag{16.24}$$

where $\bar{n} = \sinh^2 r$. This suggests that we need $\bar{n} \gg 1$. In other words, we need initial states of very high average energy. This is a general feature of estimating elapsed local time.

What measurements should we actually make? There is no point in photon counting as it is insensitive to this transformation. Homdyne detection would require knowing the parameter in order to choose the correct quadrature phase. It turns out that the Susskind-Glogower POVM in Sect. 1.6 is optimal but of course is unphysical. In fact it is generally the case that choosing a POVM that commutes with the operator canonically conjugate to the generator of unitary transformations is always best.

16.2.2 Single Parameter Non-unitary Transformations

Consider the one parameter non unitary operation defined as

$$\rho_o(\theta) = \sum_k \Upsilon_k(\theta)\rho_i\Upsilon_k^\dagger(\theta) \tag{16.25}$$

An example is given in in Sect. 7.1.

$$\hat{\Upsilon}(n|\theta) = \frac{1}{\sqrt{n!}}(1-e^{-\theta})^{n/2}e^{-\theta a^\dagger a/2}a^n \tag{16.26}$$

where the sum is $n = 0, 1, 2, \ldots$. which describes a photon loss process where the probability to absorb a photon is $1 - e^{-\theta}$. It is easy to se that

$$\frac{d\rho(\theta)}{d\theta} = a\rho(\theta)a^\dagger - \frac{1}{2}(a^\dagger a\rho(\theta) + \rho(\theta)a^\dagger a) \tag{16.27}$$

The rate of change of statistical distance is

$$\left(\frac{ds}{d\theta}\right)^2 = \mathrm{tr}[a\rho a^\dagger \mathcal{L}_\rho(a\rho a^\dagger)] - 2\langle a^{\dagger\,2}a^2\rangle + \langle (a^\dagger a)^2\rangle \tag{16.28}$$

If we start in a coherent state $|\alpha_0\rangle$ solution to (16.27) is $\rho(\theta)=|\alpha_0 e^{-\theta/2}\rangle\langle\alpha_0 e^{-\theta/2}|$. As this is a pure state it has only a single unit eigenvalue. We find that

$$\left(\frac{ds}{d\theta}\right)^2 = |\alpha_0|^2 e^{-\theta} \tag{16.29}$$

The parameter uncertainty bound is then

$$\mathbb{E}[\delta\theta^2] \geq \frac{e^\theta}{Nn_0} \tag{16.30}$$

where $n_0 = |\alpha_0|^2$ is the initial mean photon number. If all photons are lost $\theta \to \infty$ and it is impossible to estimate θ.

16.3 Kinetic Uncertainty Relations

In many quantum optics experiments, the measurement record is a stochastic process for example a homodyne photo-current $J(t)$, (see Sect. 7.3). The source of the light could be controlled by a parameter that we need to estimate. For example, the detuning of a laser drive from an intra-cavity dipole emitter could be estimated using homodyne detection of the emitted light. In this case we could integrate the measurement current over a time T to get a random variable $x(T)$ the statistics of which can be used to infer the relevant parameter using the QCR bound [3]. In this case the bound will need to reflect irreversible dynamics of the cavity.

As an example we consider the case of a coherently driven single mode cavity with damping rate κ containing a two level system (see Fig. 16.4). The question we ask is: is there a universal bound for parameter estimatoin in this case regardless of what integrated current we choose?

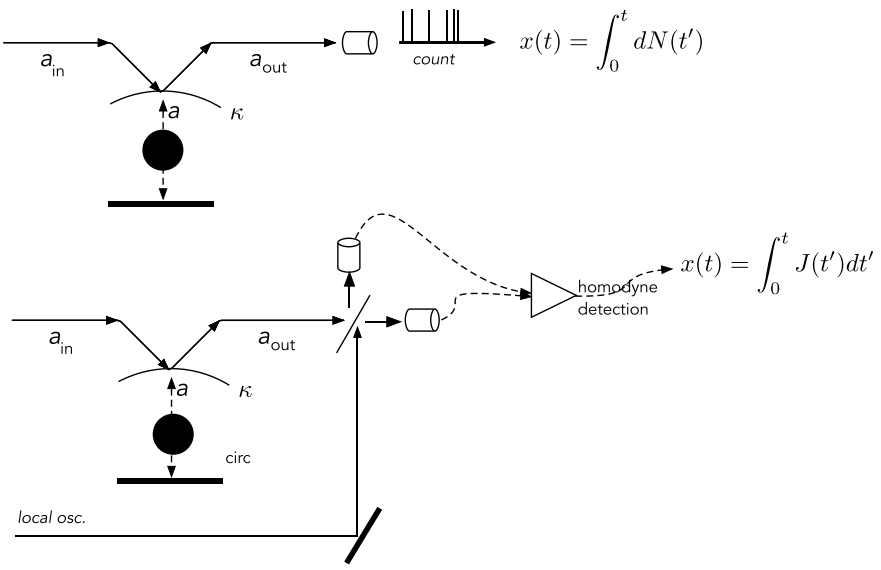

Fig. 16.4 A driven cavity containing a single two level atom emits a field into the environment. This may be subject to photon counting or homodyne detection. In both case we wish to infer some parameter of the irreversible dynamics from the integrated photo current or homodyne currrent that produces a random variable $x(t)$

This problem was first posed in a quantum optical setting by Gammelmark and Molmer [3]. It also arises in the study of stochastic thermodynamics where the answer is given in terms of entropy production [4]. Not surprisingly it can be formulated in terms of the Fisher information associated with the statistics of $x(t)$.

Hasegawa [4] showed that under physically realistic assumptions

$$\frac{\mathbb{V}[x]}{\mathbb{E}[x]^2} \geq \frac{\mu}{T(K+Q)} \tag{16.31}$$

where T is the integration time and $\mu = 1$ for integrating a photon counting measurement and $\mu = 1/4$ for a integrating a homodyne current. Here K arises purely from classical stochastic processes, for example, decay of photons into the environment, while Q captures quantum coherence terms and arises from the Hamiltonian part of the dynamics. These quantities are determined entirely by the master equation that describes the source of the measurement current. We will refer to K, Q as the classical and quantum activation respectively.

As an example we consider the interaction picture master equation describing the a two-level atom in a highly damped cavity and driven cavity (see Sect. 9.2),

$$\frac{d\rho}{dt} = -i\frac{\Delta}{2}[\sigma_z, \rho] - i\Omega[\sigma_+ + \sigma_-, \rho] + \gamma\mathcal{D}[\sigma_-]\rho \tag{16.32}$$

where Ω is the Rabi frequency, the detuning is $\Delta = \omega_a - \omega_L$ and ω_L is the carrier frequency of the driving field and ω_a is the atomic transition frequency. In this case

$K = \gamma\, p_{e,ss}$ where $p_{e,ss}$ is the steady state probability to find the atom in the excited state. The classical and quantum activation are then given by

$$K = \frac{4\gamma\Omega^2}{4\Delta^2 + \gamma^2 + 8\Omega^2} \tag{16.33}$$

$$Q = \frac{128\Omega^4\left[4\Delta^4 + \Delta^2(\gamma^2 + 32\Omega^2) + (\gamma^2 + 4\Omega^2)^2\right]}{\gamma(4\Delta^2 + \gamma^2 + 4\Omega^2)} \tag{16.34}$$

Hasegawa also proved an important connection to the field of stochastic thermodynamics. This relates the bound in (16.31) to the entropy production Σ in the steady state,

$$\frac{\mathbb{V}[x]}{\mathbb{E}[x]^2} \geq \frac{2\mu}{T\Sigma} \tag{16.35}$$

We thus see that decreasing the lower bound is achieved by making the entropy production rate in the environment as large as possible. We will consider how this works in the case of clock design in the next section.

16.4 Quantum Optical Clocks

Form the perspective of quantum optics, a clock is a quantum sensor to estimate a period or frequency of a periodic process that is as precise as possible. This task can be related to the kinetic uncertainty relation discussed in the previous section. In the case of a clock the sensor is typically a counter for some sustained temporal process. The process itself can be quite varied but for an autonomous periodic clock it is often a dissipative dynamical structure known as a limit cycle [5]. Microwave generators achieve this using a DC drive to a circuit with negative differential resistance over some voltage range. This is a form of amplification that leads to a limit cycle formation in which a dissipative nonlinear system undergoes a Hopf bifurcation to a one dimensional attractor.

As we saw in Chap. 10, a good example is a laser which exhibits a fixed point to limit cycle bifurcation in a semi-classical description of its dynamics (see (10.23)). The laser is an autonomous clock in that it can reach a non-thermal equilibrium steady state due to a population inversion maintained by two thermal baths at different temperature. Above threshold, the laser exhibits phase diffusion due entirely to quantum noise. This ultimately limits its precision as a clock, although in a real artefact many technical noise sources are likely to limit its performance. The laser exhibits another important aspect of a quantum clock: the nature of the measurement is important. There is no point counting photon emission from a laser. To use it as a clock you need to make a phase-dependent measurement such as homodyne detection or a Ramsey fringe interferemetor.

The laser phase diffusion rate decreases as the mean photon number in the cavity increases (see (10.33)). This is a generic feature of all limit cycle clocks and leads

to fluctuations in the period of the extracted clock signal and a Lorentzian line shape for the power noise spectrum. We will consider the statistics of the period first.

The period is the time taken for a monitored oscillatory variable to change its phase by 2π. Fluctuations in phase of the oscillation mean it sometimes gets to 2π a bit too early or a bit too late. This is a first passage time problem: what is the probability distribution for the time T taken for the phase to first reach 2π starting from a zero point. In the case of a limit cycle, the resulting distribution in periods is given by the Wald distribution (see Chap. 10).

In the case of clocks built from limit -cycle dynamics, this is given by [6],

$$W(T,\alpha,\lambda) = \sqrt{\frac{\lambda}{2\pi}} T^{-3/2} \exp\left[-\frac{\lambda}{2\alpha^2 T}(T-\alpha)^2\right] \qquad t \geq 0.$$

where α, λ are positive real parameters (λ is called the spread parameter). The mean and variance are

$$\mathbb{E}[T] = \alpha, \qquad \mathbb{V}[T] = \frac{\alpha^3}{\lambda} \tag{16.36}$$

In the case of a laser $\alpha = \frac{2\pi}{\omega_c}$, where ω_c is the laser cavity frequency, and $\lambda = \pi^2/\Gamma$, where Γ is related to the mean photon number in the cavity $\bar{n}$ and the gain G as $\Gamma = G/(8\bar{n})$.

We define a clock quality N as the square of the signal-to-noise ratio.

$$N = \frac{\mathbb{E}[T]^2}{\mathbb{V}[T]^2} = \lambda/\alpha \tag{16.37}$$

A good clock is one for which $\lambda \gg \alpha$. In the case of a laser

$$N = \frac{\pi\omega}{2\Gamma} \tag{16.38}$$

We now turn to the noise power spectrum. The phase variable on the limit cycle is defined in terms of the complex amplitude of the laser cavity field $\alpha(t) = r_0 e^{i\phi(t)}$ where

$$d\phi = -i\omega dt + \frac{\sigma}{r_0} dW \tag{16.39}$$

where ω is the frequency on the limit cycle and σ^2 is the variance in the noise. For a thermal clock $\sigma^2 \propto k_B T$. In the case of a quantum clock this is not the case, for example, in a laser $r_0 = \sqrt{\bar{n}}$ and $\sigma^2 = G/2$. The Ito stochastic differential equation for $\alpha(t)$ is the Kubo oscillator (See [7] p. 104).

$$d\alpha = i\alpha(t)d\theta(t) = i(\omega dt + \frac{\sigma}{r_0} dW)\alpha(t) \tag{16.40}$$

The stationary two-time correlation function for heterodyne detection is given by

$$\mathbb{E}[\alpha^*(0)\alpha(\tau)] = e^{i\omega t - \frac{\sigma^2}{2r_0^2}|\tau|} \tag{16.41}$$

The noise power spectrum is the Fourier transform of this

$$P(\Omega) = \frac{r_0^2}{\pi} \frac{\gamma}{\gamma^2 + (\omega - \Omega)^2} \tag{16.42}$$

where the line width is

$$\gamma = \frac{\sigma^2}{4r_0^2} \tag{16.43}$$

a Lorentzian. In the case of a laser $\gamma = G/(8\bar{n})$.

16.4.1 FPT Uncertainty Relation

Various authors [8] have shown that the quantity, N satisfies an uncertainly relation closely related to a KUR,

$$N \leq \mathbb{E}[T](K + Q) \tag{16.44}$$

when the clock signal is derived from measurements made on the field emitted by a source that obeys a Markov master equation. As a simple example we consider a clock made up of photon emissions from the cavity in Fig. 16.4, in the bad cavity limit, and thermally driven. The two-level atom that obeys the master equation, (9.40),

$$\dot{\rho} = -\frac{i\omega_a}{2\hbar}[\sigma_z, \rho] + \gamma(\bar{n} + 1)\mathcal{D}[\sigma_-]\rho + \gamma\bar{n}\mathcal{D}[\sigma_+]\rho \tag{16.45}$$

where γ is the spontaneous emission rate and $\bar{n}$ is the mean thermal occupation of the cavity at the atom resonance frequency. In the eigenstates of the atomic energies this is a two state markov stochastic process,

$$\dot{p_g} = \nu p_e - \mu + p_g = -\dot{p_e} \tag{16.46}$$

where $\nu = \gamma(\bar{n} + 1)$, $\mu = \gamma\bar{n}$ are the transition rates from $e \to g$ and $g \to e$ respectively. When the atom makes a transition from one falling edge to the next a photon is emitted and we regard each of these as a 'tick' of the clock. The distributions of the period T defined this way is given by

$$P(T) = \frac{\mu\nu}{\nu - \mu}(e^{-\mu T} - e^{-\nu T}) \tag{16.47}$$

In the high temperature limit $\nu \to \mu$, this becomes

$$P(T) = \mu^2 T e^{-\mu T}. \tag{16.48}$$

The mean and variance of this distribution are

$$\mathbb{E}[T] = \frac{2}{\mu}, \quad \mathbb{V}[T] = \frac{2}{\mu^2}. \tag{16.49}$$

Thus $N = 2$ for this aperiodic clock. In this case $K = \mu$, $Q = 0$ and the FPT bound is saturated.

A more interesting case was studied experimentally in [9]. A driven superconducting transmon two-level system in a coplanar microwave cavity was described by the master equation

$$\frac{d\rho}{dt} = -i[\Omega\sigma_x + \Delta\sigma_z, \rho] + \Gamma D[\sigma_z]\rho = L\rho, \tag{16.50}$$

where Ω is the Rabi frequency, Δ is the Stark shift, Γ is the dephasing rate determined entirely by the σ_z-QND measurement back action. In the experiment, spontaneous emission of the transmon qubit was negligible. Given that this model is only subject to dephasing, it is easy to show that the steady state is just the maximally mixed state $\rho_{ss} = \frac{I}{2}$. There are two types of dynamics; underdamped, $\Gamma < 2\Omega$, which exhibits oscillations and over-damped, $\Gamma > 2\Omega$ with a monotonic approach to the steady state.

We will suppose that the system is being continuously measured via Homodyne detection and is described by the stochastic master equation

$$d\rho_J = -i[\Omega\sigma_x + \Delta\sigma_z, \rho_J]dt + \Gamma D[\sigma_z]\rho_J dt + \sqrt{\Gamma}(\sigma_z\rho_J + \rho_J\sigma_z - 2\mathrm{tr}[\sigma_z\rho_J])dW, \tag{16.51}$$

where dW is a Weiner process, and the index J indicates that we are conditioning on the Homodyne current

$$J(t)dt = 2\sqrt{\Gamma}\mathrm{tr}[\sigma_z\rho_J]dt + dW. \tag{16.52}$$

This problem was discussed in Sect. 11.2.1 and we use that model to illustrate the role of FPT uncertainty relations for understanding precision. As defined by He et al. [9], the precision of the clock can be measured by the signal-to-noise ratio (SNR) in the first passage time for the clock to undergo a tick and tock. This corresponds to the time it takes for the system to traverse a longitudinal angle of $\theta = 2\pi$, which we will denote as τ. Thus the quality of the clock is measured as

$$N = \frac{\mathbb{E}[\tau]^2}{\mathrm{Var}[\tau]}. \tag{16.53}$$

If we ignore the multiplicative noise term in the conditional dynamics, the statistics follows a Wald distribution in the underdamped oscillatory regime ($\Gamma < 2\Omega$),

$$P(\tau) = \sqrt{\frac{\pi}{\Gamma\tau^3}}\exp\left(-\frac{(2\pi - 2\Omega\tau)^2}{4\Gamma\tau}\right), \tag{16.54}$$

with mean and variance given as:

$$\mathbb{E}[\tau] = \frac{\pi}{\Omega}, \quad \mathrm{Var}[\tau] = \frac{\pi\Gamma}{2\Omega^3}. \tag{16.55}$$

Thus $N = 2\pi\left(\frac{\Omega}{\Gamma}\right)$. A direct simulation of the stochastic differential equations indicates that this is a good approximation when Γ is very small.

The FPT uncertainty relation [8] gives, $N \leq (K + Q)$, where

$$K = \Gamma\,, \qquad Q = \frac{4\Omega^2}{\Gamma}\,, \tag{16.56}$$

Not surprisingly, for a good clock we need $\Omega \gg \Gamma$.

In the quantum jump regime we define one period to be the time from one downward transition to the next. The Markov transition rate, μ, can be used to calculate a FPT distribution:

$$P(T) = \mu^2 T e^{-\mu T}\,, \tag{16.57}$$

where the transition rate is $\mu = \Gamma\Omega^2/(\Gamma^2 + \Delta^2)$ Then

$$\mathrm{E}[T] = \frac{2}{\mu}, \quad \mathrm{Var}[T] = \frac{2}{\mu^2}, \quad N = 2\,. \tag{16.58}$$

This is the expected result for a Markov process clock. This system enables us to move from an oscillatory clock, when the measurement dephasing is weak, to a quantum jump clock for which the measurement dephasing is very large. Changing the measurement process changes the nature of a quantum clock.

16.5 Non Linear Quantum Sensors via Machine Learning

Many sensors operate with linear response for which the measured variable is proportional to the parameter to be estimated. The rise of machine learning has led to the concept of a smart sensor [10] that moves beyond this. More broadly, machine learning is impacting many areas of quantum technology [11].

We will discuss a machine learning enhancement for single photon scanning of a phase image [12]. A phase image encodes the data in the spatial distribution of phase changes in an optical wave after reflection. In the single photon case, the phase changes lead to an intensity modulation of the reflected pulse. Using a time resolved Raman single photon detector (see Sect. 14.2) a control pulse can be optimised using a machine learning to extract the spatially dependent parameters encoding the image. As an example, will assume that these are the detuning from the pulse carrier frequency and the line-width of a reflecting optical cavity. Single photon pulses, as opposed to weak coherent pulses, offer a number of advantages.

The scheme is depicted in Fig. 16.5. A single photon Raman pulse produces a sequence of identical single photon pulse with temporal function $\nu(t)$. The reflected single photon pulse has a different temporal function $\xi(\mathbf{f}_T, t)$ that depend on the true parameters $\mathbf{f}_T = (\kappa, \Delta)$ of the cavity currently under scan. The reflected pulses arrive back at a Raman single photon detector controlled by a classical coherent pulse with temporal shape $\mu(\mathbf{f}, t)$. The error channel is a reflection from this detector and a machine leaning algorithm changes the parameters $\mathbf{f}$ until the error is minimised.

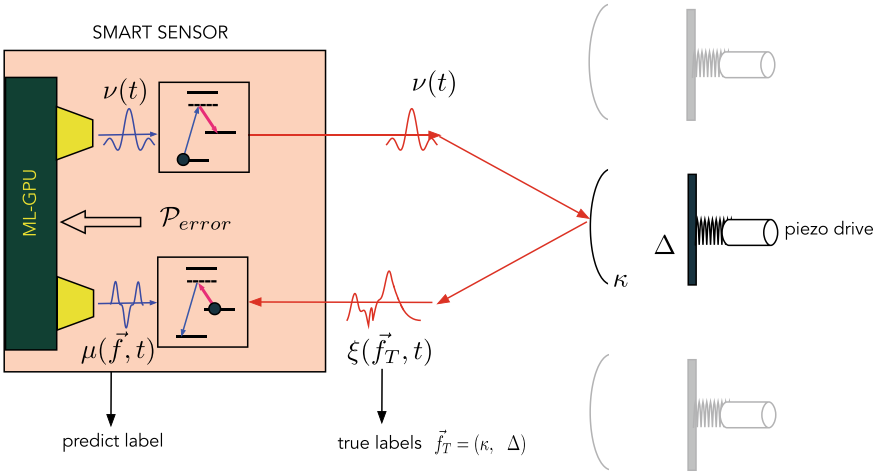

Fig. 16.5 A sequence of identical single photo pulses are reflected from an array of single-sided cavities, with a spatially varying piezo-modulation of the detuning from the carrier frequency. The image is encoded in the detuning Δ and the line-width κ of each cavity. These change the temporal response of each cavity distorting the intensity of the single photon pulse upon reflection.A machine learning scheme based on Raman single photon detectors can estimate the parameters κ, Δ for each cavity

When this is reached the energy loss due to photo reflection is minimised. The overall detector has learned the true parameters with a low probability of error.

In analysing this scheme is important to include thermal effects in both the detectors and the optical fields. The error probability is given by [12]

$$P_e^{(Q)}(t) = \frac{1+\bar{n}}{1+2\bar{n}} - \frac{4\eta\Gamma}{\kappa_d}\tanh\left(\frac{\hbar\omega_d/k_BT}{2}\right), \tag{16.59}$$

where $\Gamma = \left|\int dt'\mu^*(\mathbf{f},t')\xi(\mathbf{f}_T,t')\right|^2$ and we have included the superscript (Q) to distinguish this scheme from an equivalent classical scheme discussed below. The parameter ω_d is the frequency of the Raman transition in the detector, κ_d is the response rate of the detector, and T is the ambient temperature and $\bar{n}$ is the average number of thermal photons in the background field. At very low temperature the error probability tends to $P_e^{(Q)}(t) = 1 - \frac{4\eta\Gamma}{\kappa}$ and is minimised when Γ is a maximum. This will occur when $\mathbf{f} = \mathbf{f}_T$.

An equivalent classical scheme would use coherent state pulses with on average $\alpha|^2$ photons per pulse. The error probability in this case is

$$P_e^{(C)}(t) = \frac{1+\bar{n}}{1+2\bar{n}} - \frac{4\eta\Gamma}{\kappa_d}e^{-4\eta\Gamma/\kappa_d}\tanh\left(\frac{\hbar\omega_d/k_BT}{2}\right), \tag{16.60}$$

In Fig. 16.6 we compare the quantum and the classical protocols in terms of the normalised parameter difference $|\mathbf{f}-\mathbf{f}_T|_N$, defined as a function of iterations i in

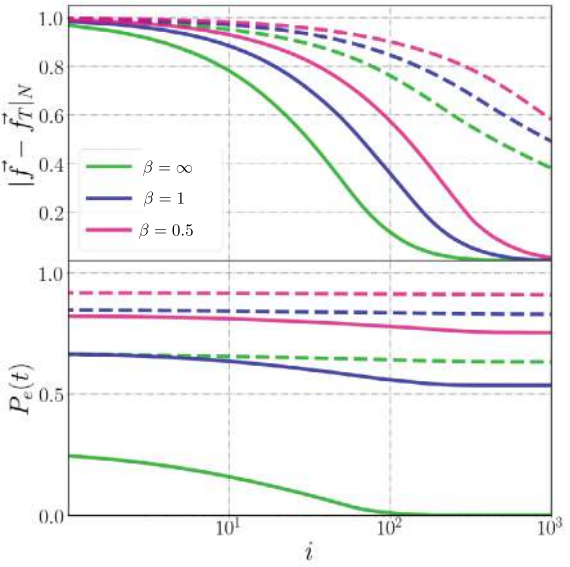

Fig. 16.6 Top: The normalized parameter difference—each parameter is dimensionless between 0 and 1—of the agent's prediction and observation, $|\mathbf{f} - \mathbf{f}_T|_N$, defined as a function of iterations i. The quantum agent (solid lines) outperforms the classical agent (dashed lines) at all temperatures, excluding the infinite temperature limit $\mu_\sigma \to 0$. Bottom: The probability of measuring an error in the incoming pulse $\xi(\mathbf{f}_T, t)$. Here $\beta = \frac{\hbar\omega_d}{2k_B T}$

the learning algorithm and the error probability also as a function of the number of iterations.

16.6 LIGO

Arguably, the largest quantum sensor existing today is LIGO (laser interferometer gravitational observatory) [13]. It consists of a Michelson-Morley interferometer, with a Fabry-Perot cavity in each arm to 'store' light, See Fig. 16.7. Each mirror is suspended and subject to a linear restoring potential. Caves [14] suggested in 1981 that squeezed light might be used to achieve better sensitivity in the interferometric detection of gravitational radiation. The result of Caves indicated that while squeezed light would not increase the maximum sensitivity of the device, it would enable maximum sensitivity to be achieved at lower laser power. Later analyses [18] demonstrated that by an optimum choice of the phase of the squeezing it is possible to increase the maximum sensitivity of the interferometer. This result was established by a full nonlinear quantum theory of the entire interferometer, including the action of the light pressure on the end mirrors. We shall demonstrate this following the treatment of Pace et al. [18].

A gravitational wave induces weak tidal forces, in a plane perpendicular to the direction of propagation. A gravitational wave passing normal to a circular arrangement of masses would periodically force the circle into an ellipse. In the case of the interferometer depicted in Fig. 16.7, the end mirrors of the two cavities are constrained by a weak harmonic potential, and lie on a circular arc separated by 90°. Thus, when a gravitational wave passes orthogonal to the plane of the interferometer, one cavity will be shortened as the other cavity is lengthened. If the intensity differ-

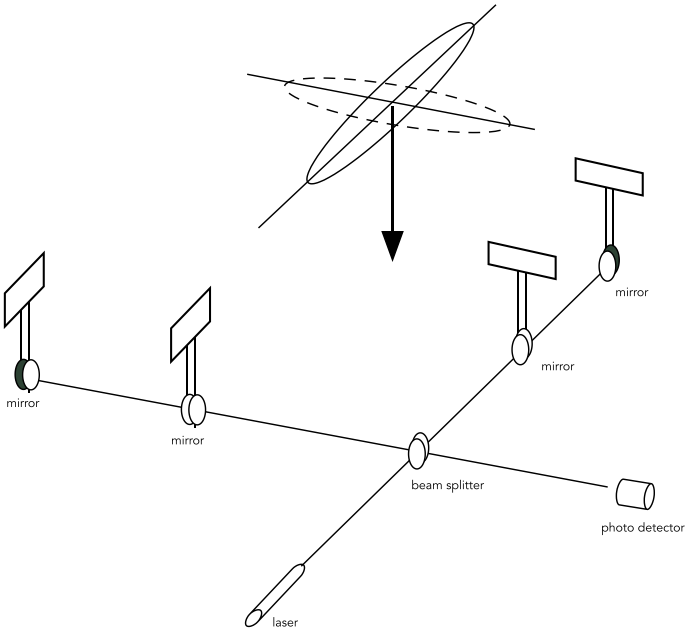

Fig. 16.7 A simplified scheme of LIGO consisting of a Michelson-Morley interferometer, with a Fabry-Perot cavity in each arm to 'store' light

ence of the light leaving each arm of the interferometer is monitored, the asymmetric detuning of each cavity caused by the moving end mirrors causes this intensity to be modulated at the frequency of the gravitational wave.

While gravitational radiation reaching terrestrial detectors is highly classical (many quanta of excitation), the interaction is weak. The relative change in the length of each cavity is then so small that it is easily lost amid a multitude of noise sources, which must somehow be reduced if any systematic effect is to be observed. To begin with, it is necessary to isolate the end mirrors from external vibrations and seismic forces. Then one must ensure that the random thermal motion of the end mirrors is negligible. Ultimately as each end mirror is essentially an oscillator, there is the zero-point motion to take account of.

Quite apart from the intrinsic noise in the motion of the end mirrors, noise due to the light also limits the sensitivity of the device. The light noise can be separated into two contributions. The measurement we ultimately perform is an intensity measurement which is limited by *shot-noise*. In the case of shot-noise, however, the signal-to-noise ratio scales as the square root of the input power, thus one might attempt to avoid this noise source by simply raising the input power. Unfortunately, increasing the input power increases the contribution from another source—*radiation pressure*. A careful study reveals that we can optimise these two complementary sources of noise. In this calculation we treat each end mirror as a damped simple harmonic oscillator subject to zero-point fluctuations and the classical driving force of the gravitational wave. We assume the thermal motion has been eliminated.

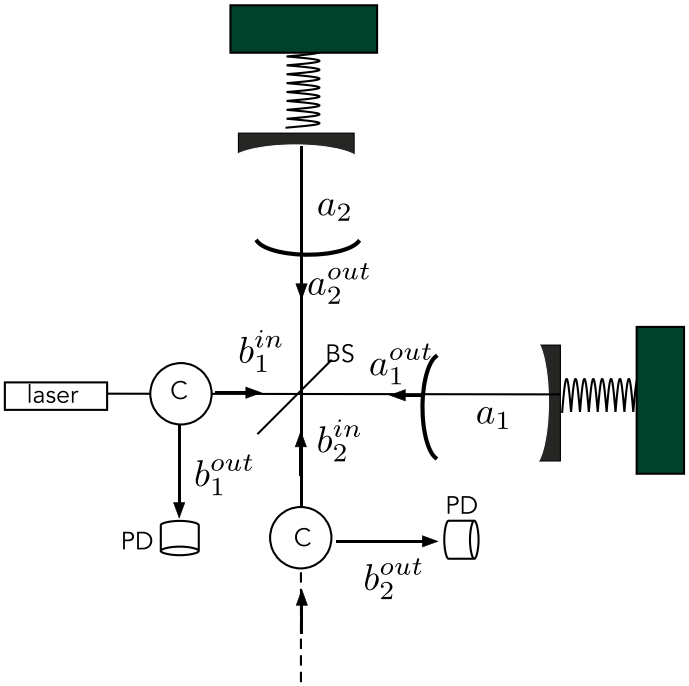

Fig. 16.8 The spatial optical modes used the quantum noise analysis. The symbol C denotes a circulator to spatially separate the input and output fields. The dashed line represents a vacuum inout. This is called the 'unused port'. The performance of the sensor can be improved by injecting squeezed light at this input

The spatial modes we will use are shown in Fig. 16.8. The measured signal is then determined by the photon number difference operator at the photo detectors (PD),

$$\hat{n}_- = b_1^{\dagger\,out} b_1^{out} - b_2^{\dagger\,out} b_2^{out} = -i\left[a_2^{\dagger\,out} a_1^{out} e^{-i\phi} - \text{h.c.}\right] \tag{16.61}$$

where where ϕ is a controlled phase shift inserted in arm 2 of the interferometer to enable the DC contribution to the output intensity difference to be eliminated. Assume that the laser is described by a coherent amplitude input with average field $E\gamma^{1/2}$, then each cavity is driven by the same amplitude that is $\epsilon = E/\sqrt{2}$ then $\langle a_k^{in}\rangle = \sqrt{\gamma}\epsilon$, such that $\langle a_k^{\dagger\,in} a_k^{in}\rangle$ has units of s^{-1}.

We turn now to a description of the intra-cavity dynamics. The end mirrors are treated as a quantised simple harmonic oscillator subject to radiation pressure forces due to the light in each cavity. Each cavity is thus a standard opto-mechanical resonator [19]. Define position and momentum operators Q, P for each mechanical oscillator. The radiation pressure force is proportional to the intra-cavity photon number. The total Hamiltonian for each cavity, in the interaction picture for the field,

then takes the form

$$H = \hbar \sum_{j=1}^{2} \Delta a_j^\dagger a_j + \Omega B_j^\dagger B_j + g_0 a_j^\dagger a_j (B_j + B_j^\dagger) \\ +(-1)^j f(t)(B_j + B_j^\dagger) - i(\epsilon^* a_j - \epsilon a_j^\dagger) \tag{16.62}$$

where ϵ is the coherent driving field for each cavity, $B_j^\dagger$, B_j are the raising and lowering operator for vibrations of the mechanical oscillator defined in terms of the position and momentum for each cavity,

$$Q_j = \left(\frac{2\hbar}{M\Omega}\right)^{1/2} (B_j + B_j^\dagger) \equiv \left(\frac{2\hbar}{M\Omega}\right)^{1/2} q_j \tag{16.63}$$

$$P_j = -i\,(\hbar M\Omega/8)^{1/2}\,(B_j - B_j^\dagger) \equiv (\hbar M\Omega/8)^{1/2}\,p_j \tag{16.64}$$

which imply that the commutation relations for the dimensionless canonical variables are $[q_j, p_j] = i$. The single photon opto-mechnical coupling rate is

$$g_0 = -\frac{\omega_0}{L}\left(\frac{2\hbar}{M\Omega}\right)^{1/2} \tag{16.65}$$

with ω_0, L the optical resonance frequency and length of the optical cavity respectively. We have take the gravitational wave to exert a time dependent force on each mirror $f(t) = f_0 \cos\omega_g t$ where $f_0 = hL\omega_g^2 \left(\frac{2M}{\hbar\Omega}\right)^{1/2}$ and h is the maximum fractional change in the length, L, of each cavity. The tidal forces acting on the mirrors are π out of phase due to the gravitational wave. For simplicity we will assume the cavities and mechanical resonators are identical.

The quantum stochastic differential equations are

$$\frac{da_j}{dt} = \epsilon - i\Delta a_j - \frac{\gamma}{2}a_j - ig_0 q_j a_j + \sqrt{\gamma}a_j^{in}, \tag{16.66}$$

$$\frac{dq_j}{dt} = \Omega p_j, \tag{16.67}$$

$$\frac{dp_j}{dt} = -\Omega q_j - g_0 a_j^\dagger a_j - (-1)^j f_0 s(t) - \Gamma_j p_j + \sqrt{\Gamma}p_j^{in} \tag{16.68}$$

where Γ is the frictional decay rate of each mechanical system (assumed to be the same for simplicity). The mechanical components correspond to the usual classical Langevin equations for frictional damping. These equations are non linear due to the opto-mechanical coupling. The corresponding semiclassical equations may not have a stable steady state, but assuming we operate in a regime where they do, we can linearise the un-driven small-amplitude dynamics around this fixed point.

The only difference between the two sets are in the phase of the driving force. In the absence of the gravitational wave we can thus treat the linearised dynamics as

the same for each opto-mechanical system and drop the subscript. Defining the new canonical operators as $\delta a = a - \alpha_0$, $\delta q = q - q_0$, $\delta p = p - p_0$ where α_0, q_0, p_0 are the semiclassical stable fixed points, see Exercise 16.3. We will now assume that we are in the highly under-damped regime for which $\Omega \ll \Gamma$.

The linearised semi-classical dynamics, in the under-damped limit, for the coupled opto-mechanical system, to lowest order in $g_0, \Gamma/\Omega$ is equivalent to

$$\frac{d}{dt}\begin{pmatrix}\delta x\\ \delta y\\ \delta q\\ \delta p\end{pmatrix} = \begin{pmatrix}-\frac{\gamma}{2} & 0 & 0 & 0\\ 0 & -\frac{\gamma}{2} & -\mu & 0\\ 0 & 0 & -\frac{\Gamma}{2} & \Omega\\ -\mu & 0 & -\Omega & -\frac{\Gamma}{2}\end{pmatrix}\begin{pmatrix}\delta x\\ \delta y\\ \delta q\\ \delta p\end{pmatrix} \tag{16.69}$$

where $\mu = 2g_0\alpha_0$ and $\alpha_0 = \frac{2\epsilon}{\gamma}$ is the steady state field amplitude in the cavity, taken real. the field quadrature fluctuation operators are defined by $\delta x = \delta a + \delta a^\dagger$ and $\delta y = -i(\delta a - \delta a^\dagger)$. It is clear that $\delta x(t) = \delta x(0)e^{-\frac{\gamma t}{2}}$. In the long-time limit, we can neglect the variables δx for the deterministic part of the motion. Secondly we note the mirror position fluctuations δq are literally coupled to δy and thus directly determine the output intensity difference signal. Finally, the fluctuations of the in-phase field variable δx drive the momentum of the mirror. This is the radiation pressure contribution. Setting $\delta x(0) = 0$, the mirror dynamics is especially simple—a damped harmonic oscillator.

When we linearise the output fields around the stationary states we find that the output signal is then determined by the operator

$$\hat{n}_- = \frac{\gamma\alpha_0}{2}(\delta y_1 - \delta y_2) - \frac{\sqrt{\gamma}\alpha_0}{2}(\delta y_1^{in} - \delta y_2^{in}) \tag{16.70}$$

where $\delta y_k = i(\delta a_k - \delta a_k^\dagger)$ and $\delta y_k^{in} = i(\delta a_k^{in} - \delta a_k^{\dagger\, in})$. We have chosen the arbitrary phase reference so that the input amplitude, and thus the steady state amplitude α_0, is real.

Each cavity may now be analysed using the input-output relations as the system is linear. The mean signal in a linearised semiclassical approximation can be shown to be [18]

$$\langle \hat{n}_-(t)\rangle = -\frac{32h\omega_0\omega_g^2 I\cos(\omega_g t + \theta + \phi)}{|\Gamma/2 + i(\omega_g - \Omega)||\Gamma/2 + i(\omega_g + \Omega)||\gamma/2 - i\omega_g|} \tag{16.71}$$

where,

$$I = \frac{4|\epsilon|^2}{\gamma^2} \tag{16.72}$$

$$\phi = -\arctan\left(\frac{\Gamma\omega_g}{\Gamma^2/4 + \Omega^2 - \omega_g^2}\right). \tag{16.73}$$

and $\theta = \arctan(\alpha_0\omega_g/\gamma)$. The signal is directly proportional to f_0 and thus to the mirror fractional displacement, h, so this is a linear sensor for the gravitational wave amplitude.

In the frequency domain we define the average signal as

$$|\langle n_-(\omega)\rangle| = S(\omega_g)\delta(\omega - \omega_g) \tag{16.74}$$

where

$$S(\omega_g) = -\frac{32h\omega_0\omega_g^2 I}{|\Lambda_+||\Lambda_-||\gamma/2 - i\omega|} \tag{16.75}$$

where

$$\Lambda_+ = \Gamma/2 + i(\omega - \Omega) \tag{16.76}$$

$$\Lambda_- = \Gamma/2 - i(\omega + \Omega) \tag{16.77}$$

while the noise power density, or signal variance is

$$V_{n_-}(\omega) = \langle n_-(\omega)n_-(\omega)^\dagger\rangle \tag{16.78}$$

Define the normalised variance by $N(\omega) = \frac{V_{n-}(\omega)}{2I}$ where I is the output intensity from each cavity. Using the input-output relations this is given by we find that this is

$$N(\omega) = 1 + \frac{16g_0^2 I\Gamma\left(\Gamma^2/4 + \Omega^2 + \omega^2\right)}{|\Lambda_+(\omega)|^2|\Lambda_-(\omega)|^2|\gamma/2 - i\omega|^2} + \frac{(16g_0^2 I)^2\Omega^2}{|\Lambda_+(\omega)|^2|\Lambda_-(\omega)|^2|\gamma/2 - i\omega|^4} \tag{16.79}$$

The first term in (16.79) is the shot-noise of the incident light on the detector. The second term is the mirror noise. It is a direct consequence of treating the mirror as a quantum harmonic oscillator damped into a zero-temperature white-noise bath. This white-noise bath produces frequency-independent fluctuations in the mirror's momentum which in turn produce small phase changes in the cavity light field and hence fluctuations in the output signal. The last term is the radiation pressure noise, which is produced by the intrinsic intensity fluctuations of the light field mode inside the cavity.

We now consider how accurate the estimation of the parameter h can be for this linear sensor. Using (16.75) we write the signal as

$$S(\omega) = f_s(\omega)h \tag{16.80}$$

Signal processing theory tells us that for a measurement of a signal at a frequency ω_g the uncertainty in the estimation is δh with

$$\delta h = \frac{\sqrt{2IN(\omega)}}{|f_s(\omega)|}\frac{1}{\sqrt{\tau/2}} \tag{16.81}$$

where the measurement time τ is much greater than the period of the gravity wave. The minimum detectable h is $h_{min} = \delta h$. We can then minimise δh as a function of mean photon number in each cavity, I (see (16.72)), which is proportional to the power of the coherent field driving the cavity. The resulting minimum detectable amplitude is [18]

$$h_{min}^2 \approx \frac{\hbar}{8M\omega_g^2 L^2 \tau \Omega^2}[2\Omega + \gamma] \tag{16.82}$$

The first term arises from the vacuum noise in the light and the second term arises form modelling the mirror as a quantised harmonic oscillator damped to a white noise bath.

Caves [14] proposed that the performance of the sensor would be improved if squeezed light was input the unused port of the interferometer, specifically, that the minimum detectable amplitude h_{min} could be achieved for lower laser power. In the case of squeezed light there is an extra parameter—the phase of the squeezing relative to the coherent amplitude of the coherent input, (see Fig. 1.1). When the minimum amplitude is also optimised with respect to this phase, we find that [18]

$$h_{min}^2 \approx \frac{\hbar}{8M\omega_g^2 L^2 \tau \Omega^2}[2e^{-2|r|}\Omega + \gamma] \tag{16.83}$$

where r is the squeezing parameter of the squeezed light injected input the empty port. The optimum phase of the squeezing with respect to the coherent field, at the optimum power, is $\pi/2$. The optimum power is independent of squeezing as the correlation term causes both the photon counting and radiation pressure noise terms to scale in exactly the same way.

Problems

16.1 The generator of displacements in quantum mechanics is the momentum operator. Show that if a displacement, x, is generated unitarily, the QCR bound for estimating this parameter is

$$\delta x^2 \geq \frac{\hbar^2}{N\langle \Delta \hat{p}^2 \rangle} \tag{16.84}$$

Investigate how cat states (Sect. 1.7) can be used to get close to this bound.

16.2 Consider the unitary squeezing transformation $S(r) = e^{r(a^2 - a^{\dagger\,2})/2}$
(a) Find the QCR bound for estimating r.
(b) If the input state is the vacuum state how close do photon number measurements get to the QCR bound?

16.3 The Bures statistical distance between two states ρ_1, ρ_2 is given by

$$(s_B(\rho_1, \rho_2))^2 = 2[1 - \mathrm{tr}\sqrt{\rho_1^{1/2}\rho_2\rho_1^{1/2}}] \tag{16.85}$$

(a) Setting $\rho_1 = |\psi\rangle\langle\psi|$ show that

$$s_B^2 = 2\left[1 - \sqrt{\langle\psi|\rho_2|\psi\rangle}\right] \tag{16.86}$$

(b) A cavity field is subject to dephasing decoherence described by the master equation

$$\dot{\rho} = -i\omega[a^\dagger a, \rho] + \Gamma\mathcal{D}[a^\dagger a]\rho \tag{16.87}$$

Solve this equation in the number basis for an initial coherent state and compute the rate of change of the Bures distance as a function of time. Interpret the results for the limits $t \to 0$ and $t \to \infty$.

16.4 Show that to lowest oder in g_0 the semiclassical fixed points for the optomechanical system of Sect. 16.6, in the absence of a gravitational wave are, $p_0 = 0, \alpha_0 = 2\epsilon/\gamma, q_0 = -g_0|\alpha_0|^2/\Omega$, where we choose $\Delta = -g_0 q_0$

References

1. C.W. Gardiner, *Handbook of Stochastic Processes for Physics Chemistry and the Natural Sciences* (Springer, 1985)
2. S.L. Braunstein, C.M. Caves, G.J. Milburn, Ann. Phys. **247** (1996)
3. S. Gammelmark, K. Molmer, Phys. Rev. Lett. **112**, 170401 (2014)
4. Y. Hasegawa, Phys. Rev. Lett. **125**, 050601 (2020)
5. G.J. Milburn, Contemp. Phys. **61**, 69 (2020)
6. Z. Aminzare , P. Holmes, V. Srivastava, *IEEE 58th Conference on Decision and Control (CDC)* (2019), p. 4717
7. C.W. Gardiner, *Handbook of Stochastic Processes for Physics, Chemistry and the Natural Sciences* (Springer, 1983)
8. T. Van Vu, K. Saito, Phys. Rev. Lett. **128**, 140602 (2022); M. Kewming, A. Kiely, S. Campbell, G.T. Landi, Phys. Rev. A **109**, L050202 (2024)
9. X. He, X.P. Pakkiam, A.A. Gangat, M.J. Kewming, G.J. Milburn, A. Fedorov, Phys. Rev. Appl. **20**, 034038 (2023)
10. Z. Ballard, C. Brown, A.M. Madni et al., Machine learning and computation-enabled intelligent sensor design. Nat. Mach. Intell. **3**, 556–565 (2021). https://doi.org/10.1038/s42256-021-00360-9
11. M. Krenn, J. Landgraf, T. Foesel, F. Marquardt, Phys. Rev. A **107**, 010101 (2023)
12. M.J. Kewming, S. Shrapnel, G.J. Milburn, Phys. Rev. A **103**, 032411 (2021)
13. https://www.ligo.caltech.edu
14. C.M. Caves, Phys. Rev. Lett. **45**, 75 (1980)
15. W.G. Unruh, in *Quantum Optics, Experimental Gravitation and Measurement Theory*, ed. by P. Meystre, M.O. Scully (Plenum, New York, 1983), p. 647
16. R.S. Bondurant, J.H. Shapiro, Phys. Rev. D **30**, 2548 (1984)
17. M.T. Jaekel, S. Reynaud, Europhys. Lett. **13**, 301 (1990)
18. A.F. Pace, M.J. Collett, D.F. Walls, Phys. Rev. A **47**, 3173 (1993)
19. W. Bowen, G.J. Milburn, *Quantum Optomechanics* (CRC Press, 2015)

Index

D. F. Walls and G. J. Milburn, *Quantum Optics*, Graduate Texts in Physics,
https://doi.org/10.1007/978-3-031-84177-4